

L. Cremer

M. Heckl

B.A.T. Petersson

Structure-Borne Sound

Structural Vibrations and Sound Radiation at Audio Frequencies

3rd edition

L.Cremer
M.Heckl
B.A.T.Petersson

Structure-Borne Sound

Structural Vibrations and Sound Radiation
at Audio Frequencies

3rd edition
With 215 figures and 13 tables



Springer

L. Cremer

M. Heckl

Prof. Dr. B.A.T. Petersson

Technische Universität Berlin
FG Technische Akustik
Einsteinufer 25
10587 Berlin
Germany

Library of Congress Control Number: 2004116521

ISBN 3-540-22696-6 **Springer Berlin Heidelberg New York**

This work is subject to copyright. All rights are reserved, whether the whole or part of the material is concerned, specifically the rights of translation, reprinting, reuse of illustrations, recitation, broadcasting, reproduction on microfilm or in other ways, and storage in data banks. Duplication of this publication or parts thereof is permitted only under the provisions of the German Copyright Law of September 9, 1965, in its current version, and permission for use must always be obtained from Springer-Verlag. Violations are liable to prosecution under German Copyright Law.

Springer is a part of Springer Science+Business Media
springeronline.com

© Springer-Verlag Berlin Heidelberg 2005
Printed in Germany

The use of general descriptive names, registered names, trademarks, etc. in this publication does not imply, even in the absence of a specific statement, that such names are exempt from the relevant protective laws and regulations and therefore free for general use.

Typesetting: Data conversion by the author.
Final processing by PTP-Berlin Protago-T_EX-Production GmbH, Germany
Cover-Design: deblik, Berlin
Printed on acid-free paper 62/3020/Yu – 5 4 3 2 1 0

Preface

The first edition of this book appeared in German in 1967. Parts were based on Prof. Lothar Cremer's work shortly after World War II, complemented by more recent research by Prof. Manfred Heckl. In 1973, the first English edition was published, translated and further complemented by Dr. Eric Ungar. Owing to the great interest with which the first English edition was received, a second edition, also in English, was issued in 1988. Apart from corrections and clarifications, the second edition also contained an update on waves in plates and shells.

Almost thirty years after the appearance of original edition, the second edition in German was published. This time, the book was given a thorough revision, whereby the material was restructured and several generalizations introduced. Although, Prof. Cremer passed away during the revision, much of his 'lines of thought' were retained also for the new sections. Another aspect observed in the revision was the computerization, making the analysis of more complicated structures more readily accessible. Importantly, however, this was employed without loosening focus on the fundamental physics. Shortly after his retirement and the publication, sadly Prof. Heckl died.

In this the third English edition, the revision of the material is continued. Moreover, the organization of the contents is modified in order better to take advantage of openings introduced by Prof. Heckl. Although significant parts have been thoroughly revised, the intention has been to preserve the style of previous editions i.e., to focus on the fundamentals to enable the reader to analyse further problems.

The author of the present third English edition is indebted to Ms. T. Lescau and Mrs. B. Töpfer-Imelmann for their ready efforts in processing the sometimes wearing text, equations and figures.

Finally, resting on the shoulders of his distinguished predecessors, it is the author's hope that this edition will prove as useful as the former.

Berlin, Summer 2004

Björn A.T. Petersson

Table of Contents

1 Introduction.....	1
2 A Little Dynamics	4
2.1 Single-Degree-of-Freedom Systems.....	4
2.2 Lagrange's Equations	9
2.3 Reciprocity and Mutual Energy.....	18
2.4 Modal Synthesis	20
2.5 Energy Considerations.....	20
2.5.1 Minimization of the Average Energy Difference (Hamilton's Principle)	22
2.5.2 The Rayleigh Quotient.....	24
References	25
3 Survey of Wave Types and Characteristics.....	27
3.1 Longitudinal Waves.....	27
3.1.1 Pure Longitudinal Waves	27
3.1.2 Quasi-Longitudinal Waves on Beams and Plates	33
3.2 Transverse Waves.....	39
3.2.1 Transverse Plane Waves	39
3.2.2 Torsional Waves	44
3.3 Bending Waves.....	49
3.3.1 Pure Bending Waves	49
3.3.2 Energy Relations.....	58
3.4 Wave Motions on Beams of Finite Length.....	60
3.4.1 Longitudinal Natural Vibrations.....	61
3.4.2 Natural Vibrations in Bending.....	67
3.5 The General Field Equations	74
3.6 Wave Field at a Free Surface.....	84
3.6.1 Reflection of Plane Waves	84
3.6.2 Excitation of an Elastic Half-Space	93
3.6.3. Surface Waves	96
3.7 Free Plate Waves	99
3.7.1 Boundary Conditions and Types of Solutions	99
3.7.2 Waves with Displacements only Parallel to the Surface	101
3.7.3 Waves with Displacements Perpendicular to the Surface	103

3.7.4 Equations of Motion for Thin Plates from the General Field Equations	109
3.8 Hamilton's Principle for the Derivation of the Equations of Motion.....	120
3.8.1 Fundamentals.....	120
3.8.2 Flat Plate with Shear Stiffness (The Corrected Bending Wave).....	121
3.8.3 Cylindrical Shells	126
3.9 Structure-Borne Sound Intensity	140
3.9.1 Fundamental Equations	140
3.9.2 Intensity in this Plates.....	141
3.9.3 Power Transmission in Thin-Walled Cylindrical Shells	145
References	147
4 Damping.....	149
4.1 Damping Mechanisms and their Mathematical Description.....	149
4.2 Complex Modulus and Wavenumbers.....	153
4.3. Resonant Vibrations of Damped Beams	161
4.3.1 Quasi-Longitudinal Waves and Torsional Waves	162
4.3.2 Bending Waves.....	169
4.4. Measurement of Complex Moduli.....	173
4.4.1 Measurements on Small Samples	174
4.4.2 Measurements on Beams	183
4.4.3 Measurements on Other than Beam-Like Samples	190
4.5 Experimental Data	191
4.5.1 Metals	191
4.5.2 Plastics	193
4.5.3 Building Materials	196
4.6 Plates with Attached Layers	197
4.6.1 Plates with Simple, Extensionally Loaded Layers	197
4.6.2 Plates with Multi-Layer Treatments	201
4.6.3 Equations of Motion of Layered Plates	208
4.7 Damping by means of Resonant Systems.....	217
4.7.1 Damping by Thick Layers (Ballast)	223
4.8 Damping at Joints	225
4.8.1 Damping by Relative Motion Normal to the Interface	226
4.8.2 Damping by Relative Motion Tangential to the Interface	230
References	232
5 Impedance and Mobility	236
5.1 Definitions	236
5.2 Measurement of Mobilities (Impedances)	238

5.2.1 Registration of Force and Velocity.....	238
5.2.2 Comparison with Known Mobilities	240
5.2.3 Other Measurement Methods	242
5.3 Input Mobility of Infinite Rods, Beams and Plates	244
5.3.1 Excitation of Quasi-Longitudinal Waves in Rods	244
5.3.2 Excitation of Bending Waves in Beams	245
5.3.3 Point Mobility of a Homogeneous Plate.....	251
5.4 Wave Impedance, Wave Mobility	256
5.4.1 Calculation of Wave Impedances and Wave Mobilities.....	256
5.4.2 Examples	257
5.4.3 Relation between Wave Mobility and Point Mobility.....	260
5.4.4 Moment Mobilities	272
5.4.5 Calculation of Impulse Response	275
5.5 Power Transmission to Infinite, Plane Structures.....	277
5.5.1 Determination of Structure-Borne Sound Power.....	277
5.5.2 Relationship with the Point Mobility.....	280
5.5.3 Interpretations and Examples	283
5.6 Summary of Impedance and Mobility Formulae; Approximations	286
5.7 Point-Excitation of Finite Systems	289
5.7.1 General Properties	290
5.7.2 Some Applications.....	294
5.7.3 Power Considerations	298
5.8 Some Specific Applications.....	306
5.8.1 Impact Excitation.....	306
5.8.2 Excitation by Sudden Release of Potential Energy	317
5.8.3 Rough Surfaces as Sources of Structure-Borne Sound.....	319
5.8.4 Parametric Excitation	322
5.8.5 Vibration Transmission from Machinery	326
References	338
 6 Attenuation of Structure-Borne Sound.....	 341
6.1 Material and Cross-Sectional Changes	341
6.1.1 Attenuation of Longitudinal Waves.....	342
6.1.2 Attenuation of Bending Waves.....	344
6.2 Right-Angled Corners and Branches	348
6.2.1 Incident Bending Wave	348
6.2.2 Incident Longitudinal Wave	353
6.2.3 Right Angled Branches with Incident Bending and Longitudinal Waves.....	354
6.3 Elastic Interlayers	359
6.3.1 Attenuation of Longitudinal Waves.....	360

6.3.2 Attenuation of Bending Waves.....	363
6.4 Blocking Masses.....	367
6.4.1 Attenuation of Longitudinal Waves.....	368
6.4.2 Attenuation of Bending Waves – Symmetric Blocking Masses	368
6.4.3 Attenuation of Bending Waves – Eccentric Blocking Masses	373
6.5 Periodic Structures.....	376
6.5.1 Periodic Mass-Spring Systems	376
6.5.2 Attenuation of Longitudinal Waves	380
6.5.3 Periodic Bending Wave-Guide	385
6.6 Hamilton's Principle for Transmission Problems.....	392
6.6.1 Procedure	392
6.6.2 An Introductory Example	394
6.6.3 Bending and Longitudinal Waves at an Eccentric Blocking Mass.....	397
6.7 Oblique Incidence.....	402
6.7.1 General Considerations	402
6.7.2 General Consequences of the Boundary Conditions	405
6.7.3 Examples	409
6.7.4 Application of Hamilton's Principle.....	420
6.8 Parallel Plates	422
6.8.1 Continuous Coupling by Elastic Interlayers	422
6.8.2 Point-Like Sound Bridges	427
6.9 Statistical Energy Analysis (SEA).....	430
6.9.1 Analogies to Statistical Room Acoustics.....	430
6.9.2 Energy Flow between Linearly Coupled Oscillators.....	434
6.9.3 Estimation of Coupling Loss Factors	437
6.9.4 Application	444
References	447
7 Sound Radiation from Structures	449
7.1 Measurement of Radiated Power.....	449
7.2 Definition and Measurement of Radiation Efficiency	451
7.3 Radiation Loss Factor.....	453
7.4 Elementary Radiators	455
7.4.1 Spherical Radiators.....	455
7.4.2 Dipole Radiators and Radiation from Forces	458
7.4.3 Infinite Plates	461
7.4.4 Cylindrical Radiators.....	465
7.4.5 Impulsive Sources	469
7.5 Plane, Baffled Radiators	472

7.5.1 The Plane Radiator as a Sum of Point Sources.....	473
7.5.2 Plane Radiators as Sum of Plane Waves	479
7.6 Radiation from Bending Waves.....	483
7.6.1 Semi-infinite plate	483
7.6.3 Modal Radiation	489
7.6.4 Radiation from Externally Excited Bending Waves.....	492
7.6.5 Comparison with Experiments	497
7.6.6 Additional Remarks on Structure-Borne Sound Radiation....	501
7.7 Fluid-Borne Sound Excitation of Structures.....	508
7.7.1 Transmission Loss of Single Leaf Wall.....	508
7.7.2 Double Walls with Sound Bridges	512
7.8 Relation between Radiation and Response.....	515
7.8.1 Reciprocity	515
7.8.2 Response and Radiation in a Reverberant Room	516
7.8.3 Directivity by Excitation and Radiation	519
7.8.4 Sound Transmission above the Critical Frequency	520
7.8.5 Transmission Loss in the Vicinity of the Critical Frequency	524
7.9 Application of Statistical Energy Analysis	525
7.9.1 Flanking Transmission	525
7.9.2 Double Walls	528
7.9.3 Multi-Layered Walls with Several Rigid Connections.....	531
References	533
8 Generation and Measurement of Structure-Borne Sound.....	536
8.1 Mechanical Measurement Methods	536
8.1.1 Registration of Motion.....	536
8.1.2 Comparison with Known Mobilities	538
8.1.3 Mechanical Transducers as Damped Mass-Spring Systems	541
8.1.4 Interaction of Transducer and Measurement Object	545
8.1.5 Immobile Reference and Rigid Termination	552
8.2 Controllable Sensors.....	553
8.2.1 Electrical Sensors	553
8.2.2 Optical Sensors	558
8.3 Excitation and Measurement of Structure-Borne Sound	560
8.3.1 Electro-Dynamic Transducers	561
8.3.2 Piezo-Electric Transducers	571
8.3.3 Electro-Static Transducers.....	578
8.3.4 Electro-Magnetic Transducers.....	583
8.3.5 Magnetostrictive Transducers.....	585
8.3.6 Elaboration on Reciprocal Transducers.....	586

8.4 Combined Quantities	589
References	591
List of Symbols and Notation.....	593
Index.....	598

1 Introduction

A major portion of the sound that reaches our ears – be it a chord from a guitar, the squeel from brakes or a lively discussion at the neighbours – originates from or is transmitted through vibrating solid structures. This field of physics, which encompasses generation, transmission, propagation and radiation of wave motions in solid structures is termed Structure-Borne Sound. In the name, the word “sound” indicates that the major emphasis is on the audible frequency range i.e., approximately between 16 Hz and 16 kHz. These limits, however, should not be taken as cast in stone. In contrast, it is often so that methods, developed for the audible range for one case, are applicable and suitable for the infra-sound (e.g. seismology) or ultra-sound (e.g. material science) ranges for other.

Even with the limits of the audible range imposed, the frequency range is very big and the field of structure-borne sound extremely rich. The latter is true for both the phenomena entangled and for the applications. The abundance of phenomena is partly a consequence of the multitude of materials and material combinations encountered, the almost unlimited structural configurations and, last but not least, the number of wave types that can exist in solids. With respect to applications, structure-borne sound is central to noise control in conjunction with practically all active artefacts, to material testing, to machine or process monitoring, to under-water radiation from ships or in conjunction with geo-prospecting, to medical diagnostics and to a specific class of fatigue problems related, for example, to aeronautics. The latter applications constitute the 'transition zone' to the field of non-linear vibrations. Although a single individual oscillation can be treated as linear, the, over time, extremely large number of oscillations will leave irreversible changes. Also in this non-linear field, the methods of structure-borne sound can be employed allowing for some minor amendments.

The associated particle oscillations and acting oscillating forces are usually very small but similarly, a limitation of the amplitude range to that of linear processes still leaves a vast range. With respect to particle motions, this range spans from 10^{-11} m for small, high frequency vibrations to 10^{-3} m by low frequency, vigorous vibrations. Accordingly, the particle velocity traverses a range from 0,1 $\mu\text{m/s}$ up to 1 m/s. Astonishingly, this means that

the acceleration can be expected to be in the range from a mm/s^2 to 10 km/s^2 . Herein are treated essentially linear processes so that a constant change in force results in a corresponding constant change in motion. If it is accounted for eventual changes in material parameters due to e.g., static loading, then most applications in practice involve linear processes. With the processes being linear, the applicability is warranted of the superposition principle.

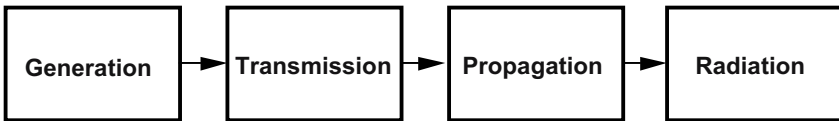


Fig. 1.1. Structural acoustic process

The structural acoustic process can be subdivided into four main stages as shown in Fig. 1.1. The first stage – generation – comprises the origin of an oscillation i.e., the mechanism behind it. The second – transmission – covers the transfer of oscillatory energy from the mechanisms of generation to a (passive) structure. In the structure, be it the passive part of the source or an attached receiving structure, the third stage – propagation – is recognised whereby energy is distributed throughout this structural system. Fourth, any structural part vibrating in a fluid environment (air) will impart power to that fluid - radiation - that is perceived as audible sound.

The complexity of the process generally calls for some kind of sub-structuring in order to concentrate on the, at each stage, essential physical phenomena. However, sub-structuring is often also dictated by the various parties involved. The source and the receiver are commonly associated with different companies, organisations or authorities with possibly different responsibilities. As an example, building services machinery can involve the manufacturer, the installation engineer, the constructor and the architect or proprietor.

Upon generalising, one may identify three types of situations;

- a machine (source) installed in a particular environment (receiver),
- a machine part (source) installed in a machinery (receiver),
- a sensitive piece of equipment (receiver) attached to a vibrating system (source).

In the first situation the source is causing unwanted sound or vibrations at or remote from the source location, e.g., a compressor in a building or a ship. The second type of situation relates to e.g., electric motors, pumps or

fans which are installed and enclosed in a unit, as for example a washing machine or a printer. Finally, the third category, which is expanding, are encountered in conjunction with precision industry such as micro-electronics and in the construction branch due to harder exploitation of land.

Although the three situations are clearly very different from the point of view of the parties involved and thus the sub-structuring will lead to different results, the subdivision of the structural acoustic process remains valid and unaffected for all situations. Moreover, the system considered as a source in one situation may contain a part which constitutes the source in another.

2 A Little Dynamics

2.1 Single-Degree-of-Freedom Systems

Precisely as for the treatment of fluid-borne sound, the kinematic and dynamic field variables constitute the primary ingredients in the treatment of structure-borne sound. An important difference is, however, that in most measurements of fluid-borne sound, the primary quantity is dynamic i.e., the sound pressure whereas it is a kinematic in measurements of structure-borne sound i.e., the displacement, velocity or acceleration. The dynamic quantities such as forces or stresses can be obtained via the constitutive relations for the material in the latter case. The reason for this difference is that the pressure is a scalar quantity and hence most manageable whilst the vectorial motion quantities, despite their direction dependence, are simpler to measure for structures.

As in classical dynamics, a corner stone for structure-borne sound is the single-degree-of-freedom system, often called the mass-spring-damper system. For such a system, the equation of motion can be written as

$$m \frac{d^2\xi}{dt^2} + r \frac{d\xi}{dt} + s\xi = F \quad (2.1)$$

where ξ is the displacement from equilibrium.

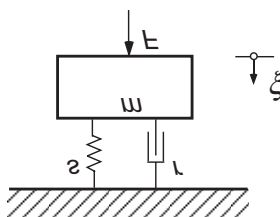


Fig. 2.1. Single-degree-of-freedom system with excitation F and displacement ξ

In this system, depicted in Fig. 2.1, the mass is denoted m , the viscous damping r and the stiffness s . If there is no excitation such that $F = 0$, the general solution is

$$\xi(t) = C_1 e^{\alpha_1 t} + C_2 e^{\alpha_2 t}.$$

Here the two constants C_1 and C_2 are to be determined from the initial conditions at time $t = 0$. α_1 and α_2 are the eigen-values i.e., the two roots of the characteristic equation

$$m\alpha^2 + c\alpha + s = 0.$$

With an external excitation ($F \neq 0$) the particular solution must be added such that

$$\xi(t) = \left[C_1 + \frac{1}{\alpha_1 - \alpha_2} g_1(t) \right] e^{\alpha_1 t} + \left[C_2 + \frac{1}{\alpha_2 - \alpha_1} g_2(t) \right] e^{\alpha_2 t},$$

where g_1 and g_2 represent the (indefinite) integrals

$$g_1 = \int \frac{F(t)}{m} e^{-\alpha_1 t} dt$$

$$g_2 = \int \frac{F(t)}{m} e^{-\alpha_2 t} dt,$$

and C_1 and C_2 , as before, are the integration constants which satisfy the initial conditions.

Assuming now that the system is subject to a steady-state harmonic excitation at the angular frequency ω such that the excitation is given in the form

$$F(t) = \hat{F} e^{j\omega t},$$

where \hat{F} is the force amplitude and

$$e^{j\omega t} = \cos \omega t + j \sin \omega t.$$

The use of the complex exponential $e^{j\omega t}$ to describe the time dependence of the physical force means that implicitly either is understood

$$F(t) = \operatorname{Re} [\hat{F} e^{j\omega t}] = \hat{F} \cos \omega t,$$

or, alternatively,

$$F(t) = \operatorname{Im} [\hat{F} e^{j\omega t}] = \hat{F} \sin \omega t.$$

The selection of the real or imaginary part is arbitrary as long as this choice is retained throughout the analysis and the physical interpretation of the results is made consistently. Herein, the first alternative will be employed.

Now, once the initial transients have faded, the steady-state response must also be harmonic of the same frequency as that of the excitation and one can assume that it can be written in the form

$$\xi(t) = D(\omega) \hat{F} e^{j\omega t},$$

where $D(\omega)$ is the complex frequency response function of the system. Upon substituting this into the equation of motion (2.1), it is clear that

$$(-\omega^2 m + j r \omega + s) D(\omega) = 1,$$

which means that

$$D(\omega) = \frac{1}{-\omega^2 m + j r \omega + s}.$$

If the undamped natural frequency squared is defined by

$$\omega_0^2 = \frac{s}{m},$$

together with the damping ratio as

$$\zeta = \frac{r}{2m\omega_0},$$

the frequency response function can be re-written as

$$D(\omega) = \frac{1}{m[-\omega^2 + 2\zeta j \omega \omega_0 + \omega_0^2]}.$$

From this complex-valued function, the amplitude ratio between the response and excitation can be developed to

$$|D| = \frac{1}{m\omega_0^2 \left[\left(2\zeta \frac{\omega}{\omega_0} \right)^2 + \left(1 - \frac{\omega^2}{\omega_0^2} \right)^2 \right]^{\frac{1}{2}}},$$

and the associated phase relation

$$\varphi_D = \arctan \left[\frac{\zeta \frac{\omega}{\omega_0}}{\left(1 - \frac{\omega^2}{\omega_0} \right)} \right].$$

So far, all what has been discussed follows the classical presentation of mechanical vibrations. For different reasons, however, use is made of velocity instead of displacement in acoustics and structure-borne sound. One such reason is that the scalar product of force and velocity yields the power, which is a convenient measure for stationary processes. Therefore, upon rewriting the equation of motion for the mass-spring-damper system in terms of the velocity,

$$\left(j\omega m + r + \frac{s}{j\omega} \right) v = F.$$

In this case, the employment of the frequency response function leads to the response

$$v(t) = Y(\omega) \hat{F} e^{j\omega t},$$

such that by means of a substitution into the equation of motion,

$$Y(\omega) = \frac{1}{j\omega m + r + \frac{s}{j\omega}}. \quad (2.2)$$

In Fig. 2.2, the magnitude and phase of this version of the frequency response function – conventionally termed the mobility – is plotted versus non-dimensional frequency ω/ω_0 for some different damping ratios. As can be seen, the low frequency region is featured by a positive slope, proportional to frequency. This corresponds to a stiffness controlled behaviour of the system i.e., the term $s/j\omega$ in the denominator is the governing for small ω . Close to the undamped natural frequency ω_0 , the response grows markedly, only constrained by the damping r . In this range, ωm and s/ω are numerically quite close but of opposite signs, precisely to cancel at the undamped natural frequency. The fact that for the damped system, the maximum of the mobility is slightly shifted from ω_0 is related to the minimum of the denominator. The maximum is shifted downwards from the frequency where the imaginary part vanishes and the phase therefore has a zero crossing. For the high frequency region, the mass term in Eq. (2.2) dominates the denominator, which means that the mobility becomes inversely proportional to frequency, resulting in a negative slope.

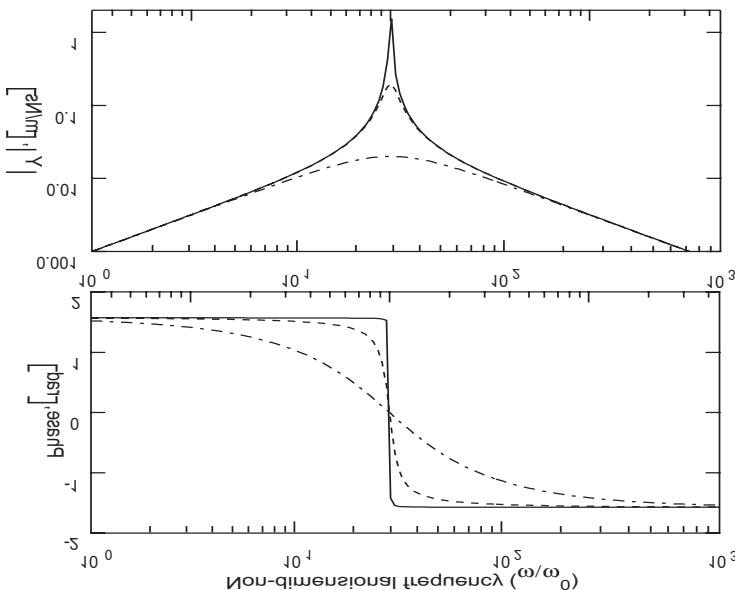


Fig. 2.2. Mobility of mass-spring-damper system for three values of damping versus non-dimensional frequency

In the phase, the stiffness controlled region is associated with a positive sign – the velocity leads the force – whereas for the mass controlled range the phase is negative – the velocity lags the force. As can be expected, there in between is a region in which the phase approaches zero and the velocity is in phase with the force. This is the resonantly or resistively controlled region where the damper essentially dictates the behavior of the system.

For the upside-down system, see Fig. 2.3, where the supporting structure realizes a constant harmonic motion, the free body diagram gives

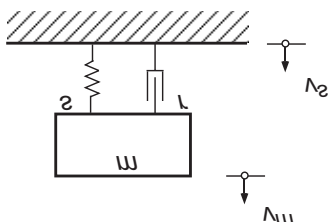


Fig. 2.3. Resiliently suspended mass with a moving base

$$(v_s - v_m)r + (v_s - v_m)\frac{k}{j\omega} = F, \quad (2.3)$$

$$j\omega mv_m = F. \quad (2.4)$$

Upon equating these linear relations the velocity ratio

$$\frac{v_m}{v_s} = \frac{\frac{1+jr\omega}{k}}{1 - \frac{\omega^2 m}{k} + \frac{j\omega r}{k}} = \frac{1}{1 - \frac{\omega^2}{\omega_0^2} + \frac{j\omega^2}{\omega_0^2} 2\zeta}$$

results, demonstrating that for frequencies below the undamped natural frequency, the velocity of the mass is essentially that of the supporting structure. For high frequencies on the other hand, the mass velocity is substantially smaller than that of the supporting structure. Only in the vicinity of the undamped natural frequency ω_0 , the mass velocity exceeds that of the supporting structure. Again the maximum is slightly displaced from the undamped natural frequency, see Fig. 2.4

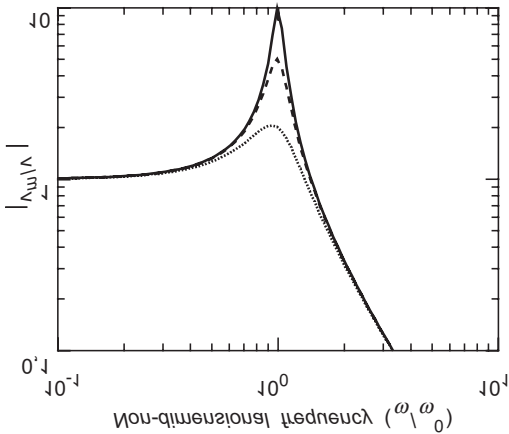


Fig. 2.4. Transfer function $H(\omega) = v_m/v_s$ for a resiliently suspended mass for three values of damping

2.2 Lagrange's Equations

Naturally, the approach of raising the equations of motion via force equilibrium can be used also for more complicated configurations than the two

previously discussed. Another possibility, which can be rather advantageous, is that termed Lagrange's equations of motion. Thereby, the explicit need of the force is removed and since the terms involved are primarily quadratic, the problem of sign errors markedly reduced. The Lagrange's equations are an alternative, energy based statement of Newton's law of motion and a derivation can start either from Newton's laws or, as will be seen in subsequently, from Hamilton's principle [2.1]. The method for deriving the equations of motion using Lagrange's equations consists of two steps:

- i) Determination of the total kinetic and potential energies of the system and
- ii) differentiation of the energies with respect to velocities and displacements.

To demonstrate the method, the system depicted in Fig. 2.5 will be considered. The total kinetic energy for the system can be written as

$$E_{kin} = \frac{1}{2} \sum_v^6 m_v v_v^2. \quad (2.5)$$

The potential energy is contained only in the springs in this case and it can be obtained via the assumption that each spring is compressed in several small steps of length Δl . After the q^{th} compression step, the total compression is $l_q = q \cdot \Delta l$ and at the end of the compression i.e., $q = Q$, the total compression is $Q\Delta l$. For each step, the compression force can be found from Hooke's law as $F_q = \Delta l \cdot s$, where s is the spring stiffness and adding all these steps the potential energy is given by

$$\begin{aligned} E_{pot} &= \sum_{q=0}^Q F_q \cdot l_q = s \sum_{q=0}^Q \Delta l \cdot l_q = s \sum_{q=0}^Q q (\Delta l)^2 = s (\Delta l)^2 \sum_{q=0}^Q q \\ &= s (\Delta l)^2 \frac{Q(Q+1)}{2} \approx \frac{1}{2} s (\Delta l \cdot Q)^2 = \frac{1}{2} s (l_Q)^2. \end{aligned}$$

The potential energy stored in a spring, therefore, is proportional to the total compression squared. When this relation is applied to the system in Fig. 2.5, the potential energy is found to be given by

$$\begin{aligned} E_{pot} &= \frac{1}{2} \left\{ s_1 (\xi_1 - \xi_2)^2 + s_2 \xi_2^2 + s_3 (\xi_1 - \xi_3)^2 + s_4 (\xi_1 - \xi_4)^2 \right. \\ &\quad \left. + s_5 (\xi_2 - \xi_5)^2 + s_6 (\xi_2 - \xi_6)^2 + s_0 (\xi_0 - \xi_1)^2 \right\}. \end{aligned} \quad (2.6)$$

It should be noted that the resulting energy is independent of whether, for example, $(\xi_1 - \xi_2)$ or $(\xi_2 - \xi_1)$ is used and the sign does not cause a

problem in this case. In the expression above are included the dummy spring s_0 and its (zero) compression. This establishes a way to account for a possible external force.

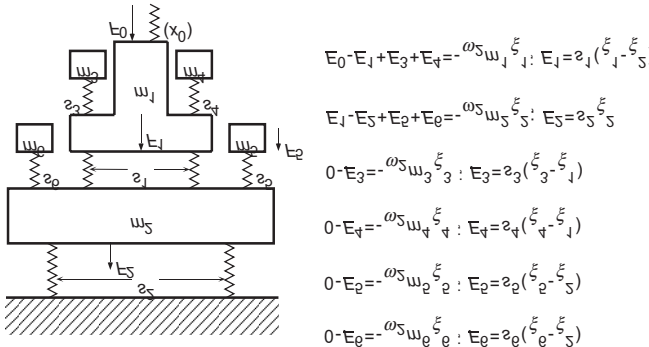


Fig. 2.5. Multi-degree-of-freedom system

As is readily found from a textbook on methods of theoretical physics, the procedure with the generalized Lagrange's equation consists in forming the expression

$$\frac{d}{dt} \frac{\partial (E_{pot} - E_{kin})}{\partial v_i} - \frac{\partial (E_{pot} - E_{kin})}{\partial \xi_i} = 0, \quad (2.7)$$

for $i = 1, 2, 3, 4, \dots$. Here, v_i and ξ_i are the unknown velocities and displacements respectively but not the prescribed and thus known displacement ξ_0 . It must be pointed out that in these calculations, v_i and ξ_i are real, time-dependent variables and no phasors.

In all cases treated herein as for many other problems in dynamics, it is possible to choose the co-ordinates in such a way that the kinetic energy depends only on the velocities whilst the potential energy only on the displacements. Equation (2.7) can accordingly be rewritten as

$$\frac{d}{dt} \frac{\partial E_{kin}}{\partial v_i} + \frac{\partial E_{pot}}{\partial \xi_i} = 0 ; i = 1, 2, 3, 4, \dots \quad (2.8)$$

Upon substituting Eqs. (2.5) and (2.6) into (2.7), the differentiations furnish six linear equations, establishing the equations of motion

$$\begin{bmatrix} a_{11} & -s_1 & -s_3 & -s_4 & 0 & 0 \\ -s_1 & a_{22} & 0 & 0 & -s_5 & -s_6 \\ -s_3 & 0 & a_{33} & 0 & 0 & 0 \\ -s_4 & 0 & 0 & a_{44} & 0 & 0 \\ 0 & -s_5 & 0 & 0 & a_{55} & 0 \\ 0 & -s_6 & 0 & 0 & 0 & a_{66} \end{bmatrix} \begin{bmatrix} \xi_1 \\ \xi_2 \\ \xi_3 \\ \xi_4 \\ \xi_5 \\ \xi_6 \end{bmatrix} = \begin{bmatrix} s_0 \xi_0 \\ 0 \\ 0 \\ 0 \\ 0 \\ 0 \end{bmatrix},$$

in which the abbreviations

$$\begin{aligned} a_{11} &= m_1 \frac{d^2}{dt^2} + s_1 + s_3 + s_4, & a_{22} &= m_2 \frac{d^2}{dt^2} + s_1 + s_2 + s_5 + s_6, \\ a_{33} &= m_3 \frac{d^2}{dt^2} + s_3, & a_{44} &= m_{14} \frac{d^2}{dt^2} + s_4, & a_{55} &= m_5 \frac{d^2}{dt^2} + s_5 \\ \text{and } a_{66} &= m_6 \frac{d^2}{dt^2} + s_6 \end{aligned}$$

have been used. An external excitation of the system can readily be accounted for by selecting the spring stiffness s_0 small so that $s_0 \xi_1 \rightarrow 0$ and ξ_0 such that the product $s_0 \xi_0$ equals the external force. By means of an inversion of the matrix, the unknown displacements can be found.

As an example, the mobility $Y = j\omega \xi_1 / F_0$ at the excitation point is shown in Fig. 2.6 for a set of given parameters.

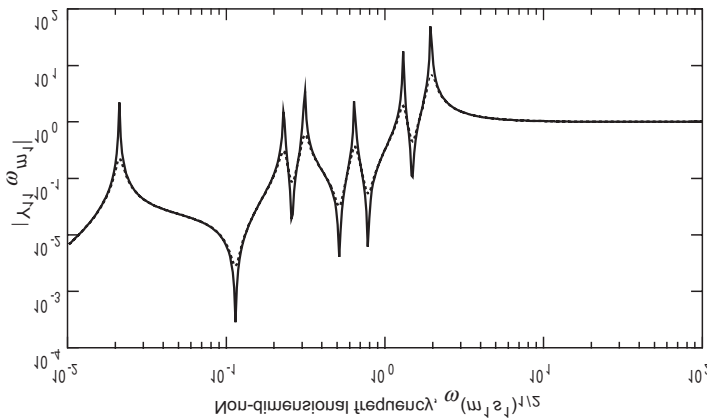


Fig. 2.6. Point mobility of the system in Fig. 2.4 at the position of F_0 . Parameters: $m_2/m_1 = 1$, $m_3/m_1 = 3$, $m_4/m_1 = 1.8$, $m_5/m_1 = 5$, $m_6/m_1 = 32$, $s_2/s_1 = 0.02$, $s_3/s_1 = 0.8$, $s_4/s_1 = 1.1$, $s_5/s_1 = 0.4$, $s_6/s_1 = 0.76$, (—) $\eta = 0.01$ and (- - -) $\eta = 0.1$

The advantage of Lagrange's equations is perhaps most easily seen when the vibration of complicated system are considered. The finite element method serves a suitable example whereby every part of the system is modelled by small elements whose motion are obtained from Eq. (2.7) or some of its derivatives. Without further pursuing the features of FEM, the strength of Lagrange's equations will be illuminated by another example where the complexity is enhanced by allowing for different translatory motions as well as rotations. Considered is the system depicted in Fig. 2.7, which can translate in the x - and y -directions as well as rotate around the z -axis. For the kinetic energy, therefore, the translatory velocities v_{cx} and v_{cy} as well as the rotatory velocity $\dot{\phi}_{cz} = d\phi_{cz} / dt$ have to be taken into account, which yields

$$E_{kin} = \frac{1}{2}m(v_{cx}^2 + v_{cy}^2) + \frac{1}{2}\Theta\dot{\phi}_{cz}^2, \quad (2.9)$$

where m is the mass and Θ the mass moment of inertia of the rigid block.

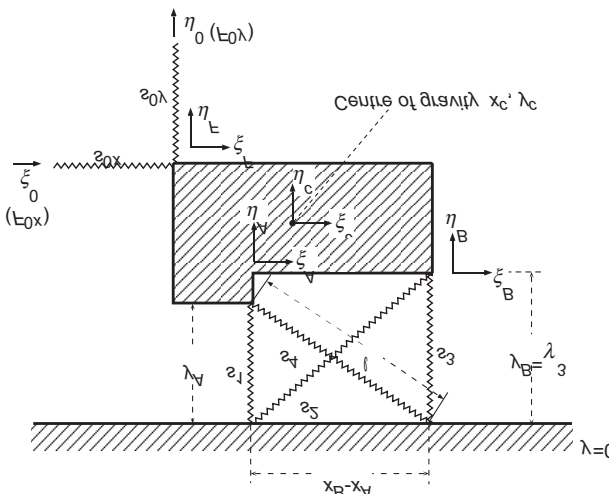


Fig. 2.7. Rigid body supported by several springs

For the potential energy a few extra steps have to be taken since the components of motion are coupled. In view of Eq. (2.6), a spring of stiffness s connecting the coordinates (x_v, y_v) with (x_μ, y_μ) gives

$$E_{pot} = \frac{s}{2} (l_c - l_e)^2$$

where l_c means the length of the spring after deformation and l_e is that at equilibrium. Relying upon Pythagoras, a virtual movement as shown in Fig. 2.8 means that

$$l_c = \left\{ [(x_v + \xi_v) - (x_\mu + \xi_\mu)]^2 + [(y_v + \eta_v) - (y_\mu + \eta_\mu)]^2 \right\}^{1/2}$$

The length of the spring at equilibrium is given by

$$l_e = \left\{ (x_v - x_\mu)^2 + (y_v - y_\mu)^2 \right\}^{1/2}$$

After substitution into the expression for the potential energy, it is found that

$$E_{pot} = \frac{s}{2} l_e^2 \left[\left\{ 1 + 2 \frac{x_v - x_\mu}{l_e^2} (\xi_v - \xi_\mu) + 2 \frac{y_v - y_\mu}{l_e^2} (\eta_v - \eta_\mu) \right\}^{1/2} - 1 \right]^2. \quad (2.10)$$

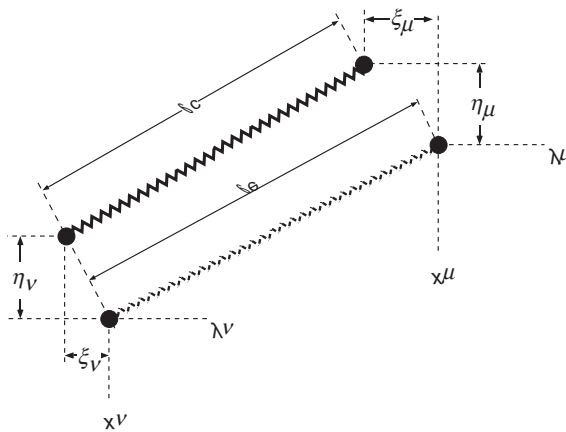


Fig. 2.8. Co-ordinates of a spring at equilibrium and in a tensioned state

Since $|x_v - x_\mu| \leq l_e$ and $|\xi_v - \xi_\mu| \ll l_e$ as well as the corresponding for y and η , all the terms with l_e^2 in the denominator are much smaller than unity and accordingly the asymptote

$$(1 + \varepsilon)^{\frac{1}{2}} \approx 1 + \frac{\varepsilon}{2},$$

is valid. Thus, the potential energy simplifies to

$$E_{pot} = \frac{s}{2} l_e^2 \left[\frac{x_v - x}{l_e^2} (\xi_v - \xi_\mu) + \frac{y_v - y_\mu}{l_e^2} (\eta_v - \eta_\mu) + R_\xi + R_\mu \right]^2$$

wherein the remainders R_ξ and R_μ represent second order terms of the motion which can be viewed as “geometric non-linearities”. Such non-linearities appear even when the spring material is completely linear. Obviously, they would play an important role whenever $|\xi_v - \xi_\mu| \geq |x_v - x_\mu|$ or $|\eta_v - \eta_\mu| \geq |y_v - y_\mu|$ i.e., when the movement is of the same order of magnitude as the smallest dimension of system. This means that for very oblique springs and large displacements the geometrical non-linearities do play a role. For instance, the geometrical non-linearities are definitely present when the displacements of a plate movement are of the same order of magnitude as the plate thickness [2.2]. Also, the amplitude dependence of the contact stiffness described by Hertz [2.3] is of this type.

In this textbook, the focus is on linear oscillations, which means that the remainders R_ξ and R_μ can be omitted such that the potential energy, stored in a spring, in a two-dimensional configuration can be written as

$$E_{pot} = \frac{s}{2} \left[\frac{x_v - x_\mu}{l_e} (\xi_v - \xi_\mu) + \frac{y_v - y_\mu}{l_e} (\eta_v - \eta_\mu) \right]^2.$$

The next step is to express the displacements ξ, η relative to an arbitrary origin for the system co-ordinates. With the assumption that the centre of gravity at equilibrium is situated at (x_c, y_c) and its displacement is (ξ_c, η_c) , see Fig. 2.9, then the rotational part of the translation is obtained from

$$\begin{aligned} \xi_R &= (x - x_c) \cos \varphi - (y - y_c) \sin \varphi - (x - x_c) \\ \eta_R &= (x - x_c) \sin \varphi + (y - y_c) \cos \varphi - (y - y_c). \end{aligned} \quad (2.11)$$

The trigonometric functions in Eq. (2.11), indeed, realizes a non-linear relationship between the rotation and the translation. For the oscillations of interest in this context, however, the approximations $\cos \varphi \approx 1$ and $\sin \varphi \approx \varphi$ are applicable and yield

$$\xi_R = -(y - y_c)\varphi,$$

$$\eta_R = (x - x_c)\varphi.$$

One can note that this kind of non-linearity comes into play by amplitudes, which are certainly larger than those associated with Eq. (2.11).

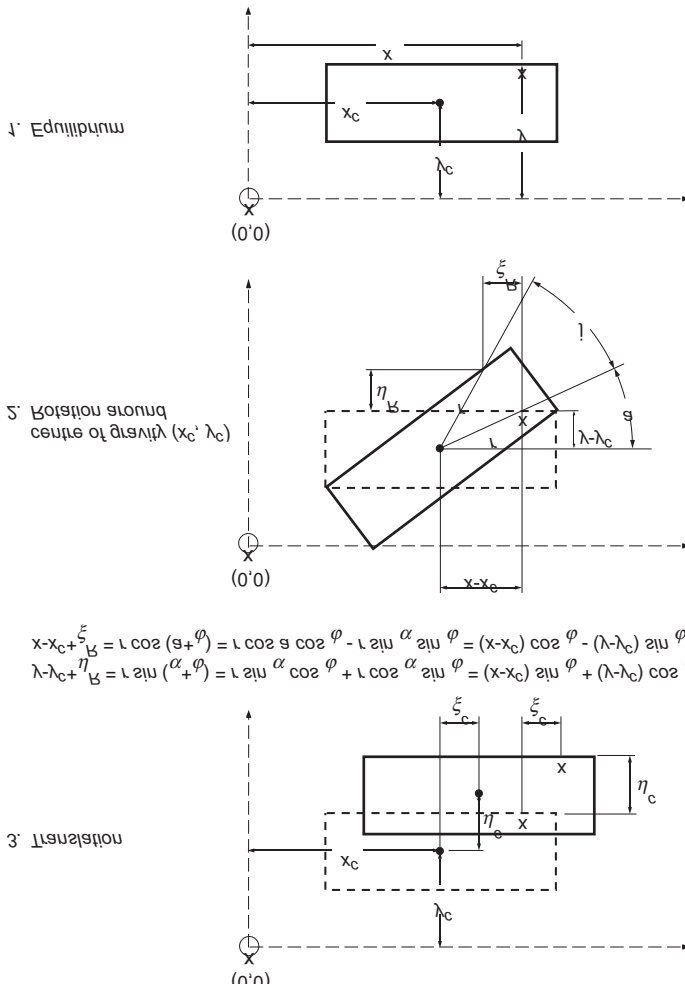


Fig. 2.9. Rotation and translation of a rigid body

By adding the translatory and rotatory parts, the net displacement of any position (x, y) on the rigid body becomes

$$\begin{aligned}\xi &= \xi_c + \xi_R = \xi_c - (y - y_c)\varphi \\ \eta &= \eta_c + \eta_R = \eta_c + (x - x_c)\varphi.\end{aligned}\quad (2.12)$$

With these components introduced in the expression for the potential energy stored in a spring and summing over the individual springs, the total potential energy of the system considered is obtained as

$$\begin{aligned}E_{pot} &= \frac{s_1}{2} \left[\frac{y_A}{l_1} \eta_A \right]^2 + \frac{s_2}{2} \left[\frac{x_B - x_A}{l_2} \xi_B + \frac{y_B}{l_2} \eta_B \right]^2 \\ &+ \frac{s_3}{2} \left[\frac{y_B}{l_3} \eta_B \right]^2 + \frac{s_4}{2} \left[\frac{x_A - x_B}{l_4} \xi_A + \frac{y_A}{l_4} \eta_A \right]^2 \\ &+ \frac{s_{0x}}{2} [\xi_F - \xi_0]^2 + \frac{s_{0y}}{2} [\eta_F - \eta_0]^2.\end{aligned}\quad (2.13)$$

In this expression s_1 to s_4 are the stiffnesses of the individual springs and l_1 to l_4 their length at equilibrium. s_{0x} and s_{0y} are the auxiliary springs for the external excitation. The explicit calculation is principally quite simple but somewhat tedious. Facilitating is a mathematical computer application with symbolic capabilities. The individual steps are:

- Substitution of (2.12) into (2.13) with $x = x_A$, $y = y_A$, $x = x_B$, $y = y_B$ and $x = x_F$, $y = y_F$ respectively.
- Substitution of the resulting total potential energy as well as the total kinetic energy in (2.9) into (2.8).
- Differentiation with respect to v_{cx} , v_{cy} , $\dot{\varphi}$, ξ_c , η_c and φ .
- Transformation to phasor notation.
- Letting the stiffnesses s_{0x} and s_{0y} approach zero with a simultaneous increase of the displacements such that the products $\xi_0 s_{0x}$ and $\eta_0 s_{0y}$ yield the forces F_{0x} and F_{0y} respectively

The resulting set of equations can be written on the form

$$\begin{bmatrix} A_{11} & A_{12} & A_{13} \\ A_{21} & A_{22} & A_{23} \\ A_{31} & A_{32} & A_{33} \end{bmatrix} \begin{Bmatrix} \xi_c \\ \eta_c \\ \varphi \end{Bmatrix} = \begin{Bmatrix} F_{0x} \\ F_{0y} \\ F_{0x} + F_{0y} \end{Bmatrix},$$

whereby $A_{\nu\mu}$ are the rather lengthy expressions containing the geometrical information.

In Fig. 2.10 are exemplified the point mobilities for two excitation positions. Observed is the strong dependence on excitation position since rotations are easily excited for this configuration. Observed are also the two 'side-resonances', which appear on either side of the main resonance. Al-

though they are clearly visible for both excitation positions, they become particularly pronounced when the excitation is remote from the centre of gravity. This is a consequence of the fact that the springs are neither symmetrically arranged nor equal. The coupling of the different degrees of freedom and thereof resulting multiple resonance's (maximum six) are often overlooked by measurements on quasi-rigid bodies and can be the reason for errors.

The procedure with the Lagrange's equations is not only a very useful tool to establish the equations of motion but is also most suitable for deriving important general theorems for linear multiple-degree-of-freedom system. Owing to the fact that those theorems are thoroughly treated in textbooks on mechanical vibration, the most important theorems are herein given without proofs.

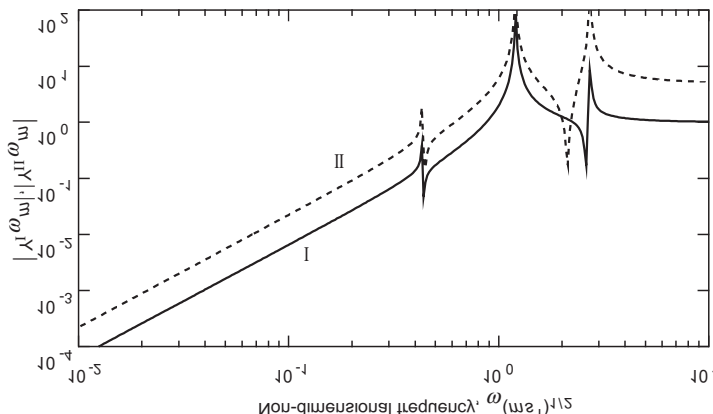


Fig. 2.10. Point mobilities at different positions of a rigid body. (—) above center of gravity and (- - -) at the edge. Parameters: $s_2 = 0.1 s_1$, $s_3 = s_1$, $s_4 = 0.2 s_1$, $r_Q = 0.23l$, $Q = mr_Q^2$

2.3 Reciprocity and Mutual Energy

Owing to the quadratic forms of the in this context interesting energy relations, the systems of equations are consistently symmetric. One of the consequences is the reciprocity principle. This principle establishes a relation between the field variables such that the excitation and response positions can be interchanged. The prerequisite is that the product of the variables to be interchanged yields the power or energy. A generalization of the recip-

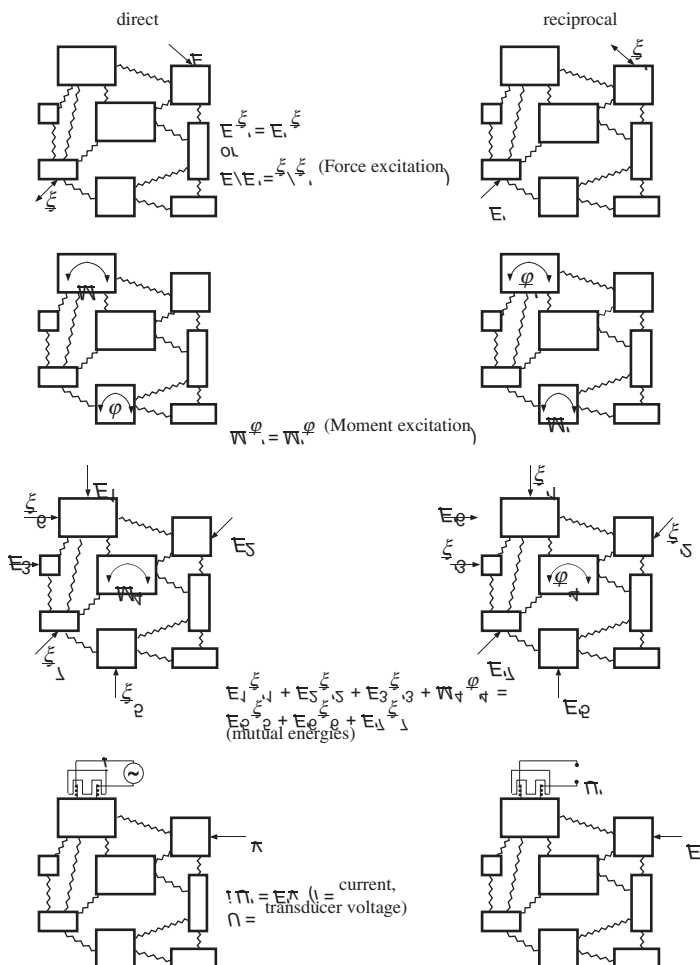


Fig. 2.11. Reciprocity and mutual energies

Reciprocity principle is the theorem of the mutual energies [2.4]. In Fig. 2.11 are exemplified the corresponding relations in phasor notation.

For systems comprising reciprocal transducers, the mutual product of current and voltage can be comprised in the reciprocity relations. The proof can be obtained via Hamilton's principle when this is employed on electrical energy reservoirs, see Eq. (8.53).

2.4 Modal Synthesis

From linear algebra it can be shown that multiple-degree-of-freedom systems exhibit a sequence of eigen-frequencies and that those frequencies are given by the singularities of the coefficient matrix [2.5]. Corresponding to every resonance frequency are one or more characteristic amplitude distributions termed eigen-vectors or modes. Furthermore, it can be shown that any amplitude distribution can be described as a sum of modes. For low frequencies, often only a few modes suffice to give a good approximation of the vibration. The advantage is that with a knowledge of the eigenfrequencies and eigen-vectors, e.g. from an FE-analysis or an experimental modal analysis, the descriptions of the low frequency behaviour is readily established [2.5, 2.6].

2.5 Energy Considerations

In the previous sections, the kinetic and potential energies were used to develop the equations of motion. This section aims at demonstrating that the energy expressions also are highly suitable for the treatment of vibration problems.

The energy flow can be predicted from the equations of motions, which represent the equilibrium of forces, through a multiplication with the velocities of the oscillators. This is readily seen for the damped mass-spring system excited by an external force F . Upon multiplying the equation of motion

$$m\xi\ddot{\xi} + r\xi\dot{\xi} + s\xi = F \quad (2.14)$$

with the velocity $\dot{\xi}$, the power balance

$$m\xi\ddot{\xi} + r\xi\dot{\xi}^2 + s\xi\dot{\xi} = \frac{1}{2} \frac{d}{dt} (m\xi^2) + \frac{1}{2} \frac{d}{dt} (s\xi^2) + r\xi^2 = F\xi\dot{\xi}$$

is obtained. By re-writing it as

$$\frac{d}{dt} \left(\frac{1}{2} m\xi^2 + \frac{1}{2} s\xi^2 \right) + r\xi^2 = F\xi\dot{\xi},$$

it is seen that this is equivalent with

$$\frac{d}{dt} (E_{kin} + E_{pot}) + W_d = W. \quad (2.15)$$

This expression reveals that the transmitted power to the system $W = F \cdot v$ is either dissipated by the damper or serves as to change the total energy combined of the kinetic and potential parts. In stationary state, the part preceded by d/dt i.e., any change in total energy vanishes per definition and the power transmission equals that dissipated. In Eqs. (2.14) and (2.15) the instantaneous values are used which means that for the employment of phasor notation, it has to be observed that power or energy are products of field variables. Therefore,

$$W = F \dot{\xi} = F \cdot v = \operatorname{Re}\{Fe^{j\omega t}\} \operatorname{Re}\{ve^{j\omega t}\},$$

since the operator $\operatorname{Re}\{ \}$ and the time base $e^{j\omega t}$ cannot be omitted.

Letting $\underline{F} = |F| e^{j\varphi}$ and $\underline{v} = |v| e^{j\psi}$ respectively, the power can be rewritten as

$$W = |\underline{F}| |\underline{v}| \operatorname{Re}\{e^{j(\omega t + \varphi)}\} \operatorname{Re}\{e^{j(\omega t + \psi)}\}$$

which is equivalent to

$$W = |\underline{F}| |\underline{v}| \cos(\omega t + \varphi) \cos(\omega t + \psi)$$

or

$$W = \frac{1}{2} |\underline{F}| |\underline{v}| [\cos(2\omega t + \varphi + \psi) + \cos(\varphi - \psi)].$$

For harmonic vibrations accordingly, the power consists of a part with the double frequency and a part that is time invariant. This means that for the usually most interesting temporal average

$$W = \frac{1}{2} |\underline{F}| |\underline{v}| \cos(\varphi - \psi) = \frac{1}{2} |\underline{F}| |\underline{v}| \operatorname{Re}\{e^{j(\varphi - \psi)}\} = \frac{1}{2} \operatorname{Re}\{|\underline{F}| e^{j\varphi} |\underline{v}| e^{-j\psi}\},$$

which clearly is equivalent to

$$W = \frac{1}{2} \operatorname{Re}\{\underline{F} \cdot \underline{v}^*\}, \quad (2.16)$$

where $*$ denotes the complex conjugate. With this relation applied to Eq. (2.15)

$$\frac{1}{2} r \operatorname{Re}\{\dot{\underline{\xi}} \cdot \dot{\underline{\xi}}^*\} = \frac{r}{2} |\dot{\underline{\xi}}|^2 = \frac{r}{2} |\underline{v}|^2 = \frac{1}{2} \operatorname{Re}\{\underline{F} \cdot \underline{v}^*\}.$$

An extension to multiple-degree-of-freedom systems is rather simple starting from Eq. (2.7) and performing the same steps after introduction of the damping terms and external forces.

2.5.1 Minimization of the Average Energy Difference (Hamilton's Principle)

One of the most important laws in physics is Hamilton's principle. When applied in classical dynamics it states that the motion of the different components of a system always adjust themselves so that an extreme value of the temporally averaged difference between kinetic and potential energy is obtained. For the cases studied in this context the extremum is always a minimum. It is astonishing that so simply stated a principle can represent such a multitude of physical processes. Furthermore, it is noteworthy that by employing Hamilton's principle, all physical processes can be described without the concept of force i.e., "without pressure or enforcement/constraint" albeit transcriptions might be required in some cases. Some implicit problems associated with the force concept are discussed in [2.7].

The mathematical representation of Hamilton's principle can be written as

$$\frac{1}{t_2 - t_1} \int_{t_1}^{t_2} (E_{kin} - E_{pot}) dt = \text{Extremum (Minimum)}. \quad (2.17)$$

Since a minimum or an extremum of a smooth, well-behaved function is featured by no or smaller than linear variations of the ordinate in its vicinity, the statement in Eq. (2.17) is equivalent to a vanishing variation of the energy difference i.e.,

$$\delta \int_{t_1}^{t_2} (E_{kin} - E_{pot}) dt = 0. \quad (2.17a)$$

The constant factor $t_2 - t_1$ thus disappears. δ denotes the variation and in the next example will be shown how it can be obtained through differentiations. Again, a single-degree-of-freedom system is considered, excited by a prescribed deformation ξ_0 of a spring s_0 as shown in Fig. 2.12. Clearly, the expression

$$\delta \int_{t_1}^{t_2} \left(\frac{1}{2} m \dot{\xi}^2 - \frac{1}{2} s \dot{\xi}^2 - \frac{1}{2} s_0 (\xi_0 - \xi)^2 \right) dt = 0 \quad (2.18)$$

is to be manipulated. For the variation, the fact that small changes (variations) of an arbitrary function $g(x_1, x_2, \dots)$ can be obtained from the changes of the arguments as

$$\delta \{g(x_1, x_2, \dots)\} = \frac{\partial g}{\partial x_1} \delta x_1 + \frac{\partial g}{\partial x_2} \delta x_2 + \dots$$

Herein, δx_1 and δx_2 etc. are the variations of the arguments. Application on Eq. (2.18) yields

$$\int_{t_1}^{t_2} \left(m\dot{\xi}\delta\dot{\xi} - s\xi\delta\xi + s_0(\xi_0 - \xi)\delta\xi \right) dt = 0 .$$

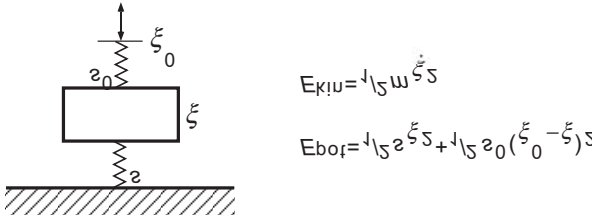


Fig. 2.12. Mass-spring system excited by means of a prescribed displacement via a spring

By means of integration by parts, the first term can be brought onto the, in this case, more useful form of

$$m \int_{t_1}^{t_2} \dot{\xi}\delta\dot{\xi} dt = m \int_{t_1}^{t_2} \frac{d\xi}{dt} \delta \left(\frac{d\xi}{dt} \right) dt = m \left[\frac{d\xi}{dt} \delta\xi \right]_{t_1}^{t_2} - m \int_{t_1}^{t_2} \frac{d^2\xi}{dt^2} \delta\xi dt .$$

If the integration limits are chosen such that the velocity $d\xi/dt$ is zero at those points, the term in the bracket vanishes and hence Eq. (2.18) becomes

$$\int_{t_1}^{t_2} \left(-m \frac{d^2\xi}{dt^2} - s\xi - s_0\xi + s_0\xi_0 \right) \delta\xi dt = 0 .$$

The expression above must be equal to zero for all, possibly time dependent, variations $\delta\xi$. This is only possible if the expression with the parenthesis is identically zero and accordingly

$$m \frac{d^2\xi}{dt^2} + s\xi + s_0\xi = s_0\xi_0$$

which is the equation of motion sought for the system in Fig. 2.12. With several masses and springs involved, the procedure is principally the same but since the corresponding operations are identical to those described previously in conjunction with the Lagrange's equations (Eq. (2.7)) it is here refrained from such developments. Subsequently, Hamilton's principle will be employed on other interesting cases.

2.5.2 The Rayleigh Quotient

So far, the important relations discussed have been derived from sums and differences of energies. In this section is described a procedure based on equality in energies [2.8, 2.9].

A prerequisite for the application of the Rayleigh quotient is the assumption that at all resonances (but not outside resonances) and free vibrations

$$\overline{E_{pot}} = \overline{E_{kin}} \quad (2.19)$$

is valid whereby the over bar denotes averaging over one or more periods of vibration.

If, for example, a multi-degree-of-freedom system vibrates at one of its eigen-frequencies ω_n then the displacement and the velocity of the v-th mass have the time dependencies

$$\xi_v(t) = \xi_{vA} \cos(\omega_n t + \phi_v); \quad v_v(t) = -\omega_n \xi_{vA} \sin(\omega_n t + \phi_v),$$

respectively. Upon averaging over one or more periods is obtained

$$\overline{\xi_v(t)^2} = \frac{1}{2} \xi_{vA}^2; \quad \overline{v_v(t)^2} = \frac{1}{2} \omega_n^2 \xi_{vA}^2.$$

Accordingly, the eigen-frequency squared (eigen-value) of a multi-degree-of-freedom system, where the v-th mass has a displacement amplitude ξ_{vA} , is given by

$$\omega_n^2 = \frac{\overline{E_{pot}}}{\frac{1}{2} \sum \frac{1}{2} m_v \xi_{vA}^2} \quad (2.20)$$

Owing to the temporal average, no phase information is required and the potential energy is also a function of the amplitude ξ_{vA} only.

The advantages of the expression in Eq. (2.20) for the estimation of eigen-frequencies (resonance frequencies) are that

- surprisingly good approximations are obtained for the first few eigen-frequencies when realistic assumptions for the amplitudes are introduced and
- expression (2.20) has the character of a minimum such that when guessed amplitudes are employed, an upper limit is found for the eigen-frequency. Indeed, this minimum character of the Rayleigh quotient can be used to find the true amplitude iteratively by means of variation until the eigen-value ω_n^2 becomes a minimum [2.1].

To highlight this, a simple mass-spring-mass system can be considered where the two masses have the amplitudes ξ_{1A} and ξ_{2A} respectively. The temporally averaged kinetic and potential energies are thus given by

$$\overline{E_{kin}} = \frac{1}{4} \omega^2 (m_1 \xi_{1A}^2 + m_2 \xi_{2A}^2); \quad \overline{E_{pot}} = \frac{1}{4} s (\xi_{1A} - \xi_{2A})^2,$$

which substituted into Eq. (2.20) yields

$$\omega_n^2 = s \frac{(\xi_{1A} - \xi_{2A})^2}{(m_1 \xi_{1A}^2 + m_2 \xi_{2A}^2)} = s \frac{(1-\alpha)^2}{m_1 + m_2 \alpha^2},$$

in which $\alpha = \xi_{2A}/\xi_{1A}$ is introduced in the last equality. To find the eigen-value ω_n^2 , α must be chosen such that a minimum is established. As can be readily demonstrated from a vanishing first derivative, there are two extremes. Those are obtained for

$$\alpha = 1 \Leftrightarrow \xi_{2A} = \xi_{1A}$$

and

$$\alpha = -m_1/m_2 \Leftrightarrow m_2 \xi_{2A} = m_1 \xi_{1A}.$$

The associated eigen-frequencies are thus found to be given by

$$\omega_n^2 = 0; \quad \omega_v^2 = s \frac{m_1 + m_2}{m_1 m_2}$$

respectively, both of which are in agreement with classical results.

References

- [2.1] Morse P.M. and Feshbach H., 1953. Methods of theoretical physics, Vol. 1, Ch. 3. McGraw-Hill, Boston MA
- [2.2] Timoshenko S.P. and Woinowsky-Krieger S., 1959. Theory of plates and shells (2nd ed.), Ch. 13. McGraw-Hill, Auckland
- [2.3] Johnson K.L., 1985. Contact Mechanics, Ch. 4. Cambridge University Press.
- [2.4] Heaviside O., 1892. Electrical Papers, Vol. 1, p. 520, Vol. 2, p. 202
- [2.5] Blevins R.D., 1979. Formulas for natural frequency and mode shape. Krieger Publishing Company, Malabar FL
- [2.6] Crandall S.H. and McCalley Jr. R.B., 1976. Shock and vibration handbook (eds. Harris, Crede), Ch. 28, Matrix methods of analysis. McGraw-Hill, New York NY
- [2.7] Hertz H., 1884. Prinzipien der Mechanik in neuen Zusammenhang dargestellt. Drei Arbeiten von Heinrich Hertz mit einem Vorwort von H.v. Helmholtz. Akademische Verlagsanstalt, Leipzig

- [2.8] Zurmühl R., 1965. Praktische Mathematik, §§31-33. Springer Verlag, Berlin.
- [2.9] Temple G. and Bickley W.G., 1956. Rayleigh's principle and its applications to engineering. Dover Publications, New York NY

3 Survey of Wave Types and Characteristics

3.1 Longitudinal Waves

3.1.1 Pure Longitudinal Waves

In solids, as in liquids and gases, there exists pure longitudinal waves that is, waves in which the direction of the particle displacements coincides with the direction of wave propagation. One may readily visualize such waves by studying the motion of two planes, which in the undisturbed medium are parallel to each other and perpendicular to the direction of propagation. In pure longitudinal wave motion, these planes experience absolute displacements from their positions of equilibrium and the distance between them also changes in general. For example, a plane which initially is at x is displaced a distance ξ , see Fig. 3.1; a second plane, which initially is at a distance dx from the first, is displaced a distance $\xi + \frac{\partial \xi}{\partial x} dx$. The material whose initial length was dx thus experiences an extensional strain ε_x in the x -direction, given by

$$\varepsilon_x = \frac{\partial \xi}{\partial x}. \quad (3.1)$$

Such a strain is associated with a stress or, more precisely, with a deviation of stress from the equilibrium condition. Unlike fluids, solids can sup-

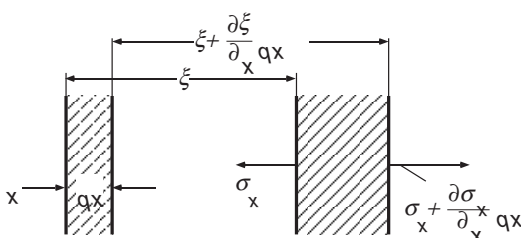


Fig. 3.1. Displacements, deformations, and stresses in longitudinal wave motion

port tensile stresses in absence of static pre-compression. Tensile stresses are usually taken as the positive normal stresses where “normal” indicates that the stress acts perpendicular to the surface. For the small deformations of interest in relation to structure-borne sound, Hooke’s law holds and the tensile stress σ_x is proportional to the extensional strain ε_x (and the compressive stress $-\sigma_x$ is proportional to the compressive strain $-\varepsilon_x$). One thus may write

$$\sigma_x = D\varepsilon_x = D \frac{\partial \xi}{\partial x}. \quad (3.2)$$

The constant D has the same dimensions as σ_x , namely force/area, and represents the longitudinal stiffness of the material. The relation between D and the usually used constants of elasticity is discussed later in this chapter.

Also the stress depends on location (x -coordinate) and a net unbalanced stress causes the element to accelerate; if ρ represents the material density, the corresponding equation of motion may be written

$$\left(\sigma_x + \frac{\partial \sigma_x}{\partial x} dx \right) - \sigma_x = \rho dx \frac{\partial^2 \xi}{\partial t^2},$$

or

$$\frac{\partial \sigma_x}{\partial x} = \rho \frac{\partial^2 \xi}{\partial t^2}. \quad (3.3)$$

The stress and the displacement thus are found to be related by two differential equations, Eqs. (3.2) and (3.3). In this derivation, the stress σ_x was treated not in terms of the location at which it occurs, which would be $(x + \xi)$, but in terms of the plane of the medium on which it acts - the plane that is indicated by its equilibrium position x . In structure-borne sound, the displacements ξ are very small compared to the distances over which there occur significant changes in the vibration field, which distances are fractions of the relevant wavelengths. Therefore, use of coordinates attached to the medium (as above) leads to the same results as use of coordinates attached to a reference frame fixed in space.

As has been shown in Chapter 2, it is convenient to describe the kinematics of a sound field in terms of the (particle) velocity

$$v_x = \frac{\partial \xi}{\partial t} \quad (3.4)$$

instead of the displacement ξ ; this velocity appears directly in the expression for the kinetic energy per unit volume,

$$e_{kin} = \frac{1}{2} \rho v_x^2. \quad (3.5)$$

Every mechanical wave motion also has potential energy associated with it. Here, the potential energy per unit volume is given by

$$e_{pot} = \int_0^{v_x} \sigma_x d\varepsilon_x = \frac{1}{2} D \varepsilon_x^2 = \frac{1}{2D} \sigma_x^2. \quad (3.6)$$

The total energy density (i.e., the total energy per unit volume) is given by the sum of these two parts,

$$e_{tot} = e_{kin} + e_{pot}, \quad (3.7)$$

and thus is completely specified only if both v_x and ε_x , or both v_x and σ_x , are given.

One now needs to consider whether one would prefer to use the strain or the stress in continuing the analysis. If one uses the strain, one obtains a certain mathematical symmetry, since the two field variables v_x and ε_x then are the derivatives of the displacement with respect to time and space, respectively. Also, one can usually measure only the strains (or deformations) directly, whereas one generally needs to deduce the stresses from the measured strains. In spite of these considerations, use of the stress as a variable in the analysis turns out to be preferable, not only because many physical boundary conditions involve the stresses directly, but also – and more significantly – because the product of stress and velocity give the power flow per unit area, i.e., the intensity of the sound field:

$$J_x = -\sigma_x v_x. \quad (3.8)$$

The negative algebraic sign here takes account of the fact that a positive (tensile) stress and a positive velocity result in energy transport in the negative x -direction.

By introducing the velocity, one may rewrite Eq. (3.3) as

$$\frac{\partial \sigma_x}{\partial x} = \rho \frac{\partial v_x}{\partial t}. \quad (3.9)$$

Similarly, one may rewrite Eq. (3.2), after differentiation with respect to time, as

$$D \frac{\partial v_x}{\partial x} = \frac{\partial \sigma_x}{\partial t}. \quad (3.10)$$

One observes that the relation between the two variables σ_x and v_x is such that the spatial derivative of one is proportional to the time derivative

of the other. This cyclic inter-relation for all is also obtained for the wave types discussed subsequently. Differentiation with respect to x or t and combination of Eqs. (3.9) and (3.10) results in the wave equation,

$$D \frac{\partial^2}{\partial x^2}(\sigma_x, v_x) = \rho \frac{\partial^2}{\partial t^2}(\sigma_x, v_x), \quad (3.11)$$

which applies for all of the field variables. One may easily verify that this equation is satisfied by all functions of the form

$$F\left(t \pm \sqrt{\frac{\rho}{D}}x\right). \quad (3.12)$$

Such functions describe waves that propagate without distortion in the positive or in the negative x -direction, depending on the algebraic sign of coefficient of x . If a certain variation with time occurs at $x = 0$, then exactly the same variation occurs also at any arbitrary location x , but delayed (or advanced) by an amount $x\sqrt{\rho/D}$. The parameter $\sqrt{D/\rho}$ thus represents the constant velocity c_L with which the disturbance propagates:

$$c_L = \sqrt{\frac{D}{\rho}}. \quad (3.13)$$

This velocity increases with increasing stiffness and decreases with increasing density. The subscript L indicates the longitudinal character of this type of wave.

The parameters D and ρ occur also in another important combination. If one considers, for example, a wave that propagates in the positive x -direction, and writes the corresponding displacement ξ as

$$\xi\left(t - \sqrt{\frac{\rho}{D}}x\right),$$

one then finds from Eq. (3.2) that the compressive stress associated with this wave is given by

$$-\sigma_x = \sqrt{D\rho}\xi'\left(t - \sqrt{\frac{\rho}{D}}x\right),$$

where the prime denotes differentiation with respect to space whereas the velocity obeys

$$v_x = \dot{\xi}\left(t - \sqrt{\frac{\rho}{D}}x\right).$$

The two field variables may be seen to depend on space and time in precisely the same way; their ratio represents a mechanical impedance per unit area and is called the “characteristic impedance” of the material:

$$Z_L'' = \frac{-\sigma_x}{v_x} = \sqrt{D\rho} = c_L \rho. \quad (3.14)$$

This proportionality of the two variables also implies that for such propagating waves, variations in the potential energy coincide in time and space with those in the kinetic energy. From the constant of proportionality one finds that these two energies are equal:

$$e_{pot} = \frac{1}{2D} \sigma_x^2 = e_{kin} = \frac{1}{2} \rho v_x^2 = \frac{1}{2} \rho \left[\dot{\xi} \left(t - \sqrt{\frac{\rho}{D}} x \right) \right]^2. \quad (3.15)$$

Finally, one also finds that the intensity

$$J = -\sigma_x v_x = Z_L'' \left[\dot{\xi} \left(t - \sqrt{\frac{\rho}{D}} x \right) \right]^2$$

and the total energy density

$$e_{tot} = \rho \left[\dot{\xi} \left(t - \sqrt{\frac{\rho}{D}} x \right) \right]^2,$$

are related by the simple expression

$$J = e_{tot} c_L. \quad (3.16)$$

Equation (3.16) demonstrates that the energy density in a propagating wave advances with the velocity c_L .

Figure 3.2 summarizes the foregoing relations for the particularly simple case of a sinusoidal wave. Here, the time-function

$$\xi(t, 0) = \hat{\xi} \sin \omega t,$$

in terms of the radian frequency ω , leads to the space-time function

$$\xi \left(t - \frac{x}{c_L} \right) = \hat{\xi} \sin \left(\omega \left(t - \frac{x}{c_L} \right) \right) \quad (3.17)$$

The ratio ω/c_L is called the wavenumber and is generally represented by a separate symbol:

$$k_L = \frac{\omega}{c_L}. \quad (3.18)$$

The wavenumber k_L is the spatial analog of the radian frequency ω ; ω is inversely proportional to the duration (period) T of a cycle,

$$\omega = \frac{2\pi}{T},$$

and the wavenumber k_L is inversely proportional to the spatial period, i.e., to the wavelength λ_L ,

$$k_L = \frac{2\pi}{\lambda_L}. \quad (3.19)$$

The wavenumber indicates how many wavelengths correspond to 2π times the unit length.

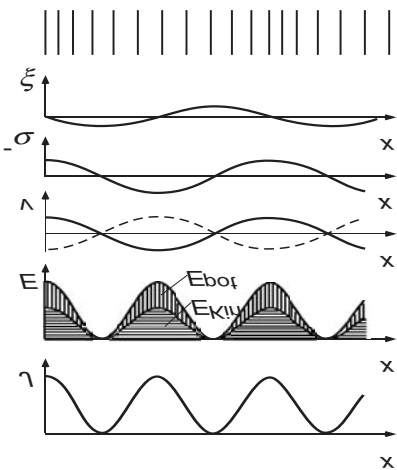


Fig. 3.2. Spatial variation of field variables and energy quantities in a sinusoidal longitudinal wave

Figure 3.2 is constructed for the instant at which the deformation is given by

$$\xi = -\hat{\xi} \sin k_L x. \quad (3.20a)$$

The top part of this figure shows this deformation in terms of the displacements of planes which are uniformly spaced at equilibrium. Below

this, the deformation is plotted as a function of x . The next lower graph shows the compressive stress distribution

$$-\sigma_x = \hat{\xi} D k_L \cos k_L x = -\hat{\sigma}_x \cos k_L x, \quad (3.20b)$$

which is shifted by $\lambda_L/4$ with respect to the deformation function. Below the graph of $-\sigma(x)$ is given a plot of the velocity

$$v_x = \hat{\xi} \omega \cos k_L x = \hat{v}_x \cos k_L x, \quad (3.20c)$$

which is in phase with the compressive stress. Below these plots of the field variables are shown the energy contributions. The curve bounding the horizontally cross-hatched area represents the kinetic energy density

$$e_{kin} = \frac{1}{2} \rho \hat{v}_x^2 \cos^2 k_L x, \quad (3.20d)$$

and the distance between the aforementioned and the topmost curve (vertically cross-hatched area) represents the potential energy density

$$e_{pot} = \frac{1}{2} \rho \hat{v}_x^2 \cos^2 k_L x. \quad (3.20e)$$

The topmost curve thus corresponds to the total energy density

$$e_{tot} = \rho \hat{v}_x^2 \cos^2 k_L x. \quad (3.20f)$$

These energies are also seen to be periodic and in phase with each other, but their wavelength is half that of the field variables. The bottom-most plot shows the intensity

$$J = c_L \rho \hat{v}_x^2 \cos^2 k_L x, \quad (3.20g)$$

which is also in phase with the aforementioned energy densities.

3.1.2 Quasi-Longitudinal Waves on Beams and Plates

The previously discussed pure longitudinal waves can occur only in solids whose dimensions in all directions are much greater than a wavelength. Thus, some seismic waves are pure longitudinal waves, but one rarely encounters practical structures that are of sufficient extent in all directions to support pure longitudinal waves at the frequencies of interest here. The largest thickness of concern in building structures, for example, is likely to be that of a heavy brick or concrete wall; about 25 cm. For this thickness and for a longitudinal wavespeed of 2500 m/s (which value is representative for such a wall and corresponds to the lowest wavespeeds in typical

building structures), one finds that the wall thickness exceeds the wavelength only at frequencies above 10,000 Hz. For most cases of interest, at least one of the dimensions is small compared with a wavelength; for plate-like structures one cross-sectional dimension is smaller than a wavelength, for beam-like structures, two.

Although an unsteady axial force acting at one end of a beam may be expected to produce primarily wave motions parallel to the beam axis, it is well-known that even in a static tensile test there occurs a contraction of the cross-section in addition to the axial extension. This contraction per unit thickness (i.e., the strains $|\varepsilon_y|$ or $|\varepsilon_z|$) are proportional to the axial strain ε_x ,

$$\varepsilon_y = \varepsilon_z = -\mu\varepsilon_x. \quad (3.21)$$

The constant of proportionality μ is a property of the material and is known as Poisson's ratio; Poisson was the first to derive a value, namely 0.25, for this constant on the basis of theoretical considerations. His value is of the same order as those actually observed, see Table 4.3. The greatest possible value that μ can take on is 0.5; this value is obtained for incompressible materials, for which the volume change associated with the cross-sectional contraction makes up for that due to the longitudinal extension. Obviously, the actual cross-sectional contractions must be less than those for an ideal incompressible material, but they are of the same order of magnitude.

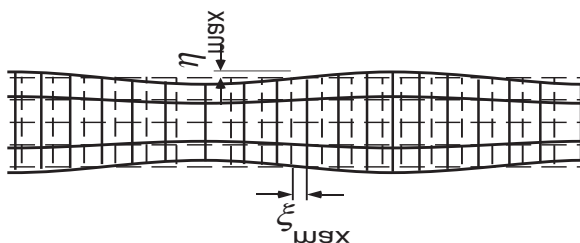


Fig. 3.3. Deformations associated with a quasi-longitudinal wave

Because of the cross-contraction phenomenon, there occur in a rod lateral displacements η and ζ in the y and z directions, in addition to the longitudinal displacements ξ of the material elements and, therefore, a wave travelling along the rod cannot be a pure longitudinal one. Rather, the wave motion appears in principle like that shown in Fig. 3.3 for a sinusoidal wave. The displacements shown in this figure are exaggerated, of

course, in order to display them more clearly; not only are the magnitudes of the displacements shown at least five orders of magnitude greater than in actuality, but also the ratio of the lateral displacement $\hat{\eta}$ to the amplitude of the longitudinal displacement $\hat{\xi}$ is shown as large as makes sense. For a circular or square rod of diameter or thickness d , and for a wavelength λ , the ratio of the transverse to the longitudinal displacement amplitude may be found from

$$|\hat{\epsilon}_y| = \frac{2\hat{\eta}}{d} = \mu |\hat{\epsilon}_x| = \mu \frac{2\pi}{\lambda} \hat{\xi},$$

to be given by

$$\frac{\hat{\eta}}{\hat{\xi}} = \frac{\pi \mu d}{\lambda}. \quad (3.22)$$

Since $\pi\mu$ is approximately equal to unity for most structural materials, one finds that the ratio of the greatest lateral displacement to the greatest longitudinal displacement is approximately equal to the ratio of the thickness of the wavelength; – and it has already been mentioned that this ratio usually is small for the audio-frequency range. The present discussion does not apply if the wavelength is of the same order as the thickness, because then the lateral displacements are no longer in phase over the cross-section and do not vary linearly with distance from the axis cf. 3.7.3. In quasi-longitudinal waves, the wave motions must be primarily longitudinal and, therefore, such waves are often also called longitudinal waves, although the “quasi-longitudinal waves” usage is to be preferred, because it indicates a deviation from the pure longitudinal waves.

Although the transverse motions may be very small, their presence has two important consequences. It is clear that only motions perpendicular to a surface can cause radiation of sound into an adjacent medium which cannot support shear stresses. Quasi-longitudinal waves can therefore radiate sound because of the cross-sectional contractions associated with them. Estimates of the magnitude of such radiation are given in Chapter 7, but it should be mentioned here that the associated radiation into air generally is insignificant unless inordinately large structure-borne sound energies are present. However, this type of radiation into water generally is not negligible, because of the considerably greater “acoustic hardness” of water. In fact, one may even make use of this radiation for measurement of the intensities of longitudinal waves propagating along a plate.

Transverse motions also cause the propagation velocities of quasi-longitudinal waves to be smaller than those of pure longitudinal waves. This difference comes about because the stiffness with which a rod resists

axial forces is smaller if the cross-section of the rod is not constrained. Because unconstrained cross-sections can easily be obtained in practice, the modulus of elasticity E was defined as the ratio of the stress to strain in the tension direction, as obtained in a simple tensile test:

$$E = \frac{\sigma_x}{\varepsilon_x} ; \quad (\sigma_y = \sigma_z = 0). \quad (3.23)$$

If, on the other hand, the lateral contraction is constrained to zero, then there results a three-dimensional instead of a one-dimensional stress condition, because then there are produced the additional normal stresses σ_y and σ_z in the directions normal to the tension direction. These stresses reduce the displacement in the x -direction by an amount which, in view of the superposition principle, corresponds to the cross-contraction they would produce if they were present by themselves. For the general case, Eq. (3.23) must be replaced by three equations:

$$\begin{aligned} E\varepsilon_x &= \sigma_x - \mu(\sigma_y + \sigma_z) \\ E\varepsilon_y &= \sigma_y - \mu(\sigma_z + \sigma_x) \\ E\varepsilon_z &= \sigma_z - \mu(\sigma_x + \sigma_y). \end{aligned} \quad (3.24)$$

For the case where no cross-sectional contraction is permitted, namely for

$$\varepsilon_y = \varepsilon_z = 0, \quad (3.25)$$

one finds by adding the last two of Eq. (3.24) that

$$(\sigma_y + \sigma_z) = \frac{2\mu}{1-\mu}\sigma_x,$$

which, after substitution into the first of these equations, leads to

$$E\varepsilon_x = \sigma_x \left(1 - \frac{2\mu^2}{1-\mu}\right).$$

Thus, the “longitudinal” stiffness D , which was introduced in Eq. (3.2) and which determines the propagation velocity of pure longitudinal waves, depends on the material parameters E and μ according to the relation

$$D = \frac{E}{1-2\mu^2/(1-\mu)} = \frac{E(1-\mu)}{(1+\mu)(1-2\mu)}. \quad (3.26)$$

Clearly, D is always greater than E . For the typical value of $\mu = 0.3$, $D/E \approx 1.35$.

Except for E taking the place of the longitudinal stiffness D , all the relations derived in Sect. 3.1.1 remain valid also for “quasi-longitudinal” waves on a rod. Instead of the tensile stress σ_x it is convenient here to introduce the longitudinal force F_x , which acts on the entire cross-sectional area S and to take this force as positive if it is compressive,

$$F_x = -S\sigma_x, \quad (3.27)$$

so that the power transported in the positive x -direction is given by the product

$$W = F_x v_x. \quad (3.28)$$

The coupled Eqs. (3.9) and (3.10) then become

$$-\frac{\partial F_x}{\partial x} = \rho S \frac{\partial v_x}{\partial t}, \quad (3.29)$$

$$-ES \frac{\partial v_x}{\partial x} = \frac{\partial F_x}{\partial t}. \quad (3.30)$$

In the development of the wave equation from these relations, the area and the algebraic sign-change drop out, and the only change that remains is replacement of D by E :

$$E \frac{\partial^2}{\partial x^2}(F_x, v_x) = \rho \frac{\partial^2}{\partial t^2}(F_x, v_x). \quad (3.31)$$

The propagation speed here is

$$c_{LII} = \sqrt{\frac{E}{\rho}}, \quad (3.32)$$

which is smaller than the speed of pure longitudinal waves. For $\mu = 0.3$, the difference between these two speeds amounts to 16 %, which is not entirely negligible. It thus is important to note which longitudinal wave speed is meant in any given situation.

In the rest of this book, Roman numeral subscripts indicating the number of directions along which the cross-sectional contraction is unconstrained will be used, in addition to the subscript L , to differentiate among the various longitudinal wavespeeds (at least where confusion may occur). Thus, the propagation speed of quasi-longitudinal waves on a rod is designated by c_{LII} in Eq. (3.32), in order to differentiate it from the speed c_L of pure longitudinal waves. Experimentally determined values of c_{LII} are given in Tables 4.3 and 4.5.

Quasi-longitudinal wave propagation on a plate constitutes a case, which lies between the two previously treated ones, because here cross-sectional contraction is unrestrained in only one direction, say, the z -direction. For this two-dimensional stress condition,

$$\varepsilon_y = 0; \sigma_z = 0. \quad (3.33)$$

The second of Eqs. (3.24) then yields

$$\sigma_y = \mu \sigma_x,$$

which, when substituted into the first of these equations, leads to

$$E\varepsilon_x = \sigma_x (1 - \mu^2).$$

One finds that here the effective modulus of elasticity is

$$\frac{E}{1 - \mu^2},$$

which lies between E and D , but nearer to E . The corresponding longitudinal wave speed

$$c_{LII} = \sqrt{\frac{E}{\rho(1 - \mu^2)}} \quad (3.34)$$

differs so little from the value c_{LII} , which applies for rods (for $\mu = 0.3$, the difference amounts to 5 %) that the difference may often be neglected in practice.

For the purpose of rewriting Eqs. (3.9) and (3.10) for plates, it is convenient to use the compressive force per unit width

$$F'_x = -\sigma_x h, \quad (3.35)$$

where h represents the plate thickness, instead of the tensile stress σ_x . Then

$$W' = F'_x v_x \quad (3.36)$$

gives the power propagating per unit width. The coupled Eqs. (3.9) and (3.10) then become

$$-\frac{\partial F'_x}{\partial x} = \rho h \frac{\partial v_x}{\partial t}, \quad (3.37)$$

$$-\frac{Eh}{1 - \mu^2} \frac{\partial v_x}{\partial x} = \frac{\partial F'_x}{\partial t}, \quad (3.38)$$

and the wave equation resulting from these may be written as

$$\frac{E}{1-\mu^2} \frac{\partial^2}{\partial x^2} (F'_x, v_x) = \rho \frac{\partial^2}{\partial t^2} (F'_x, v_x). \quad (3.39)$$

The case of the plate differs from that of a rod in that the cross-sectional contractions occur in only one direction, but it also follows from Eqs. (3.24) (appropriately modified for this case) that the cross-sectional contraction ε_z for a plate is larger than the two equal contractions for a rod; namely, for a plate,

$$\varepsilon_z = -\frac{\mu}{1-\mu} \varepsilon_x. \quad (3.40)$$

In effect, the material in this case “makes better use” of the one direction it can move to “get out of the way”. For $\mu = 0.3$, this increase in the cross-sectional contraction amounts to 43 %, but does not change significantly the previous estimates of the kinematic relations. However, this difference should be considered in calculations of sound radiation, which, at any rate, always is greater for plate-like than for beam-like structures, because for beams the fluid motions on two opposite sides may cancel each other in the acoustic nearfield.

3.2 Transverse Waves

3.2.1 Transverse Plane Waves

Solids do not only resist changes in volume but also changes in shape. This resistance to changes in shape comes about because, unlike a liquid or gas, a solid can support tangential stresses on any cutting plane, even with the material at rest. Because these tangential stresses oppose “shearing” displacements parallel to the cutting plane, they are called shear stresses. It is the shear stresses, which make it possible for solids to exist in the shape of rods, plates, shells, etc. It is also because of shear stresses that transverse plane wave motions can occur in solid bodies, where the direction of propagation (here again taken as the x -direction) is perpendicular to the direction of the displacement η (here taken as the y -direction). Since the transverse displacements of two planes, a distance dx apart, differ by an amount $\partial\eta/\partial x dx$, an element, which originally was a rectangle with sides dx and dy , is distorted into a parallelogram. The acute angle of this parallelogram differs from a right angle (see Fig. 3.4) by the shear angle

$$\gamma_{xy} = \frac{\partial \eta}{\partial x}. \quad (3.41)$$

One may observe that here the deformation is not associated with a change in volume.

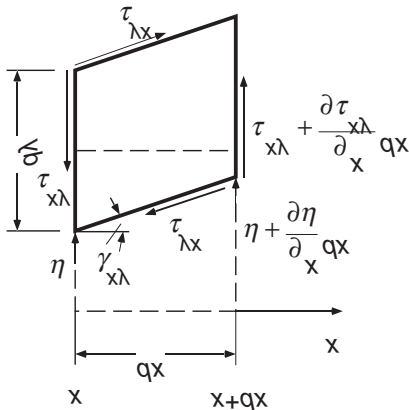


Fig. 3.4. Displacements, deformations, and stresses in transverse wave motion

On the other hand, there does occur a “rotation” of the element by the (of course, very small) angle $\gamma_{xy}/2$. Therefore, transverse waves are also known as “rotational” waves, see Sect. 3.5.

The previously discussed shear deformations always are associated with shear stresses τ_{xy} and τ_{yx} , where the first subscript indicates the axis normal to the plane on which the stress acts, and the second indicates the direction of the stress. Moment equilibrium of the element $dx dy$ requires that the shear stresses on two perpendicular planes must be of equal magnitude. These stresses are proportional to the strain γ_{xy} they produce, so that one may write

$$\tau_{xy} = \tau_{yx} = G\gamma_{xy}, \quad (3.42)$$

or, with the aid of Eq. (3.41),

$$\tau_{xy} = G \frac{\partial \eta}{\partial x}. \quad (3.42a)$$

The constant of proportionality G again has the dimension of a stress and is known as the shear modulus.

If one replaces the displacement in the y -direction by the corresponding velocity

$$v_y = \frac{\partial \eta}{\partial t}, \quad (3.43)$$

then one may write the result of a differentiation of Eq. (3.42a) with respect to time as

$$G \frac{\partial v_y}{\partial x} = \frac{\partial \tau_{xy}}{\partial t}. \quad (3.44)$$

This differential equation replaces Eq. (3.10). Correspondingly, the version of Newton's law in Eq. (3.9) is replaced by the equation

$$\frac{\partial \tau_{xy}}{\partial x} = \rho \frac{\partial v_y}{\partial t}, \quad (3.45)$$

which one may obtain by noting that the difference between the shear stresses which act on two planes separated by a distance dx accelerate the element in the y -direction. Combination of the coupled Eqs. (3.44) and (3.45) again yields a wave equation

$$G \frac{\partial^2}{\partial x^2}(\tau_{xy}, v_y) = \rho \frac{\partial^2}{\partial t^2}(\tau_{xy}, v_y), \quad (3.46)$$

from which one finds that the propagation speed in this case is given by

$$c_T = \sqrt{\frac{G}{\rho}}, \quad (3.47)$$

where the constant G appears instead of D or E . The subscript T is used to indicate transverse waves and experimentally determined values of c_T are given in Table 4.3.

Although G at a first glance may appear to be a new material property, which is independent of those discussed previously, this is not the case. That G must be related to E may be deduced by noting that normal stresses are always associated with shear stresses, and vice versa. In longitudinal waves there occur also shear stresses, and in pure transverse waves there occur normal stresses. It is therefore incorrect to call pure transverse waves shear waves. Normal or shear stresses occur by themselves only on planes which are either parallel or perpendicular to the direction of propagation. In general, the stresses at a given point in a solid depend on the orientation of the hypothetical cutting plane through that point. Consider, for example,

the diagonal planes of a square whose edges are subject only to shear stresses, see Fig. 3.5a.

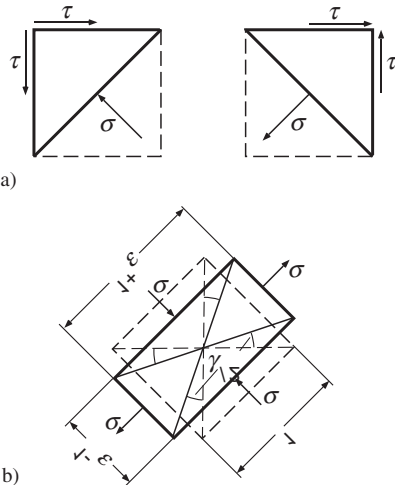


Fig. 3.5. Relations between a) normal and shear stresses; b) extensional strains and shear angles

Equilibrium of the forces demands that depending on which diagonal is being considered there act on the diagonal plane a compressive or a tensile stress, which is equal to the shear stresses acting on the edges:

$$2\tau \cos 45^\circ = \frac{\sigma}{\cos 45^\circ}; \quad \tau = \sigma.$$

The $\cos 45^\circ$ term on the left-hand side results from the taking of force components, that on the right-hand side accounts for the greater surface area on the diagonal. Also the deformation of a differential rectangle depends on its orientation relative to the stresses. Under plane stress conditions, a square with edges parallel to the aforementioned diagonals experiences a normal (extension or contraction) strain, which may be found from Eq. (3.24) to be given by

$$\varepsilon = \frac{\sigma(1+\mu)}{E}.$$

These strains, however, are related to the angle γ , as evident from Fig. 3.5b, as

$$\frac{1-\varepsilon}{1+\varepsilon} = \tan\left(45^\circ - \frac{\gamma}{2}\right) \approx \frac{1-\gamma/2}{1+\gamma/2},$$

which means that

$$\varepsilon = \frac{\gamma}{2}.$$

If one combines these equations with

$$\tau = G\gamma,$$

then one obtains the desired relation between G and E :

$$G = \frac{E}{2(1+\mu)}. \quad (3.48)$$

One may observe that the shear modulus is always considerably smaller than the modulus of elasticity E , and thus much smaller than the longitudinal stiffness D . The propagation speed c_T of transverse waves, therefore, also is smaller than that of quasi-longitudinal waves,

$$\frac{c_T}{c_{LII}} = \sqrt{\frac{G}{E}} = \sqrt{\frac{1}{2(1+\mu)}}, \quad (3.49a)$$

$$\frac{c_T}{c_{LI}} = \sqrt{\frac{G(1-\mu^2)}{E}} = \sqrt{\frac{1-\mu}{2}}, \quad (3.49b)$$

and much smaller than that of pure longitudinal waves,

$$\frac{c_T}{c_L} = \sqrt{\frac{G}{D}} = \sqrt{\frac{1-2\mu}{2(1-\mu)}}. \quad (3.50)$$

For $\mu = 0.3$, the foregoing ratios become

$$c_T/c_{LII} = 0.620, \quad c_T/c_{LI} = 0.592, \text{ and } c_T/c_L = 0.535.$$

From the similarity of the form of the equations one may determine without a detailed analysis that in a sinusoidal transverse wave the distribution of kinetic and potential energy is the same as in sinusoidal longitudinal waves as shown in Fig. 3.2.

Plane transverse waves also can occur only in bodies, which are large compared to the wavelength in all three dimensions. However, a free surface, which is parallel to the propagation and displacement directions (here, parallel to the x - y plane), has no effect on this type of wave. Plane transverse waves thus also can occur in flat plates of uniform thickness.

Since the motions at the surfaces of the plates in such cases are purely tangential, the motions can neither excite an ambient, non-viscous fluid nor can these motions be excited by the fluid.

3.2.2 Torsional Waves

Another type of transverse waves occurs when a narrow beam is excited by a torque or a torsional moment i.e., a moment, which varies with time and whose axis coincides with the axis of the beam. In such wave-motions, cross-sections rotate about the axis of the beam, so that all points on a cross-section experience circumferential displacements, which increase with the distance from the beam axis. If the beam axis coincides with the x -axis as in Fig. 3.6a, then the y - and z -components of these displacements may be written as

$$\eta = -\chi z, \quad (3.51a)$$

$$\zeta = \chi y, \quad (3.51b)$$

where χ represents the angular displacement, in radians, from the equilibrium position.

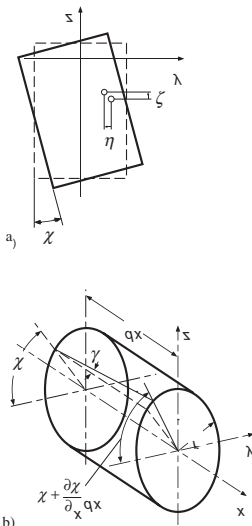


Fig. 3.6. Rotation of cross-section in torsion (a) and relation between change in rotation and shear angle (b)

For circular or annular cross-sections, it follows from rotational symmetry that none of the points in a cross-sectional plane are displaced out of that plane, so that

$$\xi = 0. \quad (3.52)$$

In this case, one may even obtain pure transverse waves. The infinite extent of the lateral displacement associated with the previously discussed plane transverse waves is here replaced by closure of these displacements around the circle. It will therefore be no surprise to find that the wave motion propagates with the speed given by Eq. (3.47).

In order to derive this result, it is convenient here – as for all configurations of finite lateral extent – to describe the system in terms of integrals of the field variables. The shear stresses, which act circumferentially everywhere on the cross-section and are proportional to the radius, may be found from Eq. (3.42) and from the relation between the angles,

$$\gamma = r \frac{d\chi}{dx}, \quad (3.53)$$

which is evident from Fig. 3.6b, to obey

$$\tau = Gr \frac{\partial \chi}{\partial x}. \quad (3.54)$$

Instead of this shear stress, one may use the torsional moment (acting about the x -axis)

$$M_x = 2\pi \int_{r_i}^{r_a} \tau r^2 dr = \frac{\pi}{2} G (r_a^4 - r_i^4) \frac{d\chi}{dx}, \quad (3.55)$$

where r_i and r_a represent the inner and outer radii of an annular cross-section.

One may note that

$$T = \frac{\pi}{2} G (r_a^4 - r_i^4) \quad (3.56)$$

represents the torsional stiffness of a rod with an annular (or circular) cross-section. Since the torque is proportional to the rate of change of the angular displacement for all cross-sectional shapes, that is,

$$M_x = T \frac{\partial \chi}{\partial x}, \quad (3.56a)$$

this proportionality serves to define a torsional stiffness for all cases. If one introduces the time-derivative of the angle of rotation χ , that is, the angular velocity about the x -axis,

$$w_x = \frac{\partial \chi}{\partial t}, \quad (3.57)$$

then one may differentiate Eq. (3.56a) with respect to time to obtain a relation between the space-wise variation of the angular velocity and the time-wise variation of the torque:

$$\frac{\partial M_x}{\partial t} = T \frac{\partial w_x}{\partial x}. \quad (3.58)$$

This partial differential equation must again be complemented by a relation between the spatial variation of the torque and the time-variation of the angular velocity. Such a relation may be obtained by equating the net moment acting on an elementary length of the rod about its axis to the angular inertia of that element. By this process one finds

$$\frac{\partial M_x}{\partial x} = \Theta' \frac{\partial w_x}{\partial t}, \quad (3.59)$$

where Θ' represents the mass moment of inertia per unit length of the rod. For a circularly symmetric cross-section with inside radius r_i and outside radius r_a this moment of inertia is given by

$$\Theta' = 2\pi\rho \int_{r_i}^{r_a} r^3 dr = \frac{\pi}{2} \rho (r_a^4 - r_i^4). \quad (3.60)$$

By combining Eqs. (3.58) and (3.59) one obtains the wave equation

$$T \frac{\partial^2}{\partial x^2} (M_x, w_x) = \Theta' \frac{\partial^2}{\partial t^2} (M_x, w_x), \quad (3.61)$$

from which it follows that the propagation speed is given by the square-root of the ratio of the torsional stiffness to the moment of inertia. As evident from Eqs. (3.56) and (3.60), which follow from the same integrations, the geometric parameters cancel each other in this ratio, so that only the material constants G and ρ remain, and

$$c_T = \sqrt{\frac{G}{\rho}}. \quad (3.62)$$

The aforementioned identical dependence of T and Θ' on geometry holds only for rotationally symmetric cross-sections. If one considers a

narrow rectangle (keeping the total area constant), its torsional stiffness decreases while its moment of inertia increases. The increase in the moment of inertia is evident from the well-known expression

$$\Theta' = \frac{\rho(bh^3 + hb^3)}{12} = \frac{\rho S^2}{12} \left(\frac{h}{b} + \frac{b}{h} \right). \quad (3.63)$$

This expression, which is symmetric with respect to the height h and the width b , takes on its minimum value for $h = b$ i.e., for a square, but even this value is larger than that for a circle of the same area. For narrow rectangles, the second term in the parentheses is negligible in comparison with the first, and the foregoing relation simplifies to

$$\Theta' = \rho \frac{bh^3}{12}. \quad (3.63a)$$

On the other hand, one obtains the following values for the torsional stiffnesses of rectangles with various ratios of h/b :

Table 3.1. Torsional stiffnesses some rectangular cross-sections

$\frac{h}{b}$	1	1.5	2	3	6
$T/(G S^2 b/h)$	0.141	0.196	0.229	0.263	0.298

As h/b approaches infinity, the torsional stiffness approaches the limiting value

$$T = \frac{Gb^3 h}{3}. \quad (3.64)$$

If one introduces values of Θ' and T given by Eqs. (3.63) and (3.64) into Eq. (3.62), then one obtains the following values for the propagation velocities c_{Tl} of torsional waves on bars with rectangular cross-sections:

Table 3.2. Torsional wave speed corrections for some rectangular cross-sections

$\frac{h}{b}$	1	1.5	2	3	6
$\frac{c_{Tl}}{c_T}$	0.92	0.85	0.74	0.56	0.32

One notes that c_{Tl} becomes smaller and smaller in comparison with the value given by Eq. (3.62), as the height-to width ratio becomes larger and

larger. For large values of h/b , one obtains from Eqs. (3.63a) and (3.64) the approximation

$$c_{Tl} = \frac{2b}{h} c_T. \quad (3.65)$$

A comparison with the values given in Eq. (3.65) shows that this approximate relation is acceptably accurate for h/b greater than 6.

The phenomena, which here have been investigated quantitatively for a rectangular cross-section, are also valid in principle for all other cross-sections with no rotational symmetry. Their moments of inertia are always greater, and their torsional stiffness always smaller than those for a circular cross-section of the same area. From the values tabled as well as given by Eq. (3.65) for a special case, one may deduce the general result that the propagation speeds of torsional waves in rods with elongated cross-sections are considerably lower than those of transverse waves.

Torsional waves in rods whose cross-sections are not rotationally symmetric are not pure transverse waves, because motions in the direction of propagation accompany them, so that

$$\xi \neq 0. \quad (3.66)$$

Surfaces which initially are planes perpendicular to the axis of the rod become curved. One may observe such distortions by twisting an eraser with a rectangular cross-section. The longitudinal displacements, of course, are again very small compared with the transverse ones, so that one may again classify all torsional waves on bars with non-rotationally-symmetric cross-sections as “quasi-transverse”. (In order to differentiate the propagation speed of such waves from c_T , the notation c_{Tl} was introduced, in analogy with the notation to differentiate c_L from c_{Ll} ; in both cases, the additional subscript l indicates that there occurs a secondary motion perpendicular to the primary motion.)

A completely rigorous analysis must also explore the validity of the assumption (which was taken from statics) that the axial displacements can propagate longitudinally without obstruction i.e., that there occur no longitudinal stresses σ_x . For the present purposes, however, it suffices to note that in every wave motion there occur opposite conditions (changes in algebraic sign) at all locations which are half a wavelength apart. Since these half-wavelengths here always are smaller than the corresponding longitudinal half-wavelengths, which determine the equalization of alternating longitudinal stresses, one may conclude that the assumption to unobstructed longitudinal stress propagation can lead to no significant discrepancies. One may also readily determine on the basis of simple estimates

that the inertia forces, which oppose the longitudinal motions, are negligibly small compared with the elastic forces.

Torsional waves on bars with non-rotationally-symmetric cross-sections also differ from those on bars with circular and annular cross-sections in another significant way. In the latter, the surface only moves tangential to itself and thus can produce no sound radiation, whereas for the former under torsion, there also occur components of motion normal to the surface. But because here regions of opposite motion perpendicular to the axis of a bar always lie close to each other, significant radiation associated with torsional waves can result only at high frequencies. (Of course, at high enough frequencies, the entire cross-section no longer vibrates in phase.)

All of the wave types discussed so far make only negligible direct contributions to the radiation of sound into air. However, they may be important as intermediate carriers of energy, which may eventually be radiated elsewhere into the surrounding medium.

3.3 Bending Waves

3.3.1 Pure Bending Waves

Of all the various wave types, bending waves, which also are called flexural waves are by far the most important for sound radiation. Because of the rather large transverse deflections associated with them, one might be inclined to include bending waves in the class of transverse waves. But such a classification would be wrong – not only because the stresses and strains that dominate the potential energy in bending waves act in the longitudinal direction, but also because the entire behaviour of such waves and the underlying differential equations differ so greatly from those of the previously discussed transverse waves that even use of a name like pseudo-transverse waves would be misleading. Flexural waves also differ no less basically from quasi-longitudinal waves. In short, flexural waves fall into a class by themselves.

Flexural waves, unlike the other wave types, must be represented by four field variables instead of two, and therefore also the boundary conditions are more complex. It is convenient to use the following four variables. The (transverse) velocity v_y of an element, the angular velocity w_z about the z -axis, which is perpendicular both to the axis of the beam and to the transverse displacement, the bending moment M_z , which acts on a cross-section (again about the z -axis), and the shear force F_y transmitted across the section. For a plate, the moments and forces are considered per unit width and are represented by M'_z and F'_y . One may select appropriate

algebraic signs by taking v_y positive in the positive y -direction, selecting w_z as positive for counter-clockwise rotation in Fig. 3.9, and choosing M_z and F_y so that the products

$$M_z \cdot w_z = W_M \quad (3.67a)$$

and

$$F_y \cdot v_y = W_F \quad (3.67b)$$

represent power flow in the x -direction. Even at this stage one observes that two different forms of power flow occur, a fact which will turn out to be of considerable importance.

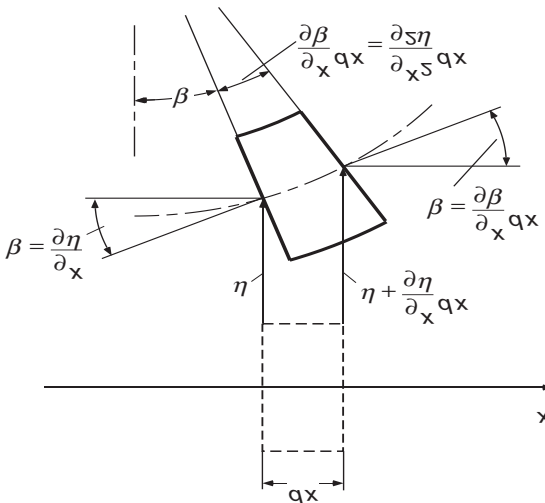


Fig. 3.7. Displacements and deformations in bending

The four field variables here are related by four differential equations, which again couple these variables cyclically. The lateral displacement η and the rotation of a cross-section through the small angle β (see Fig. 3.7) are related by the approximate expression

$$\beta = \frac{\partial \eta}{\partial x}. \quad (3.68)$$

Differentiation with respect to time then leads to the following relation between the angular and lateral velocities:

$$w_z = \frac{\partial v_y}{\partial x}. \quad (3.69)$$

The rate of change of the angular velocity with distance is equal to the time-wise rate of change of the curvature, because for small lateral displacements η , both can be represented in terms of $\partial^2\eta/\partial x^2$:

$$\frac{\partial w_z}{\partial x} = \frac{\partial^2 v_y}{\partial x^2} = \frac{\partial}{\partial t} \left(\frac{\partial^2 \eta}{\partial x^2} \right). \quad (3.70)$$

As is shown in elementary strength of materials, the curvature depends primarily on the local bending moment and is proportional to it i.e.,

$$\frac{\partial^2 \eta}{\partial x^2} = -\frac{M_z}{B}. \quad (3.71)$$

The negative algebraic sign results from taking M_z positive for power flow in the positive x -direction i.e., from taking M_z positive on the left (smaller x) surface of an element as shown in Fig. 3.9 if M_z acts in the same direction as w_z . This direction of M_z , however, is opposite to that which produces a positive curvature.

The constant of proportionality B is called the bending stiffness or flexural stiffness. This stiffness may be determined on the basis of the experimentally verified assumptions that plain sections remain plane and merely rotate by an angle $\partial\eta/\partial x$ (so that two neighbouring sections rotate with respect to each other by an amount $\partial^2\eta/\partial x^2 dx$) and that this rotation affects only the extensions or compressions in the axial direction. The additional deformations that result from shear displacements produced by the shearing forces may be neglected, provided that the bending wavelength is large compared with the cross-sectional dimensions; this relative size of wavelength may be considered as a necessary condition “pure bending waves”.

The strains ε_x in the axial direction increase linearly with the distance y from a neutral fiber,

$$\varepsilon_x = -y \frac{\partial^2 \eta}{\partial x^2}. \quad (3.72)$$

For symmetric cross-sections, the neutral fibre is located at the midpoint of the section, see Fig. 3.8. The negative algebraic sign indicates the occurrence of compression at locations above the neutral fibre i.e., for positive y there occur compressive strains. The same sign applies also for the tensile and compressive stresses,

$$\sigma_x = E\varepsilon_x = -Ey \frac{\partial^2 \eta}{\partial x^2}. \quad (3.73)$$

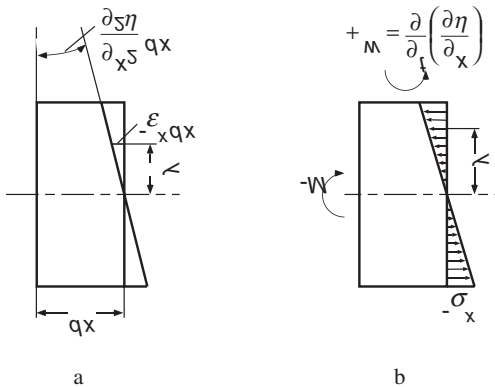


Fig. 3.8. Distribution of a) strain and b) stress over cross-section

For plane bending of plates, one must again replace E by $E/(1-\mu^2)$, in order to account for the fact that cross-sectional contraction is prevented in one direction. One may obtain the bending moments by multiplying the stresses σ_x by the lever y , see Fig. 3.8 and summing them over the area of the cross-section:

$$M_z = \int_S \sigma_x y \, dS = -E \frac{\partial^2 \eta}{\partial x^2} \int_S y^2 dS = -EI \frac{\partial^2 \eta}{\partial x^2}. \quad (3.74)$$

In this expression, I is the second moment of area about the z -axis. As is observed from a comparison of Eqs. (3.71) and (3.74), the bending stiffness of the system is given by the product of the material related Young's modulus and cross-sectional shape related second area moment I

$$B = EI = E \int_S y^2 dS \quad (3.75)$$

The second moment of area for a rectangular cross-section of height h and width b , a tube with inner radius r_i and outer r_o as well as a solid cylinder of radius r_o are given by:

$$\frac{bh^3}{12}; \quad \frac{\pi}{4} (r_o^4 - r_i^4); \quad \frac{\pi}{4} r_o^4 \quad (3.76)$$

For complicated cross-sectional shapes, the second area moment can be taken from a handbook but also calculated analytically or numerically employing Eq. (3.75). It should be noted that the reference $y = 0$ for the integration must first be estimated from

$$\int_s E y dS = 0 \quad (3.76a)$$

This procedure is also applicable when multi-layered beams are considered, where Young's modulus E is a function of y .

Upon differentiating (3.71) with respect to time and introducing the rotational velocity from (3.70) one obtains

$$\frac{\partial M_z}{\partial t} = -B \frac{\partial w_z}{\partial x}. \quad (3.77)$$

The expression relating the shear force F_y to the bending moment M_z may also be obtained from static bending theory. This relation results from the moment equilibrium of an element of length dx , as shown in Fig. 3.9 together with the positive direction, and can be written as

$$M_z - \left(M_z + \frac{\partial M_z}{\partial x} dx \right) - F_y dx = 0 \quad (3.78)$$

yielding

$$F_y = -\frac{\partial M_z}{\partial x} \quad (3.78a)$$

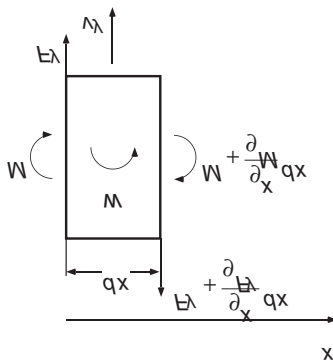


Fig. 3.9. Field variables for a beam element in bending indicating the positive directions

For the dynamics, also an inertia term have to be included on the right hand side of (3.78), which amounts to

$$I \rho dx \frac{\partial w_z}{\partial t}$$

but, as will be shown later, the kinetic energy associated with such rotational motion can be neglected in comparison with that associated with translational motion as long as the bending wavelength is large composed with the cross-sectional dimensions cf., Sect. 3.8.2.

Finally, is needed a relation between the shear force and the transverse velocity to complete the cycle of equations. This relation may be obtained from an application of Newton's second law to an element of the beam, see Fig. 3.9,

$$F_y - \left(F_y + \frac{\partial F_y}{\partial x} dx \right) = m' dx \frac{\partial v_y}{\partial t} \quad (3.79)$$

which reduces to

$$\frac{\partial F_y}{\partial x} = m' \frac{\partial v_y}{\partial t}. \quad (3.79a)$$

Here,

$$m' = \rho S \quad (3.80)$$

is the mass per unit length.

The combination of Eqs. (3.69), (3.77), (3.78a) and (3.79a) furnishes the one-dimensional form of the bending wave equation, which is valid for all field variables

$$-B \frac{\partial^4}{\partial x^4} (v_y, w_z, M_z, F_y) = m' \frac{\partial^2}{\partial t^2} (v_y, w_z, M_z, F_y) \quad (3.81)$$

This equation resembles the usual wave equations only in that the time derivative is of second order. In contrast to the other wave equations, the left-hand side of Eq. (3.81) involves the fourth derivative with respect to space and appears with a negative sign. This algebraic sign, which affects the basic character of the solutions, is not the result of arbitrary choices of signs for the field variables and cannot be changed by modified choices.

The fact that the spatial and temporal derivatives appear with different orders implies that the wave motion is dispersive. Furthermore, the dispersion, in general, cannot be given a simple functional description.

On the other hand, Fourier analysis is still applicable such that any time dependence can be decomposed in pure tonal components and the propagation of those temporally sinusoidal components investigated.

The spatial variation of temporally waves can readily be shown to allow also sinusoidal forms i.e., sinusoidal flexural waves are also possible. By substituting

$$v_y = \hat{v}_y \sin(\omega t - kx + \varphi_v) \quad (3.82)$$

in (3.81), it is seen that the velocity assumed satisfies the wave equation for arbitrary amplitudes and phase angles as long as the angular frequency and wave number characterizing the temporal and spatial periodicity respectively, obey

$$\frac{B}{m'} k^4 = \omega^2 \quad (3.83)$$

Also in this case, the ratio of angular frequency to wavenumber

$$\frac{\omega}{k} = c \quad (3.84)$$

represents the speed with which one has to move to remain at the same phase of the sinusoidal wave motion. This ‘phase speed’ of bending waves, designated by subindex B thus depends on frequency as seen from Eq. (3.83),

$$c_B = \sqrt[4]{\frac{B}{m'}} \sqrt[2]{\omega}. \quad (3.85)$$

Such a phase speed clearly represents speed of propagation only of one infinite sinusoidal wave. Waveforms that in a Fourier analysis sense are composed of various sinusoidal components always distort since high frequency components propagate with higher speed than those of low frequency.

In optics, the corresponding process, is called dispersion and this concept is carried over to all wave carrying systems with frequency dependent phase speed.

For a plate of thickness h , Eq. (3.85) can be simplified to

$$c_B \approx \sqrt{1.8 c_{LI} h f} = c_{LI} \sqrt{\frac{1.8 h}{\lambda_{LI}}} \quad (3.85a)$$

In Fig. 3.10 are shown some bending wave speeds for plates of various materials as function of the product of thickness and frequency. The curves are approximately valid also for beams with rectangular cross-sections since Poisson’s contraction only has a minute effect. In the figure, moreover, the frequency independent phase speeds of waves in air and water are included as is the limit of validity of the Kirchhoff bending theory cf., (3.196b).

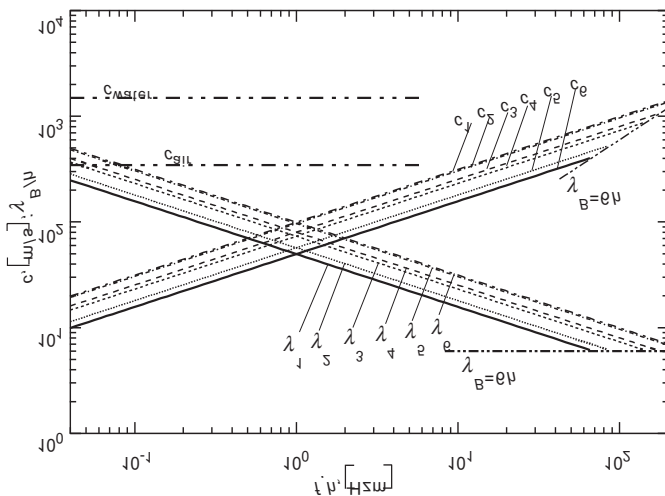


Fig. 3.10. Flexural wave speed (c_1 to c_6) and normalized wavelength (λ_1 to λ_6) for plates of various materials versus product of thickness and frequency. (1) Steel, aluminium, (2) glass, (3) brass, dense concrete, (4) brick stone, chipboard, (5) light-weight concrete, Gypsum board, perspex and (6) lead

Besides the theoretical case of an infinite sinusoidal wave, there is another special case, in which it is meaningful to consider a definite propagation speed. This is the case, in which a wave motion occurs composed of several components of slightly differing periodicity. Intuitively, one could jump to the conclusion that these phase speeds have a small variation around some mean which also could be used as a mean speed. Unfortunately, it is a bit more involved as can be gathered from the simplest case with two superimposed, equally strong components, of frequencies ω_1 and ω_2 and wavenumbers k_1 and k_2 . Such a superposition results in a modulation

$$\begin{aligned} & \sin(\omega_1 t - k_1 x) + \sin(\omega_2 t - k_2 x) \\ &= 2 \sin\left(\frac{\omega_1 + \omega_2}{2} t - \frac{k_1 + k_2}{2} k\right) \cos\left(\frac{\omega_1 - \omega_2}{2} t - \frac{k_1 - k_2}{2} x\right), \end{aligned} \quad (3.86)$$

which means that a sinusoidal carrier wave of the mean frequency $(\omega_1 + \omega_2)/2$ and of the mean wave number $(k_1 + k_2)/2$ is amplitude modulated by the substantially lower wavenumber $(k_1 - k_2)/2$. This envelope curve, however, is of primary interest since it determines the average energy transport. Although the carrier wave indeed propagates with the average phase speed

$$c = \frac{\omega_1 + \omega_2}{k_1 + k_2}, \quad (3.87)$$

the envelope curve, which encloses the group of the wave peaks, propagates at the ‘group speed’

$$c_g = \frac{\omega_1 - \omega_2}{k_1 - k_2} = \frac{\Delta\omega}{\Delta k}. \quad (3.88)$$

This group velocity can be considerably larger as well as considerably smaller than the phase speed. In the limiting case, where the frequencies and wavenumbers are arbitrarily close to each other, c_g is given by the derivative

$$c_g = \frac{d\omega}{dk} \quad (3.88a)$$

The group speed as defined here does not apply only to the envelope function of a modulation given by Eq. (3.86) but in general is applicable to the envelope function of all processes composed of arbitrarily many adjacent wave trains of arbitrary amplitudes and phases. The group speed is also applicable to continuous spectra which have negligible components outside of the immediate vicinity of the carrier frequency. Such individual wave-groups are of significant interest since they represent the only type of excitation signals for which dispersive systems exhibit clearly defined transit times.

From Eq. (3.83), the group velocity of bending waves c_{gB} obeys

$$c_{gB} = 2\sqrt{\frac{B}{m'}}k = 2c_B, \quad (3.89)$$

which thus is twice the phase speed. In Fig. 3.11a, this relation is exemplified. The upper and lower curves represent two points in time respectively, which are displaced half a period of the carrier wave. Therefore, the carrier wave is shifted half a wavelength of the carrier wave rightwards whereas thereby, the envelope curve is shifted the double distance. The lower part of Fig. 3.11b shows a continuous wavenumber spectrum - in this case represented by a Gaussian error curve. The significant position of this curve encompasses only a small wavenumber range. There above is the dispersion relation $\omega(k)$ plotted and indicated is the difference between group and phase speeds via the associated angles.

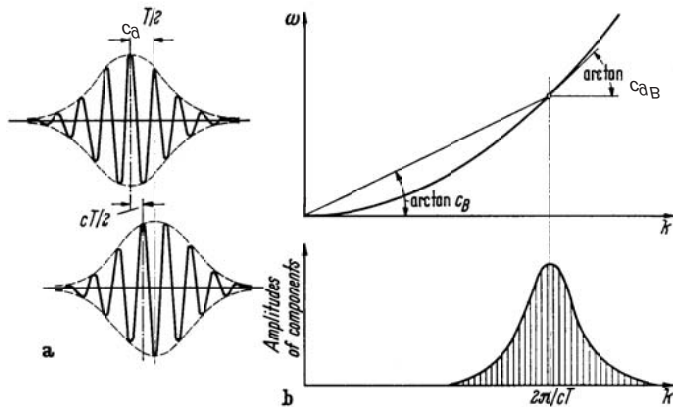


Fig. 3.11. Illustration of the difference between group and phase speeds

3.3.2 Energy Relations

The fact that the energy is propagated with the group speed can be demonstrated by means of the energy relations that holds for pure sinusoidal waves. These energy relations for bending waves differ markedly from those of the previously discussed wave types as is observed from a comparison of Fig. 3.12 pertaining to bending waves and Fig. 3.2 associated with a longitudinal wave. The sinusoidal displacement in the former case can be written as

$$\eta = \hat{\eta} \sin(\omega t - kx). \quad (3.90)$$

At the top of Fig. 3.12 is shown the corresponding deformation at time $t = 0$. Next follow the spatial distributions of the translational velocity, the rotational velocity, the bending moment and the cross-sectional force. Pairwise, F_y and v_y are in phase as are M_z and w_z but group-wise a quarter period out-of-phase. These phase relations lead to a remarkable property of the energy flow composed of

$$\begin{aligned} W_F &= F_y v_y = \hat{\eta}^2 B \omega k^3 \cos^2 kx = \hat{F}_y \hat{v}_y \cos^2 kx \\ W_M &= M_z w_z = \hat{\eta}^2 B \omega k^3 \sin^2 kx = \hat{M}_z \hat{w}_z \sin^2 kx \end{aligned} \quad (3.91)$$

Their sum, however, establishes a time-invariant power

$$W = W_F + W_M = \hat{\eta}^2 B \omega k^3 \quad (3.92)$$

For the sinusoidal flexural wave, the energy flow does not vary with the period $\lambda/2$ between zero and a maximum value but is spatially constant.

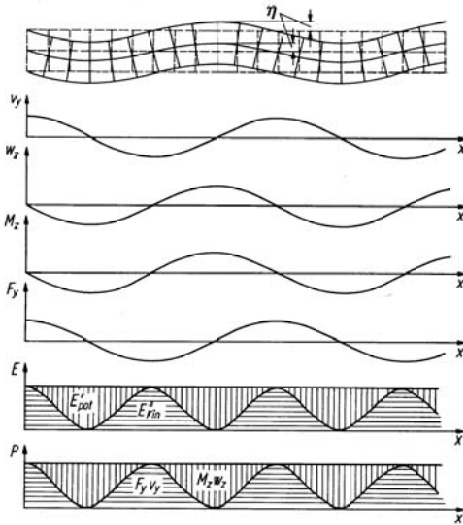


Fig. 3.12. Field variable and energy distribution of a sinusoidal flexural wave

Accordingly, the same must be true also for the sum of potential and kinetic energy. Per unit length, the latter amounts to

$$SE_{kin,T} = \frac{m'}{2} v_y^2 = \frac{m'}{2} (\omega \eta)^2 \cos^2 kx = \frac{\rho S}{2} \hat{v}_y^2 \cos kx \quad (3.92a)$$

and is essentially governed by the translational energy. Upon comparing it with that associated with rotations

$$SE_{kin,R} = \frac{\rho I}{2} w_z^2 = \frac{\rho I}{2} k^2 \hat{v}_y^2 \sin^2 kx,$$

it is noted that the rotational energy maximum is a factor

$$\frac{\text{Max}(\bar{E}_{kin,R})}{\text{Max}(E_{kin,T})} = \left(\frac{2\pi \sqrt{I/S}}{\lambda} \right)^2$$

smaller. Owing to the fact that the rotational energy grows towards the boundaries, an average value is understood, which is denoted by an over bar. As has already been mentioned, in pure bending the cross-sectional

dimensions must be small compared with the wavelength. For this reason, Eqs. (3.85) and (3.89) are also only valid in the range where the calculated wave speeds are substantially below that of the longitudinal wave, c_L . The potential energy, on the other hand, is controlled by the axial stresses and strains,

$$S\bar{E}_{pot} = \frac{1}{2} \int_S \sigma_x \varepsilon_x dS = \frac{E}{2} \left(\frac{\partial^2 \eta}{\partial x^2} \right)^2 \int_S y^2 dS = \frac{B}{2} k^4 \hat{\eta}^2 kx. \quad (3.92b)$$

Both the energy components vary between zero and a maximum value with period of $\lambda/2$. This maximum value is, furthermore, in both cases the same, which can be seen by substituting expression (3.83) in the relation for the potential energy. The two energy components oscillations are quarter wavelength displaced, however, and where the beam, for example, has its maximum curvature and is about to change the direction of motion and thus momentarily at rest, the potential energy is a maximum. Thus, the sum of the two energy components is a constant,

$$\begin{aligned} S\bar{E}_{tot} &= \left(S\bar{E}_{pot} + S\bar{E}_{kin} \right) = \frac{\hat{\eta}^2}{2} \left(m' \omega^2 \cos^2 kx + B k^4 \sin^2 kx \right) \\ &= \frac{B}{2} k^4 \hat{\eta}^2. \end{aligned} \quad (3.92c)$$

This is illustrated in Fig. 3.12 with horizontally and vertically hatched regions. The constant energy per unit length can be found to be related to the constant energy flow W as

$$W = 2 \frac{\omega}{k} S\bar{E}_{tot} = 2 c_B S\bar{E}_{tot} = c_{gb} S\bar{E}_{tot}, \quad (3.93)$$

and the power transmission is again determined by the group speed.

3.4 Wave Motions on Beams of Finite Length

Waves that propagate in one direction, which have been the subject of discussion until now, can occur only as long as they encounter no change in the wave carrying system. Every homogeneous wave guide, however, have ends and at those ends the wave motion always change direction, usually also its amplitude and phase, and often even its basic characters.

This section deals only with the one-dimensional case, and for the sake of further simplicity, only with waves in beams of the types treated in Sects. 3.1.2, 3.2.2, and 3.3.1, in the presence of ideal boundary conditions.

3.4.1 Longitudinal Natural Vibrations

It is convenient to begin by considering a quasi-longitudinal wave arriving at the end of a beam at $x = 0$, which end may be either free or clamped (i.e., built into a rigid body). At a rigidly constrained end, the velocity must vanish whereas at a free end, the force. For airborne sound in ducts, rigid ends can be approximated well in practice, but for sound in liquid – and even more so for sound in solids – free ends can be obtained much more easily. It is therefore preferable, particularly because experimental verifications will also be of interest, to study first a beam with a free, for which the boundary conditions are

$$F = 0 \quad ; \quad x = 0. \quad (3.94)$$

These conditions must be satisfied at all times. However, the arriving wave

$$F_+ \left(t - \frac{x}{c} \right),$$

where the subscript + indicates that the waves propagates in the positive x -direction, cannot satisfy the boundary conditions by itself. An additional wave, which propagates in the negative x -direction,

$$F_- \left(t + \frac{x}{c} \right),$$

must be added. Then

$$F(x, t) = F_+ \left(t - \frac{x}{c} \right) + F_- \left(t + \frac{x}{c} \right), \quad (3.95)$$

and satisfaction of the boundary condition of Eq. (3.94) requires that

$$F_-(t, 0) = -F_+(t, 0). \quad (3.96a)$$

Thus, as far as the force is concerned, the wave merely changes its sign becomes “ideally reflected”.

One may now determine the behaviour of the velocity, by noting first that the velocity in the arriving wave has the same dependence as the force,

$$v_+ = \frac{1}{\rho S c_L} F_+ \left(t - \frac{x}{c} \right),$$

as is evident from Eq. (3.14) for a pure longitudinal wave, and as may be easily derived from Eqs. (3.29) and (3.30). In the reflected wave, however, the ratio of v_- to F_- occurs with a changed algebraic sign,

$$v_- = \frac{-1}{\rho S c_L} F_- \left(t + \frac{x}{c} \right),$$

because in this wave energy is transported in the negative direction. At the boundary, therefore,

$$v_-(t, 0) = v_+(t, 0). \quad (3.96b)$$

Thus, while the force vanishes at the boundary, the velocity there is twice that of the arriving wave:

$$v(t, 0) = 2v_+(t, 0). \quad (3.97)$$

An assumption of zero motion at $x = 0$ would have led to a doubling of the force at this end.

The equations for torsional waves, which are discussed in Sect. 3.2.2, are analogous to those for quasi-longitudinal waves, and this analogy also holds for the boundary conditions at free and clamped ends where either the moment M or the angular velocity w vanishes. Without needing to analyse torsional waves in detail, one may therefore conclude that torsional waves also experience ideal reflection at free or rigid ends. Also, M changes sign at a free end, but w does not, and the reverse is true at clamped end. Similarly, the angular velocity is doubled at a free end, and the moment, at a clamped end.

A wave propagating on a beam which has the same type of boundary at both ends is reflected similarly at both ends. After two reflections, the wave again propagates in the same direction as originally, and both field variables again have the original algebraic sign. This implies that everywhere each field variable varies periodically in time. The period,

$$T = \frac{2l}{c}, \quad (3.98a)$$

corresponds to the time taken by the wave to propagate to one end, from there in the reverse direction to the other end, and from there again to its starting place, all with the same velocity c .

Because every periodic process with frequency

$$f_1 = \frac{1}{T} = \frac{c}{2l} \quad (3.98b)$$

can be analysed in terms of sinusoidal components with frequencies

$$f_n = n \frac{c}{2l}, \quad (3.98c)$$

one is led to consider the character of these component waves or, the character of the vibrations that result from these waves in the presence of the boundary conditions. Because these vibrations are characteristic of the particular beam under consideration, they are called characteristic vibrations. Since such vibrations can occur “naturally” in absence of external driving forces, they are also called natural vibrations.

In the simplest case, such as that of pendulum or an elastically supported mass, constrained to move in only one direction, the natural vibration obeys

$$u = \hat{u} \cos(\omega t + \varphi_u) \quad (3.99a)$$

for every field variable u (displacement, velocity, restoring force, etc.). The natural vibrations of systems with m independent degrees of freedom, m independent co-ordinates are required, all varying sinusoidally in time, generally with different amplitudes. In the absence of energy losses i.e., in undamped natural vibrations all co-ordinates of the same type transverse their extreme (and their zero) values simultaneously. Therefore, if one takes the time origin $t = 0$ at an instant when all co-ordinates pass through their extreme values, and if one admits positive and negative values for the amplitudes \hat{u} , then one may choose $\varphi_u = 0$ and write for any coordinate, say, the k^{th} ,

$$u_k = \hat{u}_k \cos \omega t. \quad (3.99b)$$

As one progresses toward a continuum, the number of degrees of freedom becomes infinite. Correspondingly, the discreet coordinate amplitudes become a continuous function of space:

$$u(x, t) = \hat{u}(x) \cos \omega t. \quad (3.99c)$$

This separation of the field behaviour into a function of space and one of time (a process named after D. Bernoulli) can provide even more insight into the concept of natural vibrations than can the decomposition of vibratory motions into propagating waves as in Eq. (3.95) (which goes back to D'Alembert).

From what has been proven so far namely, that the time variation of each field variable is periodic with the period $2l/c$ and may be analysed in terms of its Fourier components, one may conclude only that these Fourier components must be of the form

$$u(x, t) = \hat{u}(x) \cos(\omega t + \varphi_u(x)). \quad (3.99d)$$

This means that one cannot exclude possible phase differences. The more general expression in (3.99d) is of importance, not only because it de-

scribes the natural vibrations of interest here, but also because it can describe any oscillation, which involves sinusoidal vibrations with time, if x is replaced by a positive vector \mathbf{r} .

The expression of Eq. (3.99d) is no longer separable into multiplicative terms, but may be written either as the sum of two such separable expressions (phase shifted in time with respect to each other),

$$u(x, t) = [\hat{u}(x) \cos \varphi_u(x)] \cos \omega t + [-\hat{u}(x) \sin \varphi_u(x)] \sin \omega t, \quad (3.99e)$$

or as the real part of a product of two quantities, each of which depends both on space and on time,

$$u(x, t) = \operatorname{Re} \left\{ [\hat{u}(x) e^{j\varphi_u(x)}] e^{j\omega t} \right\} = \operatorname{Re} \{ \hat{u}(x) e^{j\omega t} \}. \quad (3.99f)$$

By extending the phasor notation introduced in Sect. 2.2, to include a location dependence, the one-dimensional wave Eqs. (3.11), (3.31), (3.46), and (3.61), reduce to the simple vibration equation

$$\frac{d^2 \hat{u}}{dx^2} + k^2 \hat{u} = 0. \quad (3.100)$$

By again considering the vibration in terms of two waves propagating in opposite directions, as in Eq. (3.95), one may write the solution of the “spatial” vibration for the special case of the longitudinal force in a beam as

$$\hat{F}(x) = \hat{F}_+ e^{-jkx} + \hat{F}_- e^{+jkx}. \quad (3.101)$$

One may observe that for the first term, which represents a wave propagating in the positive x -direction, the phase must increase with increasing x , because a given phase arrives later at a location for which x is larger.

The first boundary condition, requiring that the axial force at $x = 0$ vanishes, implies that the two phasors \hat{F}_+ and \hat{F}_- must have opposite algebraic signs, as in Eq. (3.96a).

Since one may also write

$$\hat{F}_- = -\hat{F}_+ \quad (3.102a)$$

as

$$\hat{F}_- = \hat{F}_+ e^{-j\pi}, \quad (3.102b)$$

one may consider the change of the sign of the force wave due to reflection as a “phase jump” of

$$\gamma = -\pi. \quad (3.102c)$$

From the first boundary condition, one may deduce that the spatial distribution of the axial force is a sinusoid, beginning at $x = 0$:

$$\underline{\hat{F}}(x) = \hat{F}_{\max} \sin kx. \quad (3.103)$$

Because of the second boundary condition, which requires vanishing of the force at $x = l$, this sinusoid also must vanish there. This requirement determines k and, therefore, the wavelengths λ

$$k_n l = n\pi; \quad l = \frac{n\lambda_n}{2}. \quad (3.104)$$

The frequencies that correspond to these values are the same as those given by Eq. (3.98c), as one would expect. These frequencies are called “natural frequencies”, “eigen-frequencies” or “characteristic frequencies”. The left-hand part of Fig. 3.13 shows the force distributions for $n = 1, 2, 3$ at the instant at which the greatest absolute values occur. The right-hand part similarly shows the corresponding velocity distributions, and thus also the displacement distributions given by

$$\hat{y}_n(x) = \hat{y}_{n\max} \cos k_n x, \quad \hat{\xi}_n(x) = \hat{\xi}_{n\max} \cos k_n x, \quad (3.105)$$

respectively the condition that the “round-trip” path length $2l$ is an integral multiple of the wavelength, which is indicated by Eq. (3.104), may also be deduced from a general, easily visualized principle which holds for all natural vibrations. This principle states that a natural vibration occurs if a propagating wave, after reflection at all boundaries along its path, returns to its starting point with the same amplitude and phase that is, if such a wave can form a *wave train that closes on itself*. In the present case, the reflections at the ends do not change the amplitudes. Therefore, formation of a closed wave-train requires only phase-matching of the wave as it closes on itself after being reflected at both ends. By applying this principle to a velocity wave, which is reflected without phase change, one obtains the relation (3.104) directly. A corresponding closed wave train for the case of $n = 2$ is illustrated in Fig. 3.14, where the rightward moving part is shown as a solid curve, the leftward moving part as a dotted curve.

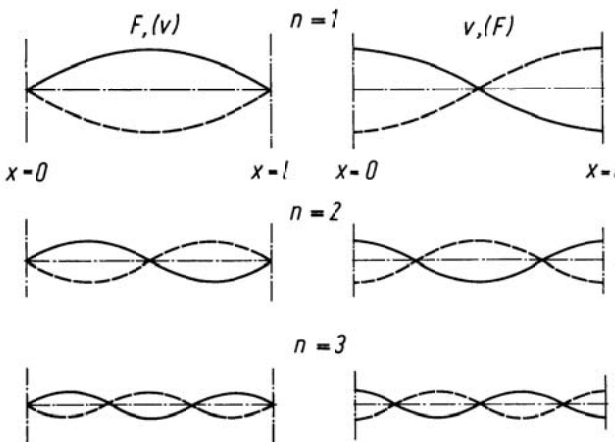


Fig. 3.13. Longitudinal natural vibrations of a rod. F, v without parentheses correspond to free end; F, v in parentheses correspond to clamped ends. (The solid and dashed curves represent conditions half a period apart.)

Application of the “wave train closure principle” to the force wave is a little more difficult, because there occur phase jumps γ_0 and γ_l at $x = 0$ and $x = l$. One must take these phase jumps into account in expressing the requirement that the wave train close on itself in phase. This leads to the general relation

$$2kl - \gamma_0 - \gamma_l = 2n\pi. \quad (3.106)$$

Because each phase jump in this case is equal to $-\pi$, Eq. (3.106) differs from Eq. (3.104) only in that it involves $n - 1$ instead of n . Since n can be any integer, the two equations amount to the same thing. One would not expect otherwise, because the natural frequencies obviously cannot depend on which variable one imposes the requirement of phase continuity.

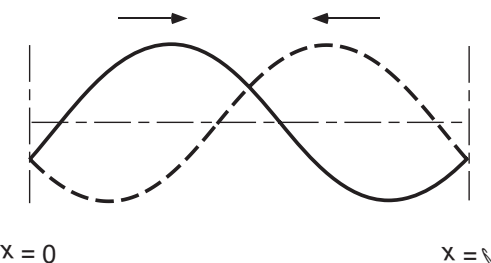


Fig. 3.14. Sketch to illustrate the principle of phase-continuous closure

From the foregoing result one may also deduce that a bar with both ends rigidly constrained has the same natural frequencies as one with free ends. One needs only to note that in an axially constrained bar, the force and velocity boundary conditions and, therefore, also the associated phase jumps, are interchanged with respect to those in a free bar.

From phase continuity at wave train closure, one also may readily determine the natural frequencies of a rod, which is clamped on one end and free on the other, irrespective of if the wave is longitudinal or torsional waves. For any field variable, one obtains a reflection with zero phase change at one end, and a phase jump of $-\pi$ at the other end. One thus obtains

$$2k_n l = (2n-1)\pi; \quad l = \frac{(2n-1)\lambda_n}{4}; \quad f_n = \frac{(2n-1)c}{4l} \quad (3.107)$$

Like the natural frequencies of a closed-ended organ pipe, the natural frequencies here are associated with the odd integers.

3.4.2 Natural Vibrations in Bending

It is instructive to turn now to flexural vibration of a beam of finite length and to determine the natural frequencies on the basis of the principle of phase continuity. For this purpose first, the phase jumps must be determined, which result from the various boundary conditions. In this case it is not sufficient to deal only with the ideal limiting cases of “clamped” or “free” ends, but also with boundaries where these descriptions apply only to the translational or to the rotational deflections.

A simple support, as represented in the upper left-hand part of Fig. 3.15, prevents a beam from deflecting vertically ($v = 0$) but permits it to rotate. Such a support therefore does not produce bending moments ($M = 0$). At a “built-in” or clamped end, as shown at the upper right of the figure, the translational and rotational displacements both vanish, and thus also the corresponding velocities ($v = 0, w = 0$). At a free end, on the other hand, the moment and the shear force vanish ($M = 0, F = 0$). Finally, at a “guided” end, as indicated schematically by guidepins in the lower right part of the figure, the beam is free to translate, but prevented from rotating. Thus, the shear force and angular velocity must vanish ($F = 0, \omega = 0$).

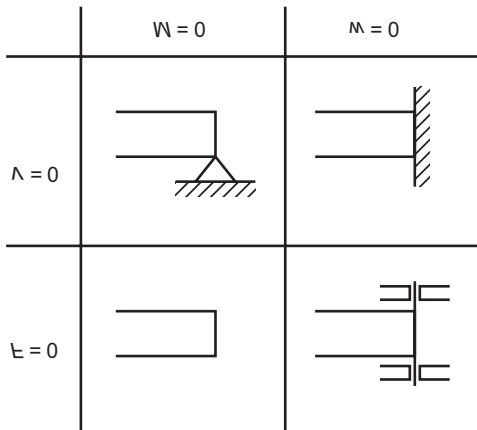


Fig. 3.15. Summary of ideal boundary conditions for bending vibrations of beams

In each of the four cases, two boundary conditions must be satisfied. Addition of a reflected wave to the incident one thus clearly is not enough. This insufficiency demonstrates how closely the doubling of the number of boundary conditions is related to the doubling of the order of the differential equation for the wave system. The differential equation also has other types of solutions than those which correspond to propagating waves.

For sinusoidal time-variation, the bending wave equation, Eq. (3.81), may be rewritten in terms of the phasors \hat{v} , \hat{w} , \hat{M} , \hat{F} . For example, for \hat{v} one obtains

$$\frac{d^4 \hat{v}}{dx^4} - k^4 \hat{v} = 0, \quad (3.108)$$

where k , which has been written in place of $\sqrt[4]{m'/B\sqrt{\omega}}$ in accordance with Eq. (3.83), represents the wavenumber of a propagating bending wave. Wave motion of the type that result from solutions of the ordinary second-order wave equation also satisfy the bending wave equation. One may arrive at this conclusion by factoring the operator that acts on the \hat{v} in Eq. (3.108) to obtain

$$\left(\frac{d^4}{dx^4} - k^4 \right) = \left(\frac{d^2}{dx^2} + k^2 \right) \left(\frac{d^2}{dx^2} - k^2 \right). \quad (3.108a)$$

The first of the factor operators corresponds to the “spatial” equation of vibrations, Eq. (3.100) i.e., it leads to propagating sinusoidal waves of the form given in Eq. (3.101) for the axial force phasor or to the following similar expression for the transverse velocity:

$$\hat{v}_l = \hat{v}_+ e^{-jkx} + \hat{v}_- e^{+jkx}.$$

Because one may obtain the second operator from the first by replacing $\pm k$ by $\pm jk$, there must also exist solutions of the form

$$\hat{v}_2 = \hat{v}_{-j} e^{-kx} + \hat{v}_j e^{+kx}$$

corresponding to the second operator. Such solutions represent fields with constant phase, which decrease exponentially with the distance from a disturbance (or an end), and which are also called “near fields”.

The general solution thus consists of four parts, corresponding to the fourth order of the differential equation

$$v = \hat{v}_+ e^{-jkx} + \hat{v}_- e^{+jkx} + \hat{v}_{-j} e^{-kx} + \hat{v}_j e^{+kx}, \quad (3.109)$$

and this solution must satisfy two independent boundary conditions at each of the two ends.

If a wave $\hat{v}_+ e^{-jkx}$ arrives from the left ($x < 0$) at an end located at $x = 0$, then there results at that location a reflected wave $\hat{v}_- e^{+jkx}$ and a near-field $\hat{v}_j e^{+kx}$, which together make it possible to satisfy the two boundary conditions there.

In some special cases, the nearfield may vanish. This happens, for example, at a simply supported end. For such an end, the boundary conditions $v = 0; M = 0$, which are equivalent to

$$v = 0; \frac{d^2 v}{dx^2} = 0, \quad (3.110a)$$

leading to the two equations

$$\hat{v}_- + \hat{v}_j = -\hat{v}_+, \quad -\hat{v}_- + \hat{v}_j = +\hat{v}_+. \quad (3.110b)$$

In these equations, the known quantities appear on the right-hand side, those to be determined appear on the left-hand side. By adding these equations, one finds

$$\hat{v}_j = 0, \quad -\hat{v}_- = \hat{v}_+, \quad (3.110c)$$

which means that the same $-\pi$ phase jump is obtained as for the velocity of longitudinal waves in a rigidly constrained beam.

The distributions indicated in the left-hand part of Fig. 3.13 therefore also correspond to the velocity and displacement of a beam that is simply supported on both ends. However, because of the dispersive nature of bending waves, the frequencies are proportional to the square of the wavenumber, according to Eq. (3.83). Therefore, the natural frequencies here are proportional to the squares of the integers:

$$f_n = \frac{1}{2\pi} \sqrt{\frac{B}{m'}} k^2 = \frac{\pi}{2} \sqrt{\frac{B}{m'} \frac{n^2}{l^2}}. \quad (3.110d)$$

For a beam with “guided” ends (lower right-hand side of Fig. 3.15), one finds the same natural frequencies, because for this case the equations for the angular velocity w are identical to those for v for a simply supported beam.

Reflection of a wave from a free end, on the other hand, gives rise to a nearfield. Since the corresponding boundary conditions,

$$\underline{M} = 0, \underline{F} = 0, \quad (3.111a)$$

may also be written as

$$\underline{M} = 0, \frac{d\underline{M}}{dx} = 0, \quad (3.111b)$$

it is convenient to describe the field in terms of the phasors for the moments in the incident wave $\hat{\underline{M}}_+ e^{-jkx}$, the reflected wave $\hat{\underline{M}}_- e^{+jkx}$, and the nearfield $\hat{\underline{M}}_j e^{jkx}$.

The boundary conditions lead to two equations

$$\begin{aligned} \hat{\underline{M}}_- + \hat{\underline{M}}_j &= -\hat{\underline{M}}_+ \\ j\hat{\underline{M}}_- + \hat{\underline{M}}_j &= j\hat{\underline{M}}_+, \end{aligned} \quad (3.111c)$$

from which one may obtain the reflected nearfield and propagating wave phasors

$$\hat{\underline{M}}_j = (-1 + j)\hat{\underline{M}}_+, \quad \hat{\underline{M}}_- = -j\hat{\underline{M}}_+ \quad (3.111d)$$

The magnitude of this nearfield phasor at the beam’s end is even greater than that for the incident wave. Although this greater magnitude extends the effective length of the nearfield, it does not change the fact that at some distance from the beam end there remains only the reflected wave, and that only the latter wave transports energy. Because the reflected energy must be equal to the incident energy, the amplitude of the reflected wave must be equal to that of the incident one. Indeed, the solution for $\hat{\underline{M}}_-$ correspond to a phase jump of $\gamma = -\pi/2$.

If one assumes that the nearfield which results at one end is negligible at the other end (an assumption which becomes increasingly valid for shorter wavelengths, that is, at higher frequencies), then wave-train closure is again obtained if the wave train closes on itself with equal phase. In this case one obtains the following approximate expression for the natural frequencies of free-free beams (i.e., beams with both ends free).

$$2k_n l \approx (2n-1)\pi, f_n = \frac{1}{2\pi} \sqrt{\frac{B}{m'}} k_n^2 \approx \frac{\pi}{8} \sqrt{\frac{B}{m'}} \frac{(2n-1)^2}{l^2}. \quad (3.111e)$$

The above relation between the wavenumber and the length of the beam is the same as that which previously was obtained for longitudinal waves in a clamped-free beam. In the latter case, the phase change of $-\pi$ was produced at one end, whereas in the present case a phase jump of $-\pi/2$ occurs at each of the two ends.

Figure 3.16 shows the velocity (or the displacement) distributions for three natural vibrations of a free-free beam. The thick curves include the nearfield contributions, whereas the thin curves correspond to only the pure propagating waves.

Although Eq. (3.111e) admits the case of $n = 1$, this case must be ruled out on physical grounds. It would imply either a rigid-body translation of the beam and thus an oscillating motion of its centre of gravity or a rigid-body rotational oscillation of the beam about its centre; the former is impossible because no external forces are present, the second, because there is no external moment.

The natural frequencies of free-free beams are approx. in the ratio 9:25:49:81... . The “overtones” thus are not related harmonically to the fundamental.

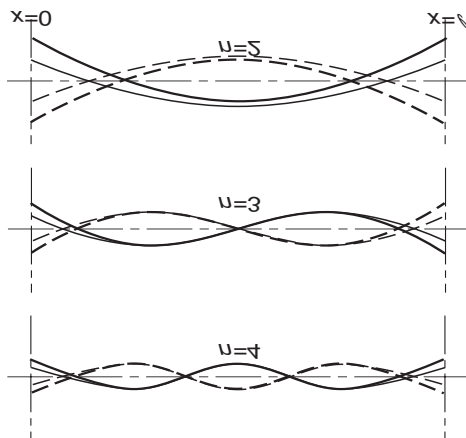


Fig. 3.16. Flexural natural vibrations of a free-free beam. Light curves: without nearfield; heavy curves: with nearfield. (Again, solid and dashed curves represent conditions half a period apart.)

For a clamped-clamped beam, the boundary conditions are

$$\underline{v} = 0, \quad \frac{d\underline{v}}{dx} = 0.$$

Therefore, if one uses v instead of M , one obtains the same results as before, and one finds that Eq. (3.111e) applies equally well also for clamped-clamped beams.

In most cases, the difference between the actual and the ideally rigid constraint at the support is likely to have a greater effect on the natural frequencies than does neglecting of the nearfield effects in the derivation Eq. (3.111e) and the exact values is generally smaller for $n > 2$ than the accuracy with which one can determine B , m' , l , or with which can measure the frequency.

Corrections to Eq. (3.111e) are of practical interest only for the lowest natural frequencies of free-free beams. It is also instructive to investigate these corrections, in order to remove any impression that the wave-train closure is only an approximation. Indeed, this principle always yields exact results also for flexural wave problems, provided one takes into account that the nearfields generated at one end still have finite values at the other and there again give rise to additional waves and nearfields.

As shown by means of (3.111c) and (3.111d), a propagating wave of amplitude \hat{M}_+ results in

$$\begin{aligned}\hat{M}_- &= j\hat{M}_+ = \hat{M}_+ e^{-j\pi/2}, \\ \hat{M}_{-j} &= -(1-j)\hat{M}_+ = -\sqrt{2}\hat{M}_+ e^{-j\pi/4},\end{aligned}\tag{3.111f}$$

as reflected propagating wave and nearfield respectively.

Upon applying this on a nearfield of amplitude \hat{M}_{+j} , the boundary conditions in (3.111b) require that $\hat{M}_{+j} + \hat{M}_{-j} + \hat{M}_- = 0$ and $-\hat{M}_{+j} + \hat{M}_{-j} + j\hat{M}_- = 0$ respectively. It follows that subsequent to the reflection are formed

$$\begin{aligned}\hat{M}_{-j} &= j\hat{M}_{+j} = \hat{M}_{+j} e^{j\pi/2}, \\ \hat{M}_- &= -(1+j)\hat{M}_{+j} = -\sqrt{2}\hat{M}_{+j} e^{j\pi/4},\end{aligned}\tag{3.111g}$$

as reflected nearfield and propagating waves respectively. The principle of phase continuity requires that after a roundtrip, comprising two reflections with the conversions from propagating wave to nearfield as well as from nearfield to propagating wave, the initial conditions are regained. Since a single passage leads to a phase shift of kl and hence a multiplication by e^{-jkl} for the propagating part and by e^{-jkl} for the nearfield, the former component of amplitude \hat{M}_+ yields

$$\begin{aligned} & \hat{M}_+ \left\{ e^{-2jkl} (-j)^2 + e^{-jkl} e^{-kl} (1+j)(1-j) \right\} \\ & - \hat{M}_+ \left\{ e^{-2jkl} j(1-j) + e^{-jkl} e^{-kl} j(1-j) \right\} \end{aligned} \quad (3.111h)$$

subsequent on a complete roundtrip. If the abbreviations P and N are introduced for the propagating wave and nearfield respectively, the separate terms in the expression correspond to PPP , PNP , PPN and NNN . In these combinations, the first letter denotes the initial wave, the second its form after the first reflection whilst the last that resulting after completing the roundtrip.

Employed on an initial nearfield of amplitude \hat{M}_{+j} follows the combinations NPP , NNP , NPN and NNN . This means that the roundtrip is described by

$$\begin{aligned} & \hat{M}_{+j} \left\{ e^{-jkl} e^{-kl} j(1+j) - e^{-2kl} j(1+j) \right\} \\ & - \hat{M}_{+j} \left\{ e^{-jkl} e^{-kl} (1-j)(1+j) + e^{-2kl} j^2 \right\}. \end{aligned} \quad (3.111i)$$

The wave-train-closure principle now requires that the sum of the propagating field components (the first brackets in the above two expressions) equal the initial amplitude \hat{M}_+ . Similarly, the sum of the nearfield components (the second brackets) must equal the amplitude \hat{M}_{+j} . Accordingly,

$$\begin{aligned} & \hat{M}_+ \left[-e^{-2jkl} + 2e^{-jkl-kl} - 1 \right] + \hat{M}_{+j} \left[j(1+j) \left(e^{-jkl-kl} - e^{-2kl} \right) \right] = 0, \\ & \hat{M}_+ \left[j(1-j) \left(e^{-2jkl} - e^{-jkl-kl} \right) \right] + \hat{M}_{+j} \left[2e^{-jkl-kl} - e^{-2kl} - 1 \right] = 0, \end{aligned}$$

for which the solution is obtained from the vanishing determinant. This means that

$$1 + e^{-2kl} + e^{-2jkl} + e^{-2kl-2jkl} - 4e^{-kl-jkl} = 0, \quad (3.111j)$$

which can readily be rewritten as [3.1]

$$\cosh kl \cos kl - 1 = 0. \quad (3.111k)$$

One may observe that for large kl this exact result reduces to

$$\cos kl = 0,$$

which was used as the basis for the previous approximate analysis. As has been noted, the difference between the exact and the approximate results is of practical interest only in relation to the first zero, for which the exact relation gives

$$k_1 l = 3\pi / 2 + 0.0176,$$

compared with the approximate value of $kl = 3\pi/2$. Thus, the exact wavenumber is about 0.37 % greater than that given by the approximation of Eq. (3.111e), and the exact natural frequency is about 0.7 % higher than the value obtained from the approximation. The exact fundamental natural frequency is given by

$$f_1 = 3.8 \sqrt{\frac{B}{m'}} \frac{1}{l^2}. \quad (3.111)$$

Finally, it is instructive to consider the case of a cantilever beam but without carrying out the corresponding analysis in full detail. In an analogous way, the characteristic equation for the cantilever beam is found to be given by

$$\cosh kl \cos kl + 1 = 0.$$

This means that the approximation

$$f_n \approx \frac{\pi}{8} \sqrt{\frac{B}{m'}} \frac{(2n-1)^2}{l^2} \quad (3.112)$$

also holds for these boundary conditions and high eigenfrequencies. The first eigenfrequency, which again is insufficiently determined from Eq. (3.112), is found to be given by

$$f_1 = 0.56 \sqrt{\frac{B}{m}} \frac{1}{l^2} \quad (3.112a)$$

for $n = 1$ in this case since no rigid body motion is possible.

3.5 The General Field Equations

The previous analyses have been based on postulating particular types of deformations, and each has lead to new types of wave propagation. Thus, one is led to inquire whether there exist arbitrarily many wave types, or – conversely – whether one may analyse all possible waves in terms of a limited number of basic types.

In order to answer this question, one must first determine what wave processes can occur in an infinite solid medium, and then investigate what effect free surfaces have on these processes.

Figure 3.17 indicates the most general deformation that a surface element $dx dy$ can have in the xy plane. For the sake of clarity, dx is shown equal in length to dy . First of all, this element is displaced by an amount ξ

in the x -direction and by an amount η in the y -direction. Because the displacements, as already discussed after Eq. (3.3), must always be small compared with the wavelength, their spatial derivatives $\partial\xi/\partial x$, $\partial\xi/\partial y$, $\partial\eta/\partial x$, $\partial\eta/\partial y$ always represent very small strains or angles. The deformations associated with these derivatives are shown in Fig. 3.17, exaggerated by several orders of magnitude for the sake of clarity. It is useful to investigate separately the three different types of deformations, as also shown at the bottom of Fig. 3.17.

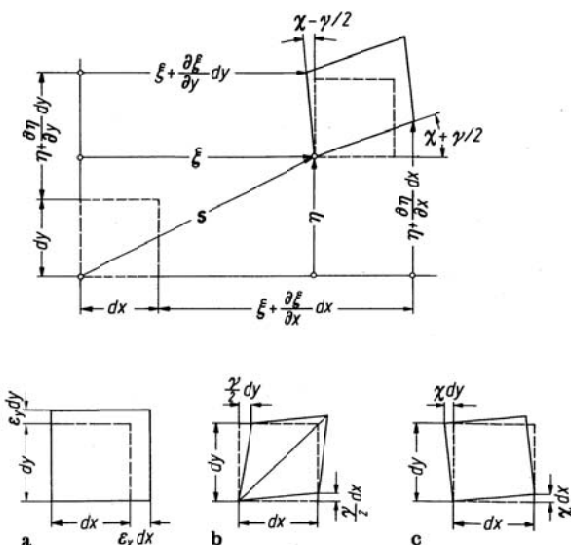


Fig. 3.17. Displacements and strains in two dimensions. a) pure extension in x - and y -directions; b) pure shear deformation; c) pure rotation about x -axis

- a) Extensions $\varepsilon_x = \partial\xi/\partial x$, $\varepsilon_y = \partial\eta/\partial y$.

Their sum corresponds to the fractional increase in the element's area, if one neglects the product $\varepsilon_x\varepsilon_y$. These strains need not be of the same magnitude, and may even have opposite signs and therefore generally imply a change in the shape i.e., a change in the ratio of length to width of the element's area.

- b) Shear, corresponding to the shear angle γ_{xy} .

This leads to an additional change in shape, namely to distortion of the original rectangle into a parallelogram. In Fig. 3.4, which dealt with a pure transverse wave, this change in shape resulted only from an η displacement, and the strain energy was due only to τ_{xy} . But because the shear stress τ_{yx} must play exactly the same role as τ_{xy} in causing

such a deformation, it is clear that one should define a pure shear deformation as one where the total shear angle γ_{xy} is equally divided over two planes which originally are perpendicular to each other, as shown in part *b* of Fig. 3.17. The distorted shape similarly should have been shown in part *a* as symmetric with respect to the original undistorted shape. There, however, the strains were so small compared with the displacements ξ and η that one could completely neglect the fact that the deformations shown in part *a* and *b* of Fig. 3.17 consist of a pure extension by $\varepsilon_x dx$ and $\varepsilon_y dy$ plus a translation by $\varepsilon_x dx/2$ and $\varepsilon_y dy/2$. But one must be careful concerning these components in analysing the changes in the angles associated with deformations like that shown in Fig. 3.4, where the deformation consists of a superposition of a pure shear deformation and a pure rotation.

c) Rotations χ_z .

As indicated in part *c* of Fig. 3.17, χ_z typically take on only very small values for elastic waves, such as pure transverse waves. One may therefore take the rotations angle χ_z (about the *z*-axis) as proportional to the components $\partial\xi/\partial y$ and $\partial\eta/\partial x$.

As may easily be seen from Fig. 3.17, these differentials obeys

$$\begin{aligned}\frac{\partial\xi}{\partial y} &= \frac{1}{2}\gamma_{xy} - \chi_z, \\ \frac{\partial\eta}{\partial x} &= \frac{1}{2}\gamma_{xy} + \chi_z.\end{aligned}\tag{3.113}$$

Their sum thus determines the shear angle,

$$\gamma_{xy} = \frac{\partial\xi}{\partial y} + \frac{\partial\eta}{\partial x},\tag{3.114a}$$

and their difference, twice the rotational angle,

$$2\chi_z = \frac{\partial\eta}{\partial x} - \frac{\partial\xi}{\partial y}.\tag{3.115a}$$

One observes that with a deformation in all three coordinate directions there is associated also an additional displacement component ζ in the *z*-direction, as well as an additional shear angle in the *yz*-plane,

$$\gamma_{yz} = \frac{\partial\eta}{\partial z} + \frac{\partial\zeta}{\partial y},\tag{3.114b}$$

and one in the *xy*-plane,

$$\gamma_{zx} = \frac{\partial \zeta}{\partial x} + \frac{\partial \xi}{\partial z}, \quad (3.114c)$$

and in general also rotations about the x -axis,

$$2\chi_x = \frac{\partial \zeta}{\partial y} - \frac{\partial \eta}{\partial z}, \quad (3.115b)$$

and about the y -axis,

$$2\chi_y = \frac{\partial \xi}{\partial z} - \frac{\partial \zeta}{\partial x}. \quad (3.115c)$$

If one writes the three displacement components in terms of a displacement vector

$$\mathbf{s} = \mathbf{i}\xi + \mathbf{j}\eta + \mathbf{k}\zeta, \quad (3.116)$$

then also, the three Eqs. (3.115) can be written as a single vector equation. $2\chi_x$, $2\chi_y$ and $2\chi_z$ are simply the components of the rotation of the displacement vector,

$$\mathbf{i}\chi_x + \mathbf{j}\chi_y + \mathbf{k}\chi_z = \frac{1}{2} \operatorname{rot} \mathbf{s}. \quad (3.117)$$

The additional extensional strain component $\varepsilon_z = \partial \zeta / \partial z$, together with ε_x and ε_y , determines the relative increase in volume of an element. This volume change is also known as the dilatation δ , and corresponds to a well-known differential operation on the vector s , namely its divergence,

$$\delta = \varepsilon_x + \varepsilon_y + \varepsilon_z = \operatorname{div} \mathbf{s}. \quad (3.118)$$

It is instructive now to determine the relations between the deformations and the stresses. The shear stresses depend on the corresponding shear angles through

$$\begin{aligned} \tau_{xy} &= \tau_{yx} = G \left(\frac{\partial \xi}{\partial y} + \frac{\partial \eta}{\partial x} \right), \\ \tau_{yz} &= \tau_{zy} = G \left(\frac{\partial \eta}{\partial z} + \frac{\partial \zeta}{\partial y} \right), \\ \tau_{zx} &= \tau_{xz} = G \left(\frac{\partial \zeta}{\partial x} + \frac{\partial \xi}{\partial z} \right). \end{aligned} \quad (3.119)$$

On the other hand, the normal stresses are coupled to each other, as a result of the Poisson effect, as has already been pointed out in Sect. 3.1.2. By

adding Eqs. (3.24) of that section and replacing E by G by means of Eq. (3.48), one obtains

$$2G(1+\mu)\delta = (1-2\mu)(\sigma_x + \sigma_y + \sigma_z).$$

If one uses this result to express the sum of the normal stresses in terms of the dilatation, then one finds from Eq. (3.24) that

$$\begin{aligned}\sigma_x &= 2G \left[\frac{\partial \xi}{\partial x} + \frac{\mu}{1-2\mu} \operatorname{div} \mathbf{s} \right], \\ \sigma_y &= 2G \left[\frac{\partial \eta}{\partial y} + \frac{\mu}{1-2\mu} \operatorname{div} \mathbf{s} \right], \\ \sigma_z &= 2G \left[\frac{\partial \zeta}{\partial z} + \frac{\mu}{1-2\mu} \operatorname{div} \mathbf{s} \right].\end{aligned}\quad (3.120)$$

To complete the description, the previously in Eqs. (3.29) and (3.45) applied dynamic relations are required. In the present three-dimensional case, are considered all normal and shear stresses acting on a volume element as well as the inertia forces per unit volume. This means

$$\begin{aligned}\frac{\partial \sigma_x}{\partial x} + \frac{\partial \tau_{xy}}{\partial y} + \frac{\partial \tau_{xz}}{\partial z} &= \rho \frac{\partial^2 \xi}{\partial t^2} \\ \frac{\partial \sigma_y}{\partial y} + \frac{\partial \tau_{yx}}{\partial x} + \frac{\partial \tau_{yz}}{\partial z} &= \rho \frac{\partial^2 \eta}{\partial t^2} \\ \frac{\partial \sigma_z}{\partial z} + \frac{\partial \tau_{zx}}{\partial x} + \frac{\partial \tau_{zy}}{\partial y} &= \rho \frac{\partial^2 \zeta}{\partial t^2}\end{aligned}\quad (3.121)$$

Upon substituting (3.119) and (3.120), making use of (3.116), results

$$G \left\{ \nabla^2 \mathbf{s} + \frac{1}{1-2\mu} \operatorname{grad} \operatorname{div} \mathbf{s} \right\} = \rho \frac{\partial^2 \mathbf{s}}{\partial t^2} \quad (3.122a)$$

or, in terms of the velocity vector,

$$G \left\{ \nabla^2 \mathbf{v} + \frac{1}{1-2\mu} \operatorname{grad} \operatorname{div} \mathbf{v} \right\} = \rho \frac{\partial^2 \mathbf{v}}{\partial t^2}, \quad (3.122b)$$

where ∇^2 is the Laplace operator. By using the velocity components $v_1 = \partial \xi / \partial t$, $v_2 = \partial \eta / \partial t$, $v_3 = \partial \zeta / \partial t$, the same expression becomes

$$\nabla^2 v_i + \frac{1}{1-2\mu} \frac{\partial}{\partial x_i} \left(\frac{\partial v_k}{\partial x_k} \right) = \frac{\rho}{G} \frac{\partial^2 v_i}{\partial t^2}; i, k = 1, 2, 3 \quad (3.122c)$$

In the last version use is made of the summation convention i.e., to sum over equal indices. This general differential equation, which all elastic oscillatory motions in the interior of a solid must satisfy, resembles the wave equations discussed in Sections 3.1 and 3.2, only in that it is also of second order with respect to space and time. It differs from them in its spatial character, in that its argument (the displacement vector) contains three components, and in that the differentiations corresponding to the vector operators extend in all coordinate directions. The latter property is characteristic of all wave problems in three-dimensional space. The fact that two operators appear on the left-hand side is characteristic of solid bodies. This indicates that the equation encompasses two wave equations simultaneously.

According to a general theorem of vector analysis, one may separate any continuous vector field into an irrotational and a divergence-free (source-free) part. If these parts are represented by \mathbf{s}_1 and \mathbf{s}_2 respectively, then the first satisfies

$$\operatorname{rot} \mathbf{s}_1 = 0, \quad (3.123a)$$

and the second

$$\operatorname{div} \mathbf{s}_2 = 0. \quad (3.123b)$$

The irrotational component therefore contains the same dilatation as the entire field,

$$\operatorname{div} \mathbf{s}_1 = \operatorname{div} \mathbf{s} = \delta \quad (3.124a)$$

and the divergence-free part contains the same rotation as the entire field,

$$\operatorname{rot} \mathbf{s}_2 = \operatorname{rot} \mathbf{s}. \quad (3.124b)$$

In terms of the vector of the angular velocity, the latter expression becomes

$$\mathbf{w} = \frac{1}{2} \operatorname{rot} \mathbf{v}_2 = \frac{1}{2} \operatorname{rot} \mathbf{v}. \quad (3.124c)$$

If one applies the divergence operation to Eq. (3.122a) once more, taking into account that

$$\operatorname{div} \nabla^2 = \nabla^2 \operatorname{div} , \quad \operatorname{div} \frac{\partial}{\partial t^2} = \frac{\partial}{\partial t^2} \operatorname{div},$$

then one obtains the three-dimensional wave equation for the dilatation:

$$G \frac{2(1-\mu)}{(1-2\mu)} \nabla^2 \delta = \rho \frac{\partial^2 \delta}{\partial t^2}. \quad (3.125)$$

This equation includes the case where the same conditions exist on every plane perpendicular to the x -axis. Then ∇^2 reduces to $\partial^2 / \partial \xi^2$, and one obtains the one-dimensional wave equation, as has already been derived in Sect. 3.1.1, as Eq. (3.11). The propagation speed obtained there, according to Eq. (3.50), is the same at that obtained here, namely that of pure longitudinal waves,

$$c_L = \sqrt{\frac{2G(1-\mu)}{\rho(1-2\mu)}}. \quad (3.126)$$

Since a three-dimensionally infinite medium was also assumed in Sect. 3.1.1, the wave type discussed there must also be subject to the present general representation. One may recognize that this previously treated wave type corresponds to a plane dilatational wave. Therefore, “pure longitudinal waves” are often called “dilatational waves”. It must remembered, however, that in finite media, other disturbances that include dilatations can also propagate at different speeds. But “pure longitudinal waves” are the only type that is “irrotational”.

A three-dimensionally infinite medium was also postulated for the pure transverse wave discussed in Sect. 3.2.1. Therefore, such a transverse wave must also satisfy Eq. (3.122a). One finds further that the two above-mentioned types of waves are the only types of plane waves that can occur in an infinite medium. By applying to Eq. (3.122a) the rotation operator and making use of the relations

$$\text{rot} \nabla^2 = \nabla^2 \text{rot}, \quad \text{rot} \frac{\partial^2}{\partial t^2} = \frac{\partial^2}{\partial t^2} \text{rot},$$

as well as the identity

$$\text{rot grad} \equiv 0,$$

one obtains the three-dimensional wave equation for $\text{rot } \mathbf{s}$,

$$G \nabla^2 (\text{rot } \mathbf{s}) = \rho \frac{\partial^2}{\partial t^2} (\text{rot } \mathbf{s}), \quad (3.127a)$$

or

$$G \nabla^2 \mathbf{w} = \rho \frac{\partial^2 \mathbf{w}}{\partial t^2}, \quad (3.127b)$$

which describe the behaviour of the source-free (non-divergent and incompressible) part of the wave field. For planar distributions of the vari-

ables, this relation reduces to Eq. (3.46), and implies that all plane rotational processes with the transverse wave velocity

$$c_T = \sqrt{\frac{G}{\rho}}. \quad (3.128)$$

Therefore, c_T is also known as the rotational wave velocity. Again, in finite media there can occur other wave types with rotational components propagating with other speeds. The solutions to Eq. (3.127) represent the only possible “source-free (non-divergent) wave motions”.

At this point it should be supplemented that in theoretical physics in particular, the strains and stresses can be elegantly written by means of 3*3 tensors. If u_i is the displacement component of the space co-ordinate x_i i.e., $u_1 = \xi$, $u_2 = \eta$, $u_3 = \zeta$ and $x_1 = x$, $x_2 = y$, $x_3 = z$ in the classical notation, then the strain tensor has the elements

$$\varepsilon_{ij} = \frac{1}{2} \left(\frac{\partial u_i}{\partial x_j} + \frac{\partial u_j}{\partial x_i} \right); i, j = 1, 2, 3. \quad (3.128a)$$

The stress-strain relations in Eqs. (3.119) and (3.120) for isotropic materials read

$$\sigma_{ij} = \frac{2G\mu}{1-2\mu} (\varepsilon_{11} + \varepsilon_{22} + \varepsilon_{33}) \delta_{ij} + 2G\varepsilon_{ij}. \quad (3.128b)$$

Herein, $\delta_{ij} = 0$ for $i \neq j$ and $\delta_{ii} = 1$ is the Kronecker delta. In tensor formalism, force equilibrium is written as

$$\frac{\partial \sigma_{ij}}{\partial x_j} = \rho \frac{\partial^2 u_i}{\partial t^2} \quad (3.128c)$$

Summation is here made for equal indices. A substitution of (3.128a, b) yields the wave Eq. (3.122c).

Although the tensor formalism is elegant and offers many advantages especially in the treatise of anisotropic and piezo-electric materials, the classical notation will be retained in this book owing to its common usage in the engineering science literature.

The question raised at the beginning of this section, concerning whether all waves may be treated in terms of a few basic types, has so far been answered only in part. It has been shown that in the interior of a solid body, only pure longitudinal and pure transverse waves can occur as plane waves. These two wave types are completely independent of each other, and therefore can be excited separately. In practice, however, one usually cannot avoid exciting both waves or, in more general terms, obtaining both

an irrotational and a source-free wave field. But because these propagate with different speeds, one can obtain separated “wave pulses” as the result of short-duration excitation, provided that the dimensions of the solid body are greater than the product of the speed difference ($c_L - c_T$) and the pulse duration. This requirement is satisfied, for example, for seismic waves in the earth, or in the testing of thick structural parts by means of ultrasound, in other words, whenever the “interior” of the solid body extends over many wavelengths in all directions.

The usually employed method to solve Eq. (3.122b) consists of introducing a scalar potential Φ and a vector potential ψ with the following properties

$$\mathbf{v}_L = \frac{d\mathbf{s}_1}{dt} = \text{grad}\Phi, \quad \mathbf{v}_T = \frac{d\mathbf{s}_2}{dt} = \text{rot } \psi, \quad \mathbf{v} = \mathbf{v}_L + \mathbf{v}_T \quad (3.129)$$

These potentials satisfy the wave Eqs. (3.125) and (3.127) respectively, analogous to the quantities δ and \mathbf{w} . The problem hence, is returned to the solution of two wave equations for which exists a battery of procedures. It should be noted, however, that any boundary condition is given by the velocity and stress. This means that since these quantities are linear combinations of Φ and ψ , there results a coupling of the two fields at boundaries of solid structures. Such conversions from one wave type to another will be further treated in the following sections.

Within the scope of this book, only plane problems will be analysed in conjunction with elastic, isotropic continua. Therefore, the vectorial nature of the vector potential can be omitted since its direction always will be perpendicular to the plane of the field. This means that as in previously studied examples, the solution of the wave equations can be constructed from one or more plane waves i.e.,

$$v_i = \hat{v}_i(k_x, k_y, k_z) e^{-jk_x x} e^{-jk_y y} e^{-jk_z z}; \quad i = 1, 2, 3. \quad (3.130)$$

The phasor notation is hereby directly introduced which means that pure harmonic processes are understood at an angular frequency ω . The time base $e^{j\omega t}$ and the prefix $\text{Re} [\dots]$ are omitted as is usual. k_x , k_y and k_z are the wavenumber components. Together they reveal the wavelength and wave direction. The expression in (3.130), of course, is not a complete solution to the wave equation. (3.122). Rather it constitutes a fundamental solution with which all other solutions can be constructed by summation or integration as Fourier series or integrals respectively. With the fundamental solution in (3.130) inserted in (3.122c)

$$\begin{aligned} \left(k_T^2 - k^2 - \frac{1}{1-2\mu} k_x^2 \right) \hat{v}_1 - \frac{1}{1-2\mu} k_x k_y \hat{v}_2 - \frac{1}{1-2\mu} k_x k_z \hat{v}_3 &= 0 \\ \frac{-1}{1-2\mu} k_y k_x \hat{v}_1 - \left(k_T^2 - k^2 - \frac{1}{1-2\mu} k_y^2 \right) \hat{v}_2 - \frac{1}{1-2\mu} k_y k_z \hat{v}_3 &= 0 \\ \frac{-1}{1-2\mu} k_z k_x \hat{v}_1 - \frac{1}{1-2\mu} k_z k_y \hat{v}_2 - \left(k_T^2 - k^2 - \frac{1}{1-2\mu} k_z^2 \right) \hat{v}_3 &= 0 \end{aligned} \quad (3.131)$$

is obtained, where $k^2 = k_x^2 + k_y^2 + k_z^2$ and $k_T^2 = \omega^2 / c_L^2$. This homogeneous set of linear equations has non-trivial solutions only when the determinant vanishes. With a few manipulations, the condition

$$(k_T^2 - k^2)^2 \left(k_T^2 - \frac{2(1-\mu)}{1-2\mu} k^2 \right) = 0$$

is obtained, which means that the admissible wavenumbers are

$$k_I^2 = k_x^2 + k_y^2 + k_z^2 = k_T^2, \quad (3.132a)$$

and

$$k_{II}^2 = k_x^2 + k_y^2 + k_z^2 = k_T^2 \frac{1-2\mu}{2-2\mu} = \frac{\omega^2}{c_L^2} = k_L^2. \quad (3.132b)$$

As can be seen, Eq. (3.132a) corresponds to a propagation of transversal waves whereas (3.132b) to that of longitudinal. Thus, the subdivision is again possible in the two wave types.

From (3.131) furthermore, it is found that certain relations exist between the phasors \hat{v}_1, \hat{v}_2 and \hat{v}_3 . By letting $k^2 = k_T^2$ in (3.131),

$$k_x \hat{v}_{1T} + k_y \hat{v}_{2T} + k_z \hat{v}_{3T} = 0, \quad (3.132c)$$

and by inserting $k^2 = k_L^2$

$$\hat{v}_{2L} = \frac{k_y}{k_x} \hat{v}_{1L}, \quad \hat{v}_{3L} = \frac{k_z}{k_x} \hat{v}_{1L}. \quad (3.132d)$$

Thence, the complete, fundamental solution in Cartesian co-ordinates to (3.122b) reads

$$v_i = \left[\hat{v}_{1L}(k_x, k_{yL}, k_z) e^{-jk_{yL}y} + \hat{v}_{1T}(k_x, k_{yT}, k_z) e^{-jk_{yT}y} \right] e^{-jk_x x - jk_z z}; i = 1, 2, 3. \quad (3.133a)$$

The additional conditions given by (3.132a, b) are

$$k_{yT}^2 = k_T^2 - k_x^2 - k_z^2, \quad k_{yL}^2 = k_T^2 \frac{1-2\mu}{2-2\mu} - k_x^2 - k_z^2 = k_L^2 - k_x^2 - k_z^2, \quad (3.133b)$$

which have to be taken into account. The fact that the index y here happens to be singled out lacks further meaning. The expressions could also have been written differently. Important is only that the wavenumber component of one direction is prescribed for (3.133a) to constitute a solution to the wave equation. The expression in (3.132c), moreover, does not reveal more than $\text{rot } \mathbf{v}_L = 0$ and, similarly, that in (3.132d) that $\text{div } \mathbf{v}_T = 0$. This can readily be demonstrated since the spatial differentiations simply are replaced by multiplications by jk_x, jk_y or jk_z respectively.

3.6 Wave Field at a Free Surface

3.6.1 Reflection of Plane Waves

As the first application of the fundamental continuum-equations, is considered the reflection of a plane wave at a free surface. Without sacrificing generality, it is assumed that the wave propagates in the x - y -plane such that all field variables are independent of the z co-ordinate. The co-ordinate system and the angles are indicated in Fig. 3.18. In this figure, are depicted wave strips for the sake of clarity although the wave fronts are considered infinite in the analysis.

The assumed two-dimensionality of the problem means that $k_z = 0$ in Eq. (3.133). Therefore, a reasonable form of the longitudinal waves – in the following termed L-waves – is

$$\begin{aligned} v_1 &= \hat{v}_{1L} e^{-jk_x x} e^{-jk_{yL} y} \\ v_2 &= \frac{k_{yL}}{k_x} \hat{v}_{1L} e^{-jk_x x} e^{-jk_{yL} y} \\ v_3 &= 0 \end{aligned} \tag{3.134}$$

in which $k_{yL} = \sqrt{k_L^2 - k_x^2}$. Herein is $k_L = \omega/c_L$ the wavenumber of L-waves (see Eq. (3.132b)), which is a material property for a given frequency. The relation in (3.132b) is already accounted for in (3.134).

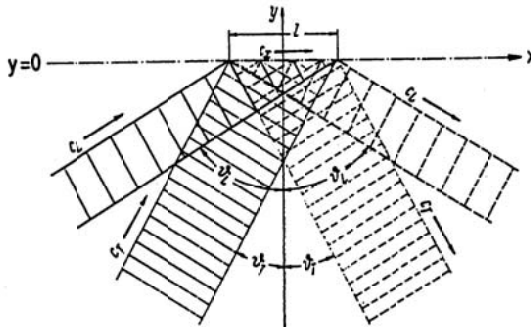


Fig. 3.18. Reflection of longitudinal and transversal waves at a free surface

In Eq. (3.134) is assumed a wave with angle of incidence ϑ_L . This is so since the wave fronts are given by the exponents i.e.,

$$\begin{aligned} k_x x + k_{yL} y &= k_L \left[\frac{k_x}{k_L} x + \sqrt{1 - \left(\frac{k_x}{k_L} \right)^2} y \right] \\ &= k_L [x \sin \vartheta_L + y \cos \vartheta_L] = \text{const.} + 2\pi t. \end{aligned} \quad (3.135)$$

These wave fronts are planes which are perpendicular to the direction of propagation. The wave fronts are also perpendicular to the particle motion (velocity vector), which is seen from a substitution of $k_x = k_L \sin \vartheta_L$ and $k_{yL} = k_L \cos \vartheta_L$ in Eq. (3.134).

3.6.1.1 Trace speed and angular relations

In the following, is required the trace wavelength λ_x . This length is the distance between two wave fronts at $y = \text{const.}$ and thus establishes the period in the x -direction. Alternatively, the wavelength is the projection of the trace wavelength on the direction of propagation. Equation (3.135) yields

$$k_L \lambda_x \sin \vartheta_L = 2\pi; \quad \lambda_x = \frac{2\pi}{k_L \sin \vartheta_L} = \frac{\lambda_L}{\sin \vartheta_L}. \quad (3.135a)$$

Herein is $\lambda_L = c_L/f$ the physical wavelength of the L-wave i.e., in the direction of propagation.

The used transformation in (3.135), $k_x = k_L \sin \vartheta_L$, means that $k_x \leq k_L$ since otherwise k_{yL} would be imaginary. That would correspond to an exponentially decaying near-field and not a propagating incident wave, which is of primary interest here. Instead of $k_x \leq k_L$, the relation $\lambda_x \geq \lambda_L$ can

be used or, if the concept of trace speed is introduced, $c_x = \lambda_s f \geq c_L$. The contradiction of either of the conditions above implies that the motion is only possible as exponentially decaying near-field, which, however, realizes a solution to the wave Eq. (3.122).

At the incidence of the L-wave on the free surface, a reflection is anticipated that fulfils the boundary conditions together with the incident wave. If it is assumed that the free surface coincides with $y = 0$ and that this surface is free of external stress or other constraints, then the boundary conditions can be expressed as

$$\sigma_y = 0, \quad \tau_{yx} = 0, \quad \tau_{yz} = 0; \quad y = 0 \text{ and } \forall x,$$

cf., Fig. 3.18. In view of Eq. (3.134), a comparatively simple solution for the total field comprising incident and reflected waves can be written on the form

$$\begin{aligned} v_1 &= \hat{v}_{1L} \left[e^{-jk_x x} e^{-jk_{yL} y} + r_{LL} e^{-j\tilde{k}_x x} e^{-j\tilde{k}_{yL} y} + r_{LT} e^{-j\bar{\tilde{k}}_x x} + e^{+j\bar{\tilde{k}}_{yL} y} \right], \\ v_2 &= \hat{v}_{1L} \left[\frac{k_{yL}}{k_x} e^{-jk_x x} e^{-jk_{yL} y} - \frac{k_{yL}}{k_x} r_{LL} e^{-j\tilde{k}_x x} e^{-j\tilde{k}_{yL} y} + \frac{k_x}{k_{yT}} r_{LT} e^{-j\bar{\tilde{k}}_x x} + e^{+j\bar{\tilde{k}}_{yL} y} \right], \end{aligned} \quad (3.136)$$

$$v_3 = 0.$$

It is thus assumed that beside the incident L-wave, exist a reflected L-wave and, additionally, an inwards propagating transversal T-wave which emanates at the free surface. The wavenumbers \tilde{k}_x and $\bar{\tilde{k}}_x$ of these new waves are still considered unknown. The remaining wavenumber components must satisfy $\tilde{k}_{yL}^2 = k_L^2 - \tilde{k}_x^2$ and $\bar{\tilde{k}}_{yT}^2 = k_T^2 - \bar{\tilde{k}}_x^2$ respectively since each of the terms in (3.136) alone must be a solution to the wave equation. r_{LL} and r_{LT} can be seen as reflection factors because the amplitudes of the inwards propagating waves are given as fractions of that of the incident wave. In the calculation of v_2 is used the relation (3.132c) for the T-wave and (3.132d) for the L-wave.

To proceed with the analysis, the stresses are required. They are obtained from (3.119) and (3.120) and can be written as

$$\begin{aligned}\frac{\partial \sigma_y}{\partial t} &= 2G \left[\frac{\partial v_2}{\partial y} + \frac{\mu}{1-2\mu} \left(\frac{\partial v_1}{\partial x} + \frac{\partial v_2}{\partial y} + \frac{\partial v_3}{\partial z} \right) \right] \\ \frac{\partial \tau_{xy}}{\partial t} &= G \left[\frac{\partial v_2}{\partial x} + \frac{\partial v_1}{\partial y} \right] \\ \frac{\partial \tau_{yz}}{\partial t} &= G \left[\frac{\partial v_2}{\partial z} + \frac{\partial v_3}{\partial y} \right],\end{aligned}\tag{3.137}$$

after conversion from displacement to velocity. Upon substituting Eq. (3.136) expressions are obtained in the form

$$\sigma_y = A_1 e^{-jk_x x} e^{-jk_{yL} y} + A_2 e^{-j\tilde{k}_x x} e^{j\tilde{k}_{yL} y} + A_3 e^{-j\bar{k}_x x} e^{j\bar{k}_{yT} y},$$

since the exponents remain unaltered in the differentiations as is the spatial dependence. Moreover, A_1 , A_2 and A_3 are independent of x and y . From the boundary conditions in this case, all the stresses must vanish at $y = 0$. This is possible if and only if $k_x = \tilde{k}_x = k_x$ such that

$$\tilde{k}_{yL} = \sqrt{k_L^2 - k_x^2} = k_{yL}, \quad \bar{k}_{yT} = \sqrt{k_T^2 - k_x^2} = k_{yT}.\tag{3.138a}$$

Accordingly, the fact that the boundary conditions apply for all of the free surface, automatically implies equality of the wavenumber components in the x -direction. This is equivalent to equality of trace wavelengths and trace speeds in view of (3.135a). The equality of trace speeds and hence also of k_x could have been derived directly from the boundary conditions. This is so since two or more waves can only satisfy a uniform, prescribed boundary condition at a plane when they propagate with equal speed along that plane.

Through (3.135), the angles of propagation can be found for the wave field components. The spatial dependence of the incident wave leads to

$$e^{-jk_x x} e^{-jk_{yL} y} = e^{-jk_L(x \sin \theta_L + y \cos \theta_L)},$$

and for the reflected L-wave follows from (3.138a) that

$$e^{-jk_x x} e^{jk_{yL} y} = e^{-jk_L(x \sin \theta_L - y \cos \theta_L)}.$$

For the, at the free surface, emanating T-wave

$$e^{-jk_x x} e^{jk_{yT} y} = e^{-jk_T(x \sin \theta_T - y \cos \theta_T)},$$

whereby $k_T \sin \theta_T = k_x$ and $k_T \cos \theta_T = k_{yT}$. The expressions reveal that the angle of reflection equals that of incidence for the L-waves but that they travel in opposite direction and that the T-wave propagates under an angle of

$$\vartheta_T = \arcsin\left(\frac{k_x}{k_T}\right) = \arcsin\left(\frac{k_L}{k_T} \frac{k_x}{k_L}\right) = \arcsin\left(\frac{k_L}{k_T} \sin \vartheta_L\right).$$

The relations above can also be written in the form

$$\sin \vartheta_T = n \sin \vartheta_L, \quad (3.138b)$$

in analogy with Snell's law wherein

$$n = \frac{k_L}{k_T} = \frac{c_T}{c_L} = \sqrt{\frac{1-2\mu}{2-2\mu}} \quad (3.138c)$$

is the index of refraction. From the range for Poisson's ratio, it follows that $0.5 \geq n^2 \geq 0$.

3.6.1.2 Reflection of L-Waves

When a plane L-wave is incident on the free surface, it is partially reflected with the reflection factor r_{LL} and partially converted into a T-wave, the relative amplitude of which is r_{LT} . Hence, the velocity field is given by Eq. (3.136) whereby

$$\begin{aligned} k_x &= \tilde{k}_x = \bar{k}_x = k_L \sin \vartheta_L, & k_{yL} &= \tilde{k}_{yL} = k_L \cos \vartheta_L, \\ k_{yT} &= \bar{k}_{yT} = k_T \cos \vartheta_T, & \sin \vartheta_T &= n \sin \vartheta_L \end{aligned} \quad (3.139)$$

from the discussion in the preceding section. Since the refraction index squared, $n^2 \leq 0.5$, a real-valued angle ϑ_T always exists.

With the expressions for the velocities in (3.136) introduced in (3.137), the stresses at the free surface are obtained as

$$\begin{aligned} \frac{\partial \sigma_y}{\partial t} &= 2jGv_{1L} \left[(1+\gamma) \left(\frac{k_{yL}^2}{k_x} - r_{LL} \frac{k_{yL}^2}{k_x} + r_{LT} k_x \right) + \gamma (-k_x - r_{LL} k_x - r_{LT} k_x) \right] e^{-jk_x x}, \\ \frac{\partial \tau_{xy}}{\partial t} &= 2jGv_{1L} \left[-k_{yL} + r_{LL} k_{yL} - r_{LT} \frac{k_x^2}{k_{yT}} - k_{yL} + r_{LL} k_{yL} + r_{LT} k_{yT} \right] e^{-jk_x x}, \end{aligned}$$

whereby $\gamma = \mu (1 - 2\mu)$. From (3.138c),

$$\left(1 + \frac{\mu}{1-2\mu} \right) = \frac{1-\mu}{1-2\mu} = \frac{1}{2n^2}$$

and making use of (3.138a) and (3.139)

$$\begin{aligned} r_{LL} (k_T^2 - 2k_x^2) - 2r_{LT} k_x^2 &= -(k_T^2 - 2k_x^2), \\ 2r_{LL} k_{yL} k_{yT} + r_{LT} (k_T^2 - 2k_x^2) &= 2k_{yL} k_{yT}, \end{aligned} \quad (3.140)$$

when the stresses at the free surfaces vanish. By solving for the reflection factors it is found that

$$\begin{aligned} r_{LL} &= \frac{-\left(k_T^2 - 2k_x^2\right)^2 + 4k_x^2 k_{yT} k_{yL}}{\text{Det}(k)} = \frac{n^2 \sin 2\vartheta_L \sin 2\vartheta_T - \cos^2 2\vartheta_T}{\text{Det}(\vartheta)}, \\ r_{LT} &= \frac{4k_{yT} k_{yL} (k_T^2 - 2k_x^2)}{\text{Det}(k)} = \frac{4n \cos \vartheta_L \cos \vartheta_T \cos 2\vartheta_T}{\text{Det}(\vartheta)}. \end{aligned} \quad (3.141a,b)$$

Herein,

$$\begin{aligned} \text{Det}(k) &= 4k_x^2 k_{yT} k_{yL} + (k_T^2 - 2k_x^2)^2, \\ \text{Det}(\vartheta) &= n^2 \sin 2\vartheta_L \sin 2\vartheta_T + \cos^2 2\vartheta_T. \end{aligned} \quad (3.141c)$$

The second version of (3.141a, b) is developed from a substitution of (3.139) into (3.140).

The reflection factors r_{LL} and r_{LT} express the amplitudes of the reflected waves relative that of the incident. In practice, also the reflection efficiency is an important quantity representing the energy ratio. The intensity in the direction of the wave propagation is given by Eq. (3.16) i.e.,

$$\begin{aligned} J_L &= e_{tot} \cdot c_L = \frac{1}{2} \rho c_L |\hat{v}_L|^2, \\ J_T &= e_{tot} \cdot c_T = \frac{1}{2} \rho c_T |\hat{v}_T|^2, \end{aligned}$$

in which $|\hat{v}_L|^2$ and $|\hat{v}_T|^2$ are the velocity magnitudes squared (peak value). The factor $\frac{1}{2}$ follows from the temporal averaging. For the energy flow also the width of the strips of the L- and T-waves must be taken into account since these are different, cf. Fig. 3.18. If the power of the incident L-wave is denoted W_{iL} , the reflected L-wave W_{rL} and the emerging T-wave W_{rT} , the efficiencies

$$\begin{aligned} \rho_{LL} &= \frac{W_{rL}}{W_{iL}} = \frac{J_{rL} \cos \vartheta_L}{J_{iL} \cos \vartheta_L} = |r_{LL}|^2 \\ \rho_{LT} &= \frac{W_{rT}}{W_{iL}} = \frac{J_{rT} \cos \vartheta_T}{J_{iL} \cos \vartheta_L} = \frac{\rho c_L |r_{LT}|^2 \left(1 + k_x^2/k_{yT}^2\right) |\hat{v}_{iL}|^2 \cos \vartheta_T}{\rho c_L \left(1 + k_{yL}^2/k_x^2\right) |\hat{v}_{iL}|^2 \cos \vartheta_L} \\ &= \frac{|r_{LT}|^2}{n} \frac{k_x^2 \cos \vartheta_T}{k_{yT}^2 \cos \vartheta_L} = |r_{LT}|^2 n \frac{\sin^2 \vartheta_L}{\cos \vartheta_T \cos \vartheta_L} \end{aligned} \quad (3.142)$$

It should be observed that ρ without index refers to the density and with index to the reflection efficiency. Upon substituting (3.141a) and (3.141b) into (3.142), it follows that

$$\begin{aligned}\rho_{LL} &= \frac{\left(n^2 \sin 2\vartheta_L \sin 2\vartheta_T - \cos^2 2\vartheta_T\right)^2}{|\text{Det}(\vartheta)|^2}, \\ \rho_{LT} &= \frac{4n^2 \sin 2\vartheta_L \sin 2\vartheta_T \cos^2 2\vartheta_T}{|\text{Det}(\vartheta)|^2},\end{aligned}\quad (3.142a)$$

respectively. By means of a few manipulations, it is readily corroborated that the energy conservation is preserved i.e., $\rho_{LL} + \rho_{LT} = 1$.

3.6.1.3 Reflection of T-Waves

If instead the incident wave is a T-wave, the analog to Eq. (3.136) reads

$$\begin{aligned}v_1 &= \hat{v}_{1T} \left[e^{-jk_{yT}y} + r_{TT} e^{jk_{yT}y} + r_{TL} e^{jk_{yL}y} \right] e^{-jk_x x}, \\ v_2 &= \hat{v}_{1T} \left[-\frac{k_x}{k_{yT}} e^{-jk_{yT}y} + \frac{k_x}{k_{yT}} r_{TT} e^{jk_{yT}y} - \frac{k_{yL}}{k_x} r_{TL} e^{jk_{yL}y} \right] e^{-jk_x x}, \\ v_3 &= \hat{v}_{3T} \left[e^{-jk_{yT}y} + r_3 e^{jk_{yT}y} \right] e^{-jk_x x}.\end{aligned}\quad (3.143)$$

The two first terms relate to the incident and reflected T-waves respectively whereas the third describes the emerging wave at the free surface, which is converted into an L-wave. For the determination of the y -component of the velocity field v_2 , again Eq. (3.132) is employed. The amplitude v_{3T} is given by the incident wave as is the case for v_{1T} and for this component of the field no L-wave will arise.

The wavenumbers and the associated angle relations are given by equality of trace speeds, as discussed in Sect. 3.6.1.1;

$$k_x = k_T \sin \vartheta_T; \quad k_{yT} = \sqrt{k_T^2 - k_x^2} = k_T \cos \vartheta_T; \quad k_{yL} = \sqrt{k_L^2 - k_x^2}. \quad (3.143a)$$

In view of the law of refraction,

$$\sin \vartheta_L = \frac{1}{n} \sin \vartheta_T = \frac{k_T}{k_L} \sin \vartheta_T \quad (3.143b)$$

such that $k_{yL} = k_L \cos \vartheta_L$ which must be augmented by a restriction. Since $n^2 \leq 0.5$, Eq. (3.143b) furnishes real-valued angles ϑ_L only in the range $0 < \vartheta_T < \arcsin n$. For the limiting angle

$$\vartheta_{Tg} = \arcsin n, \quad (3.143c)$$

ϑ_L equals $\pi/2$. This means that the secondary L-wave runs parallel with the free surface. The angular range is not wide for the secondary L-wave. Typically the limiting angle is about 35° for a Poisson's ratio of $\mu = 0.25$. With a larger angle of incidence, the angle relations cannot be applied. The expressions for the wavenumbers, however, are still applicable and show that for $\vartheta_T > \vartheta_{Tg}$, k_x is larger than k_L and hence k_{yL} becomes imaginary, corresponding to a nearfield. In the following section this issue is considered in some more detail.

If, again, Eq. (3.143) is introduced in (3.137), one obtains

$$\begin{aligned} 2r_{TT}k_x^2 - r_{TL}(k_T^2 - 2k_x^2) &= -2k_x^2, \\ r_{TT}(k_T^2 - 2k_x^2) + 2r_{TL}k_{yL}k_{yT} &= (k_T^2 - 2k_x^2), \\ r_3 &= 1, \end{aligned} \quad (3.144)$$

at the free surface in a similar way as that leading to (3.140). From this can be developed,

$$\begin{aligned} r_{TT} &= \frac{-4k_x^2 k_{yL} k_{yT} + (k_T^2 - 2k_x^2)^2}{\text{Det}(k)} = -r_{LL}, \\ r_{TL} &= \frac{4k_x^2 (k_T^2 - k_x^2)}{\text{Det}(k)} = 4n^2 \frac{\sin^2 \vartheta_L \cos 2\vartheta_T}{\text{Det}(\vartheta)}, \\ r_3 &= 1. \end{aligned} \quad (3.145)$$

Since the z -component of the incident T-wave is totally reflected ($r_3 = 1$) its influence is fairly straightforwardly encompassed. Hence, to keep the mathematical description brief, the reflection efficiencies in the energy relations will be developed only for the case in which $v_3 = 0$. After some small manipulations is obtained

$$\begin{aligned} \rho_{TT} &= \frac{W_{rT}}{W_{iT}} = |r_{TT}|^2, \\ \rho_{TL} &= \frac{W_{rL}}{W_{iT}} = \frac{c_L}{c_T} \frac{\cos \vartheta_L \cos \vartheta_T}{\sin^2 \vartheta_L} |r_{LT}|^2, \end{aligned}$$

such that, again, energy is conserved and $\rho_{TT} + \rho_{TL} = 1$.

3.6.1.4 Reflection Factors and Efficiencies

Figure 3.19 shows the calculated reflection efficiencies for a Poisson's ratio of $\mu = 0.25$. With the graphical layout used, it is readily seen that energy is conserved in accordance with $\rho_{LL} + \rho_{LT} = 1$ and $\rho_{TT} + \rho_{TL} = 1$ respectively. Also, can be noted that $\rho_{TL} = \rho_{LT}$ which is a consequence of the principle of reciprocity as well as the fact that the energy relations remain unaltered by a time reversal (the film is played backwards). For practice, it is facilitating that the reflection factors and efficiencies are independent of frequency at the free surface and hence apply to arbitrary signals. The reflection of a z -component of an incident T-wave is complete with the reflection factor $r_3 = 1$. This part is therefore not considered in the power considerations and discussions of the reflection efficiencies.

The question remains, however, what happens to an incident T-wave at a larger angle than the limiting of Eq. (3.143c). In this case,

$$k_{yL} = \sqrt{k_L^2 - k_x^2} = -j\sqrt{k_x^2 - k_L^2} = -jk_T \sqrt{\sin^2 \theta_T - n^2}. \quad (3.146a)$$

The last root is in the interesting range, $\theta_T > \theta_{Tg}$, purely real. Its sign is given by the physical requirement that the amplitude must decline for growing negative y . Accordingly, the y dependence of the longitudinal wave motion take the form

$$r_{TL} e^{jk_T y} = r_{TL} e^{\sqrt{k_x^2 - k_L^2} y}; \quad y < 0. \quad (3.146b)$$

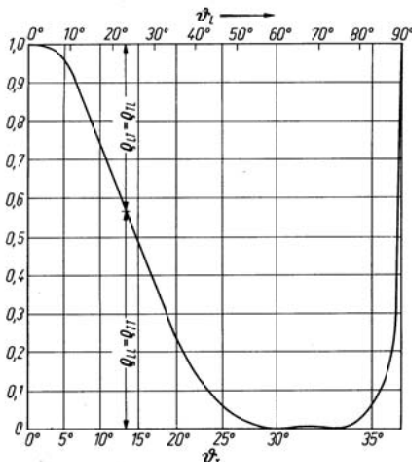


Fig. 3.19. Reflection efficiency at a free surface as function of angle of incidence; $\mu = 0.25$. Top: Longitudinal wave. Bottom: Transversal wave

This means an exponentially decaying nearfield, which already at a distance of $1/(k_x^2 - k_L^2)^{1/2}$ has decayed an e^{th} of the original. This type of wave motion is also called “surface wave” owing to some resemblance with the gravitational waves seen on the sea surface. The waves propagating obliquely from the surface towards the interior in contrast are called “body” or “bulk” waves.

The conditions for the occurrence of a nearfield – i.e., $k_L^2 < k_x^2$ – is identical to $\lambda_L > \lambda_T \sin \theta_T = \lambda_x$. The fact that an exponentially decaying nearfield arises whenever the trace wavelength of the excitation is smaller than the “natural” or free wavelength of the medium will be encountered in numerous air- and structure-borne sound problem.

Upon substituting the imaginary value of k_{yL} , an expression is found for ρ_{TT} in the form $|(jA + B)/(-jA + B)|^2$, which with A and B real gives $\rho_{TT} = 1$. For an angle $\theta_T > \theta_{Tg}$, a total reflection takes place of the incident T-wave. In parallel there exists the exponentially decaying nearfield having the character of a longitudinal wave motion but propagating no energy in the y -direction. For wave trains of finite width, however, the surface wave must first be developed. Therefore, the reflection at the left boundary cannot be instantaneously complete as is also the case at the right where it cannot be abruptly disengaged since the surface wave must be distorted by radiation. This situation is not only qualitatively but also quantitatively analogous to that of a mass-spring system by pulse excitation. The SDOF system must first – in that case temporally – reach the resonance amplitude and, subsequent to the disengagement of the excitation, have a gradual decay.

Yet another feature of the surface wave should be pointed out. The components in the x and y directions exhibit a phase difference of $\pi/2$. From (3.132d)

$$\frac{\hat{v}_{2L}}{\hat{v}_{1L}} = \frac{k_y}{k_x}, \quad (3.147)$$

which, for surface waves, is purely imaginary since k_y is imaginary. This means that v_1 and v_2 do not combine to a resulting velocity with an unambiguous direction but instead the particles exhibit elliptical orbits.

3.6.2 Excitation of an Elastic Half-Space

The reflection of L - and T -waves treated in the previous sections are of significant importance but of at least equal importance is the behaviour of an externally excited elastic half-space. Considered is an isotropic elastic

continuum, occupying the semi-infinite space $y < 0$, which is excited by an external force distribution, see Fig. 3.20. For simplicity, it is assumed that the force distribution takes the form of a plane wave of angular frequency ω and wavenumbers k_x and k_z with the associated trace wavelengths λ_x and λ_z respectively.

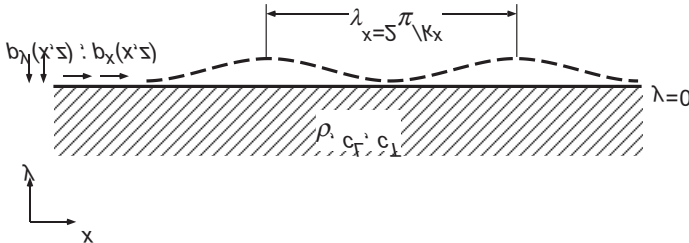


Fig. 3.20. Excitation of an elastic half-space by an external force distribution in terms of a plane wave

At the surface $y = 0$ hence, the exciting normal stress is $p_y = \hat{p}_N e^{-jk_x x} e^{-jk_z z}$, shear stress in x -direction $p_x = \hat{p}_{Tx} e^{-jk_x x} e^{-jk_z z}$ and shear stress in z -direction $p_z = \hat{p}_{Tz} e^{-jk_x x} e^{-jk_z z}$. Owing to the equality of trace wavelengths and trace speeds, the velocity field must have the same x and z dependence and this not only at the surface but for all planes $y \leq 0$. Furthermore, since both L - and T -waves are possible, the following velocity fields are to be assumed

$$\begin{aligned} v_1(x, y, z) &= \left[\hat{v}_{1L} e^{jk_{yL} y} + \hat{v}_{1T} e^{jk_{yT} y} \right] e^{-jk_x x} e^{-jk_z z}, \\ v_2(x, y, z) &= \left[\hat{v}_{1L} \frac{-k_{yL}}{k_x} e^{jk_{yL} y} + \left(\hat{v}_{1T} \frac{k_x}{k_{yT}} + \hat{v}_{3T} \frac{k_z}{k_{yT}} \right) e^{jk_{yT} y} \right] e^{-jk_x x} e^{-jk_z z}, \\ v_3(x, y, z) &= \left[\hat{v}_{1L} \frac{k_z}{k_x} e^{jk_{yL} y} + \hat{v}_{3T} e^{jk_{yT} y} \right] e^{-jk_x x} e^{-jk_z z}, \end{aligned} \quad (3.147a)$$

whereby the relations in Eqs. (3.132c,d) have been used taking the signs associated with the direction of propagation into account. The wavenumbers in the y -direction are given by

$$k_{yL} = \begin{cases} \sqrt{k_L^2 - k_x^2 - k_z^2} \\ j\sqrt{k_x^2 + k_z^2 - k_L^2} \end{cases}, \quad k_{yT} = \begin{cases} \sqrt{k_T^2 - k_x^2 - k_z^2} \\ j\sqrt{k_x^2 + k_z^2 - k_T^2} \end{cases}, \quad (3.147b)$$

of which the second form is valid when $k_x^2 + k_z^2$ is larger than k_L^2 and k_T^2 respectively. Since there are no restrictions on the excitation wavenumbers

k_x and k_z , both forms of the radicals are possible. Also, those waves having opposite signs of the wavenumbers k_{yL} and k_{yT} would be solutions to the wave Eq. (3.122a) but since they represent waves propagating from infinity towards the surface, they are omitted in this case.

The three unknowns in Eq. (3.147a) can be determined from the conditions at the surface where the elastic stresses of the half-space must equal those externally applied, implying that

$$\begin{aligned}\sigma_y(x, 0, z) &= p_y(x, z), \\ \tau_{xy}(x, 0, z) &= p_x(x, z), \\ \tau_{yz}(x, 0, z) &= p_z(x, z).\end{aligned}\quad (3.147c)$$

It is hence necessary to express the elastic stresses in the velocities via the constitutive relations (3.137). After some manipulations, observing that differentiations with respect to time corresponds to multiplication by $j\omega$ in the phasor notation, one finds that

$$\begin{aligned}\hat{v}_{1L}(-k_T^2 + 2k_x^2 + 2k_z^2) + \hat{v}_{1T}2k_x^2 + \hat{v}_{3T}2k_xk_z &= \frac{\omega k_x}{G}\hat{p}_N, \\ \hat{v}_{1L}2k_{yL}k_{yT} - \hat{v}_{1T}(-k_T^2 + 2k_x^2 + k_z^2) - \hat{v}_{3T}k_xk_z &= \frac{\omega k_{yT}}{G}\hat{p}_{Tx}, \\ \hat{v}_{1L}2k_{yL}k_{yT}\frac{k_z}{k_x} - \hat{v}_{1T}k_xk_z - \hat{v}_{3T}(-k_T^2 + k_x^2 + 2k_z^2) &= \frac{\omega k_{yT}}{G}\hat{p}_{Tz}.\end{aligned}\quad (3.148a)$$

The determinant of this set of linear equations is

$$\text{Det} = -2k_{yT}^2 \left[(k_T^2 - 2k_x^2 - 2k_z^2)^2 + 4k_{yL}k_{yT}(k_x^2 + k_z^2) \right]. \quad (3.148b)$$

From Eqs. (3.148) the unknown amplitudes can be determined and thence the velocities in (3.147a). As an example, the velocity component perpendicular to the surface is obtained as

$$\begin{aligned}v_2(x, y, z) &= -\frac{\omega \hat{p}_N}{G \text{Det}} k_{yL} k_T^2 \\ &\times \left[(k_T^2 - 2k_x^2 - 2k_z^2)e^{jk_{yL}y} + 2(k_x^2 + k_z^2)e^{jk_{yT}y} \right] e^{-jk_x x} e^{-jk_z z},\end{aligned}\quad (3.148c)$$

in a case where the tangential excitation components are identically zero i.e., $p_x = p_z = 0$. From this expression, the ratio of normal stress to normal velocity component that is, the wave impedance, can be found to be given by

$$\hat{Z} = \frac{p(x, z)}{v_2(x, 0, z)} = \frac{G}{\omega} \frac{(k_T^2 - 2k_x^2 - 2k_z^2)^2 + 4k_{yL}k_{yT}(k_x^2 + k_z^2)}{k_{yL}k_T^2}, \quad (3.148d)$$

for the excitation considered. With the procedure employed here, the structure-borne sound field in a half-space, excited by plane waves, can be treated for arbitrary combinations of the excitation components \hat{p}_N , \hat{p}_{Tx} and \hat{p}_{Tz} . Also other kinds of problems can be handled, in which partly the stress and partly the velocities at the surface are prescribed. If, for instance, it is requested that \hat{p}_N takes on a specific value and simultaneously the shear deformation at the surface should vanish, then the resulting set of linear equations to be solved consists of the first row of Eq. (3.148a) together with

$$\begin{aligned} v_1(x, 0, z) &= (\hat{v}_{1L} + \hat{v}_{1T}) e^{-jk_x x} e^{-jk_z z} = 0 \Leftrightarrow \hat{v}_{1L} + \hat{v}_{1T} = 0, \\ v_3(x, 0, z) &= \left(\frac{k_z}{k_x} \hat{v}_{1L} + \hat{v}_{3T}\right) e^{-jk_x x} e^{-jk_z z} = 0 \Leftrightarrow k_z \hat{v}_{1L} + k_x \hat{v}_{1T} = 0. \end{aligned}$$

The above procedure is also applicable when the boundary conditions are given in terms of an impedance. The prerequisite is always, however, that plane waves are present such that the same exponentials for x and z are common for all expressions.

3.6.3. Surface Waves

From an examination of the impedance \hat{Z} can be gained an impression of the amplitudes resulting in the excited half-space. It is shown in Fig. 3.21 for a two-dimensional case i.e., where k_z is set to zero. From this Figure and the formulae in (3.148c, d), the following observations can be made:

- For $k_x^2 \ll k_L^2$ or $\lambda_x \gg \lambda_L$, the L - and T -waves propagates with the direction cosines $\cos\theta_L = k_{yL}/k_L$ and $\cos\theta_T = k_{yT}/k_T$ respectively. As a rough approximation $\hat{Z} \approx \rho c_L$.
- For $k_x^2 = k_L^2$ or $\lambda_x = \lambda_L$, $\hat{Z} = \infty$ irrespective of Poisson's ratio and the surface appears rigid.
- For $k_L^2 < k_x^2 < k_T^2$ i.e., $\lambda_L > \lambda_x > \lambda_T$, the T -waves propagates whereas only evanescent L -waves exist (near-fields). The wave impedance is complex.
- For $k_x^2 = k_T^2$ or $\lambda_x = \lambda_T$, the T -waves are grazing ($\theta_T = 90^\circ$) and the L -waves are evanescent.

For $k_x^2 > k_T^2$ or $\lambda_x < \lambda_T$, only evanescent waves occur and \hat{Z} is purely imaginary. In the vicinity of $k_x = k_T$, however, another feature arises owing to the vanishing impedance and this is briefly discussed in the following since it is of great practical importance in conjunction with seismic and ground-borne waves as well as in ultrasonic applications.

As for any set of linear equations, it has to be considered if the determinant to Eq. (3.148a) will become zero for real-valued k_x and k_z . From Eq.

(3.148b), it is seen that in the range of propagating waves i.e., where k_{yL} or k_{yT} or both are real, the determinant is non-zero since either both terms within brackets are positive or one is real and the other imaginary. When both k_{yL} and k_{yT} are imaginary, however, the situation is different and a zero-crossing is found for

$$(k_T^2 - 2k_R^2)^2 = 4k_R^2 \sqrt{k_R^2 - k_T^2} \sqrt{k_R^2 - k_L^2},$$

where $k_R^2 = k_x^2 + k_z^2$. Upon squaring both sides of the expression, it is seen that the condition for a vanishing of the determinant is given by the equation

$$16k_R^6(k_T^2 - k_L^2) + 8k_R^4(2k_L^2k_T^2 - 3k_T^4) + 8k_R^2k_T^6 - k_T^8 = 0. \quad (3.149)$$

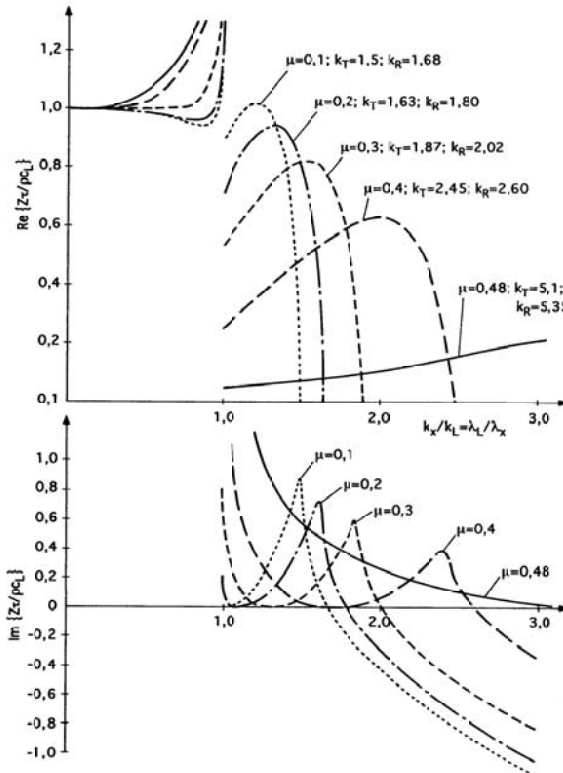


Fig. 3.21. Wave impedance of an elastic half-space at the stress-free surface

This third order equation in k_r^2 has a positive real root which is close to k_T^2 . It thus exists a realizable excitation for which the determinant vanishes and which leads to arbitrarily large amplitudes of a surface wave, namely $k_x^2 + k_z^2 = k_r^2$. After its discoverer, this wave is named the Rayleigh wave [3.2]. Its wavenumber k_r and its wave speed c_R is found by solving Eq. (3.149) and for some different values of Poisson's ratio the following relative wave speeds are obtained:

Table 3.3. Rayleigh wave speeds for some values of Poisson's ratio

μ	0	0.1	0.2	0.3	0.4	0.5
c_R/c_T	0.874	0.887	0.91	0.928	0.943	0.955

Approximately, the Rayleigh wave speed is given by

$$c_R \approx c_T \frac{(0.874 + 1.12\mu)}{1 + \mu} \quad (3.149a)$$

and it can be noted that it is independent of frequency and only slightly smaller than that of the transversal wave. The penetration depth of the Rayleigh wave is given by the wavenumber components in the y -direction $2\pi/\sqrt{k_r^2 - k_L^2}$ and $2\pi/\sqrt{k_r^2 - k_T^2}$. In Fig. 3.22 is illustrated the deformation pattern for a Rayleigh wave and it can be seen that the displacements become smaller with increasing depth.

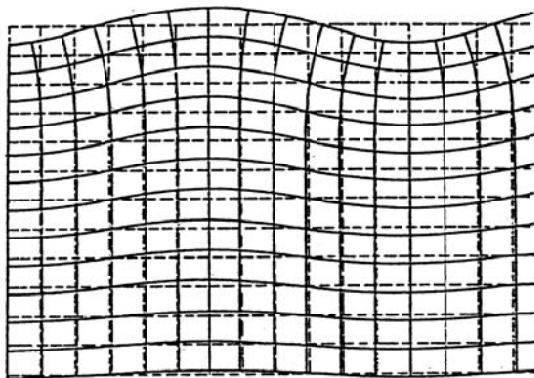


Fig. 3.22. Deformation pattern for a Rayleigh wave

3.7 Free Plate Waves

3.7.1 Boundary Conditions and Types of Solutions

In mechanics, one defines a “plate” as a homogeneous isotropic elastic continuum, bounded by two free parallel planes. The distance between these planes is designated by h and to facilitate the mathematical treatment, the origin of the co-ordinate system is set to coincide with the plane of symmetry between the two free planes. This means that the plate surfaces are situated at $y = \pm h/2$ respectively. For the treatment, moreover, it is assumed that only plane waves are present of angular frequency ω and that all processes are independent of the z co-ordinate. Therefore, the associated wave number component k_3 vanishes. This does not mean, however, that no motions can occur in the z -direction.

For shear waves it might be the prevailing situation. It is merely to understand that all quantities are equal in this direction and that the wave fronts are perpendicular to the cross-sectional plane at $z = 0$ for the plane waves considered here.

Since the plates of interest in this analysis can be arbitrarily big in x - and z -directions and are limited only in the y -direction, waves (and near-fields) can propagate in both positive and negative y -direction. This leads to the general assumption for the velocity components

$$\begin{aligned} v_1(x, y) &= (\hat{v}_L e^{jk_{yL}y} + \hat{v}_{T-} e^{jk_{yT}y} + \hat{v}_{L+} e^{-jk_{yL}y} \hat{v}_{T+} e^{-jk_{yT}y}) e^{-jk_x x}, \\ v_2(x, y) &= \left(-\frac{k_{yL}}{k_x} \hat{v}_{L-} e^{jk_{yL}y} + \frac{k_x}{k_{yT}} \hat{v}_{T-} e^{jk_{yT}y} + \frac{k_{yL}}{k_x} \hat{v}_{L+} e^{-jk_{yL}y} - \frac{k_x}{k_{yT}} \hat{v}_{T+} e^{-jk_{yT}y} \right) e^{-jk_x x}, \\ v_3(x, y) &= (\hat{v}_{3-} e^{jk_{yT}y} + \hat{v}_{3+} e^{-jk_{yT}y}) e^{-jk_x x}. \end{aligned} \quad (3.150)$$

The six unknown amplitudes of the velocity components are to be obtained from the boundary conditions. If it is assumed that the stresses are prescribed at the free surfaces then the boundary conditions are

$$\begin{aligned} \sigma(x, h/2, z) &= \hat{p}_+ e^{-jk_x x}, \tau_{xy}(x, h/2, z) = \hat{p}_{xy+} e^{-jk_x x}, \\ \tau_{yz}(x, h/2, z) &= \hat{p}_{yz+} e^{-jk_x x}, \\ \sigma(x, -h/2, z) &= \hat{p}_- e^{-jk_x x}, \tau_{xy}(x, -h/2, z) = \hat{p}_{xy-} e^{-jk_x x}, \\ \tau_{yz}(x, -h/2, z) &= \hat{p}_{yz-} e^{-jk_x x}, \end{aligned} \quad (3.151)$$

see Fig. 3.23. The analysis is similar also when other variables are prescribed. Whenever the x -dependence is in the simple form used, it always consists of solving a set of linear equations.

In Eq. (3.151) the boundary conditions all have the same x -dependence as of the assumed solution in (3.150). For other x -dependencies, the prescribed conditions must first be Fourier transformed to be brought in the form of the assumed solution, cf. Sect. 4.4.3. Intricate it would be, however, to take into account any sideways boundary conditions. In this case the boundaries are at infinity and hence not considered. With Eq. (3.150) substituted into the fundamental stress relations (3.119) and (3.120), observing the boundary conditions in (3.151), emerges

$$\begin{aligned} \frac{\omega \hat{p}_+ k_x}{G} &= -A \hat{v}_{L-} e^{jL} + 2k_x^2 \hat{v}_{T-} e^{jT} - A \hat{v}_{L+} e^{-jL} + 2k_x^2 \hat{v}_{T+} e^{-jT}, \\ \frac{\omega \hat{p}_- k_x}{G} &= -A \hat{v}_{L-} e^{-jL} + 2k_x^2 \hat{v}_{T-} e^{-jT} - A \hat{v}_{L+} e^{jL} + 2k_x^2 \hat{v}_{T+} e^{jT}, \\ \frac{\omega \hat{p}_{xy+} k_{yT}}{G} &= 2k_{yL} k_{yT} \hat{v}_{L-} e^{jL} + A \hat{v}_{T-} e^{jT} - 2k_{yL} k_{yT} \hat{v}_{L+} e^{-jL} - A \hat{v}_{T+} e^{-jT}, \\ \frac{\omega \hat{p}_{xy-} k_{yT}}{G} &= 2k_{yL} k_{yT} \hat{v}_{L-} e^{-jL} + A \hat{v}_{T-} e^{-jT} - 2k_{yL} k_{yT} \hat{v}_{L+} e^{jL} - A \hat{v}_{T+} e^{jT}, \\ \frac{\omega \hat{p}_{yz+}}{G} &= -k_x (\hat{v}_{3-} e^{jT} + \hat{v}_{3+} e^{-jT}), \\ \frac{\omega \hat{p}_{yz-}}{G} &= -k_x (\hat{v}_{3-} e^{-jT} + \hat{v}_{3+} e^{jT}). \end{aligned} \quad (3.152)$$

Herein are introduced the abbreviations

$$k_{yL} h/2 = L \quad , \quad k_{yT} h/2 = T \quad \text{and} \quad A = k_T^2 - 2k_x^2$$

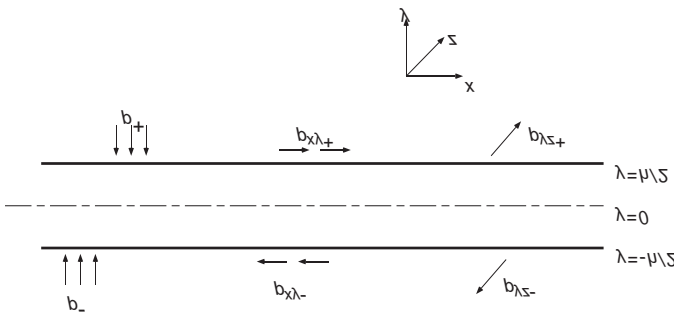


Fig. 3.23. Normal and tangential stresses at the plate surfaces

3.7.2 Waves with Displacements only Parallel to the Surface

As in Sect. 3.6, the conditions are particularly simple when the displacements are parallel to the surface i.e., there exists only the component v_3 . Upon solving the two latter equations in (3.152) and substituting into the last of (3.150) is obtained

$$v_3(x, y) = \frac{-1}{\sin k_{yT} h} [\hat{p}_{xz+} \sin k_{yT} (y + h/2) - \hat{p}_{xz-} \sin k_{yT} (y - h/2)] \frac{\omega}{Gk_x}. \quad (3.153a)$$

So-called free plate waves exist when a finite motion is possible also in the absence of excitation provided a loss-free medium. Evidently, the conditions are

$$\sin k_{yT} h = 0,$$

meaning that

$$k_{yT} h = \sqrt{k_T^2 - k_x^2} h = k_T h \cos \vartheta_T = m\pi, \quad (3.153b)$$

where $m = 0, 2, 4\dots$ establish a cross-sectionally symmetric field while $m = 1, 3, 5\dots$ an anti-symmetric.

The case $m = 0$ implies a uniform velocity across the complete plate thickness and thus also uniform shear stress. This corresponds to a slice of thickness h from a plane transversal wave. Also in view of the given boundary conditions, such a slice is admissible since the shear stresses present, τ_{xz} and τ_{zx} , only arise on surfaces $x = \text{const.}$ and $z = \text{const.}$ but not on surfaces $y = \text{const.}$.

With the exception of the case $m = 0$, these types of plate waves can be considered as superpositions of two crossing transverse waves impinging on the surfaces at an angle ϑ_T . This gives the trace velocity for both

$$c_x = \frac{c_T}{\sin \vartheta_T} = \frac{c_T}{\sqrt{1 - (m\lambda_T / 2h)^2}}, \quad (3.153c)$$

a relation which also encompasses the $m = 0$ case.

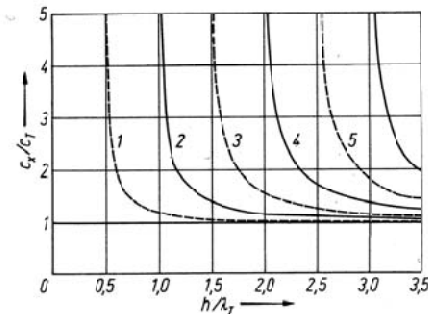


Fig. 3.24. Dispersion diagram for free transversal waves with displacements parallel to the surface (----) symmetric and (---) anti-symmetric modes

Figure 3.24 shows the corresponding dispersion diagram. The fact that the trace velocity in the x -direction c_x can exceed the phase speed c_T is not a contradiction of physics. The energy of a plate wave associated with pure shear deformations propagates with the group velocity as was discussed at the end of Sect. 3.3. In this case it means that

$$c_{gx} = \frac{d\omega}{dk_x} = \left(\frac{dk_x}{d\omega} \right)^{-1} \quad (3.154a)$$

Following from (3.153c), $k_x = [k_T^2 - (m\pi/h)]^{1/2}$ whereby $k_T = \omega/c_T$ such that

$$c_{gx} = \frac{c_T k_x}{k_T} = c_T \sqrt{1 - (m\lambda_T / 2h)^2} = c_T \sin \vartheta_T \leq c_T. \quad (3.154b)$$

This enables a simple geometrical interpretation of the group speed in the x -direction, given by Schoch [3.3] as the speed of an energy package, which criss-crosses back and forth across the thickness of the plate thickness under the incidence angle ϑ_T like a billiard ball bouncing obliquely between the walls. Such an illustrative interpretation, however, should not mislead thoughts that the rigorous wave theoretical treatise merely confirms observations made by elementary geometric ray tracing. Ray tracing is not limited to a particular angle whereas plate waves at a given frequency always propagate in discrete directions. Furthermore, the pair of crossing waves form specific sinusoidal or cosinusoidal distributions over the cross-section, which also must match those of an external excitation if a single specific plate wave should be excited. This cannot be obtained from ray tracing. On the contrary, ray tracing is only valid for the description of wave propagation when the wavelength is small in comparison with

all geometrical dimensions involved i.e., the ray width and plate thickness h in this case. For large h/λ_T , trains of plane transversal waves of finite width propagating at arbitrary angles, may be described by sets of superimposed plate waves, as discussed for infinite continua in Sect. 3.2.1.

3.7.3 Waves with Displacements Perpendicular to the Surface

Of much greater practical importance than the previously considered case is when displacement components occur which are perpendicular to the plate surfaces. This is so since such components can be excited by dynamic processes in the ambient medium as well as excite them also when that medium cannot support shear stresses.

The general treatise of plate waves which exhibit displacements in the xy -plane is complicated by the fact that two conditions at each boundary have to be satisfied by two wave types. As was discussed earlier, the two types, moreover, can appear as surface or volume waves [3.4]. For the dispersion diagram, which shall be developed, therefore, three ranges must be distinguished, giving the following table, cf. Sect. 3.6.3

Table 3.4. Three regions for plate waves

	Irrational Part	Divergence-Free Part
$c_x > c_L$	Longitudinal volume waves	Transverse volume waves
$k_x^2 < k_L^2$		
$c_L > c_x > c_T$	Surface waves	Transverse volume waves
$k_L^2 < k_x^2 < k_T^2$		
$c_T > c_x$	Surface waves	Surface waves
$k_x^2 > k_T^2$		

The dispersion problem consists of determining $\hat{v}_{L+}, \hat{v}_{L-}, \hat{v}_{T+}, \hat{v}_{T-}$ from the first four equations in (3.152). In this pursuit, it is convenient to replace the exponentials with the associated trigonometric functions. Then, the first equation is added to and subtracted from the second respectively, the third similarly added to and subtracted from the fourth. In this way is obtained

$$\begin{aligned}
 -A(\hat{v}_{L-} + \hat{v}_{L+})\cos L + 2k_x^2(\hat{v}_{T-} + \hat{v}_{T+})\cos T &= \frac{\omega k_x}{2G}(\hat{p}_+ + \hat{p}_-), \\
 2k_{yT}k_{yL}(\hat{v}_{L-} + \hat{v}_{L+})\sin L + A(\hat{v}_{T-} + \hat{v}_{T+})\sin T &= \frac{\omega k_{yT}}{2jG}(\hat{p}_{xy+} + \hat{p}_{xy-}), \\
 -A(\hat{v}_{L-} - \hat{v}_{L+})\sin L + 2k_x^2(\hat{v}_{T-} - \hat{v}_{T+})\sin T &= \frac{\omega k_x}{2jG}(\hat{p}_+ - \hat{p}_-), \\
 2k_{yT}k_{yL}(\hat{v}_{L-} - \hat{v}_{L+})\cos L + A(\hat{v}_{T-} - \hat{v}_{T+})\cos T &= \frac{\omega k_{yT}}{2jG}(\hat{p}_{xy+} - \hat{p}_{xy-}).
 \end{aligned} \tag{3.155}$$

Hereby, the equations are brought into two independent pairs, which readily can be solved. In this context the study is confined to the free plate waves, which means that those wavenumbers are sought leading to non-trivial solutions. Mathematically, this is again found from the vanishing determinants to the two pairs of equation

$$\begin{aligned} \text{Det } I &= \sin L \sin T \left[-\left(k_T^2 - 2k_x^2 \right)^2 \cot L - 4k_x^2 k_{yL} k_{yT} \cot T \right], \\ \text{Det } II &= \cos L \cos T \left[-\left(k_T^2 - 2k_x^2 \right)^2 \tan L - 4k_x^2 k_{yL} k_{yT} \tan T \right]. \end{aligned} \quad (3.156a, b)$$

In the expressions above, $A = k_T^2 - 2k_x^2$ is back substituted but the abbreviations $L = k_{yL} h/2$ and $T = k_{yT} h/2$ are retained.

Equating (3.156a, b) to zero furnishes the wavenumbers of the free plate waves and

$$\frac{\tan T}{\tan L} = -\frac{4k_x^2 k_{yL} k_{yT}}{\left(k_T^2 - 2k_x^2 \right)^2}, \quad (3.156c)$$

$$\frac{\tan L}{\tan T} = -\frac{4k_x^2 k_{yL} k_{yT}}{\left(k_T^2 - 2k_x^2 \right)^2}. \quad (3.156d)$$

The cosine and sine factors in Eqs. (3.156a, b) results in no additional roots of the determinant. Equations (3.156c, d) therefore establish all the roots and it is sufficient that one of the two equations vanishes for a free plate wave to exist and propagate. If, for example, Eq. (3.156c) vanishes, then the two first equations in (3.155) have non-trivial solutions for a vanishing right-hand-side. At the same time, trivial solutions can be chosen for the latter two such that $\hat{v}_{L-} = \hat{v}_{L+}$ and $\hat{v}_{T-} = \hat{v}_{T+}$ result. This means that for those free plate waves governed by Eq. (3.156c), the motion is given in the form

$$\begin{aligned} v_1(x, y) &= 2 \left[\hat{v}_L \cos k_{yL} y + \hat{v}_T \cos k_{yT} y \right] e^{-jk_x x}, \\ v_2(x, y) &= 2j \left[\frac{k_{yL}}{k_x} \hat{v}_L \sin k_{yL} y + \frac{k_x}{k_{yT}} \hat{v}_T \sin k_{yT} y \right] e^{-jk_x x}. \end{aligned} \quad (3.157)$$

These waves represents the symmetric modes.

If, in contrast, (3.156d) vanishes, the same reasoning applies but with cosine and sine interchanged in (3.157). In such a case the anti-symmetric modes are promoted.

The dispersion equation, yielding the wavenumbers of the free plate waves could have been developed also employing the wave train closure

principle. For this, forwards propagating and reflected waves are assumed as in Sect. 3.4.1 and the wavenumber and angles respectively sought, for which the phase change due to reflection and propagation is multiples of 2π . This approach is here not chosen as it is interest also to encompass the case of forced vibration.

To further evaluate Eqs. (3.156c, d) usually numerical methods are employed. An example, taken from [3.5] is presented in Fig. 3.25.

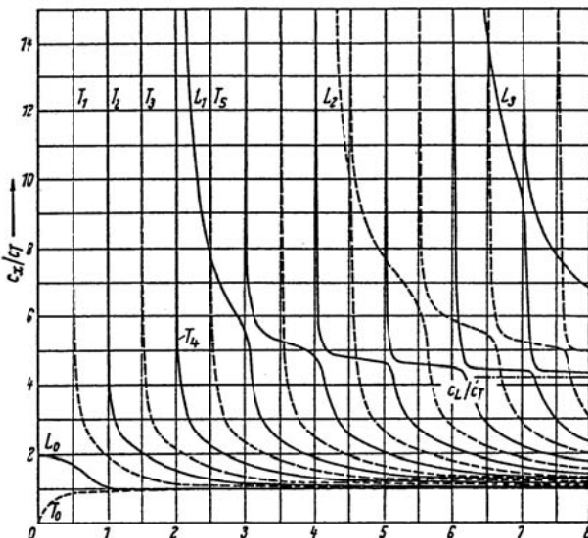


Fig. 3.25. Dispersion diagram for free plate waves comprising displacements perpendicular to the surface, after [3.5]. (—) symmetric and (---) anti-symmetric modes

For specific values of the trace wavenumber in the x -direction $k_x = \omega/c_x$ it is easy to find the corresponding values of $k_T = \omega/c_T$. For $k_x = 0$, for example, are $k_{yT} = k_T$ and $k_{yL} = k_L$. Thereby vanishes the right-hand side of Eq. (3.156c) and hence, the governing equations for the free wavenumbers read $\tan T = 0$ and $\tan L = \infty$ for the symmetric modes whereas $\tan L = 0$ and $\tan T = \infty$ for the anti-symmetric. The frequencies corresponding to this trace wavenumber i.e., for a trace speed of $c_x = \infty$, are

$$\begin{aligned}
 \frac{k_T h}{2} &= \pi v \Rightarrow \omega = \frac{2\pi c_T}{h} v, \\
 \frac{k_L h}{2} &= \frac{\pi}{2}(2v+1) \Rightarrow \omega = \frac{\pi c_L}{h}(2v+1), \\
 \frac{k_L h}{2} &= \pi v \Rightarrow \omega = \frac{2\pi c_L}{h} v, \\
 \frac{k_T h}{2} &= \frac{\pi}{2}(2v+1) \Rightarrow \omega = \frac{\pi c_T}{h}(2v+1)
 \end{aligned} \tag{3.158a}$$

A closed form approximation is also possible for thin plates and low frequencies. With the tangential functions series expanded to first order,

$$\frac{k_{yT} h}{k_{yL} h} = -\frac{4k_x^2 k_{yT} k_{yL}}{(k_T^2 - 2k_x^2)^2}$$

and

$$(k_T^2 - 2k_x^2)^2 = -4k_x^2 (k_L^2 - k_x^2)$$

respectively. It follows that

$$k_x^2 = \frac{k_T^4}{4(k_T^2 - k_L^2)} \tag{3.158b}$$

leading to

$$\frac{c_x}{c_T} = \frac{k_T}{k_x} = 2\sqrt{1-h^2} = \sqrt{2/(1-\mu)} ; k_T h \ll 1.$$

It is easy to convince oneself that this means that $c_L > c_x > c_T$ and that $c_x = c_{LI}$, see Eq. (3.34). For thin plates, the symmetric mode is hence identical to the tensional wave. It consists of a rotational free pair of surface wave because of $k_x > k_L$ or $c_x < c_L$ and of two crossing transversal waves since $k_x < k_T$ or $c_x > c_T$.

If also the cubic terms are taken into account in the series expansion of the tangential functions then

$$k_x^2 = \frac{k_T^4}{4(k_T^2 - k_L^2)} \left[1 + \frac{1}{3} \left(k_T \frac{h}{2} \right)^2 \frac{1-2n^2}{4(1-n^2)} \right]$$

or

$$c_x = c_{LI} \left[1 - \frac{1}{6} \left(\frac{k_L h}{6} \right)^2 \left(\frac{\mu}{1-\mu} \right)^2 \right] \quad (3.158c)$$

respectively. With a typical Poisson's ratio of $\mu = 0.3$ it means that a phase speed deviation of around 3% of that of c_{LI} first then arises when $\lambda_{LI} < 3h$.

To find an approximative solution for the anti-symmetric mode (3.156d) at low frequencies, it is necessary to expand the tangential function to third order already for the simplest approximation i.e.,

$$\frac{\tan L}{\tan T} \approx \frac{k_{yL} h / 2}{k_{yT} h / 2} \frac{1 + \frac{1}{3} \left(\frac{k_{yL} h}{2} \right)}{1 + \frac{1}{3} \left(\frac{k_{yT} h}{2} \right)} = - \frac{4 k_x^2 k_{yL} k_{yT}}{(k_T^2 - 2 k_x^2)^2} \quad (3.159a)$$

In this case it follows that,

$$k_T^4 + \frac{h^2}{12} \left[k_L^2 k_T^4 + k_x^2 (3k_T^4 - 4k_L^2 k_T^2) + 4k_x^4 (k_L^2 - k_T^2) \right] = 0$$

For the approximation of interest where $k_x^2 \gg k_T^2$, it sufficient to retain the highest order of k_x in the bracket, which yields

$$k_x^4 = 3 \frac{k_T^4}{h^2} \frac{1}{k_T^2 - k_L^2} = 3 \frac{k_T^4}{k_T^2 h^2} \frac{1}{1 - n^2}. \quad (3.159b)$$

By using the relations (3.34), (3.48), (3.75), (3.83) and (3.138c), this means that the trace speed approaches

$$c_x^2 = \frac{1}{6} \frac{\omega^2 h^2 G}{\rho (1-\mu)} = \frac{1}{12} \frac{\omega^2 h^2 E}{\rho (1-\mu^2)} = \frac{B' \omega^2}{m''} = c_{LI} \frac{\omega^2 h^2}{12}; k_T h \ll 1 \quad (3.159c)$$

Herein, B' is the bending stiffness of the plate and m'' the mass per unit area.

From (3.159) is readily seen that for thin plates are $k_x > k_T > k_L$ such that $c_x > c_T > c_L$. Therefore, the T - and L -waves can only appear as near-fields. These combine in such a way that an anti-symmetric motion results having the form and propagation speed of the flexural wave. In this case also, the approximation is limited to the range in which $k_x^2 > k_T^2$ or $c_x < c_T$. An error analysis will be presented in Sect. 3.8.2.

The flexural wave and the symmetric longitudinal wave are clearly recognized in Fig. 3.25 where they are denoted by T_0 and L_0 respectively. Not equally clear is that the T_0 branch asymptotically tends to that of the Rayleigh wave and not to that of the slightly higher shear wave.

In this high frequency range, the dispersion diagram more and more resembles Fig. 3.24 and one is almost inclined to assume that the type T -waves approach $c_x = c_T$ whilst the type L -waves $c_x = c_L$. The latter is however not the case. Instead, is revealed by numerical calculations that all curves for the high orders step-wise approach $c_x = c_L$ whereby one curve succeeds the other. These steps not only approach the asymptote $c_x = c_L$ at $k_7 h \rightarrow \infty$ but far earlier. The approach follows approximately the relation

$$c_x = \frac{c_L}{\sin \vartheta_L}, \quad (3.160)$$

which is analogous to that in Eq. (3.153c) and which is a necessary condition for the formation of obliquely propagating waves as discussed in that context.

The first dispersion curves of this kind i.e., T_1 , L_1 and T_2 , obtained by Götz [3.6] from measurements ($n = c_T/c_L = 0.53$) and point-wise graphically collated, did not clearly reveal such a tendency. It became evident, however, from the curves reaching T_7 and L_3 , computed a couple of years later by Firestone [3.7] for steel ($n = 0.49$). Most clearly, though, the tendency is observed in the results of Naake and Tamm, here reproduced in Fig. 3.25. This is not only because the dispersion curves are presented up to T_{15} but also because they are calculated for the very small value of $n = 0.24$ i.e., $\mu = 0.47$.

In contrast to Fig. 3.24, the curves in Fig. 3.25 clearly show that the previously denoted T - and L -type waves, in general do not consist of pure transversal or longitudinal wave fields but are rather composed of both.

The fact that the flexural and Rayleigh waves do not reach the $c_x = c_T$ limit is not a contradiction. It simply becomes surface waves of the rotational free part of the volume waves.

Tamm and Weiss [3.8], moreover, have calculated the group speeds for the plate waves in Fig. 3.25, obtained from the dispersion diagram employing Eq. (3.154a). The results are presented in Fig. 3.26, for which the following remarks apply. No group speed exceeds the phase speed of the longitudinal wave c_L . This wave speed appears only as the common asymptote to the successive steps of the adjacent curves. The envelope to these steps approximately obeys

$$c_x = c_L \sin \vartheta_L. \quad (3.161)$$

At very high frequencies accordingly, obliquely propagating longitudinal rays may be constructed from plate waves. The same thing is true for the curves, which approach from below the genuine asymptote represented by the transverse wave speed c_T , even if it is temporarily exceeded. The

fact that the quasi-longitudinal and bending waves ends at the somewhat lower Rayleigh wave speed which exhibits no dispersion, is shadowed in the figure by the convergence of the many curve branches.

In practice, most structure-borne sound problems only concerns the limiting cases of quasi-longitudinal and bending waves when h/λ_T is small.

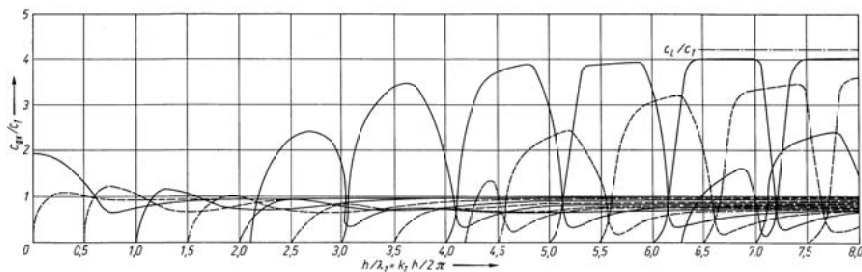


Fig. 3.26. Dispersion diagram for the group velocities corresponding to Fig. 3.25 [2.10]

3.7.4 Equations of Motion for Thin Plates from the General Field Equations

3.7.4.1 Quasi-Longitudinal and Shear Waves in Uniform, Isotropic Plates

In the preceding section were determined the dispersion curves for arbitrary thick strata of homogeneous, isotropic media from the field equation. In the following, these equations are employed for the derivation of the equations of motion of thin plates i.e., plates of thickness small in comparison with the wavelength cf., [3.9]. The required equations are the constitutive and the dynamic force equilibrium relations i.e., (3.119), (3.120) and (3.121) respectively. For a prescribed harmonic motion of angular frequency ω , the basic equations read

$$\begin{aligned} \frac{\sigma_x}{2G} &= (\alpha + 1) \frac{\partial \xi}{\partial x} + \alpha \eta' + \alpha \frac{\partial \zeta}{\partial z}, \\ \frac{\sigma_y}{2G} &= \alpha \frac{\partial \xi}{\partial x} + (\alpha + 1) \eta' + \alpha \frac{\partial \zeta}{\partial z}, \\ \frac{\sigma_z}{2G} &= \alpha \frac{\partial \xi}{\partial x} + \alpha \eta' + (\alpha + 1) \frac{\partial \zeta}{\partial z} \\ \frac{\tau_{xy}}{G} &= \xi' + \frac{\partial \eta}{\partial x}, \quad \frac{\tau_{yz}}{G} = \zeta' + \frac{\partial \eta}{\partial z}, \quad \frac{\tau_{xz}}{G} = \frac{\partial \xi}{\partial z} + \frac{\partial \zeta}{\partial x} \end{aligned} \quad (3.162a)$$

and

$$\begin{aligned}-\omega^2 \rho \xi &= \frac{\partial \sigma_x}{\partial x} + \tau_{xy}' + \frac{\partial \tau_{xz}}{\partial z}, \\ -\omega^2 \rho \eta &= \frac{\partial \tau_{xy}}{\partial x} + \sigma_y' + \frac{\partial \tau_{yz}}{\partial z}, \\ -\omega^2 \rho \zeta &= \frac{\partial \tau_{xz}}{\partial x} + \tau_{xy}' + \frac{\partial \sigma_z}{\partial z}.\end{aligned}\quad (3.162b)$$

Herein is introduced

$$\frac{\mu}{1-2\mu} = \alpha \quad (3.162c)$$

as an abbreviation. With the phasor notation, the time differentiation is replaced by a multiplication by $j\omega$. Differentiation with respect to y , moreover, is abbreviated by a ‘prime’ owing to its special role and frequency in the subsequent development.

Upon employing the above relations to the case of a flat plate of thickness h as depicted in Fig. 3.23, the stresses at the surfaces $y = \pm h/2$ can be expanded in Taylor series such that

$$\begin{aligned}\sigma_y(h/2) &= \sigma_y(0) + \frac{h}{2} \sigma_y'(0) + \frac{h^2}{8} \sigma_y''(0) + \frac{h^3}{48} \sigma_y'''(0) + \dots = p_+, \\ \sigma_y(-h/2) &= \sigma_y(0) - \frac{h}{2} \sigma_y'(0) + \frac{h^2}{8} \sigma_y''(0) - \frac{h^3}{48} \sigma_y'''(0) + \dots = p_-.\end{aligned}\quad (3.163a)$$

Herein, p_+ and p_- denote the applied normal stress. By means of addition and subtraction of the two lines in (3.163a) one obtains

$$\sigma_y(0) = -\frac{h^2}{8} \sigma_y''(0) + \frac{p_+ + p_-}{2}, \quad \sigma_y'(0) = -\frac{h^2}{24} \sigma_y'''(0) + \frac{p_+ - p_-}{h} \quad (3.163b)$$

In the same manner, the shear stresses acting at the surfaces $y = \pm h/2$ yield

$$\begin{aligned}\tau_{yx}(0) &= -\frac{h^2}{8} \tau_{xy}'' + \frac{p_{yx+} + p_{yx-}}{2}, \quad \tau_{yx}'(0) = -\frac{h^2}{24} \tau_{yx}'''(0) + \frac{p_{yx+} - p_{yx-}}{h} \\ \tau_{yz}(0) &= -\frac{h^2}{8} \tau_{yz}'' + \frac{p_{yz+} + p_{yz-}}{2}, \quad \tau_{yz}'(0) = -\frac{h^2}{24} \tau_{yz}'''(0) + \frac{p_{yz+} - p_{yz-}}{h}\end{aligned}\quad (3.163c)$$

With the abbreviations for the various stresses in Fig. 3.23,

$$\begin{aligned}p_+ + p_- &= p_D, \quad p_+ - p_- = p_B, \quad p_{yx+} + p_{yx-} = p_1, \\ p_{yx+} - p_{yx-} &= p_2, \quad p_{yz+} + p_{yz-} = p_3, \quad p_{yz+} - p_{yz-} = p_4,\end{aligned}\quad (3.164)$$

introduced in (3.163a) to (3.163c) and the Eq. (3.162b) substituted, is obtained

$$\begin{aligned}-\omega^2 \rho \xi &= \frac{\partial \sigma_x}{\partial x} + \frac{\partial \tau_{xz}}{\partial z} - \frac{h^2}{24} \tau_{xy}''' + \frac{p_2}{h}, \\-\omega^2 \rho \eta &= -\frac{h^2}{8} \frac{\partial \tau_{xy}''}{\partial x} - \frac{h^2}{24} \sigma_y''' - \frac{h^2}{8} \frac{\partial \tau_{yz}}{\partial z} + \frac{1}{2} \frac{\partial p_1}{\partial x} + \frac{p_B}{h} + \frac{1}{2} \frac{\partial p_3}{\partial z}, \\-\omega^2 \rho \zeta &= \frac{\partial \tau_{xz}}{\partial x} + \frac{\partial \sigma_z}{\partial z} - \frac{h^2}{24} \tau_{yz}''' + \frac{p_4}{h}.\end{aligned}\quad (3.165)$$

In order to establish a set of equations of motion from (3.165), it is suitable to rewrite the normal and shear stresses such that all differentials with respect to y are eliminated at the final stage. Hereby, it should be observed that in the plane $y = 0$, there can only occur displacements and stresses as well as their x and z derivatives. For the sake of convenience, the argument (0) appearing in Eqs. (3.163b, c) is omitted in the following.

With the relation (3.163b) introduced in the second equation of (3.162a) it follows that

$$-\frac{h^2}{16G} \sigma_y'' + \frac{p_D}{4G} = \alpha \frac{\partial \xi}{\partial x} + (\alpha + 1) \eta' + \alpha \frac{\partial \zeta}{\partial z},$$

which means that as h approaches zero

$$\begin{aligned}\eta' &= \frac{-\alpha}{\alpha + 1} \left(\frac{\partial \xi}{\partial x} + \frac{\partial \zeta}{\partial z} \right) + \frac{p_D}{4G(\alpha + 1)} \\&= \frac{-\mu}{1 - \mu} \left(\frac{\partial \xi}{\partial x} + \frac{\partial \zeta}{\partial z} \right) + \frac{1 - 2\mu}{8G} \frac{1 + \mu}{1 + \mu} p_D.\end{aligned}\quad (3.166)$$

Thereby, η' can be eliminated from the rest of the equations in (3.162a) and after some manipulation it is found that

$$\begin{aligned}\frac{\sigma_x}{G} &= \frac{2}{1 - \mu} \left(\frac{\partial \xi}{\partial x} + \mu \frac{\partial \zeta}{\partial z} \right) + \frac{\mu}{1 - \mu} \frac{p_D}{2G}, \\ \frac{\sigma_z}{G} &= \frac{2}{1 - \mu} \left(\mu \frac{\partial \xi}{\partial x} + \frac{\partial \zeta}{\partial z} \right) + \frac{\mu}{1 - \mu} \frac{p_D}{2G}, \\ \frac{\tau_{xz}}{G} &= \left(\frac{\partial \xi}{\partial z} + \frac{\partial \zeta}{\partial x} \right).\end{aligned}\quad (3.167)$$

Upon combining Eqs. (3.165) and (3.167), the simplest form of equation of motion for a flat plate emerges when all terms of order h^2 or higher are omitted. This means that

$$\begin{aligned}\frac{-\omega^2 \rho}{G} \xi &= \frac{2}{1-\mu} \frac{\partial^2 \xi}{\partial x^2} + \frac{\partial^2 \xi}{\partial z^2} + \frac{1+\mu}{1-\mu} \frac{\partial^2 \zeta}{\partial x \partial z} + \frac{\mu}{1-\mu} \frac{1}{2G} \frac{\partial p_D}{\partial x} + \frac{p_2}{Gh}, \\ \frac{-\omega^2 \rho}{G} \zeta &= \frac{1+\mu}{1-\mu} \frac{\partial^2 \xi}{\partial x \partial z} + \frac{2}{1-\mu} \frac{\partial^2 \zeta}{\partial z^2} + \frac{\partial^2 \zeta}{\partial x^2} + \frac{\mu}{1-\mu} \frac{1}{2G} \frac{\partial p_D}{\partial z} + \frac{p_4}{Gh}.\end{aligned}\quad (3.168a)$$

A rearrangement of these expressions yields

$$\begin{aligned}\left(\frac{2}{1-\mu} \frac{\partial^2}{\partial x^2} + \frac{\partial^2}{\partial z^2} + k_T^2 \right) \xi + \frac{1+\mu}{1-\mu} \frac{\partial^2 \zeta}{\partial x \partial z} &= -\frac{1}{G} \left[\frac{\mu}{2(1-\mu)} \frac{\partial p_D}{\partial x} + \frac{p_2}{h} \right], \\ \frac{1+\mu}{1-\mu} \frac{\partial^2 \xi}{\partial x \partial z} + \left(\frac{2}{1-\mu} \frac{\partial^2}{\partial z^2} + \frac{\partial^2}{\partial x^2} + k_T^2 \right) \zeta &= -\frac{1}{G} \left[\frac{\mu}{2(1-\mu)} \frac{\partial p_D}{\partial z} + \frac{p_4}{h} \right].\end{aligned}\quad (3.168b)$$

Herein, k_T is the shear or transversal wavenumber cf., Sect. 3.2.1. The fact that shear and extensional waves combine can be seen by, for example, letting $\partial/\partial z = 0$, which means that all quantities are constant in the z -direction. This leads to

$$\begin{aligned}\left(\frac{2}{1-\mu} \frac{\partial^2}{\partial x^2} + k_T^2 \right) \xi &= -\frac{1}{G} \left[\frac{\mu}{2(1-\mu)} \frac{\partial p_D}{\partial x} + \frac{p_2}{h} \right], \\ \left(\frac{\partial^2}{\partial x^2} + k_T^2 \right) \zeta &= -\frac{p_4}{Gh}.\end{aligned}\quad (3.169)$$

The second equation is seen to be the shear wave equation with the excitation p_4/Gh . Owing to

$$k_T^2 \frac{1-\mu}{2} = \omega^2 \rho \frac{1-\mu}{2G} = \omega^2 \rho \frac{1-\mu^2}{2G(1+\mu)} = \frac{\omega^2 \rho}{E} (1-\mu^2) = \frac{\omega^2}{c_{LI}^2} = k_{LI}^2,\quad (3.170a)$$

see Eqs. (3.48) and (3.34), the first equation in (3.169) turns into

$$\left(\frac{\partial^2}{\partial x^2} + k_{LI}^2 \right) \xi = -\frac{\mu(1+\mu)}{2E} \frac{\partial p_D}{\partial x} - \frac{1-\mu^2}{E} \frac{p_2}{Gh},\quad (3.170b)$$

whereby k_{LI} is the wavenumber of the quasi longitudinal or extensional wave in a thin plate. Thus, the one-dimensional extensional wave equation is obtained. The first part of the excitation depends on the normal stress and comes into play through cross-sectional contraction whilst the second is associated with forces parallel with the plane of the plate cf., Eqs. (3.39) and (3.40) as well as Fig. 3.23. That also the two wave types combine in the two-dimensional case is readily demonstrated by seeking those solutions which represent free plane waves i.e., the excitation is removed. By introducing

$$\xi = \hat{\xi}_0 e^{-jk_x x} e^{-jk_z z}, \zeta = \hat{\zeta}_0 e^{-jk_x x} e^{-jk_z z}, \quad (3.171)$$

in Eq. (3.168b), it is found that

$$\begin{aligned} \left(\frac{2}{1-\mu} k_x^2 + k_z^2 - k_T^2 \right) \hat{\xi}_0 + \frac{1+\mu}{1-\mu} k_x k_z \hat{\zeta}_0 &= 0, \\ \frac{1+\mu}{1-\mu} k_x k_z \hat{\xi}_0 + \left(\frac{2}{1-\mu} k_z^2 + k_x^2 - k_T^2 \right) \hat{\zeta}_0 &= 0. \end{aligned} \quad (3.172)$$

These two equations have non-trivial solutions only when the determinant of the coefficients vanishes. Rewriting $2/(1 - \mu)$ as $1 + (1 + \mu)/(1 - \mu)$, the characteristic equation in k_x and k_z becomes

$$\left(k_x^2 + k_z^2 - k_T^2 + \frac{1+\mu}{1-\mu} k_x^2 \right) \left(k_x^2 + k_z^2 - k_T^2 + \frac{1+\mu}{1-\mu} k_z^2 \right) - \left(\frac{1+\mu}{1-\mu} k_x k_z \right)^2 = 0. \quad (3.173)$$

This expression is of the form $(a + b)(a + c) - bc = a(a + b + c) = 0$. Hence, the pair of equations in (3.172) has non-trivial solutions if either $a = 0$ or $(a + b + c) = 0$ i.e.,

$$\begin{aligned} k_x^2 + k_z^2 &= k_T^2, \\ k_x^2 + k_z^2 + \frac{1+\mu}{1-\mu} (k_x^2 + k_z^2) &= \frac{2}{1-\mu} (k_x^2 + k_z^2) = k_T^2 \Rightarrow k_x^2 + k_z^2 = k_{LI}^2, \end{aligned} \quad (3.174a)$$

respectively. The first of these solutions represents shear waves whilst the second extensional waves. From the outcome of the analysis so far, it can be concluded that the motions of the neutral layer of a thin plate are described by Eq. (3.168b). Also is clarified that the (3.167) establishes the relation between the forces $F_x = -\sigma_x h$ in the x -direction see Eq. (3.35) and $F_z = -\sigma_z h$ in the z -direction. This relation turns into (3.38) as expected.

The so called plate waves consist of shear and extensional waves having free wavenumber and the phase speeds given by (3.174a, b). When also the motion at the plate surfaces in the y -direction, resulting from the cross-sectional contraction, is of interest, Eq. (3.166) gives

$$\eta(\pm h/2) = -\frac{\pm\mu h}{2(1-\mu)} \left(\frac{\partial \xi}{\partial x} + \frac{\partial \zeta}{\partial z} \right) + \frac{h}{8G} \frac{1-2\mu}{1+\mu} p_D. \quad (3.175)$$

3.7.4.2 Bending Waves in Flat Isotropic Plates

To analyse the bending motion of a plate, it is necessary to determine the displacement η of its neutral layer. As indicated by the middle expression

in Eq. (3.165), the derivatives of the normal and tangential stresses are required

$$-\omega^2 \rho h = -\frac{h^2}{8} \left[\frac{\partial \tau_{xy}''}{\partial x} + \frac{1}{3} \sigma_3''' + \frac{\partial \tau_{yz}''}{\partial z} \right] + \frac{p_B}{h}. \quad (3.176)$$

For reasons of brevity it is here assumed that the normal stresses at the upper and lower surfaces are equal in magnitude and that all shearing stresses p_1, p_2, p_3 and p_4 vanishes.

Fortunately, no principal difficulties arise in the determination of τ_{yx}'' etc. since these quantities are multiplied by the factor h^2 and accordingly the stresses need be determined only up to the order h^0 . In the following development, one may furthermore set the plate thickness h equal to zero to retain the precision desired i.e., Eq. (3.166) to (3.168) can be used to determine τ_{yx}'' . In principle, it is then possible to use the results recurrently to obtain approximations up to order h^4 . The drawback, however, is that the expressions become rather lengthy and intractable.

The first derivative with respect to the y -direction of the stresses sought immediately follows from (3.162b)

$$\begin{aligned} \tau_{xy}' &= -\frac{\partial \sigma_x}{\partial x} - \frac{\partial \tau_{xz}}{\partial z} - \omega^2 \rho \xi, \\ \sigma_y' &= -\frac{\partial \tau_{xy}}{\partial x} - \frac{\partial \tau_{yz}}{\partial z} - \omega^2 \rho \eta, \\ \tau_{yz}' &= -\frac{\partial \tau_{xz}}{\partial x} - \frac{\partial \sigma_z}{\partial z} - \omega^2 \rho \zeta. \end{aligned} \quad (3.177)$$

In order to carry out the next differentiation, first the $\xi', \eta', \zeta', \sigma_x', \sigma_z'$ must be determined. This is not difficult since $\tau_{yx} = \tau_{yz} = 0$ to the required precision, which means that

$$\xi' = -\frac{\partial \eta}{\partial x}, \quad \zeta' = -\frac{\partial \eta}{\partial z} \quad (3.178a)$$

follows from the last equation in (3.162a). Moreover, with $p_+ = -p_-$ i.e., $p_D = 0$ follows from Eq. (3.166) that

$$\eta' = \frac{-\mu}{1-\mu} \left(\frac{\partial \xi}{\partial x} + \frac{\partial \zeta}{\partial z} \right). \quad (3.178b)$$

The condition $p_D = 0$ in (3.167) furthermore implies that

$$\frac{\sigma_x'}{G} = \frac{-2}{1-\mu} \left(\frac{\partial^2 \eta}{\partial x^2} + \mu \frac{\partial^2 \eta}{\partial z^2} \right), \quad \frac{\sigma_z'}{G} = \frac{-2}{1-\mu} \left(\mu \frac{\partial^2 \eta}{\partial x^2} + \frac{\partial^2 \eta}{\partial z^2} \right), \quad (3.179)$$

$$\frac{\tau_{xy}'}{G} = -2 \frac{\partial^2 \eta}{\partial x \partial z},$$

using Eq. (3.175). Upon introducing this in (3.177) together with (3.178) one obtains

$$\begin{aligned} \tau_{xy}'' &= \frac{2G}{1-\mu} \frac{\partial \nabla^2 \eta}{\partial x} + \omega^2 \rho h \frac{\partial \eta}{\partial x}, \\ \tau_{zy}'' &= \frac{2G}{1-\mu} \frac{\partial \nabla^2 \eta}{\partial z} + \omega \rho h \frac{\partial \eta}{\partial z}. \end{aligned} \quad (3.180)$$

Herein,

$$\nabla^2 = \frac{\partial^2}{\partial x^2} + \frac{\partial^2}{\partial z^2}$$

is the two-dimensional Laplace operator.

With a further substitution of (3.180) into the mid equation of (3.177), taking into account that

$$\eta'' = \frac{-\mu}{1-\mu} \left(\frac{\partial \xi'}{\partial x} + \frac{\partial \zeta'}{\partial z} \right) = \frac{\mu}{1-\mu} \nabla^2 \eta, \quad (3.181)$$

it follows from (3.178a, b) that the third derivative of the normal stress in the y -direction is

$$\sigma_y''' = \frac{-2G}{1-\mu} \nabla^4 \eta - \frac{\mu}{1-\mu} \omega^2 \rho \nabla^2 \eta. \quad (3.182)$$

Finally, is obtained the equation for bending motion of a plate by substituting (3.182) and (3.180) in (3.176),

$$\frac{h^3}{16} \frac{2G}{1-\mu} \frac{2}{3} \nabla^4 \eta + \frac{h^3}{48} \frac{3-4\mu}{1-\mu} \omega^2 \rho \nabla^2 \eta - \omega^2 \rho \frac{h}{2} \eta = \frac{p_B}{2}, \quad (3.183a)$$

or,

$$\frac{E}{1-\mu^2} \frac{h^3}{12} \nabla^4 \eta + \frac{h^3}{24} \frac{3-4\mu}{1-\mu} \omega^2 \rho \nabla^2 \eta - \omega^2 \rho h \eta = p_B. \quad (3.183b)$$

In this equation, $B' = Eh^3/[12(1-\mu^2)]$ is the bending stiffness and $m'' = \rho h$ the mass per unit area. $p_B = p_+ - p_-$ describes the external forces exerted onto the plate. This means that Eq. (3.183b) can be rewritten in the form

$$\frac{B'}{m''} \nabla^4 \eta - \omega^2 \eta = \frac{P_+ - P_-}{m''} - \text{correction} \approx \frac{P_B}{m''}. \quad (3.184a)$$

As is seen from a comparison with Eq. (3.81), the first two terms correspond to the ordinary flexural wave equation. The correction term on the right hand side represents a portion of the effects of shear stresses cf., Sect. 3.8.2. These effects becomes significant when the bending wavelength is smaller than six times the plate thickness and can therefore often be neglected.

In order to enable the employment of Eq. (3.183) also for the solution of boundary value problems where forces and moments are prescribed, it remains to establish expressions also for these quantities. The cross-sectional rotation is given by

$$-\beta_x = \xi' = -\frac{\partial \eta}{\partial x}, \quad -\beta_z = \zeta' = -\frac{\partial \eta}{\partial z} \quad (3.184b)$$

for the small amplitudes of interest. In view of (3.74), the moments are analogously given by the product of local stress and distance from the neutral layer

$$\begin{aligned} M_{xz} &= \int_{-h/2}^{h/2} \sigma_x y dy = \frac{-2G}{1-\mu} \left(\frac{\partial^2 \eta}{\partial x^2} + \mu \frac{\partial^2 \eta}{\partial z^2} \right) \int_{-h/2}^{h/2} y^2 dy = -B' \left(\frac{\partial^2 \eta}{\partial x^2} + \mu \frac{\partial^2 \eta}{\partial z^2} \right), \\ M_{zx} &= \int_{-h/2}^{h/2} \sigma_z y dy = \frac{-2G}{1-\mu} \left(\mu \frac{\partial^2 \eta}{\partial x^2} + \frac{\partial^2 \eta}{\partial z^2} \right) \int_{-h/2}^{h/2} y^2 dy = -B' \left(\mu \frac{\partial^2 \eta}{\partial x^2} + \frac{\partial^2 \eta}{\partial z^2} \right), \\ M_{xx} = -M_{zz} &= \int_{-h/2}^{h/2} \tau_{xz} y dy = 2G \frac{\partial^2 \eta}{\partial x \partial z} \int_{-h/2}^{h/2} y^2 dy = -B' (1-\mu) \frac{\partial^2 \eta}{\partial x \partial z}. \end{aligned} \quad (3.184c)$$

In the above expressions σ_x' , σ_z' and τ_{xz}' are introduced from (3.179) considering that $\sigma_x = \sigma_x' y$, $\sigma_z = \sigma_z' y$, $\tau_{xz} = \tau_{xz}' y$ apply in the approximation used here. Furthermore, is used the flexural stiffness of a plate

$$B' = \frac{E}{1-\mu^2} \frac{h^3}{12} = \frac{2G}{1-\mu} \frac{h^3}{12}. \quad (3.184d)$$

From the moments, the cross-sectional forces are obtained as

$$\begin{aligned} Q_x &= -\frac{\partial M_{xz}}{\partial x} - \frac{\partial M_{zz}}{\partial z} = B' \frac{\partial \nabla \eta}{\partial x}, \\ Q_z &= -\frac{\partial M_{zx}}{\partial z} - \frac{\partial M_{zz}}{\partial x} = B' \frac{\partial \nabla \eta}{\partial z} \end{aligned} \quad (3.184e)$$

cf., Fig. 3.27.

In summary, it can be stated that the motion of a thin plate is well described by (3.168b) and (3.184a-e) whereby (3.168b) yields the in-plane motions whilst (3.184a) those out-of-plane. The accuracy is satisfactory for most engineering application provided the plate thickness is smaller than a sixth of the wavelength.

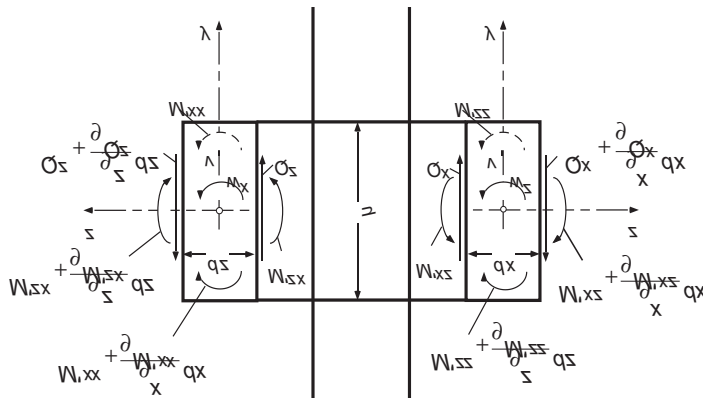


Fig. 3.27. Velocities, moments and forces for a plate in bending

3.7.4.3 Flexural Waves in Flat, Orthotropic Plates

Plates are termed orthotropic when the bending stiffness differs in two orthogonal directions. Typical examples are corrugated plates and plates with stiffeners in one direction as in the decks of a ship, cf. Fig. 2.28. The analysis in this section concerns configurations, for which the corrugation or stiffener distance is substantially smaller than the wavelength. If this condition is not met, the structure is rather to be considered as a periodic system, at least in the case of stiffened plates, see Sect. 6.5. The equation of motion for orthotropic plates can be derived in precisely the same manner as that of an isotropic plate; only the stress-strain relations have to be slightly modified

$$\begin{aligned}\sigma_x &= \sigma'_x \cdot y = \left(-\frac{E_x}{1-\mu^2} \frac{\partial^2 \eta}{\partial x^2} - E_\mu \frac{\partial^2 \eta}{\partial z^2} \right) y, \\ \sigma_z &= \sigma'_z \cdot y = \left(-E_\mu \frac{\partial^2 \eta}{\partial x^2} - \frac{E_z}{1-\mu^2} \frac{\partial^2 \eta}{\partial z^2} \right) y, \\ \tau_{xz} &= \tau'_{xz} \cdot y = -2Gy \frac{\partial^2 \eta}{\partial x \partial z}.\end{aligned}\quad (3.185)$$

E_x and E_z are the Young's moduli for the x - and z -directions respectively, which can be measured using the conventional test on rod samples cut in the two directions respectively. The cross-contractional modulus E_μ and the shear modulus are more intricate. Commonly, they are approximated or assessed from the eigen-modes of an orthotropic plate i.e., from the eigenfunctions of (3.186).

With Eq. (3.185) inserted in the relations (3.176), (3.177) and (3.180), which are valid also for orthotropic, thin plates, then with the exception for the $\omega^2\rho$ -term, the flexural wave equation for an orthotropic plate is obtained as [3.10-3.13]

$$B_x' \frac{\partial^4 \eta}{\partial x^4} + 2(B_\mu' + 2B_G') \frac{\partial^4 \eta}{\partial x^2 \partial z^2} + B_z' \frac{\partial^4 \eta}{\partial z^4} - \omega^2 m'' \eta = p(x, z, t). \quad (3.186)$$

Herein, B_x' is the bending stiffness in one direction, B_z' that in the perpendicular direction, B_μ' denotes to the stiffness relating to E_μ whereas B_G' takes the shear stiffness into account. For a plate of thickness h and of orthotropic material with the moduli E_x , E_z , E_μ and shear modulus G , it follows from (3.185) that

$$B_x' = \frac{E_x}{1-\mu^2} \frac{h^3}{12}, \quad B_z' = \frac{E_z}{1-\mu^2} \frac{h^3}{12}, \quad B_\mu' = E_\mu \frac{h^3}{12}, \quad B_G' = G \frac{h^3}{12}. \quad (3.186a)$$

As an example can be mentioned that for a three-layer plywood laminate the following approximate values apply

$$E_x \approx 130, \quad E_z \approx 11, \quad E_\mu \approx 3, \quad G \approx 7.5 \text{ GPa}.$$

For corrugated or stiffened plates of homogeneous material with Young's modulus E , Poisson's ratio μ the formulae in Fig. 3.28 are found in the literature. With the exception of the term $\omega^2\rho\eta$, all other terms involving $\omega^2\rho$ in Eqs. (3.177), (3.180) and (3.182) are omitted in the developments since the thereby expressed shear stress corrections anyhow would be incorrect for corrugated and stiffened plates.

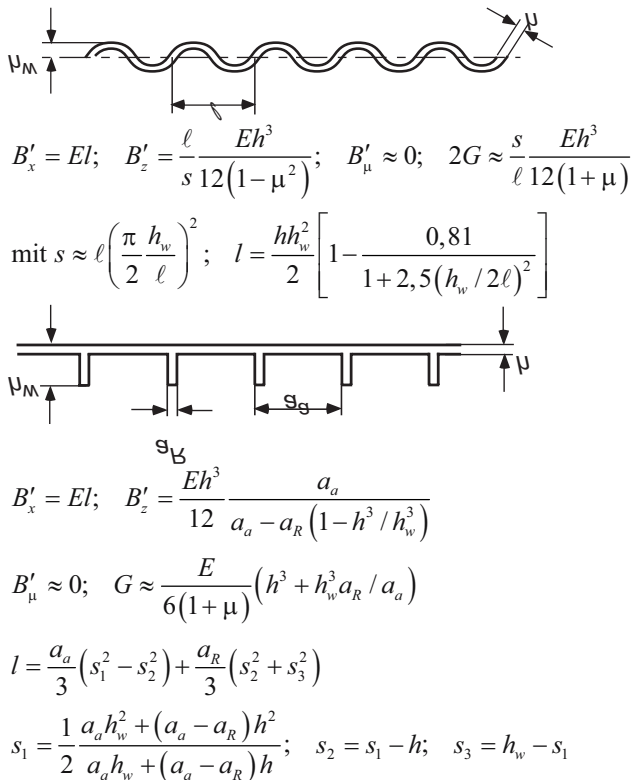


Fig. 3.28. Bending stiffness of corrugated and stiffened plates (l and a_a must be substantially smaller than the flexural wavelength)

3.7.4.4 Thin Prestressed Plates on Winkler Bed

The methods of the previous sections can be employed to develop the equations of motion for a plate of bending stiffness B' , prestressed with a (positive) tensile or a (negative) compressional stress and when this plate, possibly also rests upon a soft layer (Winkler bed) of stiffness s'' per unit area. Simpler still, Hamilton's principle [3.14] can be used as discussed in the next section. The result, given here without proof, reads

$$B\nabla^4\eta - T'\nabla^2\eta + s''\eta + m''\frac{\partial^2\eta}{\partial t^2} = p(x, z, t) \quad (3.187)$$

for the motion out of the plane of the plate. The units of the quantities used are: B' [Nm], T' [N/m], s'' [N/m³], m'' [kg/m²], η [m] and p [N/m²]. $p(x, z, t)$ is the externally applied pressure.

It is clear that Eq. (3.187) combines the plate Eq. in (3.184a) and a membrane equation. Included is also an additional reaction force $s'' \eta$. By introducing the conventional exponential solution, the dispersion equation is found for $p(x, z, t) = 0$ to be

$$B' \left(k_x^2 + k_z^2 \right)^2 + T' \left(k_x^2 + k_z^2 \right) - \left(\omega^2 m'' - s'' \right) = 0, \quad (3.187a)$$

revealing the possible free wavenumbers. A closer scrutiny of this expression leads to the following findings:

- Propagating waves are only possible when

$$\omega^2 > \frac{s'' - T'^2 / 4B'}{m''},$$

which, for vanishing prestress, means that the frequency must be higher than $\sqrt{s'' / m''}$. For lower frequencies only evanescent waves exist.

- A consequence of the limiting frequency just defined is that, in contrast to the plate without a Winkler bed, the wave speed does not decrease below a certain limiting value, also for very low frequencies. For plates without prestress ($T' = 0$), the limiting phase speed is $c_{B\min} = (2 s'' B' / m'')^{1/4}$ which is reached at $\omega_{\min}^2 = 2 s'' / m''$. For railway rails the minimum phase speed is typically some 100 m/s and the cut-on occurs in the range 50 to 100 Hz.
- When the plate is compressed ($T' < 0$), it appears somewhat more flexible. Theoretically, a vanishing wavenumber is possible but has to be ruled out on physical grounds since the plate will buckle.
- Upon combining a membrane equation comprising the prestresses T'_x and T'_z with the equation of motion for orthotropic plates in (3.186) the applicability of Eq. (3.187) can be further extended.

3.8 Hamilton's Principle for the Derivation of the Equations of Motion

3.8.1 Fundamentals

As was already stated in Sect. 2.5.1, Hamilton's principle realizes one of the most important relations of physics. It is therefore to be anticipated that it is applicable also in structure-borne sound. As far as discretizations of a structure are concerned, the use of Hamilton's principle has experienced a renaissance in recent years since the application of the finite element method (FEM) can be seen as an employment of the principle. Despite this, FEM will not be a topic in this book because a large number of publi-

cations is devoted to the method. Instead, the wave equations will be developed from Hamilton's principle in Chapters 3 and 4 whereby the plate and the shell serve as examples, cf. Sect. 4.6.3. In Sect. 6.6, moreover, a further use will be demonstrated.

Naturally, also the wave equations employed in previous sections could have been derived from Hamilton's principle but besides the physics of structure-borne sound, also different methods should be presented.

In mechanics the Hamilton's principle reads, cf. Sect. 2.5.1

$$\delta \int_{t_1}^{t_2} (E_{kin} - E_{pot}) dt + \int_{t_1}^{t_2} \delta W dt = 0. \quad (3.188)$$

Herein, E_{kin} and E_{pot} are the total kinetic and potential energies of the system respectively. W is the externally supplied work. The symbol δ means that a variation is undertaken. Equation (3.188) thus states that a mechanical system adjusts itself such that the variation vanishes of $(E_{kin} - E_{pot})$ and W respectively. In particular, $(E_{kin} - E_{pot})$ is a minimum when no energy is imparted on the system externally. The task consists of expressing E_{kin} , E_{pot} and W in terms of the field variables e.g., ξ , η and ζ and to perform the variation – a kind of differentiation.

3.8.2 Flat Plate with Shear Stiffness (The Corrected Bending Wave)

In conjunction with the bending wave equation in Sect. 3.3, it was pointed out that the simple bending theory loses its validity at high frequencies because the phase speed according to (3.85) would exceed all limits. This deficiency can partly be remedied by introducing a finite shear stiffness in the y -direction and, in addition, taking the rotational inertia into account. The co-ordinate system used in this case is shown in Fig. 3.29. Assumed is only that the motion η is constant over the thickness of the plate and that the displacements in the plane of the plate are composed of a displacement in the mid-plane ξ_M and rotational motions with angles φ_x and φ_z . For the displacements ξ , η and ζ of a volume element with co-ordinates x , y , z one has

$$\xi = \xi_M + \varphi_x y, \quad \eta = \eta, \quad \zeta = \zeta_M + \varphi_z y. \quad (3.189)$$

The kinetic energy thereby becomes

$$\begin{aligned}
 E_{kin} &= \frac{\rho}{2} \int (v_x^2 + v_y^2 + v_z^2) dxdydz \\
 &= \frac{\rho}{2} \int [\dot{\xi}_M + y\dot{\varphi}_x]^2 + \dot{\eta}^2 + [\dot{\zeta}_M + y\dot{\varphi}_z]^2 dxdydz \\
 &= \frac{\rho}{2} \int \dot{\xi}_M^2 + \dot{\eta}^2 + \dot{\zeta}_M^2 + \frac{h}{12} (\dot{\varphi}_x^2 + \dot{\varphi}_z^2) dxdz.
 \end{aligned} \tag{3.190a}$$

In the last version of (3.190a) the integration across the cross-section is undertaken from $-h/2$ to $+h/2$.

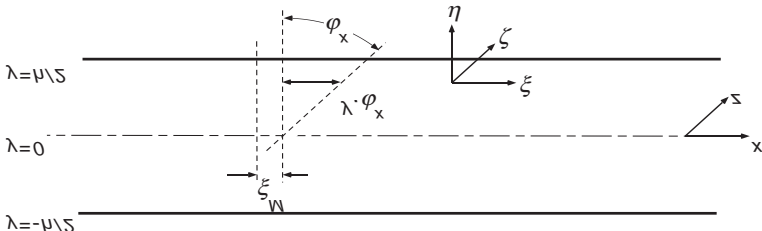


Fig. 3.29. Co-ordinate system for the derivation of the ‘corrected bending wave’ equation

For the potential energy of a volume element, the different stresses with the accompanying strains ε and γ are to be multiplied and added, cf. (3.115) and (3.120). Generally,

$$E_{pot} = \frac{1}{2} \int [\sigma_x \varepsilon_x + \sigma_y \varepsilon_y + \sigma_z \varepsilon_z + \tau_{xy} \gamma_{xy} + \tau_{yz} \gamma_{yz} + \tau_{xz} \gamma_{xz}] dxdydz. \tag{3.190b}$$

For thin plates with stress-free surfaces, σ_y can be set to zero for the complete cross-section. Thence, (3.178b) follows from (3.120) which resubstituted in (3.120) gives

$$\sigma_x = \frac{E}{1-\mu^2} \left(\frac{\partial \xi}{\partial x} + \mu \frac{\partial \zeta}{\partial z} \right), \quad \sigma_z = \frac{E}{1-\mu^2} \left(\mu \frac{\partial \xi}{\partial x} + \frac{\partial \zeta}{\partial z} \right). \tag{3.190c}$$

Regarding the shear stresses, the general expressions in Eq. (3.119) are used. The strains and shear angles read

$$\begin{aligned}\varepsilon_x &= \frac{\partial \xi}{\partial x} = \frac{\partial \xi_M}{\partial x} + y \frac{\partial \varphi_x}{\partial x}, \quad \varepsilon_z = \frac{\partial \zeta}{\partial z} = \frac{\partial \zeta_M}{\partial z} + y \frac{\partial \varphi_z}{\partial z}, \\ \gamma_{xy} &= \frac{\partial \xi}{\partial y} + \frac{\partial \eta}{\partial x} = \varphi_x + \frac{\partial \eta}{\partial x}, \quad \gamma_{yz} = \frac{\partial \zeta}{\partial y} + \frac{\partial \eta}{\partial z} = \varphi_z + \frac{\partial \eta}{\partial z}, \\ \gamma_{xz} &= \frac{\partial \xi}{\partial z} + \frac{\partial \zeta}{\partial x} = \frac{\partial \xi_M}{\partial z} + y \frac{\partial \varphi_x}{\partial z} + \frac{\partial \zeta_M}{\partial x} + y \frac{\partial \varphi_z}{\partial x}.\end{aligned}\quad (3.190d)$$

With these expression inserted in (3.190b), results after integration over the cross-section

$$\begin{aligned}E_{pot} &= \frac{1}{2} \frac{Eh}{1-\mu^2} \int (\xi_{M,x}^2 + 2\mu \xi_{M,x} \zeta_{M,z} + \zeta_{M,z}^2) dx dz \\ &\quad + \frac{Gh}{2} \int (\xi_{M,z}^2 + \zeta_{M,x}^2)^2 dx dz \\ &\quad + \frac{1}{2} \frac{Eh}{1-\mu^2} \frac{h^2}{12} \int [\varphi_{x,x}^2 + 2\mu \varphi_{x,x} \varphi_{z,z} + \varphi_{z,z}^2 + \frac{1-\mu}{2} (\varphi_{x,z} + \varphi_{z,x})^2] dx dz \\ &\quad + \frac{Gh}{2} \int [(\varphi_x + \eta_{,x})^2 + (\varphi_z + \eta_{,z})^2] dx dz.\end{aligned}\quad (3.190e)$$

In this expression the notation “,” is used in indices to denote differentiations with respect to the subsequent co-ordinate.

The first and second lines in (3.190e), relate to the potential energy of the in-plane waves. The third line describes the potential energy of the ordinary Kirchhoff's bending theory whereas the last line gives the Timoshenko-Mindlin correction [3.15], stemming from the finite shear stiffness.

Upon undertaking the variation after substitution in (3.188), a set of expressions results in the following form:

$$\begin{aligned}\delta \int \left(\frac{\partial \xi_M}{\partial x} \right)^2 dx dz dt &= \int 2 \left(\frac{\partial \xi_M}{\partial x} \right) \delta \left(\frac{\partial \xi_M}{\partial x} \right) dx dz dt \\ &= \int 2 \left(\frac{\partial \xi_M}{\partial x} \right) \delta \xi_M dz dt \Big|_{x_1}^{x_2} - 2 \int \left(\frac{\partial^2 \xi_M}{\partial x^2} \right) \delta \xi_M dx dz dt \\ &= -2 \int \left(\frac{\partial^2 \xi_M}{\partial x^2} \right) \delta \xi_M dx dz dt.\end{aligned}$$

Herein, first, the variation is performed according to the product rule (analogous to that in a differentiation). Then, an integration by parts is made and finally, it is assumed that the field quantities vanish at the limits of integration, equivalent to a vanishing variation.

By means of the corresponding procedure is obtained

$$\begin{aligned}\delta \int \frac{\partial \xi_M}{\partial x} \frac{\partial \zeta_M}{\partial z} dx dz dt &= - \int \frac{\partial^2 \xi_M}{\partial x \partial z} \delta \zeta_M dx dz dt - \int \frac{\partial^2 \zeta_M}{\partial x \partial z} \delta \xi_M dx dz dt, \\ \delta \int \varphi_x \frac{\partial \eta}{\partial x} dx dz dt &= - \int \frac{\partial \varphi_x}{\partial x} \delta \eta dx dz dt - \int \frac{\partial \eta}{\partial x} \delta \varphi_x dx dz dt,\end{aligned}\quad (3.190f)$$

and a set of similar expressions.

Regarding the external work W , it is assumed that it is solely due to distributed forces i.e., pressure. Since work is the product of force and displacement,

$$W = \int (p_B \eta + p_2 \xi_M + p_4 \zeta_M) dx dz \quad (3.191)$$

As in Fig. 3.23 and in Eq. (3.164), p_B is the external pressure in the y -direction and p_2 and p_4 are the pressures in the x - and z - directions respectively. Upon undertaking the same manipulation as in Eq. (3.190f), it is found that

$$\int_{t_1}^{t_2} \delta W dt = \int (p_B \delta \eta + p_2 \delta \xi_M + p_4 \delta \zeta_M) dx dz dt. \quad (3.192)$$

where the pressure need not be varied since it is prescribed.

By combining all equations, beginning with (3.188), is obtained an expression in the form

$$\int [A_1 \delta \xi_M + A_2 \delta \eta + A_3 \delta \zeta_M + A_4 \delta \varphi_x + A_5 \delta \varphi_z + p_B \delta \eta + p_2 \delta \xi_M + p_4 \delta \zeta_M] dx dz dt = 0$$

This formula reveals why all variations in (3.190f) are transposed to the quantities ξ_M , η , ζ_M , φ_x , φ_z . Pivotal is namely that Hamilton's principle must be valid for any variation. For instance, also for the variation $\delta \xi_M \neq 0$ but $\delta \eta = \delta \zeta_M = \delta \varphi_x = \delta \varphi_z = 0$. It follows that $A_1 + p_2$ must vanish since $\delta \xi_M$ is arbitrary. This argument, applied on $\delta \eta$ etc., shows that the factors in front of the variations $\delta \xi_M$, $\delta \eta$ and the other must vanish independently. With the expressions for A_1 to A_5 introduced, from Eq. (3.188) to (3.190), result

$$\begin{aligned}
\delta\xi_M : \rho \ddot{\xi}_M - \left[\frac{E}{1-\mu^2} \frac{\partial^2}{\partial x^2} + G \frac{\partial^2}{\partial z^2} \right] \xi_M - \frac{1+\mu}{1-\mu} G \frac{\partial^2 \zeta_M}{\partial x \partial z} &= \frac{p_2}{h} \\
\delta\zeta_M : -\frac{1+\mu}{1-\mu} G \frac{\partial^2 \xi_M}{\partial x \partial z} + \rho \dot{\zeta}_M - \left[\frac{E}{1-\mu^2} \frac{\partial^2}{\partial z^2} + G \frac{\partial^2}{\partial x^2} \right] \zeta_M &= \frac{p_4}{h} \\
\delta\eta : \rho h \ddot{\eta} - Gh \nabla^2 \eta - Gh \frac{\partial \varphi_x}{\partial x} - Gh \frac{\partial \varphi_z}{\partial z} &= p_B \quad (3.193) \\
\delta\varphi_x : Gh \frac{\partial \eta}{\partial x} + \rho I \ddot{\varphi}_x + \left[G \left(h - I \frac{\partial^2}{\partial z^2} \right) - B' \frac{\partial^2}{\partial x^2} \right] \varphi_x - \frac{1+\mu}{2} B' \frac{\partial^2 \varphi_z}{\partial x \partial z} &= 0 \\
\delta\varphi_z : Gh \frac{\partial \eta}{\partial z} - \frac{1+\mu}{2} B' \frac{\partial^2 \varphi_x}{\partial x \partial z} + \rho I \ddot{\varphi}_z + \left[G \left(h - I \frac{\partial^2}{\partial x^2} \right) - B' \frac{\partial^2}{\partial z^2} \right] \varphi_z &= 0
\end{aligned}$$

where $B' = EI/(1 - \mu^2)$ is the bending stiffness of the plate and $I = h^3/12$ the second area moment. As can be observed, the two first equations are fully decoupled from the rest. Owing to the fact that these are identical to the equations of motion for the in-plane waves, cf. Eq. (3.186b), they will not be discussed further in this context.

The three remaining equations form relations between the displacement η and the two rotations φ_x and φ_z . They hence describe the bending motion. It would be possible to retain them in the present form as a system of differential equations. This would indeed give the advantage that the relationship is seen between the cross-sectional force, established from the variation $\delta\eta$, and the moments from the variations of the rotations. It is customary, however, to bring them together in one differential equation of higher order. Therefore, the expressions are rewritten as

$$\begin{aligned}
Gh \left(\nabla^2 \eta + \frac{\partial \varphi_x}{\partial x} + \frac{\partial \varphi_z}{\partial z} \right) &= \rho h \ddot{\eta} - p_B \\
\frac{B'}{2} \left[(1-\mu) \nabla^2 \varphi_x + (1+\mu) \left(\frac{\partial^2 \varphi_z}{\partial x \partial z} + \frac{\partial^2 \varphi_x}{\partial z^2} \right) \right] - Gh \left(\varphi_x + \frac{\partial \eta}{\partial x} \right) &= \rho I \ddot{\varphi}_x \quad (3.194a) \\
\frac{B'}{2} \left[(1-\mu) \nabla^2 \varphi_z + (1+\mu) \left(\frac{\partial^2 \varphi_x}{\partial x \partial z} + \frac{\partial^2 \varphi_z}{\partial z^2} \right) \right] - Gh \left(\varphi_z + \frac{\partial \eta}{\partial z} \right) &= \rho I \ddot{\varphi}_z
\end{aligned}$$

where use is made of the relation $GI = B' (1 - \mu)/2$. By differentiating the penultimate equation with respect to x and the last with respect to z , a subsequent addition yields

$$\begin{aligned}
Gh (\nabla^2 \eta + \psi) &= \rho h \ddot{\eta} - p_B, \\
B' \nabla^2 \psi - Gh (\nabla^2 \eta + \psi) &= \rho I \ddot{\psi}, \quad (3.194b)
\end{aligned}$$

where the abbreviation,

$$\psi = \frac{\partial \varphi_x}{\partial x} + \frac{\partial \varphi_z}{\partial z}, \quad (3.194c)$$

is introduced for clarity. From an elimination of ψ it is found that

$$B' \nabla^4 \eta - \left(\frac{B' \rho}{G} + \rho I \right) \nabla^2 \ddot{\eta} + \rho h \ddot{\eta} + \rho I \frac{\rho}{G} \ddot{\eta} = p_B + \frac{B'}{Gh} \nabla^2 p_B - \frac{\rho I}{Gh} \ddot{p}_B \quad (3.195)$$

This formula, which in the one-dimensional case dates back to Timoshenko [3.12] and to Mindlin [3.15] in the two-dimensional, furnishes an improvement of the simple bending wave Eqs. (3.81) and (3.184a) respectively. It takes the shear stiffness into account via terms involving I . Of the two, the latter, already derived by Rayleigh, is the least important.

Often, the modified shear stiffness G^* cf., Sect. 3.2.2, is introduced in Eq. (3.195) instead of the ordinary shear modulus G . In this way, the flexural wave speed approaches the Rayleigh wave speed at high frequencies.

To assess how much (3.195) deviates from (3.81) and (3.184a) respectively, a one-dimensional case without external excitation can be considered, Upon letting $\eta \sim e^{j\omega t} e^{-jk_s x}$, the dispersion equation results as

$$k_C^4 - \omega^2 k_C^2 \left[\frac{1}{c_T^2} + \frac{1}{c_{LH}^2} \right] - k_B^4 + \frac{\omega^4}{c_{LH}^2 c_T^2} = 0 \quad (3.196a)$$

Herein, k_B is the non-corrected flexural wave number according to (3.83) and k_C the free wave number of flexural waves in thick plates. This means that the wave speed of the corrected flexural wave is approximated by

$$c_C \approx c_B \left[1 - \frac{1}{2} c_B^2 \left(\frac{1}{c_T^2} + \frac{1}{c_{LH}^2} \right) \right] \approx c_B \left[1 - 4(h/\lambda_B)^2 \right] \quad (3.196b)$$

A 10% deviation is accordingly first then approached when the wavelength λ_B becomes smaller than six times the plate thickness; $\lambda_B < 6h$. Further aspects of plates with finite shear stiffness are given in Sect. 4.4.3.1.

3.8.3 Cylindrical Shells

3.8.3.1 Fundamental Equations

In Figs. 3.30 and 3.31 are depicted, the polar co-ordinates and the displacement variables – ξ tangential, η radial and ζ axial – appropriate for cylindrical shells. The conversion to Cartesian co-ordinates for very large radii is given by $r\vartheta \rightarrow x$, $r \rightarrow y$, $\zeta \rightarrow z$.

To be able to employ Hamilton's principle, the potential energy is required, given by the stresses and strains. This means that the general stress-strain relations have to be developed in polar co-ordinates. As can be seen from Fig. 3.30, the strain in radial direction is

$$\varepsilon_r = \frac{1}{\Delta r} \left[\left(\eta + \frac{\partial \eta}{\partial r} \Delta r \right) - \eta \right] = \frac{\partial \eta}{\partial r} \quad (3.197a)$$

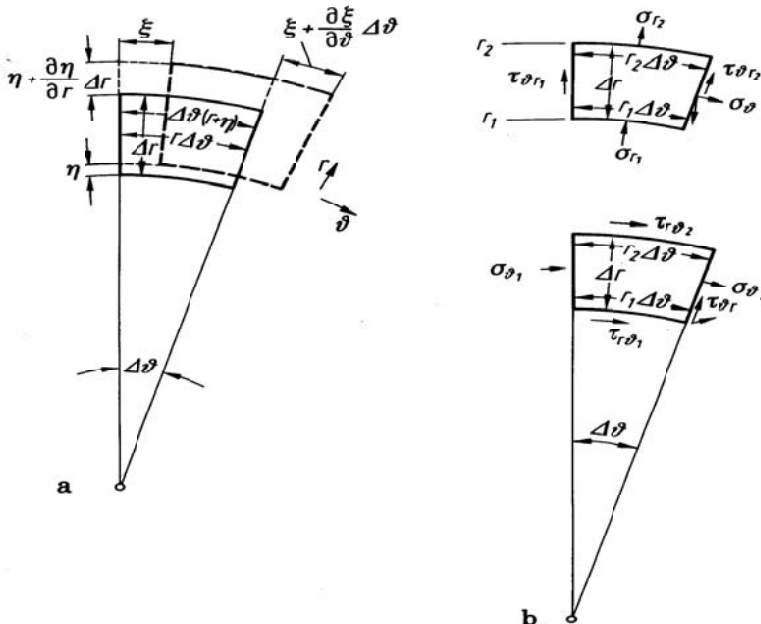


Fig. 3.30. Deformation (a) of a volume element in polar co-ordinates and normal and shear stresses (b)

The tangential strain consists of two parts. The first occurs for pure radial motion because the element is elongated,

$$\varepsilon_{\theta 1} = \frac{1}{r \nabla^2 \vartheta} \left[\nabla^2 \vartheta (r + \eta) - r \nabla^2 \vartheta \right] = \frac{\eta}{r}.$$

The second comes about due to motion in tangential direction whereby

$$\varepsilon_{\theta 2} = \frac{1}{r \nabla^2 \vartheta} \left[\left(\xi + \frac{\partial \xi}{\partial \theta} \nabla^2 \vartheta \right) - \xi \right] = \frac{1}{r} \frac{\partial \xi}{\partial \theta}.$$

Accordingly, the tangential strain becomes

$$\varepsilon_{\vartheta} = \varepsilon_{\vartheta 1} + \varepsilon_{\vartheta 2} = \frac{\eta}{r} + \frac{1}{r} \frac{\partial \xi}{\partial \vartheta} \quad (3.197b)$$

By a similar consideration for the shear deformation, it is found in analogy with (3.162a) that the stress-strain relations in polar co-ordinates are given by [3.9, 3.16-18]

$$\begin{aligned} \frac{\sigma_{\vartheta}}{2G} &= (\alpha + 1)\varepsilon_{\vartheta} + \alpha\varepsilon_r + \alpha\varepsilon_z = (\alpha + 1)\left(\frac{\eta}{r} + \frac{1}{r} \frac{\partial \xi}{\partial \vartheta}\right) + \alpha \frac{\partial \eta}{\partial r} + \alpha \frac{\partial \zeta}{\partial z}, \\ \frac{\sigma_r}{2G} &= \alpha\varepsilon_{\vartheta} + (\alpha + 1)\varepsilon_r + \alpha\varepsilon_z = \alpha\left(\frac{\eta}{r} + \frac{1}{r} \frac{\partial \xi}{\partial \vartheta}\right) + (\alpha + 1) \frac{\partial \eta}{\partial r} + \alpha \frac{\partial \zeta}{\partial z}, \\ \frac{\sigma_z}{2G} &= \alpha\varepsilon_{\vartheta} + \alpha\varepsilon_r + (\alpha + 1)\varepsilon_z = \alpha\left(\frac{\eta}{r} + \frac{1}{r} \frac{\partial \xi}{\partial \vartheta}\right) + \alpha \frac{\partial \eta}{\partial r} + (\alpha + 1) \frac{\partial \zeta}{\partial z}, \\ \frac{\tau_{\vartheta r}}{G} &= \gamma_{\vartheta r} = r \frac{\partial}{\partial r} \left(\frac{\xi}{r} \right) + \frac{1}{r} \frac{\partial \eta}{\partial \vartheta} = \frac{\partial \xi}{\partial r} - \frac{\xi}{r} + \frac{1}{r} \frac{\partial \eta}{\partial \vartheta}, \\ \frac{\tau_{rz}}{G} &= \gamma_{rz} = \frac{\partial \zeta}{\partial r} + \frac{\partial \eta}{\partial z}, \\ \frac{\tau_{\vartheta z}}{G} &= \gamma_{\vartheta z} = \frac{\partial \xi}{\partial z} + \frac{1}{r} \frac{\partial \zeta}{\partial \vartheta}, \end{aligned} \quad (3.198a)$$

where $\alpha = \mu/(1 - 2\mu)$. Henceforth, it is assumed that the thickness of the shell h is substantially smaller than the radius of curvature and the wavelength, see Fig. 3.31. For such a case, σ_r can be set to zero when the shell is free of external stresses i.e., a state of plane stress. In analogy with (3.190c) it follows that

$$\begin{aligned} \sigma_{\vartheta} &= \frac{E}{1-\mu^2} (\varepsilon_{\vartheta} + \mu\varepsilon_z) = \frac{E}{1-\mu^2} \left(\frac{\eta}{r} + \frac{1}{r} \frac{\partial \xi}{\partial \vartheta} + \mu \frac{\partial \zeta}{\partial z} \right), \\ \sigma_z &= \frac{E}{1-\mu^2} (\mu\varepsilon_{\vartheta} + \varepsilon_z) = \frac{E}{1-\mu^2} \left(\mu \frac{\eta}{r} + \mu \frac{1}{r} \frac{\partial \xi}{\partial \vartheta} + \frac{\partial \zeta}{\partial z} \right), \end{aligned} \quad (3.199)$$

whilst the shear stresses remain unaltered.

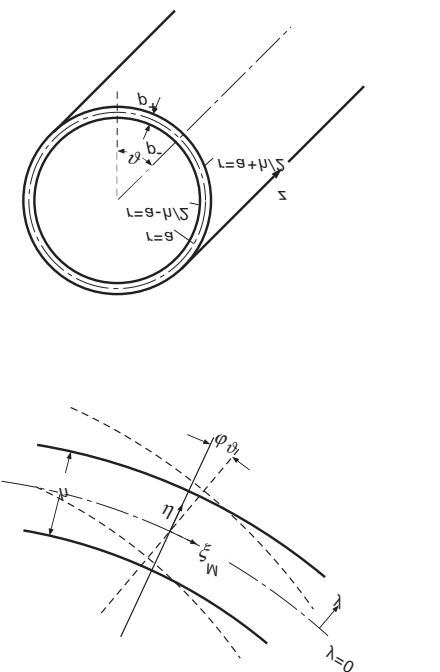


Fig. 3.31. Displacement co-ordinates for a thin-walled shell

The proceeding analysis follows that of the preceding section. Thus, the radial component η is constant over the cross-section whereas the tangential and axial motion will consist of an “in-plane” part and bending part, which depends linearly on the radius cf., (3.189),

$$\begin{aligned}\xi &= \frac{r}{a} \xi_M + (r-a) \varphi_\theta, \\ \zeta &= \zeta_M + (r-a) \varphi_z.\end{aligned}\quad (3.200a)$$

Accordingly, there are again five independent variables i.e., the motion of the mid-plane of the shell ξ_M , η and ζ_M and rotations φ_θ and φ_z . The shell radius is assumed constant in this analysis, Fig. 3.31. With (3.200a) substituted into the equations for the strain (3.197) and approximating

$$(r-a) = y, \quad \frac{1}{r} \approx \frac{1}{a} \left(1 - \frac{y}{a}\right), \quad \frac{a}{r} \approx 1 - \frac{y}{a}, \quad \frac{r-a}{r} \approx \frac{y}{a}, \quad (3.200b)$$

the strains and shear angles become

$$\begin{aligned}\varepsilon_{\vartheta} &= \frac{1}{a} \left(1 - \frac{y}{a} \right) \eta + \frac{1}{a} \frac{\partial \xi_M}{\partial \vartheta} + \frac{y}{a} \frac{\partial \varphi_{\vartheta}}{\partial \vartheta}, \quad \varepsilon_z = \frac{\partial \zeta_M}{\partial z} + y \frac{\partial \varphi_z}{\partial z}, \\ \gamma_{r\vartheta} &= \left(1 - \frac{y}{a} \right) \varphi_{\vartheta} + \frac{1}{a} \left(1 - \frac{y}{a} \right) \frac{\partial \eta}{\partial \vartheta}, \quad \gamma_{rz} = \varphi_z + \frac{\partial \eta}{\partial z}, \\ \gamma_{z\vartheta} &= \left(1 + \frac{y}{a} \right) \frac{\partial \xi_M}{\partial z} + y \frac{\partial \varphi_{\vartheta}}{\partial z} + \frac{1}{a} \left(1 - \frac{y}{a} \right) \frac{\partial \zeta_M}{\partial \vartheta} + y \frac{\partial \varphi_z}{\partial \vartheta}.\end{aligned}\tag{3.201}$$

Thereby are terms involving y^2 omitted. Furthermore, since ξ_M and ζ_M are constant across the cross-section, their derivatives vanish in the radial direction. It should also be noted that $\partial \xi / \partial r = 1$.

The next step to use Hamilton's principle for the derivation is to express the energies. The kinetic energy is obtained as

$$\begin{aligned}E_{kin} &= \frac{\rho}{2} \int_0^{2\pi} \int_{-h/2-L}^{h/2} \int_0^L \left(\dot{\xi}^2 + \dot{\eta}^2 + \dot{\zeta}^2 \right) ad\vartheta dy dz = \\ &\quad \frac{\rho h}{2} \int_0^{2\pi} \int_0^L \left[\dot{\xi}_M^2 + \dot{\eta}^2 + \dot{\zeta}_M^2 + I' \left(\dot{\varphi}_{\vartheta}^2 + \dot{\varphi}_z^2 + \frac{2}{a} \dot{\xi}_M \dot{\varphi}_{\vartheta} \right) \right] ad\vartheta dz,\end{aligned}\tag{3.202a}$$

and the potential energy

$$\begin{aligned}E_{pot} &= \frac{1}{2} \int_0^{2\pi} \int_{-h/2-L}^{h/2} \int_0^L \left(\sigma_{\vartheta} \varepsilon_{\vartheta} + \sigma_z \varepsilon_z + \tau_{r\vartheta} \gamma_{r\vartheta} + \tau_{rz} \gamma_{rz} + \tau_{z\vartheta} \gamma_{z\vartheta} \right) ad\vartheta dy dz = \\ &= \frac{1}{2} \int_0^{2\pi} \int_{-h/2-L}^{h/2} \int_0^L \left[\frac{E}{1-\mu^2} \left(\varepsilon_{\vartheta}^2 + \varepsilon_z^2 + 2\mu \varepsilon_{\vartheta} \varepsilon_z \right) + G \left(\gamma_{r\vartheta}^2 + \gamma_{rz}^2 + \gamma_{z\vartheta}^2 \right) \right] ad\vartheta dy dz\end{aligned}\tag{3.202b}$$

In Eq. (3.202a) is $I' = h^2/12$ introduced.

By substituting Eq. (3.201) in (3.202b) and integrating with respect to y , a lengthy expression results, which contains the displacements ξ_M , η etc. as well as their spatial derivatives. The subsequent treatment is as for (3.190) to (3.192) i.e., the variation is undertaken and an integration by parts such that the variation refers to the field variables. Use is also made of the fact that the values of the integrand at the limits 0 and 2π are equal due to the periodicity and that $+L$ and $-L$ are so remote that all field variables have decayed and the variations vanish. As in Eq. (3.193), a system of linear differential equations results in the independent variables ξ_M , η , ζ_M , φ_{ϑ} and φ_z . Abbreviated, this reads

$$\begin{bmatrix} A_{11} & A_{12} & A_{13} & A_{14} & A_{15} \\ A_{21} & A_{22} & & & \vdots \\ \vdots & \ddots & & \ddots & \vdots \\ \vdots & & \ddots & & \vdots \\ A_{51} & & & A_{55} & \end{bmatrix} \begin{bmatrix} \xi_M \\ \zeta_M \\ \eta \\ \varphi_9 \\ \varphi_z \end{bmatrix} = \begin{bmatrix} 0 \\ 0 \\ -p_B(1-\mu^2)/Eh \\ 0 \\ 0 \end{bmatrix} \quad (3.203)$$

Herein, the coefficients are

$$A_{11} = -\frac{\partial^2}{\partial s^2} - \alpha_- (1 + \beta^2) \frac{\partial^2}{\partial z^2} + \frac{1 + \beta^2}{c_{LI}^2} \frac{\partial^2}{\partial t^2},$$

$$A_{12} = (-\alpha_+ - \beta^2 \alpha_-) \frac{\partial^2}{\partial s \partial z} = A_{21},$$

$$A_{13} = -\frac{1}{a} \frac{\partial}{\partial s} = A_{31}, \quad A_{14} = \beta^2 a \left(-\alpha_- \frac{\partial^2}{\partial z^2} + \frac{1}{c_{LI}^2} \frac{\partial^2}{\partial t^2} \right) = A_{41},$$

$$A_{15} = -\beta^2 a \alpha_- \frac{\partial^2}{\partial s \partial z} = A_{51}, \quad A_{22} = -\frac{\partial^2}{\partial z^2} - \alpha_- (1 + \beta^2) \frac{\partial^2}{\partial s^2} + \frac{1}{c_{LI}^2} \frac{\partial^2}{\partial t^2},$$

$$A_{23} = -\frac{\mu}{a} \frac{\partial}{\partial z} = A_{32}, \quad A_{24} = \beta^2 a \alpha_- \frac{\partial^2}{\partial s \partial z} = A_{42},$$

$$A_{25} = \beta^2 a \alpha_- \frac{\partial^2}{\partial s^2} = A_{52}, \quad A_{33} = -\left\{ \frac{1 + \beta^2}{a^2} - \alpha_- \left[(1 + \beta^2) \frac{\partial^2}{\partial s^2} + \frac{\partial^2}{\partial z^2} \right] + \frac{1}{c_{LI}^2} \frac{\partial^2}{\partial t^2} \right\},$$

$$A_{34} = [\alpha_- + \beta^2 (1 + \alpha_-)] \frac{\partial}{\partial s} = A_{43}, \quad A_{35} = (\alpha_- + \mu \beta^2) \frac{\partial}{\partial z} = A_{53},$$

$$A_{44} = \alpha_- (1 + \beta^2) - I' \frac{\partial^2}{\partial s^2} - \alpha_- I' \frac{\partial^2}{\partial z^2} + \frac{I'}{c_{LI}^2} \frac{\partial^2}{\partial t^2},$$

$$A_{45} = -\alpha_+ I' \frac{\partial^2}{\partial s \partial z} = A_{54}, \quad A_{55} = \alpha_- - I' \frac{\partial^2}{\partial z^2} - \alpha_- I' \frac{\partial^2}{\partial s^2} + \frac{I'}{c_{LI}^2} \frac{\partial^2}{\partial t^2},$$

$$\alpha_- = \frac{1-\mu}{2}, \quad \alpha_+ = \frac{1+\mu}{2}, \quad \beta^2 = \frac{h^2}{12a^2}, \quad I' = \frac{h^2}{12} = \beta^2 a^2,$$

$$\frac{\partial}{\partial s} = \frac{1}{a} \frac{\partial}{\partial \vartheta}, \quad s = a\vartheta$$

3.8.3.2 Special Cases

The rather extensive system of Eq. (3.203) permits the following conclusions:

- a) The system is symmetric as usual for wave equations derived by means of Hamilton's principle for stationary or uniformly moving media.

- b) As the wall thickness tends to zero $h \rightarrow 0$, $\beta = 0$ and $I' = 0$ and $\varphi_3 = -\partial\eta/\partial s$ as well as $\varphi_z = -\partial\eta/\partial z$. Thence, Eq. (3.203) turns into the membrane equation [3.18].

$$\begin{aligned} & \left[-\frac{\partial^2}{\partial s^2} - \frac{1-\mu}{2} \frac{\partial^2}{\partial z^2} + \frac{1}{c_{LI}^2} \frac{\partial^2}{\partial t^2} \right] \xi_M - \frac{1+\mu}{2} \frac{\partial^2 \zeta_M}{\partial s \partial z} - \frac{1}{a} \frac{\partial \eta}{\partial s} = 0, \\ & -\frac{1+\mu}{2} \frac{\partial^2 \xi_M}{\partial s \partial z} + \left[-\frac{\partial^2}{\partial z^2} - \frac{1-\mu}{2} \frac{\partial^2}{\partial s^2} + \frac{1}{c_{LI}^2} \frac{\partial^2}{\partial t^2} \right] \zeta_M - \frac{\mu}{a} \frac{\partial \eta}{\partial z} = 0, \quad (3.204a) \\ & \frac{1}{a} \frac{\partial \xi_M}{\partial s} + \frac{\mu}{a} \frac{\partial \zeta_M}{\partial z} + \left[\frac{1}{a^2} + \frac{1}{c_{LI}^2} \frac{\partial^2}{\partial t^2} \right] \eta = \frac{p_B (1-\mu^2)}{Eh}, \end{aligned}$$

which is fully valid for numerous applications.

- c) When the radius grows large i.e., $a \rightarrow \infty$, all terms involving $1/a$ and β disappears. The remaining expressions are identical to those for in-plane waves (3.168b) and the Mindlin-Timoshenko bending wave description (3.195).
- d) Upon approximating $h/a \approx 0$ in Eq. (3.203) for non-vanishing h , all terms involving β and I'/a vanish while those with I' remains. If, in addition, the terms representing the rotational inertia i.e., $(I'/c_{LI}^2) \partial^2/\partial t^2$ as is the case for the simple bending theory, one obtains the “Donell-Mushtari equation” [3.19, 3.20]. It differs from Eq. (3.204a) merely in that the η term in the last relation takes the form

$$\left[\frac{1}{a^2} + I' \left(\frac{\partial^2}{\partial s^2} + \frac{\partial^2}{\partial z^2} \right) + \frac{1}{c_{LI}^2} \frac{\partial^2}{\partial t^2} \right] \eta. \quad (3.204b)$$

Thereby, is taken into account the bending of the cylinder wall.

- e) For a transition to a ring, $\partial/\partial z = 0$ is employed and c_{LI} as well as $E/(1-\eta^2)$ are replaced by c_{LII} and E respectively owing to the cross-sectional contraction in axial direction cf., Eq. (3.32) to (3.34). Thereby, two independent expressions result: Shear in axial direction

$$\frac{\partial^2 \zeta_M}{\partial s^2} - \frac{2}{(1-\mu)c_{LI}^2} \frac{\partial^2 \zeta_M}{\partial t^2} = \frac{\partial^2 \zeta_M}{\partial s^2} - \frac{1}{c_T^2} \frac{\partial^2 \zeta_M}{\partial t^2} = 0 \quad (3.204c)$$

and motion in tangential and radial directions

$$\begin{aligned} & \left[\frac{\partial^2}{\partial s^2} - \frac{1+\beta^2}{c_{LII}^2} \frac{\partial^2}{\partial t^2} \right] \xi_M - \left[\frac{1}{a} \frac{\partial}{\partial s} + \frac{I'}{ac_{LII}^2} \frac{\partial^3}{\partial s \partial t^2} \right] \eta = 0, \\ & \left[\frac{1}{a} \frac{\partial}{\partial s} + \frac{I'}{ac_{LII}^2} \frac{\partial^3}{\partial s \partial t^2} \right] \xi_M + \left[\frac{1}{a^2} + \beta^2 \left(\frac{1}{a} + a \frac{\partial^2}{\partial s^2} \right)^2 + \frac{1}{c_{LII}^2} \frac{\partial^2}{\partial t^2} - \frac{I'}{c_{LII}^2} \frac{\partial^4}{\partial s^2 \partial t^2} \right] \eta = \frac{P_B}{Eh}. \quad (3.204d) \end{aligned}$$

To arrive at these expressions, the last three equations in (3.203) are added to account for the rotational energy. Moreover, the approximation $\varphi_9 = -\partial\eta/\partial s$ is introduced as employed in simple bending theory.

- f) Besides the shell Eq. (3.203) presented and the simplified versions in Eqs. (3.204), the literature comprises a suite of other formulae, which differ in the terms involving β^2 [3.21]. As long as the wavelengths and the radius of curvature are larger than six times the shell thickness, however, no significant differences arise.

3.8.3.3 Phase Speeds

To better understand the shell equations it is suitable to consider their features for the special case of plane waves spiralling along a cylinder. It is thus assumed that the field variables $\xi, \eta, \zeta, p_B, \varphi_2$ and φ_9 take the form

$$\left(\hat{\xi}, \hat{\eta}, \hat{\zeta}, \hat{p}_B, \hat{\varphi}_z, \hat{\varphi}_9 \right) e^{-jk_z z} e^{jns/a} e^{j\omega t}. \quad (3.205)$$

Herein, index M is omitted for brevity. For an infinitely long cylinder, the associated waves propagate with the speed $c_z = \omega/kz$ in the axial direction and exhibit $2n$ nodes over the perimeter, see Fig. 3.32a. They can be imagined as screw-formed propagating disturbances of “threading” $\lambda_z = 2\pi/kz$. In the literature appears often $\cos ns/a$ or $\sin ns/a$ instead of $e^{jns/a}$ but also $\cos n\theta$ or $\sin n\theta$ for symmetric and antisymmetric problems. For the general case, however, the notation $e^{jns/a}$ is most suitable and for the dispersion diagrams and wave impedances this does not lead to any differences.

Upon inserting (3.205) in Eq. (3.203) and simultaneously letting $\varphi_9 = -\partial\eta/\partial s$ and $\varphi_z = -\partial\eta/\partial z$ as is customary in conjunction with simple bending theory, is obtained

$$\begin{pmatrix} a_{11} & -a_{12} & -ja_{13} \\ -a_{12} & a_{22} & -ja_{23} \\ ja_{13} & ja_{23} & a_{33} \end{pmatrix} \begin{pmatrix} \hat{\xi} \\ \hat{\zeta} \\ \hat{\eta} \end{pmatrix} = \begin{pmatrix} 0 \\ 0 \\ \hat{p}_B v / \omega^2 \rho h \end{pmatrix}. \quad (3.206a)$$

The manipulations required to arrive at this system of equations consists in differentiating the fourth equation with respect to s , the fifth with respect to z and adding the last three of the resulting expressions. In Eq. (3.206a),

$$\begin{aligned}
a_{11} &= n^2 + \alpha_- k_z^2 a^2 - v^2 + \beta^2 (\alpha_- k_z^2 a^2 - v^2), \\
a_{12} &= \alpha_+ n k_z a + \beta^2 \alpha_- n k_z a, \\
a_{13} &= n + \beta^2 n (2\alpha_- k_z^2 a^2 - v^2), \\
a_{22} &= k_z^2 a^2 + \alpha_- n^2 - v^2 + \beta^2 \alpha_- n^2, \\
a_{23} &= -\mu k_z a + 2\beta^2 \alpha_- n^2 k_z a,
\end{aligned} \tag{3.206b}$$

and

$$a_{33} = 1 - v^2 + \beta^2 \left[1 - 2n^2 - 2\mu k_z^2 a^2 + (k_z^2 a^2 + n^2 - v^2)(k_z^2 a^2 + n^2) \right].$$

In addition, $v = \omega a / c_{LI} = \omega / \omega_{ring}$, is a non-dimensional frequency based on the ring frequency $\omega_{ring} = c_{LI}/a = 2\pi f_{ring}$.

The determinant of (3.206a) is given by

$$\text{Det} = a_{33} (a_{11} a_{22} - a_{12}^2) - 2a_{12} a_{13} a_{23} - a_{11} a_{23}^2 - a_{22} a_{13}^2 \tag{3.206c}$$

and its vanishing furnishes the wave numbers of the free waves, which can exist in loss-free media also in the absence of excitation. With (3.206b) in (3.206c), a fourth-order polynomial in $(k_z a)^2$ is obtained. Accordingly, four free waves can exist at most at every frequency. At least one thereof, does not propagate implying an exponentially decaying nearfield. For the remaining three propagating waves, the dispersion diagram in Fig. 3.32 is obtained by equating (3.206c) to zero. Shown is the phase speed for the axial direction instead of the associated wavenumber for a Poisson's ratio of $\mu = 0.3$ and normalized with respect to c_{LI} . The following conclusions can be drawn from the curves.

- a) The branches denoted by T which come down from infinity at $v^2 = n^2(1-\mu)/2$ approach asymptotically $c_z = c_{LI} \sqrt{(1-\mu)/2}$. They correspond to pure transversal waves (no compression of the material, see Sect. 3.2.1).
- b) The branches denoted by L which come down from infinity at $v^2 = 1 + n^2$ approach asymptotically $c_z = c_{LI}$. They correspond to quasi-longitudinal waves (see Sect. 3.1.2).
- c) For low frequencies is obtained the relation

$$c_z = \sqrt[4]{\omega^2 a^2 / 2c_{LI}^2}$$

for $n = 1$. Since $a^2/2$ is the square of the radius of gyration of a thin-walled cylinder, this relation constitutes the flexural wave speed of a cylindrical shell vibrating as a beam.

- d) A fundamental role plays the non-dimensional frequency $v = 1$ i.e., the ring frequency $f_{ring} = c_{LI}/2\pi a$ where the cylinder perimeter equals one wavelength of the longitudinal wave.

- e) For $n = 0$ there exist at low frequencies longitudinal waves of speed $c_z = c_{L1} \sqrt{1 - \mu^2} = \sqrt{E/\rho}$ and torsional waves of speed $c_z = c_{L1} \sqrt{1 - \mu/2} = \sqrt{G/\rho}$. In the first case, a volume element of the cylinder wall moves in radial direction – breathing mode – neglecting the comparatively much smaller cross-contraction. In the second, the motion is torsional.

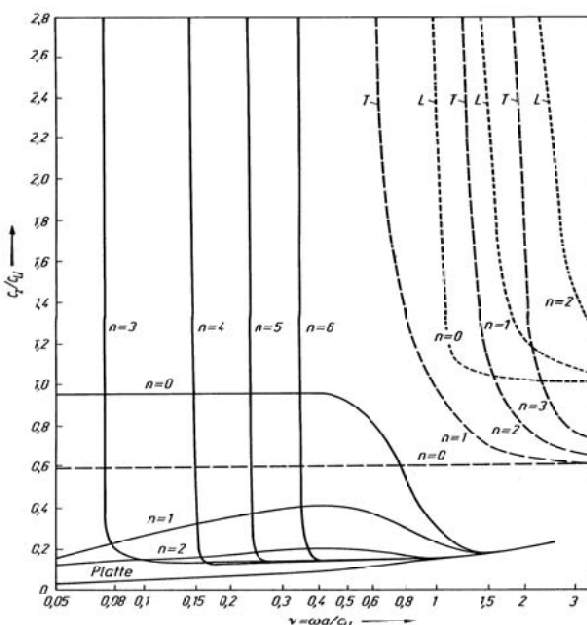
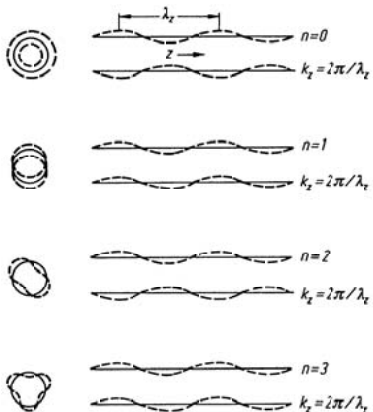


Fig. 3.32. Spatial displacements of modes $n = 0, 1, 2, 3$ and dispersion diagram according to (3.206c) for $a = 15$ and $\mu = 0.3$

- f) For $n \geq 2$, the characteristic Eq. (3.206) yields three groups of dispersion curves. The first two – long and short dashed curves in Fig. 3.32 – were discussed in a) and b). The third group – solid curves – is only possible above the associated ring-resonance frequencies, see Eq. (3.210c). All the solid curves approach that of the bending wave speed of a plate of thickness h – also drawn solid – at high frequencies.
- g) At frequencies above $v > 2$, the dispersion curves are practically identical to those of a flat plate of thickness h and width πa exhibiting bending and in-plane waves. The boundary condition for the strip are those shown in Fig. 3.15 top left or bottom right. In this frequency range, therefore, the cylinder wall can be treated as a flat plate. The dispersion curves obtained from the characteristic Eq. (3.206) are corroborated by experimental results.

3.8.3.4 Wave Impedances

In addition to the phase speeds, Eq. (3.206a) also furnishes the so-called wave impedance, cf. Sect. 5.4. It is defined by

$$Z_{\sim} = \frac{\hat{P}_B}{\hat{v}_r} = \frac{\hat{P}_B}{j\omega\hat{\eta}} \quad (3.207)$$

i.e., the ratio of the exciting pressure amplitude \hat{P}_B to the resulting radial velocity amplitude \hat{v}_r for an infinitely extended cylinder. For discrete n , Eq. (3.206a) gives

$$Z_{\sim n} = \frac{\rho h}{jv^2} \left[a_{33} - \frac{2a_{12}a_{13}a_{23} + a_{11}a_{23}^2 + a_{22}a_{13}^2}{a_{11}a_{22} - a_{12}^2} \right], \quad (3.208)$$

from which a good approximation is found to be [3.21]

$$Z_{\sim n} \approx \frac{\omega\rho h}{jv^2} \left\{ -v^2 + \beta^2 \left[(n^2 + k_z^2 a^2)^2 - \frac{n^2(4-\mu)-2-\mu}{2(1-\mu)} \right] + \left[\frac{(1-\mu^2)}{2} \left[\frac{1-\mu}{2} k_z^2 a^2 - v^2 \right] k_z^2 a^2 - \left[\frac{1-\mu}{2} (k_z^2 a^2 + n^2) - v^2 \right] v^2 \right] \right\}. \quad (3.209)$$

The wave impedance indicates whether a cylinder will be strongly or weakly excited by a pressure of the form (3.205); small and large $Z_{\sim n}$ respectively. From $Z_{\sim n} = 0$, the wavenumbers of the free waves can be de-

terminated and, in turn, the dispersion curves can be generated by using $c_x / c_{LI} = v / k_z a$ for given values of n .

3.8.3.5 Resonance Frequencies

The resonance frequencies of a circular ring can be obtained from Eqs. (3.204c, d) by setting $p_B = 0$ and employing the solution given by (3.205). From Eq. (3.204c) it is found that

$$-\frac{n^2}{a^2} + \frac{\omega^2}{c_T^2} = 0,$$

giving the possible resonance frequencies for the particle motion in axial direction

$$\omega_{n,III}^2 = n^2 c_T^2 / a^2. \quad (3.210a)$$

For the other, important motion components, the dispersion equation is obtained in a similar manner as (3.206). It is sufficient to put $k_z = 0$ since no z dependence exists. Some further manipulations yield the characteristic equation

$$v^4 \left[1 + \beta^2 (1 + n^2) \right] - v^2 \left[n^2 + 1 - 2\beta (n^2 - 1)^2 \right] + n^2 \beta^2 (1 - n^2)^2 = 0.$$

By focussing on thin-walled cylinders ($\beta^2 \ll 1$), the approximations

$$\begin{aligned} v_{nl}^2 &= \frac{\omega_{nl}^2}{c_{LI}^2} a^2 \approx n^2 + 1, \\ v_{nll}^2 &= \frac{\omega_{nll}^2}{c_{LI}^2} a^2 \approx \beta^2 \frac{n^2 (n^2 - 1)^2}{n^2 + 1} \end{aligned} \quad (3.210b, c)$$

result for the quasi-longitudinal and flexural motion respectively. Thus, the resonances are determined.

It should be pointed out, however, that the ring resonances are not accurately predicted by means of the approximation for the wave impedance in (3.209) for $k_z = 0$. The error amounts to 14 % for $n = 2$, 4 % for $n = 3$, 2 % for $n = 4$ and is smaller than 1.5 % when $n \geq 5$.

As for slender beams, the calculation of the eigen-frequencies of a cylindrical tube of length l_z can be readily made only for two ideal boundary conditions. This means that the eigen-functions

$$\begin{aligned}\xi(\vartheta, z) &= \xi_{m,n} \sin \frac{m\pi z}{l_z} \sin n\vartheta, \\ \eta(\vartheta, z) &= \eta_{m,n} \sin \frac{m\pi z}{l_z} \cos n\vartheta, \\ \zeta(\vartheta, z) &= \zeta_{m,n} \cos \frac{m\pi z}{l_z} \cos n\vartheta,\end{aligned}\quad (3.211)$$

apply or the corresponding ones in which the terms $\cos(m\pi z/l_z)$ and $\sin(m\pi z/l_z)$ are interchanged.

The eigen-functions in (3.211) imply that the tube wall at $x = 0$ and $x = l_z$ are simply supported and, simultaneously the axial motion is unconstrained, see Fig. 3.15, top-left. With the sine and cosine functions interchanged the eigen-functions satisfy guided tube ends and blocked with respect to axial motion $\zeta(\varphi, 0) = \zeta(\varphi, l_z) = 0$, see Fig. 3.15, bottom-right.

A similar analysis as that of the preceding section can be used also in this case to determine the resonance frequencies. The only modification necessary is that $k_z a$ is replaced by $m\pi a/l_z$. The resonance frequencies then correspond to those values of v for which the wave impedance in Eq. (3.208) vanishes. This means that the resonance frequencies correspond to the intersections of the dispersion curves c_z/c_{LI} in Fig. 3.32 with curves $v l_z/m\pi a$ since

$$\frac{c_z}{c_{LI}} = \frac{\omega a}{c_{LI} m\pi a} \frac{l_z}{m\pi a} \Leftrightarrow m\pi = \frac{\omega}{c_z} l_z = k_z l_z \Leftrightarrow m\lambda_z = 2l_z$$

at these points. For the flexural motion of primary interest, the resonance frequencies are closely approximated by [3.22]

$$\begin{aligned}v_{n,m}^2 &= \frac{\omega_{n,m}^2 a^2}{c_{LI}} \approx \frac{(m\pi a/l_z)^4}{\left[(m\pi a/l_z)^2 + n^2 \right]^2} + \beta^2 \left\{ \left[(m\pi a/l_z)^2 + n^2 \right]^2 \right. \\ &\quad \left. - \frac{n^2(4-\mu)-2-\mu}{2(1-\mu)} \right\},\end{aligned}\quad (3.212a)$$

whereas for the other types of motion,

$$\begin{aligned}v_{n,m}^2 &\approx \frac{1-\mu}{2} \left[(m\pi a/l_z)^2 + n^2 \right], \\ v_{n,m}^2 &\approx 1 + \left[(m\pi a/l_z)^2 + n^2 \right].\end{aligned}\quad (3.212b)$$

The formulae in (3.212) encompass for $n = 0$ the very important ring frequency $v = 1$ as $m\pi a/l_z$ tends to zero. Other expressions for resonance fre-

quencies as well as comparison of different shell equations can be found in [3.21].

From the results of a few calculated examples, it is clear that the resonances for long tubes ($l_z > 10 a$) tend to occur just above the corresponding ring frequencies of Eq. (3.210b). Additionally, it is realized that $\omega_{n1,m} > \omega_{n2,m}$ even if $n_1 < n_2$. Thus, it is possible that two modes of the same number m of nodes in axial direction but of differing nodes in circumferential exhibit the highest resonance for the smaller n .

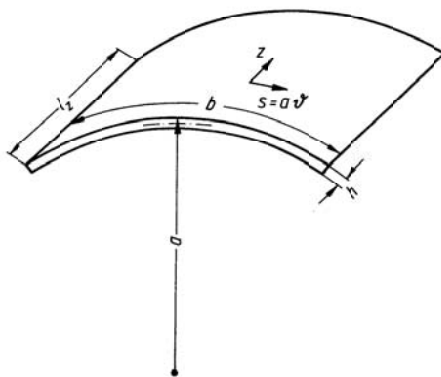


Fig. 3.33. Notations for a cylinder segment

Equations (3.212a, b) also apply for segments of cylindrical shells owing to the fact that the basic differential equations are the same. For a cylindrical segment of arc and edge lengths b and l_z as sketched in Fig. 3.33, the eigen-functions

$$\begin{aligned}\xi &= \xi_{m1,m2} \sin \frac{m_1 \pi z}{l_z} \sin \frac{m_2 \pi s}{b}, \\ \eta &= \eta_{m1,m2} \sin \frac{m_1 \pi z}{l_z} \cos \frac{m_2 \pi s}{b}, \\ \zeta &= \zeta_{m1,m2} \cos \frac{m_1 \pi z}{l_z} \sin \frac{m_2 \pi s}{b},\end{aligned}\tag{3.213}$$

apply for $m_{1,2} = 1, 2, 3, \dots$ provided that the boundary conditions fulfil

$$\begin{aligned}\xi = \eta = 0, \quad \frac{\partial^2 \xi}{\partial z^2} = \frac{\partial^2 \eta}{\partial z^2} = 0, \quad \frac{\partial \zeta}{\partial z} = 0; \quad z = 0, l_z, \\ \xi = \eta = 0, \quad \frac{\partial^2 \xi}{\partial s^2} = \frac{\partial^2 \eta}{\partial s^2} = 0, \quad \frac{\partial \zeta}{\partial s} = 0; \quad s = 0, b.\end{aligned}$$

This means that the supports present no moments with respect to radial and axial motions and no forces to the tangential. It is readily verified that the eigen-functions in (3.213) satisfy the spatial dependencies of the cylindrical shell equations and lead to a characteristic equation of the same form as that for a complete cylinder, the only alteration being that n is replaced by $m_2\pi a/b$ and m by m_1 .

It is easy to demonstrate that as the radius of curvature tends to infinity, $a \rightarrow \infty$, the expressions for flexural as well as shear and extensional resonances given above collapse into those of a flat plate.

Unfortunately, no simple expressions are available for other boundary conditions but it can be mentioned that the resonance frequencies rise considerably as the tangential motion at edges $x = 0$ and $x = b$ are restrained [3.23]. In this context, it is of interest to consider also doubly curved shells. Without derivation [3.24], are given the resonance frequencies for bending waves for a rectangular patch with radii of curvature a_1 and a_2 having simple supports along all edges,

$$\omega_{m_1, m_2}^2 \approx c_{LI}^2 \left\{ \frac{\left[\frac{1}{a_1} \left(\frac{m_1 \pi}{l_z} \right)^2 + \frac{1}{a_2} \left(\frac{m_2 \pi}{b} \right)^2 \right]^2}{\left[\left(\frac{m_1 \pi}{l_z} \right)^2 + \left(\frac{m_2 \pi}{b} \right)^2 \right]^2} + \frac{h^2}{12} \left[\left(\frac{m_1 \pi}{l_z} \right)^2 + \left(\frac{m_2 \pi}{b} \right)^2 \right]^2 \right\}. \quad (3.214)$$

3.9 Structure-Borne Sound Intensity

3.9.1 Fundamental Equations

The well-thumbed definition of the intensity vector for air-borne sound can readily be extended to the structure-borne sound case [3.25-3.27],

$$\overline{\mathbf{J}_{air}} = \overline{p \cdot \mathbf{v}} = (\overline{pv_x}, \overline{pv_y}, \overline{pv_z}). \quad (3.215)$$

In the structure-borne case, however, it is necessary to take into account that the dynamic quantities are not represented by the pressure but the

stress tensor. In Cartesian co-ordinates, therefore, the general definition of the three components of the intensity vector reads

$$\begin{aligned} J_x &= -\left[\overline{\sigma_x v_x} + \overline{\tau_{xy} v_y} + \overline{\tau_{xz} v_z}\right] \\ J_y &= -\left[\overline{\tau_{xy} v_x} + \overline{\sigma_y v_y} + \overline{\tau_{yz} v_z}\right] \\ J_z &= -\left[\overline{\tau_{xz} v_x} + \overline{\tau_{yz} v_y} + \overline{\sigma_z v_z}\right]. \end{aligned} \quad (3.216)$$

In this text only the temporal average of the stress and velocity product will be considered and referred to as the intensity. Instantaneous intensity as well as the imaginary intensity will not be treated [3.28, 3.29].

As can be observed, the intensity is formed by the scalar product of the force acting on a surface element and the velocity at that surface. The overbar denotes that each term is temporally averaged. The negative sign in front stems from the fact that σ and τ are defined positive as extensional stresses and hence act like elemental forces opposite a positive velocity cf., Eqs. (3.27), (3.28) and (3.35).

A special case of Eq. (3.216) was treated previously in Sect. 3.1.1 whereby the intensity was given in a pure longitudinal wave, for which $v_y = v_z = 0$ and $J_x = -\sigma_x v_x$. Also shown in this context was that the intensity equals the power transmitted through a surface element. This statement also holds in the three-dimensional case for the separate directions. It should be noted, however, that the vector resulting from the components J_x, J_y, J_z , not necessarily is perpendicular to the wave front, in contrast to the analogous airborne intensity cf., [3.29].

3.9.2 Intensity in this Plates

Due to the severe difficulties to measure stresses and velocities interior to a structure without detrimentally disturbing the field, the following treatise is confined to thin plates and thin-walled shells for which the measurements can be undertaken comparatively easy at the surfaces. The analysis, moreover, is confined to the x -component of the intensity since the y -component vanishes and the z -component readily is obtained from a replacement of x by z for homogeneous media. The notation is the same as in Sect. 3.8.2 and is found in Fig. 3.29 as well as in Eqs. (3.189-3.190d).

Upon substituting these expressions into Eq. (3.216) is obtained

$$\begin{aligned} -J_x &= \frac{E}{1-\mu^2} \left(\frac{\partial \xi_M}{\partial x} + y \frac{\partial \varphi_x}{\partial x} + \mu \frac{\partial \zeta_M}{\partial z} + \mu y \frac{\partial \varphi_z}{\partial z} \right) (\dot{\xi}_M + y \dot{\varphi}_x) \\ &\quad + G \left[\left(\varphi_x + \frac{\partial \eta}{\partial x} \right) \dot{\eta} + \left(\frac{\partial \xi_M}{\partial z} + y \frac{\partial \varphi_x}{\partial z} + \frac{\partial \zeta_M}{\partial x} + y \frac{\partial \varphi_z}{\partial x} \right) (\dot{\zeta}_M + y \dot{\varphi}_z) \right]. \end{aligned} \quad (3.217)$$

Herein, the differentiation with respect to time is denoted by a dot i.e., $v_x = \dot{\xi}_M + y \dot{\varphi}_x$, $v_y = \dot{\eta}$ and $v_z = \dot{\zeta}_M + y \dot{\varphi}_z$. Equation (3.217) furnishes the intensity in a plane $y = \text{const}$. Of greater practical interest, however, is the cross-sectionally integrated power per unit width,

$$W'_x = - \int_{-h/2}^{h/2} J_x dy. \quad (3.218)$$

With Eq. (3.217) inserted in (3.218), the power per unit width becomes

$$\begin{aligned} \frac{W'_x}{h} &= \frac{E}{1-\mu^2} \overline{\left(\frac{\partial \xi_M}{\partial x} + \mu \frac{\partial \zeta_M}{\partial z} \right) \dot{\xi}_M} + G \overline{\left(\frac{\partial \xi_M}{\partial z} + \frac{\partial \zeta_M}{\partial x} \right) \dot{\zeta}_M} \\ &\quad + \frac{EI'}{1-\mu^2} \overline{\left(\frac{\partial \varphi_x}{\partial x} + \mu \frac{\partial \varphi_z}{\partial z} \right) \dot{\varphi}_x} + G \overline{\left(\varphi_x + \frac{\partial \eta}{\partial x} \right) \dot{\eta}} + GI \overline{\left(\frac{\partial \varphi_x}{\partial z} + \frac{\partial \varphi_z}{\partial x} \right) \dot{\varphi}_z} \end{aligned} \quad (3.219)$$

In this expression $I' = h^2/12$ is the radius of gyration squared and stems from the integration of y^2 -terms whereas all y -terms vanish.

The terms of the first line in Eq. (3.219) both depend only on the motion of the neutral layer of the structure and thus represent the power carried by the in-plane waves cf., Sect. 3.7.4.1. In contrast, those of the second line are all associated with the flexural motion and can be rewritten such that only the translatory motion perpendicular to the surface η appears. Also, it is suitable to alter the factor $G(\varphi_x + \partial\eta/\partial x)$ to improve on its present appearance as $\infty \cdot 0$.

Upon back-tracking this expression it is seen that

$$\begin{aligned} G \overline{\left(\varphi_x + \frac{\partial \eta}{\partial x} \right) \dot{\eta}} &= \frac{1}{h} \int \overline{\tau_{xy} \dot{\eta}} dy = - \frac{\overline{\dot{\eta}}}{h} \int \overline{\tau_{xy}} dy \\ &= - \frac{1}{h} \overline{\dot{\eta} Q_x} = - \frac{B'}{h} \frac{\partial}{\partial x} \overline{\left(\frac{\partial^2 \eta}{\partial x^2} + \frac{\partial^2 \eta}{\partial z^2} \right)} \dot{\eta}. \end{aligned} \quad (3.220)$$

In this, the fact is used that the cross-sectionally integrated shear stress equals the total force at the cross-section Q_x given by Eq. (3.184e), see Fig. 3.27. Another possibility to arrive at this form would be to rewrite the first line in Eq.(3.193) as

$$Gh\left(\varphi_x + \frac{\partial \eta}{\partial x}\right) = \left(GI \frac{\partial^2}{\partial z^2} + B' \frac{\partial^2}{\partial x^2}\right)\varphi_x + \frac{1+\mu}{2} B' \frac{\partial^2 \varphi_z}{\partial x \partial z} - \rho I \ddot{\varphi}_z \quad (3.221)$$

With the approximations $\varphi_x = -\partial \eta / \partial x$ and $\varphi_z = -\partial \eta / \partial z$, applicable for thin plates, the right hand side of (3.221) turns into (3.220) with the negligible difference of the small term $\rho I \ddot{\varphi}_x$ associated with the approximation, and Eq. (3.219) finally becomes [3.26]

$$\begin{aligned} \frac{W'_x}{h} &= \frac{E}{1-\mu^2} \left(\frac{\partial \xi_M}{\partial x} + \mu \frac{\partial \zeta_M}{\partial z} \right) \dot{\xi}_M + G \left(\frac{\partial \xi_M}{\partial z} + \frac{\partial \zeta_M}{\partial x} \right) \dot{\zeta}_M \\ &+ \frac{B'}{h} \left[\left(\frac{\partial^2 \eta}{\partial x^2} + \mu \frac{\partial^2 \eta}{\partial z^2} \right) \frac{\partial \dot{\eta}}{\partial x} + (1-\mu) \frac{\partial^2 \eta}{\partial x \partial z} \frac{\partial \dot{\eta}}{\partial z} - \frac{\partial}{\partial x} \left(\frac{\partial^2 \eta}{\partial x^2} + \frac{\partial^2 \eta}{\partial z^2} \right) \dot{\eta} \right] \end{aligned} \quad (3.222a)$$

For the one-dimensional case and pure bending, it is readily found that

$$W_{xB} = B \left(\frac{\partial^2 \eta}{\partial x^2} \frac{\partial \dot{\eta}}{\partial x} - \frac{\partial^3 \eta}{\partial x^3} \dot{\eta} \right)$$

is in agreement with the previous results in (3.91) or (3.91a).

Equation (3.222a) demonstrates that measurement of structure-borne sound power is not so simple even for thin plates. This is due to the averaging of lateral motions ξ , ζ and their derivatives measured at the plate surfaces $y = \pm h/2$, which yield the quantities ξ_M and ζ_M . Moreover is required the translation η to its third order spatial derivative with a high degree of accuracy cf., Figs. 8.42 and 8.43.

If bending wave nearfields are disregarded, then

$$\frac{\partial^2 \eta}{\partial x^2} = -k_B^2 \eta = -\omega \sqrt{\frac{m'}{B}} \eta \quad (3.223a)$$

applies in the one-dimensional case, for regions more than half a wavelength away from structural discontinuities and excitations. This means that (3.222b) becomes

$$W_{xB} = -\omega \sqrt{m' B} \left(\eta \frac{\partial \dot{\eta}}{\partial x} - \frac{\partial \eta}{\partial x} \dot{\eta} \right), \quad (3.223b)$$

which can be further simplified by making use of the chain rule

$$\frac{\partial}{\partial t} \left(\eta \frac{\partial \eta}{\partial x} \right) = \frac{\partial \eta}{\partial x} \frac{\partial}{\partial t} + \eta \frac{\partial^2}{\partial x \partial t} = \dot{\eta} \frac{\partial \eta}{\partial x} + \eta \frac{\partial \dot{\eta}}{\partial x} \quad (3.223c)$$

and observing that every arbitrary function of time $g(t)$, oscillating around zero will vanish when averaged,

$$\overline{\frac{\partial}{\partial t} g(t)} = \frac{1}{T} \int_{t_1}^{t_2} \frac{\partial}{\partial t} g(t) dt = \frac{1}{T} [g(t_2) - g(t_1)] \approx 0. \quad (3.223d)$$

Implicit is that the average is taken over a long time. With this relation, then

$$\overline{\frac{\partial}{\partial t} \left(\eta \frac{\partial \eta}{\partial x} \right)} = 0 = \overline{\dot{\eta} \frac{\partial \eta}{\partial x}} + \eta \overline{\frac{\partial \dot{\eta}}{\partial x}} \Leftrightarrow \overline{\dot{\eta} \frac{\partial \eta}{\partial x}} = -\eta \overline{\frac{\partial \dot{\eta}}{\partial x}} \quad (3.223e)$$

From Eq. (3.223b) [3.25] therefore

$$W_{xB} = 2\omega \sqrt{m'B} \overline{\frac{\partial \eta}{\partial x} \dot{\eta}} = -2\omega \sqrt{m'B} \overline{\frac{\partial \dot{\eta}}{\partial x} \eta} \quad (3.223f)$$

applies for the farfield in the one-dimensional case.

Upon employing two accelerometers with identical amplitude and phase characteristics, placed a small distance Δx apart, a good approximation for the power transmitted is given by

$$W_{xB} = -2\omega \sqrt{m'B} \frac{\eta_1 + \eta_2}{2} \frac{1}{\Delta x} \overline{\int_{-\infty}^t (a_2 - a_1) d\tau}, \quad (3.224)$$

provided that $\Delta x \ll \lambda_B/10$. Herein, η_1, η_2 are the measured displacements and a_1, a_2 the accelerations. Use is also made of the approximation

$$\frac{\partial \dot{\eta}}{\partial x} \approx \frac{\dot{\eta}_2 - \dot{\eta}_1}{\Delta x}, \quad \dot{\eta} = v = \int_0^t a d\tau.$$

For a narrow frequency band, $\eta \approx -a/\omega^2$, such that

$$W_{xB} \approx \frac{\sqrt{m'B}}{\omega} \frac{1}{\Delta x} \overline{\int_{-\infty}^t (a_1 + a_2) d\tau} \quad (3.224a)$$

With the exception of the factor in front, this is the same formula as is used in the airborne sound case, with the acceleration substituted instead of pressure. Outside regions with significant, nearfields, it is thus possible to assess the power carried by bending waves applying the same signal processing equipment as is used for airborne sound intensity. Also, as in the airborne sound intensity context [3.28], it is finally possible to put

$$\int_{-\infty}^t a_1 d\tau = g_1(t) \Rightarrow a_1 = \frac{\partial g}{\partial t},$$

which means that

$$\begin{aligned}
 W_{xB} &= \frac{\sqrt{m'B}}{\omega\Delta x} \left[\overline{\frac{\partial g_1}{\partial t} g_2} + \overline{\frac{\partial g_2}{\partial t} g_1} - \overline{\frac{\partial g_1}{\partial t} g_1} - \overline{\frac{\partial g_2}{\partial t} g_2} \right] \\
 &= \frac{\sqrt{m'B}}{\omega\Delta x} \left[2 \overline{\frac{\partial g_1}{\partial t} g_2} - \overline{\frac{\partial(g_1 g_2)}{\partial t}} + \frac{1}{2} \overline{\frac{\partial g_2^2}{\partial t}} - \frac{1}{2} \overline{\frac{\partial g_1^2}{\partial t}} \right] \\
 &= 2 \frac{\sqrt{m'B}}{\omega\Delta x} a_1 \int_{-\infty}^t a_2 d\tau.
 \end{aligned} \tag{3.224b}$$

As in Eq. (3.223d), the averaged time derivatives cancel.

From a transition to power-spectral densities, it is possible to show that the power spectrum W_{xB} (ω) is proportional to the imaginary part of the cross-power spectrum between the two accelerations. This is most readily demonstrated in that a single frequency is considered i.e.,

$$\begin{aligned}
 a_1 &= \operatorname{Re} [\hat{a}_1 e^{j\omega t}] = \frac{1}{2} [\hat{a}_1 e^{j\omega t} + a_1^* e^{-j\omega t}], \\
 a_2 &= \operatorname{Re} [\hat{a}_2 e^{j\omega t}] = \frac{1}{2} [\hat{a}_2 e^{j\omega t} + a_2^* e^{-j\omega t}].
 \end{aligned}$$

Substitution into Eq. (3.224a) yields

$$W_{xB}(\omega) = \frac{\sqrt{m'B}}{\omega\Delta x} |\hat{a}_1| |\hat{a}_2| \sin(\varphi_2 - \varphi_1), \tag{3.224c}$$

in which $(\varphi_2 - \varphi_1)$ is the usually small phase difference between the two accelerations.

3.9.3 Power Transmission in Thin-Walled Cylindrical Shells

In cylindrical co-ordinates, the general expressions for the components of the intensity vector read

$$\begin{aligned}
 J_\theta &= - \left[\overline{\sigma_\theta \dot{\xi}} + \overline{\tau_{r\theta} \dot{\eta}} + \overline{\tau_{z\theta} \dot{\zeta}} \right], \\
 J_r &= - \left[\overline{\tau_{r\theta} \dot{\xi}} + \overline{\sigma_r \dot{\eta}} + \overline{\tau_{rz} \dot{\zeta}} \right], \\
 J_z &= - \left[\overline{\tau_{z\theta} \dot{\xi}} + \overline{\tau_{rz} \dot{\eta}} + \overline{\sigma_z \dot{\zeta}} \right],
 \end{aligned} \tag{3.225}$$

and are analogous to those in Eq. (3.216). The following analysis is confined to thin-walled cylinders, free from excitations on the cylinder wall. For such cases, there is no power transmitted in the radial direction i.e.,

$J_r = 0$. The stress and strain relations in Eqs. (3.198) to (3.201), moreover, can also be employed in this context owing to the vanishing radial stress, $\sigma_r = 0$. With those expressions introduced in (3.225), some manipulations yield the principal power transmission in axial direction as

$$\begin{aligned} \frac{W'_z}{h} &= \frac{E}{1-\mu} \overline{\left(\frac{\partial \zeta_M}{\partial z} + \mu \frac{\partial \xi_M}{\partial s} \right) \dot{\zeta}_M} + G \overline{\left((1+\beta^2) \frac{\partial \xi_M}{\partial z} + (1-\beta^2) \frac{\partial \zeta_M}{\partial s} \right) \dot{\xi}_M} \\ &+ \frac{EI'}{1-\mu^2} \overline{\left(\frac{\partial \varphi_z}{\partial z} + \mu \frac{\partial \varphi_\theta}{\partial s} \right) \dot{\varphi}_z} + G \left(\varphi_z + \frac{\partial \eta}{\partial z} \right) \dot{\eta} + GI' \overline{\left(\frac{\partial \varphi_z}{\partial s} + \frac{\partial \varphi_\theta}{\partial z} \right) \dot{\varphi}_\theta} \\ &+ \frac{EI'}{1-\mu^2} \frac{\mu}{a} \overline{\left(\eta \dot{\xi}_M - \frac{I'}{a} \eta \dot{\varphi}_z \right)} \\ &+ \frac{GI'}{a} \left[\overline{\left(\frac{\partial \varphi_z}{\partial s} + \frac{\partial \varphi_\theta}{\partial z} \right) \dot{\xi}_M} - \overline{\left(\frac{\partial \zeta_M}{\partial s} - \frac{\partial \xi_M}{\partial z} \right) \dot{\varphi}_\theta} \right]. \end{aligned} \quad (3.226)$$

The first line of this expression describes the in-plane intensity in the absence of radial motion of the cylinder. In the second, is contained that associated with bending motion. This is clearly seen from a comparison of Eqs. (3.226) and (3.219) whereby it is taken into account that the power in z -direction is considered in the latter. The last two lines, finally, represent mixed terms which vanish as the radius a tends to infinity, $a \rightarrow \infty$.

To proceed with the analysis, the cross-sectional force is in this case obtained from the equation of motion for the system i.e., from (3.203). By calculating $G(\varphi_z + \partial\eta/\partial z)$ from the last of the expressions and subsequently introducing the approximations $\varphi_z = -\partial\eta/\partial z$ and $\varphi_\theta = -\partial\eta/\partial s$, the power transmitted is obtained as

$$\begin{aligned} \frac{W'_z}{h} &= \frac{E}{1-\mu^2} \left[\overline{\frac{\partial \zeta_M}{\partial z} \dot{\zeta}_M} + \mu \overline{\frac{\partial \xi_M}{\partial s} \dot{\zeta}_M} \right] + G \left[\overline{\frac{\partial \xi_M}{\partial z} \dot{\xi}_M} + \overline{\frac{\partial \zeta_M}{\partial s} \dot{\xi}_M} \right] \\ &+ \frac{EI'}{1-\mu^2} \left[\overline{\left(\frac{\partial^2 \eta}{\partial z^2} + \mu \frac{\partial^2 \eta}{\partial s^2} \right) \dot{\eta}} - \overline{\left(\frac{\partial \nabla^2 \eta}{\partial z} - \frac{1}{c_{LI}^2} \frac{\partial^3 \eta}{\partial z \partial t^2} \right) \dot{\eta}} + (1-\mu) \overline{\frac{\partial^2 \eta}{\partial s \partial z} \frac{\partial \dot{\eta}}{\partial s}} \right] \\ &+ \frac{E}{1-\mu^2} \frac{\mu}{a} \left[\overline{\eta \dot{\zeta}_M} + \frac{I'}{a} \overline{2\eta \frac{\partial \dot{\eta}}{\partial z}} \right] + \frac{GI'}{a} \left[\overline{\frac{\partial \zeta_M}{\partial s} \frac{\partial \dot{\eta}}{\partial s}} - \overline{\frac{\partial^2 \zeta_M}{\partial s^2} \dot{\eta}} \right]. \end{aligned} \quad (3.227)$$

Practical measurements according to this expression are highly complicated and time-consuming. Most often, therefore, the simplified one-dimensional formulae (3.224) to (3.224c) are employed to assess the order of magnitude and, above all, the direction of the intensity.

As in the case of airborne sound intensity, structure-borne intensity due to multiple tonal coherent sources must be treated cautiously. Any phase

shift between the sources may result in highly differing directivity of the intensity.

References

- [3.1] Morse P.M., 1948. Vibration and sound, Ch. 4. McGraw-Hill, New York NY
- [3.2] Rayleigh J.W.S., 1885. On waves propagated along the plane surface of an elastic solid. Proc. Mathematical Society London, 17, 4-11
- [3.3] Schoch A., 1950. Periodische Wellen im schubspannungsfreien planparallelen Schichten. Ergebnisse der exakten Naturwissenschaften, 23, p. 172
- [3.4] Achenbach J.D., 1975. Wave propagation in elastic solids. North-Holland, Amsterdam
- [3.5] Naake H.J. and Tamm K., 1958. Sound propagation in plates and rods of rubber-elastic materials. Acustica, 8, p. 65
- [3.6] Götz J., 1943. Über den Schalldurchgang durch Metallplatten in Flüssigkeiten bei schrägem Einfall einer Welle. Akustische Zeitschrift, 8, p. 145
- [3.7] Firestone F.A., 1948. Tricks with the supersonic reflectoscope. Non-destructive testing, 7, p. 5
- [3.8] Tamm K. and Weiss O., 1959. Untersuchungen über periodische Wellen, exponentielle und komplexe Nahfelder im begrenzten Festkörper. Acustica, 9, p. 275
- [3.9] Epstein P.S., 1942. On the theory of elastic vibrations in plates and shells. Journal of Mathematics and Physics, 21, p. 198
- [3.10] Huber M.T., 1914. Die Grundlagen einer rationellen Berechnung der kreuzweise bewehrten Eisenbetonplatte. Zeitschrift des Österreichischen Ingenieur- und Architekten-Vereins, 30, p. 557
- [3.11] Hearmon R.F.S. and Adams E.H., 1952. The bending and twisting of an isotropic plates. British Journal of Applied Physics, 3, p. 155
- [3.12] Timoshenko S.P. and Woinowsky-Krieger S., 1959. Theory of plates and shells (2nd ed.), Ch. 11. McGraw-Hill, Auckland
- [3.13] Heckl M., 1960. Untersuchungen an orthotropen Platten. Acustica, 10, 109-115
- [3.14] Heckl M., 1990. Einfache Anwendung des Hamiltonschen Prinzips bei Körperschallproblemen. Acustica, 72, 189-196
- [3.15] Mindlin R.D., 1951. Influence of rotatory inertia and shear on flexural motions of isotropic, elastic plates. Journal of Applied Mechanics, 18, p. 155
- [3.16] Junger M.L. and Feit D., 1972. Sound structures and their interaction, Ch. 9. MIT Press, Cambridge MA
- [3.17] Love A.E.H., 1948. A treatise on the mathematical theory of elasticity, Ch. XXIII. Dover Publications, New York NY
- [3.18] Rayleigh J.W.S., 1945. Theory of sound (2nd ed.), Vol. 1, §235e. Dover Publications, New York NY
- [3.19] Cremer L., 1955. Theorie der Luftschalldämmung zylindrischer Schalen. Acustica, 5, p. 245

- [3.20] Donell L.H., 1939. Discussion of thin shell theory. Proc. 5th International Congress on Applied Mechanics, p. 66
- [3.21] Leissa A.W., 1973. Vibration of shells. NASA-SP 288
- [3.22] Heckl M., 1962. Vibrations of point-driven cylindrical shells. Journal of the Acoustical Society of America, 34, 1553-1557
- [3.23] Cremer L., 1984. Physics of the violin, §3.3. MIT Press, Cambridge MA
- [3.24] Reissner E., 1955. On transverse vibration of thin, shallow elastic shells. Quarterly Applied Mathematics, 13, p. 169
- [3.25] Noiseux D.U., 1970. Measurement of power flow in uniform beams and plates. Journal of the Acoustical Society of America, 47, p. 238
- [3.26] Pavic G., 1976. Measurement of structure borne wave intensity, part I: Formulation of the methods. Journal of Sound and Vibration, 49, p. 221
- [3.27] Pavic G., 1986. The influence of curvature on structure-borne acoustical power propagation in a cylindrical circular shell. Proc. 12th International Congress on Acoustics, Paper D6-6. Toronto
- [3.28] Fahy F.J., 1995. Sound intensity (2nd ed.). E & FN Spon, London
- [3.29] Maysenhölder W., 1994. Körperschallenergie. Grundlagen zur Berechnung von Energiedichten und Intensitäten. S. Hirzel Verlag, Stuttgart

4 Damping

4.1 Damping Mechanisms and their Mathematical Description

The previous chapter, which dealt with the various types of waves that can occur in a solid body, in all cases made use of some form of Hooke's law that is, it always involved proportionality between stress and strain. Hooke's law, like most laws of physics, is exact only for ideal situations, which represent limiting conditions for practical situations. For the topics treated in the previous chapter, the deviations from Hooke's law exhibited by actual structures are unimportant. However, in relation to processes that, for example, take place over relatively long times one finds that the relations derived in the previous chapter are unsatisfactory. Although it is evident even from cursory observation that every oscillation decays with space and time, the previously derived relations (for example, Eqs. (3.11) and (3.12)) imply that a motion continues forever once it has been started.

The present chapter deals with the aforementioned decay, which is associated with conversion of the energy contained in a given oscillation into a different form of energy. This conversion usually is called damping or dissipation. "Damping" and "dissipation" usually refer only to conversion of mechanical energy into heat. These terms are generally not applied to energy losses that occur as a result of reflection at discontinuities (see Chapter 6), which process is usually described as "attenuation".

Although damping occurs in all types of oscillations, this chapter is concerned only with processes in which mechanical energy is converted into heat. Thus, radiation damping and similar processes are not considered here. The damping of isotropic solids is treated first; then follows a discussion of multilayer systems, for example, plates with damping layers, which are of great practical importance.

Mechanical damping is of interest not only in relation to the control of vibrations and noise, but also for studies of the structure of materials particularly high-polymers and in relation to quality control monitoring.

The question of how the basic equations of elasticity (in the simplest case, Eq. (3.2)) may be modified in order to take into account damping

phenomena has concerned physicists for a long time. As early as 1874, O. E. Meyer [4.1] suggested that a viscous friction force should be taken to act in addition to the elastic forces. Since such a friction force is proportional to the time derivative of the strain, Eq. (3.2) would then be rewritten as the later denoted Kelvin-Voigt model [4.2]

$$\sigma = D \left(\varepsilon + \vartheta \frac{d\varepsilon}{dt} \right). \quad (4.1)$$

For the sinusoidal time variations, which are of greatest interest,

$$\varepsilon = \hat{\varepsilon} \cos \omega t, \quad (4.2)$$

is obtained

$$\begin{aligned} \sigma &= D\hat{\varepsilon} (\cos \omega t - \omega \vartheta \sin \omega t) \\ &= D\hat{\varepsilon} \sqrt{1 + \omega^2 \vartheta^2} \cos(\omega t + \arctan \omega \vartheta). \end{aligned} \quad (4.3)$$

Thus, for the given periodic strain variation, the stress and strain are not in phase with each other. As will be shown later, this phase difference implies that mechanical energy is transformed into heat in the course of such oscillations.

Equations (4.1) and (4.3) are not quite satisfactory, because it turns out that the parameter ϑ in reality is strongly frequency dependent. Viscous forces, moreover, within solid bodies are somewhat difficult to imagine. For this reason, Boltzmann [4.3] suggested a different type of relation between stress and strain. He reasoned that the force that produces a given strain does not depend only on that strain, but also on the previous strains i.e., the “strain history”. Following Boltzmann and assuming that the effects of the prior strains may be superposed linearly, the dependence of the stress $\sigma(t)$ at time t on the strain $\varepsilon(t)$ at time t and on the strain $\varepsilon(t-\Delta t)$ at the earlier time $(t-\Delta t)$ as can be written as

$$\sigma(t) = D_1 \varepsilon(t) - \int_0^\infty \varepsilon(t-\Delta t) \varphi(\Delta t) d(\Delta t). \quad (4.4)$$

The function $\varphi(\Delta t)$ describes the “after-effect” of a strain and the form of this function determines the stress-strain relation. One may note that the above reduces to Hooke’s law for $\varphi(\Delta t) \equiv 0$, as one would expect.

Of the many “after-effect functions” $\varphi(\Delta t)$ that are possible in principle, only one, the so-called “relaxation function”, is physically meaningful. If a strain is imposed on a material, then there occur certain molecular processes (displacements, distortions of crystal lattices, changes in molecular structure, excitation of certain molecular oscillations, etc.), which are ex-

cited gradually, and which then also decay gradually. If the applied strain, for example, causes a molecule chain to oscillate, one may assume that these oscillations will decay exponentially. The corresponding after-effect function then may be written as

$$\varphi(\Delta t) = \frac{D_2}{\tau} e^{-\Delta t/\tau}, \quad (4.5)$$

where D_2 is a constant and τ is the so-called relaxation time, which in the present example is a sort of decay time of molecular oscillations. The form of the stress history for a given strain is shown in Fig. 4.1, for two examples.

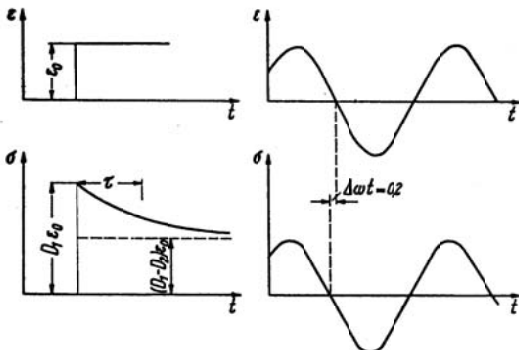


Fig. 4.1. Variations of strain and stress with time for a prescribed step-function displacement (left) and sinusoidal displacement (right). Parameters: $D_1 = 2D_2$, $\omega\tau = 0.2$

The left-hand part of the figure indicates the force that is required to produce a step-function jump in the strain from 0 to ε_0 . One finds that the initial force is relatively large, but that the force decreases as the body “gets used to” its new state.

The right-hand part of the figure illustrates the stress history for a periodic strain. Because this case is particularly important, it is of interest to analyse it in some detail. Upon introducing Eqs. (4.2) and (4.5) into (4.4), the stress becomes

$$\begin{aligned}\sigma(t) &= D_1 \hat{\varepsilon} \cos \omega t - \frac{D_2}{\tau} \hat{\varepsilon} \int_0^{\infty} \cos \omega(t-\Delta t) e^{-\Delta t/\tau} d(\Delta t) \\ &= \left(D_1 - \frac{D_2}{\omega^2 \tau^2 + 1} \right) \hat{\varepsilon} \cos \omega t - D_2 \frac{\omega \tau}{\omega^2 \tau^2 + 1} \hat{\varepsilon} \sin \omega t.\end{aligned}\quad (4.6)$$

Relaxation processes thus lead to a phase shift and therefore to dissipation of mechanical energy. The amount of mechanical energy that is transformed into heat depends on the second term of Eq. (4.6) and thus essentially on the relaxation time and on frequency. For molecular vibrations, these times obviously are very short, but the times τ corresponding to changes in molecular structure may be very long. Relaxation times may be of the order of hours and days, but also of the order of nanoseconds.

Equations (4.4) and (4.5) permit one to describe all observed stress and strain relations, provided that one accounts for all of the relaxation processes that occur simultaneously i.e., Eq. (4.5) is replaced by a sum of similar expressions with different relaxation times. Therefore, the relaxation model of after-effects may be taken as valid in general.

Unfortunately, the stress-strain relations given so far in Eqs. (4.1) and (4.4) lead to relatively complicated expressions if one tries to use them to derive a wave equation. As is evident from Eqs. (3.9) and (3.10), use of the viscous model of Eq. (4.1) leads to a differential equation of third order, whereas use of the after-effect model of Eq. (4.4) leads even to an integro-differential equation.

Besides the viscous and the relaxation models in (4.1) and (4.4) respectively, there is a number of other suggestions for the mathematical description of damping. Amongst those are the models of Maxwell [4.4] and Zener [4.5] for which the stress-strain relations read

$$\begin{aligned}\frac{d\varepsilon}{dt} &= \frac{1}{D} \frac{d\sigma}{dt} + \frac{1}{\nu} \sigma, \\ \sigma + \tau_1 \frac{d\sigma}{dt} &= D \left(\varepsilon + \tau_2 \frac{d\varepsilon}{dt} \right),\end{aligned}\quad (4.7)$$

respectively. Herein, ν denotes the dynamic viscosity while τ_1 and τ_2 are relaxation times. The Maxwell model is primarily used in the description of creep and the Zener model is a combination of that of Eq. (4.1) and the Maxwell model.

4.2 Complex Modulus and Wavenumbers

Fortunately, the difficulties associated with the stress-strain relations discussed above can be avoided, if one limits oneself to periodic processes and introduces a complex modulus. As has been pointed out earlier, however, other time dependencies can be handled by means of superposition. Equation (4.3), as well as Eq. (4.6), indicates that the primary effect of damping is the production of a phase difference between stress and strain. One may express this fact very conveniently in complex notation, by writing

$$\sigma(t) = \operatorname{Re} \left\{ D \hat{\epsilon} e^{j\omega t} \right\} = D' \hat{\epsilon} \cos \omega t - D'' \hat{\epsilon} \sin \omega t, \quad (4.8)$$

where

$$D = D' + jD'' = D'(1 + j\eta) \quad (4.8a)$$

represents the complex modulus of elasticity. The quantity $\eta = D''/D'$ is the so-called loss factor, which is used widely throughout the rest of this book (in textbooks on polymers often the loss factor is denoted d). It should be noted, however, that the complex modulus may lead to causality problems by a transformation from frequency domain to time domain when the loss factor is not known precisely.

Table 4.1. Frequency dependence of complex moduli and loss factor

Type	D'	D''	η
Voigt-Kelvin	D	$D\omega\vartheta$	$\omega\vartheta$
Maxwell	$D \frac{\omega^2 v^2 / D^2}{1 + \omega^2 v^2 / D^2}$	$D \frac{\omega v / D}{1 + \omega^2 v^2 D^2}$	$D/\omega v$
Boltzmann	$D_1 - \frac{D^2}{1 + \omega^2 \tau^2}$	$D_2 \frac{\omega \tau}{1 + \omega^2 \tau^2}$	$\frac{D_2 \omega \tau}{D_1 - D_2 + D_1 \omega^2 \tau^2}$
constant loss factor η_0	D	$\eta_0 D$	η_0

In Table 4.1 are shown the real and imaginary parts of the complex Young's modulus as well as the loss factor for the models described above. Figure 4.2a depicts the frequency dependencies and 4.2b the force transmissibility for a single-degree-of-freedom system, containing a spring element incorporating the different damping models. The Zener model is not explicitly included in the table and graphs since it is represented by the Boltzmann model using the substitution $D_2/D_1 = (\tau_2 - \tau_1)/\tau_2$.

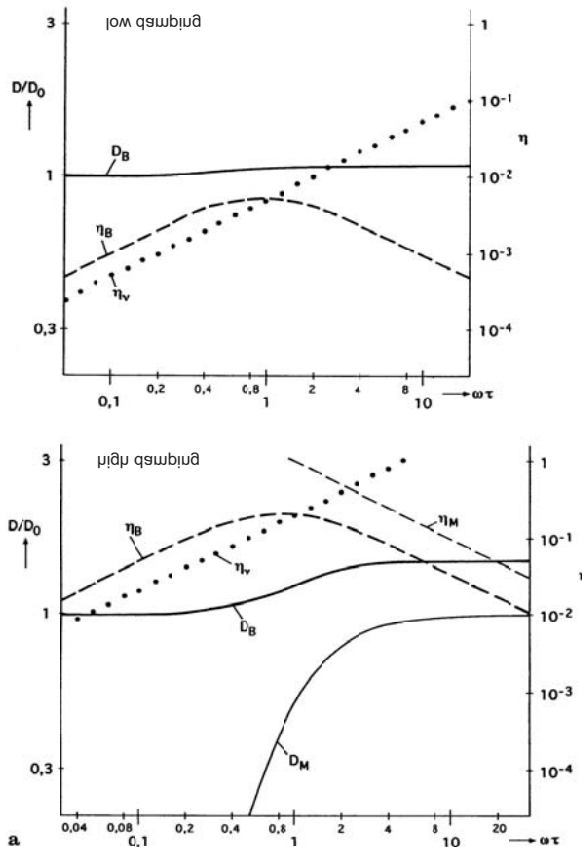


Fig. 4.2a. Frequency dependence of the real part of the normalized complex modulus and loss factor. D_V, η_V – Voigt-Kelvin, D_B, η_B – Boltzmann and D_M, η_M – Maxwell

It is seen in Fig. 4.2a that the Boltzmann model increases by a factor of $(1 + \eta_{\max})/(1 - \eta_{\max})$ in the vicinity of $\omega\tau = 1$ and that there the loss factor is a maximum. For the force transmissibility in Fig. 4.2b it is observed that the Voigt-Kelvin model does not lead to the typical isolation effect that is present at high frequencies for the other models.

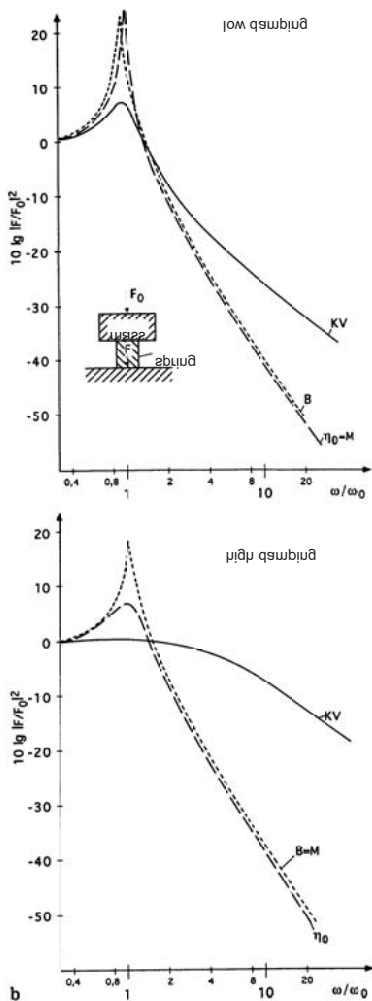


Fig. 4.2b. Force transmissibility for a SDOF system. KV – Voigt-Kelvin, B – Boltzmann, M – Maxwell and η_0 – constant loss factor

If one substitutes the modulus of elasticity D , as defined above, into the wave equation, one finds that the propagation speed becomes complex. Thus, instead of Eq. (3.13) is obtained

$$\underline{c}_L = c'_L + jc''_L = \sqrt{\frac{D}{\rho}} = \sqrt{\frac{\sqrt{D'^2 + D''^2} + D'}{2\rho}} + j\sqrt{\frac{\sqrt{D'^2 + D''^2} - D'}{2\rho}}. \quad (4.9)$$

For weak damping, that is $D' \gg D''$ or $\eta \ll 1$, one may approximate Eq. (4.9) by

$$\underline{c}_L \approx \sqrt{\frac{D'}{\rho}} \left(1 + j \frac{\eta}{2} \right). \quad (4.9a)$$

Even for $\eta = 0.5$, this approximation deviates from the exact value only by about 4 %. Errors that exceed 10 % result only for $\eta > 1$. The wavenumber also becomes complex, of course, namely,

$$\underline{k}_L = \frac{\omega}{\underline{c}_L} = k'_L - jk''_L \approx \omega \sqrt{\frac{\rho}{D'}} \left(1 - j \frac{\eta}{2} \right). \quad (4.10)$$

For propagation in the positive x -direction, the above expression must be multiplied by -1 , for propagation in the negative x -direction, by $+1$.

Similar expressions hold also for quasi-longitudinal waves on plates and beams, as well as for torsional and transverse waves. An additional simplification occurs for homogeneous isotropic materials, because the loss factors associated with extension and shear of such materials generally are found to be equal. (For anisotropic solids, this is generally not the case.) For transverse waves, in the presence of weak damping, one finds

$$\underline{c}_T \approx \sqrt{\frac{G'}{\rho}} \left(1 + j \frac{\eta}{2} \right); \quad \underline{k}_T \approx \pm \omega \sqrt{\frac{\rho}{G'}} \left(1 - j \frac{\eta}{2} \right). \quad (4.11)$$

For pure bending waves, introduction of the appropriate complex modulus into Eq. (3.85) yields

$$\underline{c}_B \approx \sqrt[4]{\omega^2 \frac{B'}{m'}} \left(1 + j \frac{\eta}{4} \right) \quad (4.12a)$$

and the corresponding wavenumber

$$\underline{k}_B \approx \sqrt[4]{\omega^2 \frac{m'}{B'}} \left(1 - j \frac{\eta}{4} \right). \quad (4.12b)$$

The physical meaning of a complex wavenumber (or of a complex propagation speed) becomes evident at once if one introduces it into the appropriate phasor relation. For plane waves propagating in the positive x -direction, which may be described by

$$u(x, t) = \operatorname{Re} \{ \hat{u} e^{j\omega t - jkx} \} = \hat{u} \cos(\omega t - kx + \varphi), \quad (4.13)$$

use of the complex wavenumber results in

$$u(x, t) = \operatorname{Re} \left\{ \hat{u} e^{j\omega t - jk'x - k''x} \right\} = \hat{u} e^{-k''x} \cos(\omega t - k'x + \varphi). \quad (4.14)$$

A complex wavenumber – that is, a complex modulus – thus implies exponential decay of propagating plane waves.

For lightly damped longitudinal, transverse and torsional waves $k'' = k'\eta / 2 = \pi\eta / \lambda$. Thus, Eq. (4.14) implies that the amplitude decays by a factor of $e^{-\pi\eta}$ within a wavelength. Within a distance Δx there therefore occurs a reduction in level by

$$\Delta L = \frac{8.7\pi\eta\Delta x}{\lambda} \text{ dB}. \quad (4.15)$$

A different expression holds for bending waves, because for these $k''_B \approx \pi\eta / 2\lambda_B$. Here the decrease in level with distance obeys

$$\Delta L_B = \frac{4.34\pi\eta\Delta x}{\lambda_B} \text{ dB}. \quad (4.16)$$

The reason that Eqs. (4.15) and (4.16) differ by a factor of 2 is that for bending waves the group speed, which determines the energy propagation, and thus also the damping is twice the phase velocity, see Eq. (3.89).

A difficulty arises, however, in relation to the nearfields of flexural waves. Namely, if Eq. (4.12b) is used to determine the nearfield wavenumber (see Eq. (3.109)), then there result nearfields of the form

$$e^{k'_B x - jk''_B x}, \quad e^{-k'_B x + jk''_B x}.$$

One obtains so-called complex nearfields, for which the amplitude decrease occurs in the direction which is opposite to propagation direction. At first glance, this result appears to have little physical meaning, because it appears to lead to increasing amplitudes. However, Tamm and Weis [4.6, 4.7] have shown that such complex nearfields occur very often at the higher-modal vibrations of plates, see Sect. 3.7. By considering the two related conjugate complex wavenumbers as corresponding to a decaying standing wave, one may remove the apparent violation of the law of conservation of energy. For the remainder of this discussion, however, complex nearfields are of relatively little interest.

For the more complicated vibrations that were treated in Sect. 3.7 (particularly in Fig. 3.25), one may also obtain the propagation speeds and damping by introduction of complex moduli. The corresponding equations, however, turn out to be very complicated. At present, solutions are available only for rubber-elastic plates ($\mu = 0.5$) with pure shear losses [4.7]. The analysis shows that with large losses the modes associated with high propagation speeds ($c \gg c_T$) are damped very strongly, so that in essence

there only remain bending or Rayleigh waves, transverse waves, and quasi-longitudinal waves.

Not only the spatial variations associated with a vibration are of interest, but also the corresponding energy relations. Consider a system that is excited so as to oscillate at a angular frequency ω , for example, a rod excited longitudinally by means of an electrodynamic shaker. The strains that occur in a given elementary volume of such a system may again be written as

$$\varepsilon(t) = \operatorname{Re} \{ \hat{\varepsilon} e^{j\omega t} \} = \hat{\varepsilon} \cos(\omega t + \varphi). \quad (4.17)$$

The corresponding stresses then obey

$$\begin{aligned} \sigma &= \operatorname{Re} \{ \underline{D} \hat{\varepsilon} e^{j\omega t} \} = \hat{\varepsilon} D' \cos(\omega t + \varphi) - \hat{\varepsilon} D'' \sin(\omega t + \varphi) \\ &= \hat{\varepsilon} D' \sqrt{1+\eta^2} \cos(\omega t + \arctan \eta + \varphi), \end{aligned} \quad (4.18)$$

see Eqs. (4.3), (4.6) and (4.8). One may note that the phase difference between stress and strain is directly related to the loss factor η . If one determines the potential energy density according to Eq. (3.6), then one obtains

$$\begin{aligned} E_{pot} &= \int_0^{\varepsilon} \sigma d\varepsilon \\ &= \frac{\hat{\varepsilon}^2 D'}{2} \left[\eta \omega t + \frac{\sqrt{1+\eta^2}}{2} \cos(2\omega t + \arctan \eta + 2\varphi) + \text{const} \right]. \end{aligned} \quad (4.19)$$

In this equation “const” represents a constant the depends on the limits of the integration and that is unimportant here. The variation of energy density with time given by Eq. (4.19) is plotted in Fig. 4.3.

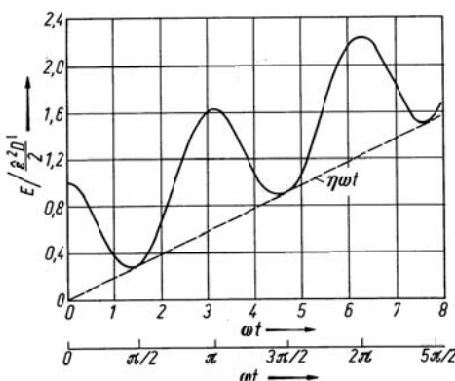


Fig. 4.3. Time-dependence of potential energy in a sinusoidally vibrating damped material. Calculated from Eq. (4.19) for $\eta = 0.2$

As evident from this figure, the average energy density increases with time. Because the amplitude of the vibration and thus the mechanical (reversible) energy remains constant, however, the additional energy supplied to the system which corresponds to the term $\eta\omega t$ in Eq. (4.19) evidently must be transformed into another form of energy (heat). The energy that the shaker continuously feeds into the sample in the last analysis serves to heat the material.

A stress-strain diagram is useful for providing further insight. If one introduces Eq. (4.17) into (4.18), one obtains

$$\sigma^2 - 2\sigma\varepsilon D' + \varepsilon^2 D'^2 (1 + \eta^2) = \eta^2 D'^2 \hat{\varepsilon}^2. \quad (4.20)$$

This equation represents an ellipse, centred at the origin, as shown non-dimensionalized in Fig. 4.4. Indicated are also the lengths of the semi-axis. The elliptical area is

$$S_E = \pi \sqrt{2} \frac{\eta}{\sqrt{2}} = \pi \eta.$$

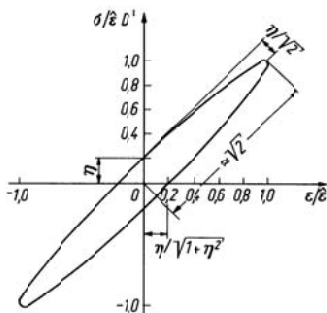


Fig. 4.4. Stress-strain curve of a dissipative material under sinusoidal loading ($\eta = 0.2$)

Since the energy E_l lost during one cycle of a vibration with period T is given by

$$E_l = \oint \sigma d\varepsilon = D' \hat{\varepsilon}^2 \oint \left(\frac{\sigma}{D' \hat{\varepsilon}} \right) d\left(\frac{\varepsilon}{\hat{\varepsilon}} \right) = D' \hat{\varepsilon}^2 S_E,$$

which corresponds precisely to the area of the ellipse, one finds that

$$E_{diss} = \pi \eta D' \hat{\varepsilon}^2. \quad (4.21)$$

The energy lost in a time interval t thus is given by $E_{diss}t/T = E_{diss}\omega t/2\pi = \hat{\varepsilon}^2 D' \eta \omega t/2$. This result corresponds exactly to the time-average value obtained from Eq. (4.19).

From these energy relations can be developed a convenient and physically meaningful definition of the loss factor. If one divides Eq. (4.21) by the (reversible) mechanical energy $E_R = D'\hat{\varepsilon}^2/2$, one obtains

$$\eta = \frac{E_d}{2\pi E_R}. \quad (4.22)$$

Thus, the loss factor indicates what fraction of the vibratory (reversible) mechanical energy is lost (i.e., converted into heat) in one cycle of the vibration. Note that the reversible energy appears in the denominator of Eq. (4.22), and not the total energy, which is usually used in definitions of efficiency. This distinction, however, is unimportant for small damping. The relation between the reversible energy and the periodically varying total energy is evident from Fig. 4.3.

In practice one is interested not only in the energy loss which occurs in a system whose vibration amplitude is kept constant by continuous external excitations, but one is also concerned with the time-wise decay of vibrations that results when the excitation is removed, so that energy is no longer supplied to the system. The over a period dissipated energy is obtained from the definition in (4.22), $E_{diss} = 2\pi\eta E_R$ such that the time dependence becomes

$$E_{diss}(t) = E_{diss} \frac{t}{T} = \omega \eta E_R t. \quad (4.22a)$$

Consider a system that vibrates at the angular frequency ω and which at time $t = 0$ has a reversible mechanical energy E_{R0} . If the system is disconnected at time $t = 0$ from all external sources, then all of its mechanical energy E_{R0} will eventually be converted into heat. In order to simplify the analysis, it is convenient to assume that the system under consideration has only one energy storage mechanism. Thus, for example, cases where energy can be stored in coupled bending waves and torsional waves are excluded here. Further, it is useful to postulate that the change in the amplitude (peak value) that occurs in one period of the oscillation is small. If the energy that is changed into heat up to time t is denoted by $E_{diss}(t)$, then the reversible energy that is left in the system at this time is $E_R(t) = E_{R0} - E_{diss}(t)$, in view of conservation of energy. The energy converted into heat during the time interval between t and $t + dt$ thus is $[E_{R0} - E_{diss}(t)] \eta \omega dt$, in view of the first term of Eq. (4.19). The total energy converted into heat up to time t is obtained by adding the losses for all earlier times,

$$E_{diss}(t) = \int_0^t [E_{R0} - E_l(t)] \eta \omega dt. \quad (4.23)$$

If one differentiates Eq. (4.23) with respect to t , one obtains a simple differential equation for $E_{diss}(t)$, which has exponential solutions, as would be expected,

$$E_{diss}(t) = E_{R0} (1 - e^{-\eta \omega t}) \quad \text{or} \quad E_R(t) = E_{R0} e^{-\eta \omega t}. \quad (4.24)$$

The energy thus decays exponentially, with a decay constant $\eta \omega$.

4.3. Resonant Vibrations of Damped Beams

One procedure that is often used for experimental determination of the loss factor involves measuring the response amplitude of a system as a function of frequency, for a constant excitation amplitude, and deducing the loss factor from the so-called bandwidth of response peaks – the half-power bandwidth. This method is well-known for measurement of the damping of systems with one degree of freedom and it is treated here in some detail, because in measurements on beams and similar structures there arise some considerations which one does not encounter for single-degree-of-freedom systems. The conversion from one damping quantity to another is facilitated by Table 4.2.

Table 4.2. Conversion formulae for damping quantities

Loss factor η =	η	b/f	$2.2/Tf$	Λ/π
Bandwidth (Hz) b =	ηf	b	$2.2/T$	$\Lambda f/\pi$
Reverberation time (sec) T =	$2.2/\eta f$	$2.2/b$	T	$6.8/\Lambda f$
Logarithmic decrement Λ =	$\eta \pi$	$\pi b/f$	$6.8/Tf$	Λ
Phase angle (rad) ϕ =	$\arctan \eta$	$\arctan(b/f)$	$\arctan(2.2/Tf)$	$\arctan(\Lambda/\pi \phi)$

λ = wavelength (m); c = phase speed (m/sec)

Additional relations:

$\underline{k}_L \approx k'_L (1 - j\eta/2)$ for longitudinal waves

$\underline{k}_B \approx k'_B (1 - j\eta/4)$ for bending waves

Level decay for plane bending waves: $D'_B = 13.6 \eta/\lambda$ [dB/m]

Level decay for longitudinal waves: $D'_L = 27.2 \eta/\lambda$ [dB/m]

$E = E' (1+j\eta)$

4.3.1 Quasi-Longitudinal Waves and Torsional Waves

Of the many methods available for the analysis of beam vibrations, the one used in this section – which deduces the vibrations of a finite beam from the behaviour of an infinite one – may be somewhat cumbersome, but provides considerable physical insight. Consider a rod, such as that shown in Fig. 4.5, excited at one end by the force

$$F = \operatorname{Re} \left\{ \hat{F} e^{j\omega t} \right\}.$$

In an infinitely long rod, such an excitation would give rise to a wave motion

$$\hat{v}_0(x) = \frac{\hat{F}}{\underline{Z}} e^{-jkx}, \quad (4.25)$$

where \underline{Z} represents the complex driving-point impedance (which takes on a complex value, because the propagation speed is complex), and \underline{k} is the complex wavenumber. For quasi-longitudinal waves, the driving-point impedance at a free end is $S p_{CLII}$.

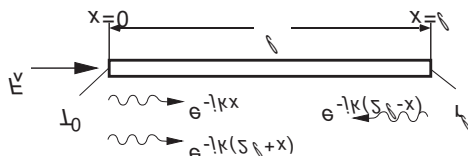


Fig. 4.5. Wave propagation along a beam

When the wave given by Eq. (4.25) arrives at the end of the rod, the velocity amplitude is

$$\frac{\hat{F}}{\underline{Z}} e^{-jk\underline{l}}.$$

The wave now is reflected, resulting in a backward travelling wave given by

$$\frac{\hat{F}}{\underline{Z}} r_l e^{-jk(2l-x)},$$

where \underline{r}_l represents the (complex) reflection coefficient at the location $x = l$. This wave is reflected once again when it reaches $x = 0$, and the doubly reflected wave obeys

$$\frac{\hat{F}}{\underline{Z}} \underline{r}_l \underline{r}_0 e^{-j\underline{k}(2l+x)},$$

where \underline{r}_0 denotes the reflection coefficient at $x = 0$. This doubly reflected wave is again reflected at $x = l$, and this process is repeated again and again, indefinitely. In the steady state, where all these components are present simultaneously, one thus obtains

$$\underline{v}(x) = \frac{F}{\underline{Z}} \left[e^{-j\underline{k}x} + \underline{r}_l e^{-j\underline{k}(2l-x)} + \underline{r}_0 \underline{r}_l e^{-j\underline{k}(2l+x)} + \underline{r}_0 \underline{r}_l^2 e^{-j\underline{k}(4l-x)} \dots \right]. \quad (4.26)$$

One may note that the first, third, fifth, ... terms of this expression form a geometric series with the ratio $\underline{r}_0 \underline{r}_l e^{-2j\underline{k}l}$ and the same holds also for the second, fourth, sixth, ... terms. Thus, by applying the summation formula for infinite geometric series, one obtains

$$\underline{v}(x) = \frac{F}{\underline{Z}} \frac{e^{-j\underline{k}x} + \underline{r}_l e^{-j\underline{k}(2l-x)}}{1 - \underline{r}_0 \underline{r}_l e^{-2j\underline{k}l}}. \quad (4.27)$$

Equation (4.27) also illustrates once again that the resonances i.e., the zeros or the minima of the denominator, correspond to the principle of wave-train closure, see Sect. 3.4. Closure of a wave train on itself here involves precisely a phase shift by $2\underline{k}l$ and reflection at both ends of the rod; one thus obtains wave train closure if $\underline{r}_0 \underline{r}_l e^{-2j\underline{k}l}$ is as close to unity as possible.

It is of interest to consider several limiting cases, in order to illustrate the general validity of Eq. (4.27). For a rod that is free at both ends ($\underline{r}_0 = \underline{r}_l = 1$) and very short ($\underline{k}l \ll 1$), one may approximate the exponential term of Eq. (4.27) by the first element of its series expansion

$$\underline{v}(x) \approx \frac{F}{\underline{Z}} \frac{1}{j\underline{k}l}. \quad (4.28)$$

For quasi-longitudinal waves, $\underline{Z} \underline{k}l = \omega_0 S l$, and the above result implies that a short rod which is free at both ends behaves essentially as a mass, as one would expect.

For a rod that is free at one end and clamped at the other ($\underline{r}_0 = 1$, $\underline{r}_l = -1$), one finds by multiplying Eq. (4.27) by $e^{j\underline{k}l}$ that

$$\underline{v}(x) = j \frac{F}{\underline{Z}} \frac{\sin \underline{k}(l-x)}{\cos \underline{k}(l-x)}. \quad (4.29)$$

In the special case of short rods ($kl \ll 1$) the velocity at $x = 0$ obeys

$$\underline{v}(0) \approx j \underline{k} l \frac{F}{Z}; \quad (4.30)$$

and for quasi-longitudinal waves, for which $\underline{Z} = S\sqrt{E\rho}$ and $k = \omega\sqrt{\rho/E}$,

$$\underline{v}(0) \approx j \frac{\omega l F}{SE}; \quad (4.31)$$

thus, such short rods behave like pure springs.

The behaviour of Eq. (4.27) in the vicinity of minima of the denominator is of particular importance in relation to measurements. In order to find these minima, one may assume that at the two ends of the rod there occur no energy losses i.e. $|r| = 1$, but only the phase shifts γ_0 and γ_1 respectively, see Sect. 3.4. If one introduces the complex wavenumber $\underline{k} = k' - jk''$ as defined in Eq. (4.10), then one may rewrite the denominator of Eq. (4.27) as

$$1 - e^{-2k''l} [\cos(2k'l - \gamma_0 - \gamma_1) - j \sin(2k'l - \gamma_0 - \gamma_1)]. \quad (4.32)$$

With small damping that is, for $k''l \ll 1$, this function takes on its minimum value i.e., the velocity reaches its maximum for

$$2k'l - \gamma_0 - \gamma_1 = 2n\pi.$$

By comparing this result with Eq. (3.106), one finds that it corresponds precisely to the resonance frequencies of undamped rods. If the damping is not small, one must find the minima of Eq. (4.32) by setting the derivative of the equation with respect to k' equal to zero. These resonance frequencies turn out to be somewhat lower than those of similar lightly damped rods.

Whether the minima of the denominator of Eq. (4.27) correspond to maxima of the velocity also depends on the observation point. The numerator of Eq. (4.27) is periodic in x , that is, there occur nodes and anti-nodes of vibration. This is illustrated in Fig. 4.6a, which shows the frequency dependence of the velocity for various amounts of damping, and in Fig. 4.6b, which shows the spatial dependence of the velocity. Both these figures pertain to a rod that is free at both ends and excited by a force of constant (frequency independent) amplitude. The corresponding velocity obeys

$$|\underline{v}(x)|^2 = \left| \frac{F}{Z} \right|^2 \frac{\cosh 2k''(l-x) + \cos 2k'(l-x)}{\cosh 2k''l - \cos 2k''l}. \quad (4.33)$$

The abscissa of Fig. 4.6a is $k'l$ (the wavenumber, multiplied by the beam length) and thus is proportional to the frequency, and the abscissa of Fig. 4.6b is $k'x$. The ordinate of these figures is the logarithm of the ratio of the velocity to an arbitrary reference velocity v_0 . One may note that the curves become flatter with increasing frequency, and eventually behave like exponentially decaying functions. For $k''/k' = 0.5$, that is for $\eta \approx 1$, the curves would exhibit no recognizable periodicity at all.

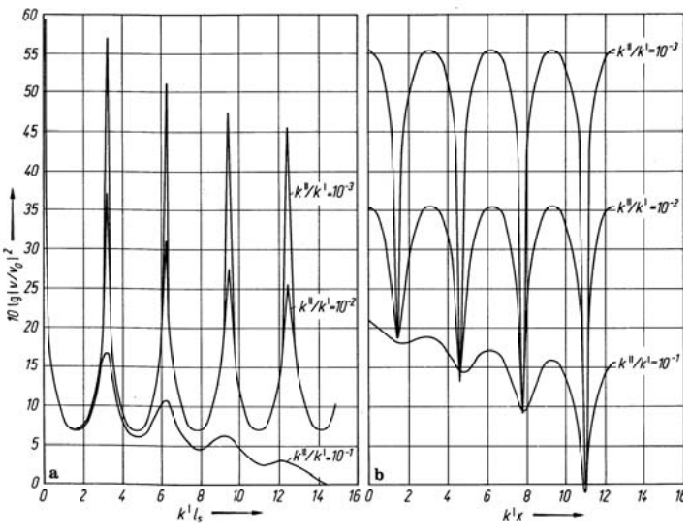


Fig. 4.6. Quasi-longitudinal or torsional vibrations of free-free beams, as determined from Eq. (33). a) Variation with frequency at $x = l$; b) Variation with position, for $k'l = 4\pi$

For small damping, one may obtain simplified expressions for the behaviour in the vicinity of resonances by developing Eq. (4.27) in a series about a resonance condition. In this development, however, one must take into account that both the numerator and the denominator depend on frequency. Assume that the velocity is measured at an anti-node i.e., a maximum in Fig. 4.6b, thus, at a position where the curve corresponding to the spatial variation is very flat and thus unaffected by small changes in $k'x$. Because of this assumption, the analysis that follows is not valid for nodal positions, since small changes in frequency lead to large changes in the numerator and denominator of Eq. (4.27). For the anti-nodes it is found that

$$\underline{v}_B = \frac{\underline{v}_0}{1 - |\underline{r}_0 \underline{r}_l| e^{-2k''l} e^{-j(2k'l - \gamma_0 - \gamma_l)}}.$$

If the damping is small, and only the behaviour in the vicinity of resonances is of interest, then one may use the approximations $e^{-2k''l} \approx 1 - 2k''l$ and $e^{-j(2k'l - \gamma_0 - \gamma_l)} \approx 1 - 2\Delta k'l$, and write

$$\underline{v}_B \approx \frac{\underline{v}}{1 - |\underline{r}_0 \underline{r}_l| (1 - 2k''l - 2j\Delta k'l)}.$$

Since this expression has its maximum value v_{\max} at resonance ($\Delta k'l = 0$),

$$\frac{\underline{v}_B}{v_{\max}} \approx \frac{1 - |\underline{r}_0 \underline{r}_l| (1 - 2k''l)}{1 - |\underline{r}_0 \underline{r}_l| (1 - 2k''l - 2j\Delta k'l)} = \frac{1}{1 + j \frac{\Delta k'l}{k''l + (1 - |\underline{r}_0 \underline{r}_l|)/2|\underline{r}_0 \underline{r}_l|k'l}},$$

from which it is found

$$\left| \frac{\underline{v}_B}{v_{\max}} \right|^2 \approx \frac{1}{1 + \left[\frac{\Delta k'}{k'} \frac{1}{(k''/k') + (1 - |\underline{r}_0 \underline{r}_l|)/2|\underline{r}_0 \underline{r}_l|k'l} \right]^2}. \quad (4.34)$$

In the vicinity of the resonance frequency, a plot of \underline{v}_B versus frequency thus has the typical resonance response character, see Fig. 4.7. The width of the resonance curve here depends on the energy losses due to reflection and internal damping. If no energy losses are due to reflections ($|\underline{r}_0 \underline{r}_l| = 1$), then Eq. (4.34) reduces to

$$\left| \frac{\underline{v}_B}{v_{\max}} \right|^2 \approx \frac{1}{1 + \left(\frac{\Delta k'}{k''} \right)^2}. \quad (4.35)$$

If the wavenumbers are expressed in terms of the frequency to which they are proportional, then $\Delta k'/k'$ becomes $\Delta f/f_n$, where Δf represents the frequency deviation measured from the peak frequency f_n . If one also sets $k'' = \eta k'/2$ (see Eq. (4.10)), one obtains

$$\left| \frac{\underline{v}_B}{v_{\max}} \right|^2 \approx \frac{1}{1 + \left(\frac{2\Delta f}{\eta f_n} \right)^2}. \quad (4.36)$$

The half-value bandwidth of the resonance curve, thus, is $b = \eta f_n$, see Fig. 4.7. Clearly, measurement of this resonant behaviour constitutes a simple

means for determining the damping, provided that the loss factor is not too great and the measurements are carried out at an anti-node.

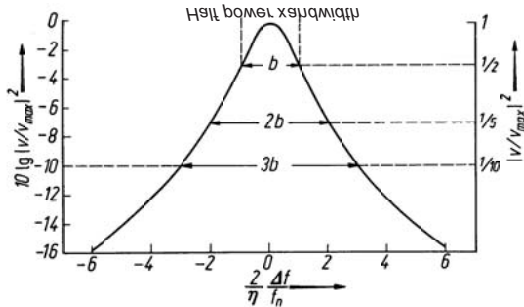


Fig. 4.7. Vibrational response of lightly damped systems in the vicinity of a resonance

For the vibrations in the vicinity of nodes, one finds that at constant frequency,

$$|\underline{v}_K|^2 \approx |\underline{v}_{\min}|^2 \left[1 + \frac{4|\underline{r}_l| e^{-2k''(l-x)}}{\left(1 - |\underline{r}_l| e^{-2k''(l-x)} \right)^2} (k\Delta x)^2 \right]. \quad (4.37)$$

for vanishingly small damping ($k'' = 0$), this reduces (for $|\underline{r}_l| \approx 1$) to

$$|\underline{v}_K|^2 \approx |\underline{v}_{\min}|^2 \left[1 + \left(\frac{2k\Delta x}{1 - |\underline{r}_l|} \right)^2 \right] = |\underline{v}_{\min}|^2 \left[1 + \left(\frac{4\pi}{1 - |\underline{r}_l|} \right)^2 \left(\frac{\Delta x}{\lambda} \right)^2 \right]. \quad (4.38)$$

For complete reflection at the end ($|\underline{r}_l| = 1$), the approximation $e^{-2k''(l-x)} = 1 - 2k''(l-x)$ may be used to obtain

$$|\underline{v}_K|^2 \approx |\underline{v}_{\min}|^2 \left[1 + \left(\frac{\Delta x}{l - x_n} \right)^2 \frac{k'^2}{k''^2} \right]. \quad (4.39)$$

As can be observed, there exists a close relation between the vibrations near a resonance and near a node. The resonance frequency f_n is analogous to the location x_n of a node, and the frequency interval Δf is analogous to the distance Δx . The fact that the expression $1 + \dots$ occurs in the numerator

in one case and in the denominator in the other makes little difference, particularly if the velocity is represented logarithmically.

There are available many methods for analysing the vibrations of a rod, in addition to that used above. Among the most important of these is the so-called “four-pole” representation. This representation can be developed by considering the wave field in a rod to be composed of forward and backward propagating waves, for which the velocity may be expressed as

$$\underline{v}(x) = \underline{v}_+ e^{-jkx} + \underline{v}_- e^{jkx}, \quad (4.40)$$

where v_+ and v_- are unknown for the present. The corresponding force that acts in the beam is given by

$$\underline{F}(x) = Z\underline{v}_+ e^{-jkx} - Z\underline{v}_- e^{jkx} \quad (4.40a)$$

where the change in the algebraic sign results from the different directions of wave propagation. The above must hold for all locations, and thus also for $x = 0$. One therefore obtains the following conditions for v_+ and v_- :

$$v_0 = v_+ + v_-, \quad F_0 = Z(v_+ - v_-).$$

If one introduces the resulting values of v_+ and v_- into Eqs. (4.40) and (4.40a), then one obtains that at the location $x = l$, for example

$$\begin{aligned} v_l &= v_0 \cos kl - j \frac{F_0}{Z} \sin kl \\ F_l &= -jZv_0 \sin kl + F_0 \cos kl. \end{aligned} \quad (4.41)$$

Equations (4.41) are a four-pole representation of the rod. They relate the velocity and the force at its beginning to the velocity and force at its end. Inversion of Eqs. (4.41) gives

$$\begin{aligned} v_0 &= v_l \cos kl + j \frac{F_l}{Z} \sin kl \\ F_0 &= jZv_l \sin kl + F_l \cos kl. \end{aligned} \quad (4.41a)$$

Of course, Eqs. (4.41a) and (4.27) always lead to the same result.

It depends on the particular problem to be solved whether Eq. (4.27) or the four-pole representation of Eq. (4.41a) is more advantageous for the analysis. Equation (4.27) is preferable if the reflection coefficients are known. If one is concerned with the transmission from one arbitrary system via the rod to another system, however, then the four-pole representation generally is more convenient.

4.3.2 Bending Waves

In order to apply the previously used analysis procedure for bending waves, one needs to replace the simple exponential functions in Eqs. (4.25) to (4.27) by the more complicated propagation functions for bending waves, which consist of nearfields and propagating waves. Because the associated manipulations are cumbersome and lengthy, it is useful to investigate bending waves on beams by means of a different approach. Equation (4.27) also gives a good approximation for bending waves on beams that are not too short, provided that the correct reflection coefficients are used. (For example, for a free-free beam, $r_0 = r_J = -j$.) This approximation only involves neglecting the nearfields; therefore the results derived in the previous section also apply to bending waves, for locations farther than a half wavelength from the beam ends.

As evident from Eq. (3.109), beam bending vibrations involve four component solutions:

$$\underline{v} = \underline{v}_+ e^{-jkx} + \underline{v}_- e^{jkx} + \underline{v}_{-j} e^{-kx} + \underline{v}_{+j} e^{kx}. \quad (4.42)$$

One may use this equation, or the equivalent expression

$$\underline{v} = \underline{v}_1 \cosh \underline{k}x + \underline{v}_2 \sinh \underline{k}x + \underline{v}_3 \cos \underline{k}x + \underline{v}_4 \sin \underline{k}x, \quad (4.42a)$$

depending on which of the two leads to simpler manipulations. The four unknowns \underline{v}_+ , \underline{v}_- , \underline{v}_{+j} , \underline{v}_{-j} , or \underline{v}_1 , \underline{v}_2 , \underline{v}_3 , \underline{v}_4 , respectively may be evaluated from the four boundary conditions. For example, for a free-free beam that is excited by a force F_0 at $x = 0$, see Sect. 3.4.2, one obtains

$$\begin{aligned} M(l) &\equiv -\frac{Bk^2}{j\omega} \left[-\underline{v}_+ e^{-jkl} - \underline{v}_- e^{jkl} + \underline{v}_{-j} e^{-kl} + \underline{v}_{+j} e^{kl} \right] = 0, \\ F(l) &\equiv \frac{Bk^3}{j\omega} \left[j\underline{v}_+ e^{-jkl} - j\underline{v}_- e^{jkl} - \underline{v}_{-j} e^{-kl} + \underline{v}_{+j} e^{kl} \right] = 0, \\ M(0) &\equiv -\frac{Bk^2}{j\omega} \left[-\underline{v}_+ - \underline{v}_- + \underline{v}_{-j} + \underline{v}_{+j} \right] = 0, \\ F(0) &\equiv \frac{Bk^3}{j\omega} \left[j\underline{v}_+ - j\underline{v}_- - \underline{v}_{-j} + \underline{v}_{+j} \right] = F_0. \end{aligned} \quad (4.43)$$

By solving Eq. (4.43) for the four unknowns, one finds after some lengthy manipulation that bending vibrations of free-free beams obey

$$\underline{v} = \frac{j\omega F_0}{Bk^3} \frac{\sinh \underline{k}l \cos \underline{k}(l-x) - \sin \underline{k}x - \cosh \underline{k}l \sin \underline{k}(l-x)}{2(1 - \cos \underline{k}l \cosh \underline{k}l)}. \quad (4.44)$$

For the location $x = l$, this result reduces to

$$\underline{v}(l) = \frac{j\omega F_0}{Bk^3} \frac{\sinh \underline{k}l - \sin \underline{k}l}{1 - \cos \underline{k}l \cosh \underline{k}l}. \quad (4.45)$$

When $kl \rightarrow 0$ i.e., for very short beams, one may show by using a series expansion including terms up to the fourth power of (kl) that

$$v(l) \approx \frac{2F_0}{j\omega m'l}. \quad (4.45a)$$

This result corresponds to rigid-body motion including rotation and translation of a rigid beam excited laterally at one end.

Figure 4.8a shows how the velocity at the end $x = l$ varies with frequency, as calculated from Eq. (4.45). Figure 4.8b shows how the velocity varies along the beam at a constant frequency corresponding to $k'l = 9\pi/2$, as calculated from Eq. (4.44). In these figures the ordinate again is the logarithm of the absolute value of the velocity, and the abscissa are $k'l$ and $k'x$, respectively. Because $k' = \sqrt{\omega / (m'/B)}$, the abscissa of Fig. 4.8a is proportional to the square-root of the frequency.

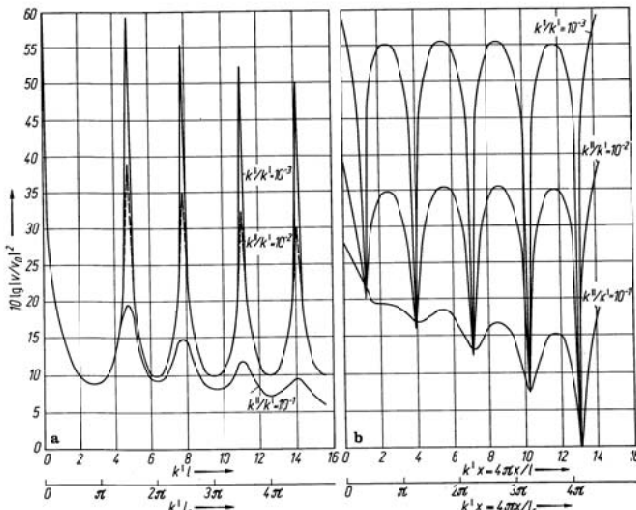


Fig. 4.8. Flexural vibrations of a free-free beam. a) Variation with frequency at $x = l$, as calculated from Eq. (4.45); b) Variation with position, for $k'l = 9\pi/2$, as calculated from Eq. (4.44)

One may derive Eq. (4.45) – but not Eq. (4.44) – considerably more rapidly with the aid of the so-called eight-pole equations [4.8]. In order to develop these equations conveniently, one may rewrite Eq. (4.42a) in terms of the following functions:

$$\begin{aligned}\frac{1}{2}(\cosh kx + \cos kx) &= C(kx), & \frac{1}{2}(\cosh kx - \cos kx) &= c(kx), \\ \frac{1}{2}(\sinh kx + \sin kx) &= S(kx), & \frac{1}{2}(\sinh kx - \sin kx) &= s(kx).\end{aligned}$$

These functions have the property that differentiation of any of them gives another function of the set, in the sequence $C(kx)$, $s(kx)$, $c(kx)$, $S(kx)$, $C(kx)$. In addition $C(0) = 1$, $S(0) = s(0) = c(0) = 0$. If the transverse velocity and the angular velocity are written as

$$\begin{aligned}\underline{v}_x &= \alpha C(kx) + \beta S(kx) + \gamma c(kx) + \delta s(kx) \\ \underline{w}_x &= k[\alpha s(kx) + \beta C(kx) + \gamma S(kx) + \delta c(kx)],\end{aligned}$$

one may observe that the velocity v_0 at the beginning of the beam is equal to α , whereas the angular velocity at the beginning of the beam is $w_0 = k\beta$. The moment and the shear force similarly may be found to be simply related to the coefficients in the foregoing expressions. After some mathematical manipulation, one may determine that

$$\begin{aligned}\underline{v}_x &= \underline{v}_0 C(kx) + \underline{w}_0 \frac{1}{k} S(kx) - \underline{M}_0 \frac{1}{jW'} c(kx) + \underline{F}_0 \frac{1}{jW' k} s(kx) \\ \underline{w}_x &= \underline{v}_0 ks(kx) + \underline{w}_0 C(kx) - \underline{M}_0 \frac{k}{jW'} S(kx) + \underline{F}_0 \frac{1}{jW'} c(kx) \\ \underline{M}_x &= -\underline{v}_0 jW' c(kx) - \underline{w}_0 \frac{jW'}{k} s(kx) + \underline{M}_0 C(kx) - \underline{F}_0 \frac{1}{k} S(kx) \\ \underline{F}_x &= \underline{v}_0 jW' k S(kx) + \underline{w}_0 jW' c(kx) - \underline{M}_0 ks(kx) + \underline{F}_0 C(kx),\end{aligned}\tag{4.46}$$

where $W' = Bk^2/\omega = \sqrt{Bm'}$.

Inversion i.e., expressing the parameters at the beginning of the beam in terms of those at the end may easily be accomplished here (as for the four-pole equations), because the determinant of the coefficients is equal to unity, in view of reciprocity. Here, the inversion merely leads to a change in the algebraic sign of the $S(kx)$ and $s(kx)$ terms.

Several approximations are of interest in relation to experimental measurements. For $k'l > \pi$, the variation with frequency of the velocity at the $x = l$ end of the beam may be written as

$$\left| \underline{v}(l) \right|^2 \approx \left| \frac{\omega F_0}{Bk^3} \right|^2 \frac{2}{\cosh 2k''l + \cos 2k'l}, \quad (4.47)$$

and the spatial variation in the region $\pi < k'x < k'l - \pi$ may be approximated by

$$\left| \underline{v}(x) \right|^2 \approx \left| \frac{\omega F_0}{Bk^3} \right|^2 \frac{\cosh 2k''(l-x) - \sin 2k'(l-x)}{\cosh 2k''l + \cos 2k'l}. \quad (4.48)$$

It is easily verified that these equations are also obtained by setting $r_0 = r_l = -j$ in Eq. (4.27). As has already been mentioned, one may apply the simpler relations of Sect. 4.3.1 to bending vibrations of long beams, if one introduces the appropriate reflection coefficients. The differences between the different wave types only become evident if one determines the frequencies and the loss factor from the wavenumbers k' and k'' . For bending waves one finds $k''/k' = \eta/4$ (see Eq. (4.12b)), unlike for longitudinal and torsional waves.

The damping of bending waves can be determined from half-value bandwidth measurements, exactly as for longitudinal and torsional waves, provided the beam is not too highly damped. The same analysis as was carried out in Sect. 4.3.1 in this case leads to

$$\frac{\underline{v}_B}{\underline{v}_{\max}} \approx \frac{1}{1 + j \frac{\Delta k l}{k'' l}}. \quad (4.49)$$

Because $k = \sqrt{\omega^4 m' / B}$, one finds that here $\Delta k = \frac{1}{2} \frac{k \Delta f}{f_n}$. Thus,

$$\left| \frac{\underline{v}_B}{\underline{v}_{\max}} \right|^2 \approx \frac{1}{1 + \left(\frac{2 \Delta f}{\eta f_n} \right)^2}. \quad (4.49a)$$

One may observe that the relation between bandwidth and loss factor for bending waves is the same as that for longitudinal and torsional waves, namely,

$$b = \eta f_n. \quad (4.50)$$

The vibrations in the vicinity of a vibration node obey the same relations as derived in Sect. 4.3.1. Therefore Eqs. (4.37) to (4.39) apply directly to bending waves, for locations outside of the nearfield regions.

The behaviour of beam vibrations in the vicinity of the various resonances is of interest not only in relation to experiments and for determination of the loss factor, but also because any vibration of a beam can be rep-

resented by a sum of its resonant or natural vibrations. This problem is treated in detail in Sect. 5.7, where it is shown that the velocity of a beam may be expressed as

$$\underline{v}(x) = \sum_{n=0}^{\infty} \frac{\underline{v}_n \phi_n(x)}{\omega_n^2 (1 - j\eta) - \omega^2}. \quad (4.51)$$

Herein, ω_n represent the radian natural frequencies of the beam, the \underline{v}_n are coefficients which are relatively independent of the frequency, and $\phi_n(x)$ represent the so-called eigenfunctions or mode shapes. Equation (4.51) applies for longitudinal and torsional waves, as well as for bending waves; one only needs to use the appropriate values for ω_n , \underline{v}_n and $\phi_n(x)$.

It may seem somewhat surprising at first glance that the velocities given by Eqs. (4.44) or (4.27) can be represented by an expression like that in (4.51), because these equations have entirely different forms. However, one may change one of these equations to the other by use of the Mittag-Leffler theorem of function theory, which states that every meromorphic function and thus also the functions $1/\sin x$ and $1/\cos x$ may be represented by an infinite sum. The actual transformation of one equation into the other involves no difficulty in principle, but is too tedious to be carried out explicitly here.

Equation (4.49a), which is most important in relation to loss factor measurement, can be obtained directly from Eq. (4.51) by neglecting all but the largest term and considering only a single point $x = x_0$. In this manner one finds

$$\underline{v}(x_0) \approx \frac{\underline{v}_n \phi_n(x_0)}{\omega_n^2 - \omega^2 - j\omega_n^2 \eta} = \frac{\underline{v}_n \phi_n(x_0)}{(\omega_n - \omega)(\omega_n + \omega) - j\omega_n^2 \eta}. \quad (4.52)$$

In the vicinity of a resonance, $\omega = \omega_n$, $\omega_n + \omega \approx 2 \omega_n$ and with $\omega_n - \omega = \Delta\omega$, it is found that

$$\underline{v}(x_0) \approx \frac{\underline{v}_n \phi_n(x_0)}{-j\omega_n^2 \eta} \frac{1}{1 + j \frac{2\Delta\omega}{\eta\omega_n}},$$

which corresponds directly to Eq. (4.49a).

4.4. Measurement of Complex Moduli

Because the complex modulus of elasticity of a material is a very important mechanical property, many techniques are available for its measure-

ment. Only the most important ones will be described here. In essence, there exist three basically different types of measurement methods. For low-frequency measurements on a sample of small dimensions, one may consider the test sample as a spring; one then needs only to determine the sample's spring constant. At intermediate and high frequencies, this approach ceases to work, because the sample then acts more like a wave-carrying distributed system than an ideal (mass-less) spring. In this upper frequency region, one therefore uses rod-shaped test samples and deduces the mechanical properties of the sample from the behaviour of longitudinal, torsional and bending waves. At very high frequencies, particularly in the ultrasonic region, where the wavelengths usually are considerably smaller than all sample dimensions, one generally determines material data by considering the test samples to be semi-infinite continua.

Only the first two types of measurements will be discussed here; for information on pure ultrasonic measurements the reader is referred to the specialized literature on the subject [4.9]. Also, no attempt will be made here to discuss the relation between mechanical properties and the structure of matter, although such topics have been the subject of great activity in the past few years and include many interesting effects e.g., coupling between sound and electron motions. Such topics belong to the field of pure physics and appear to have little application to noise control practice. On the other hand, investigations of the structure of high-polymer materials by means of structure-borne sounds measurements have led to the development of materials, which are of direct interest for structure-borne sound attenuation purposes, and such materials will be discussed in some detail.

4.4.1 Measurements on Small Samples

4.4.1.1 Stress-Strain Curve

A direct method for determination of the complex modulus of elasticity is shown schematically in Fig. 4.9. The test sample is rigidly fixed at one end, and excited by a periodic force F at the other. From the absolute values of the force and of the resulting displacement $\Delta\xi$ one may determine the absolute value of the modulus of elasticity from

$$\frac{|F|}{|\Delta\xi|} = |E| \frac{S}{l} = \frac{S}{l} E' \sqrt{1 + \eta^2}. \quad (4.53)$$

S represents the cross-sectional area and l the length of the test sample and from the phase angle φ between the force and the displacement one may find the loss factor as

$$\eta = \tan \varphi. \quad (4.54)$$

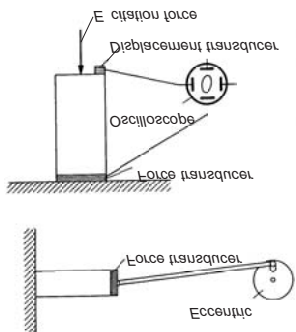


Fig. 4.9. Measurement of complex modulus via the stress-strain curve

Usually, electrodynamic shakers are most convenient for providing the required oscillatory force, and electromechanical transducers are used for sensing force and displacement. It thus is relatively easy to convert all mechanical quantities into electrical ones, to amplify without introducing significant phase shifts, and to measure them. For the signal processing, real-time FFT-analyser are suitable and furnishes readily the frequency response function sought, cf. Sects. 2.1 and 5.2. A frequency response function defined as the complex ratio of force to displacement represents directly the complex dynamic stiffness sought. Somewhat more physically direct perhaps but significantly more time consuming is the employment of an oscilloscope where the excitation and response signals are fed to the horizontal and vertical plates of the cathode ray tube. The oscilloscope output is an ellipse from which the real and imaginary parts of the complex modulus can be determined as given by Eq. (4.20) and illustrated in Fig. 4.4. In addition, one may easily recognize irregularities such as nonlinearities due to buckling of the test sample, higher order vibrations, resonances in the support system from distortions of the ellipse.

One may also excite the test sample in bending or torsion and deduce the complex bending stiffness and the complex shear modulus from the measured forces, moments, and translational or rotational displacements. Instead of applying a periodic force, one may also apply a periodic dis-

placement, for example, by means of an eccenter, see the lower part of Fig. 4.9. This arrangement also permits the application of a static preload without great difficulty.

The most significant problems with this type of measurement are associated with the accuracy to which the phase angle must be measured and with supporting the sample "rigidly". A "rigid support" is just as impossible to realize as, e.g., an absolute vacuum. In order to measure loss factors of the order $\eta \approx 10^{-2}$ with a 10 % accuracy, a value typical for example, for wood, the accuracy with which the phase angle between the force and displacement must be determined should be better than 0.6 degrees. Although, high-performance electronic equipment can achieve such an accuracy, losses in the sample support commonly contribute with larger phase shifts. Therefore, the applicability of the method is limited to relatively soft material with not too small loss factors such as rubber [4.10]. The lowest resonance frequency of the measurement set-up, moreover, must of course be considerably above the highest frequency of interest. Attention must also be paid the fixturing of the sample end. Upon applying a clamping support, the length of the test sample is no longer precisely defined since also the clamped part of the sample will participate in the deformation. It is thus advisable to use slender samples where such end effects are comparatively small. Unfortunately, slender samples are prone to buckling. If, on the other hand, use is made of short pad-shaped test samples other problems are introduced. For instance, the cross-sectional contraction of the sample is impeded at the contact area with the support yielding a locally enlarged modulus of elasticity. In particular, this effect must be considered for rubber samples where the Poisson's ratio is close to 0.5.

The length of the sample imposes a limit on the applicability of this measurement technique. As shown by Eq. (4.29), the stiffness of a sample that is clamped at one end is given by $\omega Z \cot kl$. Because $kl = 2\pi l/\lambda$, Eq. (4.53) ceases to apply if the length of the test sample approaches the longitudinal wavelength or the bending or torsional wavelength, in bending or torsional tests. From a series expansion of $\cot kl$ one may find that the fractional error due to the finite length of the sample is of the order of $k^2 l^2 / 3$. For a sample whose length is $1/50^{\text{th}}$ of the wavelength, this error is about 0.5 percent whereas for a sample length $1/10^{\text{th}}$ of the wavelength, the error amounts to 13 percent.

The method described above has one great advantage; namely, it permits one to change the measurement frequency continuously without changing the sample. One may thus determine the frequency dependence of the modulus and of the loss factor without difficulty over the entire measurement range of the apparatus. This is not the case for all the resonance methods.

4.4.1.2 Frequency Response Measurements in a Mass-Spring-Mass Rig

Due to the large difficulties in realizing a rigid support as employed in Fig. 4.9, is commonly used a measurement rig with dynamically free terminals. The simplest form of such a rig is the mass-spring-mass system. Two examples of such a rig type are shown in Fig. 4.10. When the masses can be considered rigid, the spring element comparatively “mass-less” and the suspension of the rig itself as well as that of any static preload dynamically free, the equations of motion read

$$\begin{aligned} j\omega m_1 v_1 + \frac{s}{j\omega} (v_1 - v_2) &= F_0, \\ j\omega m_2 v_2 + \frac{s}{j\omega} (v_2 - v_1) &= 0. \end{aligned} \quad (4.55)$$

This means that all the suspensions are made extremely soft such that there is no dynamic interference in the measurement range from the support or preload body.

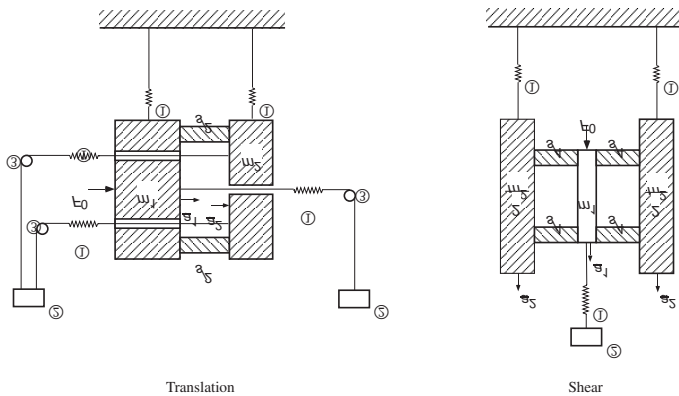


Fig. 4.10. Measurement of frequency response functions a_1/F_0 , a_2/F_0 or transfer function a_1/a_2 , in a mass-spring-mass system. ① suspension, ②preload and ③ pulleys

From Eq. (4.55) is obtained

$$\begin{aligned} v_1 &= F_0 \frac{j\omega m_2 + s/j\omega}{s(m_1 + m_2) - \omega^2 m_1 m_2}, \\ v_2 &= F_0 \frac{s/j\omega}{s(m_1 + m_2) - \omega^2 m_1 m_2}. \end{aligned} \quad (4.56)$$

As can be seen, there is an antiresonance at $\omega_A^2 = s/m_2$ which means that the velocity v_1 vanishes. Also, a resonance occurs at $\omega_R^2 = \underline{s}(m_1 + m_2)/m_1 + m_2$. At those two frequencies, the dynamic stiffness can be determined from Eq. (4.56). A more direct way to determine the dynamic stiffness, however, is obtained via the frequency response functions $\underline{a}_1/\underline{F}_0$ and $\underline{a}_2/\underline{F}_0$ or via the transfer functions $\underline{a}_1/\underline{a}_2$. Introducing $\underline{a} = j\omega\underline{v}$ instead of the velocities in Eq. (4.56) yields

$$\begin{aligned}\underline{s} &= \omega^2 m_2 \frac{1 - m_1 \underline{a}_1 / \underline{F}_0}{1 - (m_1 + m_2) \underline{a}_1 / \underline{F}_0}, \\ \underline{s} &= -\omega^2 m_2 \frac{m_1 \underline{a}_2 / \underline{F}_0}{1 - (m_1 + m_2) \underline{a}_2 / \underline{F}_0}, \\ \underline{s} &= \omega^2 m_2 \frac{1}{1 - \underline{a}_1 / \underline{a}_2}.\end{aligned}\tag{4.57}$$

Of the above forms, the last is the most convenient since it only involves the acceleration ratio and only requires a simple calibration.

The lower limiting frequency is set by the stiffness of the elastic suspension and 1 Hz is possible without greater difficulty. It should be observed the losses in the suspension elements should be small in order not to influence the measurements. Such a suspension, for example, can be realized by means of air springs (balloon). The upper frequency limit is given by the eigen-frequencies of the masses, which most often corresponds to bending resonances. It is preferable to try to achieve as symmetric a rig as possible to avoid rotational oscillations. Advisable is to ascertain the amount of contamination due to such rotations prior to the actual test or to perform a modal analysis.

The influence of sample size in comparison with the wavelength, as mentioned in Sect. 4.4.1.1, is also important for measurements in a mass-spring-mass rig. It can be reduced by adding the mass of the test sample proportionally to the two masses.

Which of the three forms in (4.57) is the more suitable depends on the specific case. In any case is a situation with $\underline{a}_1 \approx \underline{a}_2$ always problematic with respect to the last form since the difference in the denominator becomes small.

The measurement of moduli via transfer functions is due to Fitzgerald [4.11] who used a specific rig. Hereby, the mechanical quantities are proportional to electrical resistances, accurately determined from a bridge-circuit.

4.4.1.3 Vibration Decay

Whereas the previously discussed methods involve measurements of both stresses and strains, only one variable (usually the strain, velocity, or acceleration) needs to be measured in all techniques based on resonances of a system. However, these techniques have the disadvantage that one can obtain data at only one frequency, namely the resonance frequency.

A well-known technique of this type makes use of a torsion pendulum (Fig. 4.11). This technique is often used for measurements on high-polymer materials at low frequencies, but is not limited to such materials. To avoid tension of the test sample due to the disc mass, the latter is placed on top and suspended by a string.

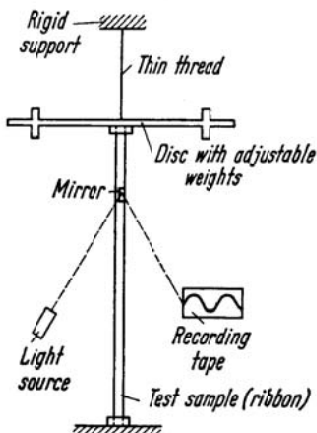


Fig. 4.11. Schematic arrangement of torsional pendulum

In tests of this type use was earlier made of an optical arrangement consisting of a light source, a small mirror, and recording paper which moves past a window at a constant velocity. The vibrations are recorded directly on this paper, and one may, for example, determine the natural frequency f_0 directly from the distance between the peaks and the known paper speed. For higher frequencies, however, electrical measurements are usually employed. The damping is usually determined in terms of the so-called logarithmic decrement, Λ , which is defined as the logarithm of the ratio of successive maxima. If A_n represents the maximum excursion measured at a certain time, and if A_{n+1} represents the maximum excursion at one period later, then Λ is defined as

$$\Lambda = \ln \left(A_n / A_{n+1} \right). \quad (4.57a)$$

For small damping, one finds from Eq. (4.24) that

$$\eta = \Lambda / \pi. \quad (4.58)$$

For large damping, inclusion of a correction leads to

$$\eta = \frac{\Lambda / \pi}{\sqrt{1 + (\Lambda / 2\pi)^2}}. \quad (4.59)$$

Because Λ can be determined rather accurately from measurement over several periods, the vibration decay technique is a simple and reasonably exact method for the loss factor η .

The second quantity of interest, the torsional stiffness T of the sample, is given by

$$|T| = (2\pi f_n)^2 \Theta \left(1 + \frac{\Lambda^2}{4\pi^2} \right), \quad (4.60)$$

where Θ represents the mass moment of inertia of the disc. The absolute value of the shear modulus is determined from the torsional stiffness and the dimensions of the sample. For ribbon-shaped test samples, as are often used,

$$|G| = G' \sqrt{1 + \eta^2} = |T| \frac{3l}{b^3 h (1 - 0.63b/h)}, \quad (4.61)$$

where l represents the length, h the width, and b the thickness of the test sample with $h > b$. (For high-polymers, the German standard DIN 53445 recommends ribbon dimensions $l \approx 60\text{mm}$, $h \approx 10\text{mm}$, $b \approx 2\text{mm}$.) For the relation between torsional stiffness and shear modulus, see also Table 3.1 and Eq. (3.64).

The primary advantage of the torsional pendulum is its great simplicity. It allows tests at many temperatures in a relatively short time, but suffers from the disadvantage that with a given sample and disc moment of inertia Θ one can obtain data at only one frequency. One can determine the frequency dependence of the modulus only rather inconveniently, by changing Θ , l , b , and h . There is virtually no lower limit for the frequency at which a torsion pendulum can be used, provided that the large discs that are needed to produce low frequencies can be made not to load the test sample excessively. Frequencies of 0.1 Hz are attainable without great difficulty.

The highest frequency at which a torsion pendulum is useful depends on the length of the test sample; for a measurement accuracy of 1 %, this length must not exceed 1/50 th of the torsional wavelength. Useful data above 500 Hz are rarely achieved with a torsion pendulum.

4.4.1.4 Resonance Frequency and Half-Value Bandwidth

The various test arrangements, in which the test sample acts as the spring in a resonant mechanical system, are closely related to the torsion pendulum in principle but differ considerably in configuration. In such set-ups, which are widely used for testing of fiber mats, foam materials, cork, etc., typically one end of the sample is fastened to a rigid support or to a large, very softly supported mass. To the other end of the sample is attached a known mass; the mass is excited by an oscillating force, and the velocity of the mass is sensed by means of a suitable transducer, see Fig. 4.12. By varying the frequency of the exciting force while holding the amplitude of the force approx. constant, a resonance frequency f_R is observed, and usually the corresponding half-value bandwidth b can be measured without great difficulty.

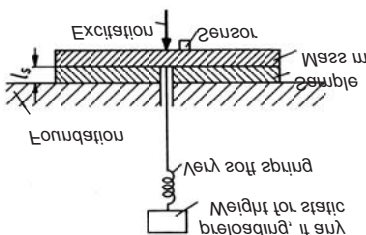


Fig. 4.12. Measurement of dynamic stiffness and loss factor via resonance frequency and bandwidth

The real part of the modulus of elasticity may be calculated from

$$E' = 4\pi^2 f_R^2 m \frac{l}{S}, \quad (4.62)$$

where l represents the thickness of the sample and S its surface area. For a sample resting on a rigid support, m represents the mass atop the sample. For a test sample resting on a softly supported mass m_u and carrying a mass m_0 , m is given by $m = m_0 m_u / (m_0 + m_u)$ cf. Fig. 4.10. When the mass

of the test sample m_s cannot be neglected, a first correction can be made by adding $m_s/3$ to the mass m for a set-up as in Fig. 4.12 whereas the sample mass is proportionally added to the two masses of the mass-spring-mass set-up. The loss factor is given by

$$\eta = \frac{b}{f_R}. \quad (4.63)$$

To achieve a higher accuracy in the measured loss factor, it is appropriate to plot the velocity ratio $|v_m/v_{m, max}|^2$ versus the square of the frequency shift $(\Delta\omega)^2$, cf. Eq. (8.22). In this way a straight line results which slope is proportional to the decay constant δ , from which the loss factor is obtained as $\eta = \delta/\pi f_r$.

In order to investigate the properties of the sample at various frequencies, one must change the mass supported by the sample. Quite often it does not suffice simply to lay additional weights atop the initial one; the weights must usually be bolted together or rigidly interconnected some other way, so that the total mass m acts as a single rigid body without resonances of its own. (One may also preload the sample statically – for example, in order to investigate the load-dependence of the behaviour of a foam mat – by connecting additional weights to the weight supported by the sample via a very soft spring, as indicated in Fig. 4.12.)

Like all measurement methods in which the loss factor is determined from the half-value bandwidth, the present method is useful only for small loss factors. If the loss factor is too large, the resonance curve becomes so flat that the bandwidth no longer can be discerned. In the best case, the relative error is of the order $\eta^2/2$.

Again, the range of applicability of the arrangements discussed here is limited by the sample thickness, which must be much smaller than the corresponding wavelength.

Practical difficulties in the use of such test arrangements also arise because of resonances of the supports and rocking motions of the sample, caused by unsymmetrical excitation. Both of these effects make it difficult to measure a single, clearly defined resonance, and thus to determine an unambiguous stiffness. In addition, care must be taken to ensure that the excitation system does not introduce extraneous damping. The damping of samples of materials that contain air (fibre mats or foams) sometimes depends markedly on sample size and geometry. For samples that have only open pores, one measures the stiffness of only the matrix material if one uses small samples and low frequencies; the air then is merely “pumped” in and out. At high frequencies, the air can no longer be moved back and forth rapidly enough; it then suffers some compression and may make a

considerable contribution to the total stiffness. For samples with closed cells, one cannot distinguish between the stiffness of the material itself and that of the enclosed air; one can only measure the total stiffness, which – like that of rubber – depends very strongly on the geometry of the sample. Such samples may behave much like liquids, i.e., they may exhibit a Poisson's ratio near 0.5.

4.4.2 Measurements on Beams

As was discussed in detail in Chapter 3, on beams are encountered primarily quasi-longitudinal waves, torsional waves, and bending waves. Surface waves occur only at relatively high frequencies. Thus, one may use the three aforementioned types of waves for measurements on beams. In practice, one usually concerns oneself only with bending waves, not only because these are most important with respect to sound radiation, but also because they can be excited most easily and most "cleanly" since their impedance is the smallest of those of the three wave types. The available bending-wave measurement techniques have been developed primarily for studying damping layers and similar noise control treatments [4.12, 4.13]. These techniques will be discussed in some detail in the following paragraphs. Techniques pertaining to torsional and quasi-longitudinal waves will be treated only cursorily.

4.4.2.1 Half-Value Bandwidth

Bending-wave resonances can be measured best on freely suspended beams, with excitation applied to one end and the resulting vibrations observed at the other, as shown schematically in Fig. 4.13.

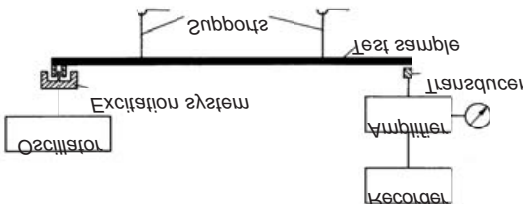


Fig. 4.13. Measurement of flexural resonance frequency and bandwidth

In this arrangement, the exciter and the sensor are at an anti-node at all frequencies; one thus avoids the difficulties associated with (frequency dependent) standing waves. Almost any electromechanical system that can be loosely coupled to the test specimen may be used as an exciter; even the electro-magnet from an earphone and a razorblade glued to the test beam will do. The loose coupling is important, because the test sample must not be damped or loaded by the excitation system. The same also holds for the sensor system. For very light samples, a capacitative sensor is usually best (a microphone mounted within 1/2 to 1 mm from the surface of the beam, in order to sense the airborne sound associated with the vibrations, constitutes an acceptable makeshift device). For large samples, other sensors may also be used. If the sensor is not to distort the measurements, its mass must be less than $M/30 n$, where M represents the total mass of the sample beam and n is the number of vibration nodes on the beam at the highest frequency of interest. Thereby, it is presumed that the mass impedance of the transducer is smaller than a tenth of the point impedance of the beam, cf. Sect. 5.3.2. One may use a somewhat heavier sensor, if one is not interested in the exact values of the higher resonance frequencies.

The suspension of the sample must be arranged so that it introduces no extraneous damping. If the loss factors to be measured are greater than 10^{-3} , then one usually may obtain acceptably low support damping simply by suspending the beam from threads in any convenient manner. For smaller loss factors and light samples, however, one must support the beam at nodal points, in order to minimize the vibratory energy extracted from the beam by the suspension system; the supports then must be moved for different resonances, see Fig. 4.13. Radiation of acoustic energy to the surrounding air may also contribute extraneous damping which is significant if one desires to measure small loss factors ($\eta < 10^{-4}$). One may reduce this radiation damping by choosing the test sample shape appropriately – or, of course, by carrying out the measurements in a vacuum. A practically simple arrangement is to insert the test sample in an upside-down-held plastic bag filled with helium, cf. [4.14].

One may determine the complex modulus simply by measuring the resonance frequencies f_n and the corresponding half-value bandwidths b . A typical amplitude-frequency curve is shown in Fig. 4.14.

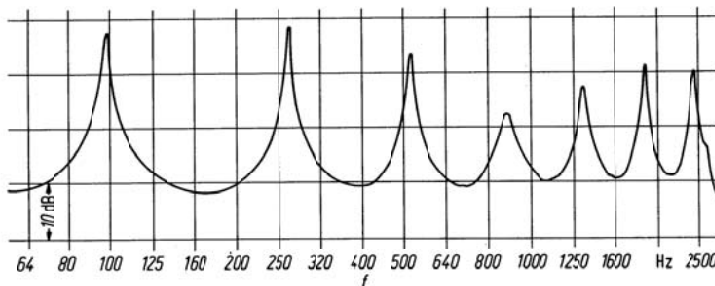


Fig. 4.14. Experimentally determined vibration response of a free-free beam (with a thin damping layer; $\eta \approx 2 \times 10^{-2}$, frequency dependent)

In view of Eq. (3.111e), the real part of the bending stiffness is found from

$$B' = m'l^4 f_n^2 \frac{64}{\pi^2 (2n-1)^4}. \quad (4.64)$$

and the loss factor from

$$\eta = \frac{b}{f_n}, \quad (4.65)$$

where m' represents the mass per unit length of the test beam, l represents its length such that $m'l$ is the total mass, n is the number of nodes, which can be determined by scanning the distribution of vibrations along the beam.

Equation (4.64) is not exact, because it neglects the slight reduction in the resonance frequency that is caused by the damping. The fractional error in the frequency associated with this approximation amounts at most to $\eta/4$ (see remarks in relation to Eq. (4.32)), but is never of great importance, because the resonance method allows measurements of loss factors only up to about 0.1. This limit stems from the fact that for large losses the vibration field is no longer resonant. Fig. 4.8a shows that for $k''/k' = 0.1$ i.e., $\eta \approx 0.4$, the rise in level hardly becomes more than 3 dB already at the third resonance. A consideration of high order terms shows that the representation of beam vibrations through a resonance curve i.e., the use of Eq. (4.49) instead of (4.47), is fully inappropriate for $k''l > 1$. The fractional error in η is approximately $n^2\eta^2/5$ in other words, if the frequency interval between resonances is of the same order as the half-value bandwidth, then one can no longer use this method.

4.4.2.2 Decay Time

For very small damping, one generally obtains more accurate results by measuring decay or reverberation times than by measuring half-value bandwidths. For $f = 100$ Hz and $\eta = 10^{-3}$, for example, the half-value bandwidth is only 0.1 Hz and thus cannot readily be measured by means of some simple apparatus. The same arrangement as described in the previous section may be used for decay measurements. Instead of determining how the amplitude varies with frequency in the vicinity of resonances, however, the decay of the vibrations is observed after the excitation is suddenly turned off. As is evident from Eq. (4.24), energy decay may be described by the function $e^{-\eta\omega t}$. Thus, the reverberation time T (within which the energy of the vibration is reduced to one millionth of its initial value) is measured as in room acoustics, and the loss factor is determined from the relation

$$\eta = \frac{\ln 10^6}{\omega T} \approx \frac{2.2}{f T}, \quad (4.66)$$

which follows from Eq. (4.24). One may, of course, also measure any other parameter that characterizes the decay process, instead of the reverberation time T , and compute η from it.

If only the loss factor is of interest and not also the bending stiffness, then only the reverberation time need be measured, for example, resulting from exciting the test sample by hammer impacts. In order to determine the frequency dependent of the loss factor, one must then filter the electrical signal picked up by the sensor. This measurement process does not yield particularly accurate results, because two or more natural vibrations with different decay times may lie within a filter bandwidth, leading to broken reverberation curves, from which the loss factor cannot be determined uniquely.

Irregularities in decay processes may also occur with periodic excitation namely, if the excitation frequency does not quite coincide with the natural frequency, see Fig. 4.15. Equation (4.24) was derived under the assumption that only one energy reservoir is present. If this is not the case, e.g., if two types of waves or several natural vibration modes are excited simultaneously as occurs with off-resonance excitation, then it may happen that mechanical energy is not only changed to heat, but also exchanged back and forth between two or more energy reservoirs, leading to rather remarkable decay curves.

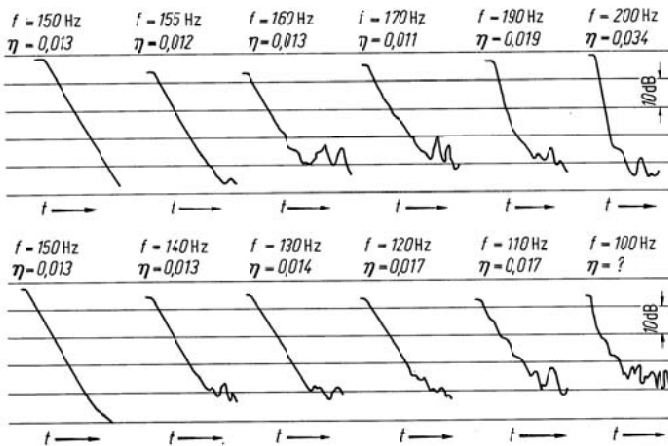


Fig. 4.15. Experimentally observed decay process near a resonance frequency of 150 Hz

In principle, reverberation time measurements are applicable up to relatively high values of the loss factor η . However, because of the inertia of the usual instrumentation, this technique generally is useful only for small damping.

4.4.2.3 Attenuation of Vibrations with Distance

In the limiting case of very long, highly damped beams, wave propagation occurs as on infinitely long beams. The velocities (or acceleration) at the two points x_0 and x_1 are related by

$$\underline{v}_1 = \underline{v}_0 e^{-j k(x_0 - x_1)} = \underline{v}_0 e^{-k''(x_0 - x_1)} e^{-j k'(x_0 - x_1)}. \quad (4.67)$$

Thus, the phase difference between these two points is given by

$$\varphi_{01} = k'(x_1 - x_0) = \frac{2\pi}{\lambda}(x_1 - x_0), \quad (4.68)$$

where λ represents the wavelength, and the reduction in amplitude obeys

$$\ln \frac{v_0}{v_1} Np = 10 \log \left| \frac{v_0^2}{v_1^2} \right| dB = 8.7 k''(x_1 - x_0) dB. \quad (4.69)$$

By measuring the phase and the amplitude reduction one may therefore determine the real and imaginary parts of the wave number.

For damping that is not extremely high, one may obtain the real part of the bending stiffness from

$$B' = \omega^2 m' \frac{1}{k'^4} = \omega^2 m' \left(\frac{x_1 - x_0}{\varphi_{01}} \right)^4 \quad (4.70)$$

and the loss factor from

$$\eta = 4 \frac{k''}{k'} = \frac{D'_B \lambda}{13.6}, \quad (4.71)$$

where D'_B represents the reduction in vibration level in decibels per unit length, that is, $(x_1 - x_0) D'_B = 10 \log \left[\left| v_0 \right|^2 / \left| v_1 \right|^2 \right] \text{dB}$.

In order to carry out this measurement, one typically excites the test beam at one end and scans the vibrations along the rod with a movable sensor as depicted in Fig. 4.16.

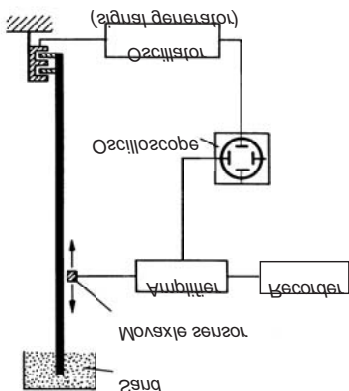


Fig. 4.16. Scanning of propagating flexural waves for measurement of wavelength and damping

If one moves the scanning sensor along the beam at a constant velocity, then one may determine D'_B , and thus k'' , directly from the slope of the recorded vibration level. Measurement of the phase difference may be accomplished simply by feeding the exciting voltage and the signal from the sensor to the two perpendicular pairs of plates of an oscilloscope and by marking on the test beam the points at which the phase difference with respect to the excitation amounts to 180° or 360° . Naturally, the phase can be registered directly also by means of a two-channel signal analyser.

Suspension of the test sample and attachment of the exciter is relatively uncritical for this type of measurement, but the scanning sensor must be relatively light. It is usually useful to embed one end of the beam in sand or some similar material, in order to reduce the reflection of waves from the end of the beam.

If reflections at the end and the associated standing waves are not eliminated, then the amplitude attenuation is not given by $e^{-k''x}$, but by the expression in the numerator of Eq. (4.48). In that case, the amplitude maxima lie on a curve given by $[\cosh 2k''(l-x)+1]^{\frac{1}{2}} = \sqrt{2} \cosh k''(l-x)$, while the minima are given by $\sqrt{2} \sinh k''(l-x)$. From these two conditions, one may determine k'' , and thus η .

The technique of measuring the level reduction with distance along the beam generally yields acceptably accurate results only for $\eta k' l > 10$. With a good sand termination, the limit may be somewhat lower. On the other hand, the half-value bandwidth method is only good up to about $\eta k' l = 2$, see also Figs. 4.8a and 4.8b. In the range between these two limits, one thus needs to vary the length of the test sample somewhat, in order to be able to use one or the other of these two methods.

4.4.2.4 Other Methods

The previously described methods for determining the elastic properties of beams vibrating in flexure are not the only possible ones. For example, one may also find the loss factor by measuring the frequency interval between response maxima and minima, the distance between the nodes of standing waves, or the mechanical driving point impedance. However, all of these methods have greater disadvantages than those described in detail above, and thus are useful only in special cases.

For quasi-longitudinal waves and torsional waves, which so far have barely been mentioned, one may also use half-value bandwidth, reverberation time, and spatial amplitude attenuation measurements. It should be noted that for such waves there applies the relation $\eta = D' \lambda / 27.2$ instead of Eq. (4.71). The same error estimates apply here as before. Care must be taken in all cases that the correct wave form is excited and measured. Particularly for inhomogeneous beams, it is very difficult to avoid exciting several wave types simultaneously, even if symmetry is carefully maintained. Measurements on quasi-longitudinal and torsional waves are generally used for very lightly damped media because of the very small associated radiation damping and at high frequencies in view of the large associated wavelengths.

4.4.3 Measurements on Other than Beam-Like Samples

On samples in the shape of plates, rings, cylinders, and the like, one can carry out measurements of the resonance frequencies, half-value bandwidths, and reverberation times much like on beam-shaped samples. However, evaluation of the results is somewhat more difficult, because simple formulas for the resonance frequencies are available only for circular and simply supported rectangular plates, and for rings. For all other configurations, one must use approximate equations for determining the modulus of elasticity from the resonance frequencies. Equations (4.65) and (4.66) apply to the evaluation of the loss factor from the half-value bandwidth, reverberation time, or decay constant, for test samples of any shape. Because the resonance frequencies of plate or shell samples are more closely spaced than those of beams, and are often distributed rather irregularly, one must take particular care to ascertain whether the interval between resonances is greater than the half-value bandwidth. Cylinders and long narrow plates, for example, exhibit a kind of band structure with clusters of resonance frequencies. The complicated distribution of the nodal lines, also often makes it difficult to find appropriate measurement points.

Curved test samples involve additional difficulties, because some of their modes may be much more strongly damped than others. In cylinders, waves which propagate in the axial direction tend to be less strongly damped than circumferential ones. For such samples one must either undertake the tedious process of determining all resonance frequencies and studying the frequency variation of the loss factor in full detail, or one may obtain a general view of the behaviour of the loss factor by exciting the test sample with third-octave or octave band noise and determining the reverberation times in these bands. The latter technique, which is analogous to reverberation measurements in room acoustics, is particularly well suited for samples with very many resonances. It is also useful for cases where there exists strong coupling between the various wave types, due to inhomogeneities and the like.

Yet another possibility relies upon measurements of the input power to the specimen and its spatial average velocity. This implies the determination of force $F(t)$ and velocity $v(t)$ to magnitude and phase at the point of excitation. The product $F(t) \cdot v(t)$ e.g., determined from the cross-spectral densities, represents the power fed to the object and thus the dissipated power under stationary conditions. With a test sample mass m , the energy is $E = 1/2 m \langle |v|^2 \rangle$, assuming a resonant response. For not too large damping, this energy approximates the reversible energy and Eq. (4.22) can be used to estimate the loss factor as

$$\eta = \frac{E_{diss}}{2\pi E_R} = \frac{W_{diss} T}{\pi m \langle |v|^2 \rangle} = \frac{2W_{diss}}{\omega m \langle |v|^2 \rangle}. \quad (4.71a)$$

4.5 Experimental Data

In the literature, material damping is characterized by several different parameters. The relations among the most important damping parameters are given in Table 4.2, in order to facilitate conversion from one to another. Most of these equations apply only for $\eta < 1$.

Table 4.3. Mechanical properties of metals at 20°C

Material	Density kg/m ³	Modulus of Elasticity N/m ²	Shear Modulus N/m ²	Poisson's Ratio	$c_{L\parallel}$ m/s	c_T m/s	Loss Factor		Remarks
							Flexural	Longitudinal	
Aluminium	2700	$72 \cdot 10^9$	$27 \cdot 10^9$	0.34	5200	3100	$0.3 \text{--} 10 \cdot 10^{-5}$	$\approx 10^{-4}$	[4.19, 20, 24]
Lead	11300	$17 \cdot 10^9$	$6 \cdot 10^9$	0.43	1250	730	$5 \text{--} 30 \cdot 10^{-2}$	$\approx 2 \cdot 10^{-2}$	[4.19] chem. pure [4.19] Antimon
Iron	7800	$200 \cdot 10^9$	$77 \cdot 10^9$	0.30	5050	3100	$1 \text{--} 4 \cdot 10^{-4}$	$2 \text{--} 6 \cdot 10^{-4}$	[4.19, 21, 24]
Steel	7800	$210 \cdot 10^9$	$77 \cdot 10^9$	0.31	5100	3100	$0.2 \text{--} 3 \cdot 10^{-4}$		[4.23]
Gold	19300	$80 \cdot 10^9$	$28 \cdot 10^9$	0.423	2000	1200	$\approx 3 \cdot 10^{-4}$		Poly-crystal
Copper	8900	$125 \cdot 10^9$	$46 \cdot 10^9$	0.35	3700	2300	$2 \cdot 10^{-3}$	$\approx 2 \cdot 10^{-3}$	single crystal
Magnesium	1740	$43 \cdot 10^9$	$17 \cdot 10^9$	0.29	5000	3100		$\approx 10^{-4}$	[4.24]
Brass	8500	$95 \cdot 10^9$	$36 \cdot 10^9$	0.33	3200	2100	$0.2 \text{--} 1 \cdot 10^{-3}$	$< 10^{-3}$	[4.19]
Nickel	8900	$205 \cdot 10^9$	$77 \cdot 10^9$	0.30	4800	2900		$< 10^{-3}$	[4.24]
Silver	10500	$80 \cdot 10^9$	$29 \cdot 10^9$	0.37	2700	1600	$\approx 4 \cdot 10^{-4}$	$< 3 \cdot 10^{-3}$	[4.22, 23]
Bismuth	9800	$3.3 \cdot 10^9$	$1.3 \cdot 10^9$	0.38	580	360		$\approx 8 \cdot 10^{-4}$	[4.24]
Zinc	7130	$13.1 \cdot 10^9$	$5 \cdot 10^9$	0.33	1350	850		$\approx 3 \cdot 10^{-4}$	[4.24]
Tin	7280	$4.4 \cdot 10^9$	$1.6 \cdot 10^9$	0.39	780	470		$\approx 20 \cdot 10^{-4}$	[4.24]

4.5.1 Metals

Although the density, modulus of elasticity and Poisson's ratio of metals and thus also the sound speed in metals, are relatively independent of the load history, duration, frequency, etc., that is by no means the case for the loss factor. Numerous and extensive investigations have shown that the interior damping of a metal is strongly affected by relatively small changes in the structure of the metal, such as may be caused by cold rolling, heat treatment and irradiation [4.5, 4.15]. The loss factor of a metal therefore cannot be considered as a material constant. On the contrary, measurements of the loss factor may be used to detect small structural changes. Such measurements are often employed in practice and constitute one ex-

ample of how acoustical measurement techniques may be of great value for metallurgical and solid-state physics investigations. Thus, the loss factor values given in Table 4.3 only provide an indication of the appropriate order of magnitude. (It is an interesting historical fact that very simple measurements on torsionally vibrating wires have long been used to detect fatigue effects) [4.16].

The physical processes that produce the damping of metals are very intricate and not yet fully understood. In addition, it is not at all easy to measure the often very small loss factors, so that some of the values given in the literature do not represent the losses in the material under investigation, but those due to the measurement apparatus (support, excitation system, etc.) or due to sound radiation (particularly for bending waves).

The primary mechanisms responsible for the damping of metals are associated with dislocations in the crystal lattice and with heat conduction between differently strained regions. Investigations concerning dislocation processes [4.16–4.19] are still ongoing, but interpretation of the heat conduction phenomena is relatively well in hand. It merely involves temperature changes produced by strains and the resulting heat conduction and the classical equation of heat conduction and linear thermo-dynamic relations apply.

Upon carrying out the corresponding analysis [4.5] it is found that the damping due to heat conduction appears as a relaxation process. Thereby, the relaxation times are

$$\begin{aligned}\tau &= (\lambda / 2\pi)^2 C_v \rho / \Lambda, \\ \tau &= (h / \pi)^2 C_v \rho / \Lambda,\end{aligned}\tag{4.72}$$

for the longitudinal and bending waves respectively. Herein, C_v is the specific heat, Λ the thermal conductivity, ρ the density, λ longitudinal wavelength and h the plate thickness. With numerical values introduced, where, for most metals $C_v \rho / \Lambda \sim 10^{-3}$, it can be established that some damping occurs at low frequencies for bending waves, typically below 200 Hz, and in the ultrasonic range for longitudinal.. The effect, however, is always small. At the relaxation maximum $\omega\tau = 1$, the loss factor is merely of the order of 10^{-3} .

The damping process associated with heat conduction is readily interpreted by recognizing that a material is cooled by an extension and heated by a compression. Thus, when the period is too short to allow for a complete equalization of temperature – isothermal case – but too long to realize ideal adiabatic conditions, then there is a small energy remainder which serves to heat the material. The fact that the wavelength appears in Eq. (4.72) on the one hand and the plate thickness on the other, stems from the

distance between elongated and compressed structural regions i.e., cool and hot zones for the two wave types respectively. For the longitudinal wave those zones are typically half a wavelength apart whereas the thickness of the structure separates them in bending.

The damping of bending waves due to heat conduction, has repeatedly been verified experimentally. However, it appears that the measured damping values agree with the theoretical ones only in the vicinity of the relaxation maximum. At higher frequencies, other damping mechanisms (heat conduction between individual crystals, dislocation processes, etc.) tend to predominate. These other mechanisms are responsible for the values given in Table 4.3, obtained under “normal” conditions.

With the exception of lead, tin, silver and copper, the loss factors of metals in general are considerably smaller than 10^{-3} .

For built-up structures such as machines and vehicles, the differences in the damping of materials are of little importance. The actual damping of such structures is not determined by the losses in the materials, but by friction at supports, interfaces, connections, etc., see Sect. 4.8.

4.5.2 Plastics

Because damping measurements have long been used as a tool in investigations of high-polymer materials, and because such materials are very often used as damping treatments, a separate discussion of this group of materials is justified. The mechanical properties of amorphous high polymers characteristically exhibit a very broad transition region between the rigid and the liquid state. In this transition region, the long and possibly cross-linked chains of molecules become increasingly mobile, and there occur relaxation mechanisms which lead to loss factors up to $\eta = 10$. The moduli of elasticity and the loss factors of such materials depend very strongly on temperature and frequency. Thus, complete description of the mechanical properties of such a material involves, for example, curves that show the frequency dependences of these properties at various constant temperatures. An example of such a set of curves, taken from Becker and Oberst [4.24], is shown in Fig. 4.17.

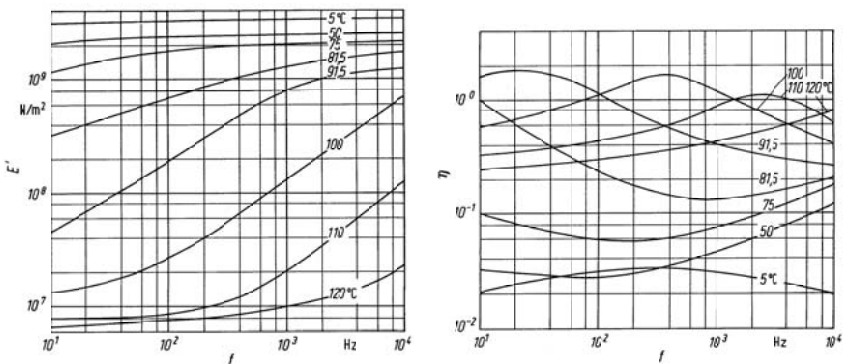


Fig. 4.17. Dependence of modulus of elasticity and loss factor of polyvinylchloride on frequency and temperature, [4.24]

Figure 4.17 illustrates the fact that the loss factor is greatest where the modulus of elasticity changes most rapidly with frequency. This sort of behaviour is exactly what one expects for a relaxation process in view of Eqs. (4.4) and (4.5), cf. Fig. 4.2a and Table 4.1. The fact that in reality there are present a multitude of relaxation processes, and not just a single one, does not affect the foregoing considerations.

Several other “laws” apply to amorphous high polymers, in addition to the relation between the loss factor and the frequency dependence of the modulus of elasticity. The most important of these laws are briefly described below.

All plastics have a so-called “freezing” point, below which their properties are much like those of glass. This freezing point or glass-transition temperature is not uniquely defined. It increases with increasing frequency, as evident in Fig. 4.17. Below the glass-transition temperature, most high polymers have a modulus of elasticity of about $5 \cdot 10^9 \text{ N/m}^2$, and a relatively small loss factor, usually less than 0.1. Plastics therefore are not suited for damping applications below their transition temperatures.

Above the glass-transition temperature, there occurs a more or less broad temperature region – the so-called “rubber-elastic” region – in which plastics behave neither entirely like solids, nor like liquids. Because plastics exhibit rather high loss factors in this region, see Table 4.4, it is this region that is best for damping applications. The moduli of elasticity in this transition region are of the order of 10^6 to 10^7 N/m^2 for “linear” materials that is, for materials with long non-cross-linked molecules. For cross-linked materials, the moduli are of the order of 10^8 N/m^2 . The modulus of elasticity of plastics which is of importance for damping layer treatments may be increased somewhat by the addition of fillers e.g., vermiculite. By

Table 4.4. Loss factor and modulus of elasticity [N/m²] at maximum damping for some high-polymers

Polyvinylchlorid (pure)	$\eta = 1.8$	$E = 3 \cdot 10^7$	at 92°C and	20 Hz
Polystyrene	$\eta = 2.0$	$E = 30 \cdot 10^7$	at 140°C and	2000 Hz
Polyisobutylene	$\eta = 2.0$	$E = 0.6 \cdot 10^7$	at 20°C and	3000 Hz
Nitrile Rubber	$\eta = 0.8$	$E = 33 \cdot 10^7$	at 20°C and	1000 Hz
Hard Rubber	$\eta = 1.0$	$E = 20 \cdot 10^7$	at 60°C and	40 Hz
Polyvinylchlorid with 30% plasticizer	$\eta = 0.8$	$E = 2 \cdot 10^7$	at 50°C and	100 Hz

this, materials with loss moduli up to about $E'' = E'\eta = 10^9$ N/m² can be obtained.

In addition, one may obtain significant changes in the temperature-variations of the properties of plastics by adding “plasticizers”. One may thus expect in principle to be able to obtain materials with optimised damping behaviour over prescribed temperature and frequency regions, by using appropriate combinations of cross-linked polymers, fillers, and plasticizers. However, both experience and theoretical considerations [4.25, 4.26] show that the temperature region in which the loss factor is high that is, the “temperature bandwidth” decreases as one increases the maximum loss factor. The variations of the loss factors with frequency behave similarly; the higher the loss factor, the smaller the bandwidth.

But there is more to the relation between the temperature and frequency variations. It was shown, particularly by Williams, Landel and Ferry [4.26], that in the transition region a temperature increase (at constant frequency) corresponds approximately to an increase in the logarithm of the frequency (at constant temperature). Thus, an increase in temperature, a reduction in the frequency, and addition of a plasticizer all have the same qualitative effect. All three changes reduce the modulus of elasticity, and all either increase or decrease the loss factor, depending on where one begins in relation to the position of the loss factor peak.

It should also be pointed out that in most cases the shear modulus is approximately 1/3 of the modulus of elasticity, and that the loss factor in shear differs only negligibly from that in tension and compression.

Beyond the rubber-elastic region, there occurs the plastic, and finally the fluid region. In these regions, any loading results in permanent deformation, and the moduli of elasticity become so small that materials in these regions are neither suitable for structural applications, nor for optimal damping treatments.

4.5.3 Building Materials

Other materials, besides metals and plastics, also are important in practice. Table 4.5 lists the moduli of elasticity and loss factors of several such materials in the audio-frequency range. The indicated values are useful only as guidelines, because the mechanical properties of material like concrete, asphalt, brick, etc. are known to depend strongly on their composition and on how they are made.

One may note that the loss factor in very many cases is of the order of 10^{-2} . Thus, this value may be used as a rough estimate for building structures, as well as for sheet-material structures.

Table 4.5 Mechanical properties of building materials

Material	Density kg/m ³	Modulus of elasticity N/m ²	c _{LII} m/s	Loss factor	Remarks
Asbestos concrete	2000	$28 \cdot 10^9$	$3.7 \cdot 10^3$	$0.7-2 \cdot 10^{-2}$	23°C, 10% Bituminous content
Asphalt	1800-2300	$7.7 \cdot 10^9$	$1.9 \cdot 10^3$	0.38	13°C, 11% Soft
		$12 \cdot 10^9$	$2.4 \cdot 10^3$	0.21	Bituminous content
		$21 \cdot 10^9$	$3.2 \cdot 10^3$	0.055	
Oak	700-1000	$2-10 \cdot 10^9$	$1.5-3.5 \cdot 10^3$	$\approx 1 \cdot 10^{-2}$	13°C, 8.5% Hard
Fiber mats, including matrix and air stiffness	50-300	$1.4-3 \cdot 10^5$		≈ 0.1	Bituminous content
Fir	400-700	$1.5 \cdot 10^9$	$\approx 2.5 \cdot 10^3$	$\approx 8 \cdot 10^{-3}$	[4.12]
Felt		$0.03 \cdot 10^9$		$\approx 6 \cdot 10^{-2}$	
Gypsum board	1200	$7 \cdot 10^9$	$2.4 \cdot 10^3$	$6 \cdot 10^{-3}$	[4.32]
Glass	2500	$60 \cdot 10^9$	$4.9 \cdot 10^3$	$0.6-2 \cdot 10^{-3}$	[4.32]
Pressed-wood panels	600-700	$4.6 \cdot 10^9$	$2.7 \cdot 10^3$	$1-3 \cdot 10^{-2}$	
Plaster	1700	$4.4 \cdot 10^9$	$1.6 \cdot 10^3$	$2-5 \cdot 10^{-2}$	
Cork	120-250	$\approx 0.025 \cdot 10^9$	$0.43 \cdot 10^3$	0.13-0.17	
Light concrete	1300	$3.8 \cdot 10^9$	$1.7 \cdot 10^3$	$1.5 \cdot 10^{-2}$	[4.32]
Plexiglas	1150	$5.6 \cdot 10^9$	$2.2 \cdot 10^3$	$2-4 \cdot 10^{-2}$	
Porous, concrete	600	$2 \cdot 10^9$	$1.7 \cdot 10^3$	$1 \cdot 10^{-2}$	[4.32]
Sand, dry	≈ 1500	$\approx 0.03 \cdot 10^9$	$0.1-0.17 \cdot 10^3$	0.06-0.12	[4.31]
Dense concrete	2300	$26 \cdot 10^9$	$3.4 \cdot 10^3$	$4-8 \cdot 10^{-3}$	[4.28. 4.31]
Plywood	600	$5.4 \cdot 10^9$	$3 \cdot 10^3$	$\approx 1.3 \cdot 10^{-2}$	[4.28. 4.21]
Brick	1900-2200	$\approx 16 \cdot 10^9$	$2.5-3 \cdot 10^3$	$1-2 \cdot 10^{-2}$	[4.28. 4.21]

4.6 Plates with Attached Layers

Whereas previous discussions dealt with more or less homogeneous materials, the discussion to follow deals with very inhomogeneous arrangements. Plates with attached layers, in particular, are of great importance for practical noise control applications. Typical configurations usually consist of a base plate (usually of metal), to which are attached one or more layers of a viscoelastic (e.g., a high-polymer) damping material and possibly additional metal plates. Such systems essentially result in a “division of labour”, where the metal plates contribute the necessary strength and the damping material produces desirable structure-borne sound properties.

It is important to note that the loss factors of plates with attached layers may differ greatly for different types of loading. It is therefore important that one knows for which type of loading a given loss factor applies. The case of a plate with a simple attached layer, as discussed in the next section, illustrates how the loss factor for longitudinal waves differs from that for bending waves for such a configuration.

4.6.1 Plates with Simple, Extensionally Loaded Layers

A simple means for increasing the damping of metal plates consists of attaching to them a so-called damping layer. The loss factor obtained by this means may be determined simply by referring to the definition in Eq. (4.22). For the case of quasi-longitudinal waves, the reversible mechanical energy is composed of the maximum potential energies in the basic plate and in the attached layer. The total reversible energy, in view of Eq. (3.6), thus is given by

$$W_R = \frac{1}{2}(E'_1 d_1 + E'_2 d_2) |\varepsilon|^2 = \frac{1}{2}(E'_1 d_1 + E'_2 d_2) \left| \frac{d\xi}{dx} \right|^2, \quad (4.73)$$

where ξ represents the maximum displacement during a period, E'_1 and d_1 represent the real part of the modulus of elasticity and the thickness of the basic plate, and E'_2 and d_2 represent these properties of the attached layer. Herein and in the following is considered the energy per unit area and to avoid confusion, W is introduced.

If the losses of the base plate are negligible, then, in view of Eq. (4.21), the energy transformed into heat per cycle of vibration may be found to obey

$$W_{diss} = \pi \eta_L E'_2 d_2 \left| \frac{d\xi}{dx} \right|^2. \quad (4.73a)$$

Thus, the loss factor η_L for longitudinal loading is given by

$$\eta_L = \frac{W_{diss}}{2\pi W_R} = \eta_2 \frac{E'_2 d_2}{E'_1 d_1 + E'_2 d_2}. \quad (4.74)$$

As one may note, this loss factor is proportional to the loss modulus $\eta_2 E'_2$. For the best material known so far, this quantity has a value of about 10^9 N/m². For sheet steel with $E_1 = 2 \cdot 10^{11}$ N/m², one finds that for $d_1 = d_2$ the loss factor amounts only to $\eta_L \approx 5 \cdot 10^{-3}$. Thus, quasi-longitudinal waves are very difficult to damp, unless they can be converted into other types of waves.

In the case of bending waves, which is considerably more important for sound radiation, the attached layer also deforms primarily in extension, as shown in Fig. 4.18. If ξ_M represents a displacement at the centre line of the attached layer, then the energy per unit area transformed into heat in one cycle is given by

$$W_{diss} = \pi \eta_2 E'_2 d_2 \left| \frac{d\xi_M}{dx} \right|^2. \quad (4.75)$$

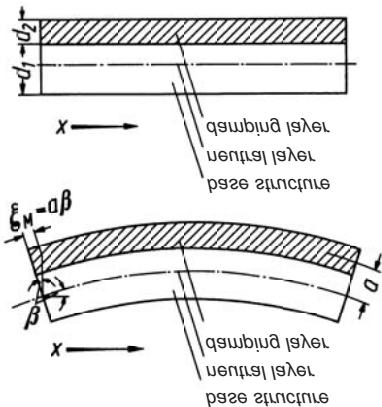


Fig. 4.18. Flexure of beam with viscoelastic layer

The reversible mechanical energy in bending, according to Eq. (3.92b), may be expressed as

$$W_R = \frac{1}{2} B \left| \frac{d^2 \eta}{dx^2} \right|^2 = \frac{1}{2} B \left| \frac{\partial \beta}{\partial x} \right|^2, \quad (4.75a)$$

where B represents the bending stiffness of the combined system consisting of the plate and the attached layer, and β represents the angle of flexure. If a denotes the distance from the neutral fiber to the centre-line of the attached layer, then $\xi_M = a\beta$. Thus, the loss factor η_B for bending waves obeys

$$\eta_B = \frac{W_{diss}}{2\pi W_R} = \eta_2 \frac{E'_2 d_2 a^2}{B}. \quad (4.76)$$

This expression contains the two quantities, a and B , that must still be evaluated. As an approximation [4.33] one may take $a = (d_1 + d_2)/2$, that is, one may assume a to be approximately equal to the distance from the middle of the basic plate to the middle of the attached layer, cf. Sect. 4.6.3.1. One may approximate B as

$$B \approx \frac{E_1 d_1^3}{12} + E_2 d_2 a^2, \quad (4.76a)$$

where the second term is of importance only for relatively thick attached layer ($d_2 > d_1$).

Figure 4.19 shows the dependence of the loss factor ratio η_B/η_2 on the thickness ratio, based on the exact analysis of Oberst [4.12]. Also shown in this figure are points for $E'_2 / E_1 = 3 \cdot 10^{-3}$. Clearly, Eq. (4.76) is a very good approximation.

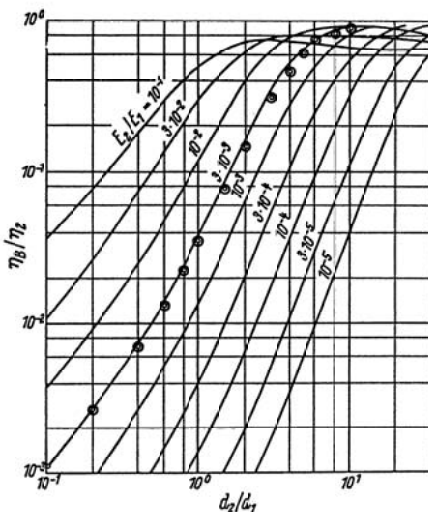


Fig. 4.19. Loss factor of beams or plates with single visco-elastic layer, after Oberst. Points show values calculated from the approximate relations, Eqs. (78) and (78a) $E'_2 / E_1 = 3 \cdot 10^{-3}$.

It is interesting to note that the loss factor for bending waves is independent of frequency, as it is for longitudinal waves, but that it is considerably higher for bending waves. Whereas for $E'_2 \eta_2 = 10^9 \text{ N/m}^2$, $d_1 = d_2$ and $E_1 = 2 \cdot 10^{11} \text{ N/m}^2$, it was previously found that the longitudinal-wave loss factor is $\eta_L \approx 5 \cdot 10^{-3}$, for the same configuration and materials the loss factor for bending waves turns out to be $\eta_B \approx 5.5 \cdot 10^{-2}$ – thus, more than 10 times greater.

Experimental measurements made on plates with attached layers have been found to be in good agreement with Fig. 4.19. Therefore, these relations may also be used for the design of damping treatments. As one may note, the total damping increases with increasing values of the product $E'_2 \eta_2$ and with increasing thickness d_2 . The damping layer therefore should not only be thick and have a high loss factor, it should also have as high a modulus of elasticity as possible. Soft materials, such as felt or soft rubber, thus are not well suited for structural damping. Useful damping materials generally consist of filled high-polymer plastics, with moduli of elasticity greater than 10^9 N/m^2 and with as high loss factors as possible.

Beside the previously discussed parameters, the separation distance a (see Fig. 4.18) also plays a significant role. Clearly, one should make a as large as possible. One can accomplish this either by increasing the thickness of the attached layer, or by using a “spacer” between the attached layer and the basic plate, Fig. 4.20. That an increase in the thickness of the attached layer increases the separation distance is obvious; the foregoing considerations also imply that one obtains the greatest amount of damping from a given thickness of damping material by applying it to only one side of the basic plate. The aforementioned spacer [4.34] essentially acts so as to amplify the motion of the basic plate, by a lever action. Ideally, the spacer should be an interlayer with a very high shear stiffness. (One typically uses a metal honeycomb structure as a spacer.) Use of a spacer increases the distance a by the thickness of the spacer, and consequently increases the loss factor considerably. If the spacer does not have a very high shear stiffness, then the increase in the loss factor is less.

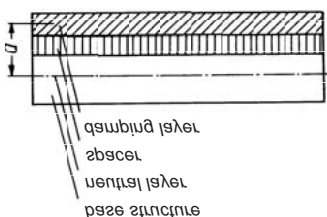


Fig. 4.20. Spacing layer for increasing the effect of a visco-elastic layer

4.6.2 Plates with Multi-Layer Treatments

It has become common practice to damp plate-like structures by attaching a layer of viscoelastic material and placing atop that layer a secondary “constraining” plate of structural material. Such arrangements are often obtained in practice by use of so-called “damping tape” (a self-adhesive, relatively thick metal foil, where the adhesive is a viscoelastic material) or in sandwich configurations which incorporate an interlayer of a highly dissipative plastic material. Also conceivable are many other “constrained layer” configurations, with or without spacers, see Fig. 4.21. In all of these constrained layer configurations, the viscoelastic material is subjected primarily to shear loading (see Fig. 4.22) caused by the covering plate extending less than the upper surface of the basic plate. The associated displacement difference ξ_2 gives rise to the shear angle $\gamma_2 = \xi_2/d_2$. By analogy to Eq. (4.21), one finds that the energy (again per unit area) that is changed into heat within the viscoelastic layer in one cycle is given by

$$W_{diss} = \pi \eta_2 G'_2 d_2 |\gamma_2|^2 = \pi \eta_2 G'_2 d_2 \left| \frac{\xi_2}{d_2} \right|^2, \quad (4.77)$$

where G_2 represents the shear modulus of the middle layer.

The reversible strain energy here, as previously, is given by

$$W_R = \frac{1}{2} B \left| \frac{d\beta}{dx} \right|^2 = \frac{1}{2} B k^2 |\beta|^2, \quad (4.78)$$

where B represents the flexural stiffness of the entire composite plate, and is made up of several parts, as will be discussed later.

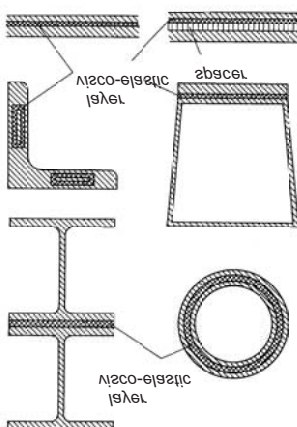


Fig. 4.21. Various configurations in which viscoelastic materials act in shear

The x -differentiation indicated in Eq. (4.78) may be carried out easily for the case where the entire composite plate vibrates only in flexure, and where the wavelengths of the motions of the two plates and of the interlayer all are the same. For the case of plane waves, from which one may obtain any desired waveform by superposition, the x -dependence of all motions is given by e^{-jkx} . Here $k = \sqrt[4]{\omega^2 m' / B}$ is the bending wavenumber, which depends on the total mass and total bending stiffness of the composite plate.

The loss factor of a composite plate, in which the energy losses are due primarily to shear of a viscoelastic interlayer, may be found from Eqs. (4.77), (4.78) and (4.22) to be given by

$$\eta = \eta_2 \frac{G'_2 d_2 |\gamma_2|^2}{B k^2 |\beta|^2}. \quad (4.79)$$

This equation still contains two unknown quantities, the flexural stiffness B of the composite plate, and the ratio of the shear angle γ_2 to the angle of flexure β . These two quantities are determined below for two special cases. Even without further analysis it is clear that the damping is enlarged by increasing the ratio γ_2/β .

4.6.2.1 Stiff Base Plate with Thin Cover Plate

If the damping treatment added to a plate is thin e.g., a damping tape, one may approximate the bending stiffness of the composite by that of the basic plate and take the extension of the viscoelastic layer as $a\beta$, see Fig. 4.22. If one takes into account that the shear forces cause the cover layer to extend by an amount ξ_3 , then one finds that the shear angle γ_2 obeys

$$d_2 \gamma_2 = \xi_2 = a\beta - \xi_3. \quad (4.80)$$

One may determine ξ_3 from the force $G_2 \gamma_2$ that acts on the cover plate and the restoring force in this plate which extends longitudinally. By replacing the inertia force in Eq. (3.3) by the shear force and using Eq. (3.2), one obtains

$$E_3 d_3 \frac{d^2 \xi_3}{dx^2} = -G_2 \gamma_2, \quad (4.81)$$

where E_3 represents the modulus of elasticity of the covering plate.

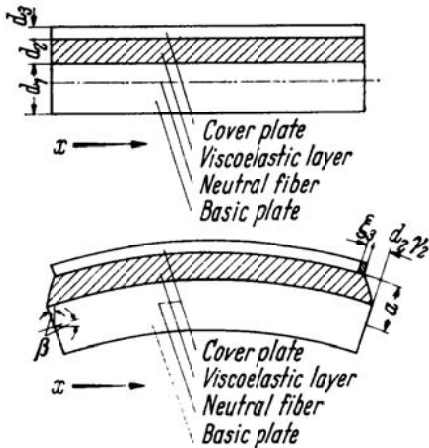


Fig. 4.22. Deformation of viscoelastic layer between two plates

Since differentiation with respect to x again is equivalent to multiplication by k , one finds from Eqs. (4.80) and (4.81) that

$$\frac{\gamma_2}{\beta} = \frac{a}{d_2} \frac{1}{1 + \frac{G_2}{E_3 d_3 d_2 k^2}}. \quad (4.82)$$

Note that the complex modulus $\underline{G}_2 = G'_2(1 + j\eta_2)$ appears above, and not the real part G'_2 of the shear modulus, as in Eqs. (4.77) and (4.79). By substituting Eq. (4.82) into (4.79), the loss factor of the composite plate can be written as

$$\eta = \eta_2 \frac{E_3 d_3 a^2 g_d}{B |1 + (1 + j\eta_2) g_d|^2}, \quad (4.83)$$

in terms of a so-called “shear parameter” g_d defined as

$$g_d = \frac{G'_2}{E_3 d_3 d_2 k^2}. \quad (4.84)$$

where index d denotes that the covering plate is thin. The shear parameter also may be expressed as

$$g_d = \frac{G'_2}{E_3 d_3 d_2 \omega} \sqrt{\frac{B}{m'}} = \frac{G'_2 \lambda^2}{4\pi^2 E_3 d_3 d_2}, \quad (4.84a)$$

where λ represents the bending wavelength of the composite plate. One may note that g_d , and therefore also the loss factor of the composite plate, depends on the frequency. In contrast, the loss factor of a plate with a single damping layer was found to be frequency independent. The variation of the loss factor with frequency, as obtained from Eq. (4.83), is shown in Fig. 4.23. As one may observe, there occurs a maximum in the damping. The frequency at which this maximum is obtained is found to obey

$$f_{\max} = \frac{1}{2\pi} \frac{G'_2 \sqrt{1+\eta_2^2}}{E_3 d_3 d_2} \sqrt{\frac{B}{m'}} \approx \frac{1}{22} \frac{c_{L1} d_1}{d_2 d_3} \frac{G'_2}{E_3} \sqrt{1+\eta_2^2}, \quad (4.85)$$

where c_{L1} represents the longitudinal wave speed in the base plate.

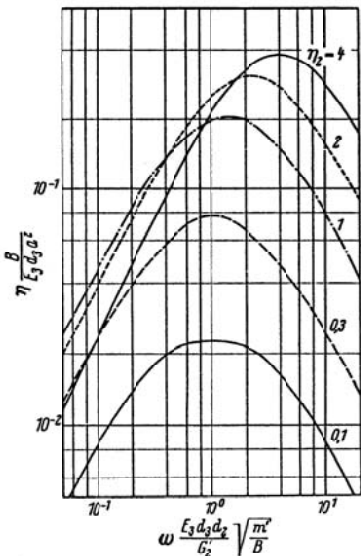


Fig. 4.23. Frequency dependence of loss factor of constrained-layer system

Since $c_{L1} \approx 5 \cdot 10^3$ m/sec for metal plates, the shear modulus of the interlayer must be much smaller than the modulus of elasticity of the covering plate, if the frequency corresponding to the damping maximum is to lie in the 100 to 1000 Hz frequency region or primary interest. The decrease in the damping on both sides of the maximum occurs relatively slowly such that the “half-value bandwidth” amounts to about 5 octaves.

There is another important difference between single-layer and multi-layer damping treatments, in addition to the frequency dependence discussed above. Whereas for a single-layer treatment the damping is proportional to the product $\eta_2 E'_2$ (see Eq. (4.76)), the damping of multi-layer treatments does not vary as the product $\eta_2 G'_2$. In fact, Eq. (4.83) indicates that the shear modulus G'_2 does not affect the magnitude of the loss factor maximum. G'_2 only determines the frequency at which this maximum occurs. In selecting viscoelastic materials here, one thus may primarily ignore the magnitude of G'_2 , and only choose a material with the largest possible loss factor η_2 . Even relatively soft plastics with $\eta_2 > 1$ may be used effectively, see Table 4.4.

The maximum damping, obtained at the optimum frequency, is given by

$$\eta_{opt} = \frac{E_3 d_3 a^2}{B} \frac{\eta_2}{2 \left(1 + \sqrt{1 + \eta_2^2} \right)}. \quad (4.86)$$

For thick base plates for which $B \approx E_1 d_1^3 / 12$ and thin covering layers for which $d_1 \gg d_2, d_1 \gg d_3$ and $a \approx d_1 / 2$, Eq. (4.86) reduces to

$$\eta_{opt} = \frac{3}{2} \frac{E_3 d_3}{E_1 d_1} \frac{\eta_2}{\left(1 + \sqrt{1 + \eta_2^2} \right)}. \quad (4.86a)$$

The greatest loss factor obtainable with $\eta_2 = 2$ (larger values are extremely rare) is about $0.9 E_3 d_3 / E_1 d_1$. By choosing appropriate dimensions, approximately 80 % of this is obtained over a rather wide band of frequencies. The “appropriate dimensions”, however, vary for different base plates and must be calculated separately for each special case.

An increase in the temperature results in a decrease in G'_2 , and thus in a lowering of the frequency at which maximum loss factor occurs.

4.6.2.2 Thick Plates with Thin Interlayer

The formulae derived in the previous section giving a loss factor proportional to $E_3 d_3$ are valid in cases where the top layer is thin and does not notably affect the compound bending stiffness. When this is not the case the formulae must be modified. Since the development is principally the same, reference is made to the literature [4.35]. The problem, moreover, is treated from another aspect in Sect. 4.6.3.2.

For the interpretation it is suitable to introduce a geometry and a shear parameter i.e.,

$$\frac{1}{h} = \frac{B_1 + B_3}{a^2} \left(\frac{1}{E_1 d_1} + \frac{1}{E_3 d_3} \right) \quad (4.87)$$

and

$$g = \frac{G'_2}{d_2 k^2} \left(\frac{1}{E_1 d_1} + \frac{1}{E_3 d_3} \right) \quad (4.87a)$$

respectively, the latter of which is analogous to that in Eq. (4.84). Herein, B_1 and B_3 are the unassembled bending stiffnesses of the base and top plates respectively and $a \approx d_2 + (d_1 + d_3)/2$ the distance to the neutral layer.

With these parameters, the loss factor of the system reads

$$\eta = \eta_2 \frac{gh}{\left| 1 + (1 + j\eta_2)g \right|^2 + gh \left[g(1 + \eta_2^2) \right]}. \quad (4.88)$$

Since

$$gh = \frac{G'_2}{d_2 k^2} \frac{a^2}{B_1 + B_3}, \quad (4.88a)$$

the analogy to (4.83) is evident. Similarly, the frequency for damping maximum is obtained by introducing

$$g_{opt} = \frac{1}{\sqrt{1+h}} \frac{1}{\sqrt{1+\eta_2^2}} \quad (4.89)$$

and the maximum by

$$\eta_{opt} = \eta_2 \frac{hg_{opt}}{2(1+g_{opt}) + hg_{opt}}. \quad (4.89a)$$

It is readily confirmed that the expressions for a thin top plate are regained for $h \ll 1$.

For the application of the expressions in (4.88) and (4.89) there is one difficulty, which relates to bending stiffness of the assembled system, required for the bending wavenumber in Eq. (4.87a). Although the complex bending stiffness can be explicitly written as

$$\underline{B} = (B_1 + B_3) \left(1 + \frac{\underline{gh}}{1 + \underline{g}} \right); \underline{g} = g(1 + j\eta_2), \quad (4.90)$$

the difficulty is not removed since g is required involving k , which in turn depends on B . It would be possible to calculate k directly (see Sect. 4.6.3)

but this implies high order polynomials and hence an iterative procedure appears easier. This means that k^2 is approached by using $B = B_1 + B_3$ or the bending stiffness from $g = g_{opt}$ as the initial value. For the special case of two equal plates i.e., $E_1 = E_3$ and $d_1 = d_3 \gg d_2$, the geometry parameter is approximately $h \approx 3$ and thence

$$\eta_{opt} = \eta_2 \frac{3}{5 + 4\sqrt{1 + \eta_2^2}} < 0.75 . \quad (4.91)$$

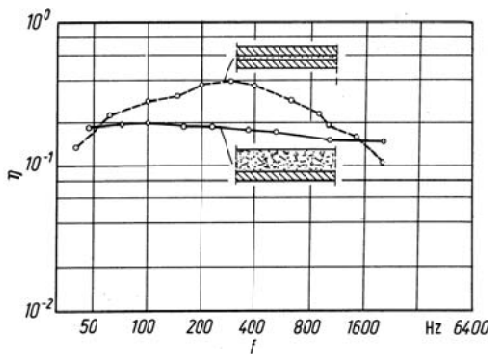


Fig. 4.24. Experimentally observed loss factors of a sandwich plate and of a plate with a simple layer ($d_2/d_1 \approx 2.5$)

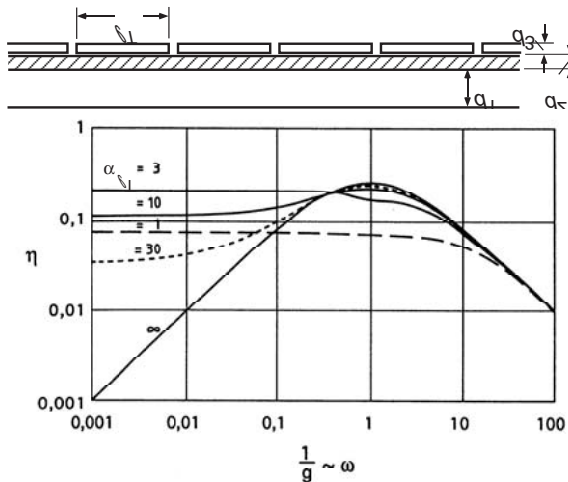


Fig. 4.25. Loss factors for a damping layer constrained by a segmented top plate. Parameter $\alpha^2 = \frac{G_2}{d_2} \left(\frac{1}{E_1 d_1} + \frac{1}{E_3 d_3} \right)$

This optimum is attained at a frequency, which is a factor four higher than that given by (4.85).

Measurement results for two plate configurations are shown in Fig. 4.24. Although the three-layer configuration exhibits an increased loss factor for a wide frequency band in comparison with that of the single-sided damped plate, the marked reduction towards low frequencies is often perceived as a disadvantage. Fortunately, this is relatively simply remedied by means of a top plate consisting of short strips. In [4.36, 4.37] is shown that such strips lead to larger shear than the corresponding all-covering top plate and thereby an enhanced low frequency damping. The most suitable strip length is $l_T = 3.3/\alpha$ where α is defined in Fig. 4.25.

In summary, one may thus conclude that three-layer plates are well suited for damping of structure-borne sound when the interlayer is developed for shearing action and the thicknesses and material properties, in particular G_2 and η_2 , can be optimised such that the loss factor maximum covers the interesting frequency range. By segmenting the top plate, the performance at low frequencies can be improved.

For equal weight, the loss factors of the three-layer plate and the single-sided damped plate are approximately equal when the best commercially available materials are used in both cases. An interesting advantage of the three-layer configuration is the high bending stiffness at low frequencies, which for equal Young's moduli of the two plates can be approximated by

$$B \approx \frac{1}{12} E_1 (d_1 + d_3)^3; g \gg 1. \quad (4.92)$$

For high frequencies, on the other hand, following Eq. (4.90)

$$B \approx B_1 + B_3 = \frac{1}{12} E_1 (d_1^3 + d_3^3); g \ll 1. \quad (4.92a)$$

This means that the, for the sound transmission loss pivotal, critical frequency is shifted upwards in frequency [4.38] cf., Chapter 7.

4.6.3 Equations of Motion of Layered Plates

4.6.3.1 Free Damping Layers

For many applications, it is insufficient with only the loss factor derived from static considerations but additional dynamic characteristics must be detailed such as the coupling between flexural and tensional waves. This means that the complete set of the equations of motion must be available.

To achieve this it is suitable to employ Hamilton's principle as was done in Sects. 2.5.1 and 3.8.

Upon assuming that the motions of the two-layer system depicted in Fig. 4.26 can be described by means of the longitudinal motion ξ_L of the plane $y = 0$, the transversal motion ξ_2 and a rotation β , the motion in the x -direction ξ_1 can be written as

$$\xi_1 = \xi_L + y\beta, \quad (4.93)$$

which is valid for any plane y . The actual position of the plane $y = 0$ with respect to the interface between the two layers is not specified. It is arbitrary and need not coincide with the neutral layer. This means, however, that the displacement ξ_L also depends on the choice of the plane $y = 0$, which will be further discussed subsequently.

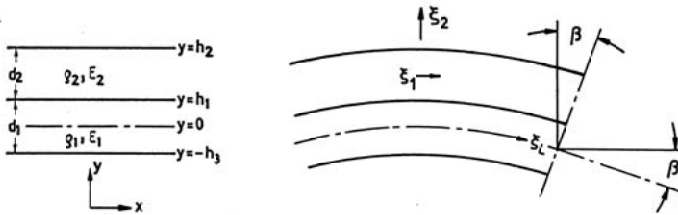


Fig. 4.26. Notations for a two-layer system with densities ρ_1 , ρ_2 and Young's moduli E_1 , E_2

For the strain, Eqs. (3.114) to (3.118) yield with the use of (4.93)

$$\begin{aligned} \varepsilon_x &= \frac{\partial \xi_1}{\partial x} = \frac{\partial \xi_L}{\partial x} + y \frac{\partial \beta}{\partial x}, \\ \gamma_{xy} &= \frac{\partial \xi_1}{\partial y} = \frac{\partial \xi_L}{\partial x} = \beta + \frac{\partial \xi_2}{\partial x}. \end{aligned} \quad (4.94)$$

A limitation to Euler-Bernoulli bending theory implies that $\gamma_{xy} = 0$ which gives

$$\beta = -\frac{\partial \xi_2}{\partial x} = -\xi_2'. \quad (4.95)$$

This is the elementary relation between the bending translation and rotation, given in Eq. (3.68) although the sign is changed due to the altered positive direction of the translation. The spatial derivative with respect to x

is abbreviated by means of a prime in this section and temporal derivatives by means of a dot.

The approximation in (4.95) could have been omitted for the further analysis. This would have meant that a similar procedure had to be employed as for the treatise of the Timoshenko beam in Sect. 3.8.2. For the sake of brevity, however, this route is discarded since no new information is revealed.

The necessary formulae for the application of Hamilton's principle on a beam of extension $-1 \leq x \leq 1$ read

$$E_{kin} = \frac{\rho_1}{2} \int_{-1-h_3}^{h_1} \int_{-h_3}^{h_1} (\dot{\xi}_1^2 + \dot{\xi}_2^2) dx dy + \frac{\rho_2}{2} \int_{-1-h_1}^{h_2} \int_{-h_1}^{h_2} (\dot{\xi}_1^2 + \dot{\xi}_2^2) dx dy, \quad (4.96)$$

and

$$\begin{aligned} E_{pot} &= \frac{E_1}{2} \int_{-1-h_3}^{h_1} \int_{-h_3}^{h_1} \varepsilon_x^2 dx dy + \frac{E_2}{2} \int_{-1-h_1}^{h_2} \int_{-h_1}^{h_2} \varepsilon_x^2 dx dy \\ &= \frac{E_1}{2} \int_{-1-h_3}^{h_1} \int_{-h_3}^{h_1} (\xi'_L - y\xi''_2)^2 dx dy + \frac{E_2}{2} \int_{-1-h_1}^{h_2} \int_{-h_1}^{h_2} (\xi'_L - y\xi''_2)^2 dx dy. \end{aligned} \quad (4.97)$$

Upon carrying out the integration with respect to y , using the abbreviations

$$\begin{aligned} m_E &= \rho_1 \int_{-h_3}^{h_1} dy + \rho_2 \int_{-h_1}^{h_2} dy = \rho_1 d_1 + \rho_2 d_2, \\ m_Z &= \rho_1 \int_{-h_3}^{h_1} y dy + \rho_2 \int_{-h_1}^{h_2} y dy = \frac{\rho_1}{2} d_1 (h_1 - h_3) + \frac{\rho_2}{2} d_2 (h_1 + h_2), \\ m_D &= \rho_1 \int_{-h_3}^{h_1} y^2 dy + \rho_2 \int_{-h_1}^{h_2} y^2 dy \\ &= \frac{\rho_1}{3} d_1 (h_1^2 - h_1 h_3 + h_3^2) + \frac{\rho_2}{3} d_2 (h_1^2 + h_1 h_2 + h_2^2), \end{aligned} \quad (4.98)$$

and, correspondingly

$$\begin{aligned} E_E &= E_1 d_1 + E_2 d_2, \\ E_Z &= \frac{E_1}{2} d_1 (h_1 - h_2) + \frac{E_2}{2} d_2 (h_1 + h_2), \\ E_D &= \frac{E_1}{3} d_1 (h_1^2 - h_1 h_3 + h_3^2) + \frac{E_2}{3} d_2 (h_1^2 + h_1 h_2 + h_2^2), \end{aligned} \quad (4.99)$$

one obtains

$$\begin{aligned} E_{kin} &= \frac{1}{2} \int_{-1}^1 \left(m_E \dot{\xi}_L^2 - 2m_Z \dot{\xi}_L \dot{\xi}_2' + m_D \dot{\xi}_2'^2 + m_E \dot{\xi}_2^2 \right) dx, \\ E_{pot} &= \frac{1}{2} \int_{-1}^1 \left(E_E \dot{\xi}_L'^2 - 2E_Z \dot{\xi}_L' \dot{\xi}_2'' + E_D \dot{\xi}_2''^2 \right) dx, \end{aligned} \quad (4.100)$$

The aim of the following steps is to rewrite the expressions involved in the variation

$$\delta \int_{t_1}^{t_2} (E_{kin} - E_{pot}) dt$$

so that only $\delta\xi_L$ or $\delta\xi_2$ appear. This is done in accordance with Sect. 3.8 regarding the derivative of the equation of motion for the Timoshenko beam. Again, this is achieved by transferring the derivatives as in Eqs. (3.190f) and (3.190g). In this manner arise linear expressions in $\delta\xi_L$ and $\delta\xi_2$ and those variations can only vanish when the factors in front equal zero i.e.,

$$\begin{aligned} E_E \ddot{\xi}_L'' - m_E \ddot{\xi}_L - m_Z \ddot{\xi}_2' + E_Z \ddot{\xi}_2''' &= 0, \\ m_Z \ddot{\xi}_L' - E_Z \ddot{\xi}_L''' - E_D \ddot{\xi}_2''' - m_E \ddot{\xi}_2'' + m_D \ddot{\xi}_2'' &= 0 = (p_A). \end{aligned} \quad (4.101)$$

This is thus the equations of motion for a two-layer beam. The pressure p_A is introduced subsequently and represents an externally applied force per unit area (or unit length) acting perpendicular to the plate or beam. It can be incorporated through the variation of the external work $\delta W = p_A \delta \xi_2$ as shown in Eq. (3.188).

As is obvious from a comparison with (3.31) and (3.81), Eq. (4.101) describe the coupling of quasi-longitudinal and flexural waves. m_E is herein the mass per unit area or length, E_E and E_D are the stiffnesses in tension or bending respectively. The coupling comes into play through E_Z and m_Z . With the exception of the special case of $E_1/\rho_1 = E_2/\rho_2$, the coupling terms cannot be made to vanish even with a suitable choice of the plane $y = 0$. This means that the bending translation ξ_2 is always coupled to a longitudinal motion in a rigorous sense. The coupling, however, can be made very small by making the plane $y = 0$ coincide with the neutral layer of the system, which in this case is given by $E_Z = 0$. From Eq. (4.99) therefore,

$$h_1 = \frac{E_1 d_1^2 - E_2 d_2^2}{2(E_1 d_1 + E_2 d_2)}, \quad (4.102)$$

since $h_3 = d_1 - h_1$ and $h_2 = d_2 + h_1$. The static bending stiffness per unit width of the double-beam thus becomes

$$E_D = B = \frac{E_1 d_1^3}{12} + \frac{E_2 d_2^3}{12} + \frac{E_2 d_2}{1 + E_2 d_2 / E_1 d_1} \left[\left(\frac{d_1 + d_2}{2} \right)^2 - \frac{d_1 d_2}{3} \right]. \quad (4.103)$$

This expression is identical to that used by Oberst [4.12] and almost alike that in Eq. (4.76a). The expression (4.103) can be used to compute the bending wavenumber and the loss factor for complex Young's moduli E_1 and E_2 . The results are identical to those of Sect. 4.6.1 and presented in Fig. 4.19. The same is true for the extensional wave at the neutral layer since, omitting the coupling i.e., with $\omega^2 m_Z = 0$, the wavenumber is given by

$$k_L^2 = \omega^2 \frac{\rho_1 d_1 + \rho_2 d_2}{E_1 d_1 + E_2 d_2}. \quad (4.104)$$

If the principally static consideration is to be avoided wherein $\omega^2 m_Z = 0$, constituting the basis for Eqs. (4.103) and (4.104), the remaining option is to determine the complex wavenumber of the free waves from (4.101). In this pursuit, the wave is assumed in the form $e^{j k x} e^{j \omega t}$, leading to

$$\begin{aligned} (\omega^2 m_E - k^2 E_E) \hat{\xi}_L - jk(\omega^2 m_Z + k^2 E_Z) \hat{\xi}_2 &= 0, \\ -jk(\omega^2 m_Z + k^2 E_Z) \hat{\xi}_L + (k^4 E_D - \omega^2 m_E - k^2 \omega^2 m_D) \hat{\xi}_2 &= 0 = (p_A). \end{aligned} \quad (4.105)$$

The determinant to this system is

$$\begin{aligned} \text{Det} = k^6 (E_Z^2 - E_E E_D) + k^4 \omega^2 (E_D m_E - 2E_Z m_Z + E_E m_D) \\ + k^2 \omega^2 [E_E m_E + \omega^2 (m_Z^2 - m_E m_D)] - \omega^4 m_E. \end{aligned} \quad (4.106)$$

It is easy to convince oneself that the coefficients of this polynomial are independent of the position of the plane $y = 0$, which is required and initially arbitrarily introduced. If the analysis is confined to the neutral layer i.e., $E_Z = 0$, Eq. (4.106) is simplified but does not split into two equations. To obtain a split, $\omega^2 m_Z$ must be set equal to zero and thus a quasi-static calculation is undertaken. By letting (4.106) equal zero, the solution $\pm k_L, \pm k_{BP}$ and $\pm jk_{BN}$ results i.e., the wavenumbers of the extensional and the propagating and evanescent flexural waves. The numerical results are very close to those resulting from a quasi-static analysis.

Equations (4.105), moreover, describe the coupling between the extensional wave motion at the neutral layer ξ_{LN} and the bending motion ξ_2 . The first equation in (4.105) yields with $E_Z = 0$

$$\frac{\hat{\xi}_{LN}}{\hat{\xi}_2} = \frac{jk\omega^2 m_Z}{\omega^2 m_E - k^2 E_E} \approx -\frac{j\omega^2 m_Z}{kE_E} \approx j\pi \frac{\rho_2 d_2}{\rho_1 d_1} \frac{\lambda(d_1 + d_2)}{\lambda_{L1}^2}. \quad (4.107)$$

λ_{L1} is here the wavelength of the longitudinal wave in beam 1 and $\lambda = 2\pi/k$ the wavelength of the motion of interest e.g., the bending of the system. For the approximation it is assumed that $\lambda_{L1} > \lambda$ and $E_1/\rho_1 > E_2/\rho_2$. It is seen that the coupling between ξ_2 and ξ_{LN} indeed exists but that it is weak, particularly at low frequencies since $\lambda < \lambda_{L1}$ as well as $d_1 + d_2 < \lambda_{L1}$. The separate treatment of the two kinds of motion, moreover, is justified by the common applications.

The wave impedance, frequently used in Sect. 4.4, can also be obtained from Eq. (4.105). With $E_Z = 0$,

$$Z_{\sim} = \frac{\hat{p}_A}{\hat{V}_A} = \frac{\hat{p}_A}{j\omega \hat{\xi}_A} = j\omega m_E \left(1 - \frac{k^4 E_D}{\omega^2 m_E} + \frac{k^2 m_D}{m_E} - \frac{k^2 \omega^2 m_Z^2}{m_E (\omega^2 m_E - k^2 E_E)} \right). \quad (4.108)$$

Upon introducing the approximations employed above and letting $k^2 m_D \ll m_E$, which is also made in ordinary bending theory, one finds

$$\begin{aligned} Z_{\sim} &= j\omega m_E \left(1 - \frac{k^4 E_D}{\omega^2 m_E} + \frac{\omega^2 m_Z^2}{E_E m_E} \right) \\ &\approx j\omega m_E \left[1 - \frac{k^4 E_D}{\omega^2 m_E} + \left\{ \frac{\rho_1 d_1}{\rho_2 d_2} \frac{\pi(d_1 + d_2)}{\lambda_{L1}} \right\}^2 \right]. \end{aligned} \quad (4.109)$$

With the exception of the last term within the brackets, this is the wave impedance of an ordinary beam. The correction due to the coupling is again small since $d_1 + d_2 \ll \lambda_{L1}$.

4.6.3.2 Three-layer plates and beams

The analysis of three-layer systems is similar to that employed for the two-layer structures in the previous section. For the former configuration, however, the shear stiffness plays a profound role and the approximation in (4.95) does not apply. With the notation given in Fig. 4.27, the motions of the three layers read

$$\begin{aligned} \xi_I &= \xi_L + y\beta_I, \\ \xi_H &= \xi_L + h_1\beta_I + (y - h_1)\beta_H, \\ \xi_M &= \xi_L + h_1\beta_I + d_2\beta_H + (y - h_1 - d_2)\beta_M. \end{aligned} \quad (4.110)$$

As before, ξ_L is the displacement in the x -direction in the plane $y = 0$, which does not necessarily coincide with the neutral layer. The position of the plane $y = 0$ i.e., the value of h_1 is again arbitrary. As in the case of two-layer structures, the displacement ξ_2 refers to the y -direction. It is the same for all layers in this treatment.

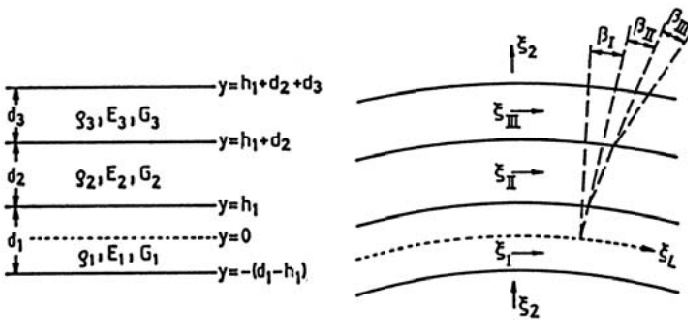


Fig. 4.27. Notations for a three-layer system with densities ρ_1, ρ_2, ρ_3 , Young's moduli E_1, E_2, E_3 and shear moduli G_1, G_2, G_3

From Eqs. (4.110), the strains become

$$\varepsilon_{Ix} = \frac{\partial \xi_L}{\partial x} = \xi'_L + y\beta'_I; \text{ analogous for } \varepsilon_{II} \text{ and } \varepsilon_{III} \quad (4.111)$$

$$\gamma_{Iy} = \frac{\partial \xi_L}{\partial y} + \frac{\partial \xi_2}{\partial x} = \beta_I + \xi'_2; \text{ analogous for } \gamma_{II} \text{ and } \gamma_{III}$$

Upon carrying out the same but substantially longer calculation as in the previous section, the equations of motion for the three-layer system result in form of second order differential equations in the variables $\xi_L, \xi_2, \beta_I, \beta_{II}$ and β_{III} . With the wave motion assumed in the form $e^{-jky} e^{j\omega t}$, a differentiation with respect to time is a multiplication by $j\omega$ and a differentiation with respect to space a multiplication by $-jk$ and the system of equations can be written as

$$\begin{pmatrix} \alpha_{11} & 0 & \alpha_{13} & \alpha_{14} & \alpha_{15} \\ 0 & \alpha_{22} & \alpha_{23} & \alpha_{24} & \alpha_{25} \\ \alpha_{13} & \alpha_{23} & \alpha_{33} & \alpha_{34} & \alpha_{35} \\ \alpha_{14} & \alpha_{24} & \alpha_{34} & \alpha_{44} & \alpha_{45} \\ \alpha_{15} & \alpha_{25} & \alpha_{35} & \alpha_{45} & \alpha_{55} \end{pmatrix} \begin{pmatrix} \hat{\xi}_L \\ \hat{\xi}_2 \\ \hat{\beta}_I \\ \hat{\beta}_{II} \\ \hat{\beta}_{III} \end{pmatrix} = \begin{pmatrix} 0 \\ p_A \\ 0 \\ 0 \\ 0 \end{pmatrix}, \quad (4.112)$$

when the system is excited by the pressure p_A in the y -direction. For a beam-like system, the coefficients are given by:

$$\begin{aligned} \alpha_{11} &= k^2 E_E - \omega^2 m_E, \quad \alpha_{13} = \left(E_E h_1 - \frac{1}{2} E_1 d_1^2 \right) k^2 - \left(m_E h_1 - \frac{1}{2} \rho_1 d_1^2 \right) \omega^2, \\ \alpha_{14} &= \left(\frac{1}{2} E_2 d_2^2 + E_3 d_2 d_3 \right) k^2 - \left(\frac{1}{2} \rho_2 d_2^2 + \rho_3 d_2 d_3 \right) \omega^2, \\ \alpha_{15} &= \frac{1}{2} E_3 d_3^2 k^2 - \frac{1}{2} \rho_3 d_3^2 \omega^2, \quad \alpha_{22} = -G_2 k^2 + \omega^2 m_E, \\ \alpha_{23} &= -jk G_1 d_1, \quad \alpha_{24} = -jk G_2 d_2, \quad \alpha_{25} = -jk G_3 d_3, \\ \alpha_{33} &= [E_E h_1^2 - E_1 d_1^2 (h_1 - d_1/3)] k^2 - [m_E h_1^2 - \rho_1 d_1^2 (h_1 - d_1/3)] \omega^2 + G_1 d_1, \\ \alpha_{34} &= \alpha_{14} h_1, \quad \alpha_{35} = \alpha_{15} h_1, \\ \alpha_{44} &= \left(\frac{1}{3} E_2 d_2^3 + E_3 d_2^2 d_3 \right) k^2 - \left(\frac{1}{3} \rho_2 d_2^3 + \rho_3 d_2^2 d_3 \right) \omega^2 + G_2 d_2, \\ \alpha_{45} &= d_2 \alpha_{15}, \quad \alpha_{55} = \frac{1}{3} E_3 d_3^3 k^2 - \frac{1}{3} \rho_3 d_3^3 \omega^2 + G_3 d_3, \\ E_E &= E_1 d_1 + E_2 d_2 + E_3 d_3, \quad m_E = \rho_1 d_1 + \rho_2 d_2 + \rho_3 d_3, \\ G_E &= G_1 d_1 + G_2 d_2 + G_3 d_3. \end{aligned}$$

Again, the free wavenumbers are determined by equating the determinant of (4.112) to zero and the loss factors are obtained the same way when the moduli are complex. Since the determinant is a fifth order polynomial in k^2 , there are five solutions at every frequency of which the quasi-longitudinal and the bending type solutions are propagating. The remaining three solutions represent exponentially decaying near fields (evanescent waves).

The wavenumbers can also be computed in analogy with Eq. (4.108). Thereby, is demonstrated that for an excitation and motion in y -direction, the free wavenumbers as well as the wave impedance are independent of the arbitrarily chosen h_1 .

A marked simplification of (4.112) results when it is assumed that no shear occurs in the top and bottom layers, I and II, as is done in simple bending theory. This means that

$$\beta_{III} = \beta_I = -\xi'_2 \Rightarrow \beta_{III} = \beta_I = jk\xi_2 \quad (4.113)$$

To maintain symmetry of the system of equations, it is suitable to multiply the third and fifth rows by jk and add them to the second. Thereby is obtained

$$\begin{pmatrix} \alpha_{11} - \frac{\alpha_{14}^2}{\alpha_{44}} jk & jk \left(\alpha_{13} + \alpha_{15} - \frac{\alpha_{14}\gamma_{23}}{\alpha_{44}} \right) \\ jk \left(\alpha_{13} + \alpha_{15} - \frac{\alpha_{14}\gamma_{23}}{\alpha_{44}} \right) & \gamma_{22} + k^2 \frac{\gamma_{25}^2}{\alpha_{44}} \end{pmatrix} \begin{pmatrix} \xi_L \\ \xi_2 \end{pmatrix} = \begin{pmatrix} 0 \\ p_A \end{pmatrix} \quad (4.114)$$

in which

$$\begin{aligned} \gamma_{22} &= -k^2 G_2 d_2 + \omega^2 m_E - k^4 [B_1 + B_3 + E_1 d_1 h_{11}^2 + E_3 d_3 h_{13}^2 + E_2 d_2 h_1^2] \\ &\quad + \omega^2 k^2 [M_1 + M_3 + \rho_1 d_1 h_{11}^2 + \rho_3 d_3 h_{13}^2 + \rho_2 d_2 h_1^2], \\ \gamma_{23} &= -G_2 d_2 + k^2 \left[E_3 d_2 d_3 h_{13} + \frac{1}{2} E_2 d_2^2 h_1 \right] - \omega^2 \left[\rho_3 d_2 d_3 h_{13} + \frac{1}{2} \rho_2 d_2^2 h_1 \right], \\ h_{11} &= h_1 - d_1 / 2, \quad h_{13} = h_1 + d_3 / 2. \end{aligned}$$

The quantities B_1 , B_3 , M_1 and M_3 are the bending stiffnesses and second mass moments of inertia of layers I and III respectively, where the intermediate layer is assumed arbitrarily soft,

$$B_1 = \frac{E_1 d_1^3}{12}, \quad B_3 = \frac{E_3 d_3^3}{12}, \quad M_1 = \frac{\rho_1 d_1^3}{12}, \quad M_3 = \frac{\rho_3 d_3^3}{12}.$$

The determinant of Eq. (4.114) is a fourth order polynomial in k^2 . Upon equating this to zero, the four solutions obtained correspond to propagating quasi-longitudinal and bending waves and evanescent bending and shear waves.

As in conjunction with Eq. (4.101), one may ask the question whether a suitable choice of h_1 leads to a decoupling of the two equations in (4.114). Again, this turns out not to be the case without allowing for a frequency dependent h_1 .

A highly useful approximation for not too high frequencies [4.39] can be achieved by letting E_2 vanish. This means that the intermediate layer is assumed to be very soft in compression. It is assumed, moreover, that all inertia terms except $\omega^2 m_E$ can be neglected i.e., $M_1 = M_3 = 0$ and $\rho_2 = \rho_3 = 0$. Hereby, the two equations in (4.114) can be decoupled by selecting h_1 such that

$$\alpha_{13} + \alpha_{15} - \frac{\alpha_{14}\gamma_{23}}{\alpha_{44}} = 0,$$

which can be shown to be equivalent to

$$h_1 = \frac{E_1 d_1^2 (1 + g_3) - E_3 d_3^2 g_3 (d_3 + 2d_2)}{2 [E_1 d_1 (1 + g_3) + E_3 d_3 g_3]}, \quad (4.115)$$

where $g_3 = G_2/(E_3 d_2 d_3 k^2)$. Equation (4.115) presents the position of the neutral layer of a three-layer beam structure. With the approximations introduced above, Eq. (4.114) yields

$$\begin{aligned} & \left[k^2 E_E - \omega^2 m_E - \frac{E_3 d_3 k^2}{1 + g_3} \right] \hat{\xi}_{LNF} = 0 \\ & \left\{ \omega^2 m_E - k^4 \left[B_1 + B_3 + g_3 \frac{E_1 d_1 E_3 d_3}{E_1 d_1 (1 + g_3) + E_3 d_3 g_3} \left(\frac{d_1}{2} + \frac{d_3}{2} + d_2 \right)^2 \right] \right\} \hat{\xi}_2 = \hat{p}_A \end{aligned} \quad (4.116)$$

The first of the two equations describes the quasi-longitudinal wave at the neutral layer of the three-layered beam. The second describes the bending wave whereby the expression within brackets corresponds to the bending stiffness in (4.90). Hence, the approximation introduced recover the simplified formulae of Sect. 4.6.2.

It should be pointed out that (4.116) implies the solutions of one second and one third order equation in k^2 since also g_3 depends on k^2 . Commonly, an initial value is inserted in g_3 and an iterative procedure is used.

4.7 Damping by means of Resonant Systems

All of the previously discussed composite plates have a rather broadband effect, as is desirable for practical applications where excitation occurs by noise. However, for narrow frequency band excitation such as by transformers and wheel squeal, it is often useful to tune the damping to the narrow band of interest, thereby sacrificing bandwidth for the sake of obtaining very high damping in the narrow band.

The simplest case of such tuned damping resonators consists of independent spring-mass systems attached to the surface that is to be damped.

Consider a rod along which are attached many independent springs and masses, as shown in Fig. 4.28. If quasi-longitudinal waves propagate along the rod, then each of the springs obeys

$$F' = \underline{s}'(\xi_S - \xi_M), \quad (4.117)$$

where F' denotes the exciting force, ξ_S and ξ_M represent the displacements of the two ends of the spring, and s' denotes the complex spring stiffness. Since all springs here act in shear, one may write

$$\underline{s}' = \underline{G}_F \frac{b}{l} = G'_F (1 + j\eta_F) \frac{b}{l}, \quad (4.118)$$

where G_F represents the shear modulus, η_F the loss factor of the spring material, l the distance between the beam and each attached mass, and b the width of the spring material.

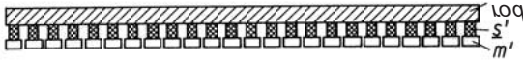


Fig. 4.28. Rod with attached damped spring-mass systems

From Newton's law, one finds that the motion of the mass obeys

$$F' = -\omega^2 m' \xi_M, \quad (4.119)$$

where the form of $e^{j\omega t}$ is understood for the motion. If one now introduces the velocity $v_S = j\omega \xi_S$, one obtains

$$F' = \frac{j\omega m' v_S}{1 - \frac{\omega^2}{\omega_0^2}}, \quad (4.120a)$$

where

$$\underline{\omega}_0^2 = \frac{s'}{m'} = \frac{G'_F b}{l m'} (1 + j\eta_F) = \omega_0^2 (1 + j\eta_F) \quad (4.120b)$$

represents the square of the complex natural frequency of each spring-mass system.

In order to determine the vibratory motion, one only needs to apply Eqs. (3.29) and (3.30), after extending these to include the force as given by Eq. (4.120a). The longitudinal motion of a beam with attached springs and masses thus obeys

$$-\frac{dF}{dx} = j\omega\rho S v_S + \frac{j\omega m'}{1 - \frac{\omega^2}{\underline{\omega}_0^2}} v_S,$$

$$-ES \frac{dv_S}{dx} = j\omega F.$$
(4.121)

Differentiation with respect to x then leads to

$$\frac{d^2 v_S}{dx^2} + \omega^2 \frac{\rho}{E} \left(1 - \frac{m'}{\rho S} \frac{\omega_0^2 (1 + j\eta_F)}{\omega^2 - \omega_0^2 - j\eta_F \omega_0^2} \right) v_S = 0.$$
(4.122)

As one would expect, for $m' = 0$ this equation reduces to the usual wave equation.

The attached springs and masses result in changing the wavenumber, which for the original untreated beam is given by $k_{L0}^2 = \omega^2 / c_0^2 = \omega^2 \rho / E$, to the new value k , which obeys

$$k^2 = k_{L0}^2 \left[1 + \frac{m'}{\rho S} \frac{(1-v^2) + \eta_F^2}{(1-v^2)^2 + \eta_F^2} - j\eta_F \frac{m'}{\rho S} \frac{v^2}{(1-v^2)^2 + \eta_F^2} \right],$$
(4.123)

where $v = \omega/\omega_0$. This change involves both the real and the imaginary part of the wavenumber. Thus, attachment of the damped springs and masses results in changing both the propagation velocity along the beam and the damping.

Figure 4.29 shows how the propagation velocity and damping vary with frequency, for the case where the attached masses in total amount to 10 % of the mass of the beam. In the vicinity of the resonance, the attached springs and masses may be seen to produce a small change in the propagation velocity and a considerably amount of damping. This damping may even become so high that the assumption of $\eta \ll 1$ originally made in the derivation does not remain valid.

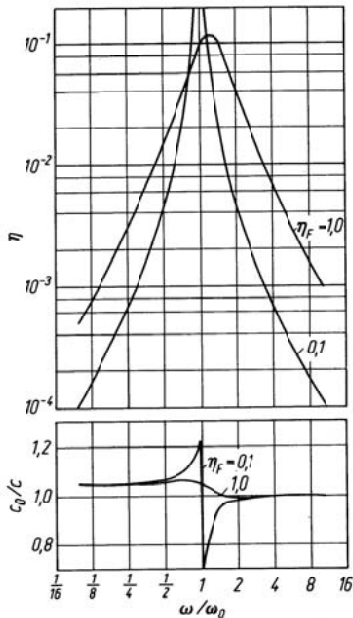


Fig. 4.29. Loss factor and propagation velocity of beam with added spring-mass systems, $m'/\rho S = 0.1$

One may readily extend Eqs. (4.117) to (4.123) to other systems attached to the beam, if these systems act independently of each other. One merely needs to use the input impedance

$$\underline{Z}' = \frac{F'}{v_S}$$

of an attached system (per unit length of the beam) in Eq. (4.118) to obtain the differential equation

$$\frac{d^2 v_S}{dx^2} + \omega^2 \frac{\rho}{E} \left(1 - j \frac{\underline{Z}'}{\omega \rho S} \right) v_S = 0, \quad (4.124)$$

which represents a generalization of Eq. (4.122). The real part of the input impedance determines the magnitude of the damping. If this impedance is purely real, the damping can be very large. The driving point impedance of a plate is an example of such a real impedance, see Eq. (4.47). Thus, one may obtain very considerable amounts of damping of quasi-longitudinal

waves by means of thin damped plates attached normal to the axis of the beam. Loss factors of 0.3 are achievable with such configurations.

The damping of the previously discussed systems may also be derived by use of the energy methods of Sect. 4.6. If the loading by the added attached springs and masses is not too great, then the reversible strain energy stored in a beam of length l may be written as

$$W_R'' = \frac{1}{2} \rho S l |v_s^2|.$$

The energy lost by the beam per unit time is given by

$$\frac{1}{2} n \operatorname{Re}\{v_s F^*\} = \frac{n}{2} |v_s|^2 \operatorname{Re}\{\underline{Z}_E\},$$

where n is the number of attached systems and \underline{Z}_E represents the driving point impedance of such systems. Thus, the energy lost per period T of the vibration is

$$W_{diss}'' = \frac{n}{2} |v_s|^2 T \operatorname{Re}\{\underline{Z}_E\} = \frac{n\pi}{\omega} |v_s|^2 \operatorname{Re}\{\underline{Z}_E\}.$$

In view of the definition, Eq. (4.22), the loss factor of the total arrangement thus is given by

$$\eta = \frac{n \operatorname{Re}\{\underline{Z}_E\}}{l \omega \rho S}. \quad (4.125)$$

Since $n\underline{Z}_E/l$ corresponds to the driving point impedance per unit length, one finds that Eqs. (4.123) and (4.125) give very nearly the same result. The small discrepancy may be ascribed to the fact that the attached systems also store reversible energy, which here has been neglected.

The same kind of analysis as was carried out above for quasi-longitudinal wave can also be performed for torsional and flexural waves. For this purpose, the forces due to the external loads are added to the inertia forces. For bending waves is obtained

$$\frac{d^4 v}{d^4 x} - k_{B0}^4 \left(1 - j \frac{\underline{Z}'}{\omega \rho S} \right) v = 0 \quad (4.126)$$

instead of Eq. (3.108). Here \underline{Z}' represents the driving-point impedance per unit length of the added system, ρS denotes the beam mass per unit length, and k_{B0} is the bending wavenumber of the original untreated beam. Clearly, the damping is again determined by the real part of the impedance. For attached simple spring-mass systems, the damping again exhibits a definite peak, and the overall behaviour is much like that indicated in Fig. 4.29.

An example of experimental results for a beam damped by attached resonators is shown in Fig. 4.30 [4.40]. The beam vibrates in flexure and has many small differently tuned sheet-metal strips attached to it, each strip being lightly damped. Nevertheless, this configuration leads to loss factors of 0.01 to 0.02. Although this value is not particularly high (the weight of the added strips was about 9 % of the weight of the beam; for the same amount of added weight one could obtain three to four times as high a loss factor by use of a simple added viscoelastic layer), this type of configuration is likely to be of practical interest for special-purpose applications, because one may obtain almost any desired frequency dependence.

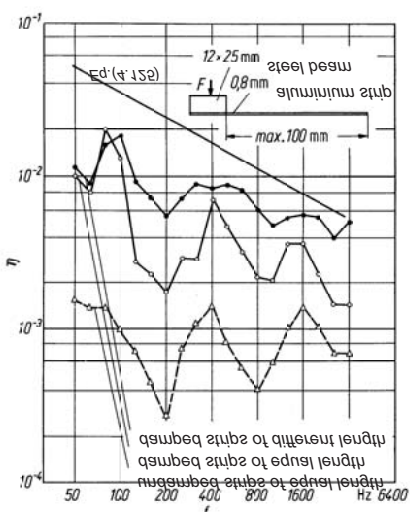


Fig. 4.30. Loss factor of beam with sheet-metal strip resonators

Another system in which the damping is of a resonant nature consists of two plates that are interconnected by resilient elements. Such plates in effect are two coupled systems, which may be described by means of two coupled bending-wave equations. The exact expressions obtained for the two bending wavenumbers are rather complicated the general case, see Sect. 6.7.1. However, it is found that the damping is greatest at

$$\omega = \omega_0 = \sqrt{\frac{s''(m_1'' + m_2'')}{m_1'' m_2''}},$$

where s'' represents the spring-constant of the interlayer per unit area, and m_1'' and m_2'' denote the masses per unit area of the two plates. ω_0 then represents the resonance frequency of the two masses interconnected by the spring. Above and below ω_0 the damping is relatively small. This fact is sometimes of importance for multi-layer plates with very soft or thick interlayers, for which the relatively high loss factors indicated in Sect. 4.6.2 is not obtained above ω_0 . One therefore should be careful not to make the interlayers of multi-layer composites too soft.

4.7.1 Damping by Thick Layers (Ballast)

For thick layers, damping is achieved by radiation of structure-borne sound energy to a material with high losses. There is thus a certain resemblance to airborne sound radiation treated in Chapter 7. For the following it is assumed that the wavelength λ_p of the vibrating structure is larger than that of the thick lossy layer c_M/f . With the quantities of Chapter 7, this means that the radiation efficiency is approximately unity, $\sigma \approx 1$. This approximation implies that the layer can be treated as a one-dimensional wave-guide of density ρ_M and the complex speed of sound c_M . When the wave-guide is free at the remote end at the distance d from the interface with the structure as depicted in Fig. 4.31, then the input impedance per unit area is

$$\underline{Z}' = j\rho_M c_M \tan(\omega d / c_M); c_M = c'_M \sqrt{1 + j\eta_M} \quad (4.128)$$

Herein, η_M is the loss factor of the layer material. If the base structure performs bending vibrations, c_M is given by the longitudinal wave speed of the layer whereas for longitudinal vibrations, the shear wave speed is to be chosen.

Upon substituting Eq. (4.128) into (4.124) or (4.126), the loss factor of the assembly can be estimated approximately. An example is shown in Fig. 4.31 where extensional waves in an aluminium rod are damped. For the damping is employed a soft rubber layer for which $c_M \approx 100$ m/s and $\eta_M \approx 0.9$. The first thickness resonance of the layer is at about 2000 Hz, $\omega d / c_M = \pi/2$. As can be observed, the loss factor diminishes rapidly below this frequency since only little energy is transmitted to the layer. Above the first thickness resonance, the subsequent resonances are barely visible owing to the high loss factor. In this frequency range it is possible to set $\text{Re}[Z'_M] \approx \rho_M c'_M$.

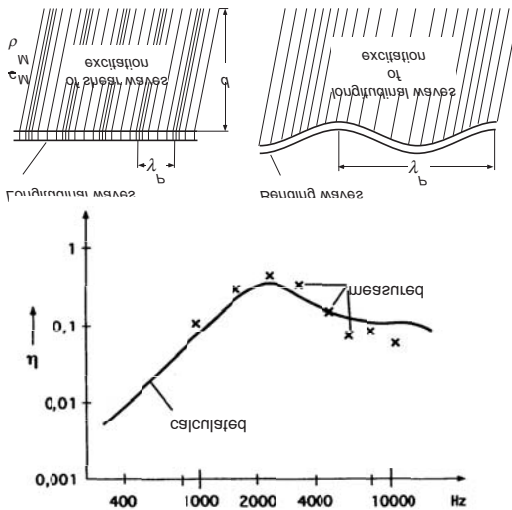


Fig. 4.31. Damping by structure-borne sound radiation to a thick layer (liner) of soft material ($\lambda_p > c_M/f$)

Compared with a free damping layer treatment of mass equal to that of the thick layer, almost the same loss factor is obtained above the first thickness resonance. Soft, lossy layers accordingly, are suitable for damping of structure-borne sound provided they are sufficiently thick. Their particular advantage is that longitudinal waves are almost as strongly damped as the flexural ones. A drawback is their space consumption; a fact that possibly can be compensated by simultaneous use as airborne sound absorbers.

In [4.41] also, those loss factors are calculated, which are obtained under consideration of the lateral coupling in the liner. In these calculations the continuum expressions are employed i.e., longitudinal and transversal motions of the liner are taken into account. A comparison of the results with those obtained using Eq. (4.128) in (4.124) or (4.126), exhibits hardly any difference. It can be shown that this is always the case whenever c_M is smaller than the governing wave speed of the base structure, the latter of which, for instance, being the bending wave speed.

The treatment of thick layers also encompasses embedding the structure or part thereof in sand. Such a solution has the advantages of being cheap and temperature robust. Also in such a case, there is a significant effect at and above the first thickness resonance and the mean of the damping is set by $\text{Re}[Z'_M] \approx \rho_M c'_M$. Here, ρ_M is the density of sand and c_M is the appropriate wave speed, which can only be quantified with difficulty. It is sug-

gested, however, that for thin, dry, uncompacted sand layers, $c_L \approx 150$ m/s, $c_T \approx 100$ m/s and $\eta \approx 0.1$ [4.42]. These values represent the most favourable case since sand is most often humid. Besides this, the sand is inevitably compacted through gravity and by being vibrated. Both effects therefore, lead to higher wave speed and thence less damping for low and intermediate frequencies. Nevertheless, commercially available dried sand remains an appreciable damping material for intermediate and high frequencies.

4.8 Damping at Joints

It is well-known that machines and technical appliances consisting of several structural parts exhibit substantially larger losses than those of the constitutive materials. As an example, the loss factor of a building is almost always about $2 \cdot 10^{-2}$ whereas systems made of steel or aluminium having a material loss factor less than 10^{-3} , show

$$\begin{aligned}\eta &\approx 5 \cdot 10^{-3}; f < 500\text{Hz} \\ \eta &\approx 2 \cdot 10^{-3}; f > 1000\text{Hz}\end{aligned}$$

in systems consisting of few, thick substructures such as a ship's hull,

$$\eta \approx 10^{-2}$$

for systems consisting of several, thick or thin parts such as a car body and

$$\begin{aligned}\eta &\approx 5 \cdot 10^{-2}; f < 500\text{Hz} \\ \eta &\approx 10^{-2}; f > 1000\text{Hz}\end{aligned}$$

for systems of several thin substructures.

Such “built-in” loss factors are the reason for lower resonant response than would be expected based on only material dissipation. They are also the reason for why damping treatments such as free damping layers, only lead to audible improvements when the loss factor of the assembly is elevated to more than 10^{-2} .

The added damping observed for built-up systems stems from the small relative motions, at interfaces between subsystems e.g., bolted or riveted joints, typically smaller than 10^{-6} m for intermediate and high frequencies. There, the thin interlayers (air, oil, dust) or contacting peaks of the surface roughnesses act as damped miniature springs or dampers. They come into play for relative motions normal or tangential to the contact surface respectively.

4.8.1 Damping by Relative Motion Normal to the Interface

Rather comprehensively investigated is the damping due to relative motion normal to an interface with a fluid film (gas pumping or squeeze film damping) [4.43-4.46]. The most essential mechanism behind the energy loss can be understood from calculating the damping of a plate vibrating in a viscous medium with prescribed velocity, see Fig. 4.32. Starting point is the linearized Navier-Stoke's equations for a compressible medium of density ρ_0 speed of sound c_0 and kinematic viscosity ν ($\nu_{\text{air}} \approx 16 \cdot 10^{-6} \text{ m}^2/\text{s}$, $\nu_{\text{water}} \approx 10^{-6} \text{ m}^2/\text{s}$)

$$\begin{aligned}\rho_0 \frac{\partial v_x}{\partial t} + \frac{\partial p}{\partial x} - \rho_0 \nu \left(\frac{\partial^2 v_x}{\partial x^2} + \frac{\partial^2 v_x}{\partial y^2} \right) &= 0, \\ \rho_0 \frac{\partial v_y}{\partial t} + \frac{\partial p}{\partial y} - \rho_0 \nu \left(\frac{\partial^2 v_y}{\partial x^2} + \frac{\partial^2 v_y}{\partial y^2} \right) &= 0, \\ \rho_0 \frac{\partial v_x}{\partial x} + \rho_0 \frac{\partial v_y}{\partial y} - \frac{1}{c_0^2} \frac{\partial p}{\partial t} &= 0.\end{aligned}\quad (4.129)$$

Restricting the analysis to harmonic vibrations such that all field variables are in the form $e^{-jk_x x} e^{-jk_y y} e^{j\omega t}$, a set of homogeneous linear equations results from (4.129) by employing the phasor notation. This set of equations has non-trivial solutions as the determinant to the coefficient matrix vanishes i.e., when

$$\begin{aligned}k_{y1}^2 &= \frac{\omega^2}{c_0^2} \frac{1}{1 + j\omega\nu / c_0^2} - k_x^2 \approx \left(\frac{\omega}{c_0} \right)^2 - k_x^2, \\ k_{y2}^2 &= \frac{-j\omega}{\nu} - k_x^2 \approx \frac{-j\omega}{\nu} \approx \left(\frac{1-j}{\delta} \right)^2.\end{aligned}\quad (4.129a)$$

The approximations introduced comes about as the kinematic viscosity ν is small and the thickness of the resulting acoustic boundary layer $\delta = \sqrt{2\nu/\omega}$ usually is of the order of 10^{-4} m whereas the wavelengths are some orders of magnitude longer. The general solution to Eq. (4.129) for harmonic motion can be written as

$$\begin{aligned}\hat{v}_x &= (A_1 e^{-jk_{y1} y} + A_2 e^{-jk_{y2} y}) e^{-jk_x x}, \\ \hat{v}_y &= (A_3 e^{-jk_{y1} y} + A_4 e^{-jk_{y2} y}) e^{-jk_x x}, \\ \hat{p} &= (A_5 e^{-jk_{y1} y} + A_6 e^{-jk_{y2} y}) e^{-jk_x x}.\end{aligned}\quad (4.129b)$$

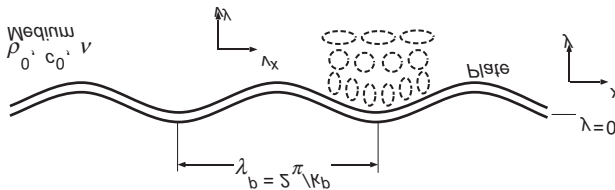


Fig. 4.32. Particle motion in a viscous medium adjacent to a vibrating plate

Upon substituting (4.129b) into (4.129), the relations

$$\begin{aligned} A_3 / A_1 &= k_{y1} / k_x, \quad A_4 / A_2 = -k_x / k_{y2}, \\ A_5 / A_1 &= \frac{\omega \rho_0}{k_x} \frac{1}{1 + j\omega v c_0^2}, \quad A_6 = 0, \end{aligned}$$

result for the so far unknown amplitudes. The latter are obtained from the boundary conditions at the plane $y = 0$. In this case, the normal velocity component must equal the plate velocity while the tangential vanishes in a viscous medium i.e.,

$$\hat{v}_y(x, 0) = \hat{v}_p e^{-jk_p x}, \quad \hat{v}_x(x, 0) = 0. \quad (4.129c)$$

$k_p = 2\pi/\lambda_p$ is the wavenumber of the plate wave and \hat{v}_p its amplitude. Upon combining the expressions, it is found that

$$\begin{aligned} \hat{v}_y(x, y) &= \frac{\hat{v}_p}{k_{y1} k_{y2} - k_p^2} \left(k_{y1} k_{y2} e^{-jk_{y1} y} - k_p^2 e^{-jk_{y2} y} \right) e^{-jk_p x}, \\ \hat{p}(x, y) &= \frac{\hat{v}_p}{1 + j\omega v / c_0^2} \frac{k_{y2}}{k_{y1} k_{y2} - k_p^2} e^{-jk_{y1} y} e^{-jk_p x}, \end{aligned} \quad (4.129d)$$

since $k_x = k_p$. As can be seen, the sound field in front of the plate consists of one part with wavenumber k_{y1} which is of the same order of magnitude as k_p and one part having very large wavenumbers k_{y2} . The former part represents either a hydrodynamic nearfield or a propagating wave radiated to the far-field and will be treated in detail in Chapter 7. The latter part is associated with the viscous boundary layer. Usually this boundary layer is neglected because its thickness δ is so small as was mentioned above. In the present case, however, it must be taken into account since the small vortices occurring in the layer convert the vibration energy into heat due to the viscosity and act like an energy sink for the plate.

To calculate the damping, it is necessary to develop the power that is transmitted from the plate to the ambient medium. In general the power is given by

$$W = \overline{\int \operatorname{Re}[p(x,0,t)] \operatorname{Re}[\dot{v}_y(x,0,t)] dx} = \frac{1}{2} \operatorname{Re} \left[\int \hat{p}(x,0) \hat{v}_y^*(x,0) dx \right]. \quad (4.129e)$$

The integration is to be taken over the total length of the plate l_p . An averaging over time is indicated by the over bar. Upon substituting the expression in (4.129d) into Eq. (4.129e) is obtained

$$W = \frac{\omega \rho_0 l_p |\hat{v}_p|^2}{2 \left(\frac{\omega^2}{c_0^2} - k_p^2 \right)} \left[\operatorname{Re} [k_{y1}] - \frac{v}{\omega} k_p^2 \operatorname{Im} [k_{y2}] - \frac{v}{\omega} k_p^2 \frac{\frac{\omega^2}{c_0^2} + k_p^2}{\frac{\omega^2}{c_0^2} - k_p^2} \operatorname{Im} [k_{y1}] \right], \quad (4.129f)$$

when the small terms $v^2 \omega^2 / c_0^4$ are neglected. Because the wavelength in the plate λ_p is substantially larger than the boundary layer thickness δ in all cases of interest in practice, $\operatorname{Im} [k_{y1}] \ll \operatorname{Im} [k_{y2}]$. This means that the first term in (4.129f) representing the radiated sound, and the second, representing the energy conversion to heat, remains whereas the third is insignificant. The loss factor can be obtained by inserting (4.129f) in the definition (4.22) observing that the dissipated energy per period T is given by $E_v = W \cdot T = 2\pi W/\omega$. Moreover, approximating the reversible energy by $E_R = \rho h |\hat{v}_p|^2 \lambda_p / 2$, it follows that

$$\eta = \frac{2W}{\omega \rho h |\hat{v}_p|^2}. \quad (4.129g)$$

Herein, ρ is the density of the plate and h its thickness. For thin plates, $|k_{y2}|^2 \gg k_p^2 \gg \omega^2/c^2$ such that $\operatorname{Re} [k_{y1}] \approx 0$ and

$$W \approx \frac{\omega \rho_0 h |\hat{v}_p|^2 \lambda_p}{4} \Rightarrow \eta \approx \frac{\rho_0 \delta}{2 \rho h}. \quad (4.129h)$$

Since the boundary layer thickness δ , as mentioned, is very small and diminishes inversely proportional to the square root of frequency, the loss factor of a system as depicted in Fig. 4.32 is also small and plays a role only for thin folios. Corresponding experiments show that (4.129h) well describes such realizations.

The situation is slightly different for double plates as shown in Fig. 4.33. The previous analysis (4.129a-h), however, applies when account is taken of the fact that for such systems there are also waves in the negative

y -direction. This means that terms involving $e^{jk_{y_1}y}$ and $e^{jk_{y_2}y}$ must be included in (4.129b). With the additional boundary conditions

$$\hat{v}_y(x, 0) = \hat{v}_{p1} e^{-jk_{p1}x}, \hat{v}_y(x, d) = \hat{v}_{p2} e^{-jk_{p2}x}, \\ \hat{v}_x(x, 0) = 0, \hat{v}_x(x, d) = 0,$$

again results a solvable set of linear equations. The explicit analysis is omitted for this case since the outcome is readily understood from Eq. (4.129h).

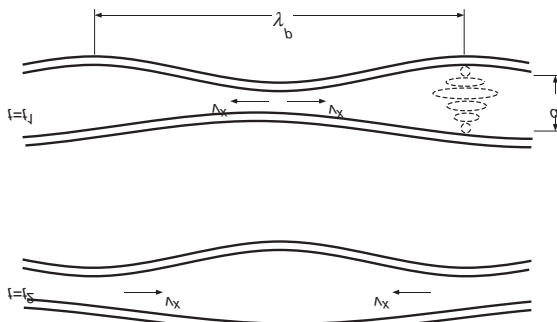


Fig. 4.33. Motion at times t_1 and t_2 for a double plate with a fluid interlayer

As is seen from the previous analysis, the damping is associated with the viscous losses arising by fluid flow in tangential direction. The same is true also for the double plates in Fig. 4.33, the only difference being that the tangential velocity is markedly larger. The reason is that the fluid only has a narrow channel of thickness d in which it can move, implying that the tangential velocity becomes much larger than that in the normal direction. It is readily shown that the flow velocity v_x in tangential direction is a factor λ_p/d larger than the normal velocity. Owing to the fact that the dissipated energy is proportional to the velocity squared, it is to be expected that the loss factor η of the double plate system is a factor of $(\lambda_p/d)^2$ larger than the value of (4.129h). This is indeed the case since the rigorous treatment [4.44-4.46] reveals a loss factor of

$$\eta \approx \frac{\rho_0 d}{\rho h} \left(\frac{\lambda_p}{2\pi d} \right)^2, \quad (4.130)$$

for a double plate system for which the gas pumping or squeeze film damping is the governing loss mechanism. In Fig. 4.34 is shown, a few ex-

perimental results [4.44] for a case where one plate could be considered rigid. Herein is observed the slope, which is proportional to $f^{-3/2}$ associated with the fact that δ as well as λ_p are inversely proportional to the square root of frequency, exhibited by both experimental and theoretical results. Figure 4.34 also includes two comparative measurements results to demonstrate that the fluid interlayer governs the damping. Squeeze film damping, however, is not the only damping mechanism for thin double plates that exhibit a relative motion in the normal direction but the most important. Other mechanism, besides gas pumping, can be assessed by modelling the interlayer as many small damped springs joining the two plates for which the discussion in conjunction with Eq. (4.127) is valid.

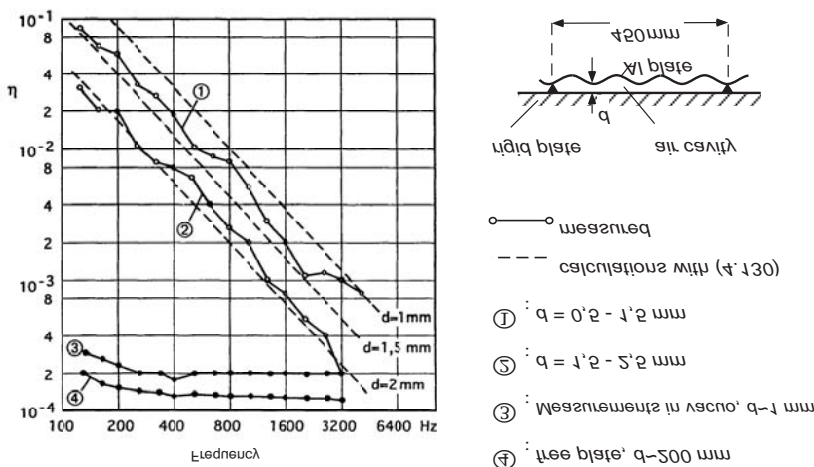


Fig. 4.34. Measured and calculated loss factor for a squeeze film damped, 1mm aluminium plate

4.8.2 Damping by Relative Motion Tangential to the Interface

For built-up systems consisting of thick substructures such as engines or industrial machines, the motion perpendicular to a junction or interface is usually very small and hence does not lead to significant damping. Instead, the tangential relative motion becomes the governing.

When an interface encompasses a thin viscous film e.g., oil, dust, etc., Sect. 4.6.2 regarding multi-layered systems apply i.e., the interlayer acts in

shear and converts a fraction of the structure-borne sound energy into heat owing to its dissipation. A theoretical assessment of the loss factors is in this case in principle possible for harmonic motion by replacing the viscosity by a complex shear stiffness.

Employing the definitions of the viscosity $\nu = \tau/v$ and the shear modulus $G = \tau/\xi$ and using the relation $\hat{\nu} = j\omega\xi$ for harmonic motion, it is found that

$$\underline{G} = j\omega\nu , \quad (4.131a)$$

which is purely imaginary. An introduction of this shear modulus in the expressions of Sect. 4.6.2 therefore implies the following substitution

$$\begin{aligned} G_2 &= j\omega\nu_2, \quad G''_2 = \eta_2 G'_2 = \omega\nu_2, \\ \eta_2 g_d &= \omega\nu_2 \frac{1}{E_3 d_3 d_2 k^2} \quad , \quad \frac{\omega\nu_2}{d_2 k^2} \left(\frac{1}{E_1 d_1} + \frac{1}{E_3 d_3} \right). \end{aligned} \quad (4.131b)$$

Numerically, one finds that the loss factor is the bigger the smaller the interlayer thickness, d_2 .

Somewhat more intricate is the situation where dry friction occurs at the interface. Two cases must be distinguished according to the present knowledge.

- a) When the amplitudes of the relative motion in tangential direction are not too small but larger than some μm , i.e. above all for low frequencies, the Coulomb friction apply. This means that the process is non-linear since the stick and slip motions follow different laws. The corresponding analysis [4.47-4.49] shows that an increase in amplitude increases the loss factor. It would lead way out of the scope of this book to include the associated analysis.
- b) For small motion amplitude, present at intermediate and high frequencies, measurements show only weak amplitude dependence of the loss factor. It thus appears possible to model the interface by many small, damped springs, as illustrated in Fig. 4.35a. The stiffness per unit area for cut steel surfaces is given approximately by the empirical formula [4.50, 4.51]

$$\frac{G_2}{d_2} = 800(p_N)^{2/3}$$

where p_N is the normal pressure in N/mm^2 and the constant such that G_2/d_2 has the proper dimension of N/mm^3 . Some measurement results are shown in Fig. 4.35b. It is expected that the interlayer stiffness increases with increasing normal pressure. The loss factor lies between 10^{-2} and 10^{-1} and tends to decrease with increasing

normal pressure. With the surface roughnesses commonly found in machine manufacturing, the interlayer stiffnesses and loss factors observed for dry joints between metals are remarkably similar. In measurements of interlayer stiffness and loss factors was observed only a negligible reduction when the average roughness was altered from 5 μm to 40 μm .

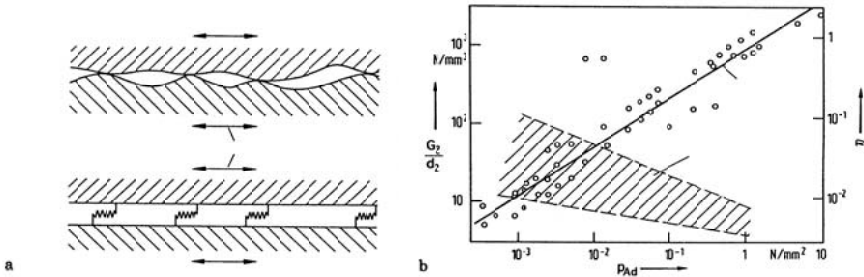


Fig. 4.35. Conditions at dry joints with tangential relative motion. (a) Idealized interface and mechanical model. (b) Stiffness and loss factor versus normal pressure

References

- [4.1] Meyer O.E., 1874. Zur Theorie der inneren Reibung. *Journal für reine und angewandte Mathematik*, 78, p. 130
- [4.2] Voigt W., 1892. Über innere Reibung fester Körper, insbesondere der Metalle. *Annalen der Physik*, 47, p. 671
- [4.3] Boltzmann L., 1876. Zur Theorie der elastischen Nachwirkung. *Annalen der Physik*, Erg. Bd. 7, p. 624
- [4.4] Maxwell J.C., 1867. On the dynamical theory of gases. *Phil. Trans. Royal Soc.*, 157, p. 49
- [4.5] Zener C., 1948. *Elasticity and Anelasticity in Metals*. University of Chicago Press, Chicago MI
- [4.6] Tamm K. and Weiss O., 1959. Untersuchungen über periodische Wellen, exponentielle und komplexe Nahfelder im begrenzten Festkörper. *Acustica*, 9, p. 275
- [4.7] Weiss O., 1959. Über die Schallausbreitung in verlustbehafteten Medien mit komplexem Schub- und Kompressionsmodul. *Acustica*, 9, p. 387
- [4.8] Cremer L., 1934. Vierpoldarstellung und Resonanzkurven bei schwingenden Stäben. *Sitzungsberichte der Preussischen Akademie der Wissenschaften, phys.-math. Kl. I*, p. 1
- [4.9] Mason W.P., 1958. *Physical acoustics and the properties of solids*. Van Nostrand, New York NY

- [4.10] DIN 53515: Bestimmung der viskoelastischen Eigenschaften von Gummi. Beuth Vertrieb, Berlin
- [4.11] Fitzgerald E.R. and Ferry J.D., 1953. Method for determining the dynamic mechanical behaviour of gels and solids at audio-frequencies—Comparison of mechanical and electrical properties. *Journal of Colloid Science*, 8, p. 1
- [4.12] Oberst H. and Frankenfeld K., 1952. Über die Dämpfung der Biegeschwingungen dünner Bleche durch festhaftende Beläge. *Acustica*, 2 Beihefte No. 4, p. 181
- [4.13] Oberst H., Becker G.W. and Frankenfeld K., 1954. Über die Dämpfung der Biegeschwingungen dünner Bleche durch fest haftende Beläge II. *Akustische Beihefte Heft 1* (in *Acustica*, 4), p. 433
- [4.14] Nijman E.J.M. and Bellussi G.N.M., 2000. Helium as good as vacuum: The poor man's approach for accurate material damping measurements. *Applied Acoustics*, 60, p. 385
- [4.15] Truell R. and Elbaum C., 1961. High frequency ultrasonic stress waves. *Handbuch der Physik* (S. Flügge ed.). Springer Verlag, Berlin
- [4.16] Love A.E.H., 1948. A treatise on the mathematical theory of elasticity, p.119. Dover Publications, New York NY
- [4.17] Lücke K., 1962. Die von den Kristallbaufehlern und insbesondere von den Versetzungen verursachten Dämpfungserscheinungen. *Metallkunde*, 53, p. 57
- [4.18] Bordoni P.G., 1960. Dislocation relaxation at high frequencies. *Nuovo Cimento*, Suppl. 1, 17, p. 43
- [4.19] Wegel R. and Walter H., 1953. Internal dissipation in solids for small cyclic strains. *Physics*, 6, p. 141
- [4.20] Zemanek Jr. J. and Rudnik I., 1961. Attenuation and dispersion of elastic waves in a cylindrical bar. *Journal of the Acoustical Society of America*, 33, p. 1283
- [4.21] Bennewitz K. and Rötger H., 1936. Über die innere Reibung fester Körper; Absorptionsfrekvenzen von Metallen im akustischen Gebiet. *Physikalische Zeitschrift*, 37, p. 578
- [4.22] Bordoni P.G., Nuovo M. and Verdini L., 1959. Relaxation of dislocations in cubic face-centered metals. *Proc. 3rd International Congress on Acoustics*, Stuttgart, Vol. 1, p. 583. Elsevier, Amsterdam (1961)
- [4.23] Förster F. and Köster W., 1937. Elastizitätsmodul und Dämpfung in Abhängigkeit vom Werkstoffzustand. *Metallkunde*, 29, p. 116.
- [4.24] Becker G.W. and Oberst H., 1956. Über das dynamisch-elastische Verhalten linear, vernetzter und gefüllter Kunststoffe. *Kolloid Zeitschrift*, 148, p. 6
- [4.25] Linhardt F. and Oberst H., 1961. Über die Temperaturabhängigkeit schwingungsdämpfender Kunststoffe. *Acustica*, 11, p. 255
- [4.26] Williams M.L., Landel R.F. and Ferry J.D., 1955. Mechanical properties of substances of high molecular weight .19. The temperature dependence of relaxation mechanisms in amorphous polymers and other glass-forming liquids. *Journal of the American Chemical Society*, 77, p.3701
- [4.27] Watters B.G., 1959. Transmission loss of some masonry walls. *Journal of the Acoustical Society of America*, 31, p. 898

- [4.28] Kuhl W. and Kaiser H., 1952. Absorption of structure-borne sound in building materials without and with sand-filled cavities. *Acustica*, 2, p. 179
- [4.29] Heckl M. and Nutsch J., 1995. Taschenbuch der Technischen Akustik, 2nd ed., Ch. 22 (M. Heckl, H.A. Müller eds.). Springer Verlag, Berlin
- [4.30] Kurtze G., 1956. Körperschalldämpfung durch körnige Medien. VDI-Berichte 8, p. 110
- [4.31] Kirstein T. and Müller H.W., 1960. Berichte des Beirats für Bauforschung beim Bundesminister für Wohnungsbau, H 13, Körperschall in Gebäuden. Ernst & Sohn, Berlin
- [4.32] Cremer L., 1963. Akustische Versuche an schwimmend verlegten Asphaltestrichen. Bitumen, 25, p. 93
- [4.33] Kerwin Jr. E.M., 1959. Damping of flexural waves by a constrained viscoelastic layer. *Journal of the Acoustical Society of America*, 31, p. 952
- [4.34] Kerwin Jr. E.M., 1959. Damping of flexural waves in plates by spaced damping treatments having spacers of finite stiffness. Proc. 3rd International Congress on Acoustics, Stuttgart, Vol. 1, p. 412. Elsevier, Amsterdam (1961)
- [4.35] Ross D., Ungar E.E. and Kerwin E.M., 1962. Structural damping. American Society of Mechanical Engineering, New York NY
- [4.36] Parfitt G.G., 1962. The effect of cuts in damping tapes. Proc. 4th International Congress on Acoustics, Copenhagen, Paper P 21
- [4.37] Zeinetdinova R.Z., Naumkina N.I. and Tartakowski B.D., 1978. Effectiveness of a vibration-absorbing coating with a cut constraining layer. *Soviet Physics Acoustics*, 24, p. 347
- [4.38] Kurtze G. and Watters B.G., 1959. New wall design for high transmission loss or high damping. *Journal of the Acoustical Society of America*, 31, p. 739
- [4.39] Mead D.J. and Markus S., 1985. Coupled flexural, longitudinal and shear wave motion in two- or three-layered damped beams. *Journal of Sound and Vibration*, 99, p. 501
- [4.40] Heckl M., 1961. Wave propagation on beam-plate systems. *Journal of the Acoustical Society of America*, 33, p. 640
- [4.41] Albrecht A. and Möser M., 1989. Die dämpfende Wirkung dicker Entdröhnschichten auf Platten. *Zeitschrift für Lärmbekämpfung*, 36, p. 73
- [4.42] Schmidt H., 1954. Die Schallausbreitung in körnigen Substanzen. *Acustica*, 4, p. 639
- [4.43] Maidanik G., 1966. Energy dissipation associated with gas-pumping in structural joints. *Journal of the Acoustical Society of America*, 40, p. 1064
- [4.44] Trochidis A., 1982. Körperschalldämpfung mittels Gas- oder Flüssigkeitschichten. *Acustica*, 51, p. 201
- [4.45] Chow L.C. and Pinnington R.J., 1987. Practical industrial method of increasing structural damping in machinery, I: Squeeze-film damping with air. *Journal of Sound and Vibration*, 118, p. 123
- [4.46] Chow L.C. and Pinnington R.J., 1987. Practical industrial method of increasing structural damping in machinery, II: Squeeze-film damping with air. *Journal of Sound and Vibration*, 118, p. 333

- [4.47] Ott D., 1978. Untersuchungen zur Schwingungsdämpfung durch Hysterese in Schraub- und Nietverbindungen. VDI-Berichte 320
- [4.48] Mindlin R.D. and Deresiewicz H., 1953. Elastic spheres in contact under varying oblique forces. Trans. ASME, Journal of Applied Mechanics, 20, p. 327
- [4.49] Gaul L., 1981. On the damping and transmission of flexural waves at structural joints. Ingenieur-Archiv, 51, p. 101
- [4.50] Petuelli G., 1983. Theoretische und experimentelle Bestimmung der Steifigkeits- und Dämpfungseigenschaften normalbelasteter Fügestellen. Diss. RWTH, Aachen
- [4.51] Schober U., 1990. Untersuchungen der Körperschalldämpfung durch Fügestellen in Motoren. Proc. of DAGA, Wien, p. 349

5 Impedance and Mobility

5.1 Definitions

In the previous two chapters is studied the wave propagation in the absence and presence of damping. Focus in this chapter is on the process preceding the propagation namely the excitation of structure-borne sound.

In practice, excitation of structure-borne sound can be due to, for example, machinery installed on foundations, in buildings, ships, vehicles etc. but also walking, knocking and magnetic forces in electrical devices constitutes excitation mechanisms. Fluid fluctuations, moreover, such as air-borne sound or pressure pulsations in liquid-filled pipes give rise to structure-borne sound excitations. Common for all these mechanisms is an exerted force or a prescribed velocity, which gives rise to a proportional motion or force respectively when extreme loads are excluded. Limiting the discussion to harmonic motions since all other time histories can be synthesized from the former, it is meaningful to introduce the point impedance or point mobility as in many other areas of physics.

The basic definitions for the mechanical impedance and mobility read

$$\underline{Z} = \frac{\hat{F}}{\hat{v}}, \quad \underline{Y} = \frac{\hat{v}}{\hat{F}} \quad (5.1)$$

respectively cf. [5.1]. Herein, \hat{F} is the complex amplitude of the force and \hat{v} that of the velocity, both at the point of excitation. The point impedance and mobility are in general complex functions of frequency since the ratios of the field variables vary with frequency.

The point quantities defined in (5.1), contrary to particle mechanics, are not unambiguous since the “point” of excitation often is a sizeable area over which the force and velocity may vary. The definitions, moreover, do not involve the area of excitation. Nonetheless, there can be substantial differences if, for example, a thin plate is excited over a small point-like area or the excitations is distributed over a large. To circumvent this ambiguity, therefore, a precise specification must be made of the excitation distribution and position.

The simplest and most commonly used specification is that the excitation is concentrated to a “point” i.e., in the structure-borne sound case, an area which is much smaller than the wavelength governing the propagation. This condition, which refers to the upper frequency limit, however, must be supplemented by one for the minimum admissible area. The finite shear stiffness of solid materials means that when a force is exerted on a mathematical point the stress becomes infinite as does the motion (a hyperfine needle will make a hole in every material). To handle this, the excitation area must be specified together with the point characteristics or, as in conjunction with the classical bending theory where the shear stiffness is assumed infinitely high, one must bear the assumptions in mind in the reporting phase. With respect to measurements, this means that the theoretical point characteristics can only then be approached when the dimensions of the excitations area are not too small. In turn, this practically means that the dimensions cannot be smaller than the plate thickness or beam depth. Section 5.4.3 will elaborate on this item further. The impedance or mobility determined from the force and velocity at such a physical point are termed point impedance or point mobility and in the following the discussion is primarily devoted to those point characteristics owing to their great importance in practice.

Besides the point characteristics, also the wave impedance or mobility as well as the characteristic impedance or mobility are of interest. The basic idea behind the former two is that for a given spatial excitation distribution $g(x, z)$, that of the response will be the same. Such a situation is only possible for infinite, homogeneous structures without discontinuities. Hence, it is possible to form a ratio of the two field variables where the spatial dependence cancels

$$\underline{Z} = \frac{\hat{F}}{\hat{v}}, \quad \underline{Y} = \frac{\hat{v}}{\hat{F}}. \quad (5.2)$$

It is clear that the dimensions of the wave impedance and the wave mobility will differ from those of the point impedance and mobility respectively. For plane problems, the function $g(x, z)$ takes the form

$$g(x, z) = e^{-jk_x x} e^{-jk_z z}, \quad (5.3)$$

implying that the wave impedance or wave mobility realize the response amplitude of a structure that is exposed to a plane wave excitation of trace wavenumbers k_x and k_z . Whilst it is only required that the excitation and response have the same frequency in the case of a point mobility or impedance, it is additionally required that the spatial distributions are the same for wave mobilities and impedances. Thereby, Eq. (5.3) establishes the, by

far, most important idealized form of excitation although the spatial distributions associated with cylindrical and spherical co-ordinates also are of importance.

The significance of the point characteristics and, yet more pronounced the wave characteristics, is seen in that they realize idealizations by means of which sources with complicated geometry can be synthesized either as sums of point sources or combinations of several plane waves. Hence, the ideal impedances or mobilities constitute fundamental building blocks for the analysis of complicated structure-borne sound problems, see Sect. 5.4.

An essential advantage of impedances or mobilities is that they enable complicated substructures to be seen as parts of a mechanical circuit diagram. With a bit of exercise, the most significant features of a system can be readily extracted from such circuit diagrams. It must be emphasized, however, that the use of mechanical circuits is not fool proof but can in situations lead to erroneous conclusion as, for example, in cases of flexure where beside forces and translational velocities also moments and rotational velocities must be taken into account.

5.2 Measurement of Mobilities (Impedances)

5.2.1 Registration of Force and Velocity

The definition in Eq. (5.1) suggests the obvious way to determine the mobility by means of simultaneous measurements of the force and the resulting velocity.

The excitation is conventionally achieved by means of an electrodynamic shaker but can be established in many other ways e.g., by means of an impact hammer.

For the registration most commonly are used a force transducer and an accelerometer of piezo-electric type. In situations involving light-weight and / or flexible measurement objects, also a so called impedance head can be employed which consists of the two aforementioned transducers in combination. The impedance head has proven less suitable, however, for massive or rigid test objects [5.2, 5.3], due to the limited stiffness of the piezo-electric crystal registering the force, see Fig. 5.1. The magnitude and phase are registered for the two electrical signals, proportional to the force and the velocity respectively. The ratio of the two signals need only be multiplied by a calibration factor, which in turn is obtained from a calibration measurement using a well defined reference mobility, for instance a mass.

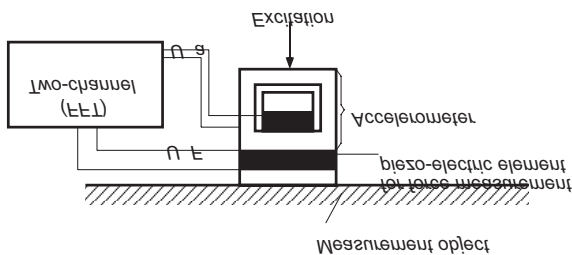


Fig. 5.1. Principal design of an impedance head

The fundamental aspect by all mobility measurements is the influence of the transducers on the dynamic behaviour of the measurement object cf., Sect. 7.2.4. Since the transducers are rigidly connected to the object, they constitute parts of the former. Thus, the measured mobility \underline{Y}_1 consists of the desired mobility \underline{Y}_0 and those of the transducers. Most often, the transducers can be considered as small masses. For two such equal masses applied to the measurement object the measured mobility is

$$\underline{Y}_1 = \underline{Y}_0 \frac{1}{1 + 2\underline{Y}_0 j\omega m} \quad (5.4)$$

Accordingly, a correct measurement result is obtained by solving Eq. (5.4) for \underline{Y}_0 . This correction is not only an extra hurdle but renders also a reduction in accuracy. The transducers hence are designed light-weight to avoid the correction. Nonetheless, a correction will become necessary for high frequencies. As an example can be mentioned that the magnitude of the mobility of a 5 mm thick aluminium plate is $1.33 \cdot 10^{-3}$ m/Ns which is comparable with that of a 20 gram transducer combination at about 5 kHz such that the correction has to be introduced for frequencies above 500 Hz to achieve some accuracy in the magnitude.

Another important aspect for mobility measurements is the connections between transducers and object. This should be as rigid as possible not to introduce an elasticity. Furthermore, the connection must be orientated such that the desired component of motion is registered.

By employing a two-channel FFT-analyser, several types of signals can be used for the excitation such as random noise or sweeps (“chirp”). The decomposition in sinusoidal components is performed by the analyser as well as the computation of the complex ratio of the two signals, which means that a wide frequency range is simultaneously encompassed.

5.2.2 Comparison with Known Mobilities

As in electronics, the mobility of a mechanical object can be assessed from a comparison with that of a known. Usually, use is made of masses of different sizes establishing accurate reference mobilities [5.4]. The only prerequisite is that the masses are really rigid such that the velocity is identical at every material point. For systems vibrating in flexure, it must be observed that in addition to translations also rotations occur which can give rise to measurement errors.

A simple method is depicted in Fig. 5.2 where a mobility of an object is compared with that of a known mass. In this set-up, a softly suspended exciter driving the test object also serves as the known mass. The exciter consists of a compact magnet with mass m_M where a coil, rigidly connected to the test object, is inserted in the annular gap. If a current is sent through the coil, a force F is exerted on the test object and by virtue of Newton's third law, an equal reaction force acts on the magnet. With the magnet very softly suspended and behaving as a rigid mass, the relation between force and velocity of the magnet is

$$\hat{F} = j\omega m_M \hat{v}_M . \quad (5.5a)$$

The velocity of the test object is on the other hand

$$\hat{v}_0 = \underline{Y}_0 \hat{F} , \quad (5.5b)$$

wherein \underline{Y}_0 is the point mobility of the object, possibly influenced by the mass of the coil. From (5.5a) and (5.5b) follows immediately that

$$\underline{Y}_0 = \frac{\hat{v}_0}{j\omega m_M \hat{v}_M} . \quad (5.5c)$$

The measurement of the mobility is turned into a relative measurement of velocities thanks to the direct comparison with the known mass. The pivotal point that the mass behaves rigidly typically limits the range of applicability to a few kilohertz.

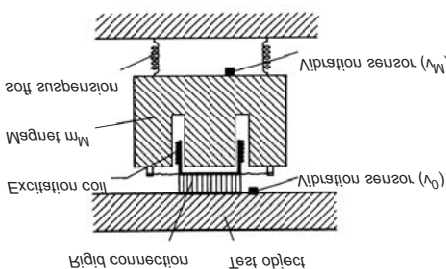


Fig. 5.2. Measurement of mobility by comparison with a known mass mobility

Another possibility to assess the mobility of an object from comparative measurements consist of registering the change in velocity arising from loading the object with a known mass. From Eq. (5.4) the mobility of a mass loaded system is given by

$$\underline{Y}_{l,1} = \frac{\hat{\underline{v}}_1}{\hat{\underline{F}}} = \underline{Y}_0 \frac{1}{1 + \underline{Y}_0 \cdot j\omega m_1}.$$

This expression is valid not only for the excitation point but for every arbitrary measurement point. The force $\hat{\underline{F}}$, however, is that one would register at the measurement point. Upon applying a second mass m_2 , keeping the exciting force constant then

$$\underline{Y}_{l,2} = \frac{\hat{\underline{v}}_2}{\hat{\underline{F}}} = \underline{Y}_0 \frac{1}{1 + \underline{Y}_0 \cdot j\omega m_2}.$$

From the ratio of the two expressions, the mobility sought is obtained as

$$\underline{Y}_0 = \frac{1 - \frac{\hat{\underline{v}}_2}{\hat{\underline{v}}_1}}{j\omega \left(m_2 \frac{\hat{\underline{v}}_2}{\hat{\underline{v}}_1} - m_1 \right)} \quad (5.6)$$

It is thus clear that the mobility \underline{Y}_0 can be obtained from a relative measurement of the velocities v_1 and v_2 in Fig. 5.3. Clearly, the measurement accuracy is improved the smaller is m_1 and the bigger is m_2 . This technique is particularly suitable for high mobilities. Examples of measurement results are given in Fig. 5.4. In this graph, however, the results are presented as impedances, which are simply the inverted mobilities since only point quantities are considered.

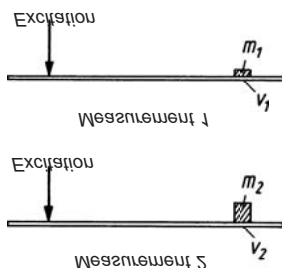


Fig. 5.3. Measurement of mobility by registration of velocity reduction due to mass loading

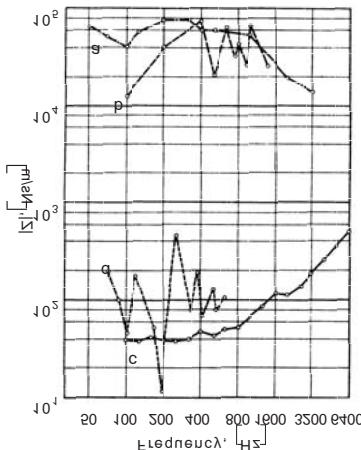


Fig. 5.4. Examples of measured impedances. a) 120mm masonry wall [5.5]. b) Submarine hull [5.6], c) 0.61mm steel plate with 7g added mass at the excitation point [5.7] and d) cello at the bridge [5.8]

5.2.3 Other Measurement Methods

The electrical impedance Z_E of an electro-dynamic shaker is made up of the internal impedance Z_{E0} with the coil blocked and a contribution due to the motion, see Sect. 8.3.1. This means that

$$Z_E = Z_{E0} - \frac{U_w}{i} \quad (5.7)$$

where U_w is the induced opposing voltage and i the current through the coil. U_w and i are related to the force and velocity by the electro-mechanical coupling relations

$$U_w = -Bl_L v \quad , \quad F = Bl_L i, \quad (5.7a)$$

cf., Eqs. (8.40a) and (8.40b). Since an electro-dynamic shaker is a passive transducer, the coupling constants are the same Bl_L , in the two relations. A substitution of (5.7a) into (5.7) yields

$$\underline{Z}_E = \underline{Z}_{E0} + \frac{(Bl_L)^2}{\underline{Z}} \quad (5.7b)$$

Thus, the mechanical impedance of an electro-dynamic shaker depends on its internal, blocked impedance Z_{E0} and on the mechanical impedance i.e., on the losses in the lead as well as on the self-induction and the character-

istics of the object attached. If Z_{E0} is sufficiently small, then one may determine the mechanical impedance directly from purely electrical impedance measurements. This approach obviously is best suited for small mechanical impedances (large mobilities) for which the second term in Eq. (5.7b) becomes large. One practical advantage of this method is that it allows mechanical power measurements i.e. the mechanical power transmitted to the excited structure, to be obtained directly from the electrical power, particularly if the electrical resistance losses are very small.

Another indirect method for determining the mechanical impedance is analogous to the impedance tube technique (Kundt's tube) in airborne acoustics. Acoustic impedances are often determined by placing the test sample at the end of a tube and measuring the standing waves in the tube. The sample impedance is then calculated from the ratio of the sound pressures at nodes and anti-nodes and from the location of the first node. For structure-borne sound, the air in the tube is replaced by a longitudinally vibrating rod and the microphone is replaced by a vibration sensor. The same ideas and formulae apply here as for the airborne sound impedance measurements, only that the characteristic impedance, of course, is that of the beam $\rho c_L S$ where ρ and c_L are the density and longitudinal wave speed of the rod respectively and S its cross-sectional area.

As elegant as this technique may appear at a first glance – only relative measurements of velocity are necessary and phase registrations are replaced by length measurements – its practical use leads to considerable difficulties. From the airborne analogue it is well known that the tube length must be approximately half a wavelength long at the lowest frequency of interest. Accordingly, a steel or aluminium rod of about 12.5 m would be required to reach a lower limiting frequency of 200 Hz. Additionally, it is generally very difficult to obtain pure longitudinal waves in a long rod, where commonly the undesired bending waves occur even with carefully adjusted, symmetric excitation.

Instead of longitudinal waves, naturally, also bending waves can be used. Because of the presence of nearfields at the ends of a beam, however, complicated and time-consuming measurement and analysis result. This approach, therefore, is of interest essentially only for the determination of the absorption coefficient α i.e., the ratio of transmitted to incident power [5.9].

The movement of the vibration sensors to the nodes and anti-nodes associated with the employment of one-dimensional wave-guides in impedance measurements, can be circumvented by using two identical transducers, which measure the velocities v_1 and v_2 at position x_1 and x_2 respectively. For positions remote from the nearfields, Eqs. (4.40) or (4.42) give

$$\begin{aligned} v_1 &= v_+ e^{-jkx_1} + v_- e^{jkx_1}, \\ v_2 &= v_+ e^{-jkx_2} + v_- e^{jkx_2}. \end{aligned} \quad (5.8)$$

This means that the two required expressions for the two unknown amplitudes v_+ and v_- are developed and can be solved in a similar manner as those of the corresponding airborne sound situation to obtain the reflection or absorption coefficients provided that $|x_1 - x_2|$ is smaller than half a wavelength [5.10]. As an example, the reflection coefficient is given by

$$r = \frac{v_-}{v_+} = -e^{jk(x_1+x_2)} \frac{(v_1/v_2)e^{jk(x_1-x_2)} - 1}{(v_1/v_2) - e^{jk(x_1-x_2)}}. \quad (5.8a)$$

5.3 Input Mobility of Infinite Rods, Beams and Plates

5.3.1 Excitation of Quasi-Longitudinal Waves in Rods

The characteristic impedance for pure longitudinal waves in an infinitely extended continuum was derived in Eq. (3.14). A completely analogous calculation applied to quasi-longitudinal waves (Sect. 3.12) results in the following expression for the input mobility of an infinitely long rod excited at one end

$$Y_{LII} = \frac{1}{m'c_{LII}} = \frac{1}{S\sqrt{E\rho}}. \quad (5.9)$$

Here, $m' = \rho S$ represents the mass per unit length of the rod, c_{LII} the longitudinal wave speed in the rod as given by Eq. (2.32) and E is the Young's modulus of the rod material.

The mobility given by Eq. (5.9) readily enables the calculation of the motion resulting when a mass m impacts on the end of three rod. If the mass impacts at time $t = 0$ with a velocity v_0 , then for $t > 0$ there acts an inertia force $m dv/dt$ on the mass and a force of the same magnitude,

$$F = \frac{v_0}{Y_{LII}} = S\sqrt{E\rho}v_0,$$

is exerted on the rod. This means that

$$m \frac{dv}{dt} + S\sqrt{E\rho}v = 0 \quad ; \quad t \geq 0, \quad (5.10)$$

which can be solved to give

$$\begin{aligned} v &= v_0 e^{-S(\sqrt{E\rho}/m)t} & ; \quad t \geq 0, \\ v &= 0 & ; \quad t < 0. \end{aligned} \quad (5.11)$$

Accordingly, the resulting motion is featured by an exponential decay which becomes larger the smaller the mass.

Of course, Eq. (5.10) and (5.11a) only apply when no plastic deformation occurs of neither mass nor rod. If such deformations do occur, then the impact is softer than that obtained on the basis of Eq. (5.11).

The impact pulse propagates along the rod entirely without distortion at the propagation speed for longitudinal waves. The velocity at any arbitrary position along the rod is thus given by

$$\begin{aligned} v &= v_0 e^{-(S\sqrt{E\rho}/mc)(ct-x)} & ; \quad x \leq ct, \\ v &= 0 & ; \quad x > ct, \end{aligned} \quad (5.11b)$$

according to Eq. (3.12). From (5.11b) one may also deduce under what conditions the result obtained for an infinite rod can be applied to a rod of finite length. The impact process can be considered essentially completed when the exponent has reached the value -2 . This occurs precisely, however, when the first shock front arrives at the position $x_l = 2m/Sp$. A reflection at this or a later position will arrive at the impact position after the impact process is completed. Since $Sp x_l$ corresponds to a portion of the rod, this means that the impact process of a finite rod of at least this length is principally the same as for an infinite. The condition thus is that the total mass of the finite rod is at least twice that of the impacting body.

The impulse shaped, particle velocity process of the longitudinally excited rod could also have been calculated in the frequency domain. In such a case the starting point is the force, which is Fourier decomposed and the resulting spectrum divided by the total impedance $j\omega m + S\sqrt{E\rho}$ at the impact. The operation results in the spectrum of the velocity, which after the inverse transform yields the time domain results of Eq. (5.11b). This procedure will be employed in the next sections.

5.3.2 Excitation of Bending Waves in Beams

The analysis of input point mobilities of beams in flexure is somewhat more involved because of the dispersive nature of the flexural wave and because of the occurrence of evanescent waves in addition to those propagating. It is convenient to begin with the equations for the velocity v , angular velocity w , bending moment M_z and shear force F_y and evaluate the un-

knowns from the related boundary conditions. From Eqs. (3.69), (3.77) and (3.78), these expressions read

$$\hat{w} = \frac{\partial \hat{v}}{\partial x}, \hat{M}_z = -\frac{B}{j\omega} \frac{\partial \hat{w}}{\partial x}, \hat{F}_y = -\frac{\partial \hat{M}_z}{\partial x}, j\omega m' \hat{v} = -\frac{\partial \hat{F}_y}{\partial x}, \quad (5.12)$$

when time differentiation is replaced by a multiplication by $j\omega$ for harmonic processes. Herein, B represents the flexural stiffness and m' the mass per unit length of the beam. In addition to Eq. (5.12) one also needs the general solution for the bending wave equation. For an angular frequency ω , Eq. (3.109) implies

$$\hat{v} = \hat{v}_+ e^{-jkx} + \hat{v}_- e^{jkx} + \hat{v}_{+j} e^{-kx} + \hat{v}_{-j} e^{kx}, \quad (5.13)$$

where $k = (\omega^2 m' / B)^{1/4}$ is the bending wavenumber.

Upon considering first the case with a semi-infinite beam i.e., a beam that extends from $x = 0$ to $x = \infty$. The excitation is applied perpendicular to the neutral layer at $x = 0$ in form of a pure force F . Owing to the fact that all excited waves propagates away from the excitation position, all terms with $+jkx$ and $+kx$ vanish which means that

$$\hat{v} = \hat{v}_+ e^{-jkx} + \hat{v}_{-j} e^{-kx}. \quad (5.14)$$

The two temporarily unknown quantities v_+ and v_{-j} are to be obtained from the boundary conditions at the point of excitation. It is clear that at this position no moment is exerted and the exciting force is F . Since

$$\hat{M}_z = -\frac{B}{j\omega} k^2 (-\hat{v}_+ e^{-jkx} + \hat{v}_{-j} e^{-kx}), \quad (5.15a)$$

and

$$\hat{F}_y = \frac{B}{j\omega} k^3 (j\hat{v}_+ e^{-jkx} - \hat{v}_{-j} e^{-kx}), \quad (5.15b)$$

the following relations are found at $x = 0$

$$\begin{aligned} -\hat{v}_+ + \hat{v}_{-j} &= 0, & j\hat{v}_+ - \hat{v}_{-j} &= \frac{j}{Bk^3} \hat{F}, \\ \hat{v}_+ &= \hat{v}_{-j} = \frac{\omega}{Bk^3(1+j)} F. \end{aligned} \quad (5.16)$$

This means that

$$\hat{v} = \frac{\omega}{Bk^3(1+j)} \hat{F} (e^{-jkx} + e^{-kx}). \quad (5.17)$$

Thus the input point mobility of the semi-infinite beams becomes

$$Y = \frac{\hat{v}(0)}{F} = \frac{\omega}{Bk^3} (1 - j) = \frac{(1 - j)}{m' c_B}, \quad (5.18)$$

where $c_B = \omega/k$ is the phase speed of the bending wave.

As is evident from Eq. (5.18), the mobility is complex and decreases with the square root of frequency, owing to the frequency dependence of the phase speed. This does not mean, however, that the mobility of a semi-infinite beam vanishes at high frequencies because above a certain frequency the Euler-Bernoulli theory and thus Eq. (5.18) ceases to be valid cf., Sect. 3.3. One may obtain expressions that remain valid up to slightly higher frequencies by employing the corrected bending wave equation cf., Sect. 3.8.3. Such an analysis is not undertaken here but is indicated later in Sect. 5.4.3.1.

For the second case in which the beam is infinitely extended and excited at $x = 0$, the analysis above cannot be directly employed. Although a cut at $x = 0$ results in two semi-infinite beams, each of which is excited by half the external force, the input mobility is not simply half of that given in Eq. (5.18). This is so since the boundary conditions for the two cases are different. For the semi-infinite beam no moment acts at $x = 0$ whereas the moment is continuous at the excitation point for the infinite one. Also required is a vanishing rotation at the point of excitation. This means that the part in the immediate vicinity of the excitation translates without rotation. Thus, the problem amounts to solving (5.14), subject to the boundary conditions,

$$\begin{aligned} \hat{w}(0) &= k(-j\hat{v}_+ - \hat{v}_{+j}) = 0, \\ \frac{\hat{F}}{2} &= \frac{Bk^3}{j\omega} (j\hat{v}_+ - \hat{v}_{+j}). \end{aligned} \quad (5.19)$$

These lead to $\hat{v}_+ = j\hat{v}_{+j} = \omega \hat{F} / (4Bk^3)$ and thence

$$\hat{v} = \frac{\omega \hat{F}}{4Bk^3} (e^{-jk|x|} - je^{-k|x|}). \quad (5.20)$$

The associated time histories of these functions are depicted in Fig. 5.5. For the input point mobility (5.20) yields

$$Y = \frac{\omega}{4Bk^3} (1 - j) = \frac{(1 - j)}{4m' c_B}. \quad (5.21)$$

This mobility hence has the same general form as that pertaining to the semi-infinite beam but is only a quarter thereof.

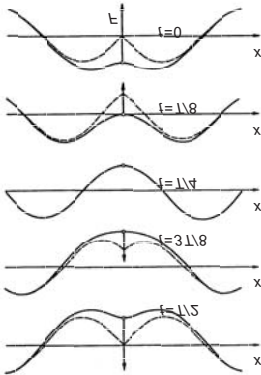


Fig. 5.5. Motion of a point-excited beam at some instances of the period T . Dashed curve represents the motion neglecting the evanescent waves

By use of the input point mobility, the power transmitted to the beam from a point force may readily be determined. This power is here due only to the product of force and velocity and no contribution is obtained from the product of moment and rotational velocity (Eq. (3.91)) since no external moment is applied. In the calculation of the force-velocity product, however, it has to be observed that consistently use is made of the complex notion whilst the power is a real-valued quantity. The power, therefore is obtained from the expression

$$W = \overline{\text{Re}[\hat{F}e^{j\omega t}]} \cdot \overline{\text{Re}[\hat{v}e^{j\omega t}]} = \frac{1}{2} \text{Re}[\hat{F}^* \hat{v}]. \quad (5.22)$$

Herein, the overbar denotes that the average is taken over several periods. Upon introducing the input mobility, the power is given by

$$W = \frac{1}{2} |\hat{F}|^2 \text{Re}[Y]. \quad (5.23)$$

This means that for the infinite beam, excited by a point force, the transmitted power amounts to

$$W = \frac{|\hat{F}|^2 \omega}{8Bk^3} = \frac{|\hat{F}|^2}{8m'c_B}. \quad (5.24)$$

Owing to the fact that the losses are not considered in the above calculations, the energy balance requires that under stationary conditions, the imparted power must equal the two-sided propagated power. From Eq.

(3.91), the one-sided propagated power amounts to $\eta^2\omega Bk^3$. Here, the displacement is denoted η and if one substitutes the velocity $v = j\omega\eta$, then \hat{v}_+ in Eq. (5.14) that represents the propagating part of the field, gives the at both sides of the beam propagated power as

$$W = \frac{2|\hat{v}_+|^2 Bk^3}{\omega} = \frac{1}{8} \frac{|\hat{F}|^2 \omega}{Bk^3} = \frac{|\hat{F}|^2}{8m'c_B}. \quad (5.25)$$

Accordingly, both methods furnish the same formula.

Finally, the vibrations of an ideal beam, excited normally by an impacting mass m , will be determined using the input mobility. Since this problem straightforwardly cannot be solved in the time domain it is suitable to treat it in the frequency domain i.e., the impulse will be considered as a sum of pure tones or more correctly, as an integral and for each tone employ the procedure discussed above. For this purpose, the Fourier transform pairs

$$\begin{aligned} F(t) &= \frac{1}{2\pi} \int_{-\infty}^{\infty} \hat{F}(\omega) e^{j\omega t} d\omega \quad , \quad \hat{F}(\omega) = \int_{-\infty}^{\infty} F(t) e^{-j\omega t} dt \\ v(t) &= \frac{1}{2\pi} \int_{-\infty}^{\infty} \hat{v}(\omega) e^{j\omega t} d\omega \quad , \quad \hat{v}(\omega) = \int_{-\infty}^{\infty} v(t) e^{-j\omega t} dt \end{aligned} \quad (5.26)$$

are introduced. Physically, the first parts of (5.26) mean that the time histories of force and velocity consist of sums of pure tones of amplitudes $\hat{F}(\omega)$ and $\hat{v}(\omega)$ respectively. The amplitude spectra are determined from the second parts of (5.26) when the time histories are known. With the mobility known as function of frequency, the response at the excitation point can be obtained from

$$\hat{v} = \frac{Y}{1 + j\omega m Y} \cdot \hat{F}. \quad (5.27)$$

Herein, Y is the beam mobility and $1/j\omega m$ the mobility of the mass because the force is exerted on both systems. In complete analogy with Eq. (5.20), also the velocity spectrum can be developed for an arbitrary position $|x| \geq 0$. For the infinite beam this means that

$$\hat{v}(x, \omega) = \frac{\hat{F}}{4m'c_B + (1+j)\omega m} (e^{-jk|x|} - je^{-k|x|}) \quad (5.28)$$

Upon substituting (5.27) or (5.28) into (5.26), the time history sought $v(x, t)$ is obtained. The above equations are valid for arbitrary time histo-

ries but specializing on an ideal impulse at time $t = 0$ i.e., $F(t) = I\delta(t)$, then

$$\hat{F}(\omega) = I \int_{-\infty}^{\infty} \delta(t) e^{-j\omega t} dt = I, \quad (5.29)$$

where $\delta(t)$ is Dirac's delta function and I the momentum transferred. By combining (5.29), (5.27), (5.26) and (5.21), the velocity at the point of impact is given by

$$v(t) = \frac{1}{2\pi} \int_{-\infty}^{\infty} \frac{I(1-j)}{4m'c_B + (1+j)\omega m} e^{j\omega t} d\omega. \quad (5.30)$$

With the abbreviations

$$\vartheta = \frac{m^2}{8\sqrt{Bm'^3}} \quad , \quad (1+j) = \sqrt{2j},$$

the integral is suitably rewritten as

$$v(t) = \frac{I}{2\pi m} \int_{-\infty}^{\infty} \frac{e^{j\omega t}}{j\omega + \sqrt{j\omega/\vartheta}} d\omega, \quad (5.31)$$

which, for instance, can be taken from a Table of integrals, and yields

$$v(t) = \frac{I}{m} e^{t/\vartheta} \left[1 - \frac{2}{\sqrt{\pi}} \int_0^{\sqrt{t/\vartheta}} e^{-\zeta^2} d\zeta \right] \quad (5.32)$$

Herein, the second term within the brackets can be recognized as the Gaussian error integral. For an estimate, it is sufficient to expand the integrand in a series leading to

$$v(t) \approx \frac{I}{m} e^{t/\vartheta} \left[1 - 2\sqrt{\frac{t}{\pi\vartheta}} \left(1 - \frac{1}{3} \frac{t}{\vartheta} + \dots \right) \right]; \quad \frac{t}{\vartheta} < 0.5,$$

$$v(t) \approx \frac{I}{m} \sqrt{\frac{\vartheta}{\pi t}} \left[1 - \frac{1}{2} \frac{\vartheta}{t} + \frac{3}{4} \left(\frac{\vartheta}{t} \right)^2 - \dots \right]; \quad \frac{t}{\vartheta} > 2.$$

In Fig. 5.6 are shown the time histories of the velocities at the point of impact for a rod and a beam respectively, both assumed excited by ideal impulses from a mass m . It is further assumed that the mass is eight times bigger than one radius of gyration long piece of the rod or beam. For a rod or beam of rectangular cross-section $h \cdot b$ and density ρ , this means a mass of $m = 8\rho h^2 b (12)^{1/2}$.

As is seen from the curves, the motion decreases much faster for a longitudinal impact than for a transversal. Hence, a longitudinal impact generally has a higher pitch than the transversal.

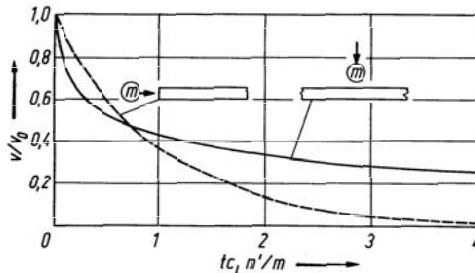


Fig. 5.6. Time history of the motion at the point of impact of a mass

5.3.3 Point Mobility of a Homogeneous Plate

In Sect. 3.7.4.2 was derived the equation of motion for plates in flexure. There, a finite shear stiffness and the rotational inertia was neglected which implies that the Eq. (3.184a) resulting has a limit of validity and that the excitation “point” cannot be too small, cf. Sect. 5.4.3. With a phasor notation, the homogeneous equation becomes

$$\nabla^4 \hat{\eta} - k_B^4 \hat{\eta} = 0. \quad (5.33)$$

One method to derive the point mobility involves solving this equation subject to the boundary conditions:

- Rotational symmetry,
- no rotation at the excitation i.e., the first spatial derivative vanishes at this point which warrants a finite amplitude
- at the excitation, the sum of the shear forces must equal the exciting force and
- the solution must satisfy the Sommerfeld radiation condition i.e., the displacement remote from the excitation behaves like a decaying wave.

To obtain a solution, Eq. (5.33) is rewritten in the operator form [5.11]

$$(\nabla^2 - k_B^2)(\nabla^2 + k_B^2)\hat{\eta} = 0.$$

This means that the fourth order differential equation is replaced by two second order equations

$$\begin{aligned}\nabla^2 \hat{\underline{\eta}}_1 + k_B^2 \hat{\underline{\eta}}_1 &= 0, \\ \nabla^2 \hat{\underline{\eta}}_2 - k_B^2 \hat{\underline{\eta}}_2 &= 0.\end{aligned}\quad (5.34)$$

The first of these equations is just the usual wave equation for non-dispersive media for which the rotationally symmetric solution is known and consists of zero order cylindrical functions. Upon considering the last boundary condition, it is found that the only admissible is the Hankel function of second kind i.e.,

$$\hat{\underline{\eta}}_1 = C_1 H_0^{(2)}(k_B r), \quad (5.35)$$

where r is the distance from the excitation point.

For the remainder of this discussion the asymptotic expressions for the Hankel function are applicable

$$\begin{aligned}H_0^{(2)}(x) &\approx \frac{-2j}{\pi} \ln \frac{x}{2} + 1 \quad ; \quad x \ll 1, \\ H_0^{(2)}(x) &\approx \sqrt{\frac{2}{\pi x}} e^{-j(x-\pi/4)} \quad ; \quad x \gg 1.\end{aligned}\quad (5.35a)$$

The solution to the second differential equation in (5.34) is readily obtained by replacing $k_B r$ with $-jk_B r$ i.e.,

$$\hat{\underline{\eta}}_2 = C_2 H_0^{(2)}(-jk_B r). \quad (5.36)$$

Using the expansion for large arguments in (5.35a) it is found that the second part tends to

$$H_0^{(2)}(-jk_B r) \approx \sqrt{\frac{2}{-\pi k_B r}} e^{j\pi/4} e^{-k_B r} = j \sqrt{\frac{2}{\pi k_B r}} e^{-k_B r}.$$

It is seen that this represents an exponentially decaying nearfield of the same kind as was found for beams. Accordingly, the total solution is given by

$$\hat{\underline{\eta}} = C_1 H_0^{(2)}(k_B r) + C_2 H_0^{(2)}(-jk_B r). \quad (5.37)$$

By applying the second boundary condition, it is found that

$$\begin{aligned}\frac{\partial \hat{\eta}}{\partial r} &= C_1 k_B \left[-j \frac{2}{\pi k_B r} + \alpha (k_B r)^n + \dots \right] - j C_2 k_B \left[\frac{2}{\pi k_B r} + \beta (k_B r)^n + \dots \right] \\ &= \frac{2j}{\pi r} (-C_1 - C_2),\end{aligned}\quad (5.38)$$

which must vanish at the excitation point so that $C_1 = -C_2$ and hence

$$\underline{\hat{\eta}} = C_1 \left[H_0^{(2)}(k_B r) - H_0^{(2)}(-jk_B r) \right]. \quad (5.39)$$

The value of Eq. (5.39) at the excitation point $r = 0$ can be obtained from the expansion of the Hankel functions

$$\begin{aligned}\underline{\hat{\eta}}(0) &= \underline{\hat{\eta}}_0 = C_1 \left[-\frac{2j}{\pi} \ln \frac{k_B r}{2} + \dots + \frac{2j}{\pi} \left(\ln \frac{k_B r}{2} + \ln(-j) + \dots \right) \right] \\ &= C_1 \frac{2j}{\pi} \ln(-j) = C_1 \frac{2j}{\pi} \ln(e^{-j\pi/2}) = C_1.\end{aligned}$$

This means that the constant C_1 equals the displacement at the excitation point such that (5.39) becomes

$$\underline{\hat{\eta}} = \underline{\hat{\eta}}_0 \left[H_0^{(2)}(k_B r) - H_0^{(2)}(-jk_B r) \right] = \underline{\hat{\eta}}_0 \Pi(k_B r). \quad (5.40)$$

Here, the propagation function $\Pi(k_B r)$ is introduced for the difference between the two Hankel functions. In Fig. 5.7 are depicted snapshots of the wave field associated with Eq. (5.40). The decay in amplitude with distance from the excitation i.e., the behaviour of $|\Pi(k_B r)|^2$, is displayed in Fig. 5.8. In this figure, moreover, the asymptotic behaviour for large arguments $k_B r$ is included. Evidently, the asymptote constitutes a very good approximation for $k_B r \geq 4$.

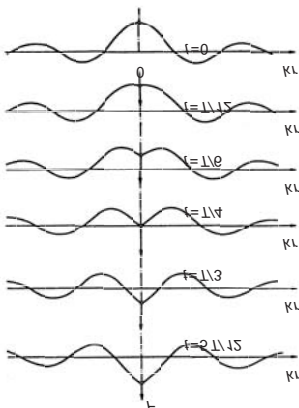


Fig. 5.7. Point excited bending waves on a plate. (T is the period)

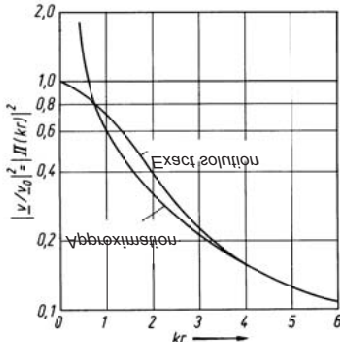


Fig. 5.8. Amplitude decay of point excited bending waves on a plate

The remaining unknown η_0 is obtained from a consideration of the fourth boundary condition. For this purpose the force F_0 is assumed to be applied over a small circular area of radius r_0 . The shear force per unit length, acting along the circumference of the circular area and over the cross-section of the plate is denoted by \underline{Q}_r . It is the same as that given by (3.184e) since the radial direction coincides with the x- or z-directions. Thus,

$$\underline{Q}_r = B' \frac{\partial \nabla^2 \underline{\eta}}{\partial r}. \quad (5.41)$$

By substituting (5.40),

$$\underline{Q}_r = -B' k_B^3 \hat{\underline{\eta}}_0 \left[\frac{\partial H_0^{(2)}(k_B r)}{\partial k_B r} + \frac{\partial H_0^{(2)}(-jk_B r)}{\partial k_B r} \right],$$

observing the relations in Eq. (5.34) $\nabla^2 H_0^{(2)}(k_B r) = -k_B^2 H_0^{(2)}(k_B r)$ and $\nabla^2 H_0^{(2)}(-jk_B r) = k_B^2 H_0^{(2)}(-jk_B r)$. Moreover, by employing the series expansions of the Hankel functions for small arguments, the shear force along the circumference of the excitation area is obtained as

$$\underline{Q}_{r_0} = \frac{4jB'k_B^2}{\pi r_0} \hat{\underline{\eta}}_0 \quad (5.42)$$

Upon multiplying (5.42) by the circumference, the third boundary condition yields

$$\hat{F}_0 = 2\pi r_0 \underline{Q}_{r_0} = 8jB'k_B^2 \hat{\underline{\eta}}_0 \quad (5.43)$$

Hereby, a physical deficiency results in that the shear stress becomes arbitrarily big for the vanishing radius, see Sect. 5.4.3.1. For the subsequent analysis, therefore, it must be presumed that the exciting force acts over a surface with dimensions much smaller than the bending wavelength but big enough to prevent shear deformations at the excitation. These prerequisites are very often met in practice. By replacing the displacement with the velocity, the input point mobility of the force excited plate can be obtained as

$$Y_0 = \frac{\hat{v}_0}{\hat{F}_0} = \frac{j\omega \eta_0}{\hat{F}_0} = \frac{\omega}{8B'k_B^2} = \frac{1}{8\sqrt{B'm''}} = \frac{k_B^2}{8\omega m''}. \quad (5.44)$$

The velocity distribution for a point excited plate is thus given by

$$\hat{v}(r) = \frac{\hat{F}_0 \omega}{8B'k_B^2} [H_0^{(2)}(k_B r) - H_0^{(2)}(-jk_B r)] = \hat{F}_0 Y_0 \Pi(k_B r). \quad (5.44a)$$

This surprisingly simple result, which is experimentally well corroborated for the high frequency range where reflections from the boundaries can be circumvented, is rather unexpected, see Fig. 5.9. The point mobility of the plate is found real-valued and independent of frequency and hence less complicated than that of a beam. The finding can be further illustrated by means of a power balance. From Eq. (5.23), the transmitted power by point-force excitation is

$$W = \frac{1}{2} \operatorname{Re} \left[\hat{F}_0^* v_0 \right] = \frac{1}{2} |\hat{F}_0|^2 \operatorname{Re}[Y_0] = \frac{|\hat{v}_0|^2}{2 \operatorname{Re}[Y_0]}. \quad (5.45)$$

At large distance R from the excitation on the other hand, the cylindrical wave behaves as a decaying plane wave such that the power transmitted through the circumference $2\pi R$ is given by (3.93)

$$W = c_{gB} S E_{kin} = 2c_B 2\pi R \rho h |\hat{v}|^2. \quad (5.46)$$

Again, c_B is the phase speed of the flexural wave in the plate and \hat{v} the velocity at distance R from the excitation. For sufficiently large R , the series expansion for Hankel function of large arguments applies and

$$\frac{\hat{v}}{\hat{v}_0} = \sqrt{\frac{2}{\pi k_B R}} e^{-j(k_B R - \pi/4)}, \quad \left| \frac{\hat{v}}{\hat{v}_0} \right|^2 = \frac{2}{\pi k_B R}. \quad (5.46a)$$

By equating (5.45) and (5.46), using (5.46a) it is found that

$$\operatorname{Re}[Y_0] = \frac{k_B}{8c_B \rho h} = \frac{k_B^2}{8\omega m''},$$

in agreement with the result in (5.44).

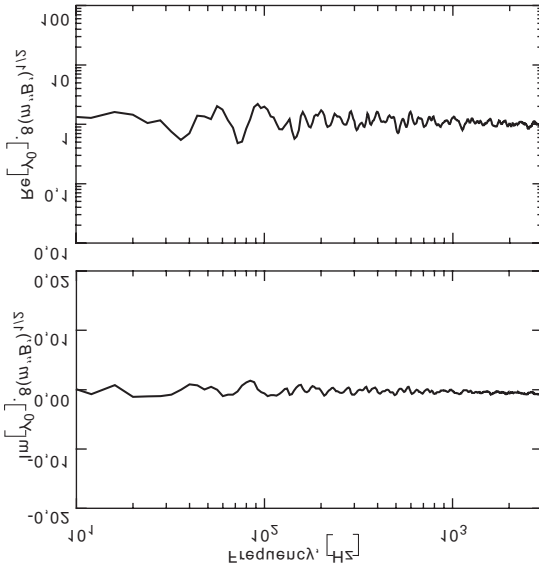


Fig. 5.9. Measured real and imaginary parts of mobility for a 4mm thick perspex plate. To approximate the infinite plate the edges were embedded in sand.

5.4 Wave Impedance, Wave Mobility

5.4.1 Calculation of Wave Impedances and Wave Mobilities

The wave impedance and wave mobility were defined by (5.2) as the ratios of pressure to velocity and velocity to pressure respectively under the condition that both quantities refer to the same frequency and spatial distribution. For an equation of motion of simple form, these ratios are readily determined since all spatial derivatives becomes multiplications with the corresponding wave-numbers.

For the thin plate, for example, the inhomogeneous equation of motion in (3.184a) can be rewritten as

$$\left(\frac{\partial^2}{\partial x^2} + \frac{\partial^2}{\partial z^2} \right)^2 \eta(x, z, t) + \frac{m''}{B'} \frac{\partial^2}{\partial t^2} \eta(x, z, t) = \frac{1}{B'} p(x, z, t), \quad (5.47)$$

where $p(x, z, t)$ is the exciting pressure distribution. By expressing the motion in terms of velocity ($v = j\omega\eta$) and assuming an excitation in the form

$$p(x, z) = \tilde{p}(k_x, k_z) e^{-jk_x x} e^{-jk_z z}, \quad (5.48)$$

Eq. (5.47) becomes

$$\left(\frac{\partial^2}{\partial x^2} + \frac{\partial^2}{\partial z^2} \right)^2 v(x, z) - k_B^4 v(x, z) = \frac{j\omega}{B'} \tilde{p}(k_x, k_z) e^{-jk_x x} e^{-jk_z z}, \quad (5.49)$$

where the bending wavenumber $k_B^4 = \omega^2 m'' / B'$ is introduced. In a case where the plate is infinite and no discontinuities or inhomogeneities are present, then and only then the spatial distribution of the response equals that of the excitation. For such a case thus, the response can be taken to be in the form

$$v(x, z) = \tilde{v}(k_x, k_z) e^{-jk_x x} e^{-jk_z z}, \quad (5.49a)$$

establishing

$$\left[(k_x^2 + k_z^2)^2 - k_B^4 \right] \tilde{v}(k_x, k_z) = \frac{j\omega}{B'} \tilde{p}(k_x, k_z). \quad (5.49b)$$

The wave mobility of a thin plate, therefore, reads

$$Y_{\sim} = \frac{\tilde{v}(k_x, k_z)}{\tilde{p}(k_x, k_z)} = \frac{j\omega}{B'} \frac{1}{\left[(k_x^2 + k_z^2)^2 - k_B^4 \right]} = \frac{1}{j\omega m''} \frac{k_B^4}{k_B^4 - (k_x^2 + k_z^2)^2}, \quad (5.50)$$

when shear stiffness and rotational inertia are disregarded. Inversely, the wave impedance of the thin plate is

$$Z_{\sim} = \frac{\tilde{p}(k_x, k_z)}{\tilde{v}(k_x, k_z)} = \frac{B'}{j\omega} \left[(k_x^2 + k_z^2)^2 - k_B^4 \right] = j\omega m'' \left[1 - \frac{(k_x^2 + k_z^2)^2}{k_B^4} \right]. \quad (5.50a)$$

5.4.2 Examples

Fully analogous, the wave mobility of an orthotropic plate can be established from (3.186)

$$Y_{\sim} = \frac{1}{j\omega m''} \frac{1}{\left[1 - \frac{B'_x}{\omega^2 m''} k_x^4 - 2 \frac{B'_u + 2B'_G}{\omega^2 m''} k_x^2 k_z^2 - \frac{B'_z}{\omega^2 m''} k_z^4 \right]}. \quad (5.50b)$$

Here, the term within brackets in the denominator is often well approximated by

$$1 - \frac{\left(\sqrt{B'_x} k_x^2 + \sqrt{B'_z} k_z^2 \right)^2}{\omega^2 m''}.$$

For a thick plate where shear stiffness and rotational inertia are taken into account, the wave impedance is given by

$$Z_{\sim} = j\omega m'' \frac{1 - \frac{(k_x^2 + k_z^2)^2}{k_B^4} + \frac{h^2}{12} \left[(k_x^2 + k_z^2) \left(1 + \frac{c_L^2}{c_T^2} \right) - \frac{\omega^2}{c_T^2} \right]}{1 + \frac{h}{12} \left[(k_x^2 + k_z^2) \frac{c_L^2}{c_T^2} - \frac{\omega^2}{c_T^2} \right]}. \quad (5.50c)$$

In this expression, $c_L^2 = E/\rho$ and $c_T^2 = G^*/\rho$ are the wave speeds for the extensional and shear waves respectively. G^* denotes that the shear distribution is taken into account rendering a slightly reduced shear modulus [3.15].

The expressions for the corresponding one-dimensional problems can be obtained by setting $k_z = 0$ and using the one-dimensional value for the bending stiffness because of the altered cross-sectional contraction.

For the parallel plates subject to an excitation perpendicular to the plate face, the wave impedance was given by Eq. (4.108) and that for a three-layered plate can easily be developed from Eq. (4.114). Yet another wave impedance or mobility is given by Eq. (3.209b) for the circular cylinder.

The wave mobilities and wave impedances discussed above, all refer to an excitation perpendicular to the surface of the structure. Although that is an important case with respect to practice, also other excitations and response components can be relevant. In-plane waves in plates obeying the wave equation in (3.168b), for instance, can be excited by shear forces parallel to the plate surface. To determine the associated wave impedance or wave mobility, a force per unit area is assumed in the x -direction

$$p_2 \sim e^{-jk_x x} e^{-jk_z z}.$$

The other two external forces p_D and p_4 are set equal to zero. Naturally, with another type of excitation it would have been possible to assume $p_D \neq 0$ whilst $p_2 = p_4 = 0$. The analysis proceeds with replacing all differen-

tiations with respect to x and z in (3.168b) by multiplications with jk_x and jk_z respectively. Then, ζ and ξ are eliminated from the resulting linear set of equations. This leads to

$$\begin{aligned} Z_{\sim\xi} &= \frac{\check{p}_2}{j\omega\xi} = j\omega\rho h \left[1 - \frac{k_x^2 + k_z^2}{k_T^2} \right] \left[1 - \frac{k_x^2 + k_z^2}{k_{Ll}^2} \right], \\ Z_{\sim\zeta} &= \frac{\check{p}_2}{j\omega\zeta} = j\omega\rho h \left[1 - \frac{k_x^2 + k_z^2}{k_T^2} \right] \left[1 - \frac{k_x^2 + k_z^2}{k_{Ll}^2} \right] \frac{1-\mu}{1+\mu} \frac{k_T^2}{k_x k_z}. \end{aligned} \quad (5.50d)$$

Finally, the wave impedance for a prestressed plate on a Winkler bed can be developed from (3.187) to be given by

$$Z_{\sim} = j\omega m'' \left[1 - \frac{B'}{\omega^2 m''} (k_x^2 + k_z^2)^2 + \frac{T}{\omega^2 m''} (k_x^2 + k_z^2) - \frac{s''}{\omega^2 m''} \right]. \quad (5.50e)$$

Hitherto, the examples treated have been two-dimensional structures for which the field variables are constant across the thickness. The wave impedance or wave mobility is of course applicable also for three-dimensional systems provided the excitation and motion have the same spatial distribution over the interface considered. Most important in this context is the semi-infinite continuum, excited at the free surface. Also in this case, it is suitable to distinguish between an excitation with a normal stress $p(x, z) = \sigma_y(x, z) = \check{\sigma} e^{-jk_x x} e^{-jk_z z}$ in the normal direction and a shear stress $p(x, z) = \tau_{xy}(x, z) = \check{\tau} e^{-jk_x x} e^{-jk_z z}$ in the tangential. From Eq. (3.148a), the wave impedance in (3.148d) results for $\sigma \neq 0$ and $\tau = 0$, which rewritten as wave mobility reads

$$Y_{\sim\sigma\eta} = \frac{j\omega\check{\eta}}{\check{\sigma}} = \frac{\omega}{G} \frac{k_T^2 k_{yL}}{\left[k_T^2 - 2(k_x^2 + k_z^2) \right]^2 + 4(k_x^2 + k_z^2) k_{yT} k_{yL}}, \quad (5.50f)$$

and with $\sigma = 0$ and $\tau \neq 0$

$$Y_{\sim\tau\xi} = \frac{j\omega\check{\xi}}{\check{\tau}} = \frac{\omega}{G} \frac{k_T^2 k_{yT}}{\left[k_T^2 - 2(k_x^2 + k_z^2) \right]^2 + 4(k_x^2 + k_z^2) k_{yT} k_{yL}}, \quad (5.50g)$$

where the notation is retained from Eqs. (3.147) and (3.138).

In the same manner also other wave mobilities can be formed, for example, $j\omega\xi/\sigma$ with $\tau = 0$ or $j\omega\eta/\tau$ with $\sigma = 0$.

The limiting case of a fluid half-space, completely free of shear is encompassed by Eq. (5.50f). Thereby it must be observed that $G \rightarrow 0$ i.e., $k_T \rightarrow \infty$ whereas $G k_T^2 = \omega^2 \rho$. For the fluid half-space the wave impedance becomes

$$Z_{\sim} = \frac{\omega\rho}{k_{yL}}. \quad (5.50h)$$

The expressions (5.50f) and (5.50g) are also valid for a viscous fluid. The only modification necessary is to substitute $j\omega v_v$ for G and $-j\omega v_v$ for k_T^2 where v_v is the kinematic viscosity of the fluid.

5.4.3 Relation between Wave Mobility and Point Mobility

The aforementioned examples and general considerations show that the wave impedance or wave mobility can be expressed as ratios of polynomials in the wavenumbers. For structures allowing for wave propagation in all directions appear also radicals of the wavenumbers as, for instance, k_{yT} and k_{yL} in Eq. (5.50f).

In the subsequent analysis, moreover, the maxima of the wave mobility (wave impedance minima) play a significant role. At those wavenumbers, a vanishingly small excitation is sufficient to drive the associated wave. Waves in the form of (5.48) or (5.49a) respectively, for which k_x and k_z realize maxima in the wave mobility, are termed “free waves”. Both propagating and evanescent waves are involved. For the former, k_x and k_z are purely real or encompass a small imaginary part associated with the dissipation whereas for the latter, k_x or k_z are imaginary. The wave mobility thus establishes a straightforward possibility to find the free wavenumbers. This is also true for less obvious cases such as the Rayleigh wave at the surface of an elastic half-space which can be determined from a vanishing denominator in (5.50f).

The wave mobilities are very useful for the analysis of structure-borne sound in (built-up) systems where the substructures do not possess inhomogeneities or discontinuities or where their influence can be neglected e.g., in conjunction with energy- or power quantities, see sections 5.5 and 5.7.3. For all such cases, the assumption of infinitely extended structures applies.

With a periodic excitation in two directions, for example, having the periods $\lambda_{x0} = 2\pi/k_{x0}$ and $\lambda_{z0} = 2\pi/k_{z0}$, then the excitation can be given in the form

$$p(x, z) = \sum_{n,m} \check{p}_{n,m} e^{-jn k_{x0} x} e^{-jm k_{z0} z}. \quad (5.51)$$

For each term in the sum in (5.51), the wave mobility expression can be used and the response amplitude becomes

$$\check{v}_{n,m} = Y_{\sim}(nk_{x0}, mk_{z0}) \check{p}_{n,m}.$$

It follows that the total response distribution is given by

$$v(x, z) = \sum_{n,m} Y_{\sim}(nk_{x0}, mk_{z0}) \check{p}_{n,m}. \quad (5.52)$$

The amplitudes of the excitation orders are obtained from the decomposition formulae

$$\check{p}_{n,m} = \frac{1}{4\pi^2} \int_0^{\lambda_{x0}} \int_0^{\lambda_{z0}} p(x, z) e^{jnk_{x0}x} e^{jm k_{z0}z} dx dz. \quad (5.53)$$

Accordingly, the problem with spatially periodic excitations has a solution since the amplitudes $p_{n,m}$ of the component waves of the excitation can be determined from Eq. (5.53), which substituted in (5.52) yields the response distribution.

For a spatially non-periodic excitation, the procedure is similar. The Fourier series is thereby replaced by a Fourier integral. Physically, (5.53) means that a prescribed excitation distribution $p_{x,z}$ is expressed as a sum (integral) of many plane waves where their amplitudes are chosen such that when added, they reconstruct $p_{x,z}$. The amplitudes are then used as previously described.

For the non-periodically distributed excitation thus, the Fourier integral is

$$p(x, z) = \frac{1}{4\pi^2} \int_{-\infty}^{\infty} \int_{-\infty}^{\infty} \check{p}(k_x, k_z) e^{-jk_x x} e^{-jk_z z} dk_x dk_z. \quad (5.54)$$

The amplitude distribution of the wave parts appearing as the integrand, also termed wavenumber spectrum, are determined by

$$\check{p}(k_x, k_z) = \int_{-\infty}^{\infty} \int_{-\infty}^{\infty} p(x, z) e^{jk_x x} e^{jk_z z} dx dz. \quad (5.55a)$$

Owing to the fact that the wave mobility formula applies for each individual wave part, the wavenumber spectrum of the response becomes

$$\check{v}(k_x, k_z) = Y_{\sim}(k_x, k_z) \check{p}(k_x, k_z). \quad (5.55b)$$

Hence, the spatial distribution of the response is obtained as

$$v(x, z) = \frac{1}{4\pi^2} \int_{-\infty}^{\infty} \int_{-\infty}^{\infty} Y_{\sim}(k_x, k_z) \check{p}(k_x, k_z) e^{-jk_x x} e^{-jk_z z} dk_x dk_z. \quad (5.55c)$$

Particularly simple is the calculation of the wavenumber spectrum in the case that the excitation is concentrated to a small area (point force) with a net force amplitude F_0 . Such an excitation can be represented by Dirac's delta function as

$$p(x, z) = F_0 \delta(x, z), \quad (5.56a)$$

stating that the excitation exists only inside the small area. This means that all components of the exciting wavenumber spectrum becomes equal

$$\check{p}(k_x, k_z) = F_0 \int_{-\infty}^{\infty} \int_{-\infty}^{\infty} \delta(x, z) e^{jk_x x} e^{jk_z z} dx dz. \quad (5.56b)$$

Following from (5.55c), the response to such an excitation thence is obtained as

$$v(x, z) = \frac{F_0}{4\pi^2} \int_{-\infty}^{\infty} \int_{-\infty}^{\infty} Y_{\sim} e^{-jk_x x} e^{-jk_z z} dk_x dk_z. \quad (5.56c)$$

Accordingly, the point mobility (impedance) can be directly obtained from Eq. (5.56c) when x and z are chosen to be at the origin,

$$Y = v(0, 0) / F_0.$$

5.4.3.1 Plate with Shear Stiffness

To calculate the integral in (5.56c) it is suitable to express the wave mobility in partial fractions and subsequently employ the method of residues. This can be elegantly illustrated in the example of a plate with shear stiffness. From (5.50c) one obtains

$$Y_{\sim} = -\frac{1}{j\omega m''} \frac{k_B^4 \alpha + k_T^2 (k_x^2 + k_z^2)}{(k_x^2 + k_z^2)^2 - (k_x^2 + k_z^2)(k_T^2 + k_L^2) - k_B^4 \alpha}$$

after some manipulations whereby $\alpha = 1 - k_T^2 h^2 / 12$. The zeroes of the denominator are found to be given by

$$k_I^2 = (k_x^2 + k_z^2)_I = \frac{k_T^2 + k_L^2}{2} + \sqrt{\left(\frac{k_T^2 + k_L^2}{2}\right)^2 + \alpha k_B^4}, \quad (5.57a)$$

$$k_{II}^2 = (k_x^2 + k_z^2)_{II} = \frac{k_T^2 + k_L^2}{2} - \sqrt{\left(\frac{k_T^2 + k_L^2}{2}\right)^2 + \alpha k_B^4}. \quad (5.57b)$$

Since the roots contained in these expressions are consistently positive, k_I is always real-valued, which means that the corresponding responses are represented by propagating waves. The wavenumber k_{II} becomes imaginary for low and intermediate frequencies realising evanescent waves as the response. At high frequencies i.e., when $\alpha < 0$ or equivalently $2\pi/k_T = \lambda_T < 1.6h$, k_{II} also becomes real-valued. This means that the Mindlin plate theory yields two propagating wave types at high frequencies. For $\alpha = 0$, the response associated with k_{II} exhibits an infinite phase speed, which reduces with increasing frequency and approaches the that of the shear- or Rayleigh wave respectively. At low frequencies, the expressions (5.57a, b) render the wavenumbers obtained from thin plate theory i.e., $k_I \approx k_B$ and $k_{II} \approx jk_B$.

Upon expressing (5.57) in terms of partial fractions, the wave mobility reads

$$Y_{\sim} = \frac{1}{j\omega m''} \frac{k_T^2(k_x^2 + k_z^2) + \alpha k_B^2}{k_I^2 - k_{II}^2} \left[\frac{1}{(k_x^2 + k_z^2) - k_I^2} - \frac{1}{(k_x^2 + k_z^2) - k_{II}^2} \right].$$

Introduced into (5.56c), the method of residues can be employed for the integration over k_z . The resulting terms can be rewritten as

$$\frac{1}{j} \int_{-\infty}^{\infty} \frac{1}{\sqrt{k_x^2 - k_I^2}} e^{-\sqrt{k_x^2 - k_I^2} k_z} e^{-jk_x x} dk_z = -\pi H_0^{(2)}(k_I \sqrt{x^2 + z^2}). \quad (5.57c)$$

By employing these expressions, the response of a point excited thick plate can be developed as

$$v(x, z) = \frac{F_0}{\omega m''} \left[\frac{k_T^2 k_I^2 + \alpha k_B^4}{k_I^2 - k_{II}^2} H_0^{(2)}(k_I r) - \frac{k_T^2 k_{II}^2 + \alpha k_B^4}{k_I^2 - k_{II}^2} H_0^{(2)}(k_{II} r) \right], \quad (5.58)$$

where $r = \sqrt{x^2 + z^2}$. The point mobility is obtained from Eq. (5.58) by taking the limiting value as x and z tend to zero. With the approximation in (5.35a) and some manipulations it follows that

$$\frac{v(r \rightarrow 0)}{F_0} = \frac{k_B^4 (A_R + jA_I)}{8\omega m'' \left[k_I^2 - \frac{1}{2}(k_T^2 + k_L^2) \right]}, \quad (5.59)$$

where the abbreviations

$$A_R = \begin{cases} \alpha + k_T^2 (2k_I^2 - k_L^2 - k_T^2) / k_B^4 & ; \quad \alpha > 0 \\ k_T^2 (2k_I^2 - k_L^2 - k_T^2) / k_B^4 & ; \quad \alpha < 0 \end{cases}, \quad (5.59a)$$

$$A_I = -\frac{2}{\pi} \left[\alpha \ln \left(\frac{k_B^2}{k_I^2} \sqrt{|\alpha|} \right) + \frac{k_T^2}{k_B^2} \{ k_I^2 \ln(k_I r) - k_H^2 \ln(k_H r) \} \right].$$

At low frequencies, $k_I^2 = k_B^2$, $\alpha = 1$, $k_I^2 = -k_H^2$ and $k_T \approx 0$ and hence $A_R = 1$ and $A_I = 0$ such that the familiar result in Eq. (5.44) is revisited.

If the fully unrealistic assumption that $G \rightarrow \infty$ and $k_T \rightarrow 0$ is not made, which is the basis for the Euler-Bernoulli bending theory, then the real part of (5.62) remains intelligible but the imaginary is remarkable since a logarithmic singularity appears. It is not a deficiency of the theory, however. Rather, a force distribution in the form of a Dirac's delta function results in extreme stresses, which would lead to a singularity (a hole) in every material with a finite shear stiffness. With the force distributed over a small area already at the beginning of the analysis, the singularity would not appear. Instead would be obtained an imaginary part of the mobility, which although dependent on the size of the excitation area, would not capture the physics. For practical measurements this means that the real part and hence the relevant quantity for the power transmission is straightforwardly assessed but that the imaginary part will vary with the size of the excitation area. Hereby, it should be observed that the theory for plates with shear stiffnesses, used in this section, is inappropriate for the quantitative description of the thickness dependent local deformation that occurs in the vicinity of a small excitation area. The issue will be revisited in the next section.

5.4.3.2 Isotropic, Elastic Half-Space

By combining Eqs. (5.55c) and (5.50f), the response at the surface of an isotropic elastic half-space, subject to only the pressure $p(x, z)$ perpendicular to the surface, is obtained as

$$v(x, z) = \frac{1}{4\pi^2 G} \int_{-\infty}^{\infty} \frac{\omega k_T^2 k_{yL} \tilde{p}(k_x, k_z) e^{-jk_x x} e^{-jk_z z}}{\left(k_T^2 - 2k_r^2 \right)^2 + 4k_r^2 k_{yL} k_{yT}} dk_x dk_z, \quad (5.60)$$

where the abbreviations $k_r^2 = k_x^2 + k_z^2$, $k_{yL}^2 = k_L^2 - k_r^2$ and $k_{yT}^2 = k_T^2 - k_r^2$ are introduced. An integration of (5.60) in closed form seem rather unlikely since k_x and k_z also appear in the radicals and thus the method of residues will not furnish the complete solution. For an excitation concentrated to a small area, an approximative [5.12] or numerical evaluation reveals that the shear and compressional waves propagate as bulk waves and the

Rayleigh wave as a surface wave as illustrated in Fig. 5.10. The wavenumber of the free Rayleigh wave is given by the real-valued zero of the denominator in (5.60). An approximation is offered by the expression in (3.149a).

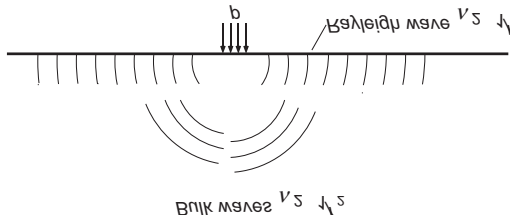


Fig. 5.10. Surface and bulk waves in a semi-infinite homogeneous elastic medium. The attenuation refers to the far field

An approximation for the mobility of the half-space, subject to an excitation perpendicular to the free surface, can be established from a comprehensive numerical analysis [5.13]

- a) Excitation with a force F , uniformly distributed over a circular area of radius a

$$\underline{Y} = \frac{\hat{v}}{\hat{F}} \approx \frac{\omega k_r}{G} (1 - \mu) [0.19 + j0.3/k_r a]. \quad (5.61)$$

- b) Excitation with a line force, uniformly distributed over a strip of width b

$$\underline{Y} = \frac{\omega}{G} (1 - \mu) \left\{ 0.463 + j1.5 \ln \left(\frac{[1.9 - 15(\mu - 0.25)^2]}{k_r b} \right) \right\}. \quad (5.62a)$$

In both these expressions, the real part is independent of the size of the excitation area as long as its dimensions are substantially smaller than the shear wavelength. This is not the case for the imaginary part since it establishes a measure of the local deformation of the structure at the excitation. Intuitively, the local deformation and thus the imaginary part, is the bigger the smaller the excitation area and the shear modulus. Interpreting the imaginary part of the mobility in (5.61) as stiffness-controlled mobility of a spring stiffness s , one finds

$$\text{Im}[Y] = \frac{\omega(1-\mu)}{Ga} 0.3 = \frac{\omega}{s},$$

giving a stiffness

$$s \approx \frac{3.3Ga}{1-\mu} \quad (5.62b)$$

for the local elasticity of the material. This result is also in agreement with that of a static deformation of the semi-infinite medium [5.14-5.16]. The stiffness in (5.62b) compares well with those obtained with the formulae given in the literature, which read

$$s = \frac{\hat{F}}{\xi_0} \approx \pi \frac{Ga}{1-\mu} , \quad s = \frac{\hat{F}}{\xi_a} \approx 5 \frac{Ga}{1-\mu} , \quad s = \frac{\hat{F}}{\xi_0} \approx 4 \frac{Ga}{1-\mu} \quad (5.63)$$

respectively. The first formula refers to a force uniformly distributed over the excitation area and the displacement at the centre. With respect to the second, the force is also uniformly distributed but the displacement ξ_a refers to that at the periphery of the area. Regarding the third formula, the force has a distribution in the form $(a^2 - r^2)^{1/2}$ which renders a uniform deformation over the excited area in the static case.

As can be observed, the imaginary part of the mobility (contact stiffness) depends on the details of the excitation in contrast to the real part, associated with the power transmission. In particular, the size of and force distribution over the excitation area are important parameters as are also the precise response position and the contact condition with respect to shear stress and tangential motion respectively. In contact mechanics cf. e.g., [5.16] and thus also in the theory of rolling contact, these effects must be carefully considered. To complicate matters further, the shear stress τ depends on the frictional forces in a complicated way which arise from the deformation in the tangential direction whereas the normal stress at the contact patch usually is known.

5.4.3.3 Orthotropic Plate, Thick Plate, Plate Strip and Tube

Upon employing the procedure described for orthotropic plates, the substitution of (5.50b) in (5.56c) yields [5.17]

$$Y = \frac{\hat{v}(r=0)}{\hat{F}} = \frac{1}{8\sqrt[4]{m''^2 B'_x B'_z}} \frac{2K(\beta)}{\pi} \approx \frac{1}{8\sqrt[4]{m''^2 B'_x B'_z}} \quad (5.64)$$

and

$$v(x, z) \approx \hat{F} Y \left[H_0^{(2)}(\gamma) - H_0^{(2)}(-j\gamma) \right],$$

with

$$\beta = \frac{1}{2} \left(1 - \frac{B'_\mu + 2B'_G}{\sqrt{B'_x B'_z}} \right), \quad \gamma = \left[\frac{\sqrt{\omega^2 m''}}{\sqrt{B'_x B'_z}} \left(\sqrt{\frac{B'_z}{B'_x}} x^2 + \sqrt{\frac{B'_x}{B'_z}} z^2 \right) \right]^{1/2}.$$

The function K is the complete elliptic integral of the first kind, which takes on a value between $\pi/2$ and 1.85 for the parameter range of interest.

The point mobility of a plate of thickness comparable with or larger than the shear wavelength can be developed by using the procedure in (5.56c). The following approximations [5.13], [5.18] illustrate the results.

- For a line excitation with a force per unit length F' , uniformly distributed over a narrow strip of width b , the mobility is

$$\underline{Y} = \frac{\hat{v}(x=0)}{\hat{F}} \approx \frac{\omega}{G} \left\{ \frac{1}{8H^{3/2}} + 0.31 \left(\frac{H}{H+1.6} \right)^2 + j \left[\frac{-1}{8H^{3/2}} + 0.16 \ln \left(\frac{\lambda_T}{b} \right) \right] \right\}. \quad (5.65a)$$

- For a point excitation with a force F , uniformly distributed over a small circular area of diameter D , the mobility is

$$\underline{Y} = \frac{\hat{v}(r=0)}{\hat{F}} \approx \frac{\omega k_T}{G} \left\{ \frac{0.063}{H^2} + \frac{1}{8} \left(\frac{H}{H+1.6} \right)^2 + j \left[\frac{0.001}{H^{1.3}} + 0.06 \frac{\lambda_T}{D} \right] \right\}. \quad (5.65b)$$

Herein, G is the shear modulus, k_T the shear wavenumber, $\lambda_T = 2\pi/k_T$ the shear wavelength, $H = k_T h/2$ and h the plate thickness. For the approximations above, obtained from a comprehensive numerical analysis, Poisson's ratio is assumed to be $\mu \approx 0.3$.

The analysis of the plate strip involves a mixed form of solution since it is finite in one direction but infinitely extended in the other, see Fig. 5.11. The procedure, however, remains applicable at least for simple boundary conditions. In analogy with Eqs. (5.48) and (5.49a), a solution is assumed in the form of the product

$$\begin{aligned} p(x, z) &= \check{p}_n(k_z) \varphi_n(x) e^{-jk_z z}, \\ v(x, z) &= \check{v}_n(k_z) \varphi_n(x) e^{-jk_z z}, \end{aligned} \quad (5.66)$$

where the eigen-function $\varphi_n(x)$ is determined by the boundary conditions. With the plate strip, depicted in Fig. 5.11, having guided edges i.e., $\partial v / \partial x = 0$ and $F \sim \partial^3 v / \partial x^3 = 0$ at $x = 0, l_s$, then

$$\varphi_n(x) = \cos \frac{n\pi}{l_s} x \quad ; \quad n = 0, 1, 2, 3, \dots \quad (5.67a)$$

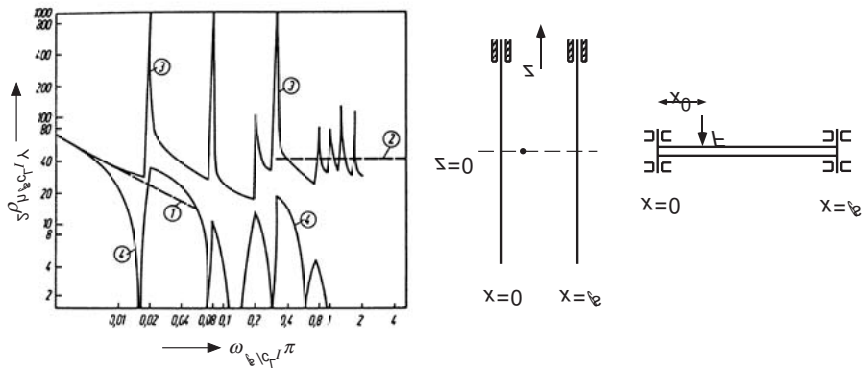


Fig. 5.11. Normalized point mobility of a plate strip of thickness h and width l_s . $h\pi / (l_s \sqrt{12}) = 0.018$. (1) Real part of the point mobility of a beam of width l_s , (2) Real part of the point mobility of an infinite plate of thickness h , (3) real part of (5.70) and (4) magnitude of the imaginary part of (5.70).

For simply supported edges ($v=0$ and $M \sim \partial^2 v / \partial x^2 = 0$; $x=0, l_s$), on the other hand, the eigen-function takes the form

$$\varphi_n(x) = \sin \frac{m\pi}{l_s} x ; \quad n = 1, 2, 3, \dots \quad (5.67b)$$

In both cases, a substitution in (5.47) yields

$$\left[- \left(\frac{m\pi}{l_s} \right)^2 - k_z^2 \right]^2 - k_B^4 \bar{v}(k_z) = \frac{j\omega}{B'} \bar{p}_n(k_z),$$

in analogy with (5.49b) since the pressure and velocity have the same spatial distribution. This means that the wave mobility becomes

$$Y_{-n} = \frac{\bar{v}_n(k_z)}{\bar{p}_n(k_z)} = \frac{j\omega}{B'} \left[\frac{1}{k_z^2 - \left(\frac{m\pi}{l_s} \right)^2 - k_B^2} - \frac{1}{k_z^2 - \left(\frac{m\pi}{l_s} \right)^2 + k_B^2} \right]. \quad (5.68)$$

An arbitrary excitation distribution can be represented a sum of terms in the form of (5.66) and

$$p(x, z) = \frac{1}{2\pi} \sum_{n=0}^{\infty} \int_{-\infty}^{\infty} \bar{p}_n(k_z) \varphi_n(x) e^{-jk_z z} dk_z, \quad (5.69)$$

in analogy with (5.55a). The transform to the wavenumber domain is the combination of a Fourier decomposition and a Fourier integral

$$\tilde{p}(k_z) = \frac{2}{l_s \varepsilon_n} \int_{-\infty}^{l_s} \int p(x, z) \varphi_n(x) e^{jk_z z} dy dz ; \varepsilon_0 = 2, \varepsilon_n = 1; n > 0, \quad (5.69a)$$

owing to the orthogonality of the involved functions.

With the pressure in (5.69) represented by a sum of terms in the form of (5.66), the response will also be given by a sum. The response of the plate strip, subject to an arbitrary pressure distribution, thus becomes

$$v(x, z) = \frac{1}{2\pi} \sum_{n=0}^{\infty} \int_{-\infty}^{\infty} Y_{\sim n}(k_z) \tilde{p}_n(k_z) \varphi_n(x) e^{-jk_z z} dk_z, \quad (5.69b)$$

with $p_n(k_z)$ given by (5.69a).

In the special case with a point force at $x = x_0, z = 0$

$$\tilde{p}_n(k_z) = \frac{2F}{l_s \varepsilon_n} \varphi_n(x_0).$$

By inserting this expression in (5.69b) together with (5.68) and applying the method of residues for the integration over k_z , the point mobility is obtained as

$$\frac{v(x_0, 0)}{F} = \underline{Y} = \frac{1}{2\rho h l_s c_B} \left[\frac{1-j}{2} \alpha + \sum_{n=1}^{\infty} \left(\frac{1}{\sqrt{1-\kappa_n^2}} - \frac{j}{\sqrt{1+\kappa_n^2}} \right) \varphi_n^2(x_0) \right]. \quad (5.70)$$

Here, $\kappa_n = n\pi / k_B l_s$ and $\alpha = \varphi_0^2(x_0)$. Upon considering the individual terms in (5.70), it is readily seen that the Helmholtz numbers $k_B l_s = n\pi$ represent important transition points i.e., the frequencies $\omega_n = (m\pi / l_s)^2 (B' / \rho h)^{1/2}$ constitute the “cut-on” frequencies for propagating modes. This is so since for $\omega > \omega_n$ or $k_B l_s > n\pi$, the first term of the sum is real realizing a bending wave energy transport to infinity. In contrast, when $\omega < \omega_n$ or $k_B l_s < n\pi$, both terms in the sum are imaginary and the n :th mode is evanescent (near-field). This nearfield is only significant in the vicinity of the excitation up to a distance of the order l_s / n . At $\omega = \omega_n$, the velocity at the excitation point becomes infinite as does the mobility. As seen from (5.68), moreover, the wave mobility becomes infinite at $\omega = \omega_n$ or $m\pi / l_s = k_B$ when k_z vanishes. This means that the motion is in phase for all positions z or, in other words, that the phase speed is infinite in the z -direction.

Also of interest is the average over frequency of the real part of the point mobility. Only terms up to and including $n = k_B l_s / \pi$ must be summed and by approximating the sum by an integration, the real part of the plate strip mobility approach that of the infinite plate in (5.44). The re-

sults are illustrated in the left part of Fig. 5.11. The point mobility is therein normalized with respect to that of an axially excited, infinite rod as are the mobilities of the elementary systems, included for comparison.

It is seen that the guided plate strip behaves as a beam at low frequencies and as an infinitely extended plate at high. With the frequency average curves plotted, the tendencies would have been even more clear.

With the thorough discussion of the plate strip as a background, the mobility of a tube can be treated easily since the analysis is almost identical. By replacing the eigen-function $\varphi_n(x)$ in Eq. (5.66) with $\exp(jns/a)$ or $\cos(ns/a)$, functions are obtained which are identical to those of (3.205). Thus, the relation

$$\check{v}_n(k_z) = Y_{-n}(n, k_z) \check{p}_n(k_z) \quad (5.71)$$

is again applicable. The only difference is that instead of (5.68), the wave impedance in (3.209b) or, more precisely, its inverse is to be used besides a translation of F/l_s to $F/2\pi a$.

For a point force excitation at $s/a = 0$ and $z_0 = 0$, the velocity is given by

$$v(0,0) = \frac{F}{2\pi^2 a} \sum_{n=0}^{\infty} \frac{1}{\epsilon_n} \int_{-\infty}^{\infty} Y_{-n}(n, k_z) dk_z ; \epsilon_0 = 2, \epsilon_n = 1; n > 0 \quad (5.71a)$$

Although it would be possible to do the integration by the methods of residues, the solution of the fourth order equation in k_z^2 involved makes such a route rather tedious. Instead it is easier to introduce a small amount of material losses such that the poles are shifted off the real axis and perform the integration numerically. An example of such a calculation is shown in Fig. 5.12. From this figure and some approximations the following findings can be listed [5.19]:

- a) The tube mobility principally shows the same trend as that of the plate strip. This is featured by the high peaks at the “ring resonances”, see Fig. 5.12 and by tending towards the point mobility of the infinite plate in an overall sense at high frequencies i.e.,

$$\operatorname{Re}[Y] \approx 1/(2.3c_{LI}\rho h^2) ; v = \frac{\omega a}{c_{LI}} > 2 \quad (5.72a)$$

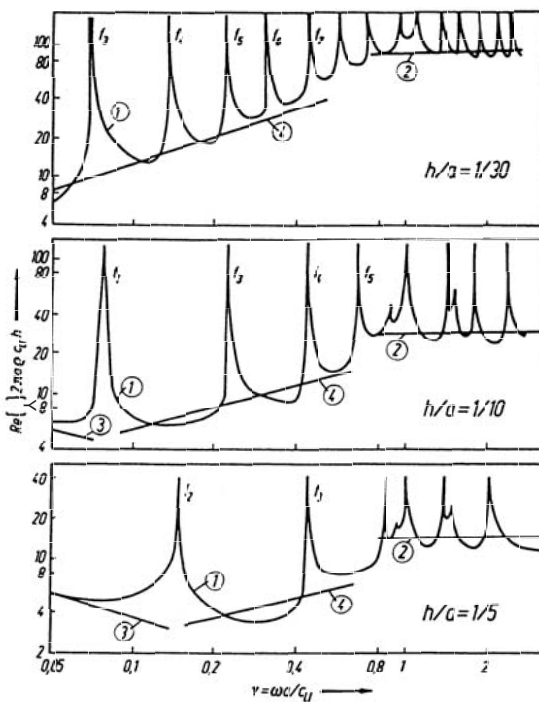


Fig. 5.12. Real part of mobility of a tube with radius a and wall thickness h . 1) Numerical results according to (5.71a) with (3.209b), 2) mobility of a plate of thickness h , 3) real part of the mobility of a tube in bending with radius of gyration $a/\sqrt{2}$, 4) approximation for the average mobility for the range $f_2 < f < \pi a/c_{L1}$. f_1, f_2, f_3, \dots denote the ring resonances according to (3.210b)

- b) At the ring resonances given by Eq. (3.210), the mobility of a tube is very high. This is particularly the case at the lower resonances, which are associated with the bending motion. Of those resonances, which are given by $v_n = (n^2 + 1)^{1/2}$ according to (3.210b) and thus are associated with the extensional motion of the tube wall, that at the so-called ring frequency at $v = 1$ is very pronounced whilst the remaining are considerably weaker.
- c) Similar to those of the plate strip, the maxima of the tube mobility are given by singularities of the dispersion equation. Except for that at the ring frequency at $v = 1$, the maxima associated with longitudinal plate waves are not very pronounced and those associated with shear waves are not evident at all in the mobility. The latter observation is

not too surprising since it is difficult to conceive how a radial excitation would give rise to pure shear motion.

- d) At low frequencies i.e., $v < 0.77h/a$, the mobility of the tube approaches that of a beam with a radius of gyration $a/\sqrt{2}$ i.e.,

$$Y \approx (1-j)/\left[2\pi a\rho h\sqrt{\omega c_{LI}a/\sqrt{2}}\right] ; \quad v < 0.77h/a \quad (5.72b)$$

- e) The maxima of the mobility are associated with “tame” poles as for the plate strip and therefore give no significant contribution to a frequency average. The frequency averaged mobility thus for many purposes may be adequately approximated by

$$\text{Re}[Y] \approx \frac{0.66}{2.3c_{LI}\rho h^2} \sqrt{\frac{\omega a}{c_{LI}}} ; \quad 0.77 \frac{h}{a} < v < 0.6 . \quad (5.72c)$$

This expression together with those in Eqs. (5.72a, b) constitute a set of approximations, which cover almost the entire frequency range.

5.4.4 Moment Mobilities

Although the previously considered impedances and mobilities for forces represent a class of great practical importance, they do not account for all possibilities even for excitations acting over very small areas. In flexural motion, moments and rotational velocities are equally important as forces and translational velocities. It is therefore essential to consider how structures respond to moment excitation and thus to study the class of moment mobilities. In analogy with Eq. (5.1) these are defined as the ratio between the resulting rotational velocity and the exciting moment

$$\underline{Y}_{wM} = \frac{\underline{w}}{\underline{M}} . \quad (5.73)$$

As for the force mobilities, the definition is applicable only for pure harmonic processes so that the time dependences cancel. The dimension of the moment mobility is [1/Nms] and hence they differ from the force mobility by m^2 .

The moment mobility is of importance, for example, in analyses of bending wave transmission from a vibrating beam to a plate, cf. Chapter 5.

As the force and moment mobilities involve all four variables of the bending wave, one might be inclined to assume that these two quantities were sufficient to completely determine the response of a system to an arbitrary combination of force and moment excitation. In particular one

might expect that the total transmitted power would be obtained by means of the two mobilities and then simply adding their contributions. Unfortunately, it is not so simple in general. Even for a semi-infinite beam, excited at the free end, it is found that a pure force excitation produces a rotational velocity and a pure moment a translational.

With an appropriate combination of force and moment, the propagating wave can be altogether suppressed leaving only an exponentially decaying nearfield such that no active power is transmitted. As seen from Eqs. (5.14) and (5.15a, b), this interesting special case where $v_+ = 0$, occurs for $F = Mk$, cf. [5.20]. It has also been shown [5.21, 5.22] that the power transmission to a plate can be reduced by employing the same or a similar ratio of force to moment when the excitation acts at or near an edge. Hence, a reduction of the power transmission can be accomplished for beams and plates subject to force or moment excitation by supplying additional appropriate moment or force excitation respectively. The significance of this interaction will also become evident in Sections 6.3 and 6.4.

In order to handle a combined moment and force excitation in completely general terms, the mobility matrix or its inverse, the impedance matrix must be introduced. Thus,

$$\begin{Bmatrix} \hat{v} \\ \hat{w} \end{Bmatrix} = \begin{bmatrix} Y_{vF} & Y_{vM} \\ Y_{wF} & Y_{wM} \end{bmatrix} \begin{Bmatrix} \hat{F} \\ \hat{M} \end{Bmatrix}, \quad (5.74)$$

in which two cross-mobility terms appear in addition to the point force and moment mobilities. For an edge-excited semi-infinite beam, $Y_{wF} = Y_{vM} = -\omega / Bk_B^2$ with units [1/Ns]. The present analysis, however, will be confined to the moment mobility and the considerations above were introduced only to clarify that the point force and moment mobilities do not suffice in the general case. For every particular case, therefore, it must be determined whether a pure force or a pure moment excitation exists otherwise the cross-mobilities must be involved. The latter mobilities are in general rather complicated functions, which vanish only in a few cases e.g., for an infinite system excited at the “centre”.

For an infinitely long beam, the moment mobility is easily determined. The analysis is the same as that in Section 5.3.2 with the difference that the conditions at the excitation point become $v(0) = 0$ and $-(B/j\omega)(\partial^2 v / \partial x^2) = M(0)$ i.e., the translatory velocity vanishes and the sum of bending moments equals the applied moment at the excitation point. In this way the moment mobility is obtained as

$$Y_{wM} = \frac{\hat{w}(0)}{\hat{M}(0)} = \frac{\omega(1+j)}{4Bk_B} = \frac{k_B^2(1+j)}{4m'c_B}. \quad (5.75)$$

The power transmitted to the beam by moment excitation thus becomes

$$W = \frac{1}{2} \operatorname{Re} \left[\hat{M}^* \hat{v} \right] = \frac{1}{2} |\hat{M}|^2 \operatorname{Re} [Y_{wM}] = \frac{\omega}{8Bk_B} |\hat{M}|^2. \quad (5.76)$$

Upon comparing (5.76) with (5.24), it is seen that for a frequency independent moment, the power transmitted increases with the square root of the frequency. Accordingly, the significance of moment excitation is enhanced at high frequencies. It should also be noted that the imaginary part of the moment mobility of a beam is stiffness controlled.

For the next examples of moment mobilities, it is suitable to proceed as in Section 5.4.3. The exciting force distribution is assumed to be that depicted at the bottom of Fig. 5.13 where two forces of equal $F = M/2a$ but opposite phase act at a small distance $2a$ establishing a moment. Instead of (5.56a),

$$p(x, z) = \frac{\hat{M}}{2a} [\delta(x+a, z) - \delta(x-a, z)]$$

is substituted in (5.55a), which, for a very small lever a i.e., a concentrated moment, gives

$$\check{p}(k_x, k_z) = \frac{\hat{M}}{2a} (e^{+jk_x a} - e^{-jk_x a}) \approx j\hat{M}k_x. \quad (5.76a)$$

By differentiating (5.56c) with respect to x , the rotational velocity around the z -axis, $w = \partial v / \partial x$, is obtained and the moment mobility follows from

$$Y_{wM} = \frac{\hat{w}(0, 0)}{\hat{M}} = \frac{1}{4\pi^2} \int Y_{\sim}(k_x, k_z) k_x^2 dk_x dk_z. \quad (5.77)$$

With the involved calculations undertaken it is found that the relation

$$\operatorname{Re}[Y_{wM}] = \alpha k_f^2 \operatorname{Re}[Y_{vF}] \quad (5.77a)$$

also holds for this case whereby k_f is the free wavenumber i.e., the singularities of the wave mobilities in Sections 5.4.1 and 5.4.2 and α a number between 0.5 and 1. Regarding the imaginary, no general statements can be made. Most often it is infinite, revealing that the idealization to a point moment through $a \rightarrow 0$ is inapplicable. For the imaginary part the approximation in (5.76a) cannot be used but the complete expression dependent on a must be introduced in (5.53a). For the real part, the distance a is of no concern as long as $k_f a \ll 1$. For the thin plate, for example, the moment mobility is given

$$Y_{wM} = \frac{\omega}{16B'} \left[1 - j \frac{4}{\pi} \ln \left(\frac{\gamma k_B a}{2} \right) \right] ; \quad \gamma = 1.781, \quad (5.77b)$$

when the plate is excited by means of a force couple.

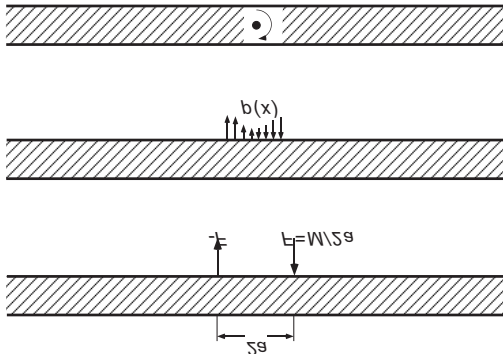


Fig. 5.13. Three examples of moment excitation

If the moment is not realized by two point forces but by another force or stress distribution, Eq. (5.77b) would have another form. Thus, the imaginary part of the moment mobility is generally also dependent on the shape of the excitation area and its distribution.

When the moment is distributed over an area of dimensions smaller than or comparable with the plate thickness a procedure similar to that yielding (5.65b) must be employed. It is found that the imaginary part of the moment mobility is surprisingly well approximated by that of an elastic half-space. An analysis similar to that in (5.60) to (5.63) provides the approximation

$$\text{Im}[Y_{wM}] \approx \frac{3}{8} \frac{\omega}{G a^3} (1 - \mu) \quad (5.77c)$$

for a circular excitation area of radius a [5.13].

5.4.5 Calculation of Impulse Response

When the excitation of a structure is not harmonic but has another time history, the motion can be determined via an additional Fourier transform over time. This means that (5.53 a, c) are to be replaced by the expressions

$$\begin{aligned}\check{p}(\omega, k_x, k_z) &= \int_{-\infty}^{\infty} \int p(t, x, z) e^{-j\omega t} e^{jk_x x} e^{jk_z z} dt dx dz, \\ v(t, x, z) &= \frac{1}{8\pi^3} \int_{-\infty}^{\infty} \int Y_{\sim}(\omega, k_x, k_z) \check{p}(\omega, k_x, k_z) e^{j\omega t} e^{-jk_x x} e^{-jk_z z} d\omega dk_x dk_z.\end{aligned}\quad (5.78)$$

Herein, $p(t, x, z)$ is the temporal and spatial function of the excitation.

Usually, the expressions in (5.78) lead to integrals, which only in rare cases can be determined analytically and a numerical analysis is most often required. Thereby, the singularities of the wave mobility can render unpleasant problems when the equation of motion does not comprise any damping (first time derivatives).

An example that can be evaluated in closed form is realized by the thin plate, which is impulse excited at $(x, z) = (0, 0)$. For such an excitation, $\check{p}(\omega, k_x, k_z) = I$. By substituting this and the wave mobility given by (5.50a) in (5.78), one finds after some manipulations and the substitution $r = \sqrt{x^2 + z^2}$ that

$$v_G(t, r) = \frac{I}{4\pi \sqrt{B' m'' t}} \sin\left(\frac{r^2}{4t} \sqrt{\frac{m''}{B'}}\right). \quad (5.79)$$

This is the Green's function for the thin plate bending wave equation. By means of the Green's function, the time dependence of the response due to an arbitrary excitation of the infinite plate can be determined. The excitation is then viewed as a sequence of many short impulses acting at the excitation points x_q, z_q at the time instances t_q and their contributions are added. Mathematically, this is a convolution which is established by the integral

$$v(t, x, z) = \iiint p(t_q, x_q, z_q) v_G(t - t_q, x - x_q, z - z_q) dt_q dx_q dz_q. \quad (5.80)$$

The time instant $t = t_q$ must be omitted from the integration since it will lead to extremely high and violently fluctuating values as seen from (5.79). This remarkable behaviour is ultimately a consequence of the approximation introduced in the Euler-Bernoulli or Kirchhoff bending theory, which lead to complications for very high frequencies or conversely, for very short times. The identity of (5.78) and (5.80) can naturally be rigorously proven.

5.5 Power Transmission to Infinite, Plane Structures

5.5.1 Determination of Structure-Borne Sound Power

5.5.1.1 Far field Approach

An approach that immediately springs to mind to determine the structure-borne sound power transmitted to infinitely extended structures consists of using the field at large distances from the source, similarly to the determination of airborne sound power transmission to a free field. The basic assumption is that at large distances, the waves behaves as plane waves for which the power readily can be assessed.

Applied on a thin plate, excited to bending vibrations, the procedure of (5.44a) is employed but instead of F_0 is used $p(x_q, z_q)dx_q dz_q$ and integrated over the excitation area. Here, p is the stress at the excitation positions (x_q, z_q) and $dx_q dz_q$ the associated surface element. Owing to the superposition principle, (5.44a) can be applied to sum over all excitation points such that

$$v(x, z) = Y_0 \iint p(x_q, z_q) \Pi(k_B r_{Aq}) dx_q dz_q \quad (5.81)$$

is obtained for an arbitrary excitation distribution, see Fig. 5.14. Herein, $Y_0 = 1/8\sqrt{m''B'}$, $\Pi(\dots)$ is the propagation function defined in (5.44a) and $r_{Aq} = \left[(x - x_q)^2 + (z - z_q)^2 \right]^{1/2}$ is the distance between the excitation and response points. As seen, Eq. (5.81) is a convolution integral, which can be rewritten in the form of (5.55c) by means of a Fourier transformation.

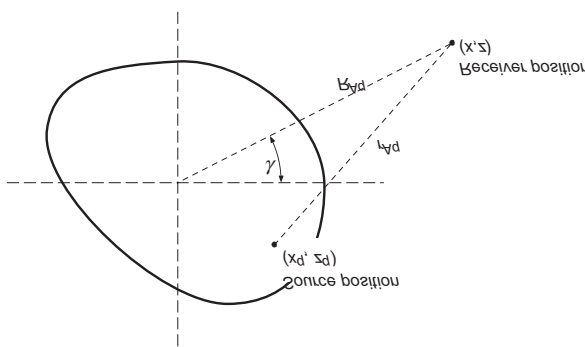


Fig. 5.14. Distributed excitation and response

In the far field where r_{Aq} is very large in comparison with the wavelength as well as the dimensions of the excitation area, the propagation function $\Pi(\dots)$ can be approximated such that

$$\begin{aligned} v(x, z) &= Y_0 \iint p(x_q, z_q) \sqrt{\frac{2}{\pi k_B r_{Aq}}} e^{-j(k_B r_{Aq} - \pi/4)} dx_q dz_q \\ &\approx Y_0 \sqrt{\frac{2j}{\pi k_B R_{Aq}}} \iint p(x_q, z_q) e^{-jk_B r_{Aq}} dx_q dz_q, \end{aligned} \quad (5.81a)$$

using the asymptotic expression in (5.35a). $R_{Aq} = (x^2 + z^2)^{1/2}$ is the (large) distance from the “centre” of the excitation area to the response position, cf. Fig. 5.14.

The formal similarity to the Rayleigh integral [5.23] for the radiation from a vibrating surface in an infinite batte is clearly seen in (5.81a). Without loss in generality, the origin can be located to the “centre” of the excitation area. This means that

$$\begin{aligned} r_{Aq} &= \left[(x - x_q)^2 + (z - z_q)^2 \right]^{1/2} = \left[x^2 + z^2 - 2xz_q - 2zz_q + x_q^2 + z_q^2 \right]^{1/2} \\ &= R_{Aq} \left[1 - \frac{2xz_q}{R_{Aq}^2} - \frac{2zz_q}{R_{Aq}^2} + \frac{x_q^2 + z_q^2}{R_{Aq}^2} \right] \\ &\approx R_{Aq} - x_q \cos\gamma - z_q \sin\gamma. \end{aligned} \quad (5.81b)$$

Thus, (5.81a) can be rewritten as

$$v(R_{Aq}, \gamma) = Y_0 \sqrt{\frac{2j}{\pi k_B R_{Aq}}} e^{-jk_B R_{Aq}} \iint p(x_q, z_q) e^{jk_B \cos\gamma x_q} e^{jk_B \sin\gamma z_q} dx_q dz_q. \quad (5.81c)$$

Compared with (5.81a), this integral is seen to be the Fourier transform at the wavenumber point $k_x = k_B \cos\gamma$, $k_z = k_B \sin\gamma$ and for the far field thence, the velocity is given by

$$v(R_{Aq}, \gamma) = Y_0 \sqrt{\frac{2j}{\pi k_B R_{Aq}}} e^{-jk_B R_{Aq}} \tilde{p}(k_B \cos\gamma, k_B \sin\gamma). \quad (5.81d)$$

The Fourier transform of the excitation, thus, is strongly linked to the directivity of the vibration velocity. It is indeed arguable that the Fourier transform of the excitation is identical to the far field characteristics for free wavenumbers.

From the vibration velocity in the far field, the power propagated by flexural waves across every portion $R_{Aq} d\gamma$ can be calculated from (3.93) since the waves can be considered plane. The total power propagated to infinity is thus given by

$$W = c_B \rho h \int_0^{2\pi} |v|^2 R_{Aq} d\gamma . \quad (5.82)$$

With (5.81d) substituted, the power transmitted is obtained from

$$W = \frac{1}{2} Y_0 \frac{1}{2\pi} \int_0^{2\pi} |\tilde{p}(k_B \cos\gamma, k_B \sin\gamma)|^2 d\gamma . \quad (5.82a)$$

Accordingly, the transmitted power only depends on the point mobility and the spectrum of the excitation at the free wavenumbers. It is easily demonstrated that (5.82) turns into (5.43) for a point force excitation.

5.5.1.2 Fourier Transforms

The approach discussed in the previous section for the determination of transmitted power can also be applied in other situations. Since knowledge of the far field velocity is required, however, it is often far from straightforward. Therefore, another approach is employed where the power is obtained directly from the wavenumber spectrum $p(k_x, k_z)$. The starting point is the definition of transmitted power at an area S given by

$$\begin{aligned} W &= \frac{1}{T} S \int_0^T \int_S p(x, z, t) v(x, z, t) dx dz dt \\ &= \frac{1}{2} \operatorname{Re} \left[\int_S \underline{p}^*(x, z) \underline{v}(x, z) dx dz \right] . \end{aligned} \quad (5.83)$$

Here, T is the averaging time, p the excitation acting at the area S and v the velocity perpendicular to the surface. The first form of (5.83) is the general whilst the second is valid for harmonic processes where the phasor notation can be used. Since the excitation vanishes outside the area S , the integration limits can be extended to infinity. By substituting (5.54) and a corresponding expression for the velocity into (5.83), one obtains

$$\begin{aligned} W &= \frac{1}{32\pi^4} \operatorname{Re} \left\{ \int \int \left[\int \int \tilde{p}^*(k_x, k_z) E^*(k_x, k_z) dk_x dk_z \right] \times \right. \\ &\quad \left. \left[\int \tilde{v}(k_x, k_z) E(k_x, k_z) dk_x dk_z \right] dx dz \right\} \\ &= \frac{1}{32\pi^4} \operatorname{Re} \left\{ \int \int \int \int \tilde{p}^*(k_x, k_z) \tilde{v}(k'_x, k'_z) E(k_x - k'_x, k_z - k'_z) dk_x dk_z dk'_x dk'_z \right\} \\ &= \frac{1}{8\pi^2} \operatorname{Re} \left\{ \int \tilde{p}^*(k_x, k_z) \tilde{v}(k_x, k_z) dk_x dk_z \right\}, \end{aligned} \quad (5.83a)$$

where all integrations extend from $-\infty$ to $+\infty$ and $E(\alpha, \beta) = e^{j\alpha x} e^{j\beta z}$.

In the development, is recurrently used the “orthogonality relation” of the exponential function, which can be made explicit by means of Dirac’s delta function

$$\int e^{j(k-k')x} dx = \int E(k-k') dx = 2\pi\delta(k-k').$$

With (5.55c) introduced in (5.83a), the general equation for the power transmitted to a structure with the wave mobility Y_{\sim} is obtained as

$$W = \frac{1}{8\pi^2} \operatorname{Re} \left\{ \int \left| \tilde{p}(k_x, k_z) \right|^2 Y_{\sim} dk_x dk_z \right\}. \quad (5.84)$$

At a first glance, Eq. (5.84) appears to furnish unrealistic results for plate-like structures since the wave mobility is purely imaginary for loss-free media, cf. Eqs. (5.50a-d). Hence, the complete integral would be imaginary and no power transmitted. Such a reasoning is incorrect, however, because although imaginary, Y_{\sim} has a singularity for real k_x and k_z in a case with no dissipation. This means that (5.84) contains a pole and the method of residues yields a non-vanishing real part. Instead of the mathematical integration method, another procedure will be employed in the next section to gain more insight into the physics.

5.5.2 Relationship with the Point Mobility

5.5.2.1 Beams and Plates

As seen in (5.50a-d), the wave impedances for beams, plates and membranes can be written in the form

$$Z_{\sim} = \frac{jQ(k_x^2, k_z^2)}{R(k_x^2, k_z^2)}, \quad (5.85)$$

where Q and R are real-valued polynomials. Upon introducing some small dissipation, represented by the loss factor η , the bending stiffness B' as well as the shear and longitudinal wave speeds c_T , c_L become complex and Z_{\sim} takes the form

$$Z_{\sim} = j \frac{Q(k_x^2, k_z^2)}{R(k_x^2, k_z^2)} + \eta A(k_x^2, k_z^2), \quad (5.85a)$$

in which A similarly is a real-valued polynomial. Substituted into Eq. (5.84) is obtained

$$W = \frac{1}{8\pi^2} \int_0^{2\pi} \int_0^\infty |\tilde{p}(k \cos\gamma, k \sin\gamma)|^2 \frac{\eta AR^2}{Q^2 + \eta^2 A^2 R^2} k dk d\gamma . \quad (5.85b)$$

Thereby, the substitutions $k_x = k \cos\gamma$ and $k_z = k \sin\gamma$ are made so that $dk_x dk_z = k dk d\gamma$ and the arguments of the polynomials are omitted for brevity.

For small loss factors, the integral is determined by the behaviour of the integrand in the vicinity of the zero of the impedance i.e., where $Q = 0$ since

$$\frac{\eta AR^2}{Q^2 + \eta^2 A^2 R^2} = \begin{cases} \eta AR^2 / Q^2 & ; \quad Q \neq 0 \\ 1/\eta A & ; \quad Q = 0 \end{cases} .$$

Evidently, the range of $Q \neq 0$ becomes less and less important whereas the range of $Q = 0$ more and more important as the loss factor is decreased. In the limiting case of a vanishingly small loss factor, the integration can be limited to the proximity of the zero since the integrand tends to zero elsewhere. It can be demonstrated that the expression above turns into a Dirac's delta function in the limiting case. The locus of $Q = 0$, however, is identical to that of the zero of the wave impedance of the structure in the absence of dissipation. In turn, the zero of the wave impedance establishes the equation for the free waves of the structure. It can hence be concluded that the integrand is significant only in the vicinity of the free wavenumbers, again denoted k_f . This means that

$$W = \frac{1}{8\pi^2} \int_0^{2\pi} \int_0^\infty |\tilde{p}(k_f \cos\gamma, k_f \sin\gamma)|^2 d\gamma \int_0^\infty \frac{\eta AR^2}{Q^2 + \eta^2 A^2 R^2} k dk , \quad (5.85c)$$

wherein it is observed that for isotropic structures, the wave impedance is only dependent on $k_x^2 + k_z^2 = k^2$ and not on γ . The remaining calculation is simple since for a point force of amplitude F_0 , the wavenumber spectrum is obtained from (5.56b), which leads to

$$W = \frac{1}{4\pi} |F_0|^2 \int_0^\infty \frac{\eta AR^2}{Q^2 + \eta^2 A^2 R^2} k dk . \quad (5.85d)$$

From the definition of the point mobility on the other hand,

$$W_F = \frac{1}{2} |F_0|^2 \operatorname{Re}[Y_0] , \quad (5.85e)$$

such that by equating (5.85d) and (5.85e), an expression is obtained for the integral, which substituted in (5.85c) yields

$$W_F = \frac{\operatorname{Re}[Y_0]}{4\pi} \int_0^{2\pi} |\tilde{p}(k_f \cos\gamma, k_f \sin\gamma)|^2 d\gamma. \quad (5.86)$$

This means that to find the power transmitted to plate-like structures, only the real part of the point mobility and the excitation wavenumber spectrum at the free wavenumbers are required. The former quantity is treated in Sect. 5.6 and the latter is found from (5.55a). Thus, for thin plates (5.86) becomes identical to (5.82a) as expected.

For orthotropic plates, a similar analysis can be undertaken, which after some co-ordinate transformation leads to

$$W_{ortho} \approx \frac{1}{4\pi} \frac{1}{8\sqrt[4]{m''^2 B'_x B'_z}} \int_0^{2\pi} |\tilde{p}(k_{fx} \cos\gamma, k_{fz} \sin\gamma)|^2 d\gamma, \quad (5.86a)$$

where the free wavenumbers in the two orthogonal directions are $k_{fx} = (\omega^2 m'' B'_x)^{1/4}$ and $k_{fz} = (\omega^2 m'' B'_z)^{1/4}$ respectively, cf. Eq. (5.50b).

5.5.2.2 Elastic Half-Space

For an elastic, semi-infinite medium and also for deep beams, thick plates and plates in contact with a deep fluid layer, the approach used in the previous section is not applicable. This is so since the wave mobility is no longer represented by polynomials in squares of the wavenumber components. Rather the wave mobilities for the present class of structures possess a real part also in the absence of damping, which corresponds to the power that propagates to infinity and which is represented by the radicals k_{yL} and k_{yT} , see Eq. (4.60). The calculation of the power, therefore, must be made according to (5.84). For the integration, it is suitable to subdivide the range. The first encompasses that in which Y_\sim has a real part. As shown by (5.50f), this is the case when k_{yT} is real i.e., $k_x^2 + k_z^2 < k_T^2$. The second is that small part around the pole where $Y_\sim \rightarrow \infty$. This is located at the wavenumber of the Rayleigh wave as demonstrated in Sect. 3.6.3 and by Eq. (5.60). Here, the approach of the previous section applies and with $k_x^2 + k_z^2 = k^2$ one finds that

$$W_{Hs} \approx \frac{1}{8\pi^2} \int_0^{k_T} \left[\int_0^{2\pi} |\tilde{p}(k \cos\gamma, k \sin\gamma)|^2 d\gamma \operatorname{Re}[Y_\sim] \right] k dk + \frac{A_{RR}}{4\pi} \int_0^{2\pi} |\tilde{p}(k_R \cos\gamma, k_R \sin\gamma)|^2 d\gamma. \quad (5.87)$$

Herein, k_R is the wavenumber of the Rayleigh wave, given by (3.149) or (5.60) and A_{RR} the real part of the input point mobility with respect to

Rayleigh waves. After some manipulations and approximations the latter can be set to

$$A_{RR} = 0.1 \frac{\omega k_T}{G} (1 - \mu) \quad (5.87a)$$

for $\mu < 0.4$. The accuracy of this approximation is not high but it is appropriate for estimations owing to its simplicity.

5.5.3 Interpretations and Examples

The essential finding of Sects. 5.5.2.1 and 5.5.2.2 is the close relationship that exists between the power transmission and the wavenumber spectrum at the free waves. This can be clearly illustrated by considering the Fourier transform i.e., the calculation with the wavenumber spectra as a sum of plane waves. The mathematical operations leading to (5.55a, b), (5.86) as well as (5.87) thus correspond to the steps depicted in Fig. 5.15 for the one-dimensional and rotationally symmetric cases respectively.

- i) The spatial distribution of the excitation is constructed from a sum of plane, infinitely extended waves; Figs. 5.15 b, c
- ii) The individual amplitudes in the wavenumber spectrum are multiplied by the wave mobility yielding the wavenumber spectrum of the velocity; Fig. 5.15e. A pivotal condition is that wavenumbers remain the same, which is only possible for structures with no discontinuities.
- iii) Of the many plane waves representing the velocity, is constructed the spatial velocity distribution; Fig. 5.15g.
- iv) Far away from the excitation area, only free waves are possible and only those propagate the power. Since no mechanism for wavenumber conversion is present for homogeneous media, the power is directly determined by the wavenumber spectrum of the excitation at the wavenumbers of the free waves.
- v) For plate-like structures there is only one or a few free wavenumbers. In an elastic half-space there are bulk waves, which have wavenumbers at the free surface fulfilling the condition $k^2 \leq k_T^2$. In addition there are surface waves (Rayleigh waves), which propagate at a single wavenumber.

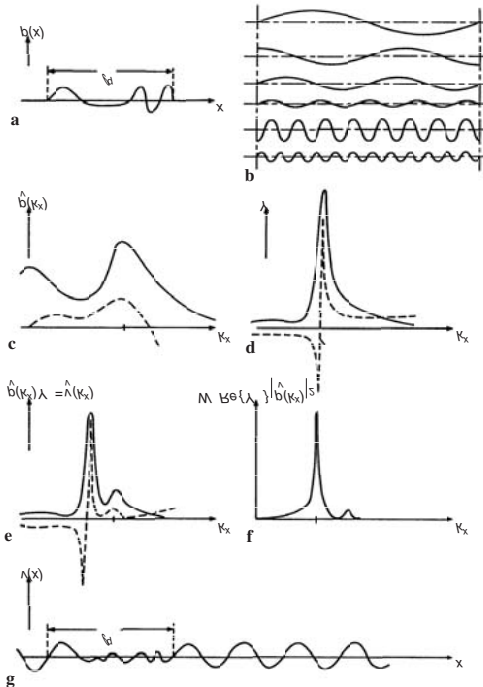


Fig. 5.15. Spatial distribution and wavenumber spectrum (WNS). a) Spatial distribution by force excitation, b) Plane waves components of amplitudes $\check{p}(k_x)$, c) WNS of distributed force excitation, d) WNS of wave mobility, e) WNS of resulting velocity, f) WNS of transmitted power and g) spatial distribution of resulting velocity

In Fig. 5.16 are shown some examples of spatial distributions and the associated wavenumber spectra. The upper part depicts excitations, which integrated over space amounts to a total force F_g . Since only the part for which $|k_x| \leq k_f$ is important for the power transmission, it is clear that the spatial distribution of the excitation is irrelevant when $k_f l_q < 1$ i.e., when the dimensions of the excitation area are less than a third of the free wavelength. As $k_f l_q$ grows large, however, the spatial distribution can be very influential. It can be expected that an excitation distribution, which conformly rises and falls, yields a relatively sparse transmission for $k_f l_q > 6$. Most disadvantageous is a concentration to a small area – point force cf., [5.24, 5.25]. This is valid, however, only for force excitation whereas a prescribed velocity excitation can gain from a concentration to a small surface owing to the influence of the total elasticity.

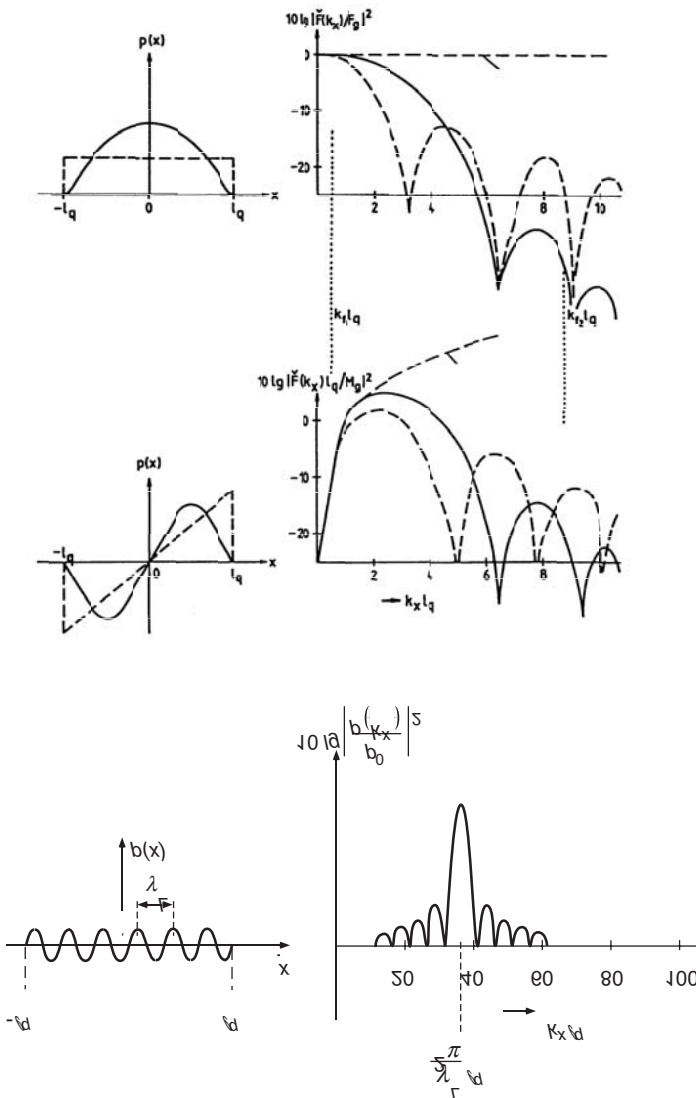


Fig. 5.16. Spatial distributions and wavenumber spectra for some different excitations

The bulk and Rayleigh waves are determined by the wavenumber ranges $k_x < k_T$ and $k_x = k_R$ respectively as shown in Eq. (5.87) for an excitation of an elastic half-space. A modification of the excitation distribution affects the excitation of bulk waves much less than that of Rayleigh waves. The

tendency is that the ratio of power propagated by Rayleigh waves to that by bulk waves will be smaller the larger the excitation area and the more uniform the excitation distribution.

In the middle part of Fig. 5.16 are shown the wavenumber spectra for a net moment

$$M_g = \int_{-l_q}^{l_q} p(x) dx \quad (5.88)$$

that remains constant but where the spatial distribution is varied. Also for this kind of excitation, the power transmission can be reduced by making the distribution as continuous and smooth as possible.

Depicted in the bottom part of Fig. 5.16 is a spatial excitation distribution resulting from, for example, fluid-borne waves impinging on a limited part of the structure. It is essential to note that little power is transmitted when the exciting wavelength is smaller than that of the free wave in the structure. The transmission is a maximum when the exciting wavelength equals that of the free wave. Additional features of the spatial distribution will be dealt with in conjunction with the reciprocal situation of radiation in Sect. 7.8.

Consistently assumed for the analysis of power transmission are infinitely extended structures without discontinuities. It will be shown in Sect. 5.7.3 that these prerequisites are less restrictive than can be anticipated. In a frequency average, namely, a not too small structure i.e., structural dimensions equal to or larger than the wavelength, appears as big as the corresponding infinite system. Applied on an airborne sound problem, this means that the power radiated by a source in a reverberation chamber equals that radiated to a free field or to an anechoic chamber, in a frequency average.

5.6 Summary of Impedance and Mobility Formulae; Approximations

To facilitate the search for impedance or mobility formulae, Table 5.1 gives an overview over the formulae and the corresponding equations. Also included is a column of “source volumes”. This comes about because the real part of the mobility can generally be written in the form

$$\operatorname{Re}[Y] = \operatorname{Re}\left[\frac{\hat{v}(0,0)}{\hat{F}_0}\right] = \frac{1}{\omega\rho V_q} \quad (5.89)$$

for a point excitation. Correspondingly, by line excitation F_l of dimensions N/m,

$$R[Y_l] = \operatorname{Re} \left[\frac{\hat{v}(0)}{\hat{F}} \right] = \frac{1}{\omega \rho S_q}. \quad (5.89a)$$

Herein, V_q is a quantity of dimensions corresponding to a volume and hence can be termed “source volume”. S_q is the corresponding quantity in two dimensions and has the dimensions of a surface,

As rough estimates, V_q and S_q can be obtained from

$$\begin{aligned} V_q &= \operatorname{Min} \left[l_x, \frac{\lambda_x}{\pi} \right] \operatorname{Min} \left[l_y, \frac{\lambda_y}{\pi} \right] \operatorname{Min} \left[l_z, \frac{\lambda_z}{\pi} \right], \\ S_q &= \operatorname{Min} \left[l_x, \frac{\lambda_x}{\pi} \right] \operatorname{Min} \left[l_z, \frac{\lambda_z}{\pi} \right], \end{aligned} \quad (5.90)$$

where l_x, l_y, l_z are the dimensions of the structure under consideration and $\lambda_x, \lambda_y, \lambda_z$ are the wavelengths of the free wave in the three spatial directions. For isotropic structures the wavelengths of the free wave are equal whereas they may differ for orthotropic or stiffened structures.

In Table 5.1 also a few cases are included that have not been treated in the text. The cases included without proof, taken from the literature, are:

- a) Beam with the shear stiffness taken into account (Timoshenko beams), excited at the centre

$$Y = \frac{1}{2\omega m'} \frac{k_T^2 + k_I k_{II}}{k_I + k_{II}} \quad (5.91)$$

where k_I and k_{II} are given by (5.57a, b)

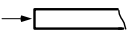
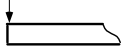
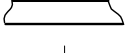
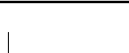
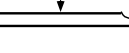
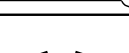
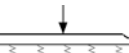
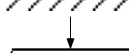
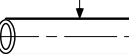
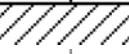
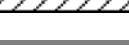
- b) Thin plate on an elastic foundation (Winkler foundation), cf. Sect. 3.7.4.4. The stiffness per unit area is s'' , the resonance frequency $\omega_0^2 = s''/m''$ and the analysis correspond to that of beams or plates with k_B^2 replaced by $k_B^2 (1 - \omega_0^2/\omega^2)^{1/2}$.

$$Y = \frac{1}{8\sqrt{B'm''}} \begin{cases} \sqrt{1 - \omega_0^2/\omega^2} & ; \quad \omega_0 < \omega \\ j\sqrt{\omega_0^2/\omega^2 - 1} & ; \quad \omega_0 > \omega \end{cases} \quad (5.92)$$

- c) Fluid of density ρ_F and wave speed c_F . Excitation at the free surface

$$\operatorname{Re}[Y] = \frac{\omega^2}{6\pi\rho_F c_F^3} \quad (5.93)$$

Table 5.1. Compilation of impedances and mobilities by point excitation

		\underline{Z}	$\text{Re } \{\underline{Y}\}$	$\text{Im } \{\underline{Y}\}$	V_q
Rod		$\rho c_L S$	$\frac{1}{\rho c_L S}$	0	$\frac{1}{2\pi} S \lambda_L$
Slender beam		$2m'c_B(1+j)$	$\frac{1}{4m'c_B}$	$\frac{-1}{4m'c_B}$	$\frac{4}{2\pi} S \lambda_B$
Slender beam		$\frac{m'c_B}{2}(1+j)$	$\frac{1}{m'c_B}$	$\frac{-1}{m'c_B}$	$\frac{1}{2\pi} S \lambda_B$
Timoshenko beam		(5.91)	(5.91)	(5.91)	--
Membrane		(5.94) für $B' \rightarrow 0$	$\frac{1}{4} \frac{\omega}{T'}$	∞	$\frac{1}{\pi^2} h \lambda_\eta^2$
Thin plate		$8\sqrt{B'm''}$	$\frac{1}{8\sqrt{B'm''}}$	0	$\frac{2}{\pi^2} h \lambda_B^2$
Thin plate		$3.5\sqrt{B'm''}$	$\frac{1}{3.5\sqrt{B'm''}}$	0	$\frac{0.9}{\pi^2} h \lambda_B^2$
Plate, finite shear stiffness		(5.59)	(5.59a)	(5.59a)	--
Plate		--	$\approx 2\omega / Eh$	--	$\frac{1}{3\pi^2} h \lambda_T^2$
Orthotropic plate		(5.64)	(5.64)	0	--
Plate on Winkler bed		(5.92)	(5.92)	(5.92)	--
Plate strip		(5.70)	(5.70)	(5.70)	--
Cylinder		--	(5.72a, b, c)	--	--
Elastic half-space		(5.61)	(5.61)	(5.62, 5.63)	$\approx \frac{\lambda_T^3}{\pi^3}$
Fluid space		--	(5.93)	∞	$\frac{3}{4\pi^2} \lambda_F^3$
Thick plate		(5.65)	(5.65)	(5.65)	--

- d) Isotropic, thin plate with bending stiffness B' and membrane stress T' . The membrane stress can also be negative but only up to the buckling load cf., Sect. 3.7.4.4.

$$Y = \frac{1}{8\sqrt{B'm''}} \frac{1}{\sqrt{1+\beta^2}} \left[1 + \frac{j}{\pi} \ln \left(\frac{\sqrt{1+\beta^2} + \beta}{\sqrt{1+\beta^2} - \beta} \right) \right] ; \quad \beta = \frac{T}{2\omega\sqrt{B'm''}} \quad (5.94)$$

- e) Thin plate excited by a force F_0 , uniformly distributed over a circular area of radius a

$$\operatorname{Re}[Y] = \frac{1}{8\sqrt{B'm''}} \left[\frac{2J_1(k_B a)}{(k_B a)} \right]^2, \quad (5.95a)$$

where $J_1(.)$ is the Bessel function of first order.

- f) Thin plate excited by a prescribed velocity v_0 over a circular area of radius $a > \lambda_B / 2$

$$\operatorname{Re}[Y] = \frac{2}{\omega m'' a \lambda_B}. \quad (5.95b)$$

5.7 Point-Excitation of Finite Systems

The problem of vibrations of systems of finite extent attracted the interest of some of the greatest physicists of previous centuries, and has served as a stimulus in many branches of physics. One may recall that the theory of mechanical waves, as it was developed by Bernoulli, D'Alambert, LaGrange, Chladni, Rayleigh, Ritz and others, contributed greatly to advancement of understanding of electromagnetic waves, and also was instrumental in the development of wave mechanics. Also, for example, electrical waves in hollow conductors are closely related to mechanical waves in rods, – and even the Klein-Gordon equation, which describes certain properties of mesons, is in its simplest form identical to the equation of motion of a string embedded in an elastic medium.

In recent decades, the rapid development of the other fields of physics has led to a decline in interest in mechanical waves and vibrations; whereas previously one tended to visualize electrical processes in terms of mechanical analogs, one nowadays often does the inverse, - for example, by treating mechanical processes in terms of electrical circuit diagrams. Nevertheless, such concepts as eigenvalues, orthogonality, etc., can still be explained and understood most easily in terms of mechanical waves. Be-

low, mechanical wave concepts will be used first to develop the general properties of vibrating systems, and then to derive some energy relations of practical importance. Instead of proceeding with full mathematical rigor, the derivations here will make use of relatively simple physical considerations. For example, the theorem that “any vibrations may be expressed in terms of a sum of eigenfunctions” will not be proven on the basis of the theory of integral equations, of self-adjoint differential equations, or of variational calculus, but the validity of this theorem will be demonstrated on the basis of simple energy considerations. Readers interested in exact mathematical representation are referred to the pertinent literature [5.26–5.28].

5.7.1 General Properties

In the analysis of wave propagation along finite beams in Sect. 3.4, it was found that there exist certain discrete preferred frequencies, the so-called “eigen-frequencies” or “natural frequencies”. These preferred frequencies may be observed in two common physical processes. If a beam e.g., a tuning fork is excited briefly, then the vibration that results after the excitation is removed produces a sound that is typical of the beam and that is made up of one or more of its eigenfrequencies. If the beam is excited continuously, as, for instance, by means of a shaker, then the resulting amplitudes depend strongly on the exciting frequency; the greatest amplitudes are obtained if the exciting frequency coincides with an eigenfrequency, which is therefore also often called a “resonance frequency” see Figs. 4.6a and 4.8a.

The magnitudes of the various eigenfrequencies depend on the type of material used, on the beam dimensions (particularly the length), and – as evident from the examples of free and simply supported beams – on the boundary conditions. As also was found, the eigenfrequencies form a sequence without an upper bound, and the higher frequencies correspond to integral multiples of a fundamental frequency only in special cases.

One only needs to remind oneself of bells, gongs, or train wheels that screech as they go around curves, in order to convince oneself that bodies with complex shapes (including, e.g., plates, rings, shells) also have eigenfrequencies. The extent to which these frequencies are observed depends, of course, on the damping and on the character of the excitation, but their existence cannot be doubted. One may therefore conclude that bodies with arbitrary shapes also exhibit eigenfrequencies, which, just as for beams, depend on the material, the dimensions, and on the boundary conditions. Unlike for beams, where the eigenfrequencies form simple sequences

which increase as n or n^2 , see Sect. 3.4, the eigenfrequencies of complex bodies are distributed considerably more irregularly.

Another important property of finite plates and shells, etc., is the occurrence of mode shapes, called “eigen-functions” in mathematics associated with the eigenfrequencies just as for beams. As the classical investigations of Chladni have shown, these mode shapes can be quite complicated and can produce rather fascinating, beautiful pictures. Detailed interpretation of the mode shapes is generally extremely difficult, and their exact prediction is possible in only a very few simple cases. Fortunately, one does not need such predictions for the problems of greatest interest here; for these problems one only needs to know that at least one eigenfunction corresponds to every eigenfrequency, and that the eigenfunctions have certain general properties, as discussed below.

For the present discussion, the eigenfunctions will be taken as dimensionless and will be denoted by $\varphi_n(x, z)$; the corresponding velocity amplitudes will be denoted by v_n , and the eigenfrequencies by ω_n . The most important characteristic of eigenfunctions is their orthogonality. This means that if $\varphi_n(x, z)$ and $\varphi_m(x, z)$ represent two eigenfunctions of the same system, and if m'' represents the mass distribution, which may depend on the coordinates x and y , then the eigenfunctions obey

$$\int_S m'' \varphi_n(x, z) \varphi_m(x, z) dx dz = 0 ; m \neq n, \quad (5.96)$$

where the integration is carried out over the entire area S of the plate, shell, etc. of interest.

In order to obtain some physical understanding of this far-reaching statement, one can consider a system, which is so excited that it vibrates precisely in its n -th mode. The total kinetic energy then is given by

$$E_{kin} = \frac{1}{2} \int_S v_n^2 m'' \varphi_n^2(x, z) dx dz. \quad (5.97a)$$

Analogously, the kinetic energy associated with a vibration in the m -th mode is given by

$$E_{kin} = \frac{1}{2} \int_S m'' v_m^2 \varphi_m^2(x, z) dx dz. \quad (5.97b)$$

Consider now that the two eigen-vibrations are excited simultaneously and that the excitation is applied exactly in the same way as in the two separate cases. Then, if the eigen-vibrations are independent of each other, the total energy must be equal to the sum of the individual energies otherwise, energy would be created or destroyed. If that is so, then

$$\begin{aligned} & \frac{1}{2} \int_S m'' v_n^2 \varphi_n^2(x, z) dx dz + \frac{1}{2} \int_S m'' v_m^2 \varphi_m^2(x, z) dx dz \\ &= \frac{1}{2} \int_S m'' [v_n \varphi_n(x, z) + v_m \varphi_m(x, z)]^2 dx dz. \end{aligned}$$

This equation can be satisfied only if

$$\int_S m'' \varphi_n(x, z) \varphi_m(x, z) dx dz = 0 \text{ for } m \neq n, \quad (5.98)$$

which relation is exactly the same as Eq. (5.96).

For the many cases where the mass distribution m'' is constant such that density and thickness are constant over the entire area, Eq. (5.98) reduces to

$$\int_S \varphi_n(x, z) \varphi_m(x, z) dx dz = 0 \text{ for } m \neq n.$$

From the foregoing derivation one may also arrive at the important conclusion that the eigenfunctions of systems which are not “closed” need not satisfy the orthogonality relation. If energy can be removed from the system, then the previously used energy relation no longer applies, and orthogonality generally is violated. Before applying orthogonality, one must always assure oneself that the system is truly a closed one. A system clearly is a closed one if its edges are completely free or completely rigidly restrained. Added masses or other non-dissipative or non-conducting impedances also extract no energy. A system is obviously “open” if it is connected to other systems. For example, a steel plate no longer may be represented as a closed system if one of its edges is imbedded in sand.

In order to apply the previously obtained results, one may first consider the completely general two-dimensional equation of motion

$$L[v(x, z)] - m'' \omega^2 v(x, z) = j\omega p(x, z), \quad (5.99)$$

where $L[\dots]$ represents a differential operator, which for homogeneous thin plates corresponds to the double Laplace operator, ω denotes the circular frequency, m'' the mass per unit area, $v(x, z)$ the phasor of velocity and $p(x, z)$ the phasor of the exciting pressure. For the sake of simplicity, phasors are not shown as underlined in the present discussion.

The fact that there exist eigenfrequencies and eigenfunctions implies that the above equation also has solutions for zero excitation i.e., for $p(x, z) = 0$. In that case, however, the equation has solutions only for certain discrete values of ω and for certain functions. The eigenfrequencies ω_n and eigenfunctions φ_n thus are defined by

$$L[\varphi_n(x, z)] - m''\omega_n^2 \varphi_n(x, z) = 0, \quad (5.100)$$

together with the applicable boundary conditions. If the boundary conditions are such that no energy can be conducted across the boundary, then also the orthogonality relation of Eq. (5.96) or (5.98) holds.

From the foregoing considerations one may deduce a very important theorem about vibrations of finite systems subject to arbitrary excitation. If one expresses an arbitrary solution $v(x, z)$ of the inhomogeneous Eq. (5.99) as a sum of eigenfunctions, by setting

$$v(x, z) = \sum_{n=1}^{\infty} v_n \varphi_n(x, z), \quad (5.101)$$

one finds by substitution into Eq. (5.99) that

$$\sum_{n=1}^{\infty} \{v_n L[\varphi_n(x, z)] - v_n m'' \omega_n^2 \varphi_n(x, z)\} = j\omega p(x, z).$$

Subtraction of Eq. (5.100) from this equation yields

$$\sum_{n=1}^{\infty} v_n m'' (\omega_n^2 - \omega^2) \varphi_n(x, z) = j\omega p(x, z).$$

If one now multiplies this equation by $v_m \varphi_m(x, z)$ and integrates over the entire region, then in view of the orthogonality relation, all terms on the left-hand vanish, except that term for which $n = m$. One thus obtains

$$v_n (\omega_n^2 - \omega^2) \int_S m'' \varphi_n^2(x, z) dx dz = j\omega \int_S p(x, z) \varphi_n(x, z) dx dz.$$

Upon introducing the so-called “norm”

$$\Lambda_n = \int_S m'' \varphi_n^2(x, z) dx dz,$$

then Eq. (5.101) can finally be rewritten as

$$v(x, z) = j\omega \sum_{n=1}^{\infty} \frac{\varphi_n(x, z)}{\Lambda_n (\omega_n^2 - \omega^2)} \int_S p(x, z) \varphi_n(x, z) dx dz. \quad (5.102)$$

Equation (5.102) represents the well-known eigen-functions expansion theorem, which states that one may express the response of a system to any arbitrary excitation in terms of the system's eigen-functions and eigen-frequencies.

Before turning to applications of this theorem, it is worth while to examine briefly the assumptions that underlie Eqs. (5.101) and (5.102). The first

assumption is that there exist an infinite number of eigen-modes, so that one can indeed form the infinite series. This assumption is not contradicted by experience; no experiments have revealed an upper bound for the eigen-frequencies, and one can conceive of no physical reason for such a bound. The validity of the second assumption – that a series of the form of Eq. (5.101) can represent any arbitrary vibratory deformation – is less obvious. The rather difficult proof, for which the reader is referred to the applicable mathematical literature [5.26–5.28] shows that the eigenfunctions constitute a “complete” set of orthogonal functions, in terms of which one may represent any arbitrary function, even if this function does not satisfy the same boundary conditions as the eigenfunctions. However, it can happen that the value of the infinite series does not converge to that of the function at some points, particularly at the boundaries, but the mean-square error is arbitrarily small and that is what counts for physical problems.

Extension of the above concepts to more than two dimensions, as well as to motions with several components, presents no difficulty [5.26].

5.7.2 Some Applications

Application of the previously obtained results may be demonstrated most simply for the case of a thin rectangular plate, simply supported at all edges as depicted in Fig. 3.15. For a plate with edge lengths l_1 and l_2 , one may take the edges as located at $x = 0, x = l_1, z = 0, z = l_2$. Just like in the one-dimensional case, the velocity and its second derivative must vanish on these edges, see Eq. (3.110a). The eigen-functions thus must satisfy these boundary conditions, in addition to the homogeneous bending-wave equation,

$$B' \nabla^4 \varphi_n(x, z) - \omega_n^2 m'' \varphi_n(x, z) = 0. \quad (5.103)$$

One may easily verify that the functions

$$\varphi_n(x, z) = \sin \frac{n_1 \pi x}{l_1} \sin \frac{n_2 \pi z}{l_2} \quad (5.104)$$

have the required properties, and that the eigenfrequencies are given by

$$\omega_n = \sqrt{\frac{B'}{m''}} \left[\left(\frac{n_1 \pi}{l_1} \right)^2 + \left(\frac{n_2 \pi}{l_2} \right)^2 \right], \quad (5.104a)$$

where the subscript n represents the double subscript n_1, n_2 .

By means of these eigen-functions, one may now find the general solution of the inhomogeneous bending wave Eq. (3.184a),

$$B' \nabla^4 v(x, z) - m'' \omega^2 v(x, z) = j\omega p(x, z),$$

subject to the aforementioned boundary conditions. From the expansion theorem in Eq. (5.102), it follows that

$$v(x, z) = \frac{4j\omega}{m'' l_1 l_2} \sum_{n=1}^{\infty} \frac{\sin \frac{n_1 \pi x}{l_1} \sin \frac{n_2 \pi z}{l_2}}{\omega_n^2 - \omega^2} \int p(x, z) \sin \frac{n_1 \pi x}{l_1} \sin \frac{n_2 \pi z}{l_2} dx dz. \quad (5.105)$$

Herein, the value $\Lambda_n = l_1 l_2 m'' / 4$ is used for the norm, as obtained with (5.104).

For the special case of greatest interest here, where the excitation is a point force $F = p(x, z) dx dz$ at the location x_0, z_0 , the integration region in Eq. (5.105) is so small that one may consider the sine functions as constant and take them outside of the integral rendering

$$\int p(x, z) \sin \frac{n_1 \pi x}{l_1} \sin \frac{n_2 \pi z}{l_2} dx dz = F \sin \frac{n_1 \pi x_0}{l_1} \sin \frac{n_2 \pi z_0}{l_2}. \quad (5.105a)$$

The velocity of the excitation point on a simply supported rectangular plate, thus, is given by

$$v(x_0, z_0) = \frac{4j\omega F}{m'' l_1 l_2} \sum_{n=1}^{\infty} \frac{\sin^2 \frac{n_1 \pi x_0}{l_1} \sin^2 \frac{n_2 \pi z_0}{l_2}}{\omega_n^2 - \omega^2}. \quad (5.106)$$

Figure 5.17 shows how this function varies with frequency, for two different excitation points on a plate for which $\pi/l_1^2 \sqrt{B'/m''} = 6$ and $l_1/l_2 = \sqrt{3}$.

One may observe that here $v(x_0, z_0)$, and thus also the driving-point impedance, is a much more complicated function of frequency and of the excitation position than for an infinite plate. For this reason, measurements of input impedances on finite systems also generally yield very complicated results, which exhibit strong frequency dependence and which also depend greatly on the location at which the excitation is applied. However, it will be shown later that in spite of this complexity, the power supplied to a finite plate (and therefore also its average velocity) is determined by the driving point impedance of an infinite plate that has the same thickness and material properties as the finite plate.

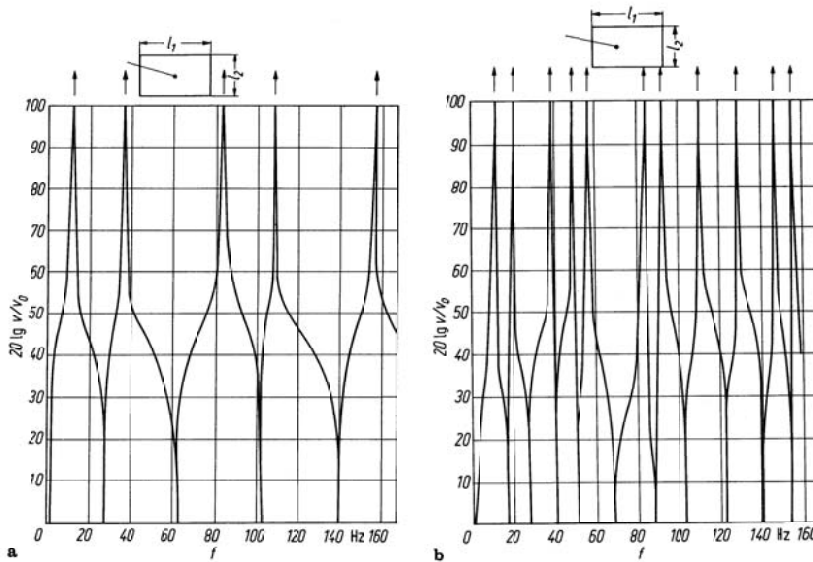


Fig. 5.17. Velocity of a simply supported, point excited plate as function of frequency. a) centre and b) off-centre excitation. $\pi \sqrt{B'} / (l_1^2 \sqrt{m''}) = 6$, $l_1/l_2 = \sqrt{3}$

The greatest amplitudes in Fig. 5.17 occur at the eigenfrequencies, as one would expect. However, one may observe by comparing the two curves that some eigenfrequencies are excited at one location, and not at the other. This phenomenon occurs because a mode obviously can not be excited by a force that acts at the mode's nodal position. This effect is encountered most often for excitation that acts in the middle, as in the illustrated example.

It can also happen that several different eigenfunctions have the same eigenfrequency. One may observe this fact if one calculates the eigenfrequencies for the example at hand from Eq. (5.104a). The values (in Hz) are shown in Table 5.2.

Table 5.2. The forty first eigen-frequencies of the simply supported rectangular plate in Fig. 5.17

$n_1 \backslash n_2$	1	2	3	4	5	6	7	8	9
1	12	21	36	57	84	117	156	201	252
2	39	48	63	84	111	144	183	228	297
3	84	93	108	129	156	189	228	273	
4	147	156	171	192	219	252	291		
5	228	237	252	273	300				

To the eigen-frequency of 84 Hz there correspond the mode shapes

$$\sin \frac{5\pi}{l_1} x \sin \frac{\pi}{l_2} z, \quad \sin \frac{4\pi}{l_1} x \sin \frac{2\pi}{l_2} z, \text{ and } \sin \frac{\pi}{l_1} x \sin \frac{3\pi}{l_2} z.$$

Similar conditions occur for 156 and 228 Hz.

Systems that have eigenfrequencies that coincide are called “degenerate”. This degeneracy, which is particularly pronounced for square plates, can also occur in rectangular plates whose edge lengths are irrational multiples of each other as is evident from the above example. One-dimensional systems, however, cannot be degenerate. Theoretically, the various eigenfrequencies all are of different magnitude only if the ratio of the squares of the edge lengths is irrational.

In determining the number of natural modes of a practical structure by counting the peaks in its response spectrum, one always obtains a number that is too small, because of coincidence of eigenfrequencies and vanishing of the response for excitation at a nodal line. The previous example shows the latter effect rather clearly; Fig. 5.17b contains only 11 peaks, whereas the table lists 20 modes with frequencies below 160 Hz. Thus, conclusions drawn from mode-counting experiments must be treated cautiously, even at low frequencies. At high frequencies, one encounters the additional problem of distinguishing eigenfrequencies that are close to each other; they may not be evident as separate peaks in the response spectrum, particularly if the test object is well damped.

The general effect of damping still remains to be considered. If one introduces the loss factor η to characterize the damping, just as in Chapter 4, one may rewrite Eq. (5.103) as

$$B'(1+j\eta)\nabla^4\varphi_n(x,z) - m''\underline{\omega}_n^2\varphi_n(x,z) = 0. \quad (5.107)$$

The differential equations of other systems may be modified similarly.

Equation (5.107) can be satisfied only if the imaginary part of the first term is cancelled by a corresponding imaginary part of the second term; this implies that $\underline{\omega}_n^2$ must be complex. Damping thus leads to complex eigenfrequencies of the form $\underline{\omega}_n = \omega_n \sqrt{1 + j\eta} \approx \omega_n (1 + j\eta/2)$, where ω_n represents the eigenfrequency in the absence of damping. Other than that, the analysis takes the same course as before. In particular, the expansion theorem is unaffected by whether $\underline{\omega}_n$ is real or complex. Thus for damped systems one may rewrite Eq. (5.102) as

$$v(x, z) = \sum_{n=1}^{\infty} \frac{\varphi_n(x, z)}{[\omega_n^2(1 + j\eta) - \omega^2]\Lambda_n} \int j\omega p(x, z) \varphi_n(x, z) dx dz. \quad (5.108)$$

This equation indicates that the plate motion may be represented by a series of damped vibrations, whereas the various series terms in Eq. (5.102) correspond to undamped vibrations. Because of the damping, the response values at the resonances here remain finite.

5.7.3 Power Considerations

The previous sections presented a general treatment of the vibrations of plates, shells and similar structures. However, one can apply the previously obtained results only rarely to practical structure-borne sound problems. Usually, there are available no simple mathematical expressions for the eigenfrequencies and eigenfunctions. Although various approximate or numerical procedures, such as the Rayleigh-Ritz and finite element methods, can be used for determining the eigenfrequencies and eigenfunctions for arbitrary boundary conditions with rather good accuracy, the amount of computation required generally is so great that they are rarely used for any but the lowest few eigenfrequencies. For the higher frequencies of interest here, one usually treats structure-borne sound problems only approximately and in terms of appropriate average values, rather than dealing with all the details of the vibrations, and in particular with their spatial distributions cf., Sect. 6.9. Quite often, one has no choice but to employ approximations, because the boundary conditions of the system may not be known well enough to permit exact calculation of the mode shapes.

Of all the various average values, the one of greatest physical importance is the spatial average of the square of the velocity. This quantity, which will be denoted by v^2 , is equal to the total energy content of the vibrating system, divided by the total mass $S\bar{m}''$ of the system. In view of Eq. (5.101), one may thus write

$$\begin{aligned}\overline{v^2} &= \frac{E_{kin}}{Sm''} = \frac{1}{Sm''} \int m'' |v(x, z)|^2 dx dz \\ &= \frac{1}{Sm''} \sum_{n,m} |v_n v_m| \left| \int m'' \varphi_n(x, z) \varphi_m(x, z) dx dz \right|^2 = \frac{1}{Sm''} \sum_n |v_n|^2 \Lambda_n.\end{aligned}\quad (5.109)$$

The double summation, extending over all combinations of m and n , here reduces to a single summation, because of the orthogonality condition. The mean-square velocity thus is equal to the sum of the squares of the velocities of the individual modes. This result is not altogether surprising, because the independence of the eigen-vibrations was used in Sect. 5.7.1 to prove the orthogonality relation.

In order to proceed further with the analysis, one requires the velocities v_n . According to Eq. (5.108) these obey

$$v_n = \frac{j\omega}{[\omega_n^2(1+j\eta) - \omega^2] \Lambda_n} \int p(x, z) \varphi_n(x, z) dx dz, \quad (5.110)$$

in the presence of damping. For the case of primary interest here, with a point-force F acting on an infinitesimally small area at the location x_0, z_0 so that $p(x_0, z_0) dx_0 dz_0 = F$, one may take $\varphi_n(x, z)$ as constant over the region of the integration, just as was done to arrive at Eq. (5.105a). Equation (5.110) then reduces to

$$v_n = \frac{j\omega F \varphi_n(x_0, z_0)}{[\omega_n^2(1+j\eta) - \omega^2] \Lambda_n}, \quad (5.110a)$$

and one may rewrite Eq. (5.109) as

$$\overline{\overline{v^2}} = \frac{F^2}{Sm''} \sum_n \frac{\omega^2 \varphi_n^2(x_0, z_0)}{\left[(\omega_n^2 - \omega^2)^2 + \eta^2 \omega_n^4 \right] \Lambda_n}. \quad (5.111)$$

For plates of uniform thickness and similar structures with constant mass m'' per unit area, Eq. (5.111) can be simplified by averaging over all possible excitation positions, rather than dealing with one specific x_0, z_0 . This second averaging process, indicated by a second over bar, leads to

$$\overline{\overline{v^2}} = \frac{1}{S} \int \overline{v^2} dx dz = \frac{\omega^2}{S^2} \frac{F^2}{m''^2} \sum_n \frac{1}{(\omega_n^2 - \omega^2)^2 + \eta^2 \omega_n^4}. \quad (5.112)$$

One may observe that this mean-square velocity response to point excitation depends only on the exciting force, the total mass, the damping, and the proximity of the excitation frequency to the various eigenfrequencies. The spatial variations of the mode shapes (eigenfunctions), on the other

hand, do not affect this response at all. One may thus consider the various modes to act as independent energy reservoirs, which are uniformly excited on the average, i.e., all receiving the same input power. The magnitudes of the resulting modal velocities then depend on the location (along the frequency axis) of the exciting frequency with respect to those of the eigenfrequencies. It must be noted, however, that uniform excitation of all modes occurs only with point forces. With other distributions of the excitation, for example with excitation by sound waves, the power may be distributed very unevenly among the various modes and the spatial variations of the eigenfunctions also tend to play important roles.

In practice, exciting forces also usually do not act at just a single frequency. Rather, they generally extend over a more or less broad frequency band. In such cases, the mean-square force F_{Δ}^2 in each frequency band $\Delta\omega$ is given instead of the total force, and one may find the mean-square velocity v_{Δ}^2 in the same frequency band by averaging Eq. (5.112) over $\Delta\omega$. For this approximate analysis, one only needs to assume that the interval from ω_1 to ω_2 is large enough so that it contains at least five natural frequencies. The square of the velocity in the frequency band $\omega_1 - \omega_2 = \Delta\omega$ is given by

$$v_{\Delta}^2 = \frac{1}{\Delta\omega} \int_{\omega_1}^{\omega_2} v^2 d\omega = \frac{F^2}{S^2 \bar{m}''^2} \sum_n \frac{1}{\Delta\omega} \int_{\omega_1}^{\omega_2} \frac{\omega^2 d\omega}{(\omega_n^2 - \omega^2)^2 + \eta^2 \omega_n^4}. \quad (5.113)$$

One may observe that the value of each of the integrals of Eq. (5.113) depends very strongly on whether the eigenfrequency ω_n is inside or outside of the integration interval. If $\omega_n < \omega_1$ or if $\omega_n > \omega_2$, then the value of the integral is very small and independent of the damping. However, if $\omega_1 < \omega < \omega_2$ and if the damping is not too great, then one may use the approximation $\omega_n^2 - \omega^2 = (\omega_n + \omega)(\omega_n - \omega) \approx 2\omega(\omega_n - \omega)$ to obtain

$$\begin{aligned} \int_{\omega_1}^{\omega_2} \frac{\omega^2 d\omega}{(\omega_n^2 - \omega^2)^2 + \eta^2 \omega_n^4} &\approx \int_{\omega_1}^{\omega_2} \frac{d\omega}{4(\omega_n - \omega)^2 + \eta^2 \omega_n^2} \\ &= \frac{1}{2\eta\omega_n} \left[\arctan \frac{2(\omega_2 - \omega_n)}{\eta\omega_n} - \arctan \frac{2(\omega_1 - \omega_n)}{\eta\omega_n} \right]. \end{aligned} \quad (5.113a)$$

By writing η in terms of the half-value bandwidth b of the resonance (see Table 4.2), one finds that the two arctangent functions approach $\pm \pi/2$ within at least 10%, if the resonance frequency ω_n differs by at least $3b$ from both ω_1 and ω_2 , one may obtain a reasonable approximation by replacing Eq. (5.113a) by $\pi/(2\eta\omega_n)$. Equation (5.113) can then approximated as

$$v_{\Delta}^2 \approx \frac{F_{\Delta}^2}{S^2 \bar{m}''^2 \Delta\omega} \sum_{n=N_1}^{N_2} \frac{\pi}{2\eta\omega_n} + \text{Remainder}, \quad (5.114)$$

where N_1 is the sequence number of the lowest, and N_2 that of the highest eigenfrequency in the region of integration, so that $N_2 - N_1 = \Delta N$ is the number of resonance frequencies in the interval $\Delta\omega$.

If one now also neglects the small remainder term of Eq. (5.114) and replaces the eigenfrequencies ω_n by the centre-frequency ω of the band under consideration, one obtains

$$v_{\Delta}^2 \approx \frac{F_{\Delta}^2}{S^2 \bar{m}''^2} \frac{\pi}{2\eta\omega} \frac{\Delta N}{\Delta\omega}. \quad (5.115)$$

For the special case of a homogeneous plate, use of the expression given in Table 5.3 here yields

$$v_{\Delta}^2 \approx \frac{F_{\Delta}^2 k_B^2}{8\omega^2 \bar{m}''^2 S\eta}. \quad (5.115a)$$

One may observe that Eq. (5.113) involves neither the eigen-functions nor the eigen-frequencies; the mean-square velocity that results from broadband excitation thus is independent of the boundary conditions, and depends only on the total mass $S\bar{m}''$, the loss factor η , the frequency and the number of resonance frequencies.

One may obtain some further physical understanding of the foregoing result by comparing it with the behaviour of a simple mass-spring-system with mass m , resonance frequency ω_0 and loss factor η . The equation of motion for such a system is

$$-\omega^2 v + \omega_0^2 (1 + j\eta) v = \frac{j\omega F}{m}.$$

If this system is excited by a broadband force, then integration over the frequency band, using the same approach as above, yields

$$v_{\Delta}^2 = \frac{1}{\Delta\omega} \int_{\omega_1}^{\omega_2} |v|^2 d\omega = \frac{F_{\Delta}^2}{m^2 \Delta\omega} \int_{\omega_1}^{\omega_2} \frac{\omega^2 d\omega}{(\omega_0^2 - \omega^2)^2 + \eta^2 \omega_0^4} \approx \frac{F_{\Delta}^2}{m^2 \Delta\omega} \frac{\pi}{2\eta\omega_0}. \quad (5.115b)$$

Comparison of this expression with Eq. (5.115) shows that the mean square velocity of a simple oscillator of mass $S\bar{m}''$, multiplied by the number of eigenfrequencies ΔN , is exactly equal to Eq. (5.115). Thus, for point excitation one may consider each mode as an independent energy content

on the average. The total energy in a frequency band then simply depends only on the number of resonance-frequencies in the band.

Table 5.3. Number of modes and modal densities

Rod (longitudinal)	$N = k_L l / \pi = \omega l / (c_L \pi)$	$\Delta N / \Delta \omega = l / (c_L \pi)$
Beam (bending)	$N = k_B l / \pi = \sqrt{\omega} l / (1.7 \sqrt{c_L h})$	$\Delta N / \Delta \omega = k_B l / (2\pi\omega)$ $= l / (3.4 \sqrt{\omega c_L h})$
Plate (bending)	$N = k_B^2 S / 4\pi = \omega S / (3.6 c_L h)$	$\Delta N / \Delta \omega = k_B^2 S / (4\pi\omega)$ $= S / (3.6 c_L h)$
Acoustic volume	$N = k_0^3 V / 6\pi^2 = \omega^3 V / (6\pi^2 c_0^3)$	$\Delta N / \Delta \omega = k_0^2 V / (2\pi^2 c_0)$ $= \omega^2 V / (2\pi^2 c_0^3)$
Ring (radial)	$N = 2k_B a = 3.7 \sqrt{\omega} a / \sqrt{c_L h}$	$\Delta N / \Delta \omega = k_B a / \omega$ $= 1.9 a / \sqrt{\omega c_L h}$
Thin-walled cylindrical shell, $v < 1$	$N \approx 3\sqrt{3} l v^{3/2} / (2\pi h)$	$\Delta N / \Delta \omega \approx 2\sqrt{\omega} l a^{3/2} / (1.6 h c_L^{3/2})$
Thin-walled cylindrical shell, $v > 1$	$N \approx \sqrt{3} l a \omega / (c_L h)$	$\Delta N / \Delta \omega \approx \sqrt{3} l a / (c_L h)$

k_L, c_L : wavenumber and sound speed for longitudinal wave,

k_0, c_0 : wavenumber and sound speed for airborne sound,

k_B, c_B : wavenumber and sound speed for bending wave,

l length, h thickness, S area, V volume, a radius and $v = \omega a / c_L$.

In addition to the mean square velocity, the power is of great practical importance. In complete generality, one may write the power supplied to a system as the real part of the product of the pressure phasor and the conjugate complex value of the velocity phasor. By expressing the velocity in terms of an eigenfunction series, the power can be written as

$$\begin{aligned} W &= \frac{1}{2} \operatorname{Re} \left\{ \int_S p(x, z) v^*(x, z) dx dz \right\} \\ &= \frac{1}{2} \operatorname{Re} \left\{ \sum_n v_n * \int_S p(x, z) \varphi_n(x, z) dx dz \right\}. \end{aligned} \quad (5.116)$$

For a point force F at the location x_0, z_0 , the foregoing integral reduces to $F\varphi_n(x_0, z_0)$. If one now substitutes v_n from Eq. (5.110), one obtains

$$W = \frac{F_\Delta^2 \eta \omega}{2} \sum_n \frac{\omega_n^2 \varphi_n^2(x_0, z_0)}{\left[(\omega_n^2 - \omega^2)^2 + \eta^2 \omega_n^4 \right] \Lambda_n}. \quad (5.117)$$

The series in Eq. (5.117) is seen to be the same as that in Eq. (5.111), except that ω^2 is replaced by ω_n^2 . However, both series yield the same result for weakly damped systems subject to excitation in a frequency band that encompasses several resonance frequencies. The same integration over frequency and over all excitation positions then yields

$$W = \frac{|F_\Delta|^2}{2} \frac{\pi}{2Sm''} \frac{\Delta N}{\Delta \omega}. \quad (5.118)$$

Herein, W represents the power in a given frequency band, for example, the power per Hz or per octave, depending upon how F_Δ is given. This result is interesting in three respects. First, it illustrates again that the natural vibration modes can be considered as a set of independent simple mass-spring-systems. The expression of Eq. (5.118) is equal to the power accepted by a simple oscillator with mass Sm'' , multiplied by the number of the excited modes. Secondly, one may find from Eqs. (5.118) and (5.115) that the input power is related to the resulting mean-square velocity simply as

$$W = \frac{1}{2} Sm'' \omega \eta v_\Delta^2. \quad (5.119)$$

Thirdly, one may find the real part of the “average” input mobility Y from Eq. (5.118). In view of the relation (5.23)

$$W = \frac{1}{2} |F|^2 \operatorname{Re} \left\{ \frac{1}{Z} \right\} = \frac{1}{2} |F|^2 \operatorname{Re} \{ Y \},$$

which means that the mobility is given by

$$\operatorname{Re} \{ Y \} = \operatorname{Re} \left\{ \frac{1}{Z} \right\} = \frac{\pi}{2Sm''} \frac{\Delta N}{\Delta \omega}. \quad (5.120)$$

Equation (5.120) is of particular interest, because it is a relation between the mobilities of finite and infinite systems. A point source exciting a very large plate, beam, etc., is likely to be affected very little by the boundaries, because they are far from the excitation position. Therefore, the power input to a large finite structure is very nearly equal to that to a similar infinite structure, at least in a frequency average sense. Thus, the point mobility Y of Eq. (5.120) must be identical to that of a corresponding infinite system. One may therefore determine the real part of the point mobility from the limiting value of $\Delta N/\Delta\omega$, and conversely. From the previously discussed physical considerations, it follows that $\Delta N/\Delta\omega$ is proportional to the area or to the length or volume, for one-dimensional or three-dimensional structures, respectively and independent of the boundary conditions [5.26].

It is instructive to illustrate the application of Eq. (5.120) to a simple case. According to Eq. (5.44), the point mobility of a homogeneous thin plate is given by $Y = 1/(8\sqrt{B'm''})$, from which one finds

$$\frac{\Delta N}{\Delta\omega} = \frac{Sm''}{4\pi\sqrt{B'm''}} = \frac{S}{4\pi} \sqrt{\frac{m''}{B'}}.$$

Thus, for plates the number of modes per unit frequency interval is constant in the limiting case. The total number of modes up to a frequency ω_1 then is

$$N = \int_0^{\omega_1} \frac{\Delta N}{\Delta\omega} d\omega = \frac{S\omega_1}{4\pi} \sqrt{\frac{m''}{B'}}.$$

One may verify that this result is correct for plates with simply supported edges by means of a simple geometrical argument, based on the so-called “modal lattice” shown in Fig. 5.18. This lattice consists of meshes of width $(\pi/l_1)\sqrt[4]{B'/m''}$ and length $(\pi/l_2)\sqrt[4]{B'/m''}$. The square of the distance from a lattice point to the origin thus is equal to

$$\left(\frac{n_1\pi}{l_1}\right)^2 \sqrt{\frac{B'}{m''}} + \left(\frac{n_2\pi}{l_2}\right)^2 \sqrt{\frac{B'}{m''}}.$$

This value may be seen to be equal to the (n_1, n_2) eigenfrequency of Eq. (5.104a). Therefore, the eigenfrequencies which fall below a given bounding value ω_1 must lie within the quarter circle with radius $\sqrt{\omega_1}$.

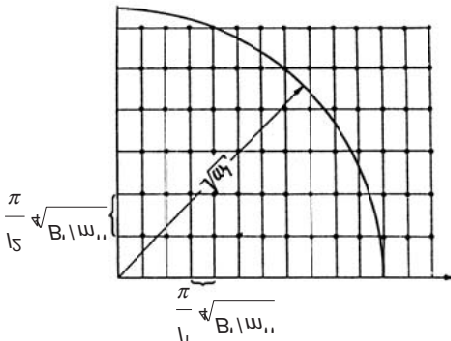


Fig. 5.18. Modal lattice for a plate

Because to each lattice point there corresponds a piece of area of magnitude $\pi^2 \sqrt{B' m'' / l_1 l_2}$ neglecting the points on the boundary, the total number of eigenfrequencies below ω_1 is given by

$$N = \frac{\pi}{4} \omega_1 \frac{l_1 l_2}{\pi^2} \sqrt{\frac{m''}{B'}} = \frac{S \omega_1}{4\pi} \sqrt{\frac{m''}{B'}}.$$

Note that eigenfrequencies that occur more than once here are counted as often as they occur. This analysis thus actually yields the number of modes (eigenfunctions). As one may note, the equations for N obtained here by two entirely different approaches are in complete agreement.

Finally, it is of interest to derive the relation between power and mean-square velocity, Eq. (5.119), by an entirely different method, and under less restrictive assumptions. One may recall that the loss factor is given by $\eta = E_{\text{diss}}/2\pi E_R$, i.e., by the ratio of the energy lost per cycle to the (reversible) energy stored, see Eq. (4.22). For small damping, the reversible energy is equal to the total energy, and for an elementary area $dx dz$ this energy is approximately $m'' v^2 dx dz / 2$. The energy that is converted into heat during a period of the vibration therefore is $m'' v^2 2\pi \eta dx dz / 2$. By dividing this energy expression by the period $T = 1/f$, where f represents the frequency (in Hz), one finds that the energy converted into heat in unit time (e.g. in a second) is $m'' v^2 \omega \eta dx dz / 2$. Therefore, the energy converted into heat in unit time for the entire area S i.e., the dissipated power, is given by

$$W_{\text{diss}} = \frac{1}{2} \omega \eta \int_S m'' v^2 dx dz = \frac{1}{2} \omega \eta m'' S \bar{v}^2. \quad (5.121)$$

It has been tacitly assumed here that the mean square velocity \bar{v}^2 can be defined and measured meaningfully. This is not the case, for example, for

a plate that is so large and so heavily damped that the velocities at different locations differ by more than an order of magnitude.

In steady state, the power W_{diss} that is converted in heat must equal the power that is supplied to the system. Therefore, Eqs. (5.119) and (5.121) must be equivalent. However, Eq. (5.121) was derived without the assumption of point-force excitation, and thus represents a generalization applicable for arbitrary excitation.

5.8 Some Specific Applications

5.8.1 Impact Excitation

In Sects. 5.3.1 and 5.3.2, the motion of a semi-infinite beam was analysed when impacted by a mass in axial and transverse directions respectively, see Fig. 5.6. An additional case of impact excitation was studied in Sect. 5.4.5, where it was demonstrated how to obtain the impulse response function for an ideal impact – Green's function – from the point mobility. For thin plates, obeying the Kirchhoff theory in a wide practically interesting frequency range, the associated Green's function could be developed in closed form.

In this section, the impact excitation by means of a rigid mass will be considered under more general conditions. Both the rigorous solution and the commonly employed approximations will be treated, taking the bounce into account.

5.8.1.1 Approximations

In Sects. 5.3.1 and 5.3.2, the problem depicted in Fig. 5.19 was considered. Thereby, the impact established by means the mass m , striking the structure with the velocity v_0 , was replaced by a configuration where the mass and structure was considered as a unit on which the impulse I was exerted. In the present analysis, a mass-less stiffness element is introduced between the impacting mass and the structure, as indicated in Fig. 5.19. This offers two advantages:

- Accountancy of the, however small, flexibility at the contact point, always present in practice resulting from, for instance, the local elasticity, cf. Eq. (5.63) and
- the numerical problems associated with the incorporation of a perfectly rigid mass.

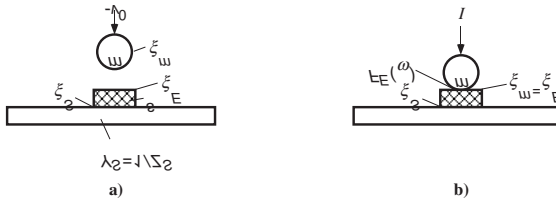


Fig. 5.19. Simplified impact model. a) A structure having the mobility Y_s impacted by a mass with velocity v_0 . The elastic layer representing the contact stiffness is monolithically joined to the structure. b) The structure is excited by an impulse $I \sim mv_0$ via the contact stiffness

The main simplification in the model depicted in Fig. 5.19 is that the bounce of the mass need not be considered. Known is therefore merely that the exciting impulse I lies between mv_0 when no bounce takes place and $2mv_0$ for a complete conservation of momentum i.e., the initial velocity of the bounce is $-v_0$. For simplicity, a value of $I = \sqrt{2}mv_0$ will be used in the subsequent analysis such that the maximum error amounts to a factor of 2. A second drawback of the model in Fig. 5.19 is the assumption that the mass will load the structure during the vibrations even if it bounces back after a short, unknown contact time.

The prediction by means of the model in Fig. 5.19 is simple. The impulse is assumed resulting from a force-time history $F(t)$ i.e.,

$$I = \int_{-\infty}^{\infty} F(t) dt. \quad (5.122a)$$

The time history is unknown and need not be known since (5.122a) is satisfied for a single impact of very short duration. By means of the force spectrum

$$F(\omega) = \int_{-\infty}^{\infty} F(t) e^{-j\omega t} dt, \quad (5.122b)$$

the following relations are applicable

$$\begin{aligned} F(\omega) - F_E(\omega) &= -\omega^2 m \xi_E(\omega), \\ \xi_E(\omega) - \xi_S(\omega) &= F_E(\omega)/s, \\ F_S(\omega) &= F_S(\omega), \quad j\omega \xi_S(\omega) = F_S(\omega) \cdot Y_S(\omega). \end{aligned} \quad (5.122c)$$

This leads to

$$v_E = j\omega \xi_E = F(\omega) \frac{Y_s + j\omega/s}{j\omega m Y_s + (1 - \omega^2 m/s)} = F(\omega) Y_I(\omega). \quad (5.123)$$

Herein, the abbreviation $Y_I(\omega)$ is introduced and denotes the point mobility of the system consisting of mass, spring and structure. The other spectral quantities can, of course, be developed in a similar manner. In the special case that the contact stiffness is very large, $s \rightarrow \infty$, it follows from Eq. (5.123) that the system mobility is influenced only by the mass and the structure.

From an inverse transform of (5.123), the time histories of forces and velocities are obtained. Here, the focus will be on averaged quantities. The energy transmitted by the impact is given by

$$\begin{aligned} E &= \int F(t) v_E(t) dt = \int \frac{1}{2\pi} \int_{-\infty}^{\infty} F(\omega) e^{j\omega t} d\omega \cdot \operatorname{Re} \left\{ \frac{1}{2\pi} \int_{-\infty}^{\infty} v_E(\omega) e^{j\omega t} d\omega \right\} dt \\ &= \frac{1}{4\pi^2} \operatorname{Re} \left\{ \iint F(\omega') v_E(\omega) e^{j(\omega' + \omega)} dt d\omega d\omega' \right\}. \end{aligned} \quad (5.124a)$$

Above is used the fact that $F(t)$ is a real-valued function. Analogous to (5.86b), the integral over time yields $2\pi\delta(\omega + \omega')$ such that after substitution from (5.123)

$$\begin{aligned} E &= \frac{1}{2\pi} \operatorname{Re} \left\{ \int_{-\infty}^{\infty} F(-\omega) F(\omega) Y_I(\omega) d\omega \right\} \\ &= \frac{1}{\pi} \int_0^{\infty} |F(\omega)|^2 \operatorname{Re}[Y_I(\omega)] d\omega. \end{aligned} \quad (5.124b)$$

In this step, use is made of $F(\omega) = F(-\omega)$ since $F(t)$ is real-valued.

The expressions in (5.122b) to (5.124b) are valid for arbitrary force-time histories. A specialisation on short impacts enables the expansion of the exponential function in a Taylor series giving

$$\begin{aligned} F(\omega) &= \int F(t) \left(1 - j\omega t - \frac{1}{2}\omega^2 t^2 \dots \right) dt \\ &= \int F(t) dt - j\omega t_I \int F(t) (t/t_I) dt - \frac{\omega^2 t_I^2}{2} \int F(t) \left(\frac{t}{t_I} \right)^2 dt \\ &= \int F(t) dt - j\omega t_I G_1 - \frac{1}{2}\omega^2 t_I^2 G_2 \approx I; \quad \omega t_I < 1 \end{aligned} \quad (5.125)$$

In the above expressions, the impact duration or contact time is introduced. Also used is the fact that the terms denoted G_1 and G_2 as well as higher order terms are all smaller than I . Hence, the analysis of short-duration im-

pact excitation is easy since the excitation spectrum $F(\omega)$ simply amounts to $I \approx \sqrt{2}mv_0$ for frequencies below $\omega = 1/t_I$.

An application of the formulae discussed is the foot-fall noise problem in apartment houses. The hammer of mass 0.5 kg of the foot-fall noise apparatus, employed in the associated measurements, strikes the floor from a height of 0.04m with an impact frequency of $f_H = 10$ Hz. A single impact approximately transmits the impulse

$$I_H \approx \sqrt{2m}\sqrt{2gh} = 0.626\text{Ns},$$

when it is assumed that the hammer neither remains on the floor nor bounces back with its impacting velocity. In the expression g is the gravitational acceleration and the last square root is the formula for the free fall velocity.

The energy transmitted per impact is given by Eq. (5.124b)

$$E_H = \frac{I_H^2}{\pi} \int_0^\infty \text{Re}[Y_I(\omega)] d\omega \quad (5.126a)$$

Upon considering the individual impacts as uncorrelated, which certainly at low frequencies is only approximately valid, then the energies can be added and the energy per unit time i.e., the power is obtained as

$$W = E_H f_H = \frac{I_H^2 f_H}{\pi} \int_0^\infty \text{Re}[Y_I(\omega)] d\omega \quad (5.126b)$$

Equation (5.126b) also represents the power spectral density for an impact sequence when the integration over frequency is omitted.

Commonly only the power $W_{\Delta f}$ in the frequency band Δf is of interest and the integrand can thus be replaced by its frequency band average value such that

$$W_{\Delta f} = \frac{I_H^2 f_H}{\pi} 2\pi\Delta f \overline{\text{Re}[Y_I(\omega)]}. \quad (5.126c)$$

For an octave band, $\Delta f = 0.707 f$ and a third-octave band $\Delta f = 0.23 f$ with f being the band centre frequency.

The expression in (5.126c), naturally, is valid also in other situations with short-duration impacts where the impact frequency and the impulse transmitted are known e.g., the “rain on the roof problem”, cf. [5.29].

By equating (5.126c) and (5.121), the average mean square velocity of a floor plate can be assessed,

$$\overline{v_{\Delta f}^2} = \frac{2W_{\Delta f}}{\omega \eta m'' S} = \frac{4I_H^2 f_H \Delta f}{\omega \eta m'' S} \overline{\text{Re}[Y_I(\omega)]}. \quad (5.126d)$$

This expression shows that the footfall noise can be reduced by increasing the mass per unit area of the plate, increasing the loss factor η and reducing the system mobility. For thin plates, such as a wooden floor, it must be noted that an increase of the impacting mass leads to a reduction of the high frequency contents i.e., impacts by big masses have a duller pitch [5.30]. Also, a soft elastic interlayer, such as a carpet, abates the noise when s is chosen to be much smaller than $\omega^2 m$.

Figure 5.20 shows the results of some examples. The mobility of the structure is here assumed to be that of an infinite, thin plate in Eq. (5.44). In the bottom part of the figure, furthermore, some measurement results are plotted, from which the effect of a soft elastic interlayer can be extracted. It must be observed that the improvement is intimately related to the mass of the hammer. For masses smaller than the 0.5 kg used in these measurements, the improvement will be less pronounced.

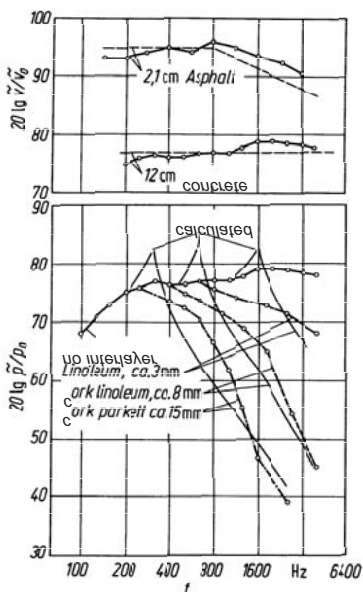


Fig. 5.20. (Top) Averaged mean square velocity level of a 12 cm concrete ceiling and of a 2.1 cm thick Asphalt floor by excitation with the standardized footfall noise apparatus. (Bottom) Measured and calculated average sound pressure level under a 12 cm concrete floor for some different elastic interlayers, excited with the standardized footfall noise apparatus

5.8.1.2 Rigorous Solution

Solving the impact problem comprising the bounce is somewhat more complicated since the equation of motion for the mass must be combined with that of the structure and since the boundary conditions abruptly changes from contact to free.

The motion of the mass m depends on the gravitation mg and the reaction force $F_E(t)$ from the structure during the contact. This means that the position $\xi(t)$ of the mass is determined by

$$m \frac{d^2\xi(t)}{dt^2} = -mg + F_E(t), \quad (5.127a)$$

see Fig. 5.19. For an oblique impact, g must be replaced by $g \sin \theta$. Otherwise the analysis remains the same. Equation (5.127a) can also be written in the form

$$\begin{aligned} \xi(t) &= \xi_0 + v_0 t + \frac{1}{m} \int_0^t [F_E(t_q) - mg] (t - t_q) dt_q \\ &= \xi_0 + v_0 t - g \frac{t^2}{2} + \frac{1}{2} \int_0^t (t - t_q) F_E(t_q) dt_q, \end{aligned} \quad (5.127b)$$

where ξ_0 and v_0 are the position and velocity at time $t = 0$ respectively. (5.127b) is obtained by integrating (5.127a) twice over time and employing Cauchy's integral formula [5.31].

To describe the motion of the contact point on the structure $\xi_E(t)$, another integral form is used,

$$\xi_E(t) = - \int_0^t F_E(t_q) \gamma_E(t - t_q) dt_q. \quad (5.127c)$$

This means that the motion at time t is determined by the sum of all previous motions at times t_q , caused by a sequence of infinitesimally short impulses $F_E(t_q) dt_q$. The negative sign in (5.127c) stems from the direction of motion chosen as positive. The convolution involves the impulse response or Green's function $\gamma(t - t_q)$, which can be derived for each structure and hence can be seen as known. The impulse response thus can be interpreted as the motion at time t resulting from a unit impulse that occurred at t_q .

The third relation necessary to solve for the three unknown quantities $\xi(t)$, $\xi_E(t)$ and $F_E(t)$ is a bit more involved. This comes from the conditions at contact which are assumed to be

$$\begin{aligned}\xi(t) &= \xi_E(t) & ; \quad t \leq t_I, \\ F_E(t) &= 0 & ; \quad t > t_I.\end{aligned}\quad (5.127d)$$

The impulse response is readily obtained from the displacement spectrum $\xi_E(\omega)$ i.e., from (5.123) by means of an inverse transform. Also, since it is defined for an ideal impact, the mass m must be set equal to zero and $F(\omega) = I$ as given by (5.125). With a unit impulse, $I = 1$, (5.123) implies that

$$\begin{aligned}\xi_E(t) &= \frac{1}{2\pi} \int \xi_E(\omega) e^{j\omega t} d\omega = \frac{1}{2\pi} \int_{-\infty}^{\infty} \left[\frac{1}{s} + \frac{Y_S}{j\omega} \right] e^{j\omega t} d\omega \\ &= \left[\frac{1}{s} \delta(t) + \frac{1}{2\pi} \int_{-\infty}^{\infty} \frac{Y_S}{j\omega} e^{j\omega t} d\omega \right] = \left[\frac{\delta(t)}{s} + \gamma_S(t) \right].\end{aligned}\quad (5.128a)$$

This means that the impulse response sought is given by the contact stiffness s , Dirac's delta function $\delta(t)$ and the impulse response of the structure without the elastic layer i.e.,

$$\gamma_S(t) = \frac{1}{2\pi} \int_{-\infty}^{\infty} \frac{Y_S}{j\omega} e^{j\omega t} d\omega, \quad (5.128b)$$

where Y_S denotes the mobility of the structure. The latter can be determined for infinite structures by using the procedures described in Sects. 5.3 and 5.4. For finite, resonant structures, however, the superposition of eigenfunctions is more suitable. It follows from Eq. (5.102) that for a harmonic point force $p = F_0(\omega)\delta(x - x_0)\delta(z - z_0)$ of frequency ω and applied at x_0, z_0 ,

$$v(x, z) = j\omega F_0(\omega) \sum_{n=1}^{\infty} \frac{\varphi_n(x, z)\varphi_n(x_0, z_0)}{\Lambda_n(\underline{\omega}_n^2 - \omega^2)} = F_0 Y_S. \quad (5.129a)$$

The next steps in the development are:

- Change to displacement i.e., $\xi = v/j\omega$,
- Concurrence of response and excitation positions i.e., $x = x_0, z = z_0$
- Explicit account of the time factor $e^{j\omega t}$

In this way, the displacement of the structure subject to pure harmonic excitation at ω becomes

$$\xi_s(x_0, z_0, \omega) = \operatorname{Re} \left\{ F_0(\omega) \sum_{n=1}^{\infty} G_n \frac{e^{j\omega t}}{\underline{\omega}_n^2 - \omega^2} \right\} \quad (5.129b)$$

where $G_n = \varphi_n^2(x_0, z_0)/\Lambda_n$. The damping is considered through assuming complex eigen-frequencies $\underline{\omega}_n$ as before.

To obtain the impulse response function, (5.129b) must be transformed to the time domain. As employed in conjunction with (5.128a), the force time history is set to be that of an ideal impact $F_0(t) = I\delta(t)$ such that the force spectrum is $F_0(\omega) = I$ and with $I = 1$ for a unit impulse, the inverse transform of (5.129b) becomes

$$\begin{aligned}\gamma_s(t) &= \frac{1}{2\pi} \int_{-\infty}^{\infty} \frac{\xi_s(x_0, z_0, \omega)}{I} e^{j\omega t} d\omega \\ &= \frac{1}{2\pi} \operatorname{Re} \left\{ \sum_n \int_{-\infty}^{\infty} G_n \frac{e^{j\omega t}}{\underline{\omega}_n^2 - \omega^2} d\omega \right\} \\ &= \sum_n \frac{G_n}{\omega_n} e^{-\eta_n \omega_n t/2} \sin \omega_n t \quad ; \quad t > 0.\end{aligned}\quad (5.129c)$$

It follows that the impulse response of the complete system, elastic layer and structure, is obtained as

$$\gamma_E(t) = \frac{\delta(t)}{s} + \sum_n \frac{G_n}{\omega_n} e^{-\eta_n \omega_n t/2} \sin \omega_n t. \quad (5.129d)$$

Thereby, the necessary relations are established to solve the problem posed. With (5.129d), the three equations describing the impact problem can be written as

$$\begin{aligned}\xi(t) &= \xi_0 + v_0 t - g \frac{t^2}{2} + \frac{1}{m} \int_0^t (t - t_q) F_E(t_q) dt_q, \\ \begin{cases} \xi(t) = \xi_E(t) & ; \quad t < t_I \\ F_E(t) = 0 & ; \quad t > t_I \end{cases}, \\ \xi_E(t) &= - \int_0^t F_E(t_q) \gamma_E(t - t_q) dt_q\end{aligned}\quad (5.130)$$

To solve Eq. (5.130) numerically, the integrals are replaced by sums. The time increment dt_q then is changed to Δ_t such that $t \rightarrow v\Delta_t$ and $t_q \rightarrow q\Delta_t$, where, of course, $v = 1, 2, 3, \dots$ and $q = 1, 2, 3, \dots$ respectively. Upon re-writing (5.130) in discretized form

$$\begin{aligned}\xi(v\Delta_t) &= A_v + H_1(v\Delta_t) F_E(v\Delta_t) + \sum_{q=1}^{v-1} H_2(q\Delta_t) F_E(q\Delta_t) \\ \xi_E(v\Delta_t) &= -\frac{1}{s} F_E(v\Delta_t) - H_3(v\Delta_t) F_E(v\Delta_t) - \sum_{q=1}^{v-1} H_4(q\Delta_t) F_E(q\Delta_t)\end{aligned}\quad (5.131a)$$

where the abbreviations

$$\begin{aligned} A_v &= \xi_0 + v_0 v \Delta_t - \frac{g}{2} (v \Delta_t)^2, \\ H_1(v \Delta_t) &= \frac{\Delta_t^2}{2m}, \quad H_2(q \Delta_t) = \frac{v - q}{m} \Delta_t^2, \\ H_3(v \Delta_t) &= \frac{\Delta_t}{2} \sum_{n=1}^{\infty} \frac{G_n}{\omega_n} e^{-\eta_n \omega_n v \Delta_t / 2} \sin \omega_n v \Delta_t, \\ H_4(q \Delta_t) &= \sum_{n=1}^{\infty} \frac{G_n}{\omega_n} \Delta_t^2 e^{-\eta_n \omega_n (v - q) \Delta_t / 2} \sin [\omega_n (v - q) \Delta_t], \end{aligned}$$

have been introduced. As is seen, the sums over time include only terms up to $q = v - 1$. At the $v : th$ iteration, they are known. The time increment Δ_t , of course, must be very small such that $\Delta_t^2 \ll m/s$ and $\omega_n \Delta_t \ll 1$.

To take the contact conditions (mid part in (5.130)) into account, a fictive force is first computed in each iteration, which would be required to bring the mass in contact with the elastic layer. When this $F_{fictive}$ is larger than zero, it is the true force. A force $F_{fictive} < 0$ would mean, that an external force be required to realize a contact. Since such an external force is absent when no adhesion is present, the contact condition is given by

$$F_E(v \Delta_t) = \begin{cases} F_{fictive} & ; \quad F_{fictive} > 0 \\ 0 & ; \quad F_{fictive} \leq 0. \end{cases} \quad (5.131b)$$

The fictive force is obtained from the equality of displacements in (5.131a) which means that

$$\begin{aligned} A_v + \frac{1}{2m} F_{fictive} \Delta_t^2 + \sum_{q=1}^{v-1} H_2(q \Delta_t) F_E(q \Delta_t) \\ = -\frac{F_{fictive}}{s} - \frac{\Delta_t}{2} F_{fictive} \sum_{n=1}^{\infty} \frac{G_n}{\omega_n} e^{-\eta_n \omega_n \Delta_t / 2} \sin \omega_n \Delta_t \\ - \sum_{q=1}^{v-1} H_4(q \Delta_t) F_E(q \Delta_t). \end{aligned} \quad (5.131c)$$

For each iteration, accordingly, $F_{fictive}$ can be calculated and thus also the true force from (5.131b). The computation, which naturally starts with $v = 1$, must be performed sequentially for $v = 2, 3, \dots$ since for each new time step, the previous forces must be known.

As soon as the forces F_E for $1 \leq q \leq v$ are known, the motion of the mass and the elastic layer can be determined. The motion of the structure at the contact point is obtained from (5.131a) as

$$\xi_s(x_0, z_0, t) = -\sum_{q=1}^v \Delta_t H_4(q\Delta_t) F_E(q\Delta_t). \quad (5.131d)$$

Upon employing the displacement version of (5.129a), the motion at an arbitrary position x, z of the structure can be obtained as

$$\xi_s(x, z, t) = -\sum_{q=1}^v \Delta_t F_E(q\Delta_t) \sum_n \frac{\varphi_n(x_0, z_0) \varphi_n(x, z)}{\Lambda_n \omega_n} e^{-\eta_n \omega_n (v-q)\Delta_t/2} \sin[\omega_n(v-q)\Delta_t] \quad (5.131e)$$

The selection of Δ_t , in principle, implies an upper frequency limit and hence it is appropriate to extend the modal summation only up to an $\omega_{n,\max}$ given by

$$\omega_{n,\max} \approx \frac{2\pi}{2\Delta_t} = \frac{\pi}{\Delta_t} \quad (5.131f)$$

Figures 5.21a, b show some results obtained by means of the expressions (5.131a-e). The following observations can be made from these two figures:

- The impacting mass exerts a short force pulse, bounces back and experiences again a free fall which leads to a new impact and so on. These force pulses are not occurring regularly due to the dependence on falling time and period of the vibration.
- The time intervals between the contacts diminishes with time – the origin of clatter – to finally bring the mass to vibrate with the structure, not included in the graphs.
- In the case of a membrane, the disturbance propagates with a constant speed (dashed lines in Fig. 5.21a) outward from the contact point and decreases gradually due to divergence. For the plate, the dispersive bending wave speed leads to a gradual fade of the signal.
- The impulse response function for the membrane exhibits a very high initial peak because the point mobility has a very large imaginary part.

The numerical analysis discussed above can be generalized to “point impacts” between two arbitrary bodies with limited modifications, provided their impulse response functions are known. Non-linear elastic layers such as e.g. Hertzian contact, moreover, can be encompassed. Finally, the sudden release of a prestressed structure can be analysed in a similar manner.

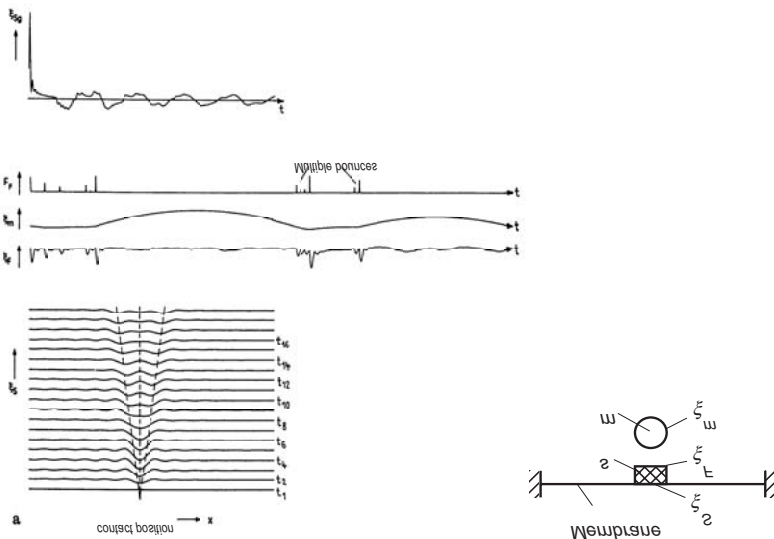


Fig. 5.21a. Impulse response γ_s , time histories of field variables F_E , ξ_m , ξ_E at the contact point and propagation of response for a mass impacting on a rectangular membrane. $\omega_E = \sqrt{s/m} = 100 \text{ rad/s}$, fundamental membrane eigen frequency = 15 rad/s

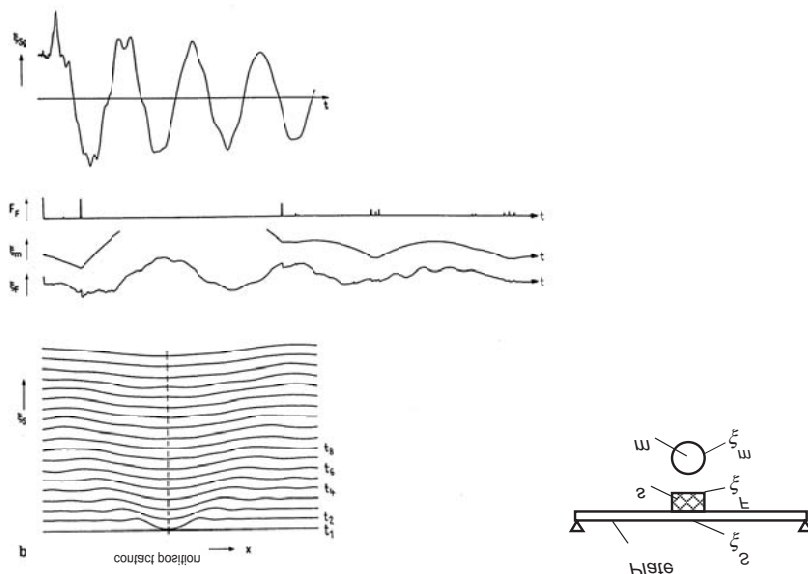


Fig. 5.21b. Impulse response γ_s , time histories of field variables F_E , ξ_m , ξ_E at the contact point and propagation of response for a mass impacting on a rectangular plate. $\omega_E = \sqrt{s/m} = 1723 \text{ rad/s}$, fundamental plate eigen frequency = 15 rad/s

5.8.2 Excitation by Sudden Release of Potential Energy

In Sect. 5.8.1.1 was analysed how a structure is excited when impacted by a mass m via an arbitrarily stiff elastic layer. The expressions (5.123) to (5.124b), derived in the frequency domain, are not only valid for force pulses but also for arbitrary force time histories, given that the force spectrum is calculated by means of Eq. (5.122b).

Besides the impact, the sudden release i.e., the vanishing of a prestressing static force F_s within a short time period, constitutes another important case in practice. Examples of such force-time histories and the corresponding spectra are shown in Fig. 5.22. For the sake of completeness also some impact force-time histories are included. Given the same net impulse, it is seen that the high frequency content is substantially less for smooth time histories than for those with abrupt steps and kinks although the mid frequency content is slightly increased. The conclusion to be drawn is that to avoid the subjectively particularly annoying high frequency components, force and velocity time histories should be kept as smooth and slow changing as possible. This can be achieved, for instance, by changes in operational processes or with elastic interlayers.

The sudden release of potential energy plays a central role in noise control of machinery in conjunction with:

- Punch presses where the punch force suddenly vanishes after piercing the work piece and press support suddenly is released and vibrates freely.
- Turning, drilling etc. where the material is not entirely homogeneous so that the tool alternatingly is stressed and released i.e., chip noise [5.32]
- Tearing and breaking where the prior to tear or break stored potential energy suddenly is released and excites mechanical parts into vibration.

When the mechanical parts do not part after the sudden release, analogous to the no bounce of the impacting mass, an uncertainty remains, which is of the order of a factor of 2.

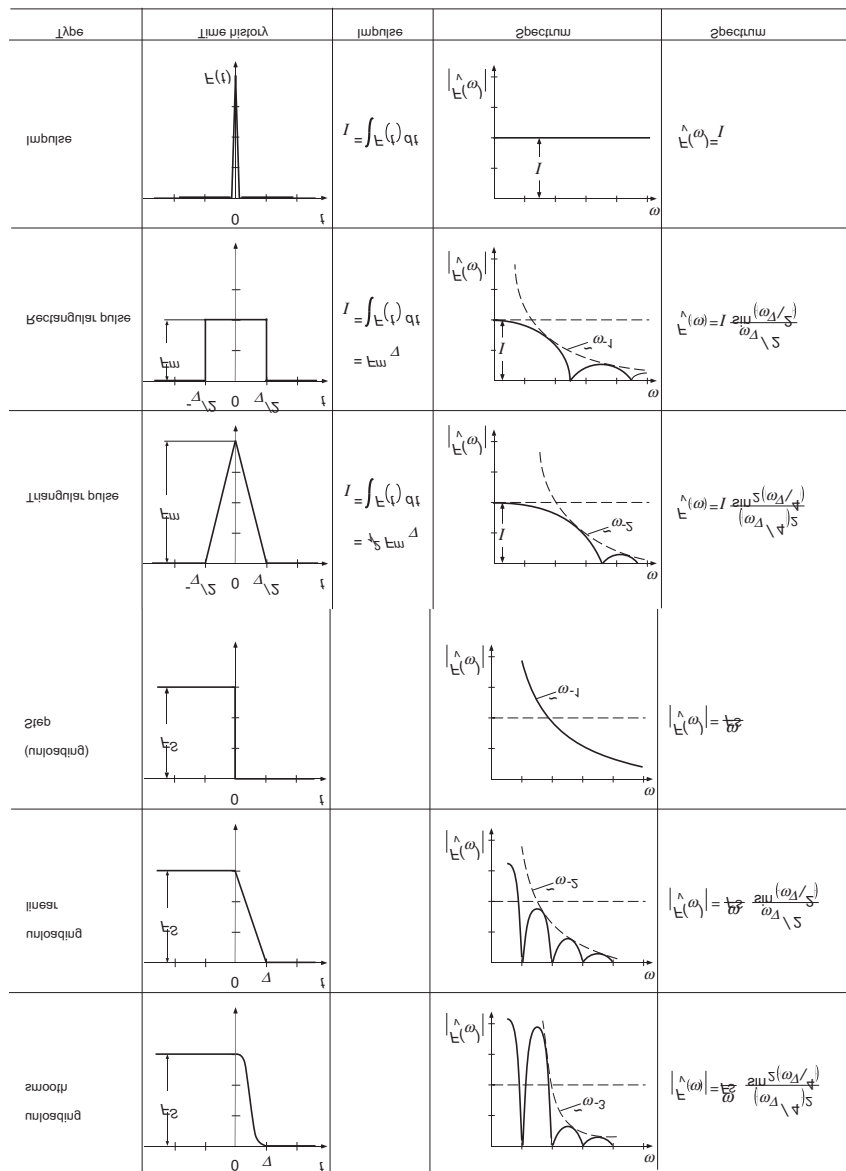


Fig. 5.22. Spectra for some idealized force-time histories

5.8.3 Rough Surfaces as Sources of Structure-Borne Sound

The excitation of structure-borne sound by rolling as well as by sliding is highly significant in practice. Prominent examples are railways, motor car tyres and roller-bearings. Rolling noise indeed, can be argued the most important source of sound since it is responsible for the major part of the traffic noise at high speeds. It is ranked as the most annoying disturbance in both national and international opinion polls.

Mechanisms that can be important in conjunction with rolling and sliding are:

- “Playback” of the surface roughness (this section)
- Parametric excitation, where the mobility of the track changes spatially and thus also in time when there is a motion cf., Sect. 5.8.4.
- Wave trace matching, where the speed of motion coincides with a wavespeed in a structure cf., Sect. 4.8.4.
- Stick-slip motion, depending on the difference between the smaller slip and the bigger stick friction, and leading to the squeal noise as well as the violin sound [5.33-5.35].

For the “playback” of surface roughness, a useful model can be developed under the following simplified conditions [5.36]:

- The contact patch can be considered a point i.e., the distance travelled $\Delta = TU$ during a period of vibration $T = 1/f$ is larger than the length of the contact l_c giving the condition

$$TU \gg l_c \Leftrightarrow f \ll U/l_c, \quad (5.132)$$

where U is the vehicle speed.

- The vehicle speed is substantially smaller than the wave speed of the participating structures.
- Only forces are present that are perpendicular to the wheel axis.
- The mobility of the road or rail surface does not vary spatially. In particular, it must be free of discontinuities.
- The contact stiffness can be approximated as a linear spring.

For a train with a speed of $U = 160 \text{ km/h} = 44.4 \text{ m/s}$ and a contact length of $12 \text{ mm} \leq l_c \leq 18 \text{ mm}$, Eq. (5.132) gives 1 kHz as an upper frequency limit for the simplified model. Thereby, a static load of about 100 kN and a wheel radius of 0.47 m are assumed as typical values.

Under these prerequisites, the excitation of structure-borne sound by rolling can be viewed as that depicted in Fig. 5.23b. Thus, a “band of roughness” is pulled with a speed U between stationary wheel and rail. The roughnesses of the band mirrors those of wheel and rail respectively.

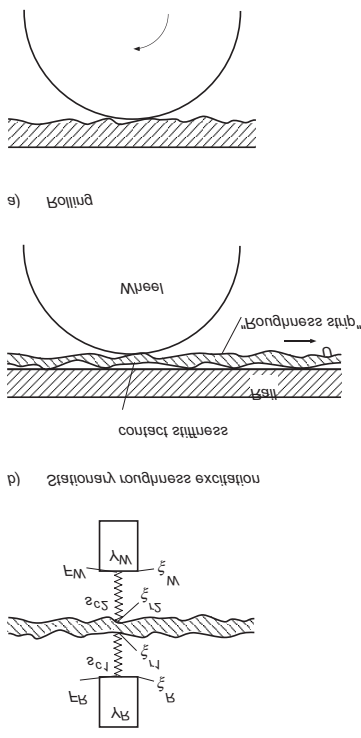


Fig. 5.23. Excitation by rolling modelled as roughness excitation a) rolling b) stationary roughness excitation c) model

With the wheel represented by the mobility Y_W , the road or rail by Y_R and the contact stiffness by the springs s_{c1} and s_{c2} respectively, the model in Fig. 5.23c can be developed.

In phasor notation, the following equations of motion can be established:

$$\text{Upper contact force } \hat{F}_W = s_{c2} (\hat{\xi}_{r2} - \hat{\xi}_W) \quad (5.133a)$$

$$\text{Lower contact force } \hat{F}_R = s_{c1} (\hat{\xi}_{r1} - \hat{\xi}_R) \quad (5.133b)$$

$$\text{Wheel response } \hat{v}_W = Y_W \hat{F}_W = j\omega \hat{\xi}_W \quad (5.133c)$$

$$\text{Road or rail response } \hat{v}_R = Y_R \hat{F}_R = j\omega \hat{\xi}_R \quad (5.133d)$$

$$\text{Force equilibrium } \hat{F}_w = \hat{F}_R \quad (5.133e)$$

$$\text{Thickness of band of roughness } \hat{\xi}_{rough} = \hat{\xi}_{r1} + \hat{\xi}_{r2} \quad (5.133f)$$

By eliminating $\hat{\xi}_{r1}$, $\hat{\xi}_{r2}$, \hat{F}_R and \hat{F}_w it is found that

$$\begin{aligned}\hat{\xi}_R &= \frac{\hat{\xi}_{rough}}{1 + \frac{Y_w}{Y_R} + \frac{j\omega}{Y_R} \left(\frac{1}{s_{c1}} + \frac{1}{s_{c2}} \right)} \\ &= \frac{\hat{\xi}_{rough} Y_R}{Y_R + Y_w + j\omega / s_c} \\ \hat{\xi}_w &= \frac{\hat{\xi}_{rough} Y_w}{Y_w + Y_R + j\omega / s_c}\end{aligned}\quad (5.134)$$

where $s_c = (1/s_{c1} + 1/s_{c2})^{-1}$ is the total contact stiffness. The total roughness $\hat{\xi}_{rough}$ is obtained from the roughnesses of the wheel and road or rail by measuring them with a sensor moved over the surfaces at a speed U_M . The resulting time signal is then spectrally decomposed. Hence, the relevant amplitude at a frequency f and a vehicle speed U is the spectral component of the roughness signal measured at frequency fU_M/U .

It follows from Eq. (5.134) that:

- The vibration amplitudes and thence also the radiated airborne sound are proportional to the roughness amplitudes. From this it is clear that for a periodic surface roughness (ripple) of roughness wavelength λ_r , the resulting tone has the frequency U/λ_r .
- The structural component with the largest mobility will be strongest excited. The wheel mobility is maximum at the resonances such that the vibrations are large at those frequencies.
- A decrease of the road or rail mobility leads to an increased wheel motion, whereas the opposite occurs when the wheel mobility is decreased. The influence on the sound radiation depends on the radiation conditions.
- A reduction of the contact stiffness e.g., through more elastic materials or other structural profiles, leads to less noise radiation since the roughness becomes better isolated.

The rolling model briefly described has proven useful for the prediction of railway noise [5.36-5.38]. For so low vehicle speeds that (5.132) is not fulfilled, a more or less empirical “contact filter” is introduced in the calculations to achieve improved predictions at high frequencies.

5.8.4 Parametric Excitation

As an example of parametric excitation, can be considered a beam resting on a non-uniform elastic foundation, which is subject to a moving point force F_0 as depicted in Fig. 5.24. The equation of motion for such a system reads (cf. Sect. 3.7.4.4)

$$B \frac{\partial^4 \xi}{\partial x^4} + m' \frac{\partial^2 \xi}{\partial t^2} + s(x) \xi = F_0 \delta(x - Ut) \quad (5.135)$$

where the external force is represented by Dirac's delta function of the speed U . The non-uniformity of the foundation stiffness is introduced through the spatial stiffness function $s(x)$.

By transforming all field variables to the frequency domain

$$\begin{aligned} \xi(x, t) &= \frac{1}{2\pi} \int \hat{\xi}(x, \omega) e^{j\omega t} d\omega, \\ \delta(x - Ut) &= \frac{1}{2\pi} \int e^{\frac{j\omega}{U}(Ut-x)} d\left(\frac{\omega}{U}\right) = \frac{1}{2\pi U} \int e^{\frac{j\omega}{U}x} e^{j\omega t} d\omega \end{aligned} \quad (5.136a)$$

Eq. (5.135) can be rewritten in terms of the spectral quantities

$$B \frac{\partial^4}{\partial x^4} \hat{\xi}(x, \omega) - [\omega^2 m' - s(x)] \hat{\xi}(x, \omega) = \frac{F_0}{U} e^{-\frac{j\omega}{U}x} \quad (5.136b)$$

giving a linear differential equation with variable constants. To obtain a general solution, a numerical procedure is required.

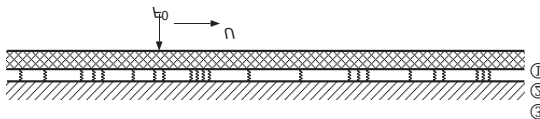


Fig. 5.24. Moving point excitation of a beam (1), on a non-uniform bed (2) and resting on a rigid foundation (3)

In this case, an iterative procedure is employed, which relies on a stiffness of the bed having a spatially constant part \bar{s} and a varying part $\varepsilon(x)\bar{s}$. Equation (5.136b) then becomes

$$B \frac{\partial^4}{\partial x^4} \hat{\xi}(x, \omega) - [\omega^2 m' - \bar{s}] \hat{\xi}(x, \omega) = \frac{F_0}{U} e^{-\frac{j\omega}{U}x} - \varepsilon(x) \bar{s} \hat{\xi}(x, \omega) \quad (5.136c)$$

As a first step, the second term on the right hand side is neglected and the solution is given by

$$\hat{\xi}(x, \omega) = \frac{F_0}{U} \frac{e^{-j\omega x/U}}{B(\omega/U)^4 - (\omega^2 m' - \bar{s})}. \quad (5.136d)$$

This solution is certainly dubious for frequencies where the denominator vanishes. However, from this so-called secular solution, it is to be expected that a pronounced vibration occurs in the vicinity of

$$B \left(\frac{\omega_{coinc}}{U} \right)^4 = \omega_{coinc}^2 m' - \bar{s},$$

or, equivalently

$$\omega_{coinc}^2 = \frac{m' \pm \sqrt{m'^2 - 4\bar{s}B/U^4}}{2B/U^4}. \quad (5.137a)$$

As is indicated by Eq. (5.137a), a coincidence phenomenon occurs due to equality of speeds of the moving force and the wave propagation. Since the root must be real-valued, coincidence cannot occur for all values of U but only for

$$U^4 > 4 \frac{\bar{s}}{m'} \frac{B}{m'},$$

or,

$$U > \sqrt[4]{2 \frac{\bar{s}}{m'} \frac{B}{m'}}. \quad (5.137b)$$

In the above expression $\omega_s = \sqrt{\bar{s}/m'}$ is the fundamental resonance frequency of the beam mass resting on the average stiffness \bar{s} of the bed. The fourth root corresponds to the flexural wave speed at this frequency.

From a numerical evaluation of (5.137b), it is clear that the inequality is not satisfied for correctly founded railway rails. Otherwise the trains would derail. For incorrectly inflated tyres, however, it is possible that the inequality is satisfied. A high vehicle speed that equals or exceeds the phase speeds of the structural waves in the tyre, yield a hazardous flutter as the consequence.

Besides airborne sound transmission through walls or plates, boundary layer noise is an additional case where the coincidence phenomenon plays a certain role. Examples are aircraft fuselages and flows in pipes and tubes. Boundary layer noise is generated when a turbulent flow strikes along a plate. The vortices can be seen as forces or pairs of forces moving with the convection speed U . The coincidence is then realized when U equals the flexural wave speed. Owing to the fact that the flow velocities can be rather high and the wall thicknesses small, giving low bending wave

speeds, this form of coincidence appear throughout the mid and high frequency ranges. In practice, however, there is no tonal effect as could be anticipated from (5.136d) since also other phenomena comes into play. Particularly, the short “life-time” of the vortices makes it difficult to survive the transient stage of the coincidence.

Upon returning to the parametric excitation it is suitable to introduce

$$\hat{\xi}(x, \omega) = \hat{\xi}_0(x, \omega) + \hat{\xi}_1(x, \omega). \quad (5.138)$$

With $\hat{\xi}_0$ satisfying the uniform part of the problem i.e., (5.136d), the governing expression for $\hat{\xi}_1$ is

$$B \frac{\partial^4 \hat{\xi}_1(x, \omega)}{\partial x^4} - (\omega^2 m' - \bar{s}) \hat{\xi}_1(x, \omega) = -\bar{s} \varepsilon(x) (\hat{\xi}_0(x, \omega) + \hat{\xi}_1(x, \omega) \omega). \quad (5.139)$$

With the second term on the right hand side neglected, (5.139) again takes the form of the equation for a beam on a uniform elastic bed, excited by a force distribution $\bar{s} \varepsilon(x) \hat{\xi}_0(x, \omega)$. This means that the larger the stiffness, the higher the vibrations and the more excited the homogeneous system becomes by the moving force.

In the absence of the last term, a solution of (5.139) is possible in the form of a spatial Fourier transform cf. Sect. 5.4.3. Here, however, the analysis will be confined to pure sinusoidal stiffness variations such that

$$\varepsilon(x) = \varepsilon_0 \sin(2\pi x / \lambda_p) = \frac{\varepsilon_0}{2j} (e^{j2\pi x / \lambda_p} - e^{-j2\pi x / \lambda_p}), \quad (5.139a)$$

where λ_p is the spatial periodicity of the stiffness variation. Upon substituting this expression and (5.136d) into (5.139), the same manipulations that led to (5.136d) yield

$$\begin{aligned} \hat{\xi}_1(x, \omega) &= -\frac{F_0}{U} \frac{\bar{s}}{2j} \frac{\varepsilon_0}{Bk_0^4 - (\omega^2 m' - \bar{s})} \times \\ &\times \left[\frac{e^{-jk_{1+}x}}{Bk_{1+}^4 - (\omega^2 m' - \bar{s})} - \frac{e^{-jk_{1-}x}}{Bk_{1-}^4 - (\omega^2 m' - \bar{s})} \right]. \end{aligned} \quad (5.139b)$$

Herein,

$$k_0 = \frac{\omega}{U}, \quad k_{1+} = \frac{\omega}{U} - \frac{2\pi}{\lambda_p}, \quad k_{1-} = \frac{\omega}{U} + \frac{2\pi}{\lambda_p}. \quad (5.139c)$$

As can be seen, the denominators may vanish at three frequencies where then large vibration amplitudes can be expected. In the frequency range of main interest where $\omega > \sqrt{\bar{s}/m'}$, the frequencies are

$$\begin{aligned}
 \text{a)} \frac{\omega}{U} &\approx \sqrt[4]{\frac{\omega^2 m'}{B}} \Leftrightarrow U = c_B, \\
 \text{b)} \frac{\omega}{U} - \frac{2\pi}{\lambda_p} &\approx \frac{\omega}{c_B} \Leftrightarrow \omega_{1+} \approx \frac{2\pi U}{\lambda_p} \frac{1}{1-U/c_B}, \\
 \text{c)} \frac{\omega}{U} + \frac{2\pi}{\lambda_p} &\approx -\frac{\omega}{c_B} \Leftrightarrow \omega_{1-} \approx -\frac{2\pi U}{\lambda_p} \frac{1}{1+U/c_B}.
 \end{aligned} \tag{5.139d}$$

For the common situation where $c_B \gg U$, the last two expressions give

$$\omega_1 \approx \frac{2\pi U}{\lambda_p} \Rightarrow f_1 \approx U/\lambda_p \tag{5.139e}$$

As is to be expected, mainly that frequency will be promoted, which corresponds to the period of the travel time from one stiffness increase to the next.

The proposed iteration scheme can be taken further and by using $\hat{\xi}_1$, an improved estimate can be obtained. The additional information gained, thereby, is limited if the basic assumption for the iteration that $\hat{\xi}_1 < \hat{\xi}_0$ is not satisfied in the vicinity of the zeroes of the denominators.

Although the analysis in this section is confined to beams, the qualitative findings can be transferred to other structures, which are exposed to some uniformly moving excitation.

- When the speed of the excitation and the wave speed are equal, a strong coincidence excitation occurs
- To first order, the parametric excitation corresponds to a force distribution in the form

$$\bar{s}\varepsilon(x)\hat{\xi}_0(x,\omega) \Rightarrow Z(x)\hat{v}_0(x,\omega), \tag{5.140}$$

acting on the homogenous structure. Thereby, $\hat{\xi}_0(x,\omega)$ and $\hat{v}_0(x,\omega)$ are the spectra of the displacement field and the velocity field respectively, resulting from the moving force F_0 . $Z(x)$ is a position dependent impedance of the foundation.

- When a parameter is spatially periodic of period λ_p as, for instance, by rail sleepers, the structure will experience strong excitation in the frequency range around U/λ_p .

The iterative procedure described is suited merely for qualitative purposes. To handle actual problems, the inhomogeneities are replaced by auxiliary forces. The computation of the auxiliary forces requires, in turn, the simultaneous solution of a more or less large set of linear equations cf. Sect. 6.5.3.

5.8.5 Vibration Transmission from Machinery

The classical approach for calculations of structure-borne sound and vibration transmission is based on the assumption of a source performing rigid body motions. A multi-point coupling between the source and the receiving structure may be reduced to a single contact point case merely by taking into account the actual number of contact points and their respective motional phase relations. These phase relations, in turn, are given by the component or components of motion considered. Although it is possible to handle all six degrees of freedom as well as the potential coupling them in between, the unwieldiness of the classical approach grows rapidly as the number of degrees of freedom included increases [5.39].

The rigid body motion underlying this approach is generally a most dubious assumption. Instead it is usually necessary to treat both the source and the receiving structure as continuous systems (flexible) even for low frequencies. Such a description of linear source and receiver systems is conveniently obtained by means of the mobilities.

The source and receiver structures are commonly coupled to each other at several discrete points. The word point is herein used in a somewhat extended meaning, denoting an area with dimensions smaller than a fraction of the governing wavelength. The physical coupling of the structural subsystems is often constituted by relatively small elastic elements (chocks, isolators, etc.) called transmission elements. For a general system, the subsystems are thus divided into the source (including possible footings), the transmission elements and the receiver. If no transmission elements are present, the interface between the source and the receiver is located below the footings. Of course, there are other divisions possible but the one described facilitates a unified treatment of rigid and resilient installations.

In the general case, the interaction between the different contact points as well as between the different components of motion must be taken into account. A thorough survey of the different approaches to treat the general case can be found in [5.40]. For the wide frequency band of interest, the handling of the general matrix formulation [5.41] results in an excessive task since not only can the contact points between the source and the receiver be quite numerous but also the six components of motion and excitation must be taken into account.

In this chapter the analysis of the transmission process will be developed. On route to the treatment of the general case will be considered first the single point interface, i.e. where the source and receiver is connected in one point, in order to throw some light on the fundamentals of the transmission of (complex) power. The next step will be the demonstration of the general matrix formulation for a multi-point, multi-component case.

It is not intended herein to fully cover all the details of the transmission process but rather to give an understanding for the basic principles. Moreover, as indicated above, the discussion is concentrated to point-like connections since one- or two-dimensional interfaces mathematically become more cumbersome.

5.8.5.1 Complex Power

For the study of transmission, two quantities generally are of interest. The first is the amplitude of the vibration at the contact point and the second is the active power fed to the receiver. The amplitude of the vibration is interesting because sensitive equipment or structural parts may be damaged or disturbed in the operation by excessive oscillations. Examples of damages and disturbances are fatigue problems and reliability conditions respectively. The active power transmitted to the receiver propagate and radiate to ambient systems such as fluid spaces with e.g. audible noise as a consequence. Both these quantities, the vibration amplitude and the active power transmitted, can be obtained from the complex power

$$\underline{Q} = W + jV = |\underline{Q}| e^{j\phi}. \quad (5.141)$$

In Eq. (5.141), W denotes the active part of the power transmitted whereas V stands for the reactive part. In the second form it is represented by its magnitude and phase.

In order to determine the complex power, the field variables at the excitation point (the contact point between the source and the receiver) must be known.

$$\underline{Q} = \frac{1}{2} \underline{F}^* \underline{v} \quad (5.142)$$

From Eq. (5.142), it is seen that the real part of \underline{Q} , the active power, is that part of the scalar product, force times velocity, where these variables act in phase and the imaginary part, the reactive power, is the part where the force and the velocity are 90° out of phase, see Fig. 5.25. The reactive part of the complex power created at the contact point is put into “nearfield” kinetic energy. Over alternate quarter cycles of the oscillation, kinetic energy is consumed by the receiver and over the two other quarter cycles the same energy is returned to the source so that no net energy flow is obtained. This part of the power, therefore, only affects the excitation region. The active part, on the other hand, stands for a net energy flow from the contact point, out in the receiver. Accordingly, the active part of the power affects the dynamic state at remote positions of the receiver as well. Since

the dynamic state at an excitation point is governed by the strength of the excitation and the dynamic characteristics of the excited structure, the complex power given by Eq. (5.142) may be written as

$$\underline{Q} = \frac{1}{2} |\underline{F}|^2 \underline{Y}, \quad (5.143a)$$

or equivalently

$$\underline{Q} = \frac{1}{2} \frac{|\underline{v}|^2}{|\underline{Y}|^2} \underline{Y}, \quad (5.143b)$$

where the point mobility of the structure has been introduced.

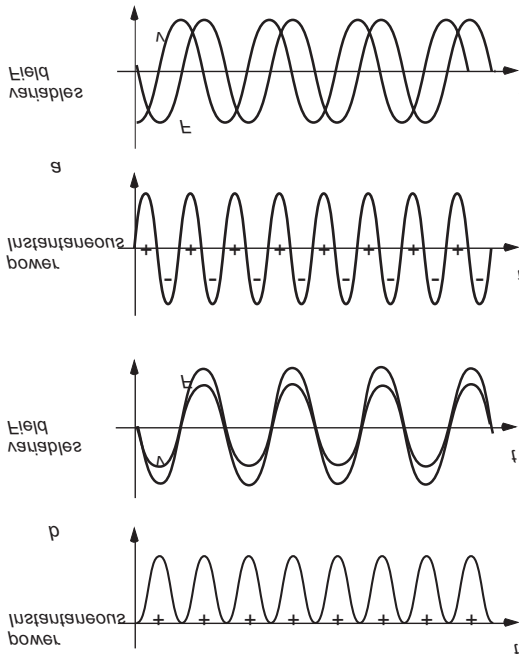


Fig. 5.25 Illustration of the complex power, (a) reactive, and (b) active

The two quantities relevant to transmission can be determined from the complex power - the vibration amplitude

$$|\underline{v}| = \sqrt{2 |\underline{Q}| |\underline{Y}|}, \quad (5.144)$$

and the active power

$$W = \operatorname{Re}[\underline{Q}] . \quad (5.145)$$

Therefore, one may conclude that in order to have a complete description of the transmission process the complex power is sought.

5.8.5.2 Single Point Case

Consider the situation where a machine – a structure- borne sound source – is connected at one point to a plate – a receiving structure. The source is presumed to exert only a translatory excitation component (vertical). Thus, no lateral (horizontal) forces and moments (rocking, twisting) components are present. This situation constitutes the fundamental model for both rigid and resilient installations.

In order to determine the power transmitted to the receiver both the actual force and velocity at the interface must be known. It is reasonable to assume that both the source and the receiver will influence the dynamic state but it is instructive to begin with two extreme cases.

5.8.5.2.1 Constant Velocity Source

If the source is disconnected from the receiver and put into operation, the velocity (at the contact point) of the free source can be registered. If, upon a subsequent connection to the receiver the same velocity is observed at the contact point, it would be tempting to use the velocity of the free source as a measure of the source strength [5.42]. If, for all possible receivers, the velocity registered at the contact point with the source and the receiver connected, is found to be equal to that registered when the source is free, the source is a constant velocity source. Intuitively, such a source is rather rare in practice but its theoretical counterpart is helpful for the understanding of the transmission process. In mathematical terms, the conditions for a constant velocity source may be stated as

$$|\underline{Y}_S| \ll |\underline{Y}_{R_i}|; \forall i, \quad (5.146a)$$

where indices S and R denote source and receiver respectively.

When the source and receiver are connected the following conditions must be valid if the two subsystems are to be rigidly joined

$$\underline{v}_S = \underline{v}_R , \quad \underline{F}_S = -\underline{F}_R .$$

Moreover, the force and the velocity at the receiver are related through the point mobility as

$$\underline{v}_R = \underline{Y}_R \underline{F}_R .$$

Since the source in this case is a constant velocity source we may immediately write

$$\underline{v}_R = \underline{v}_0 ,$$

and hence

$$\underline{F}_R = \frac{\underline{v}_0}{\underline{Y}_R} .$$

Finally, the complex power sought is obtained by substitution in Eq. (5.142)

$$\underline{Q} = \frac{1}{2} \left(\frac{\underline{v}_0}{\underline{Y}_R} \right)^* \underline{v}_0 = \frac{1}{2} \frac{|\underline{v}_0|^2}{|\underline{Y}_R|^2} \underline{Y}_R . \quad (5.147a)$$

Interpreting the result, it is seen that for an idealized constant velocity source, the power transmitted is independent of the source mobility. The magnitude of the complex power increases with the mean square velocity but decreases with the magnitude of the mobility. The phase of the complex power is equal to the phase of the receiver mobility. Taking the real part of \underline{Q} yields

$$W = \frac{1}{2} \frac{|\underline{v}_0|^2}{|\underline{Y}_R|^2} \operatorname{Re}[\underline{Y}_R] ,$$

and it is seen that the active power transmission increases with an increased real part of the receiver mobility and decreases with the magnitude squared. Hence, in order to reduce the active power transmitted the imaginary (reactive) part of the receiver mobility should be as large as possible.

A further discussion concerning the vibration amplitude clearly is meaningless when the source is of constant velocity type.

5.8.5.2.2 Constant Force Source

Similarly, the situation where the force exerted on the receiver does not change by varying the receiver is theoretically acceptable. If, for all receivers, the same force is registered at the contact point as that registered when the source is operating on a perfectly rigid, immobile foundation, the source is termed a constant force source. Thus, the conditions to be fulfilled for characterizing the source as a constant force source is

$$|\underline{Y}_S| \gg |\underline{Y}_{R_i}| ; \forall i . \quad (5.146b)$$

In this situation

$$\underline{F}_R = \underline{F}_0 ,$$

where \underline{F}_0 is the force produced by the constant force source. Using the receiver mobility one obtains by substitution in Eq. (5.142) that

$$\underline{Q} = \frac{1}{2} |\underline{F}_0|^2 \underline{Y}_R \quad (5.147b)$$

Thus, for a given force the power transmission is reduced by a decreased receiver mobility. The phase of the complex power, in this case also, is that of the receiver mobility. Taking the real part of the complex power in (5.147b), it is seen that only the real part of the mobility is of interest. Hereby, the more reactive the receiver mobility, the less active power is transmitted.

With respect to the vibration amplitude at the contact point, Eq. (5.144) implies that

$$|\underline{v}| = |\underline{F}_0| |\underline{Y}_R| ,$$

which is obvious from the definition of the point mobility. Therefore, a reduction of the magnitude of the mobility in the case of a constant force source decreases the vibration amplitude.

5.8.5.2.3 Non-idealized Source

As pointed out, the two extremes analysed above are rarely found in practice. This is because structural design is conventionally based on static requirements, leading to structural elements of similar proportions. Therefore, it is important that the theoretical basis includes the common case of non-idealized sources.

Again, by assuming that the source can be suspended freely and operated under normal conditions, the velocity of the free source is registered at the contact point i.e., $\underline{v}_S = \underline{v}_{FS}$. As soon as it is connected, the receiver gives rise to a reaction force which acts on the source. With the convention of positive direction as in Fig. 5.26, the velocity at the connection point becomes $\underline{v}_S = \underline{v}_{FS} + \underline{Y}_S \underline{F}_S$. Analogously, the velocity at the contact point of the receiver is $\underline{v}_R = \underline{Y}_R \underline{F}_R$. With the interface conditions that the velocities are to be equal and that the forces must be equal in magnitude but opposing each other, one finds that

$$\underline{F}_R = \frac{\underline{v}_{FS}}{(\underline{Y}_S + \underline{Y}_R)} .$$

Physically this means that the velocity of the free source has to move both subsystems in the connected state. By means of the receiver mobility, the velocity of the receiver can be found to be

$$\underline{v}_R = \frac{\underline{v}_{FS}}{(\underline{Y}_S + \underline{Y}_R)} \underline{Y}_R.$$

Therefore, upon substitution in Eq. (5.142), the two previous relations give

$$\underline{Q} = \frac{|\underline{v}_{FS}|^2 \underline{Y}_R}{2 |\underline{Y}_S + \underline{Y}_R|^2}. \quad (5.148)$$

This result means that for the non-idealized source, both the source and receiver mobilities govern the power transmission. The phase of the complex power, however, has not been changed but is still equal to that of the receiver mobility.

The vibration amplitude at the contact point is obtained from

$$|\underline{v}_R| = \frac{|\underline{v}_{FS}| |\underline{Y}_R|}{|\underline{Y}_S + \underline{Y}_R|},$$

which states that a reduction is achieved principally by an increase of the source mobility simultaneously as the receiver mobility is decreased. The word principally is introduced since not only the magnitudes of the mobilities are involved but also the phases which affect the denominator.

The active power transmitted to the receiver is obtained as before by taking the real part of \underline{Q} yielding

$$W = \frac{1}{2} \frac{|\underline{v}_{FS}|^2}{|\underline{Y}_S + \underline{Y}_R|^2} \operatorname{Re}[\underline{Y}_R].$$

It is seen that besides the real part of the receiver mobility, the interaction between the source and the receiver is important. If e.g., both mobilities are essentially reactive of the same order of magnitude and, in addition, of opposite sign, then the denominator becomes fairly small and the active power transmitted grows drastically. It is thus demonstrated that as soon as the source and receiver mobilities are of the same order of magnitude, their interaction will be significant.

5.8.5.3 Transmission Elements

The most commonly applied technique to reduce structure-borne sound transmission in practice is the introduction of resilient transmission elements or vibration isolators. In other cases, aligning elements called

chocks (carefully grinded blocks of steel) are inserted but also pipes, cables and shallow air cavities must be regarded as transmission elements. Perhaps the most intuitive transmission element still is the isolator (rubber-, foam- or steel spring). As will be demonstrated, the introduction of resilient transmission elements should not be considered as a first step on the route towards a reduced transmission.

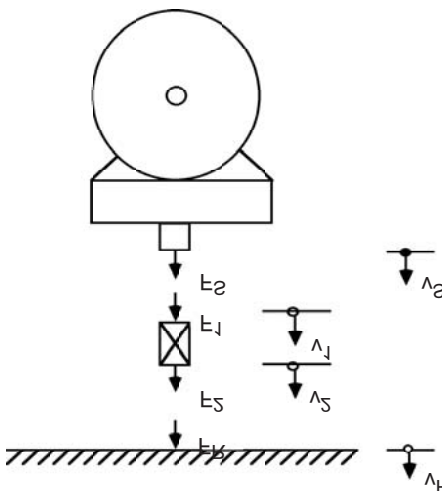


Fig. 5.26 Source-receiver interface involving a transmission element

Consider again the variables at the interface of the source and receiver, this time with a linearly elastic transmission element introduced, as shown in Fig. 5.26. By using the previously raised relations for the dynamic state at the contact point of the source and receiver,

$$\underline{v}_S = \underline{v}_{FS} + \underline{F}_S \underline{Y}_S, \quad \underline{v}_R = \underline{Y}_R \underline{F}_R,$$

together with

$$\underline{v}_1 = \underline{F}_1 \underline{Y}_{11} + \underline{F}_2 \underline{Y}_{12},$$

and

$$\underline{v}_2 = \underline{F}_2 \underline{Y}_{22} + \underline{F}_1 \underline{Y}_{21},$$

for the transmission element, the power transmitted to the receiver can be determined. In these equations \underline{Y}_{ij} are the point mobilities where both the excitation and the force are registered at the same end of the transmission element and \underline{Y}_{ij} are the transfer mobilities relating the excitation at one

end (j th) to the response at the other (i th). Hence, the transmission element is completely characterized (unidirectional motion) by its mobility matrix

$$\begin{bmatrix} \underline{Y}_T \end{bmatrix} = \begin{bmatrix} \underline{Y}_{11} & \underline{Y}_{12} \\ \underline{Y}_{21} & \underline{Y}_{22} \end{bmatrix}. \quad (5.149)$$

For a passive, linear element the reciprocity principle applies (cf. Chapter 2), which states that

$$\frac{\underline{v}_1}{F_2} = \frac{\underline{v}_2}{F_1}.$$

Accordingly, the transfer mobilities \underline{Y}_{12} and \underline{Y}_{21} are equal. If, in addition, the transmission element is symmetric, the two point mobilities are equal.

From the conditions at, now, the two interfaces

$$\underline{v}_S = \underline{v}_1, \quad F_S = -\underline{F}_1,$$

and

$$\underline{v}_R = \underline{v}_2, \quad F_R = -\underline{F}_2,$$

the force exerted on the receiver is found to be

$$\underline{F}_R = \frac{\underline{v}_{FS} \underline{Y}_{21}}{\left[(\underline{Y}_S + \underline{Y}_{11})(\underline{Y}_R + \underline{Y}_{22}) - \underline{Y}_{12} \underline{Y}_{21} \right]}.$$

The complex power transmitted to the receiver therefore becomes

$$\underline{Q} = \frac{(\tilde{v}_{FS})^2 |\underline{Y}_{21}|^2}{\left| (\underline{Y}_S + \underline{Y}_{11})(\underline{Y}_R + \underline{Y}_{22}) - \underline{Y}_{12} \underline{Y}_{21} \right|^2} \underline{Y}_R. \quad (5.150)$$

By introducing the complex power transmitted without any transmission element given in Eq. (5.148), (5.150) can be rewritten as

$$\underline{Q} = \underline{Q}_o \frac{|\underline{Y}_S + \underline{Y}_R|^2 |\underline{Y}_{21}|^2}{\left| (\underline{Y}_S + \underline{Y}_{11})(\underline{Y}_R + \underline{Y}_{22}) - \underline{Y}_{12} \underline{Y}_{21} \right|^2},$$

where the fraction represents the transmission efficiency τ for the transmission element given by

$$\tau = \frac{|\underline{Y}_S + \underline{Y}_R|^2 |\underline{Y}_{21}|^2}{\left| (\underline{Y}_S + \underline{Y}_{11})(\underline{Y}_R + \underline{Y}_{22}) - \underline{Y}_{12} \underline{Y}_{21} \right|^2}.$$

The transmission efficiency demonstrates the fact that a vibration isolation must be considered as a late step in reducing the power transmission since

generally the interaction (coupling) between the source and receiver mobilities will influence the efficiency. Note that the transmission efficiency is different from the force or displacement transmissibility [5.43], which considers control of one field variable only.

A special case of interest in conjunction with vibration isolation with resilient element is the case where a proper selection of installation points has been made on the assumption of a rigid installation. If then the introduction of resilient elements is considered, it is often possible to select a transmission element where all the mobilities are larger than those of the source and the receiver. In such a case, the transmission efficiency may be approximated by

$$\tau' = |\underline{Y}_S + \underline{Y}_R|^2 \frac{|\underline{Y}_{21}|^2}{|\underline{Y}_{11}\underline{Y}_{12} - \underline{Y}_{12}\underline{Y}_{21}|^2},$$

where the second factor is equal to the magnitude of the *transfer impedance* squared of the transmission element (the ratio of force at a blocked end to the velocity at the excited end).

This transfer impedance, in turn, will be mainly governed by the stiffness of the (resilient) transmission element. It is important to note, however, that the mobility mismatch condition implied often does not hold and therefore it is in general safer to resort to Eq. (5.150).

In some instances also, it may be very difficult to use resilient elements “springy” enough to ensure a small power transmission. This is, for example, the situation where the stability requirements or transient shock regulations are firm. Naturally, a too springy transmission element will create serious problems if internal or external excitation components appear close in frequency to that of the mounted resonance. So far, only one component of motion has been considered and it is worth emphasizing that in conjunction with stability questions the other components as well as coupled motion should be taken into account.

5.8.5.4 Matrix Formulation of the General Transmission Problem

As stated at the beginning, the general transmission problem concerns the description of power transmission between a source system and a receiving system via all connections (interfaces). Basically, these connections can be point-, line- or surface-like. The present analysis will be restricted to point-like connections where the assignment of discrete velocities and forces is appropriate.

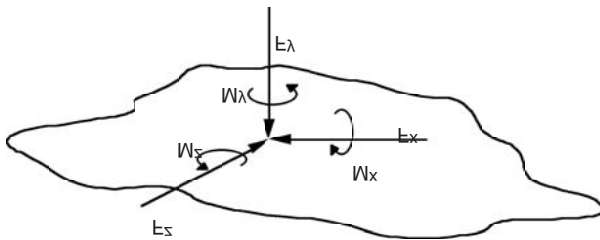


Fig. 5.27 Point excitation, general case

In the preceding sections the presumption of a single connection (contact point) and a single component of excitation and motion was made. It was pointed out, however, that such a condition is rarely encountered in practice. Rather, the general situation is that depicted in Fig. 5.27. This means that there will be 6 point mobilities required at each point. In addition, the general case comprises N contact points and it is reasonable to expect that what happens in one point is not unaffected by the processes at the others. Thus, the interaction illustrated Fig. 5.28 has to be taken into account. Accordingly there will be several transfer mobilities to take into account, $(N - 1)$ for each component. Moreover, as indicated in Fig. 5.28, an interaction may also take place between different components at different points and on top of all there is a possibility that the different components at the same point will interact. Hence, the two subsystems, the source and the receiver, structurally are characterized by two, $6N \times 6N$ mobility matrices.

For linear structures, the reciprocity principle implies that not only the matrices are square matrices but also symmetric about the main diagonal,

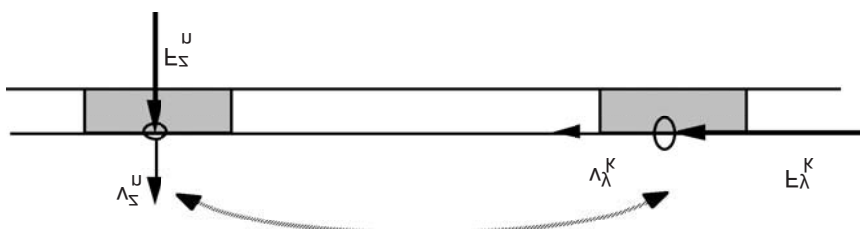


Fig. 5.28 Illustration of the interaction between different contact points.

i.e., $\underline{Y}_{ij} = \underline{Y}_{ji}$. Each matrix, therefore, consists of $(6N+1)3N$, generally unknown mobility elements.

In the assembled state, the field variables at the contact points can be represented by $\underline{\mathbf{v}}$ and $\underline{\mathbf{F}}$ i.e., the complex velocity and force vectors. Therefore, the total complex power in the general case is given by

$$\underline{Q} = \frac{1}{2} \underline{\mathbf{v}}^T \underline{\mathbf{F}}^*. \quad (5.151)$$

Using the mobility matrices for the source and receiver, $\underline{\mathbf{Y}}_S$, $\underline{\mathbf{Y}}_R$, one obtains

$$\underline{\mathbf{v}}_S = \underline{\mathbf{v}}_{FS} + \underline{\mathbf{Y}}_S \underline{\mathbf{F}}_S,$$

and

$$\underline{\mathbf{v}}_R = \underline{\mathbf{Y}}_R \underline{\mathbf{F}}_R,$$

which manifest similar forms as those of the single point case. As before, the conditions at the interface (multi-point) are given by

$$\underline{\mathbf{v}}_S = \underline{\mathbf{v}}_R, \quad \underline{\mathbf{F}}_S = -\underline{\mathbf{F}}_R,$$

such that

$$\begin{aligned} \underline{\mathbf{F}}_R &= \{\underline{\mathbf{Y}}_S + \underline{\mathbf{Y}}_R\}^{-1} \underline{\mathbf{v}}_{FS}, \\ \underline{\mathbf{v}}_R &= \underline{\mathbf{Y}}_R (\underline{\mathbf{Y}}_S + \underline{\mathbf{Y}}_R)^{-1} \underline{\mathbf{v}}_{FS}. \end{aligned}$$

This means that the total complex power is found from

$$\underline{Q} = \frac{1}{2} \left(\underline{\mathbf{v}}_{FS}^T \underline{\mathbf{Y}}_R^T (\underline{\mathbf{Y}}_S + \underline{\mathbf{Y}}_R)^{-1T} (\underline{\mathbf{Y}}_S + \underline{\mathbf{Y}}_R)^{-1*} \underline{\mathbf{v}}_{FS}^* \right). \quad (5.152)$$

In principle, the matrix expression (5.152) is straightforward but the solution involves formally an inversion and requires comprehensive computer facilities for the accurate handling of large numbers of contact points. The matrix elements are complex functions of frequency but not all are significant. Since the elements do not have the same dimension, the matrices must be conditioned prior to any evaluation. The incompatibility of the elements, of course, makes comparisons amongst the elements meaningless and thus any attempt to simplify such as by rank ordering the paths is cumbersome. These drawbacks and the intransparency of the matrix form regarding dominating paths and components of motion and excitation has promoted several studies of reformulations and approximations e.g., [5.44–5.46].

References

- [5.1] Gardonio P. and Brennan M.J., 2002. On the origins and development of mobility and impedance methods in structural dynamics. *Journal of Sound and Vibration*, 249, p. 557
- [5.2] Brownjohn J.M.W., Steele G.H., Cawley P. and Adams R.D., 1980. Errors in mechanical impedance data obtained with impedance heads. *Journal of Sound and Vibration*, 73, p. 461
- [5.3] Petersson B.A.T., 1984. The prerequisites for measuring mobility using annular transducer accessories. *Journal of Sound and Vibration*, 94, p. 495
- [5.4] Heckl M., 1956. Messungen an Schallbrücken zwischen Estrich und Rohdecke. *Acustica*, 6, p. 91
- [5.5] Elling W., 1954. Die Bestimmung grosser mechanischer Eingangsimpedanzen fester Körper im Frequenzband 50-3000 Hz, *Acustica*, 4, p 396
- [5.6] Muster D., 1958. Mechanical Impedance measurements. Colloquium on mechanical impedance methods for mechanical vibrations (R. Plunkett ed.). The American Society of Mechanical Engineers, Annual meeting, New York NY
- [5.7] Kuhl W., 1958. Über die akustischen und technischen Eigenschaften der Nachhallplatte. *Rundfunktechnische Mitteilungen*, 2, p. 111
- [5.8] Eggers F., 1959. Untersuchung von Corpus-Schwingungen am Violoncello. *Acustica*, 9, p. 453
- [5.9] Vogel S., 1956. Messleitungen für Biegewellen. *Acustica*, 6, p. 511
- [5.10] Scheuren J., 1989. Aktive Beeinflussung der Ausbreitung von Biegewellen. Diss. TU-Berlin, Berlin
- [5.11] Cremer H. and Cremer L., 1948. Theorie der Entstehung des Klopfschalls, *Frequenz*, 2, p. 61
- [5.12] Lamb H., 1904. On the propagation of tremors over the surface of an elastic solid. *Phil. Trans. Royal Society*, A203, p.1
- [5.13] Petersson B.A.T. and Heckl M., 1996. Concentrated excitation of structures. *Journal of Sound and Vibration*, 196, p. 295
- [5.14] Boussinesq J., 1885. Application des Potentiels à l'Etude de l'Equilibre et du Mouvement des Solides Elastiques. Gautier-Villars, Paris
- [5.15] Timoshenko S.P. and Goodier J.N., 1970. Theory of elasticity, Ch. 12. McGraw-Hill Book Company, Auckland
- [5.16] Johnson K.L., 1985. Contact Mechanics, Ch. 2. Cambridge University Press, New York NY
- [5.17] Heckl M., 1960. Untersuchungen an orthotropen Platten. *Acustica*, 10, p. 109
- [5.18] Ljunggren S., 1983. Generation of waves in an elastic plate by a vertical force and by a moment in the vertical plane. *Journal of Sound and Vibration*, 90, p. 559
- [5.19] Möser M., Heckl M. and Ginters K-H., 1986. Zur Schallausbreitung in flüssigkeitsgefüllten kreiszylindrischen Rohren. *Acustica*, 60, p. 34

- [5.20] Petersson B.A.T., 1992. Structural acoustic power transmission by point moment and point force excitation; Part 1: Beam- and frame-like structures. *Journal of Sound and Vibration*, 160, p. 43
- [5.21] Eichler E., 1964. Plate-edge admittances. *Journal of the Acoustical Society of America*, 36, p. 344
- [5.22] Petersson B.A.T., 1992. Structural acoustic power transmission by point moment and point force excitation; Part 2: Plate-like structures. *Journal of Sound and Vibration*, 160, p. 67
- [5.23] Stenzel H. and Brosze O., 1958. *Leitfaden zur Berechnung von Schallvorgängen*. Springer Verlag, Berlin
- [5.24] Hammer P. and Petersson B.A.T., 1988. Strip excitation; Part II: Upper and lower bounds for power transmission. *Journal of Sound and Vibration*, 129, p. 133
- [5.25] Petersson B.A.T. and Hammer P., 1991. Strip excitation of slender beams. *Journal of Sound and Vibration*, 150, p. 217
- [5.26] Courant R. and Hilbert D., 1953. *Methods of Mathematical Physics*, Vol. I. John Wiley & Sons, New York NY
- [5.27] Morse P.M. and Feshbach H., 1953. *Methods of theoretical physics*, Vol. 1, Chs. 5-8. McGraw-Hill, Boston MA
- [5.28] Rayleigh J.W.S., 1945. *Theory of sound* (2nd ed.), Vols. 1, 2. Dover Publications, New York NY
- [5.29] Petersson B.A.T., 1995. Building Acoustics, Vol. 2, 585-623. The liquid drop impact as a source of sound and vibration
- [5.30] Gösele K., Reiher H. and Jekle R., 1960. Schalltechnische Untersuchungen an Holzbalkendecken. *Berichte aus der Bauforschung*, Heft 14. Ernst & Sohn, Berlin
- [5.31] Morse P.M. and Feshbach H., 1953. *Methods of theoretical physics*, Vol. 1, Chs. 4. McGraw-Hill, Boston MA
- [5.32] Weck M. and Humpert R., 1989. Geräuschemission von Werkzeugmaschinen bie der Bearbeitung II. *Schriftenreihe Bundesanstalt für Arbeitsschutz*, Fb 582. Wirtschaftsverlag, Bremerhaven
- [5.33] McIntyre M.E., Schumacher R.T. and Woodhouse J., 1983. On the oscillations of musical instruments. *Journal of the Acoustical Society of America*, 74, p. 1325
- [5.34] Fingberg U., 1990. Ein Modell für das Kurvenquietschen bei Schienenfahrzeugen. *Fortschritt-Berichte VDI*, Reihe 11, 140
- [5.35] Heckl M.A. and Abrahams I.D., 2000. Curve squeal of trains, part 1: Mathematical model for its generation. *Journal of Sound and Vibration*, 229, p. 669
- [5.36] Remington P., 1987. Wheel/rail rolling noise, I: Theoretical analysis. *Journal of the Acoustical Society of America*, 81, p. 1805
- [5.37] Thompson D.J., 1993. Wheel-rail noise generation, part I: Introduction and interaction model. *Journal of Sound and Vibration*, 161, p. 387
- [5.38] Thompson D.J. et al., 1994. TWINS, Track-wheel interaction noise software. User manual and theoretical manual. TNO Institute of Applied Physics, Delft

- [5.39] Timoshenko S.P. and Young D.H., 1955. Vibration problems in engineering. D. van Nostrand Company Inc., Princeton
- [5.40] Petersson B. , 1990. Procedures for sound path quantification; definition of state-of-the-art. Part 5: Structure-borne sound transmission between machinery and foundations revisited; in particular rigid paths. Institute of Applied Physics, The Netherlands, TPD-SA-RPT-91-017
- [5.41] Sykes A.O., 1968. Development and application of linear multi-thermal network theory to vibration problems. Discs., The Catholic University of America, Washington D.C.
- [5.42] Mondot J-M. and Petersson B., 1987. Characterization of structure borne sound sources: The source descriptor and the coupling function. Journal of Sound and Vibration, 114, p. 507
- [5.43] Beranek L., 1976. Noise and Vibration Control. McGraw-Hill, New York NY
- [5.44] Petersson B. and Plunt J., 1982. On effective mobilities in the prediction of structure-borne sound transmission between a source structure and a receiving structure, Part I. Journal of Sound and Vibration, 82, p. 517
- [5.45] Moorhouse A. T. and Gibbs B. M., 1995. Towards a practical characterization for structure-borne sound sources based on mobility techniques. Journal of Sound and Vibration, 185, p. 737
- [5.46] R. A. Fulford and B. M. Gibbs, 1997. Structure-borne sound power and source characterisation in multi-point-connected systems, part 1: Case studies for assumed force distributions. Journal of Sound and Vibration, 204, p. 659

6 Attenuation of Structure-Borne Sound

6.1 Material and Cross-Sectional Changes

The previous chapter dealt with the most important aspects of excitation and transmission of structure-borne sound. It is thus logical to proceed with a consideration of the subsequent fate of the excited waves. Waves propagating along real structures soon encounter material or structural changes or both. At each such discontinuity, the incident wave is partially reflected such that the energy transmitted across is reduced. The discontinuity thus realizes some attenuation. The present chapter deals with these attenuating effects, which are of particular importance for structural design. It addresses the problem of predicting the inherent attenuation in a given structure and that of design.

It is clearly not possible to analyse all the various boundary conditions that occur in practice in detail. Only the most basic and typical will be discussed. Unfortunately, one cannot apply the results derived for these cases to other similar ones because small changes in boundary conditions can lead to large changes in the attenuation, as will be shown. The analyses presented, however, are expected to provide the general insight with which configurations not explicitly treated here can be dealt with.

In principle, all attenuation analyses follow the same route, which is also applicable for scattering problems.

- a) An incident wave of unit amplitude is prescribed.
- b) General wave fields with unknown coefficients (amplitudes) are assumed for the reflection and transmission respectively. With the exception of Sects. 6.5, 6.6 and 6.9 it is also assumed that the transmitted field consists of outward propagating and evanescent waves only.
- c) The boundary conditions are taken into account, through equality of velocities, forces (stresses) and moments at the discontinuity. Hereby the number of equations must equal the number of unknown amplitudes.
- d) The unknown coefficients of the reflected and transmitted wave fields are determined from the set of equations developed in c). Owing to the applicability of the superposition principle for linear proc-

esses, this means the simultaneous solution of a set of linear equations. For most cases in practice, the assumption of linear processes is justified. One exception is the thin plate undergoing large amplitude vibrations at low frequencies.

- e) By means of the amplitudes, determined in d), the energy based reflection and transmission efficiencies are calculated.

Since the attenuation of structure-borne sound mostly is frequency dependent, the analyses are carried out with waves at a frequency. For brevity, moreover, the operation $\text{Re} [\dots e^{j\omega t}]$ is omitted as is the under bar denoting a complex quantity.

6.1.1 Attenuation of Longitudinal Waves

The subsequent analysis, which is carried out for rods, is also valid for plates and normal incidence upon the discontinuity. The only modification is that Young's modulus E must be replaced by $E/(1 - \mu^2)$. Since $1 - \mu^2$ approximately amounts to 0.9, the difference will be negligible in most cases.

For the longitudinal wave experiencing a change in material properties and / or cross-section, the analyses is analogous to that of plane waves in ducts. Thus, the wave fields on either side of the discontinuity in Fig. 6.1 are set to be given by

$$\begin{aligned} v_1 &= v_{1+}e^{-jk_1x} + v_{1-}e^{+jk_1x} & ; \quad x \leq 0, \\ v_2 &= v_{2+}e^{-jk_2x} & ; \quad x \geq 0. \end{aligned} \quad (6.1)$$

According to Eq. (3.30), the axial forces are obtained as

$$\begin{aligned} F_1 &= Z_1 \left(v_{1+}e^{-jk_1x} - v_{1-}e^{+jk_1x} \right) & ; \quad x \leq 0, \\ F_2 &= Z_2 v_{2+}e^{-jk_2x} & ; \quad x \geq 0, \end{aligned} \quad (6.2)$$

where

$$Z_1 = \rho_1 c_{L1} S_1 \quad , \quad Z_2 = \rho_2 c_{L2} S_2 \quad (6.3)$$

are the wave impedances of the two parts and S_1 and S_2 are their cross-sectional surfaces respectively.

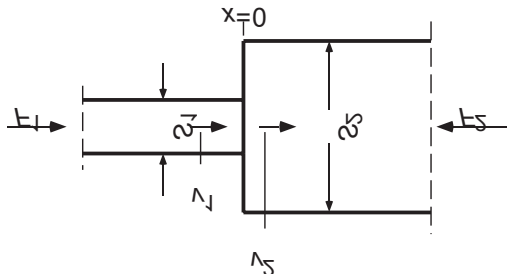


Fig. 6.1. Transmission of longitudinal waves at a cross-sectional area change of a rod

With a rigid connection at the discontinuity, the first boundary condition is

$$v_1(x=0) = v_2(x=0). \quad (6.4)$$

At the interface between the two parts, also the normal stresses would be equal. A small distance away, however, the total cross-sectional force will be distributed over a larger surface in the right hand part such the stress is reduced. This means that

$$F_1(x=0) = F_2(x=0) \Leftrightarrow -S_1\sigma_1(x=0_-) = -S_2\sigma_2(x=0_+). \quad (6.5)$$

By substituting (6.1) and (6.2) into (6.4) and (6.5), the amplitude of the transmitted wave is obtained as

$$v_{2+} = v_{1+} \frac{2Z_1}{Z_1 + Z_2}. \quad (6.6)$$

With the incident and transmitted power given by

$$W_{1+} = \frac{1}{2} \operatorname{Re}[Z_1] |v_{1+}|^2, \quad W_{2+} = \frac{1}{2} \operatorname{Re}[Z_2] |v_{2+}|^2, \quad (6.7)$$

the transmission efficiency $\tau = W_{2+}/W_{1+}$ is obtained as

$$\tau = \frac{Z_2}{Z_1} \left(\frac{2Z_1}{Z_1 + Z_2} \right)^2 = \frac{4}{\left(\sqrt{Z_1/Z_2} + \sqrt{Z_2/Z_1} \right)^2}. \quad (6.8)$$

This expression can also be derived from the ratio v_1/v_{1+} , obtained by eliminating v_{2+} , which defines the reflection coefficient r cf., Sects. 3.6 and 4.3. Thereby

$$r = \frac{Z_1 - Z_2}{Z_1 + Z_2}. \quad (6.9)$$

The square of this expression, which represents the ratio of reflected power to the incident, is termed the reflection efficiency

$$\rho = |r|^2. \quad (6.10)$$

Since the non-reflected power must equal that transmitted in the present case, the transmission efficiency can be obtained also as

$$\tau = 1 - \rho = 1 - |r|^2, \quad (6.11)$$

which subsequently leads to (6.8).

The relation in (6.11) is not valid for all attenuation problems, however. For discontinuities involving dissipative structural parts, the non-reflected part of the power encompasses both that dissipated and that transmitted.

The attenuation offered by a single cross-sectional area change is not particularly large. With the area ratio denoted by $\Delta = S_1/S_2$ for beams or $\Delta = h_1/h_2$ for plates introduced in (6.8),

$$\tau = \frac{4}{(\Delta^{-1/2} + \Delta^{1/2})^2}. \quad (6.8a)$$

The transmission loss, defined by

$$R = 10 \log(1/\tau) \text{ dB}, \quad (6.8b)$$

thus amounts to only 0.5 dB for an area ratio of 2. This estimate shows how limited the attenuation is also for substantial cross-sectional area changes as seen from a design point of view. It is to be noted that the transmission loss or transmission efficiency must be distinguished from changes of the observable field variables. From (6.6), for instance, it is clear that the reduction of the velocity across the discontinuity is markedly larger. It must be borne in mind, however, that this discrepancy also depends on the fact that the power is propagated over a larger cross-section. When subsequently the cross-section is reduced again, the field variables may rise in amplitude and the small attenuation is better depicted.

6.1.2 Attenuation of Bending Waves

For bending waves, analogies to the theory of airborne sound do not exist. This is already therein manifested that the number of boundary conditions

rises from two to four. In a case with pure bending wave transmission across a discontinuity, not only the transverse velocities and forces must be considered but also the rotations and moments as illustrated in Fig. 6.2. This means that at the interface

$$v_{y1} = v_{y2} \quad , \quad F_{y1} = F_{y2}, \quad (6.12)$$

as well as

$$w_{z1} = w_{z2} \quad , \quad M_{z1} = M_{z2}. \quad (6.13)$$

To satisfy these four boundary conditions, the solution assumed must consist of four unknown amplitudes. In Sect. 3.4.2 the complete reflection of bending wave was analysed. Besides the propagating waves appeared also evanescent waves (quasi-stationary nearfields) as solutions. Accordingly, the velocity fields must take the form

$$\begin{aligned} v_{y1} &= v_{1+} \left[e^{-jk_1 x} + r e^{jk_1 x} + r_j e^{k_1 x} \right] \quad ; x \leq 0 \\ v_{y2} &= v_{1+} \left[t e^{-jk_2 x} + t_j e^{-k_2 x} \right] \quad ; x \geq 0 \end{aligned} \quad (6.14)$$

The first condition in (6.12) thus means that

$$r + r_j - t - t_j = -1. \quad (6.15a)$$

Next step in the analysis consists of determining the rotational velocity w_z , the moment M_z and the cross-sectional force F_y . As shown in Sect. 3.3.1, these quantities are derivatives of the transverse velocity given by

$$w_z = \frac{\partial v_y}{\partial x}, \quad M_z = -\frac{B}{j\omega} \frac{\partial^2 v_y}{\partial x^2}, \quad F_y = \frac{B}{j\omega} \frac{\partial^3 v_y}{\partial x^3} \quad (6.16)$$

Upon substituting (6.14) and considering the conditions in (6.12) and (6.13) it is found that

$$jk_1 r + k_1 r_j + jk_2 t + k_2 t_j = jk_1, \quad (6.15b)$$

$$B_1 k_1^2 r - B_1 k_1^2 r_j - B_2 k_2^2 t + B_2 k_2^2 t_j = -B_1 k_1^2, \quad (6.15c)$$

$$-jB_1 k_1^3 r + B_1 k_1^3 r_j - jB_2 k_2^3 t + B_2 k_2^3 t_j = -jB_1 k_1^3, \quad (6.15d)$$

for the rotational velocities, the moments and the forces respectively.

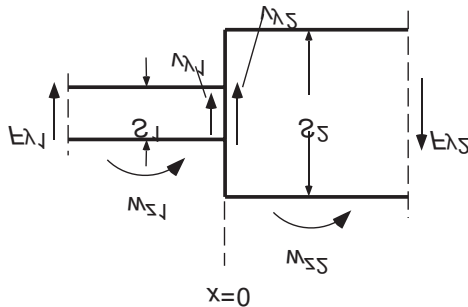


Fig. 6.2. Transmission of bending waves at a cross-sectional area change of a beam

Whilst the power transmission for longitudinal waves can be characterized by a single constant, the impedance ratio Z_1/Z_2 , there are always two such ratios necessary in the bending wave case. From the set of Eqs. (6.15), these can be identified as

$$\kappa = \frac{k_2}{k_1} = \sqrt[4]{\frac{m'_2 B_1}{m'_1 B_2}} = \frac{\lambda_1}{\lambda_2},$$

and

$$\psi = \frac{k_2^2 B_2}{k_1^2 B_1} = \sqrt{\frac{m'_2 B_1}{m'_1 B_2}}.$$

In the latter ratio, the quantities $(m'B)^{1/2}$ can be said to represent the characteristic impedance with respect to bending waves and will be termed the bending wave impedances

$$Z'_{B_1} = \sqrt{m'_1 B_1} \quad , \quad Z'_{B_2} = \sqrt{m'_2 B_1} .$$

The analogy to the impedance for longitudinal waves is incomplete, however, since the bending wave impedances do not represent the ratio between the force and velocity of a positively travelling wave but is rather a geometric mean of the force and moment impedances.

With the introduction of the ratios κ and ψ in (6.15) and developing the numerator and denominator determinants corresponding to the coefficients sought, one obtains the reflection coefficient for propagating waves as

$$r = \frac{2\psi(1-\kappa^2) - j\kappa(1-\psi)^2}{\kappa(1+\psi)^2 + 2\psi(1+\kappa^2)}, \quad (6.17)$$

and that with respect to reflected evanescent waves as

$$r_j = \frac{\kappa(1-\psi^2) - j\kappa(1-\psi^2)}{\kappa(1+\psi)^2 + 2\psi(1+\kappa^2)}. \quad (6.18)$$

Similarly, the transmission coefficient for propagating waves is found to be given by

$$t = \frac{2(1+\kappa)(1+\psi)}{\kappa(1+\psi)^2 + 2\psi(1+\kappa^2)}, \quad (6.19)$$

whereas that with respect to the nearfield is given by

$$t_j = \frac{2(1-\psi) - j2\kappa(1-\psi)}{\kappa(1+\psi)^2 + 2\psi(1+\kappa^2)}. \quad (6.20)$$

Of primary interest is of course the transmission efficiency. It can either be found from $1 - |r|^2$ or from multiplying t^2 by the ratio $(m'_2 c_2)/(m'_1 c_1) = \kappa\psi$ since the power is given by the product $m'c$ for a given velocity amplitude cf., Eq. (3.93). Irrespective of way, the transmission efficiency is obtained as

$$\tau = \left[\frac{2\sqrt{\kappa\psi}(1+\kappa)(1+\psi)}{\kappa(1+\psi)^2 + 2\psi(1+\kappa^2)} \right]^2. \quad (6.21)$$

In this context, the discussion will be limited to the case of equal material properties on either side of the discontinuity but with a change of the cross-sectional area or plate thickness respectively. By introducing the parameter Δ as defined in conjunction with Eq. (6.8a), κ becomes $\Delta^{-1/2}$ and ψ is Δ^2 . This means that the transmission efficiency simplifies to

$$\tau = \left[\frac{\Delta^{-5/4} + \Delta^{-3/4} + \Delta^{3/4} + \Delta^{5/4}}{\Delta^{-2}/2 + \Delta^{-1/2} + 1 + \Delta^{1/2} + \Delta^2/2} \right]^2, \quad (6.22)$$

which again is reciprocally symmetric.

In Fig. 6.3, the transmission efficiency for this case is shown together with that for longitudinal waves. Whilst the bending wave transmission occurs almost unimpeded for small area or thickness changes, it is seen that the increase in attenuation for large area or thickness ratios is larger

for bending waves than for longitudinal. Theoretically, the transmission efficiency amounts to 0.07 ($R = 23$ dB) for a ratio of $\Delta = 150$. Such an area change, however, which is hardly realistic from a practical point of view, would probably imply a violation of the assumptions underlying the theory and interface corrections would be required. For equal material properties, area or thickness ratios larger than 5 are hardly conceivable, furnishing a maximum attenuation of 3 dB.

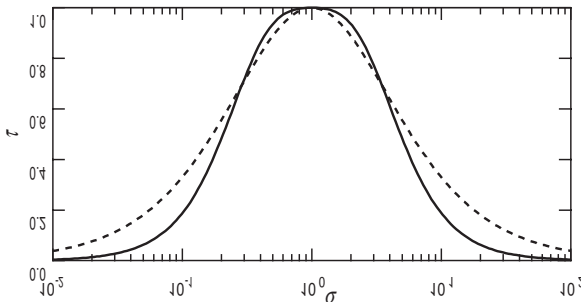


Fig. 6.3. Transmission efficiency of a cross-sectional area change as function of the area ratio. (---) bending and (- - -) longitudinal waves

The formula in (6.22) has been experimentally corroborated for sufficiently long beams [6.1]. It has also been successfully applied in the estimation of flanking transmission in building acoustic measurement facilities where the test wall is placed in an opening of a thick partitioning wall [6.2].

6.2 Right-Angled Corners and Branches

6.2.1 Incident Bending Wave

Of even greater practical importance than the previously discussed discontinuities established by changes in material properties or cross-sectional area are those established by structural components that meet at right angles. Such a configuration is realized, for example, by adjacent walls of a room, the ceiling or floor and the supporting walls and beams in a truss, see Fig. 6.4. To gain some insight into the corresponding phenomena is

considered a simple corner formed by two beams or plates, possibly with differing material properties and thicknesses. For a rigid connection such that a bending moment is transmitted, it follows that

$$M_{z1} = M_{z2}, \quad (6.23a)$$

as well as continuity in rotational velocity,

$$\omega_{z1} = \omega_{z2}. \quad (6.23b)$$

Thus, these two boundary conditions remain the same as in the previous section. With respect to the other boundary conditions, it must be observed that not only forces and velocities are present, which act perpendicular to the neutral layers of the adjoining structural components but also those that act parallel there to. This means that longitudinal waves arise with the associated transmission and reflection as discussed in Sect. 6.1.1.

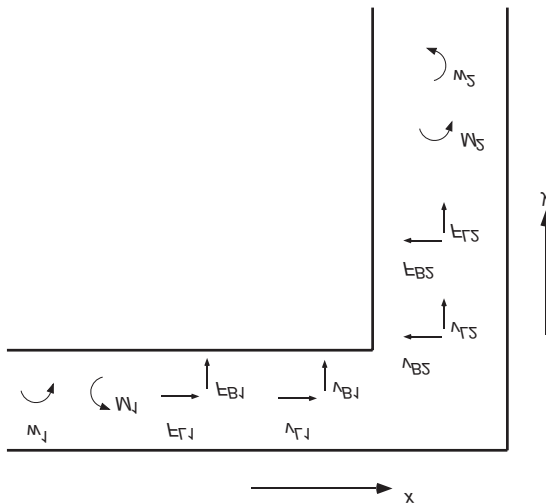


Fig. 6.4. Transmission at a flexurally rigid corner

With the notation introduced in Fig. 6.4, the field assumed for the horizontal part can be described by

$$\begin{aligned} v_{B_1}(x) &= v_{B_{1+}} \left(e^{-jk_1 x} + r e^{jk_1 x} + r_j e^{k_1 x} \right), \\ v_{L_1}(x) &= v_{B_{1+}} r_{BL} e^{jk_{1L} x}, \end{aligned} \quad (6.24a)$$

and for the vertical by

$$\begin{aligned} v_{B_2}(y) &= v_{B_{1+}} \left(t e^{-jk_2 y} + t_j e^{-k_2 y} \right), \\ v_{L_2}(y) &= v_{B_{1+}} t_{BL} e^{-jk_{2L} y}. \end{aligned} \quad (6.24b)$$

It is here observed that the incident wave is a flexural wave of amplitude $v_{B_{1+}}$ and that the longitudinal waves arising are propagating from the corner with amplitudes $v_{B_{1+}} r_{BL}$ and $v_{B_{1+}} t_{BL}$ respectively.

Besides the already in (6.23a,b) introduced boundary conditions, the following relations must hold

$$F_{L1} = -F_{B2}, \quad F_{B1} = F_{L2}, \quad v_{L1} = -v_{B2}, \quad v_{B1} = v_{B2}, \quad (6.23c-f)$$

where the sign is given by the chosen directions, see Fig. 6.4. The signs are selected such that by simply rotating the vertical part 90° the directions for the horizontal are preserved.

To determine the unknown reflection and transmission factors, the fields in (6.24) are substituted into (6.15) and into (3.30) regarding the longitudinal waves. By employing the boundary conditions in (6.23), the following set of linear equations is obtained

$$\begin{aligned} \frac{B_1 k_1^2}{B_2 k_2^2} (1 - r + r_j) &= -t + t_j, \\ \frac{k_1}{k_2} (-j + jr + r_j) &= -jt - t_j, \\ -\frac{E_1 S_1 k_{L1}}{\omega} r_{BL} &= -\frac{B_2 k_2^3}{j\omega} (jt - t_j), \\ \frac{B_1 k_1^3}{j\omega} (j - jr + r_j) &= -\frac{E_2 S_2 k_{L2}}{\omega} t_{BL}, \\ r_{BL} &= -(t + t_j), \\ 1 + r + r_j &= t_{BL}. \end{aligned}$$

With the abbreviations, defined above

$$\Psi = \frac{B_2 k_2^2}{B_1 k_1^2}, \quad \kappa = \frac{k_2}{k_1},$$

and additionally

$$\begin{aligned} \frac{E_1 S_1 k_{L1}}{B_2 k_2^3} &= \frac{m'_1 c_{L1}^2 \omega k_2^4}{c_{L1} \omega^2 m'_2 k_2^3} = \frac{m'_1 c_{L1}}{m'_2 c_{B2}} = \frac{1}{\beta_1}, \\ \frac{E_2 S_2 k_{L2}}{B_1 k_1^3} &= \frac{m'_2 c_{L2}}{m'_1 c_{B1}} = \frac{1}{\beta_2}, \end{aligned} \quad (6.25)$$

the equations for the reflections and transmissions factors reduce to

$$\begin{aligned} \frac{1}{\psi}(-1-r+r_j) &= -t+t_j, \quad \frac{1}{\kappa}(-j+jr+r_j) = -jt-t_j, \\ -\frac{1}{\beta_1}(t+t_j) &= t+jt_j, \quad 1-r-jr_j = \frac{1}{\beta_2}(1+r+r_j), \end{aligned} \quad (6.26)$$

when r_{BL} and t_{BL} are eliminated. After some further manipulations it is found that

$$\begin{aligned} t &= 2 \frac{\beta_1 + \beta_2 - j(1 - \beta_1 \beta_2)}{N}, \\ r &= \frac{\psi(1 - 2\beta_2 - \beta_1 \beta_2) + \kappa(1 + 2\beta_1 - \beta_1 \beta_2)}{N}, \\ &\quad + j \frac{\psi(1 + \beta_1 - \beta_1 \beta_2) - \kappa(1 - \beta_2 - \beta_1 \beta_2)}{N}, \end{aligned} \quad (6.27a, b)$$

$$\begin{aligned} r_j &= \frac{-1 + \beta_2 - r(1 + \beta_2)}{1 + j\beta_2}, \\ t_j &= \frac{-1 - \beta_1}{1 + j\beta_1} t, \end{aligned} \quad (6.27c, d)$$

wherein

$$\begin{aligned} N &= -\psi(1 + \beta_1 + 2\beta_2 + \beta_1 \beta_2) \\ &\quad - \kappa(1 + 2\beta_1 + \beta_2 + \beta_1 \beta_2) + j(\psi + \kappa)(1 - \beta_1 \beta_2). \end{aligned}$$

By observing that for the power propagated by flexural waves and by longitudinal waves

$$W_B = 2m'c_Bv_B^2, \quad W_L = m'c_Lv_L^2, \quad (6.28)$$

respectively, the reflection and transmission efficiencies are derived as

$$\begin{aligned} \rho_{BB} &= \frac{W_{B1-}}{W_{B1+}} = |r|^2, \quad \tau_{BB} = \frac{W_{B2}}{W_{B1+}} = \frac{2m'_2 c_{B2}}{2m'_1 c_{B1}} |t|^2 = \kappa \psi |t|^2, \\ \rho_{BL} &= \frac{W_{L1}}{W_{B1+}} = \frac{m'_1 c_{L1}}{2m'_1 c_{B1}} |r_{BL}|^2 = \frac{c_{L1}}{2c_{B1}} |1 + t_j|^2, \\ \tau_{BL} &= \frac{W_{L2}}{W_{B1+}} = \frac{m'_2 c_{L2}}{2m'_1 c_{B1}} |t_{BL}|^2 = \frac{1}{2\beta_2} |1 + r + r_j|^2. \end{aligned} \quad (6.29)$$

As expected from an energy conservation point of view and as is readily demonstrated by some small calculation

$$\rho_{BB} + \tau_{BB} + \rho_{BL} + \tau_{BL} = 1. \quad (6.30)$$

In Fig. 6.5 is exemplified the transmission efficiency τ_{BB} and the velocity ratio $|v_{B1+}|^2/|v_{B2}|^2$. The former quantity is a power ratio whereas the latter is a ratio between two mean square velocities. The velocity ratio constitute an easily measured quantity when the two structural parts are several wavelengths long and the receiver is moderately damped.

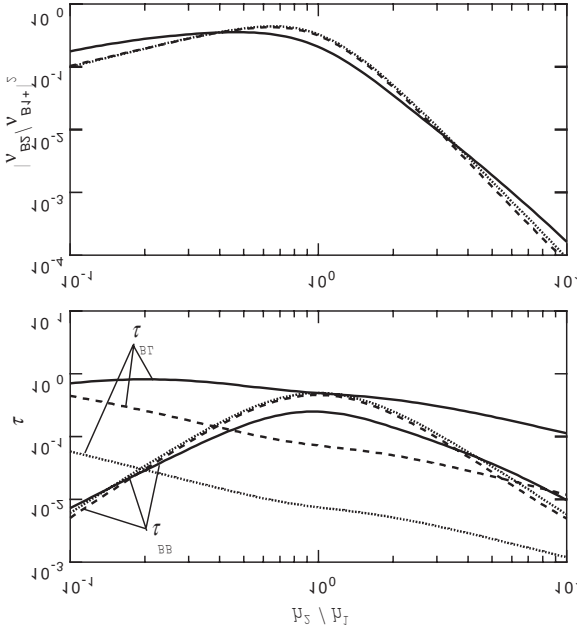


Fig. 6.5. Mean square velocity ratio and transmission efficiency for a bending wave incident upon a corner made up by beams of the same material. (....) $\sqrt{1.8h_l f / c_L} = 0.003$, (---) $\sqrt{1.8h_l f / c_L} = 0.03$ and (—) $\sqrt{1.8h_l f / c_L} = 0.3$

With equal thickness for the two parts, the different reflection and transmission efficiencies are plotted as functions of normalised frequency in Fig. 6.6. It is seen that for low frequencies, the coupling is small between bending and longitudinal waves, ρ_{BL} and τ_{BL} . The corresponding asymptotic values for ρ_{BB} and τ_{BB} are given by

$$\rho_{BB} \approx \frac{\psi^2 + \kappa^2}{(\psi + \kappa)^2}, \quad \tau_{BB} \approx \frac{2\kappa\psi}{(\psi + \kappa)^2}, \quad (6.31)$$

which are valid for β_1 and β_2 less than 0.05.

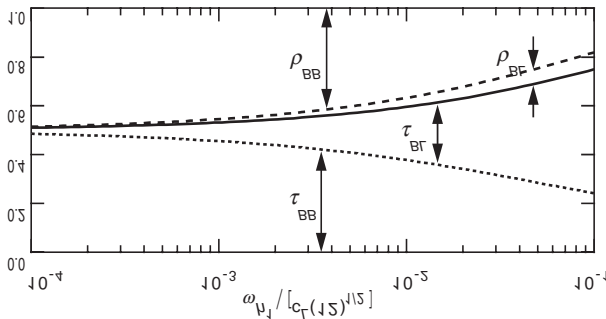


Fig. 6.6. Energy distribution for a bending wave incident upon a corner made up by two equal beams ($h_1 = h_2$)

6.2.2 Incident Longitudinal Wave

In the previous section the structure-borne sound transmission across a corner was considered for an incident bending wave. It was found that longitudinal waves were excited particularly at high frequencies. It is thus of interest to clarify the transmission of longitudinal waves, which are incident upon a corner. To obtain some insight, again two long beams or plates are joined at right angle. The analysis is almost identical to that for the incident bending wave. Specifically, the boundary conditions in (6.23a-f) remain valid. The only difference is that (6.24) is replaced by

$$\begin{aligned} v_{B1}(x) &= v_{L1+} \left(r e^{j k_1 x} + r_j e^{k_1 x} \right), \\ v_{L1}(x) &= v_{L1+} \left(e^{-j k_{1L} x} + r_{LL} e^{j k_{1L} x} \right), \\ v_{B2}(y) &= v_{L1+} \left(t e^{-j k_2 y} + t_j e^{-k_2 y} \right), \\ v_{L2}(y) &= v_{L1+} t_{LL} e^{-j k_{2L} y}. \end{aligned} \quad (6.32)$$

For the usually interesting case with equal thickness on either side of the corner, for which $\psi = \kappa = 1$ and $\beta_1 = \beta_2 = \beta$, the reflection and transmission efficiencies read

$$\begin{aligned}
 \tau_{LB} &= \frac{W_{B2}}{W_{L1+}} = \frac{5\beta + 8\beta^2}{2 + 6\beta + 9\beta^2} = \tau_{BL}, \\
 \rho_{LB} &= \frac{W_{B1}}{W_{L1+}} = \frac{\beta}{2 + 6\beta + 9\beta^2} = \rho_{BL}, \\
 \tau_{LL} &= \frac{W_{L2}}{W_{L1+}} = \frac{\beta^2}{2 + 6\beta + 9\beta^2} \ll \tau_{LB}, \\
 \rho_{LL} &= \frac{W_{L1-}}{W_{L1+}} = \frac{2}{2 + 6\beta + 9\beta^2} \ll \rho_{LB}.
 \end{aligned} \tag{6.33}$$

The relations $\tau_{LB} = \tau_{BL}$ and $\rho_{LB} = \rho_{BL}$ are found from a comparison with (6.29) or as a consequence of the reciprocity principle. The frequency dependencies of τ_{LB} , ρ_{LB} and τ_{LL} are shown in Fig. 6.7.

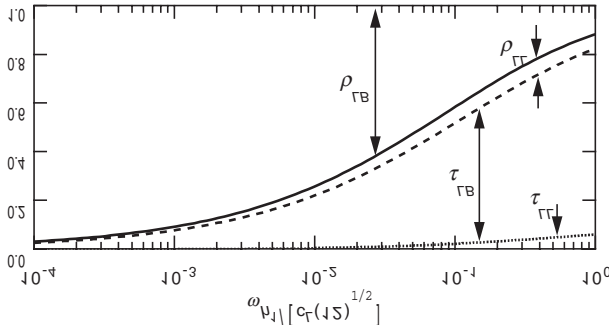


Fig. 6.7. Energy distribution for a longitudinal wave incident upon a corner made up by two equal beams ($h_1 = h_2$)

6.2.3 Right Angled Branches with Incident Bending and Longitudinal Waves

The analysis of structure-borne sound transmission at discontinuities was detailed in the two previous sections. Here T and $+$ junctions will be treated simultaneously. A T -junction can be considered as a crossing where one branch is missing.

With the notations defined in Fig. 6.8, the fields involved can be assumed as

$$\begin{aligned}
v_{B1}(x) &= v_{B1+} \left(A_B e^{-jk_1 x} + r e^{jk_1 x} + r_j e^{k_1 x} \right), \\
v_{L1}(x) &= v_{B1+} \left(A_L e^{-jk_{L1} x} + r_{BL} e^{jk_{L1} x} \right), \\
v_{B2}(y) &= v_{B1+} \left(t_2 e^{-jk_2 y} + t_{2j} e^{-k_2 y} \right), v_{L2}(y) = v_{B1+} t_{2BL} e^{-jk_{L2} y}, \\
v_{B3}(x) &= v_{B1+} \left(t_3 e^{-jk_3 x} + t_{3j} e^{-k_3 x} \right), v_{L3}(x) = v_{B1+} t_{3BL} e^{-jk_{L3} x}, \\
v_{B4}(y) &= v_{B1+} \left(t_4 e^{-jk_4 y} + t_{4j} e^{-k_4 y} \right), v_{L4}(y) = v_{B1+} t_{4BL} e^{-jk_{L4} y}.
\end{aligned} \tag{6.34}$$

In the set of equations above, a bending wave of amplitude A_B is incident from $x = -\infty$ as well as a longitudinal wave of amplitude A_L . If only one wave type is present, the amplitude of the other vanishes. v_{B1+} is a unit velocity which subsequently cancels. In analogy with (6.23 a-f), the boundary conditions in the case read

$$\begin{aligned}
M_1 &= M_2 + M_3 + M_4, \\
w_1 &= w_2, \quad w_1 = w_3, \quad w_1 = w_4, \\
F_{L1} &= -F_{B2} + F_{L3} - F_{B4}, \quad F_{B1} = F_{L2} + F_{B3} + F_{L4}, \\
v_{L1} &= -v_{B2}, \quad v_{L1} = v_{L3}, \quad v_{L1} = -v_{B4}, \\
v_{B1} &= v_{L2}, \quad v_{B1} = v_{B3}, \quad v_{B1} = v_{L4}.
\end{aligned} \tag{6.35}$$

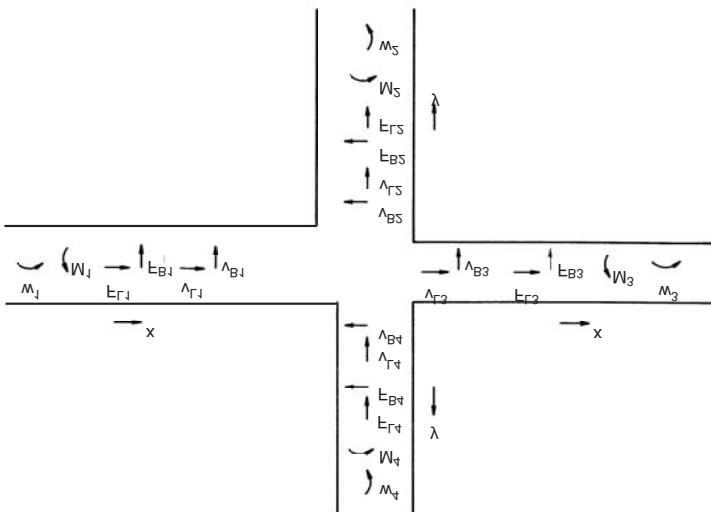


Fig. 6.8. Transmission at a rigid beam (plate) crossing

In total there are 12 equations for the 12 unknowns in the set (6.34), which after some evident simplifications leads to the linear set of equations

$$\mathbf{At} = \mathbf{b}, \quad (6.36)$$

besides the relations $t_{2BL} = t_{4BL} = A_B + r + r_j$ and $t_{3BL} = A_L + r_{BL}$. The coefficient matrix \mathbf{A} comprises the following elements

$$\begin{aligned} a_{11} &= -1 - \psi_3, \quad a_{12} = 1 - \psi_3, \quad a_{13} = 2\psi_2, \\ a_{14} &= 2\psi_3, \quad a_{15} = 2\psi_4, \quad a_{16} = \psi_2 + \psi_4, \\ a_{21} &= j, \quad a_{22} = 1, \quad a_{23} = (-1 + j)\kappa_2, \quad a_{26} = -\kappa_2, \\ a_{31} &= j + \kappa_3, \quad a_{32} = 1 + \kappa_3, \quad a_{34} = \kappa_3(-1 + j), \\ a_{41} &= j, \quad a_{42} = 1, \quad a_{45} = -\kappa_4(1 - j), \quad a_{46} = -\kappa_4, \\ a_{51} &= -1 - B_2 - jB_3 - B_4, \quad a_{52} = -j - B_2 - jB_3 - B_4, \\ a_{54} &= B_3(-1 + j), \quad a_{63} = L_2(-1 + j), \quad a_{65} = -L_4(1 - j), \\ a_{66} &= jL_2 + L_3 + jL_4 + 1, \end{aligned}$$

and \mathbf{t} is a column vector with the elements $\mathbf{t}^T = \{r \ r_j \ t_2 \ t_3 \ t_4 \ r_{BL}\}$. Also \mathbf{b} is a column vector where the elements are

$$\begin{aligned} b_1 &= A_B(1 + \psi_3) - A_L(\psi_2 + \psi_4), \quad b_2 = jA_B + A_L\kappa_2, \\ b_3 &= A_B(j - \kappa_3), \quad b_4 = jA_B - A_L\kappa_4, \\ b_5 &= A_B(-1 + B_2 + jB_3 + B_4), \quad b_6 = A_L(1 - jL_2 - L_3 - jL_4). \end{aligned}$$

The abbreviations used read

$$\begin{aligned} \psi_2 &= \frac{B_2 k_2^2}{B_1 k_1^2}, \quad \psi_3 = \frac{B_3 k_3^2}{B_1 k_1^2}, \quad \psi_4 = \frac{B_4 k_4^2}{B_1 k_1^2}, \\ \kappa_2 &= \frac{k_2}{k_1}, \quad \kappa_3 = \frac{k_3}{k_1}, \quad \kappa_4 = \frac{k_4}{k_1}, \\ L_2 &= \frac{m'_1 c_{B2}}{m'_1 c_{L1}}, \quad L_3 = \frac{m'_3 c_{L3}}{m'_1 c_{L1}}, \quad L_4 = \frac{m'_4 c_{B4}}{m'_1 c_{L1}}, \\ B_2 &= \frac{m'_2 c_{L2}}{m'_1 c_{B1}}, \quad B_3 = \frac{m'_3 c_{B3}}{m'_1 c_{B1}}, \quad B_4 = \frac{m'_4 c_{L4}}{m'_1 c_{B1}}. \end{aligned} \quad (6.37)$$

Figures 6.9 a,b show the results for some examples, partially displayed logarithmically as transmission loss. Therein, the practically common configuration is investigated for which the structural members 1 and 3 are equal as are 2 and 4 if present. In the legend to Fig. 6.9b are also supplied some asymptotic expressions which are valid for an incident bending wave ($A_L = 0$) and $1.8 h_1 f/c_L < 0.01$.

In Fig. 6.10 are additionally shown some measurements results [6.3], obtained for perspex beams. To reduce the influence of reflections in members 2, 3 and 4, the beam ends were embedded in a mix of sand and sawdust over a length of 2.5 m.

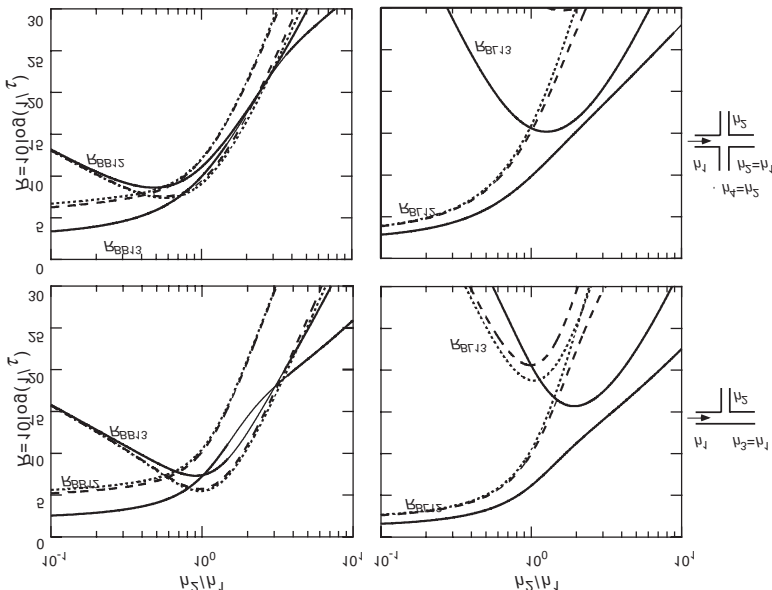


Fig. 6.9a. Transmission loss for a wall-crossing (top) and a T-junction (bottom) with all branches of the same material. Incident bending wave ($A_L = 0$). (....) $\sqrt{1.8h_l f / c_L} = 0.003$, (---) $\sqrt{1.8h_l f / c_L} = 0.03$ and (—) $\sqrt{1.8h_l f / c_L} = 0.3$

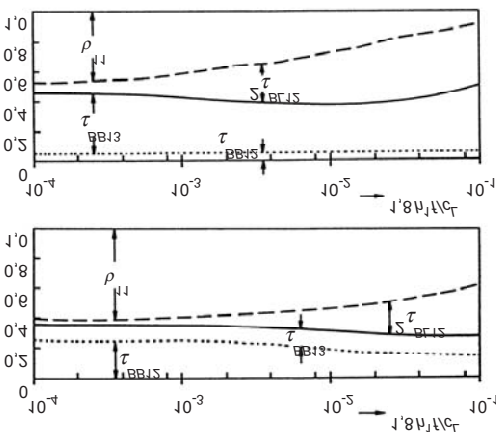


Fig. 6.9b. Energy distribution for bending waves incident upon a wall-crossing with all branches of the same material. Top: $h_2/h_1 = 0.316$. Bottom: $h_2/h_1 = 1$. ($\tau_{BL13} \approx 0$, $\rho_{BL11} \approx 0$). Asymptotic expressions for a wall-crossing

$$\begin{aligned}\tau_{BB12} &= 0.5 \left(\kappa_2 / \psi_2 + 2 + \psi_2 / 2\kappa_2 \right)^{-1}, \\ \tau_{BB13} &= 0.5 \left(1 + 2\psi_2 / \kappa_2 + \psi_2^2 / \kappa_2^2 \right)^{-1},\end{aligned}$$

and a *T*-junction

$$\begin{aligned}\tau_{BB12} &= \left(\sqrt{2\kappa_2 / \psi_2} + \sqrt{\psi_2 / 2\kappa_2} \right)^{-1}, \\ \tau_{BB13} &= \left(2 + 2\psi_2 / \kappa_2 + 0.5\psi_2^2 / \kappa_2^2 \right)^{-1}.\end{aligned}$$

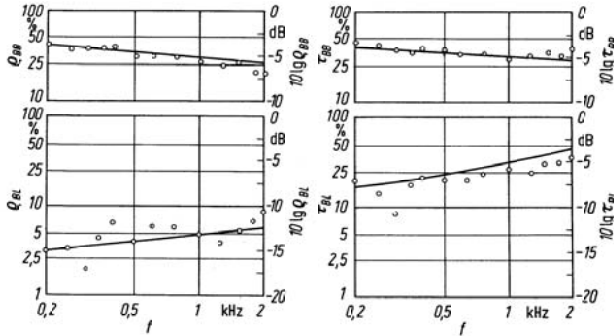


Fig. 6.10. Comparison of calculated (----) and measured (o) reflection and transmission efficiencies

Shown in Fig. 6.11 are some measured results for the velocity level difference between either side of a wall-crossing, which is a measure of the flanking transmission. Included in the figure are also calculated values for a brick wall crossing with $\rho = 1800 \text{ kg/m}^3$ and $c_L = 3000 \text{ m/s}$, which is very similar to concrete. It is to be noted for this comparison of calculated and measured results that whilst the calculations pertain to normal wave incidence on the crossing, many different angles of incidence are present in the measurements enhancing the transmission loss. On the other hand, the transmitted waves are partially reflected at subsequent discontinuities, which leads to lower than predicted transmission loss.

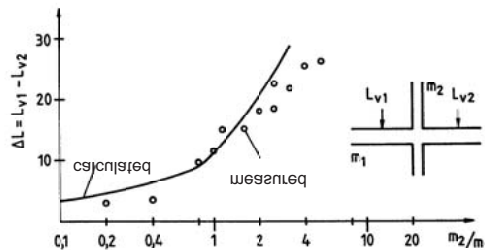


Fig. 6.11. Transmission loss at a wall-crossing with masses per unit area of m_1 and m_2 respectively. After [6.2]

6.3 Elastic Interlayers

The two previous sections show that a change in material, structural thickness and direction of structural parts do not lead to substantial structure-borne sound attenuation for practically conceivable changes. This finding is also in agreement with common experience, particularly from concrete buildings.

In order to achieve greater attenuation, special means are required such as use of elastic interlayers, which is the approach most commonly employed. The approach is based on the observation that large reflections are obtained by drastic changes in impedances as revealed by Eq. (6.9). Owing to the fact that primary structures made of steel or concrete are acoustically “hard”, only acoustically “soft” materials can provide useful attenuation. From this viewpoint an air gap (vacuum) between two solid structures would be optimal. Since such a separation is mostly unrealistic in practice from static considerations, acoustically soft but solid materials must be applied. It should be emphasized that although statically, an air gap is practically equivalent to a vacuum, this equivalence does not hold dynamically. This is so since the rapidly reversing displacements associated with a sound field make it impossible for the air to escape the gap, in contrast to the quasi-static situation where the air can flow laterally or through pores. Thus, the dynamic stiffness of an air gap approaches that of a cylinder with a tightly fitting piston. This stiffness is large enough to realize significant sound transmission.

6.3.1 Attenuation of Longitudinal Waves

The method chosen here to analyse the transmission through plane parallel layers is based on Sect. 6.1.1. In view of the mathematical labor it is not the most elegant. Thereby, the elastic layer is seen as a double change in material where the resulting multiple reflections are taken into account.

From Eq. (6.6), an incident longitudinal wave of amplitude v_{1+} gives rise to a wave in the interlayer with the velocity

$$v_{2\infty} = \frac{2Z_1}{Z_1 + Z_2} v_{1+} \quad (6.38)$$

whereby the index ∞ denotes that the expression is valid only for an infinitely extended receiving medium. When this primary wave reaches the other end of the interlayer, a transmitted wave arises and with the roles of Z_1 and Z_2 now interchanged, the velocity is

$$v_{3\infty} = \frac{2Z_2}{Z_1 + Z_2} v_{2\infty} = \frac{4Z_1 Z_2}{(Z_1 + Z_2)^2} v_{1+} \quad (6.39)$$

The transmission efficiency for such a transmission through an interlayer corresponding to a cascading of two similar discontinuities would thus be equal to the square of the transmission efficiency for one discontinuity given by Eq. (6.8). This reasoning, however, is not correct as can be expected from the fact that the length l of the interlayer does not appear in (6.39). Rather must be considered the fact that the primary wave in the interlayer, which is reflected over and over again at the two ends with the reflection factor

$$r = \frac{Z_2 - Z_1}{Z_1 + Z_2}, \quad (6.40)$$

loses energy at those reflections.

The resultant wave propagating in the positive x -direction hence is composed of an infinite number of components where their relative phases are determined by the total “round-trip” distance $2l$, the phase speed c_2 of the interlayer material and any phase changes produced at the reflection. Accordingly,

$$v_{2+} = v_{2\infty} \left(1 + r^2 e^{-j2k_2 l} + r^4 e^{-j4k_2 l} + \dots \right) \quad (6.41)$$

Since $r^2 < 1$, this geometric series converges to

$$v_{2+} = \frac{v_{2\infty}}{1 - r^2 e^{-j2k_2 l}}. \quad (6.42)$$

By applying Eq. (6.6) to this resultant wave that impinges at the far end of the interlayer, the wave transmitted to the remote part of the structure is obtained as

$$v_{3+} = v_{2+} e^{-jk_2 l} \frac{2Z_2}{Z_1 + Z_2} \quad (6.43)$$

where Z_2 and Z_1 are interchanged to adapt to the present case.

Upon combining Eqs. (6.38) and (6.40) to (6.43), the transmission efficiency sought is found to be given by

$$\tau = \left| \frac{v_{3+}}{v_{1+}} \right|^2 = \left| \frac{4Z_1 Z_2 e^{-jk_2 l}}{(Z_1 + Z_2)^2 - (Z_2 - Z_1)^2 e^{-2jk_2 l}} \right|^2 = \frac{1}{\cos^2 k_2 l + \frac{1}{4} \left(\frac{Z_1}{Z_2} + \frac{Z_2}{Z_1} \right)^2 \sin^2 k_2 l} \quad (6.44)$$

This relation, which is applicable for any interlayer, shows that total transmission i.e., $\tau = 1$, occurs not only for complete impedance matching where $Z_1 = Z_2$ but also for other impedance ratios when the sine function vanishes i.e., at $k_2 l = n\pi$. These thickness resonances corresponds to the natural vibrations of the interlayer cf., Sect. 3.4. The dissipative losses of elastic materials effectively prevent total transmission at the resonances. With the loss factor and complex wavenumber $k_2 = k_2 (1-j\eta)$ of Chapter 4 introduced, the first maxima of the transmission efficiency is approximately given by

$$\tau_{\max} = \frac{1}{1 + \frac{\pi\eta Z_1}{4Z_2}}. \quad (6.45)$$

This is valid provided the material properties are independent of frequency; a condition that is far from always fulfilled.

Most often, the elastic interlayers are so thin that the approximations $\cos k_2 l \approx 1 - (k_2 l)^2/2$ and $\sin k_2 l \approx k_2 l$ are valid. This means that the transmission efficiency in (6.44) takes the form

$$\tau = \frac{1}{1 - (k_2 l)^2 + \frac{1}{4} \left(\frac{Z_1}{Z_2} + \frac{Z_2}{Z_1} \right)^2 (k_2 l)^2}. \quad (6.46)$$

As is to be expected, the transmission efficiency decreases with increasing length or thickness of the interlayer. Since every dimension in a wave field should be compared with the governing wavelength and the wavelength of the longitudinal wave in the present case is inversely proportional to fre-

quency, the thickness dependence is the same as the frequency dependence. Moreover, it makes no difference whether Z_2 is greater or smaller than Z_1 or, if the materials are the same, whether the cross-sectional area of the interlayer is larger or smaller than that of the primary structure.

For an elastic layer or a cross-sectional reduction to realize a practically appreciable attenuation, Z_2 is always that small compared with Z_1 that (6.46) can be further simplified into

$$\tau = \left[1 + \left(\frac{Z_1 k_2 l}{2 Z_2} \right)^2 \right]^{-1} = \left[1 + \left(\frac{\omega Z_1 l}{2 E_2 S_2} \right)^2 \right]^{-1} = \left[1 + \left(\frac{\omega Z_1}{2 s_2} \right)^2 \right]^{-1}. \quad (6.47)$$

From the last expression it is clear that the stiffness $s_2 = E_2 S_2 / l$ of the thin interlayer controls the transmission.

One could have obtained the expression in (6.47) more simply by considering *á priori* only the stiffness of the interlayer. The forces on either side of the interlayer must then be equal

$$F_1 = F_{1+} + F_{1-} = F_3 \quad (6.48)$$

and related to its compression via its stiffness as

$$\frac{v_1 - v_3}{j\omega} = \frac{1}{S_2} F_3. \quad (6.49)$$

By noting that

$$v_1 = v_{1+} + v_{1-} = \frac{1}{Z_1} (F_{1+} - F_{1-}) \quad (6.50)$$

and

$$v_3 = \frac{F_3}{Z_1}, \quad (6.51)$$

Eq. (6.48) can be rewritten as

$$F_{1+} - F_{1-} = F_3 \left(1 + \frac{j\omega Z_1}{S_2} \right),$$

which together with (6.48) furnishes a relation between the incident and transmitted parts, from which the transmission efficiency in (6.47) is recovered.

As pointed out, the approach of summing the multiply reflected waves in (6.41) is not the most elegant. Alternatively, one may assume the force and velocity fields

$$\begin{aligned} v_2 &= Ae^{-jk_2x} + Be^{jk_2x}, \\ F_2 &= Z_2(Ae^{-jk_2x} - Be^{jk_2x}) \end{aligned} \quad (6.52)$$

for the interlayer and apply expressions corresponding to Eqs. (6.1) and (6.3) for the longitudinal waves before and after the layer. The resulting four unknown coefficients are then determined by the conditions of equality in force and velocity at the interfaces on either side of the elastic layer. Instead of (6.52) it would have been possible to write the velocity and force as

$$\begin{aligned} v_2(x) &= v_2(0)\cos k_2x - j\frac{F_2(0)\sin k_2x}{Z_2}, \\ F_2(x) &= -jZ_2v_2(0)\sin k_2x + F_2(0)\cos k_2x. \end{aligned} \quad (6.53)$$

Herein, $v_2(0)$ and $F_2(0)$ are the velocity and force at the incident side of the elastic layer respectively. This so called four-pole representation has some advantages when several finite rods and elastic layers are combined. For the airborne sound analogue of reactive silencer, the transmission theory of acoustic filters is far developed [6.4, 6.5].

6.3.2 Attenuation of Bending Waves

The finding that an elastic interlayer can be regarded as a partitioning spring for longitudinal waves at not too high frequencies, can be transferred to the case of incident bending waves. The simple bending wave theory is valid only for such frequencies. For an elastic interlayer of length comparable with the flexural wavelength, the analysis can be performed as described in conjunction with Eqs. (6.52) and (6.53). This means that the wave fields in the structures on either side of the elastic layer are assumed analogous to those in (6.14) and the field in the layer is described by (4.42) and (4.43) or (4.46). From continuity in motion and equilibrium of forces at the two ends of the layer, the unknown coefficients can be solved. It should be pointed out, however, that a limiting value process with respect to short or thin layers furnish an incorrect result because shear stiffness and rotational inertia are not encompassed by the simple bending theory. For such a limiting value process, Timoshenko theory must be employed.

As in the case of a single cross-sectional area change, the first two boundary conditions for a thin, mass-less, elastic layer are

$$F_{y1} = F_{y2} \quad , \quad M_{z1} = M_{z2}, \quad (6.54a)$$

since such a layer does not affect the transfer of forces and moments. The kinematic variables on the two sides of the elastic layer differ by the deformations of the layer, the latter of which are proportional to the forces and moments, meaning that

$$\nu_{y1} - \nu_{y2} = j\omega F_2 / K , \quad w_{z1} - w_{z2} = j\omega M_2 / C . \quad (6.54b)$$

In these relations, K is the shear stiffness and C the rotational stiffness, which, by means of Eqs. (3.42), (3.73) and (3.74), can be obtained via

$$\frac{F_{y2}}{K} = \frac{\nu_{y1} - \nu_{y2}}{j\omega} = \gamma l_z , \quad \frac{F_{y2}}{K} = \frac{1}{K} \int \tau dS = \frac{1}{K} \int G\gamma dS = \frac{G\gamma S}{K} , \quad (6.55a)$$

$$\Delta l_z = \frac{w_{z1} - w_{z2}}{j\omega} = \frac{\sigma l_z}{E} \Rightarrow \sigma = \frac{w_{z1} - w_{z2}}{j\omega} \gamma \frac{E}{l_z} , \quad (6.55b)$$

$$M_{zz} = \int \sigma y dS = \frac{w_{z1} - w_{z2}}{j\omega} \frac{E}{l_z} \int y^2 dS = \frac{w_{z1} - w_{z2}}{j\omega} \frac{EI}{l_z} . \quad (6.55c)$$

Herein, γ is the shear angle, τ the shear stress, Δl_z the change in length at the cross-sectional co-ordinate y and σ the normal stress also at this co-ordinate. Furthermore, E is the Young's modulus of the layer material, G its shear modulus, μ Poisson's ratio, l_z the equilibrium length of the layer, S its cross-sectional area and I the second area moment. By dividing (6.55a) by (6.55b) and comparing (6.55c) with (6.54b) it is found that

$$K = \frac{GS}{l_z} = \frac{E}{2(1+\mu)} \frac{S}{l_z} , \quad C = \frac{EI}{l_z} \left(= \frac{ESh^2}{12l_z} \right) , \quad (6.56)$$

with the last part of the second expression in (6.56) pertaining to rectangular cross-sections.

The proceeding steps of the analysis follow those in Sect. 6.1.2 i.e., (6.14) is substituted into (6.54a) and the unknown reflection and transmission coefficients are determined from the resulting set of linear equations. The, in this context, two most important coefficients read

$$\begin{aligned} r &= (-v + \varepsilon^2 v^3 + \varepsilon^2 v^4 / 2) / N , \\ t &= -j(4 + v - \varepsilon^2 v^3) / N , \end{aligned} \quad (6.57)$$

where $N = (v + \varepsilon^2 v^3) - j(4 + v - \varepsilon^2 v^3 - \varepsilon^2 v^4 / 2)$ and the abbreviations

$$v = \frac{k_1 B_1}{C} = \frac{k_1 l_z E_1}{E} \left(= \frac{k_1 h}{2\varepsilon} \right) , \quad \varepsilon = \frac{C}{B_1} \sqrt{\frac{C}{K}} = \frac{E}{E_1 l_z} \sqrt{\frac{2I(1+\mu)}{S}} \left(\approx \frac{E}{E_1} \frac{h}{2l_z} \right) \quad (6.58)$$

with the expressions within brackets referring to rubber-like interlayers with $\mu \approx 0.5$ of rectangular cross-section and with the same cross-sectional area as the primary structure.

Provided the interlayer can be regarded as loss-free i.e., E and G are real-valued, the expressions in (6.57) can be shown to possess the following characteristics:

- a) Energy conservation

$$|r|^2 + |t|^2 = 1, \quad (6.59a)$$

- b) orthogonality

$$|r + t| = 1. \quad (6.59b)$$

Together with (6.59a), this means that the phasors r and t are perpendicular.

- c) Vanishing attenuation at low frequencies or for stiff interlayers since for $v \sim k_1 l_z \rightarrow 0$ and thence $\sqrt{\omega} l_z \rightarrow 0$,

$$t \rightarrow 1 - jv / 4. \quad (6.59c)$$

- d) Attenuation proportional to $\sqrt{\omega}$ at high frequencies since

$$t \rightarrow 2/v \sim 1/k_1 l_z \sim 1/\sqrt{\omega}$$

for $v \rightarrow \infty$. This frequency dependence is hardly attainable in practice since the elementary bending theory ceases to be valid.

- e) Existence of total transmission since the reflection factor vanishes for

$$-v + \varepsilon^2 v^3 + \varepsilon^2 v^4 / 2 = 0 \Rightarrow v^3 + 2v^2 = 2/\varepsilon^2 \quad (6.59e)$$

A good approximation of (6.59e) is

$$v_{\text{tr}} \approx \sqrt[3]{2/\varepsilon^2} \quad (6.59f)$$

since $E \ll E_1$ and most commonly therefore $\varepsilon \ll 1$.

- f) Existence of total attenuation since the transmission factor vanishes for

$$4 + v - \varepsilon^2 v^3 = 0 \quad (6.59g)$$

A good approximation or first iteration for (6.59g) is

$$v_{\text{ta}} \approx 1/\varepsilon \quad (6.59h)$$

From (6.58) one finds the corresponding bending wavelength to be

$$\lambda_{lta} \approx \pi h$$

for a rectangular cross-section. This value is always beyond the limit of applicability of the elementary bending theory.

The existence of total reflection and total transmission, does not mean, however, that the discontinuity is motionless or follows precisely the motion of the incident wave respectively at the corresponding frequencies. Rather, the propagating and evanescent waves combine in such a way that the motion of the discontinuity avert transmission and reflection of energy respectively.

Indeed, it is possible to realize trapped modes in a very long beam equipped with two identical elastic interlayers, sufficiently far apart to ensure negligible evanescent waves. This is a vibration for which the energy is confined to the region between the layers. For longitudinal waves in one-dimensional wave guides, evanescent waves do not occur and hence total reflection does not exist such that trapped modes cannot be realized.

Figure 6.12 shows the bending wave transmission loss for some examples of elastic interlayers. The cross-section is taken to be rectangular. The frequency of total transmission is clearly seen whereas that of total attenuation falls outside the range of validity, given by $hf/c_L < 0.05$. The positively sloping part of the curves is acceptably approximated by

$$R_B \approx \left[16 - 20 \log(\varepsilon) + 30 \log\left(\frac{hf}{c_L}\right) \right] \text{dB} \quad (6.60)$$

Also included are the measured results from [6.6], which demonstrate a good agreement between theory and experiment.

A similar approximation for longitudinal waves is readily obtained from (6.46) as

$$R_L = 10 \log\left(\frac{1}{\tau_L}\right) \approx \left[10 - 20 \log(\varepsilon) + 20 \log\left(\frac{hf}{c_L}\right) \right] \text{dB} \quad (6.61)$$

which is valid for the range in which $R_L > 6$ dB. Since hf/c_L in the present analysis is consistently much less than unity, the transmission loss in (6.60) is always smaller than that of (6.61). Accordingly, longitudinal waves are more easily attenuated by means of elastic interlayers than bending waves.

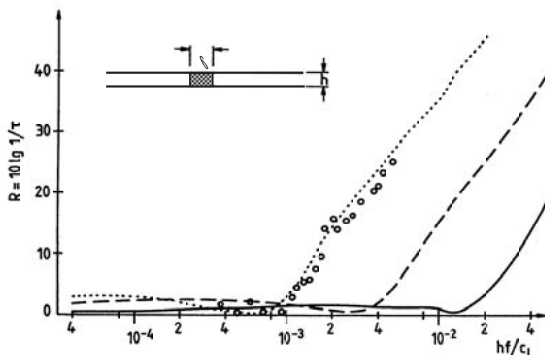


Fig. 6.12. Bending wave transmission loss for some different elastic interlayers. (....) $\epsilon = 10^{-4}$, (- - -) $\epsilon = 10^{-3}$ and (----) $\epsilon = 10^{-2}$. o o o measured values from [6.6]

6.4 Blocking Masses

Although elastic interlayers in structures may be very effective for the attenuation of structure-borne sound, they entail a considerable disadvantage in that they reduce the static structural stability. The elastic layers are necessarily more compliant than the primary structural components and hence cannot be used in load-carrying structural members. Any rigid connection in parallel with the elastic layer deteriorates the attenuation even if it is only a single nail or screw.

Even more impractical would be elastic interlayers in ship structures. Not only must the static stability be guaranteed but also is required that the structure is water tight. Ship structures obviously must be continuous. It is well known from continuous pipes or ducts that the structure-borne sound transmission is profound, partially due to the limited internal losses in commonly used materials. By analogy, it would be expected that the structure-borne transmission between bow and stern be large. Surprisingly, however, this is not the case as is demonstrated by measurements, particularly for high frequencies. Evidently, the many stiffeners or ribs that interrupt the continuity of the hull each reflect some incident energy such that a considerably net attenuation is obtained.

6.4.1 Attenuation of Longitudinal Waves

The effects of blocking masses on longitudinal waves can be straightforwardly determined from Eq. (6.44), applicable for transmission through arbitrary material or area changes. By letting Z_2 become large compared with Z_1 , (6.44) reduces to

$$\tau = \left[1 + \left(\frac{Z_2 k_2 l_z}{2 Z_1} \right)^2 \right]^{-1} = \left[1 + \left(\frac{\omega m}{2 Z_1} \right)^2 \right]^{-1}. \quad (6.62)$$

Herein,

$$m = Z_2 l_z / c_2 = \rho S l_z, \quad (6.63)$$

is the mass of the interlayer, now acting as a blocking mass. The transmission efficiency also could have been derived from Eq. (6.2) subject to the boundary conditions

$$v_1 = v_2, \quad F_1 - F_2 = j\omega m v. \quad (6.64)$$

The subsequent analysis amounts to the solution of a set of linear equations.

Somewhat discouraging, however, the transmission efficiency for longitudinal waves according to (6.62) is close to unity even for substantial masses.

6.4.2 Attenuation of Bending Waves – Symmetric Blocking Masses

With respect to bending waves, the situation is more favourable. For such waves, even a single mass can produce substantial attenuation in the audible frequency range. This is due to the total reflection effect, discussed in Sect. 6.3.2, and which is specific for the bending wave. Thereby, the wave energy is fully obstructed whilst the mass motion as well as the forces remain finite. Also the inverse effect occurs for blocking masses. This total transmission appears below the total reflection in frequency, which means that a single mass acts like a low-pass filter [6.7].

The analysis of the attenuation realized by blocking masses of mass m and mass moment of inertia Θ is analogous to that described in Sect. 6.3.2. The only modification necessary is to replace the boundary conditions in (6.54a,b) by

$$\begin{aligned} v_{y1} &= v_{y2} \quad , \quad w_{z1} - w_{z2} \\ F_{y1} - F_{y2} &= j\omega m v_{y2} \quad , \quad M_{z1} - M_{z2} = j\omega \Theta w_{z2} \end{aligned} \quad (6.65)$$

This means that the motion on either side of the rigid mass is the same whereas the forces and moments differ by the translational and rotational inertia respectively. By employing (6.14) and (6.16), the application of the boundary conditions again yields a set of linear equations, from which the reflection and transmission coefficients are solved. Alternatively, use can be made of the conversions

$$\begin{aligned} \Theta &\rightarrow 1/K \quad , \quad m \rightarrow 1/C \quad , \quad m' = \rho S \rightarrow 1/B, \\ v_y &\rightarrow -jM_z \quad , \quad w_z = jF_y, \end{aligned}$$

with which (6.65) is turned into (6.54) and the results of the analysis in Sect. 6.3.2 can be transferred directly. Irrespective of the approach, the result can be written as

$$\begin{aligned} r &= (-\mu + \vartheta^2 \kappa^3 + \vartheta^2 \kappa^4/2)/N, \\ r_j &= [(-\vartheta^2 \kappa^3 - \vartheta^2 \kappa^4/2) + j(\kappa - \vartheta^2 \kappa^4/2)]/N, \\ t &= -j(4 + \kappa - \vartheta^2 \kappa^3)/N, \\ t_j &= (\vartheta^2 \kappa^3 + j\kappa)/N, \\ N &= (\kappa + \vartheta^2 \kappa^3) - j(4 + \kappa - \vartheta^2 \kappa^3 - \vartheta^2 \kappa^4/2). \end{aligned} \quad (6.66)$$

Moreover are introduced the abbreviations

$$\kappa = k_1 \frac{m}{m'} \quad , \quad \vartheta = \frac{m}{m'} \sqrt{\frac{\Theta}{m}}, \quad (6.67)$$

cf., Eqs. (6.57) and (6.58).

The most important factors in this context r and t can be shown to possess the following characteristics:

a) Energy conservation

$$|r|^2 + |t|^2 = 1. \quad (6.68a)$$

b) Orthogonality

$$|r + t| = 1. \quad (6.68b)$$

c) Vanishing attenuation at low frequencies and for small masses provided also the square of the radius of gyration Θ/m is small, which is typically the case. For $\kappa \sim k_1 m / m' \rightarrow 0$ and thus $\sqrt{\vartheta} \rightarrow 0$,

$$t \rightarrow 1 - j\kappa / 4. \quad (6.68c)$$

d) Attenuation proportional to $\sqrt{\omega}$ at high frequencies since

$$t \rightarrow 2/\kappa \sim 1/\sqrt{\omega} \quad (6.68d)$$

for large κ .

e) Existence of total transmission since the reflection coefficient vanishes for

$$\kappa^3 + 2\kappa^2 = 2/\vartheta^2. \quad (6.68e)$$

f) Existence of total reflection since the transmission coefficient vanishes for

$$4 + \kappa - \vartheta^2 \kappa^3 = 0. \quad (6.68f)$$

An approximation for the roots to this equation or a valid initial value for an iterative solution is given by

$$\kappa_{ta} \approx 2 + 1/\vartheta. \quad (6.68g)$$

After substitution of κ and ϑ , (6.68g) corresponds to a wavelength of

$$\lambda_{ta} = 2\pi \sqrt{\Theta/m}. \quad (6.68h)$$

g) With the beam simply supported at a point, this corresponds to a configuration for which $\vartheta \rightarrow 0$ and $\kappa \rightarrow \infty$. Thence,

$$t = -j(1-j) \quad (6.68i)$$

which leaves a transmission loss of 3 dB.

As for the elastic interlayer, the existence of a frequency of total transmission and an always higher frequency of total reflection implies particular combinations of propagating and evanescent waves at the blocking mass. Similarly, trapped modes can appear in this case as well.

In Fig. 6.13, the transmission loss is shown for some different blocking masses, symmetrically attached with respect to the neutral layer of the beam. For these examples as well, the structural cross-section is taken to be rectangular and the equally rectangular masses are of the same material as the primary structure.

As is seen, the frequency of total reflection is clearly manifested for all examples. In contrast the frequency of total transmission is less obvious in the figure since the transmission loss is usually smaller than 0.5 dB below this frequency.

The transmission loss is well approximated by

$$R_B \approx 10 \log \left(\frac{\kappa^2}{4} \right) = 7.5 + 20 \log \left(\frac{m}{\rho_1 h_1^2} \right) + 10 \log \left(\frac{h_1 f}{c_L} \right) \quad (6.69)$$

in the range roughly two octaves above the frequency of total reflection. For comparison, Eq. (6.62) leads to the transmission loss

$$R_L = -10 \log \left[1 + \left(\frac{\pi h_1 f}{c_L} \frac{m}{\rho_1 h_1^2} \right)^2 \right] \quad (6.70)$$

for longitudinal waves. In these expressions, the blocking masses are taken per unit width.

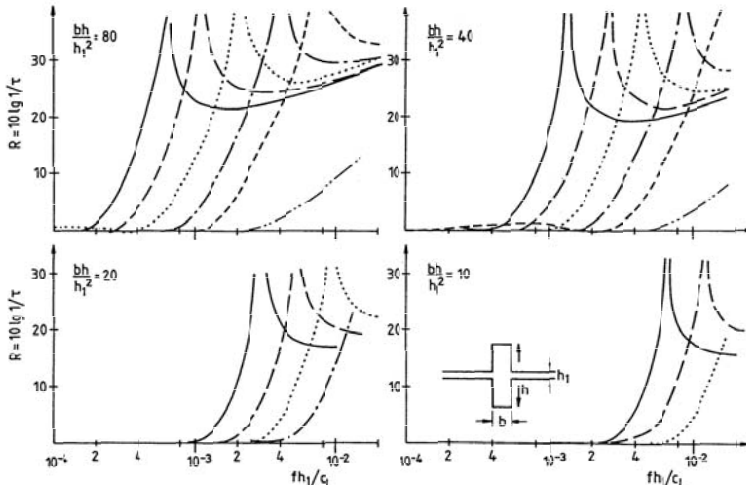


Fig. 6.13. Bending wave attenuation for symmetrically attached, rectangular blocking masses of the same material as the beam. (- - -) $h/b = 1$, (- - - -) $h/b = 2$, (....) $h/b = 4$, (— —) $h/b = 8$, (—) $h/b = 16$ and (- - - - -) longitudinal wave attenuation

It should be pointed out that the attenuation is drastically reduced when the masses or their attachment to the beam are not perfectly rigid. In such a case, all material points do not participate fully in the rotational motion. Ultimately, the effect of a blocking mass relies on the beam being “clamped” at a position, which is possible only if beam and mass constitute a unit. The clamping refers, of course, to both the translational and the

rotational motion. It is insufficient, for instance, with a vanishing translation but a finite rotational stiffness of the attachment. This is shown by the specific case with a pivoted blocking mass for which $\Theta = 0$ and thus $\vartheta \approx 0$. Under such conditions, Eq. (6.66) yields

$$t \approx -j \frac{4+\kappa}{\kappa - j(4+\kappa)} \Rightarrow |t|^2 = \tau = \frac{1}{1+\kappa^2/(4+\kappa)} > 0.5$$

The corresponding transmission loss is only about 3 dB, a result, moreover, also found for a crossing of a stiff and a flexible beam, see R_{BB13} in Fig. 6.9a.

Figure 6.14 displays two additional measurements results. The first represents a blocking mass as rigidly connected as possible whereas the second is connected with a finite rotational stiffness allowing for a difference in rotational velocity between the mass and the beam.

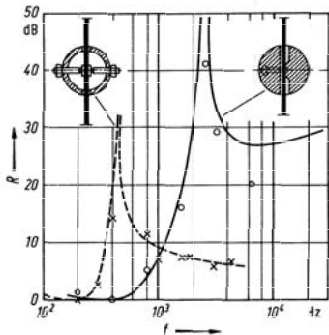


Fig. 6.14. Measured and calculated transmission loss for symmetrically attached blocking masses. (oooo) rigid connection and (xxxx) flexible connection

The influence of the finite rotational stiffness can readily be taken into account in the analysis by generalizing the boundary conditions in (6.65) to encompass arbitrary force and moment impedances for the blocking element. The two last equations in (6.65) are thereby replaced by

$$F_{y1} - F_{y2} = Z_{Fv} v_{y2} \quad , \quad M_{z1} - M_{z2} = Z_{Mw} w_{z2} \quad (6.71)$$

The alteration has no effect on the final Eqs. (6.66) provided that

$$\kappa = -j \frac{k_1 Z_{Fv}}{\omega m'} = -j \frac{Z_{Fv}}{m' c_B} \quad , \quad \vartheta = j\omega \frac{m'}{Z_{Fv}} \sqrt{\frac{Z_{Mw}}{Z_{Fv}}} \quad (6.72)$$

For the flexible connected mass of mass moment of inertia Θ , the moment impedance can be written

$$Z_{Mw} = \frac{M}{w} = j\omega\Theta \frac{1}{1 - (\omega/\omega_0)^2} \quad (6.73)$$

where $\omega_0^2 = s_w/\Theta$ is the square of the rotational resonance frequency with s_w being the rotational stiffness of the connection. Upon substituting (6.73) into (6.72) the dashed curve in Fig. 6.14 is obtained where the resonance frequency is taken to be $\omega_0 = 1000\pi$. By appropriately selecting the rotational stiffness of the connection, the frequency of total reflection can be shifted substantially downwards in frequency. Such a shift, however, is always on behalf of the bandwidth and the high frequency attenuation.

6.4.3 Attenuation of Bending Waves – Eccentric Blocking Masses

The eccentric blocking mass differs from the symmetric in one pivotal aspect. With an eccentrically located centre of gravity as depicted in Fig. 6.15, the forced rotation due to the flexural wave leads to an axially orientated acceleration. This means that an axial force is exerted on the beam resulting in a secondary longitudinal wave. The effect has been examined experimentally [6.8] in a reciprocal manner. By means of an incident longitudinal wave, a secondary flexural wave was catalyzed, which is more easily registered experimentally. This is so since for a primary flexural wave, the conversion can be described by

$$\tau_{BL} = \frac{c_L v_{2L+}^2}{2c_B v_{1B+}^2}, \quad (6.74)$$

whereas the equally large transmission efficiency for a primary longitudinal wave reads

$$\tau_{LB} = \frac{2c_B v_{2B+}^2}{c_L v_{1L+}^2}. \quad (6.75)$$

It follows that the measured velocity level differences are given by

$$[\Delta L_{v+}]_{BL} = 20 \log \frac{v_{1B+}}{v_{2L+}} \text{dB} = R_{BL} + 10 \log \frac{c_L}{2c_B} \text{dB} \quad (6.76a)$$

and

$$[\Delta L_{v+}]_{LB} = 20 \log \frac{v_{1L+}}{v_{2B+}} \text{ dB} = R_{LB} - 10 \log \frac{c_L}{2c_B} \text{ dB} \quad (6.76b)$$

in the two situations respectively, whereby

$$R_{BL} = 10 \log \frac{1}{\tau_{BL}} = R_{LB} = 10 \log \frac{1}{\tau_{LB}}. \quad (6.76c)$$

Whilst the secondary, longitudinal velocity can be lower than the background noise in the first situation, the primary, longitudinal and secondary, bending velocities are of the same order of magnitude. Alike many other, this example shows the great value of the reciprocity principle for experiments.

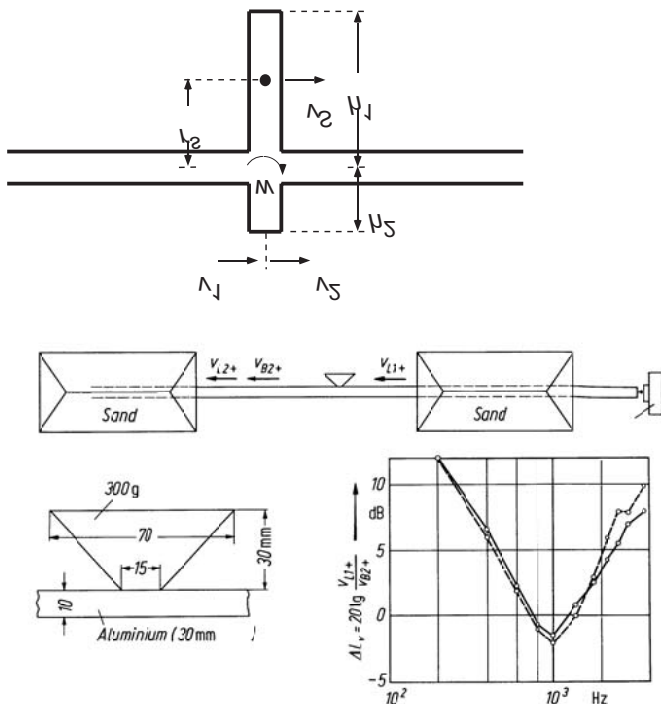


Fig. 6.15. (a) Motion of an eccentrically positioned blocking mass on a longitudinally excited rod. (b) Experimental demonstration of wave conversion. After [6.8]

Also for the analysis, the second situation proves more transparent. First, the longitudinal motion at the connection point must obey

$$v_1 = v_{1+} + v_{1-} = v_{2+} = v_2. \quad (6.77a)$$

Owing to the eccentricity, a rotation w occurs at the connection point. With r_s denoting the distance from the point of motion (centre of rod) to the centre of gravity of the mass, the velocity at the latter point is

$$v_s = v_1 - r_s w. \quad (6.77b)$$

Second, the difference in forces between the two rod parts must equal the inertia force of the blocking mass

$$F_1 - F_2 = F_{1+} + F_{1-} - F_2 = j\omega m v_s, \quad (6.77c)$$

which is exerted at the centre of gravity. The longitudinal forces, moreover, are related to the velocities by the impedances

$$F_{1+} = v_{1+} Z_{Fv}, \quad F_{1-} = -v_{1-} Z_{Fv}, \quad F_2 = v_2 Z_{Fv}, \quad (6.77d)$$

whereby, it is observed that the direction F_{1-} is in the negative x -direction. Upon substitution in (6.77c) and elimination of v_{1-} and v_s by means of (6.77a) and (6.77b)

$$2v_{1+} = \left(2 + \frac{j\omega m}{Z_{Fv}} \right) v_2 - \frac{j\omega m}{Z_{Fv}} r_s w. \quad (6.78)$$

The third relation necessary between v_2 and w arises from the moment

$$M = j\omega m r_s v_2, \quad (6.79a)$$

which must equal that given by the moment impedance multiplied by the rotational velocity

$$j\omega m r_s v_2 = Z_{Mw} w. \quad (6.79b)$$

The moment impedance in this case is composed of the rotational inertia of the eccentric mass and the moment impedance of the beam in flexure discussed in Sect. 5.4.4,

$$Z_{Mw} = j\omega \Theta + \frac{2B}{c_B} (1-j). \quad (6.79c)$$

This means that v_2 in Eq. (6.78) can be eliminated establishing

$$\frac{v_{1+}}{w} = \left(1 + \frac{j\omega m}{2Z_{Fv}} \right) \frac{Z_{Mw}}{j\omega m r_s} - \frac{j\omega m}{2Z_{Fv}} r_s. \quad (6.80)$$

It should be noted that the mass moment of inertia refers to the point of rotation i.e., the centre of the rod and not to the centre of gravity. Hence,

$$\Theta = \int_{h_1}^{h_2} y^2 dm \quad (6.81a)$$

where the origin is at the centre of the rod. For a rectangular blocking mass as depicted in Fig. 6.15 one obtains

$$\Theta = m(h_2^2 - h_1 h_2 + h_1^2)/3 \quad , \quad r_s = (h_1 - h_2)/2. \quad (6.81b)$$

In order to arrive at the transmission efficiency it must be observed that the transmitted bending wave power i.e., half of the total power transmitted for an excitation by means of a prescribed rotational velocity w is given by

$$W_{2B+} = \frac{1}{2} W_B = \frac{1}{4} \operatorname{Re}[Z_{Mw}] |w|^2. \quad (6.82a)$$

The incident longitudinal power is

$$W_{1L+} = \frac{1}{2} Z_{Fv} |v_{1+}|^2. \quad (6.82b)$$

This means that the transmission efficiency is finally obtained as

$$\tau_{LB} = \frac{1}{2} \operatorname{Re} \left[\frac{Z_{Mw}}{Z_{Fv}} \right] \left(1 + \frac{j\omega m}{2Z_{Fv}} \right) \frac{Z_{Mw}}{j\omega m r_s} - \frac{j\omega m r_s}{2Z_{Fv}} \right]^{-2}. \quad (6.83)$$

6.5 Periodic Structures

The stiffeners in ship and aircraft structures, the attenuation of which gave rise to the investigation of blocking masses, are periodically distributed. Also in high-rise buildings such periodic structures are common e.g., reinforced floors. The question is justified thus to what extent the periodicity enhances or possibly reduces the attenuation due to resonances in the intermediate substructures.

Mathematical approaches for dealing with periodic structures are well developed and applied since long in electrical transmission theory and in solid state physics.

6.5.1 Periodic Mass-Spring Systems

The best known example of a “longitudinal periodic system” consists of a beam with periodic changes in the cross-section as depicted in Fig. 6.16. As long as the wavelength λ_L is large compared with the lengths l_m and l_s

of the different parts, those with the cross-sections acts as masses whereas those with small as springs. It is thus possible to represent the periodic system in terms of mechanical circuit elements as a series array of masses and springs.

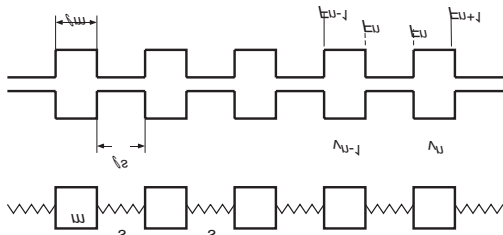


Fig. 6.16. Periodic mass-spring system with the notation used

Analysis of such cascaded systems, involving a finite number of not necessarily equal elements leads to as many dynamic and kinematic equations as there are independent field variables. This means that the mathematics can be quite comprehensive. The problem of propagation along infinite cascades of equal components, however, lends itself to relatively simple analysis based on the field equations for continuous systems discussed in Chapter 3. A distinction is though that instead of differential equations one obtains difference equations in the case of periodic structures.

For the problem studied, the equation of motion for a mass can be written as

$$F_n - F_{n+1} = j\omega m v_n \quad (6.84)$$

and the force – velocity relation for a spring with stiffness s as

$$v_{n-1} - v_n = \frac{j\omega}{s} F_n. \quad (6.85)$$

As for the wave transmission problem, the solution may be taken in the exponential form, which means that the ratio of the value of a field variable at the input point of an element to that at the output is the same for all elements i.e.,

$$F_{n+1} = F_n e^s, \quad v_{n-1} = v_n e^{-s}. \quad (6.86)$$

This reduces Eqs. (6.84) and (6.85) to two linear equations in terms of F_n and v_n ,

$$\begin{aligned} (1 - e^g) F_n - j\omega m v_n &= 0, \\ -\frac{j\omega}{s} F_n + (e^{-g} - 1) v_n &= 0, \end{aligned} \quad (6.87)$$

which have non-trivial solutions for a vanishing determinant,

$$\text{Det} = e^g + e^{-g} - 2 + \frac{\omega^2 m}{s} = 0.$$

This conditions for the, in general, complex propagation constant g can also be written in the form

$$\cosh g = 1 - 2\omega^2 / \omega_l^2 \quad (6.88a)$$

wherein the “limiting frequency”

$$\omega_l = 2\pi f_l = 2\sqrt{s/m} \quad (6.88b)$$

has been introduced.

The meaning of ω_l becomes clear when the real and imaginary parts of g are distinguished

$$g = a + jb, \quad (6.89a)$$

whereby a is the “attenuation constant” rendering an exponential amplitude decay and b is the “phase constant”. Thence, Eq. (6.88a) can be re-written as

$$\cosh a \cos b + j \sinh a \sin b = 1 - 2\omega^2 / \omega_l^2. \quad (6.89b)$$

Since the right-hand side is purely real, the imaginary part on the left-hand side must vanish i.e., either the attenuation constant is

$$a = 0 \quad (6.90a)$$

or the phase constant takes the values

$$b = n\pi \quad ; \quad n = 0, 1, 2, \dots \quad (6.90b)$$

The first condition is only possible for frequencies below and the second only for frequencies above the limiting frequency.

In the first region, which may be called “transmission region” there occurs only a phase change between consecutive elements, as is found from a substitution of (6.90a) in (6.89b),

$$b = \arccos\left(1 - \frac{2\omega^2}{\omega_l^2}\right) = 2 \arcsin\left(\frac{\omega}{\omega_l}\right). \quad (6.91a)$$

For frequencies well below the limiting frequency this expression reduces to the linear relation

$$b = 2 \frac{\omega}{\omega_l} = \omega \sqrt{\frac{m}{s}} . \quad (6.91b)$$

A phase constant that varies linearly with frequency simply implies a constant phase speed and thus a constant propagation speed,

$$\begin{aligned} c &= \frac{\omega}{b} (l_m + l_s) = \omega_l (l_m + l_s) / 2 \\ &= \sqrt{\frac{s}{m}} (l_m + l_s) . \end{aligned} \quad (6.91c)$$

Near the limiting frequency, the phase constant increases more rapidly until it reaches the value π at the limiting frequency. There above, it remains at π implying that the field variables of adjacent periodic elements are always of opposite phase cf., Fig. 6.17.

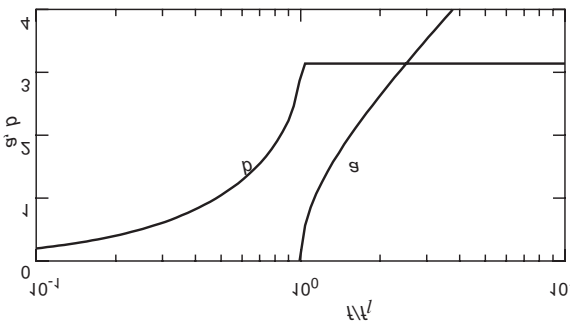


Fig. 6.17. Attenuation and phase constants of a low-pass filter

In contrast, the attenuation constant α increases rapidly with increasing frequency in the attenuation region as is seen by inserting Eq. (6.90b) in (6.89b)

$$\alpha = \operatorname{arccosh} \left(\frac{2\omega^2}{\omega_l^2} - 1 \right) = 2 \operatorname{arcsinh} \left(\frac{\omega}{\omega_l} \right) . \quad (6.91d)$$

Because the attenuation is large at frequencies above the limiting frequency but small below, a system like that depicted in Fig. 6.16 may be called a “low pass” system as its electrical analog.

With respect to attenuation, it is beneficial with an as low as possible limiting frequency. If the material of the masses and springs is the same, then this desirable condition can only be achieved by means of large changes in the cross-sectional area or large element lengths. With $m = \rho S_m l_m$ and $s = E S_s / l_s$, Eq. (6.88b) can be written as

$$\omega_l = 2c_L \sqrt{\frac{S_s}{S_m}} \frac{1}{\sqrt{l_m l_s}}, \quad (6.92a)$$

which, in the case of a cylindrical elements of diameters D and d respectively, simplifies to

$$\omega_l = 2c_L \frac{d}{D} \frac{1}{\sqrt{l_m l_s}}. \quad (6.92b)$$

As is seen, the periodic mass-spring system can be designed such that the limiting frequency and thus the propagation speed can be widely varied. There are limitations, however, since the analysis above is based on lumped elements i.e., the lengths l_m and l_s must be much shorter than half a longitudinal wavelength. Additionally, the cross-sectional area S_m cannot be made arbitrary big since then the element will no longer behave as a rigid body but a flexible structure exhibiting modes.

Despite the limitations, it is possible to realize periodic structures with very low phase speeds. As an example can be mentioned the torsional wave periodic system consisting of a slender steel rod and comparatively large discs [6.9], for which the propagation speed is merely 20 m/s and the limiting frequency 11 kHz. The corresponding analysis only requires the replacement of the axial force F by the torsional moment M , the axial velocity v by the rotational w , the mass m by the mass moment of inertia $\Theta = \pi \rho D^4 l_m / 32$ and the stiffness s by the torsional stiffness $T = \pi G d^4 / 32 l_s$, in cylindrical case where G is the shear modulus. It follows that

$$\omega_l = 2\sqrt{\frac{T}{\Theta}} = 2c_T \left(\frac{d}{D} \right)^2 \frac{1}{\sqrt{l_m l_s}} , \quad c = \sqrt{\frac{T}{\Theta}} (l_m + l_s). \quad (6.93)$$

6.5.2 Attenuation of Longitudinal Waves

For the simplest, continuous, periodic system only quasi-longitudinal waves are considered or when rotational motions, torsional waves. The wave field in each part must consist of one positively and one negatively propagating wave with wavenumbers $k = \omega/c_L$ and $-k = -\omega/c_L$ respectively.

There are different methods to analyse the propagation in the configuration depicted in Fig. 6.18. First, a method is employed, in which the propagation is expressed as a function of the transmission coefficients defined in Sects. 6.3.1 and 6.3.2. It is assumed that the positively propagating wave has its origin at the left end where it has the amplitude v_{+n} and $v_{+(n-1)}$ respectively. For the negatively propagating wave, the origin is assumed at the right end having the amplitude v_{-n} and $v_{-(n-1)}$. Accordingly,

$$\begin{aligned} v_n(x) &= v_{+n} e^{-jk(x-l_{nL})} + v_{-n} e^{jk(x-l_{nR})}, \\ v_{n-1}(x) &= v_{+n} e^{-g} e^{-jk(x-l_{n-1L})} + v_{-n} e^{-g} e^{jk(x-l_{n-1R})}, \end{aligned} \quad (6.94)$$

where the periodicity relation in (6.86) is used.

Since the amplitude v_{+n} is composed of that of the wave transmitted from the element $(n-1)$ of amplitude $t v_{+(n-1)} = t v_{+n} e^{-g}$ and that of the reflected wave having the amplitude $r v_{-n}$, it can be expressed as

$$v_{+n} = v_{+n} e^{-g} t e^{-jk(l_{nL}-l_{n-1L})} + v_{-n} r e^{jk(l_{nL}-l_{nR})}. \quad (6.95a)$$

Similarly, the amplitude of the reflected wave in the element $(n-1)$ can be written as

$$v_{-(n-1)} = v_{+n} e^{-g} r e^{-jk(l_{nL}-l_{n-1L})} + v_{-n} t e^{jk(l_{nL}-l_{nR})}. \quad (6.95b)$$

Observing that $l_{nL} - l_{n-1L} = l_p$ and $l_{nL} - l_{nR} = -l_p$, it follows that

$$\begin{aligned} v_{+n} &= v_{+n} e^{-g} t e^{-jkl_p} + v_{-n} r e^{-jkl_p}, \\ v_{+n} e^{-g} &= v_{+n} e^{-g} r e^{-jkl_p} + v_{-n} t e^{-jkl_p}. \end{aligned} \quad (6.96)$$

This homogeneous set of linear equations has a non-trivial solution for a vanishing determinant, which means that

$$\cosh g = \frac{1}{2} \frac{e^{jkl_p} + (t^2 - r^2) e^{-jkl_p}}{t}. \quad (6.97)$$

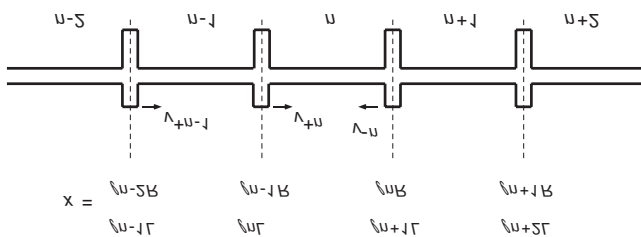


Fig. 6.18. Periodic longitudinal wave-guide with the notation used

For conservative discontinuities, Eq. (6.97) can be simplified by invoking energy conservation. If a wave of amplitude A is incident on a discontinuity then

$$|A|^2 = |Ar|^2 + |At|^2 \quad (6.98a)$$

as demonstrated in Sects. 6.2 and 6.4. With a wave B impinging simultaneously on the discontinuity from the other side, the in both directions emanating waves are $Ar + Bt$ and $At + Br$ respectively. Following energy conservation

$$|A|^2 + |B|^2 = |Ar + Bt|^2 + |At + Br|^2, \quad (6.98b)$$

and with (6.98a) and a corresponding expression for the B wave introduced on the left hand side, it is found that

$$|Ar|^2 + |At|^2 + |Br|^2 + |Bt|^2 = |Ar + Bt|^2 + |At + Br|^2. \quad (6.98c)$$

By separating the generally complex reflection and transmission coefficient in real and imaginary parts i.e., $r = r' + jr''$ and $t = t' + jt''$, it follows from (6.98c) that

$$r't' + r''t'' = 0. \quad (6.98d)$$

In the complex plane, therefore, the vectors r and t are perpendicular to each other as was seen also in Eqs. (6.67b) and (6.76b). Hence, it is also possible to write

$$t = |t|e^{j\phi} \quad , \quad r = |r|e^{j\phi + j\pi/2} \quad , \quad t^2 - r^2 = |t|^2 e^{2j\phi} + |r|^2 e^{2j\phi} = e^{2j\phi} \quad (6.98e)$$

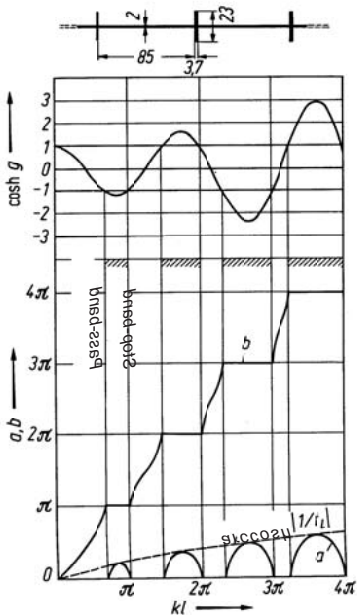
and when substituted in (6.97), it is found that

$$\cosh g = \frac{1}{2} \frac{e^{jkl_p} + e^{2j\phi} e^{-jkl_p}}{t} = \frac{1}{2} \left[\frac{e^{jkl_p}}{|t|e^{j\phi}} + \frac{e^{-jkl_p}}{|t|e^{-j\phi}} \right] = \operatorname{Re} \left[\frac{e^{jkl_p}}{t} \right]. \quad (6.99)$$

Use is here made of the fact that the sum of a complex number and its conjugate becomes twice the real part.

As an example of the application of (6.99), Fig. 6.19 shows $\cosh g$ as well as the attenuation constant a and the phase constant b for a specific case. In addition is included the curve $\operatorname{arccosh}|1/t|$ which is expected to realize the upper limit for the attenuation. From Eq. (6.99) and Fig. 6.19, together with some calculations of other examples, the following conclusion can be drawn for the behaviour of periodic systems carrying longitudinal or torsional waves:

- a) Contrary to periodic systems made of lumped subsystems, a sequence of pass- and stop bands appear.
- b) In the stop bands, the phase is constant whereas it grows in the pass bands.
- c) The maximum amplitude ratio for adjacent subsystems is given by $\cosh g = |1/t|$.
- d) On average, the frequency separation between consecutive onsets of the stop bands is set by $\Delta kl_p = (\Delta\omega/c) l_p = \pi$, associated with the periodicity of the exponential function in (6.99).



From Eq. (6.94), the forces are obtained as

$$\begin{aligned} F_n(x) &= \rho c S \left[v_{+n} e^{-jk(x-l_{nL})} - v_{-n} e^{jk(x-l_{nR})} \right], \\ F_{n-1}(x) &= \rho c S \left[v_{+n} e^{-g} e^{-jk(x-l_{(n-1)L})} - v_{-n} e^{-g} e^{jk(x-l_{(n-1)R})} \right]. \end{aligned} \quad (6.100)$$

The boundary conditions at the discontinuity $x = l_{nL} = l_{(n-1)R} = 0$ offer the necessary relations to develop the set of linear equations. For blocking masses m , for instance, continuity in velocity and equilibrium in forces require

$$\begin{aligned} v_n(0) &= v_{n-1}(0), \\ F_{n-1}(0) - F_n(0) &= j\omega m v_n(0). \end{aligned} \quad (6.101a)$$

With the chosen origin, $l_{(n-1)L} = -l_p$ and $l_{nR} = l_p$ such that when (6.94) and (6.100) are inserted in (6.101a), the system of equation becomes

$$\begin{aligned} v_{+n} + v_{-n} e^{-jkl_p} &= v_{+n} e^{-g} e^{-jkl_p} + v_{-n} e^{-g}, \\ v_{+n} e^{-g} e^{-jkl_p} - v_{-n} e^{-g} - v_{+n} + v_{-n} e^{-jkl_p} &= \frac{j\omega m}{\rho c S} \left(v_{+n} + v_{-n} e^{-jkl_p} \right). \end{aligned} \quad (6.101b)$$

From a vanishing determinant it is found that

$$\cosh g = \cos kl_p - \frac{\omega m}{2\rho c S} \sin kl_p. \quad (6.101c)$$

By employing the transmission coefficient associated with this structural configuration

$$t = \left(1 + \frac{j\omega m}{2\rho c S} \right)^{-1}$$

in Eq. (6.99), it is readily ascertained that (6.101c) and (6.99) are identical.

Yet another method should be briefly outlined for the analysis of periodic systems. In this method, the four-pole representations are required of the two building blocks constituting a subsystem, in this case a rod of length l_p and a mass. In the following example, however, the analysis is somewhat generalized in that both building blocks are represented by their respective four-pole. With the notation defined in Fig. 6.20, the forces and velocities at the ends of the building blocks can be written in the form

$$\begin{pmatrix} v_A \\ F_A \end{pmatrix} = \begin{pmatrix} \alpha_{11} & \alpha_{12} \\ \alpha_{21} & \alpha_{22} \end{pmatrix} \begin{pmatrix} v_B \\ F_B \end{pmatrix}, \quad \begin{pmatrix} v_B \\ F_B \end{pmatrix} = \begin{pmatrix} \beta_{11} & \beta_{12} \\ \beta_{21} & \beta_{22} \end{pmatrix} \begin{pmatrix} v_c \\ F_c \end{pmatrix}. \quad (6.102a)$$

The matrix elements can be obtained from (4.41). Thus, $\alpha_{11} = \alpha_{22} = \cos k_A l_A$, $\alpha_{12} = j(\sin k_A l_A) / \rho_A c_A S_A$ and $\alpha_{21} = -j\rho_A c_A S_A \sin k_A l_A$. Similarly are $\beta_{11} = \beta_{22} = \cos k_B l_B$, $\beta_{12} = j \sin k_B l_B / \rho_B c_B S_B$ and $\beta_{21} = -j\rho_B c_B S_B \sin k_B l_B$.

To arrive at the characteristic equation for the periodic system, the two relations in (6.102a) are simply multiplied and the periodicity relations $v_A = e^g v_c$ and $F_A = e^g F_c$ observed, which leads to

$$e^g \begin{pmatrix} v_c \\ F_c \end{pmatrix} = \begin{pmatrix} \alpha_{11} & \alpha_{12} \\ \alpha_{21} & \alpha_{22} \end{pmatrix} \begin{pmatrix} \beta_{11} & \beta_{12} \\ \beta_{21} & \beta_{22} \end{pmatrix} \begin{pmatrix} v_c \\ F_c \end{pmatrix}. \quad (6.102b)$$

Again, the expression for g sought is developed from setting the determinant equal to zero.

Which of the methods described above is the more suitable in a specific case depends on the question posed and on the available data. For numerical processing, the four-pole formulation is convenient since no analytical steps are involved and the programming is straightforward.

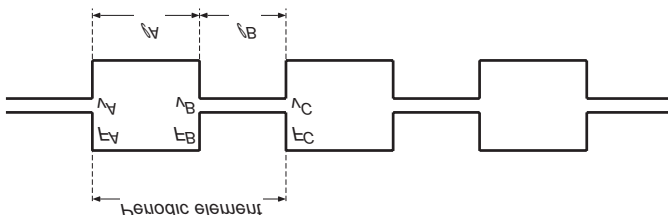


Fig. 6.20. Notations for a four-pole representation of a periodic system carrying longitudinal waves

6.5.3 Periodic Bending Wave-Guide

For wave-guides carrying flexural waves, also moments and rotational velocities are present as field variables beside the forces and translational velocities. Although this complicate the analysis, the previously treated methods remain applicable. For periodic subsystems that are long enough for the nearfields to decay within their length i.e., the length of the subsystem is longer than half a bending wavelength, Eq. (6.99) can be applied directly. It is only to replace the longitudinal wavenumber and the transmission coefficient by those of the bending wave e.g., those in (6.57) and (6.66) because the energy ratio is preserved correctly by (6.99).

For exact calculations, the four-pole formulation is extended to an eight-pole dito. The expression required are given in Sect. 4.3.2 [6.10]. By sub-

stituting $-l_A$ for x in Eq. (4.46) for a beam of length l_A as depicted in Fig. 6.21, the eight-pole description is obtained as

$$\begin{Bmatrix} v_A \\ w_A \\ M_A \\ F_A \end{Bmatrix} = \begin{pmatrix} C_A & -S_A/k & c_A/jZ_{cb} & -s_A/jZ_{cb}k \\ -ks_A & C_A & kS_A/jZ_{cb} & c_A/jZ_{cb} \\ -jZ_{cb}c_A & jZ_{cb}s_A/k & C_A & S_A/k \\ -jZ_{cb}ks_A & jZ_{cb}c_A & ks_A & C_A \end{pmatrix} \begin{Bmatrix} v_B \\ w_B \\ M_B \\ F_B \end{Bmatrix}. \quad (6.103)$$

Herein, $C_A = [\cosh kl_A + \cos kl_A]/2$, $c_A = [\cosh kl_A - \cos kl_A]/2$, $S_A = [\sinh kl_A + \sin kl_A]/2$, $s_A = [\sinh kl_A - \sin kl_A]/2$, $Z_{cb} = \sqrt{Bm}$ and k is the bending wavenumber. When also the second building block of the subsystem is a beam, possibly of another material and with a different cross-section, the second eight-pole expression is similar to that in (6.103), the difference being that the matrix elements are modified.

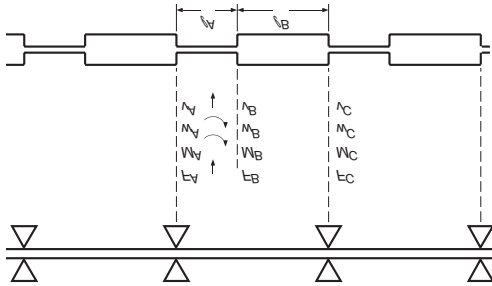


Fig. 6.21. Periodic bending wave-guide. Top, one periodic element consisting of two different beams. Bottom, one periodic element consisting of a beam and a blocking mass

Another important configuration in practice is that where the wave-guide consists of a beam with periodically spaced masses. In such a case, the relations between the field variables on either side of a mass can be written as

$$\begin{Bmatrix} v_B \\ w_B \\ M_B \\ F_B \end{Bmatrix} = \begin{pmatrix} 1 & 0 & 0 & 0 \\ 0 & 1 & 0 & 0 \\ 0 & j\omega\Theta & 1 & 0 \\ j\omega m & 0 & 0 & 1 \end{pmatrix} \begin{Bmatrix} v_C \\ w_C \\ M_C \\ F_C \end{Bmatrix}, \quad (6.104)$$

in accordance with (6.65). Upon denoting the column vectors and matrices \mathbf{v}_A , \mathbf{v}_B , \mathbf{v}_C and \mathbf{M}_A , \mathbf{M}_B respectively, the characteristic equation is obtained as

$$e^g \mathbf{v}_C = \mathbf{M}_A \mathbf{M}_B \mathbf{v}_C, \quad (6.105)$$

in analogy with (6.102). In Fig. 6.22 are shown the results for two different configurations.

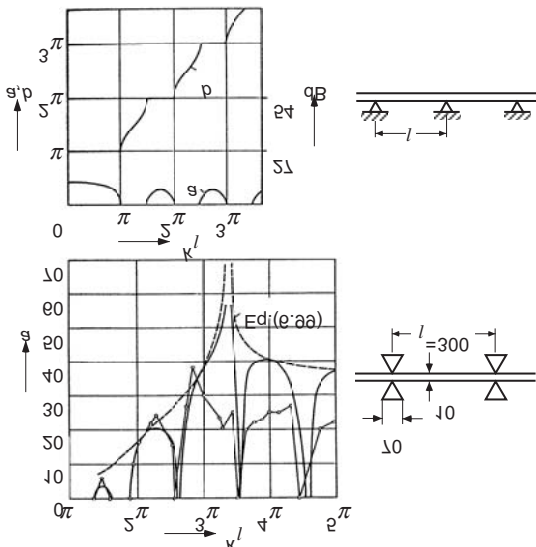


Fig. 6.22. Calculated attenuation per subsystem of a periodic flexural wave-guide.
a) Simple supports and b) symmetric blocking masses of mass 0.6 kg on a steel beam. (—) calculated from (6.105), (---) from (6.99) and (o-o) measured

From these results and those of some additional calculations as well as the form of (6.105), some general findings can be noted.

- Two attenuation constants exist for periodic, flexural wave-guides, one of which is too large to be practically interesting.
- As for the periodic wave-guide carrying longitudinal waves, the pass- and stop band alternate.
- With the properties for the bending wave substituted, Eq. (6.99) represents the envelope to the attenuation. Only the first pass- and stop band must be determined from the more complete expression (6.105).
- For a beam, which is periodically simply supported or equivalently, $m \rightarrow \infty$ and $\Theta \rightarrow 0$ in (6.104), a stop band exists up to $kl_A = \pi$. For the upper stop bands, the maximum attenuation is given by $\cosh \alpha = \sqrt{2}$ since $t = -j(1-j)$ in view of (6.68i) cf., Fig. 6.22a.

For beams [6.8], the measured and calculated results are in agreement regarding the positions of pass- and stop bands. On the other hand, the attenuation in the stop bands, which theoretically often would amount to 100 dB after a few subsystems, is not realized in practice since other wave types e.g., longitudinal waves are excited due to eccentricities. The latter are transmitted unattenuated and re-excite bending waves at the subsequent discontinuities cf., Sect. 6.6.3 and Fig. 6.27.

As is seen, the expression in (6.99) constitutes the envelope to the attenuation at high frequencies where the evanescent waves have decayed between consecutive discontinuities. The starting point for such an analysis is the basic relations in Eqs. (3.69) and (3.77) to (3.79) for the simple bending wave i.e.,

$$w_z = \frac{\partial v_y}{\partial x} \quad , \quad \frac{\partial M_z}{\partial t} = -B \frac{\partial w_z}{\partial x}, \quad (6.106a)$$

$$-\frac{\partial M_z}{\partial x} = F_y \quad , \quad \frac{\partial F_y}{\partial x} = m' \frac{\partial v_y}{\partial t}. \quad (6.106b)$$

To take the influence of the discontinuities into account, are added to the dynamic relations in (6.106b) the “smeared” moments M_D/l_A and forces F_D/l_A resulting from the discontinuities. Thereby, it is natural to distribute the actually point-wise acting moments and forces over the periodic length l_A whereby the relations in (6.106b) are moments and forces per length. By means of phasor notation and impedances for the moments and forces, it is found that

$$-\frac{\partial M_z}{\partial x} = F_y + \frac{M_D}{l_A} = F_y + \frac{Z_{Mw}}{l_A} w_z \quad , \quad -\frac{\partial F_y}{\partial x} = j\omega m' v_y + \frac{Z_{Fv}}{l_A} v_y. \quad (6.106c)$$

Furthermore, a combination of (6.106a) and (6.106c) yields the equation of motion for the “smeared”, periodic bending wave-guide cf., Sect. 4.7

$$B \frac{\partial^4 v_y}{\partial x^4} - \omega^2 m' v_y - j\omega \frac{Z_{Mw}}{l_A} \frac{\partial^2 v_y}{\partial x^2} + j\omega \frac{Z_{Fv}}{l_A} v_y = 0. \quad (6.106d)$$

Upon employing the usual wave field, the dispersion equation becomes

$$\left[Bk^4 - \omega^2 m' \left(1 + \frac{Z_{Fv}}{j\omega m' l_A} + \frac{Z_{Mw}}{j\omega m' l_A} k^2 \right) \right] v_y = 0. \quad (6.106e)$$

Hence, the bending wavenumbers k can be determined and thence the generally complex propagation constant $jg = kl_A$ for the wave guides at low frequencies i.e., for $\text{Im}[kl_A] < 1$.

In most cases, $Z_{Mw} k^2 < Z_{Fv}$ such that

$$k^4 \approx \frac{\omega^2 m'}{B} \left(1 + \frac{Z_{Fv}}{j\omega m' l_A} \right)$$

results approximately. For discontinuities consisting of springs, $Z_{Fv} = s/j\omega$, which means that for $\omega^2 < s/m' l_A$, the wavenumber always has an imaginary part, implying that no wave motion occurs cf., Sect. 3.7.4.4.

Owing to the rather lengthy analysis, the issue of concentrated excitation of periodic systems will not be considered. The reason for lengthy analysis is that the periodicity is disturbed by the excitation. From a multiplication of a large number of transmission matrices, similar to those in (6.102) to (6.105), however, the possibility remains to undertake the analysis. Often thereby, numerical problems occur due to multiplication of possibly large terms by $\cosh kl_A$. In such cases it is suitable to employ the procedure outlined below, in which one large matrix is developed instead of matrix multiplications.

For this purposes, the discontinuities are substituted by the forces and moments resulting, which are applied to the uniform beam. This means that the analysis of the periodic system is turned into that of a uniform beam subject to the original excitation F_0 and some yet unknown forces F_v and moments M_v . With the velocity response due to a force acting at a point x_v given by

$$v_{Fv}(x) = \frac{\omega F_v}{4Bk^3} (e^{-jk|x-x_0|} - j e^{-k|x-x_v|}) = Y_{vF}(x|x_v) F_v, \quad (6.107a)$$

in accordance with (5.23) and that due to a moment by

$$v_{Mv}(x) = Y_{vM}(x|x_v) M_v, \quad (6.107b)$$

the net translational and rotational response is obtained as

$$\begin{aligned} v(x) &= F_0 Y_{vF}(x|x_0) - \sum_{v=1}^N F_v Y_{vF}(x|x_v) - \sum_{v=1}^N M_v Y_{vM}(x|x_v), \\ w(x) &= F_0 Y_{wF}(x|x_0) - \sum_{v=1}^N F_v Y_{wF}(x|x_v) - \sum_{v=1}^N M_v Y_{wM}(x|x_v). \end{aligned} \quad (6.108)$$

Herein,

$$\begin{aligned}
 Y_{vF}(x|x_v) &= \frac{\omega}{4Bk^3} (e^{-jk|x-x_v|} - je^{-k|x-x_0|}), \\
 Y_{wM}(x|x_v) &= \frac{\omega}{4Bk} (e^{-jk|x-x_v|} + je^{-k|x-x_v|}), \\
 Y_{wF}(x|x_v) &= -j \frac{\omega}{4Bk^2} (e^{-jk|x-x_v|} - e^{-k|x-x_v|}) \operatorname{sgn}(x-x_v),
 \end{aligned} \tag{6.109}$$

are the mobilities pertaining to the point excited, infinite beam and

$$\operatorname{sgn}(x-x_v) = \begin{cases} -1 & ; \quad x < x_v \\ +1 & ; \quad x > x_v \end{cases},$$

is the signum function resulting from the differentiation of a function involving an absolute value.

With the responses of the possibly differing discontinuities expressed in terms of the associated mobilities as

$$v(x_\mu) = Y_{F\mu} F_\mu, \quad w(x_\mu) = Y_{M\mu} M_\mu; \quad 1 \leq \mu \leq N, \tag{6.110}$$

the set of linear equations for the solution of the unknown auxiliary forces and moments can be written as

$$\begin{aligned}
 F_\mu Y_{F\mu} + \sum_{v=1}^N F_v Y_{vF}(x_\mu|x_v) + \sum_{v=1}^N M_v Y_{vM}(x_\mu|x_v) \\
 = F_0 Y_{vF}(x_\mu|x_0), \\
 M_\mu Y_{M\mu} + \sum_{v=1}^N F_v Y_{wF}(x_\mu|x_v) + \sum_{v=1}^N M_v Y_{wM}(x_\mu|x_v) \\
 = F_0 Y_{wF}(x_\mu|x_0).
 \end{aligned} \tag{6.111}$$

By means of this set of $2N$ equations, the unknown auxiliary forces and moments can be solved for and subsequently be substituted into (6.108) to obtain the vibration field of the periodic structure.

Figure 6.23 shows the results from such an analysis. In the analysis, the properties of a typical railway rail supported by a mass (sleeper) via a spring (rail interlayer). Furthermore, the mass rests on a rigid foundation through a secondary spring. The two springs are assumed damped with a dissipation corresponding to that found in practice implying that an attenuation is obtained also in the pass bands.

For this example, a comparatively strong attenuation can be observed at low frequencies owing to the translatory support cf., Fig. 6.22a. This means that a stop band exists for low frequencies. Around 200 Hz, the attenuation is marginal to increase markedly again around 500 Hz; almost 40

dB decrease within 15 discontinuities. At about 1.4 kHz, standing waves can be observed because half a wavelength then approximately equals the periodicity.

From the analysis also the point mobility can be established. It is found that:

- It is position dependent between two consecutive discontinuities,
- it is purely imaginary in the stop bands and
- it differs only marginally from that of the homogeneous beam in the pass bands.

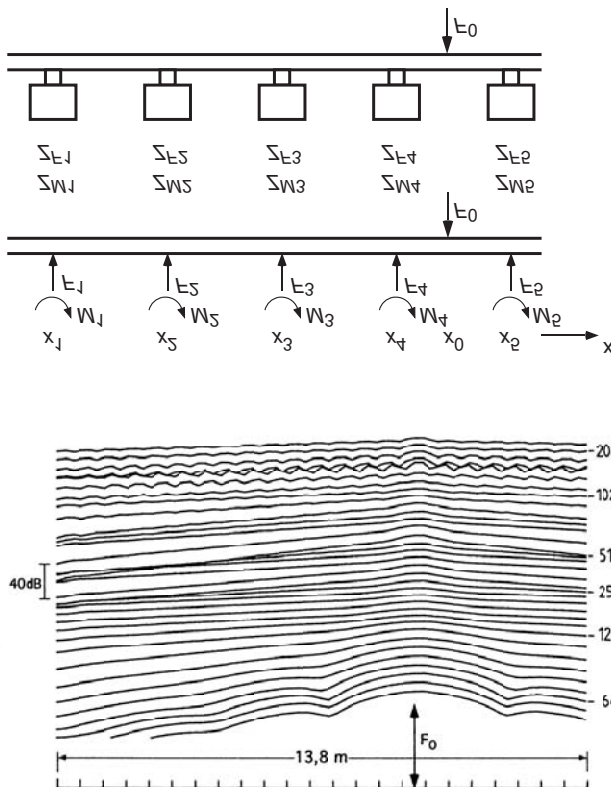


Fig. 6.23. Velocity level reduction for a periodic system subject to transverse point force excitation (longitudinal waves omitted) calculated from (6.108-6.111) spatial period 0.6m. Flexural wavelength of the homogeneous beam $\lambda = 45 /f[m]$

6.6 Hamilton's Principle for Transmission Problems

6.6.1 Procedure

For the application of Hamilton's principle in conjunction with structure-borne sound transmission problems, the specific boundary conditions at the discontinuities must be simultaneously considered in the schemes employed in Sects. 2.2 or 3.8.1 or 4.6.3. In a variational analysis sense, a minimum of the Hamiltonian is sought subject to defined constraints i.e., the boundary conditions. The appropriate tool in this pursuit is Lagrange's multiplier e.g., [6.11]. Thus, when the v-th boundary condition is given in the form $g_v = 0$, then the equation

$$\frac{1}{T} \int_0^T (E_{kin} - E_{pot}) dt + \sum_v (\lambda_v^* g_v + \lambda_v g_v^*) = \text{Min.} \quad (6.112)$$

Herein, E_{kin} and E_{pot} are the kinetic and potential energies of the vibrating masses, springs, rods and beams. T is the integration time and λ_v Lagrange's multiplier. It appears here as a pure mathematical factor or, following [6.11], "as a particularly elegant way to circumvent the irritating requirements imposing the asymmetry". It will be seen, however, that the multipliers correspond to physically meaningful quantities such as forces, moments or similar, less a factor. Beside $\lambda_v g_v^*$ appears also $\lambda_v^* g_v$ in Eq. (6.112) warranting that all quantities are real and thus that the minimum is physically meaningful.

The following analysis presumes pure harmonic processes of angular frequency ω . This means that with the use of the phasor notation, the real part is understood. By means of the following identities this does not introduce any complications. From

$$\begin{aligned} \xi(x, t) &= \text{Re} [\underline{\xi}(x) e^{j\omega t}] = \frac{1}{2} [\underline{\xi}(x) e^{j\omega t} + \underline{\xi}^*(x) e^{-j\omega t}], \\ \zeta(x, t) &= \text{Re} [\underline{\zeta}(x) e^{j\omega t}] = \frac{1}{2} [\underline{\zeta}(x) e^{j\omega t} + \underline{\zeta}^*(x) e^{-j\omega t}], \end{aligned} \quad (6.113a)$$

it follows that

$$\begin{aligned} \frac{1}{T} \int_0^T \xi^2(x, t) dt &= \frac{1}{2} |\underline{\xi}(x)|^2, \quad \frac{1}{T} \int_0^T \left[\frac{\partial \xi(x, t)}{\partial t} \right]^2 dt = \frac{\omega^2}{2} |\underline{\xi}(x)|^2, \\ \frac{1}{T} \int_0^T \zeta(x, t) \xi(x, t) dt &= \frac{1}{4} [\underline{\zeta}(x) \underline{\xi}^*(x) + \underline{\zeta}^*(x) \underline{\xi}(x)]. \end{aligned} \quad (6.113b)$$

It should be noted that the integration time must comprise an integer number of periods.

The free longitudinal waves in a finite rod obey

$$\xi(x, t) = \operatorname{Re} \left[(A_L e^{-jk_2 x} + B_L e^{jk_2 x}) e^{j\omega t} \right]. \quad (6.114)$$

Therefore the time averaged Hamiltonian for a rod extending from l_l to l_n ($l_l < l_n$) becomes

$$H_L = \frac{1}{T} \int_0^T [E_{kin} - E_{pot}] dt = \frac{1}{T} \int_0^T \left[\int_{l_l}^{l_n} \frac{\rho S}{2} \left(\frac{\partial \xi(x, t)}{\partial t} \right)^2 dx - \int_{l_l}^{l_n} \frac{\rho S}{2} \left(\frac{\partial \xi(x, t)}{\partial x} \right)^2 dx \right] dt \quad (6.115)$$

In view of (6.113), substitution of (6.114) yields

$$H_L = \alpha_L \left[A_L B_L^* e^{-jk_L(l_l + l_n)} + A_L^* B_L e^{jk_L(l_l + l_n)} \right]; \\ \alpha_L = \frac{1}{2} \rho S \omega c_L \sin k_L (l_l - l_n), \quad (6.116)$$

since $E = \rho \omega^2 / k_L^2$.

For finite beams exhibiting free bending waves at a frequency ω , the transverse motion is given by

$$\zeta(x, t) = \operatorname{Re} \left[(A_B e^{-jk_B x} + B_B e^{jk_B x} + C_B e^{-k_B(x-l_l)} + D_B e^{k_B(x-l_n)}) e^{j\omega t} \right] \quad (6.117)$$

The time-averaged Hamiltonian for an Euler-Bernoulli beam extending from $x = l_l$ to $x = l_n$ is given by

$$H_B = \frac{1}{T} \int_0^T [E_{kin} - E_{pot}] dt = \frac{1}{T} \int_0^T \left[\int_{l_l}^{l_n} \frac{\rho S}{2} \left(\frac{\partial \zeta(x, t)}{\partial t} \right)^2 dx - \int_{l_l}^{l_n} \frac{\rho S}{2} \left(\frac{\partial \zeta(x, t)}{\partial x} \right)^2 dx \right] dt \quad (6.118)$$

After some algebraic manipulations one finds that

$$H_B = \frac{\omega^2 \rho S}{2k_B} \left[(A_B^* C_B + B_B^* C_B^*) I_C^* + (A_B^* D_B + B_B^* D_B^*) I_D^* + (A_B C_B^* + B_B^* C_B) I_C + (A_B D_B^* + B_B^* D_B) I_D \right], \quad (6.119)$$

where

$$I_C = \frac{e^{-jk_B l_n} e^{-k_B(l_l - l_n)} - e^{-jk_B l_l}}{1+j}, I_D = -\frac{e^{-jk_B l_n} - e^{-jk_B l_l} e^{-k_B(l_l - l_n)}}{1-j}. \quad (6.120)$$

The exponential terms associated with C_B and D_B are thereby written in a form that they do not exceed unity on the interval $l_l < x < l_n$. Possible numerical overflow for large $k_B l_0$ are thus avoided.

6.6.2 An Introductory Example

Consider for simplicity the longitudinally vibrating rod having a cross-sectional area change, as depicted in Fig. 6.24. To be able to apply the analysis in different cases, it is assumed that the left part of the rod is excited by a prescribed motion ξ_{E1} via the spring s_1 . Similarly, the right end experiences the prescribed motion ξ_{E2} via the spring s_2 . Following (6.114), the motion in the left-hand part can be written as

$$\xi_1(x, t) = \operatorname{Re} \left[(A_{L1} e^{-jk_{L1}x} + B_{L1} e^{jk_{L1}x}) e^{j\omega t} \right], \quad (6.121)$$

such that the potential energy and the Hamiltonian for the spring becomes

$$\begin{aligned} H_{s1} &= -\frac{1}{T} \int_0^T E_{pot} dt = -\frac{1}{T} \frac{s_1}{2} \int_0^T [\xi_{E1} - \xi_1(l_1, t)]^2 dt \\ &= -\frac{s_1}{4} \left| \xi_{E1} - \xi_1(l_1) \right|^2 = -\frac{s_1}{4} \left| \xi_{E1} - A_{L1} e^{-jk_{L1}l_1} - B_{L1} e^{jk_{L1}l_1} \right|^2. \end{aligned} \quad (6.122a)$$

Analogously, that for the right-hand spring at $x = l_{n2}$ reads

$$H_{s2} = -\frac{s_2}{4} \left| \xi_{E2} - A_{L2} e^{-jk_{L2}l_{n2}} - B_{L2} e^{jk_{L2}l_{n2}} \right|^2. \quad (6.122b)$$

The boundary condition at the interface between the two parts of the rod $x_1 = x_2 = 0$ is

$$\xi_1 = \xi_2 \Leftrightarrow A_{L1} + B_{L1} - A_{L2} - B_{L2} = 0. \quad (6.122c)$$

Hence, all components of the function to minimize are established and by involving (6.112)

$$\begin{aligned} H_{L1} + H_{L2} + H_{s1} + H_{s2} + \lambda^* \left(\frac{A_{L1} + B_{L1} - A_{L2} - B_{L2}}{A_{L1} + B_{L1} - A_{L2} - B_{L2}} \right)^* &= \text{Min.} \end{aligned} \quad (6.123a)$$

By introducing (6.116) and (6.122a, b), it is explicitly obtained

$$\begin{aligned}
& \sum_{q=1}^2 \left\{ \alpha_{Lq} \left[A_{Lq} B_{Lq}^* e^{-jk_{Lq}(l_{q1} + l_{q2})} + A_{Lq}^* B_{Lq} e^{jk_{Lq}(l_{q1} + l_{q2})} \right] \right\} \\
& - \frac{s_1}{4} \left| \xi_{E1} - A_{L1} e^{-jk_{L1}l_{11}} - B_{L2} e^{jk_{L1}l_{11}} \right|^2 \\
& - \frac{s_2}{4} \left| \xi_{E2} - A_{L2} e^{-jk_{L2}l_{22}} - B_{L2} e^{jk_{L2}l_{22}} \right|^2 \\
& + \lambda^* (A_{L1} + B_{L1} - A_{L2} - B_{L2}) + \lambda (A_{L1}^* + B_{L1}^* - A_{L2}^* - B_{L2}^*) = \text{Min.}
\end{aligned} \tag{6.123b}$$

It is evident that this expression is purely real.

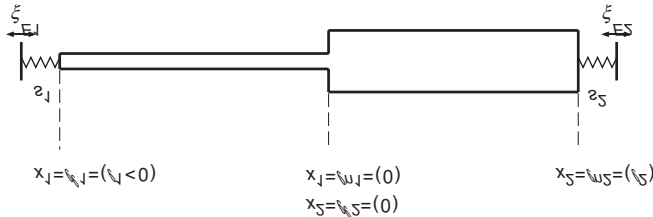


Fig. 6.24. Notations used in Eqs. (6.121) to (6.125)

To obtain the minimum, (6.123b) is differentiated with respect to the unknown amplitudes and factors and the resulting expressions equated to zero. Hereby, it must be considered that the unknowns are complex, which means that $A = A' + jA''$, $A^* = A' - jA''$, $B = B' + jB''$, $B^* = B' - jB''$, $\lambda = \lambda' + j\lambda''$ and $\lambda^* = \lambda' - j\lambda''$ where A' , A'' etc. are purely real.

To minimize a function $f(A, A^*, B, B^*, \lambda, \lambda^*)$, the differentiations must be equated to zero in the form

$$\begin{aligned}
0 &= \frac{\partial f}{\partial A'} = \frac{\partial f}{\partial A} \frac{\partial A}{\partial A'} + \frac{\partial f}{\partial A^*} \frac{\partial A^*}{\partial A'} = \frac{\partial f}{\partial A} + \frac{\partial f}{\partial A^*}, \\
0 &= \frac{\partial f}{\partial A''} = \frac{\partial f}{\partial A} \frac{\partial A''}{\partial A''} + \frac{\partial f}{\partial A^*} \frac{\partial A^*}{\partial A''} = j \left(\frac{\partial f}{\partial A} - \frac{\partial f}{\partial A^*} \right),
\end{aligned} \tag{6.124}$$

as well as those involving $B', B'', \lambda', \lambda''$. By dividing the last part by j and subtracting the result from the first

$$0 = \frac{\partial f}{\partial A^*}.$$

In such a way, the purely real and imaginary expressions in (6.124) can be summarized in one complex equation. This reduces the algebraic labour

since only differentiations with respect to A^* , B^* and λ^* have to be made. The minimization accordingly yields the following set of equations

$$\begin{aligned}
 \frac{\partial}{\partial A_{L1}^*}: & \alpha_{L1} B_{L1} e^{jk_{L1}(l_{n1}+l_{n1})} + \\
 & \frac{s_1}{4} e^{jk_{L1}l_{n1}} \left(\xi_{E1} - A_{L1} e^{-jk_{L1}l_{n1}} - B_{L1} e^{jk_{L1}l_{n1}} \right) + \lambda = 0, \\
 \frac{\partial}{\partial B_{L1}^*}: & \alpha_{L1} A_{L1} e^{-jk_{L1}(l_{n1}+l_{n1})} + \\
 & \frac{s_1}{4} e^{-jk_{L1}l_{n1}} \left(\xi_{E1} - A_{L1} e^{-jk_{L1}l_{n1}} - B_{L1} e^{jk_{L1}l_{n1}} \right) + \lambda = 0, \\
 \frac{\partial}{\partial A_{L2}^*}: & \alpha_{L2} B_{L2} e^{jk_{L2}(l_{n2}+l_{n2})} + \\
 & \frac{s_2}{4} e^{jk_{L2}l_{n2}} \left(\xi_{E2} - A_{L2} e^{-jk_{L2}l_{n2}} - B_{L2} e^{jk_{L2}l_{n2}} \right) + \lambda = 0, \\
 \frac{\partial}{\partial B_{L2}^*}: & \alpha_{L2} A_{L2} e^{-jk_{L2}(l_{n2}+l_{n2})} + \\
 & \frac{s_2}{4} e^{-jk_{L2}l_{n2}} \left(\xi_{E2} - A_{L2} e^{-jk_{L2}l_{n2}} - B_{L2} e^{jk_{L2}l_{n2}} \right) + \lambda = 0, \\
 \frac{\partial}{\partial \lambda^*}: & A_{L1} + B_{L1} - A_{L2} - B_{L2} = 0.
 \end{aligned} \tag{6.125}$$

From these five equations, the five unknown quantities sought A_{L1} , B_{L1} , A_{L2} , B_{L2} and λ , can be determined. A simplification can be made when the stiffnesses s_1 and s_2 are unimportant for the result. Then, they can be set so small but ξ_{E1} and ξ_{E2} large so that products in the form $s_1 A_{L1}$, $s_1 B_{L1}$, $s_2 A_{L2}$ and $s_2 B_{L2}$ can be neglected whilst $s_1 \xi_{E1}$ and $s_2 \xi_{E2}$ remain finite. This is a small trick to encompass an external excitation without extending the Hamiltonian to include the work of forces. In this way also infinite rods can be simulated. It is, for example, possible to require that no backwards propagating waves exist in the left-hand part of the rod such that $B_{L2} = 0$. This is achieved by setting ξ_{E2} such that the incident wave is “caught” as is done in conjunction with active control of sound. In that case the unknown are A_{L1} , B_{L1} , A_{L2} , ξ_{E2} and λ . Practically, this simply means that the column with ξ_{E2} is substituted for the column associated with B_{L2} in the coefficient matrix. Also after such a manipulation, (6.125) is solvable and furnishes the reflection and transmission coefficients as $r = B_{L1}/A_{L1}$ and $t = A_{L2}/A_{L1}$ respectively. The results are, of course, identical to those in Eqs. (6.9) to (6.11).

It is also interesting to examine Lagrange's multiplier λ . Disregarding the factor $\frac{1}{4}$, it can be shown that it equals the force acting at the discontinuity $x_1 = x_2 = 0$. This is not so surprising since (6.123b) takes the dimension of work implying that $\lambda^* A_{L1}$ etc. also must represent some work. With A_{L1} having the dimension of displacement, λ must have the dimension of force. That this quantity, initially introduced as a purely mathematical factor, proves to correspond to a force is nothing new. In [6.12], Sommerfeld introduces "the pressure as a Lagrange's multiplier".

In this context it should be pointed out that Hamilton's principle can be employed for all structure-borne sound problems without the explicit use of forces and moment etc. but solely involving displacement variables. This might require the somewhat artificial detour over springs with prescribed displacements as used in this section. Naturally, the excitation can also be introduced as was done in Eq. (3.188).

6.6.3 Bending and Longitudinal Waves at an Eccentric Blocking Mass

Consider the system shown in Fig. 6.25 consisting of the two rods exhibiting longitudinal ξ and bending ζ motions. The second index denotes the part of the rod. The excitation (or sink) is realised by means of the springs s_{L1}, s_{B1}, s_{L2} and s_{B2} .

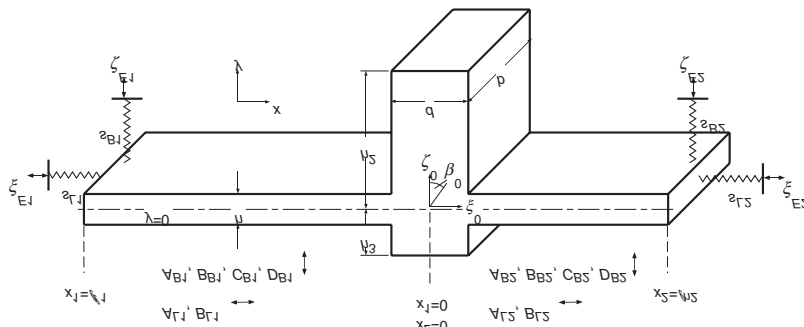


Fig. 6.25. Beam with an eccentric blocking mass with the notation used

For the analysis is required, moreover, the kinetic energy of the blocking mass. It is composed of the longitudinal motion ξ_0 , the bending motion ζ_0 and the rotation β_0 and can be written as

$$E_{Mkin} = \frac{\rho bd}{2} \left[\int_{-h_3}^{h_2} \left(\frac{\partial \zeta_0}{\partial t} \right)^2 dy + \int_{-h_3}^{h_2} \left(\frac{\partial \xi_0}{\partial t} + y \frac{\partial \beta_0}{\partial t} \right)^2 dy \right]. \quad (6.126a)$$

By carrying out the integration, introducing the phasor notation and employing the identities in (6.113) one obtains

$$\begin{aligned} H_M = \frac{1}{T} \int_0^T E_{Mkin} dt &= \frac{M\omega^2}{4} \left[\underline{\zeta}_0 \underline{\zeta}_0^* + \underline{\xi}_0 \underline{\xi}_0^* + \frac{h_2 - h_3}{4} \left(\underline{\xi}_0 \underline{\beta}_0^* + \underline{\xi}_0^* \underline{\beta}_0 \right) \right. \\ &\quad \left. + \frac{1}{3} (h_2^2 - h_2 h_3 + h_3^2) \underline{\beta}_0 \underline{\beta}_0^* \right], \end{aligned} \quad (6.126b)$$

where $M = \rho bd(h_2 + h_3)$ is the total mass of the blocking element.

Finally, the boundary conditions at the discontinuity are required for the neutral layer i.e., where the motion is given by ξ_0 , ζ_0 and β_0 . For continuity, the motion components on either side must equal such that with the usual wave fields (6.114) and (6.117) assumed, this gives, at $x_1 = x_2 = 0$

$$\begin{aligned} \xi_{01} - \xi_{02} = 0 &\Leftrightarrow g_1 = A_{L1} + B_{L1} - A_{L2} - B_{L2}, \\ \zeta_{01} - \zeta_{02} = 0 &\Leftrightarrow g_2 = A_{B1} + B_{B1} + C_{B1} e^{k_{B1} l_{11}} + D_{B1} \\ &\quad - A_{B2} - B_{B2} - C_{B2} - D_{B2} e^{-k_{B2} l_{n2}}, \\ \beta_{01} - \beta_{02} = 0 &\Leftrightarrow g_3 = k_{B1} \left[-jA_{B1} + jB_{B1} - C_{B1} e^{k_{B1} l_{11}} + D_{B1} \right] \\ &\quad - k_{B2} \left[-jA_{B2} + jB_{B2} - C_{B2} - D_{B2} e^{-k_{B2} l_{n2}} \right]. \end{aligned} \quad (6.127)$$

No complications arise from a generalization to configurations involving obliquely adjoining beams. It must merely be observed that motion components in the two directions must equal.

By means of (6.116), (6.119), (6.122), (6.126b) and (6.127), the function to be minimized can be developed,

$$\begin{aligned} H_{B1} + H_{B2} + H_{L1} + H_{L2} + H_{sL1} + H_{sL2} + H_{sB1} + H_{sB2} + H_M \\ + \sum_{v=1}^3 (\lambda_v^* g_v + \lambda_v g_v^*) = \text{Min.} \end{aligned} \quad (6.128a)$$

In somewhat elaborated form this expression reads

$$\begin{aligned} \sum_{v=1}^2 \beta_v (h_{Bv} + h_{Bv}^*) + \sum_{v=1}^2 \alpha_{Lv} (h_{Lv} + h_{Lv}^*) - \sum_{v=1}^2 \frac{s_{Lv}}{4} h_{Lsv} h_{Lsv}^* \\ - \sum_{v=1}^2 \frac{s_{Bv}}{4} h_{Bsv} h_{Bsv}^* + \sum_{v=1}^3 (\lambda_v g_v^* + \lambda_v^* g_v) \\ + \gamma_1 \left[\underline{\zeta}_0 \underline{\zeta}_0^* + \underline{\xi}_0 \underline{\xi}_0^* + \frac{h_2 - h_3}{4} \left(\underline{\xi}_0 \underline{\beta}_0^* + \underline{\xi}_0^* \underline{\beta}_0 \right) + \frac{h_2^2 - h_2 h_3 + h_3^2}{2} \underline{\beta}_0 \underline{\beta}_0^* \right] = \text{Min.} \end{aligned} \quad (6.128b)$$

Herein,

$$\begin{aligned}
 \beta_v &= \frac{\omega^2 \rho_v s_v}{2k_{Bv}}, \alpha_{L_v} = \frac{\omega^2 \rho_v s_v}{2k_{L_v}} \sin[k_{L_v} (l_m - l_n)], \gamma_1 = \frac{M\omega^2}{4}, \\
 h_{Bv} &= (A_{Bv}^* C_{Bv} + B_{Bv} C_{Bv}^*) I_{Cv}^* + (A_{Bv}^* D_{Bv} + B_{Bv} D_{Bv}^*) I_{Dv}^*, \\
 I_{Cv} &= \frac{E_{Bnv} N_v - E_{Bnv}}{1+j}, I_{Dv} = \frac{E_{Bnv} - E_{Bnv} N_v}{1-j}, \\
 E_{Bnv} &= e^{-jk_{Bv} l_m}, E_{Bnv} = e^{-jk_{Bv} l_n}, \\
 N_v &= e^{-k_{Bv} (l_m - l_n)}, h_{L_v} = A_{L_v} B_{L_v}^* E_{L_v}, E_{L_v} = e^{-jk_{L_v} (l_m - l_n)}, \\
 \zeta_0 &= A_{B1} + B_{B1} + C_{B1} e^{k_{B1} l_1} + D_{B1}, \xi_0 = A_{L1} + B_{L1}, \\
 \underline{\beta}_0 &= k_{B1} (-jA_{B1} + jB_{B1} - C_{B1} e^{k_{B1} l_1} + D_{B1}), \\
 h_{Bs1} &= \zeta_{E1} - A_{B1} e^{-jk_{B1} l_1} - B_{B1} e^{jk_{B1} l_1} - C_{B1} - D_{B1} e^{k_{B1} (l_1 - l_{n1})}, \\
 h_{Bs2} &= \zeta_{E2} - A_{B2} e^{-jk_{B2} l_{n2}} - B_{B2} e^{jk_{B2} l_{n2}} - C_{B2} e^{k_{B2} (l_{n2} - l_{n1})} - D_{B2}, \\
 h_{Ls1} &= \xi_{E1} - A_{L1} e^{-jk_{L1} l_1} - B_{L1} e^{jk_{L1} l_1}, \\
 h_{Ls2} &= \xi_{E2} - A_{L2} e^{-jk_{L2} l_{n2}} - B_{L2} e^{jk_{L2} l_{n2}}.
 \end{aligned} \tag{6.128c}$$

These expression are written such that they readily can be extended to include more beam elements.

To determine the minimum, the derivatives are formed with respect to the unknown A_{B1}^* , B_{B1}^* ... D_{B2}^* , λ_1^* , λ_2^* and λ_3^* and equated to zero. At this step of the analysis, which is preferably commissioned to a symbolic algebra solver, are developed the $2 \cdot 6 + 3 = 15$ linear equations having symmetric coefficients. Also the solution can be performed numerically with the commonly available programmes.

Numerical difficulties arise at the singularities of matrix, which correspond to system resonances. This can be circumvented by introducing some damping i.e., k_L and k_B are made complex or at least one of the external sources acts as a sinc. For the following results, for example, the reflected waves in the second beam element is cancelled by choosing ξ_{E2} and ζ_{E2} such that $B_{L2} = B_{B2} = 0$. Mathematically, this means that the amplitudes ξ_{E2} and ζ_{E2} are transferred to the unknown, practically established by means of a simple column exchange in the matrix formed from Eq. (6.128b). Similarly, ξ_{E1} or ζ_{E1} can be chosen such that only incident bending or longitudinal waves respectively exist in the first beam element. Accordingly, the same conditions are achieved as those employed in Sects. 6.1 and 6.4.

A good check of the calculated results is the energy conservation. This means that the sum of the incident powers must equal the sum of transmitted and reflected powers i.e.,

$$\begin{aligned} & 2|A_{B1}|^2 \beta_1 + 2|B_{B2}|^2 \beta_2 + |A_{L1}|^2 \alpha_1 + |B_{L2}|^2 \alpha_2 \\ & = 2|B_{B1}|^2 \beta_1 + 2|A_{B2}|^2 \beta_2 + |B_{L1}|^2 \alpha_1 + |A_{L2}|^2 \alpha_2, \end{aligned} \quad (6.129)$$

where $\alpha_v = \omega^2 \rho_v^2 s_v / 2 k_{L1}$.

For the part of the power carried by bending waves, a factor 2 appears because the power here propagates with the group speed $2\omega/k_B$.

Another possible check is given by the reciprocity principle. Its satisfaction is readily examined by means a few manipulations.

In Figs. 6.26 a and b are shown some results obtained with the procedure described. These results give some impression of the influence of the eccentricity of the blocking mass and the angle between the beam elements. It is observed that the larger the eccentricity, resulting from an increased radius of gyration, the lower the blocking frequency whilst the high frequency attenuation remains unaffected. Also, the conversion from bending to longitudinal waves is not particularly pronounced. When the eccentricity already is significant, a further increase has only limited effect on the conversion.

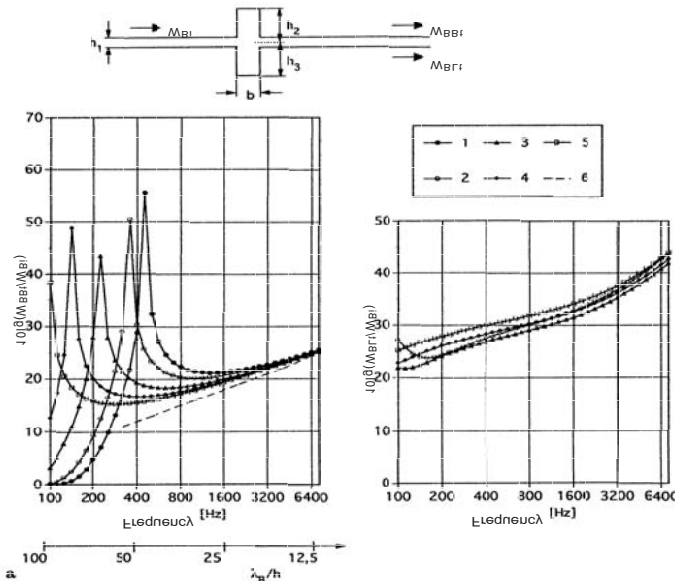


Fig. 6.26a. Bending wave attenuation and conversion at an eccentric blocking mass. $b = 2 h_1$, 1) $h_2 = h_3 = 15 h_1$; 2) $h_2 = 20 h_1$, $h_3 = 10 h_1$; 3) $h_2 = 25 h_1$, $h_3 = 5 h_1$; 4) $h_2 = 30 h_1$, $h_3 = 0$; 5) $h_2 = 35 h_1$, $h_3 = -5 h_1$; 6) Asymptote in (6.68d)

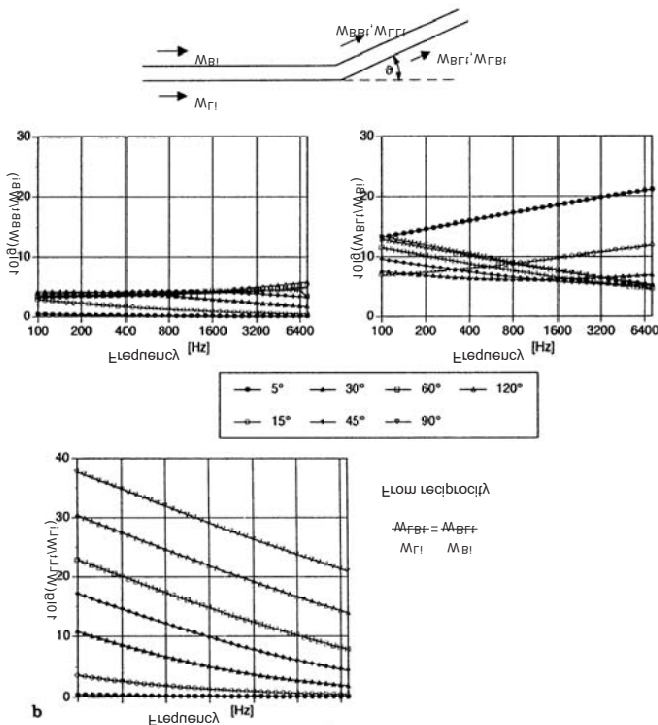


Fig. 6.26b. Attenuation and conversion of bending and longitudinal waves at an angle discontinuity

For the inclined beams it is evident that the angle affects the transmission of longitudinal waves whereas that of flexural waves remains essentially uninfluenced.

Figure 6.27 show additional examples. In this case, the analysis is extended to several beam elements. The procedure, however, remains unaltered although the numerical labour grows markedly with the number of unknown; $6 + 9(n - 1)$ for n beam elements. In this figure, the parameters were set such that for a single blocking mass, the unrealistically high attenuation of 15 – 20 dB is achieved at high frequencies. As is seen, the transmission loss per element is additive for the symmetric configuration and results in fully unrealistic values in the stop bands. For the eccentric configuration involving equally heavy masses as the symmetric, in contrast, the limiting attenuation is reached after about two spatial periods. That the excitation of longitudinal waves constitutes the reason, is found not only in measurements [6.8] but also in the analysis, which clearly

shows that after about three spatial periods, the power propagated by longitudinal waves is substantially bigger than that carried by flexural waves.

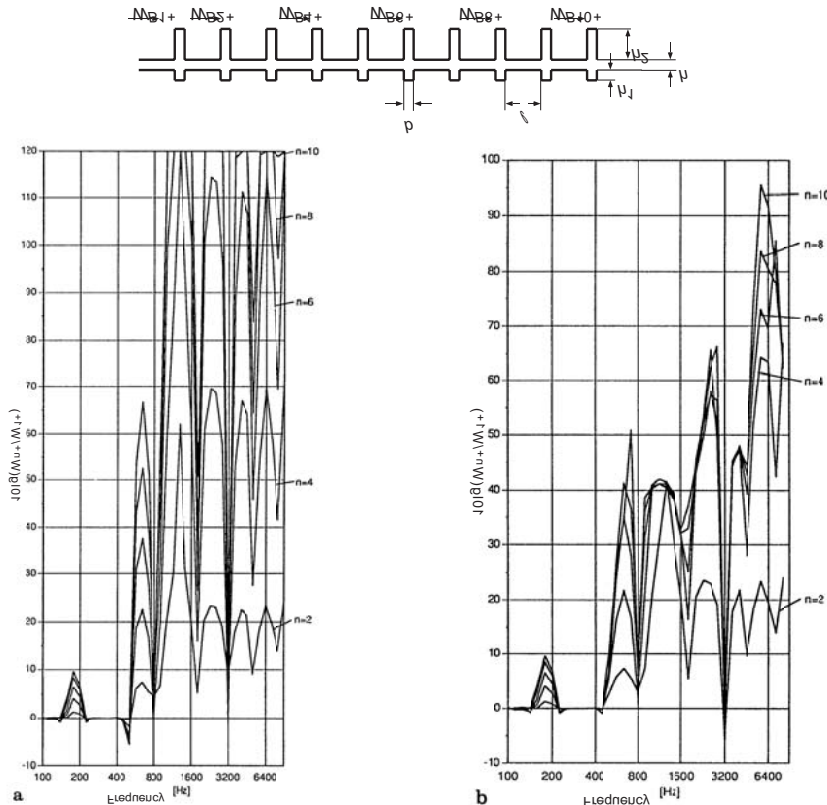


Fig. 6.27. Propagation of bending waves along a beam with periodic masses. $l = 0.3\text{m}$, $h = 0.01\text{m}$, $b = 0.02\text{m}$. a) Symmetrically attached masses $h_2 = h_3 = 0.1\text{m}$, b) eccentrically attached masses $h_2 = 0.1\text{m}$, $h_3 = 0\text{m}$

6.7 Oblique Incidence

6.7.1 General Considerations

It is now instructive to consider bending waves propagating along plates and impinging obliquely on straight boundaries or interfaces. This generalization obviously is of great practical importance because normal inci-

dence is only one rare special case of interest for plate-like structures. If a plate is excited at a point, the energy propagates from the excitation point in all directions in the plate. A rectangular boundary thus intercepts waves at all possible angles, partially after multiple reflections.

In contrast to statistical room acoustics, grazing incidence is no more probable than incidence from any other direction including the normal. As in room acoustics, however, an element of length l of the boundary intercepts only the projection $l \cos \theta$ of the incident wave as illustrated in Fig. 6.28. Therefore, normal incidence is of greatest importance in the two-dimensional case. If the transmission efficiency is τ for the boundary element and angle of incidence considered and the energy per unit area $e'' [\text{J/m}^2]$ is uniformly distributed over all angles of incidence, the fraction of power transmitted for the angular segment $d\theta$ corresponds to $d\theta/2\pi$. Hence, the power transmitted through the element l is given by

$$W = \frac{c_g e'' l}{2\pi} \int_{-\pi/2}^{\pi/2} \tau(\theta) \cos \theta d\theta = \frac{c_g e'' l}{2\pi} \int_{-1}^1 \tau(\sin \theta) d(\sin \theta), \quad (6.130)$$

where c_g denotes the group speed. The second form of the expression suggests that it is useful to express and plot the transmission efficiency as function of $\sin \theta$ so that the area under the resulting curve corresponds directly to the average transmission efficiency

$$\tau_m = \frac{\int_0^1 \tau(\sin \theta) d(\sin \theta)}{\int_0^1 d(\sin \theta)} = \int_0^1 \tau(\sin \theta) d(\sin \theta). \quad (6.131a)$$

Similarly, may be defined the average absorption efficiency

$$\alpha_m = \int_0^1 \alpha(\theta) d(\sin \theta). \quad (6.131b)$$

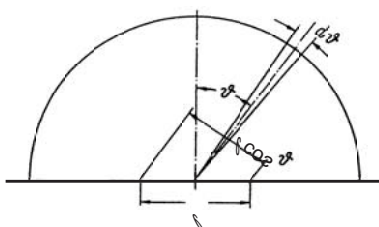


Fig. 6.28. Weighting for the process of averaging over angle of incidence

As in statistical room acoustics, the question may be addressed of how much energy per unit area e'' is induced in a plate of area S due to a continuous power input W_0 . Neglecting the losses that occur during propagation, the input power must equal the sum of power lost at the boundaries given by (6.130), with the transmission efficiency replaced by the absorption efficiency. If the average absorption efficiency is used instead of the integral form of Eq. (6.130), the power balance can be expressed as a sum over boundary parts

$$W_0 = \frac{c_g e''}{\pi} \sum l_k \alpha_{mk}. \quad (6.132)$$

This means that the stationary energy per unit area is determined by the power imparted and the boundary characteristics

$$e'' = \frac{\pi W_0}{c_g \sum l_k \alpha_{mk}}. \quad (6.133)$$

Also the increase or decrease in the energy per unit area can be determined that occurs in those time periods when e'' deviates from that given by (6.133) such that a difference arise between the right and left hand side. This difference leads to a corresponding growth or decay of the total energy $e'' S$ in the plate,

$$W_0 - \frac{c_g e''}{\pi} \sum l_k \alpha_{mk} = S \frac{de''}{dt} \quad (6.134)$$

In particular it is found for the reverberation process discussed in Sect. 4.4.1.3, which occurs when the power input is suddenly removed, that

$$e'' = e_0'' e^{-\delta t} \quad (6.135)$$

where $\delta = (c_g / \pi S) \sum l_k \alpha_{mk}$. The corresponding reverberation time T_{60} , defined for a decay by 60 dB,

$$T_{60} = 6 \frac{\pi S}{c_g \sum l_k \alpha_{mk}} \ln(10) = 13.8 \frac{\pi S}{c_g \sum l_k \alpha_{mk}} \quad (6.136)$$

is proportional to the area and inversely proportional to the sum $\sum l_k \alpha_{mk} = a$, which can be considered as the “equivalent absorption length”. By introducing the spatially averaged absorption efficiency,

$$\bar{\alpha}_m = \frac{\sum l_k \alpha_{mk}}{\sum l_k}, \quad (6.137)$$

as well as the total perimeter $L = \sum l_k$, Eq. (6.136) can be rewritten as

$$T_{60} = \frac{13.8 \pi S}{c_g L} \frac{1}{\bar{\alpha}_m}. \quad (6.138)$$

Upon comparing this expression with that for the reverberation time of a room of volume V and surface area S

$$T_{60} = \frac{13.8}{c_g} \frac{4V}{S} \frac{1}{\bar{\alpha}_m}, \quad (6.139)$$

it is clear that the volume of the room is analogous to the plate area, the surface area analogous to the perimeter of the plate but that the numerical factors differ. Whilst the mean free path for a room is given by

$$l_m = \frac{4V}{S}, \quad (6.140a)$$

that for a plate obeys [6.13]

$$l_m = \frac{\pi S}{L}. \quad (6.140b)$$

The latter result will be used in conjunction with the treatment of the statistical energy analysis (SEA) in Sect. 6.9.

6.7.2 General Consequences of the Boundary Conditions

6.7.2.1 Wavenumber and Angle

Consider two semi-infinite plates, which are connected along the axis at $x = 0$ as depicted in Fig. 6.29. For homogeneous plates and an angle of incidence θ_1 , one can distinguish between the incident wave

$$A_{B1} e^{-jk_{x1}x} e^{-jk_z z} = A_{B1} e^{-jk_{x1}x} E_z, \quad (6.141a)$$

the reflected wave

$$B_{B1} e^{jk_{x1}x} E_z = r A_{B1} e^{jk_{x1}x} E_z, \quad (6.141b)$$

the transmitted propagating wave

$$A_{B2} e^{-jk_{x2}x} E_z = t A_{B1} e^{-jk_{x2}x} E_z, \quad (6.141c)$$

and the to both sides emanating evanescent waves

$$\begin{aligned} C_{B2} e^{-k_{N2}x} E_z &= t_j A_{B1} e^{-k_{N2}x} E_z, \\ D_{B1} e^{k_{N1}x} E_z &= r_j A_{B1} e^{k_{N1}x} E_z. \end{aligned} \quad (6.141d)$$

The identical z dependence for all wave parts is abbreviated E_z . The amplitude of the incident wave as well as its wavenumber component in the x -direction k_{x1} are prescribed by the form of the excitation. The latter can also be expressed in terms of the angle of incidence as

$$k_{x1} = k_{B1} \cos \vartheta_1. \quad (6.141e)$$

The other amplitudes or equivalently, the reflection factors r , r_j and transmission factors t , t_j must be determined from the boundary conditions, which can be summarized as:

- The relations in (6.141a) to (6.141d) must satisfy the equation for free bending waves i.e., the homogeneous version of (3.184a). This determines the unknown k_z , k_{x2} , k_{N1} , k_{N2} .
- At the interface at $x = 0$, the motions must be continuous and forces as well as moments must establish an equilibrium. These conditions yield the equations for r , t , r_j and t_j .

An important prerequisite is the common spatial periodicity along the interface for all waves. Only for an equality of the wavenumber component k_z , describing the spatial periodicity in the z -direction, equality of motions can be fulfilled. This can also be described as all waves having the same “trace” velocity c_z in the z -direction. Such a situation stands and falls with homogeneity of the plates and uniformity of the boundary conditions at the interface $x = 0$. When one of these prerequisites is not fulfilled, it is no longer a reflection and attenuation problem of plane waves but a markedly more complicated scattering problem, for which new waves with other wavenumbers must be taken into account.

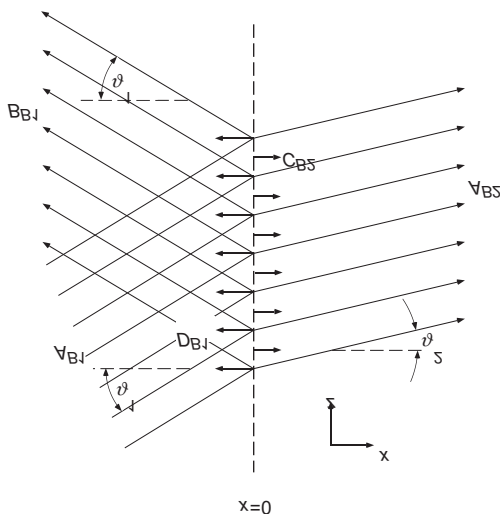


Fig. 6.29. Reflection and transmission at an interface between two different plates

Upon substituting (6.141a) into (3.184a) with different right hand side one finds that

$$(-k_{x1}^2 - k_z^2)^2 - k_{B1}^4 = 0 \Rightarrow k_z = \sqrt{k_{B1}^2 - k_{x1}^2} = k_{B1} \sin \vartheta_1. \quad (6.142a)$$

Herein, k_{B1} is the bending wavenumber of the plate at the side $x < 0$ cf., (3.83). Also obtained are

$$(-k_{x2}^2 - k_z^2)^2 - k_{B1}^4 = 0 \Rightarrow k_{x2} = \sqrt{k_{B2}^2 - k_z^2} = k_{B2} \sqrt{1 - \frac{k_{B1}^2}{k_{B2}^2} \sin^2 \vartheta_1}, \quad (6.142b)$$

$$(k_{N1}^2 - k_z^2)^2 - k_{B1}^4 = 0 \Rightarrow k_{N1} = \sqrt{k_{B1}^2 + k_z^2} = k_{B1} \sqrt{1 + \sin^2 \vartheta_1}, \quad (6.142c)$$

$$(k_{N2}^2 - k_z^2)^2 - k_{B2}^4 = 0 \Rightarrow k_{N2} = \sqrt{k_{B2}^2 + k_z^2} = k_{B2} \sqrt{1 + \frac{k_{B1}^2}{k_{B2}^2} \sin^2 \vartheta_1}. \quad (6.142d)$$

Three phenomena are noteworthy in conjunction with (6.142).

- Since all expressions in (6.141) contain the factor $E_z = \exp(-jk_z z)$, the problem is principally one-dimensional.
- In contrast to the one-dimensional wave propagation in beams hitherto treated, the absolute values of the wavenumbers for evanescent and propagating waves are not equal.
- As for other wave phenomena, total reflection can occur i.e., solely evanescent waves exist in the indirectly excited plate field. The condition for this is that (6.142b) is imaginary, which means that

$$k_{B1} \sin \vartheta_1 > k_{B2} \Leftrightarrow \sin \vartheta_1 > \frac{k_{B2}}{k_{B1}} = \frac{c_{B1}}{c_{B2}} = \sqrt{\frac{m_2'' B_1'}{m_1'' B_2'}} = \frac{h_1}{h_2} \sqrt{\frac{c_{L1}}{c_{L2}}}. \quad (6.143)$$

This is completely analogous to the refraction of electro-magnetic waves (Snell's law). In the present case and plate fields of equal materials, the critical angles for total reflection are listed in Table 6.1 for some thickness ratios.

Table 6.1. Critical angles for total reflection at an interface between two plates of equal materials

h_1/h_2	1.1	1.2	1.5	2	3	5
ϑ_{Cr}	72°	66°	55°	45°	35°	26°

6.7.2.2 Amplitudes

The Eqs. (6.141) contain four unknown amplitudes although it appears as if six were required to satisfy the boundary conditions, velocity and rotational velocities in two directions, the moments M_{xx} and M_{xz} as well as the force F_x . This is a delusion, however, since the variables are partially dependent. The rotational velocity in the z -direction is obtained as

$$\frac{\partial v}{\partial z} = -jk_z v,$$

and, hence, is not an independent variable but completely determined through k_z and by the behaviour of v . Similarly, the torsional moment per unit width, given by (3.184c)

$$M_{xx} = \frac{B'(1-\mu)}{j\omega} \frac{\partial^2 v}{\partial x \partial z} = -\frac{B'(1-\mu)}{\omega} k_z \frac{\partial v}{\partial x} = -\frac{B'(1-\mu)}{\omega} k_z w_x \quad (6.144a)$$

is not an independent variable. For the boundary conditions therefore, only the velocity v , the rotational velocity in the x -direction, the moment

$$M_{xz} = -\frac{B'}{j\omega} \left(\frac{\partial^2 v}{\partial x^2} + \mu \frac{\partial^2 v}{\partial z^2} \right) = -\frac{B'}{j\omega} \left(\frac{\partial^2 v}{\partial x^2} - \mu k_z^2 v \right), \quad (6.144b)$$

and the shear force

$$Q_x = \frac{B'}{j\omega} \left(\frac{\partial^3 v}{\partial x^3} + \frac{\partial^3 v}{\partial x \partial z^2} \right) = \frac{B'}{j\omega} \left(\frac{\partial^3 v}{\partial x^3} - k_z^2 w_x \right), \quad (6.144c)$$

need be considered cf., Eqs. (3.184c, d).

On the other hand, this means that the three dynamic quantities M_{xx} , M_{xz} , and Q_x cannot act independently at the edge of a plate. Intuitively, for example, one would expect all three to vanish at a free edge. This dilemma is resolved by the shear force Q_x and the torsional moment M_{xz} combining to a resulting net action whereby the force is associated with the vertical shear stresses whereas the moment is associated with those acting horizontally above and below the neutral layer. This corresponds to St. Venant's principle, which states that first at a distance of some plate thicknesses from the boundary, the stress field approach that assumed in classical bending theory and which was adhered to in developing the boundary conditions. At such distances, on the other hand, the actual stress field at boundary does not matter. Also, the principle was employed as only equality of bending moments was required at cross-sectional area changes without bothering about the non-linear stress growth in the immediate vicinity of the discontinuity. A linear stress variation across the cross-section is es-

tablished a few plate thickness away from the discontinuity. Therefore, the present form of boundary conditions only make sense for wavelengths that are large compared with the plate thickness. This is also the requirement for the simple bending wave equation.

In the present analysis accordingly, the torsional moments resulting from the horizontal shear stresses (top part of Fig. 6.30), are qualitative equal to those due to the vertical shear stresses (mid part of Fig. 6.30). The related but opposing moments will compensate each other, limited by their differential difference. This means that torsional moments can be promoted or compensated by additional vertical forces per unit length and by concentrated forces at corners, which do not appear in this context owing to the arbitrary large side ways extension.

For all external forces and hence also for those appearing in the boundary conditions, it is the supporting force per unit length

$$F_x = Q_x - \frac{\partial M_{xx}}{\partial x} = \frac{B'}{j\omega} \left(\frac{\partial^3 v}{\partial x^3} - (2 - \mu) k_z^2 \frac{\partial v}{\partial x} \right) \quad (6.145)$$

and not the shear force, which is of interest.

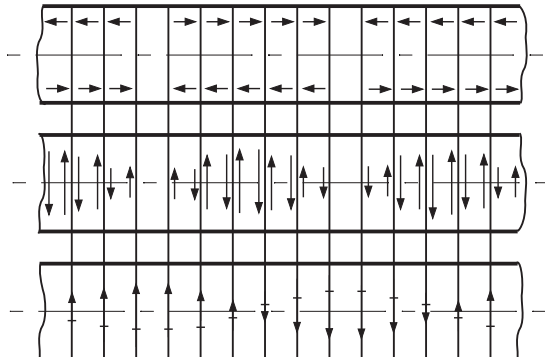


Fig. 6.30. Reaction forces (bottom) at a plate interface, composed of torsional moments (top) and shear forces (middle)

6.7.3 Examples

6.7.3.1 Bending Wave Transmission at Corners and Branches

As for the corresponding beam configurations, the boundary conditions at the interface $x = 0$ are:

- a) Vanishing velocity $v_1(0, z) = 0, v_2(0, z) = 0$,
- b) equality of rotational velocities $w_1(0, z) = w_2(0, z)$ and
- c) equality of moments $M_{xz1}(0, z) = M_{xz2}(0, z)$.

With Eq. (6.141) they yield the following relations cf., (6.144b)

$$\begin{aligned} v_1 &= 0 \Rightarrow 1 + r + r_j = 0 \\ v_2 &= 0 \Rightarrow t + t_j = 0 \\ w_1 = w_2 &\Rightarrow -jk_{x1}(1-r) + k_{N1}r_j = -jk_{x2}t - k_{N2}t_j \\ M_{xz1} = M_{xz2} &\Rightarrow -\frac{B'_1}{j\omega} \left[-k_{x1}^2(1+r) + k_{N1}^2r_j - \mu k_z^2 0 \right] \\ &= -\frac{B'_2}{j\omega} \left[-k_{x2}^2t + k_{N2}^2t_j - 0 \right] \end{aligned} \quad (6.146)$$

After some manipulations, using the relation from (6.142) $k_{N1}^2 + k_{x1}^2 = k_{B1}^2 + k_z^2 + k_{B1}^2 - k_z^2 = 2k_{B4}^2$ and similar relations for the second plate, it is found that

$$\begin{aligned} t &= \frac{2jk_{x1}}{k_{N2} + \Psi k_{N1} - j(k_{x2} + \Psi k_{x1})} \\ &= \frac{2j \cos \vartheta_1}{\left(\sqrt{\kappa^2 + \sin^2 \vartheta_1} + \Psi \sqrt{1 + \sin^2 \vartheta_1} \right) - j \left(\sqrt{\kappa^2 - \sin^2 \vartheta_1} + \Psi \cos \vartheta_1 \right)}, \end{aligned} \quad (6.147a)$$

and

$$r = \frac{-\sqrt{\kappa^2 + \sin^2 \vartheta_1} - \Psi \sqrt{1 + \sin^2 \vartheta_1} + j \left(\sqrt{\kappa^2 - \sin^2 \vartheta_1} - \Psi \cos \vartheta_1 \right)}{\left(\sqrt{\kappa^2 + \sin^2 \vartheta_1} + \Psi \sqrt{1 + \sin^2 \vartheta_1} \right) - j \left(\sqrt{\kappa^2 - \sin^2 \vartheta_1} - \Psi \cos \vartheta_1 \right)}. \quad (6.147b)$$

Herein, the abbreviations

$$\Psi = \frac{B'_2}{B'_1} \frac{k_{B2}^2}{k_{B1}^2} = \sqrt{\frac{m''_2 B'_2}{m''_1 B'_1}}, \quad \kappa = \frac{k_{B2}}{k_{B1}} = \frac{c_{B1}}{c_{B2}} \quad (6.147c)$$

are used cf., (6.18) and (6.20).

The transmission efficiency, of particular importance for the power transmission, again, can be obtained from $1 - |r|^2$ or from

$$\tau = \kappa \Psi \frac{\cos \vartheta_1}{\cos \vartheta_2} |t|^2 = \frac{\Psi \sqrt{\kappa^2 - \sin^2 \vartheta_1}}{\cos \vartheta_1} |t|^2, \quad (6.148a)$$

where account must be taken of the additional fact that a unit length of the boundary line intercepts different projected lengths of the incident and transmitted waves as indicated in Fig. 6.28. Either way is obtained

$$\tau = \frac{2\Psi \sqrt{\kappa^2 - \sin^2 \theta_i} \cos \theta_i}{\Psi^2 + \Psi \left[\sqrt{(\kappa^2 + \sin^2 \theta_i)(1 + \sin^2 \theta_i)} + \sqrt{(\kappa^2 - \sin^2 \theta_i) \cos \theta_i} \right] + \kappa^2}. \quad (6.148b)$$

By expressing the dependence on the angle of incidence in terms of $\sin \theta_i$, to facilitate the averaging in accordance with (6.129a) and abbreviating this by s , the foregoing result can be rewritten as

$$\tau = \frac{2\Psi \sqrt{\kappa^2 - s^2} \sqrt{1-s^2}}{\Psi^2 + \Psi \left[\sqrt{(\kappa^2 + s^2)(1+s^2)} + \sqrt{(\kappa^2 - s^2)(1-s^2)} \right] + \kappa^2}. \quad (6.148c)$$

This expression is easily verified by letting $\sin \theta_i = s = 0$ whereby (6.148c) reduces to (6.31).

For the special case where the two joined plates are alike so that

$$\Psi = \kappa = 1, \quad (6.148d)$$

Eq. (6.148c) becomes

$$\tau = \frac{1}{2} \cos^2 \theta_i = \tau(0) \cos^2 \theta_i,$$

and is represented by curve a in Fig. 6.31. This simple angle dependence also results when only

$$\kappa = 1, \quad (6.149a)$$

in which case always

$$\tau = \frac{2\Psi}{(\Psi + 1)^2} \cos^2 \theta_i = \tau(0) \cos^2 \theta_i. \quad (6.149b)$$

This expression also applies for all right-angled branches and intersections where all component plates have the same properties. For branches as depicted in the bottom part of Fig. 6.9a, however, the moment relation in (6.146) must be modified to

$$M_{xz1} = M_{yz2} + M_{xz3} = 2M_{yz2}, \quad (6.150a)$$

whilst the relation for intersections (upper part of Fig. 6.9a) reads

$$M_{xz1} = M_{yz2} + M_{xz3} + M_{yz4} = 3M_{yz2}, \quad (6.150b)$$

which merely means that $\Psi = 2$ or $\Psi = 3$ in Eqs. (6.157) and (6.158) respectively.

This first example demonstrates that the transmission efficiency does not increase with increasing angle of incidence as is the usual case for air-borne sound. The average transmission efficiency as obtained from Eq. (6.129a), is here smaller than that for normal incidence,

$$\tau_m = \tau(0) \int_0^1 \cos^2 \vartheta d(\sin \vartheta) = \frac{2}{3} \tau(0).$$

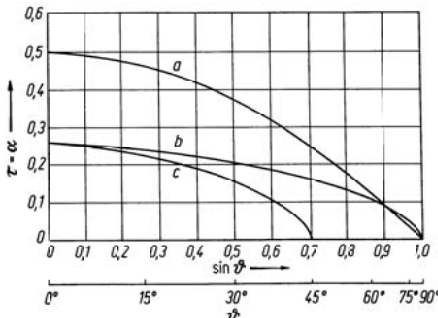


Fig. 6.31. Flexural wave transmission efficiency of a right-angle corner for oblique incidence. (a) $h_2 = h_1$, (b) $h_2 = h_1/2$ and (c) $h_2 = 2h_1$

As soon as the simplification of (6.149a) does not apply, the angle dependence not only becomes more complicated but the single parameter description of the normal incidence fails. In such a case, Ψ and κ have totally different influence on the angle dependence. Moreover, h_1/h_2 and h_2/h_1 are not interchangeable as is evident from curves *b* and *c* in Fig. 6.31. These curves, which represent the transmission efficiencies for $h_2/h_1 = 1/2$ and $h_2/h_1 = 2$ respectively, begin at the same value for normal incidence. For the latter case, however, the bending wave speed in the second branch is $\sqrt{2}$ times that of the configurations with $h_2/h_1 = 2$ and the limiting angle for total reflection is attained at $\arcsin(1/\sqrt{2}) = 45^\circ$. Beyond this angle, $j\sqrt{\kappa^2 - \sin^2 \vartheta_1}$ must be replaced by $\pm\sqrt{\sin^2 \vartheta_1 - \kappa^2}$ and thence, $|r| = 1$. This means that total reflection prevails in this angular range.

Regarding the phenomenon of total reflection it must also be noted that the relations above were derived on the basis of infinitely extended boundaries, just as the Fresnel expressions in optics. With finite lengths, or with cylindrical wave fronts, rays at the ends tend to broaden, often quite considerably at the limiting angle for total reflection. This broadening can cause some of the energy, propagating towards the boundary at the limiting angle of incidence, to be deflected along the boundary and then continuously reflect at the limiting angle.

One special case of plate branches deserves mentioning in this context since it only involves a small alteration of the boundary conditions. This is the configuration where one plate is rigidly connected to a second perpendicular one, which extends in both directions. Again, Eq. (6.146a) must be replaced by (6.150a) but without restricting Ψ and κ . This merely means that Ψ is replaced by 2Ψ in the final result, yielding

$$\tau_{12} = \frac{4\Psi \sqrt{\kappa^2 - s^2} \sqrt{1-s^2}}{4\Psi^2 + 2\Psi \left[\sqrt{(\kappa^2 + s^2)(1+s^2)} + \sqrt{(\kappa^2 - s^2)(1-s^2)} \right] + \kappa^2} \quad (6.152)$$

Upon letting $\sin \vartheta_1 = s = 0$, the normal incidence expression is recovered.

6.7.3.2 Conversion of In-Plane Waves at Corners

As in the case of normal incidence and beam problems, additional secondary waves generally arise also at interfaces between semi-infinite plates. Owing to the two dimensions, two new wave types can be excited namely longitudinal and transversal waves. In Sect. 3.7.4.1 these waves were treated and collectively termed in-plane waves in conjunction with Eq. (3.168b). Restricting the discussion to free plane waves, which have the wavenumber component k_z in the z -direction, it is readily found that (3.168b) yields

$$\begin{aligned} j\omega\xi &= v_I(x, z) = \left[A_L E_{L+} + B_L E_{L-} - (A_T E_{T+} - B_T E_{T-}) \frac{k_z}{k_{Tx}} \right] E_z, \\ j\omega\zeta &= v_{II}(x, z) = \left[(A_L E_{L+} - B_L E_{L-}) \frac{k_z}{k_{Tx}} + A_T E_{T+} + B_T E_{T-} \right] E_z, \end{aligned} \quad (6.153a)$$

in the absence of an excitation. Herein, A_L and B_L are the amplitudes of the longitudinal waves propagating in positive and negative directions respectively. A_T and B_T are similarly the transversal wave amplitudes. According to (3.174), the wavenumbers in the x -direction for both wave types are given by

$$k_{Lx} = \sqrt{k_{L1}^2 - k_z^2} = \sqrt{\frac{1-\mu}{2} k_T^2 - k_z^2} , \quad k_{Tx} = \sqrt{k_T^2 - k_z^2} . \quad (6.153b)$$

Additionally are used the abbreviations

$$E_{L+} = \frac{1}{E_{L-}} = e^{-jk_{Lx}x} , E_{T+} = \frac{1}{E_{T-}} = e^{-jk_{Tx}x} , E_z = e^{-jk_z z} . \quad (6.153c)$$

For the attenuation problem considered, for which there are only incident bending waves, only such in-plane waves can occur which emanate at the interface $x = 0$. This means that the in-plane wave velocities in the two plates are given by

$$\begin{aligned} v_{I1}(x, z) &= \left[B_{L1} E_{L1-} + B_{T1} E_{T1-} \frac{k_z}{k_{T1x}} \right] E_z , \\ v_{I2}(y, z) &= \left[A_{L2} E_{L2+} - A_{T2} E_{T2+} \frac{k_z}{k_{T2y}} \right] E_z , \\ v_{II1}(x, z) &= \left[-\frac{k_z}{k_{L1x}} B_{L1} E_{L1-} + B_{T1} E_{T1-} \right] E_z , \\ v_{II2}(y, z) &= \left[\frac{k_z}{k_{L2y}} A_{L2} E_{L2+} + A_{T2} E_{T2+} \right] E_z . \end{aligned} \quad (6.153d)$$

From (6.153a-d) it is seen that the longitudinal waves are propagating for real-valued k_{Lx} only. Similarly, the shear waves are propagating for real-valued k_{Tx} only. Since the wavenumber component k_z , which is common for all motions, is determined by the angle of incidence of the primary bending wave in accordance with (6.142a),

$$\begin{aligned} k_{L1}^2 - k_{B1}^2 \sin^2 \vartheta_1 > 0 &\Leftrightarrow \sin \vartheta_1 < \frac{c_{B1}}{c_{L1}} , \\ k_T^2 - k_{B1}^2 \sin^2 \vartheta_1 > 0 &\Leftrightarrow \sin \vartheta_1 < \frac{c_{B1}}{c_T} , \end{aligned} \quad (6.154a)$$

must be fulfilled for propagating waves in both plates. In these expressions, c_{B1} , c_{L1} and c_T are the phase speeds of the bending, longitudinal and shear waves respectively. The conditions in (6.154a) can be interpreted easily by introducing the trace velocity of the primary bending wave i.e., the wave speed projected on the z -direction

$$c_z = \frac{\omega}{k_z} = \frac{\omega}{k_{B1} \sin \vartheta_1} = \frac{c_{B1}}{\sin \vartheta_1} . \quad (6.154b)$$

It is clear that a wave is propagating only when its phase speed is smaller than the trace velocity. Otherwise, regions with positive and negative phases are closer than half a wavelength and compensate each other, realizing nearfields but no far field cf., the so called “hydro-dynamic short-circuiting” in Sect. 7.4.3.

Owing to the fact that for equal materials, the various phase speeds obey $c_B < c_T < c_{L1}$, there is always a limiting angle. Upon considering the condition for different angles of incidence, it is seen that almost only in the vicinity of normal incidence all wave types are propagating i.e.,

$$0 < \vartheta_1 < \vartheta_L \quad ; \quad \vartheta_L \arcsin\left(\frac{c_{B1}}{c_{L1}}\right) = \arcsin\left(\frac{\lambda_{B1}}{\lambda_{L1}}\right) \leq 20^\circ.$$

In the range

$$\vartheta_L < \vartheta_1 < \vartheta_T \quad ; \quad \vartheta_T \arcsin\left(\frac{c_{B1}}{c_T}\right) = \arcsin\left(\frac{\lambda_{B1}}{\lambda_T}\right) \leq 35^\circ,$$

only shear and bending waves yield far field. For $\vartheta_1 > \vartheta_T$ only the bending wave propagates. Whether or not the waves are transmitted to an adjoined plate, moreover, depends also on the limiting angle given by (6.143). The values given in the relations above represent limits in practice, associated with the condition that elementary bending theory is valid only up to about $\lambda_B < \lambda_L/3$ cf., Eq. (3.196). For thin plates and not too high frequencies, the limits will not be reached. In turn, this means that the in-plane wave excitation is confined to a very narrow angle segment.

To determine the eight unknown amplitudes B_{B1} , D_{B1} , A_{B2} and C_{B2} in (6.141b-d) and B_{L1} , B_{T1} , A_{L2} and A_{T2} in (6.153d) or the corresponding reflection and transmission factors, the augmented set of boundary conditions at $x = 0$ must be applied. In addition to (6.146) appear equality of translatory and rotational velocities in all directions besides equality of moments and forces i.e.,

$$\begin{aligned} v_{B1} &= v_{I2} \quad , \quad v_{I1} = v_{B2} \quad , \quad v_{H1} = v_{H2}, \\ w_1 &= w_2 \quad , \quad M_{xz1} = M_{yz2}, \\ F_{B1} &= F_{I2} \quad , \quad F_{I1} = F_{B2} \quad , \quad F_{H1} = F_{H2}, \end{aligned} \tag{6.155}$$

where the forces associated with the in-plane waves are simply obtained from a multiplication of the stresses by the plate thickness.

The rather tedious analysis is not recapitulated here but can be found in [6.7]. An example is shown in Fig. 6.32, taken from that work. To bring out the effects, the analysis is made for such a high frequency that the limit of validity of the elementary bending theory is reached. As in Fig. 6.6, the

various reflection and transmission efficiencies are overlaid. It is observed in this example that the longitudinal waves do not participate in the energy flow beyond 19.5° i.e., $\tau_{BL} = \rho_{BL} = 0$ and beyond 33° neither the shear waves, $\tau_{BT} = \rho_{BT} = 0$. The values for the normal incidence are in agreement with those in Fig. 6.6 for $\beta^2 = 1/9 \approx 0.11$, corresponding to $\lambda_B = 6h$.

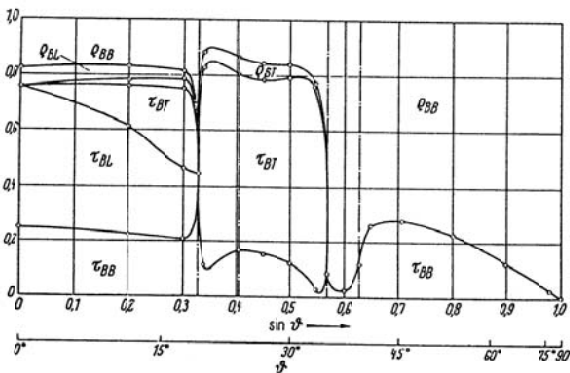


Fig. 6.32. Variation of reflection and transmission efficiencies with angle of incidence, accounting for secondary longitudinal and transversal waves

6.7.3.3 Transmission at Stiffeners

As an additional example is considered a plate with a reinforcing or stiffening beam attached. The discussion will be confined to a configuration consisting of two semi-infinite, equal plates with an incident bending wave at an angle θ ($\theta = \theta_1 = \theta_2$). Furthermore is employed, the very large simplification of a symmetrically located stiffener as depicted in Fig. 6.33. In such a way, the occurrence of in-plane waves is circumvented. As in Sect. 6.4, the width b is taken to be small and the junction between plate and beam rigid.

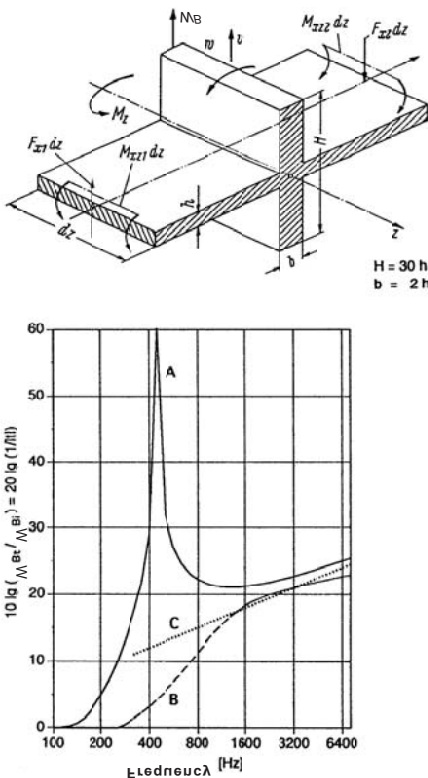


Fig. 6.33. Bending wave transmission across a symmetric stiffener. (A) normal incidence, (B) average for all angles of incidence and (C) approximation $\tau = |t|^2 \approx (2m''/m'k_B)^2$

In accordance with Sect. 6.7.2.1, the wave fields in the two plates can be written as

$$\begin{aligned} v_{B1}(x, z) &= A_{B1} \left[e^{-jk_x} + re^{jk_x} + r_j e^{k_N x} \right] E_z, \\ v_{B2}(x, z) &= A_{B1} \left[te^{-jk_x x} + t_j e^{-k_N x} \right] E_s, \end{aligned} \quad (6.156a)$$

where

$$k_x = k_B \cos \vartheta, \quad k_z = k_B \sin \vartheta, \quad k_N = k_B \sqrt{1 + \sin^2 \vartheta}. \quad (6.156b)$$

Since the two semi-infinite plates are equal and the stiffener assumed homogeneous such that no scattering occurs, the indices 1 and 2 are omitted. For the determination of the unknown amplitudes or factors, again two dy-

namic and two kinematic boundary conditions are required. The kinematic conditions read

$$v_{B1}(0, z) = v_{B2}(0, z) \Rightarrow 1 + r + r_j - t - t_j = 0, \quad (6.157a)$$

and

$$\left. \frac{\partial v_{B1}}{\partial x} \right|_{x=0} = \left. \frac{\partial v_{B2}}{\partial x} \right|_{x=0} \Rightarrow -jk_x + jrk_x + r_j k_N + jtk_x + t_j k_N = 0. \quad (6.157b)$$

For the dynamic boundary condition associated with the cross-sectional force, it must be taken into account that the difference in forces between the two sides of the stiffener constitute the driving force for the stiffener, In view of (6.145) therefore

$$p_s = F_{x1} - F_{x2} = \frac{B'}{j\omega} \left\{ \frac{\partial^3 (v_{B1} - v_{B2})}{\partial x^3} - (2 - \mu) k_z^2 \frac{\partial (v_{B1} - v_{B2})}{\partial x} \right\} A_{B1}. \quad (6.157c)$$

By substituting (6.156a) it follows that

$$\begin{aligned} p_s &= \frac{B'}{j\omega} \left\{ jk_x^3 (1 - r) + k_N^3 r_j - jk_x^3 t + k_N^3 t_j - (2 - \mu) k_z^2 \cdot 0 \right\} A_{B1} E_z \\ &= \frac{B'}{j\omega} \left\{ jk_x (k_B^2 - k_z^2) (1 - r + t) + k_N (k_B^2 + k_z^2) (r_j + t_j) \right\} A_{B1} E_z \\ &= \frac{B'}{j\omega} \left\{ k_B^2 (jk_x - jk_x r - jk_x t + k_N r_j + k_N t_j) + k_z^2 \cdot 0 \right\} A_{B1} E_z, \end{aligned} \quad (6.157d)$$

whereby (6.156b) and (6.157b) are used.

The force per unit length p_s acts perpendicular to the stiffener and since this can be considered as a beam, the bending wave Eq. (3.81) furnishes the necessary relations. Rewriting (3.81) in term of phasor notation and including the excitation on the right-hand side one obtains

$$\frac{B}{j\omega} \frac{\partial^4 v_{Bs}}{\partial z^4} + j\omega m' v_{Bs} = p_s, \quad (6.157e)$$

with v_{Bs} denoting the velocity along the stiffener. By employing the exponential form for the wave field in the z -direction and introducing the wave impedance from Sect. 5.4.1 this reduces to

$$Z_\sim \cdot v_{Bs} = p_s \quad ; \quad Z_\sim = j\omega m' \left(1 - \frac{k_z^4}{k_{Bs}^4} \right), \quad (6.157f)$$

where $k_{Bs} = \sqrt[4]{\omega^2 m' / B}$ is the bending wavenumber of the stiffener. Owing to the rigid connection between beam and plate, $v_{B1}(0) = v_{Bs} = v_{B2}(0)$. From (6.157d-f) it follows finally that

$$\frac{B'k_z^2}{j\omega} (jk_x - jk_x r - jk_x t + k_N r_j + k_N t_j) = Z_{\sim}(t + t_j), \quad (6.157g)$$

in view of (6.157a).

Regarding the second dynamic boundary condition related to the moment, the procedure is similar. The driving moment for the stiffener follows from (6.144b) as

$$\Delta M_s = M_{xz1} - M_{xz2} = -\frac{B'}{j\omega} \left\{ \frac{\partial^2 (v_{B1} - v_{B2})}{\partial x^2} - \mu k_z^2 \cdot 0 \right\} E_z. \quad (6.157h)$$

A relation between the driving moment and the rotational velocity of the stiffener w_{xs} is obtained from the harmonic, inhomogeneous form of the torsional wave Eq. (3.61)

$$T \frac{\partial^2 w_{xs}}{\partial z^2} + \omega^2 \Theta' w_{xs} = -j\omega \Delta M_s.$$

With the wave field in the exponential form, a torsional wave impedance of the stiffener is obtained as

$$Z_{-T} = \frac{\Delta M_s}{w_{xs}} = j\omega \Theta' \left(1 - \frac{T k_z^2}{\Theta' \omega^2} \right) = j\omega \Theta' \left(1 - \frac{k_z^2}{k_{Ts}^2} \right), \quad (6.157i)$$

in which $k_{Ts} = \sqrt{\omega^2 \Theta' / T}$ is the torsional wavenumber of the stiffener having the torsional stiffness T and the mass moment per unit length Θ' . Upon combining (6.157h-i) and observing (6.157a-b), it is found that

$$-\frac{B'k_z^2}{j\omega} (-1 - r + t + r_j - t_j) = Z_{-T} (-jk_x t - k_N t_j). \quad (6.157j)$$

The relations (6.157a, b, g, j) establish the four linear equations for determining t , r , r_j and t_j . The former two are found to be given by

$$t = \frac{j\alpha [4 + \gamma - \beta]}{j\alpha [4 + \gamma - \beta - \beta\gamma/2] - [\gamma + \alpha^2 \beta - \beta\gamma (1 - \alpha^2)/4]} \quad (6.158a)$$

$$r = \frac{\gamma - \alpha^2 \beta - \beta\gamma (1 - \alpha^2)/4}{j\alpha [4 + \gamma - \beta - \beta\gamma/2] - [\gamma + \alpha^2 \beta - \beta\gamma (1 - \alpha^2)/4]},$$

with

$$\begin{aligned}\alpha &= \frac{k_x}{k_N} = \frac{\cos \vartheta}{\sqrt{1 + \sin^2 \vartheta}}, \\ \beta &= \frac{\Theta' k_B^3}{m''} \sqrt{1 + \sin^2 \vartheta} \left(1 - \frac{k_B^2 \sin^2 \vartheta}{k_{Ts}^2} \right), \\ \gamma &= \frac{m' k_B}{m''} \frac{1}{\sqrt{1 + \sin^2 \vartheta}} \left(1 - \frac{k_B^4 \sin^4 \vartheta}{k_{Bs}^2} \right),\end{aligned}\quad (6.158b)$$

where m'' represents the mass per unit area of the plate.

Figure 6.33 shows the calculated transmission efficiency. From this figure and similar examples and from the structure of (6.158a) the following observations can be made:

- The total attenuation phenomenon disappears in an average over the angle since it occurs only in a very narrow angle segment.
- For grazing incidence ($\vartheta \approx 90^\circ$) there is no transmission because $\alpha \rightarrow 0$.
- Two trace matchings exist. The trace speed of the bending wave in the plate $c_z = c_B / \sin \vartheta$ equals either the bending wave or the torsional wave speed of the stiffener. In such a case, $\beta = 0$ or $\gamma = 0$ respectively. At high frequencies total transmission occurs in the vicinity of those points.
- The total transmission leads to an attenuation, averaged over the angle, which is smaller than that of normal incidence in a wide frequency range. This effect and the excitation of other wave types for asymmetric stiffeners constitute the reason why the average attenuation of structure-borne sound in stiffened structures does not differ markedly from that of unstiffened [6.8].

6.7.4 Application of Hamilton's Principle

The analysis method for structure-borne sound problems treated in Sect. 6.6 is also applicable for the oblique incidence. The procedure can be summarized as:

- a) Wave fields are assumed for the displacements in the three coordinate directions. For the bending motion, for example, (6.125) is replaced by

$$\eta(x, z, t) = \operatorname{Re} \left\{ \left[A_B e^{-jk_B x} + B_B e^{jk_B x} + C_B e^{-k_N (x-l_i)} + D_B e^{k_N (x-l_n)} \right] E_z e^{j\omega t} \right\}. \quad (6.159a)$$

Equation (6.153a) applies for the in-plane waves if it is divided by $j\omega$ to obtain the displacement, the time factor $e^{j\omega t}$ is included and the real

part taken. For potential stiffener, vibrating in bending and torsion, the wave fields are described by

$$\eta_s(x=0, z, t) = \operatorname{Re} \left\{ A_{Bs} E_z e^{j\omega t} \right\}, \quad w_s(x=0, z, t) = \operatorname{Re} \left\{ A_{Ts} E_z e^{j\omega t} \right\}. \quad (6.159b)$$

It is noted that the wavenumber component k_z is common in the entire domain since only plane waves exist and no scattering occurs.

- b) To establish the Hamiltonian, the equations of motion for the plate are substituted into (3.190a) and (3.190e) respectively. Limiting the precision to that of Kirchhoff's plate theory, the terms involving φ_x and φ_z in (3.190e) associated with the Mindlin correction, can be omitted. Also, the curvatures simplify to the respective spatial derivatives of η . The Hamiltonian of possible stiffeners is obtained from (6.118) and (6.115) for bending and torsion respectively. In the latter, however, the mass per unit length ρS must be replaced by the mass moment of inertia per unit length, ES by the torsional modulus and the displacement by the rotation.
- c) The boundary conditions relating to the displacements and rotations are taken into account by means of Lagrange's multipliers cf., Eqs. (6.128 a-c). The boundary conditions regarding moments and forces are not required, which is an advantage of the method.
- d) The external excitation and any elimination of waves with sines are introduced as displacements via springs or terms of the virtual work supplied cf., (3.188).
- e) By differentiating the function composed of the individual energies and additional constraints with respect to the unknown amplitudes and Lagrange's multipliers, the minimum is determined. The resulting set of linear equations is then solved by means of some suitable method.

Hamilton's principle commonly leads to more equations than the method employed in Sect. 6.7.3.3. This drawback, which becomes insignificant with the inescapable numerical handling, is fully compensated by compatibility of the method with numerical procedures and the less error-prone derivation path.

6.8 Parallel Plates

6.8.1 Continuous Coupling by Elastic Interlayers

For all double-plate structures such as double panel walls and machine enclosures, the plates involved have their mid-planes parallel to each other. In such designs one of the plates is usually supported by or coupled to the other by means of studs or common frames. Even if the two plates are separated by a highly elastic interlayer, the coupling may be significant. Such a coupling must also be taken into account if there is only air in the cavity. With air only, the coupling indeed can be stronger than when a sound absorbing fibrous mat occupies the cavity.

The configuration with a fibrous mat can be viewed as numerous, adjacent, independently compressible springs as is illustrated in Fig. 6.34. This model applies when the thickness is small. In view of the loose structure of the mats, such a modelling is intuitively reasonable. The stiffness per unit area s'' of the interlayer then consists of two parts. First, the stiffness of the fibres and second, that of the trapped air in pores leading to

$$s'' = s''_s + s''_a. \quad (6.160a)$$

The latter can be obtained as

$$s''_a = \frac{K}{\sigma d}, \quad (6.160b)$$

where K is the compression modulus of air, σ the porosity,

$$\sigma = \frac{\text{volume of pore}}{\text{total volume}}, \quad (6.160c)$$

which rarely deviates markedly from unity and d the thickness of the cavity.

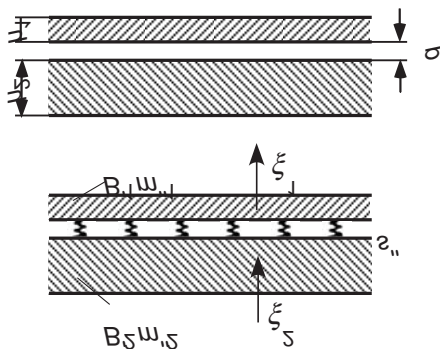


Fig. 6.34. Model for a floating floor

At low frequencies, of primary interest in this context, compression predominantly occurs isothermally because of the thermal conductivity and heat capacity of the fibres and K is equal to the static pressure of the air i.e., approximately 10^5 Pa. At high frequencies the compression process is adiabatic, increasing K by a factor of 1.4, a difference that is of little concern for the present discussion.

Compression of the air trapped in the fibre layer occurs essentially without lateral coupling because sidewise flow is constrained by the flow resistance of the fibrous layer. A flow resistance of above 10 kNs/m^4 suffices to prevent the lateral coupling. This is often exceeded by common fibre materials.

To determine the motion of two infinite plates, coupled by a fibrous layer, use is made of the plate Eqs. (3.184a) or (5.47) or (5.49). The upper plate is excited by an external force per unit area p and the stress at the interlayer, proportional to the relative displacement of the plates $s''(\eta_1 - \eta_2)$. On the lower plate acts only the interlayer stress when the radiation loading is neglected. Thus, the system of equations reads [6.14]

$$\begin{aligned} B'_1 \nabla^4 \xi_1 - \omega^2 m'_1 \xi_1 &= p - s''(\xi_1 - \xi_2), \\ B'_2 \nabla^4 \xi_2 - \omega^2 m''_2 \xi_2 &= s''(\xi_1 - \xi_2), \end{aligned} \quad (6.161a)$$

for harmonic processes. The analysis is identical to that of an excited single plate in Sect. 5.4. This means that exponential fields are assumed for the force as well as the resulting motion following (4.51) and (4.52a). If, simultaneously, the motion is expressed in terms of the velocity $v_{1,2} = j\omega \xi_{1,2}$, the coupled equations become

$$\begin{aligned} \left[(-k_x^2 - k_z^2)^2 - k_{BB1}^4 \right] v_1 - \frac{s''}{B'_1} v_2 &= \frac{j\omega}{B'_1} p, \\ \left[(-k_x^2 - k_z^2)^2 - k_{BB2}^4 \right] v_2 - \frac{s''}{B'_2} v_1 &= 0, \end{aligned} \quad (6.161b)$$

where the arguments for v and p are omitted for brevity. The wavenumbers

$$k_{BB1}^4 = \frac{\omega^2 m'_1}{B'_1} \left(1 - \frac{\omega_1^2}{\omega^2} \right), \quad k_{BB2}^4 = \frac{\omega^2 m''_2}{B'_2} \left(1 - \frac{\omega_2^2}{\omega^2} \right) \quad (6.162a)$$

correspond to those of either plate resting on an elastic layer backed by an immobile foundation cf., Sect. 3.7.4.4. The eigen-frequencies

$$\omega_1 = \sqrt{s''/m'_1}, \quad \omega_2 = \sqrt{s''/m''_2} \quad (6.162b)$$

are those of the plates undergoing spatially uniform vibrations. As is seen from (6.162a), k_{BB} is real only for frequencies $\omega > \omega_1$ and $\omega > \omega_2$ respectively.

In analogy with (5.50), the wave mobilities follow from (6.161b) as

$$\begin{aligned} Y_{\sim 1} &= \frac{v_1}{p} = \frac{j\omega}{B'_1} \frac{\left(k_x^2 + k_z^2\right)^2 - k_{BB2}^4}{\left[\left(k_x^2 + k_z^2\right)^2 - k_I^4\right] \left[\left(k_x^2 + k_z^2\right)^2 - k_{II}^4\right]}, \\ Y_{\sim 2} &= \frac{v_2}{p} = \frac{j\omega s''}{B'_1 B'_2} \frac{1}{\left[\left(k_x^2 + k_z^2\right)^2 - k_I^4\right] \left[\left(k_x^2 + k_z^2\right)^2 - k_{II}^4\right]}. \end{aligned} \quad (6.163a)$$

Herein, k_I^4 and k_{II}^4 are the zeroes of the determinant to (6.161b) given by

$$k_{I,II}^4 = \frac{1}{2} \left(k_{BB1}^4 + k_{BB2}^4 \right) \pm \sqrt{\frac{1}{4} \left(k_{BB1}^4 - k_{BB2}^4 \right)^2 + \frac{\omega_1^2 \omega_2^2 m_2'' m_1''}{B'_1 B'_2}} \quad (6.163b)$$

For equal plates such that $B'_1 = B'_2 = B'$ and $m_1'' = m_2'' = m''$, one obtains

$$k_I^4 = \frac{\omega^2 m''}{B'}, \quad k_{II}^4 = \frac{\omega^2 m''}{B'} \left(1 - 2 \frac{\omega_1^2}{\omega^2} \right) \quad (6.163c)$$

In coupled wave problems, equations are encountered that have the same structure as those pertaining to two simple, coupled systems e.g., two coupled pendula. Just as there occur two eigen-frequencies for two coupled oscillators, which differ little from those of the uncoupled systems when the coupling is weak, there occur two wavenumbers in the present case, which reduce to the wavenumbers k_{B1} and k_{B2} when the layer stiffness vanishes i.e., $\omega_1 = \omega_2 = 0$. However, since ω_1 and ω_2 appear in ratios to ω , the same transition also occurs for large frequencies.

By means of the wave mobilities, the response to an arbitrary excitation can be determined by integrating over wavenumber space in accordance with (5.55c). For a point force excitation F_0 of the top plate, its velocity is obtained from

$$v_1(x, z) = \frac{F_0}{4\pi^2} \frac{j\omega}{B'_1} \iint \frac{k^4 - k_{BB2}^4}{\left(k^4 - k_I^4\right) \left(k^4 - k_{II}^4\right)} e^{-jk_x x} e^{-jk_z z} dk_x dk_z, \quad (6.163d)$$

where the abbreviation $k^2 = k_x^2 + k_z^2$ is used. For the further analysis it is suitable to rewrite the fraction as

$$\begin{aligned} \frac{k^4 - k_{BB2}^4}{(k^4 - k_I^4)(k^4 - k_H^4)} &= \frac{1}{k_I^4 - k_H^4} \left(\frac{k^4 - k_{BB2}^4 - k_I^4 + k_I^4}{k^4 - k_I^4} - \frac{k^4 - k_{BB2}^4 - k_H^4 + k_H^4}{k^4 - k_H^4} \right) \\ &= \frac{k_I^4 - k_{BB2}^4}{k_I^4 - k_H^4} \frac{1}{k^4 - k_I^4} - \frac{k_H^4 - k_{BB2}^4}{k_I^4 - k_H^4} \frac{1}{k^4 - k_H^4}. \end{aligned}$$

Beside the factors that do not involve k^4 , there remain integrals in the form

$$\frac{F_0 j\omega}{4\pi B'_1} \iint \frac{1}{k^4 - k_I^4} e^{-jk_x x} e^{-jk_z z} dk_x dk_z = \frac{F_0 \omega}{8k_I^2 B'_1} \Pi(k_I r),$$

similar to that resulting for the homogeneous plate, established by substituting (5.50) into (5.56c).

In this way, the following responses are obtained after some manipulations

$$\begin{aligned} v_1(r) &= \frac{F_0 \omega}{8B'_1(k_I^4 - k_H^4)} \left[\frac{k_I^4 - k_{BB2}^4}{k_I^2} \Pi(k_I r) - \frac{k_H^4 - k_{BB2}^4}{k_H^2} \Pi(k_H r) \right], \\ v_2(r) &= \frac{F_0 \omega s''}{8B'_1(k_I^4 - k_H^4) B'_2} \left[\frac{\Pi(k_I r)}{k_I^2} - \frac{\Pi(k_H r)}{k_H^2} \right], \end{aligned} \quad (6.164a)$$

where $r = \sqrt{x^2 + z^2}$ is the distance between excitation and response points and $\Pi(\cdot)$ the propagation function defined in (5.44a).

Of primary interest with respect to practice is the case with weak coupling i.e., high attenuation, obtained for $\omega > \omega_1$ and $\omega > \omega_2$. For differing plate properties such that $k_1 \neq k_2$, the plate response approach

$$\begin{aligned} v_1(r) &\approx \frac{F_0 \omega}{8B'_1 k_I^2} \Pi(k_I r), \\ v_2(r) &\approx -\frac{F_0 \omega s''}{8B'_1 B'_2 (k_I^4 - k_2^4)} \left[\frac{\Pi(k_I r)}{k_I^2} - \frac{\Pi(k_2 r)}{k_2^2} \right]. \end{aligned} \quad (6.164b)$$

As is seen, the response of the upper plate is equal to that of the free plate where the connected plate has no influence. In contact, the wave field in the bottom plate is composed of two waves, with wavenumbers k_1 and k_2 emanating from the excitation position. The former is a forced wave whereas the latter is free.

In practice, usually the improvement is of interest when introducing a secondary plate such as, for example, in conjunction with floating floors. For the directly excited, untreated reference bottom plate, the response is given by

$$v_{20}(r) = \frac{F_0 \omega}{8B'_1 k_2^2} \Pi(k_2 r),$$

such that the improvement is obtained as

$$\frac{v_2(r)}{v_{20}(r)} = \frac{s''}{\omega^2 m''_1} \left(1 - \frac{m''_2 B'_1}{m''_1 B'_2} \right)^{-1} \left[1 - \left(\frac{m''_2 B'_1}{m''_1 B'_2} \right)^{1/2} \frac{\Pi(k_1 r)}{\Pi(k_2 r)} \right]. \quad (6.165a)$$

When the added plate is significantly more flexible than the bottom reference plate ($B'_1 \ll B'_2$), which is commonly the case in practice, (6.165a) condenses to the surprisingly simple form

$$\frac{v_2(r)}{v_{20}(r)} \approx \frac{\omega_1^2}{\omega^2} = \frac{s''}{\omega^2 m''_1}. \quad (6.165b)$$

It is noteworthy that the improvement for such designs is independent of the properties of the reference plate. This means that it is possible to define as well as measure an improvement for an elastic layer and a top plate, which is applicable also in other situations [6.15, 6.16].

Equation (6.165b) and its applicability as a practical measure of the improvement is clearly confirmed by measurements on plates with marked material losses as illustrated in the bottom part of Fig. 6.35. For low material losses as in the upper part of the figure, the modal behaviour, not accounted for in the present analysis, gives rise to additional transmission, in particular at high frequencies.

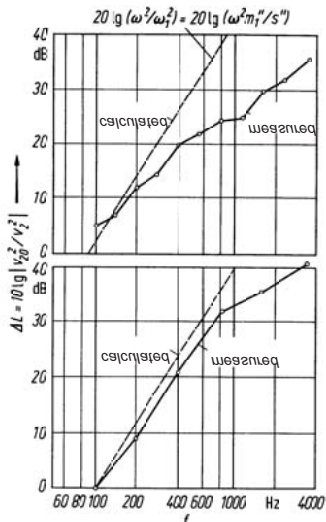


Fig. 6.35. Insertion loss for a floating floor. 35mm concrete floating floor on a 130mm concrete deck with a glass wool interlayer (1 kg/m^2) (top), 50mm concrete slab supported by 200mm wooden joists (bottom)

It must be emphasized that the fact that (6.165b) also describes the behaviour of a two-degree-of-freedom system with one small and one big mass should not lead to the conclusion that the elastic coupling between two parallel plates is identical to the coupling between two rigid masses. The differences are the following:

- In the lower plate two waves with wavenumbers k_1 and k_2 establish the response. Solely in the special case where $m''_2 B'_1 \ll m''_1 B'_2$, the forced vibrations of wavenumbers k_1 due to the top plate can be neglected.
- A short analysis of (6.164a) shows that in the case of equal plates, for which $k_I^2 - k_H^2 = 2\omega_1^2 m''_1 / B'_1$, the average attenuation is small. This is fundamentally different from the situation with two elastically coupled masses. For the wave motion there is continuously an interaction between the two plates.

Figure 6.35 shows two of the many measurement results where the applicability of Eq. (6.165b) is demonstrated with respect to the low frequency range of primary concern in practice. The deviations are mainly due to the finite size of the measured plates. The resulting modal behaviour means, moreover, that the top plate contributes with sound radiation above its critical frequency [6.17, 6.18].

Another reason for deviations can be the neglect of lateral coupling in the analysis, which overestimates the stiffness of the elastic layer and hence manifests itself as a reduced attenuation [6.18].

6.8.2 Point-Like Sound Bridges

Double shell structures considered herein, often involve more or less rigid connections. So called sound bridges can be statically motivated or be due to manufacturing imperfections. Whatever background, they affect the attenuation negatively, particularly at high frequencies since they short-circuit the elastic layer [6.19, 6.20].

As an idealized model can be considered two infinite plates connected via an elastic layer and a point-like sound bridge as illustrated in Fig. 6.36. The sound bridge is assumed to be a short rod carrying longitudinal waves. With the bridge having a Young's modulus E_b and density ρ_b , connected rigidly to both plates, the forces and velocities at the two ends are given by the four-pole Eqs. (4.41)

$$\begin{aligned} F_{b2} &= F_{b1} \cos k_b d - jZ_b v_{b1} \sin k_b d [= F_{b1} - j\omega m_b v_{b1}], \\ v_{b2} &= \frac{-jF_{b1} \sin k_b d}{Z_b} + v_{b1} \cos k_b d \left[= -\frac{j\omega}{s_b} F_{b1} + v_{b1} \right]. \end{aligned} \quad (6.166)$$

Herein,

$$k_b = \omega \sqrt{\rho_b / E_b} , \quad Z_b = S_b \sqrt{\rho_b E_b}$$

are the longitudinal wavenumber and impedance, respectively. The expressions in brackets, moreover, are valid in the practically important case of short bridges or low frequencies at which $k_b d \ll 1$, $m_b = \rho_b S_b d$ is the net mass and $s_b = S_b E_b / d$ the net stiffness.

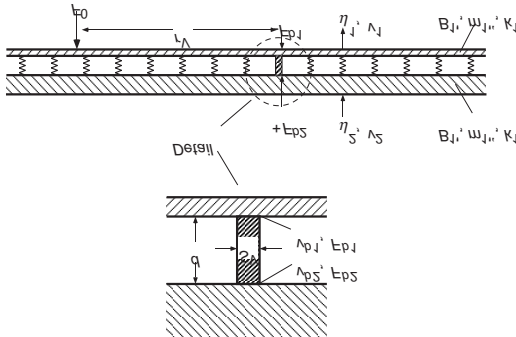


Fig. 6.36. Model for parallel plates with a point-like sound bridge

In the analysis, the response of the point-excited parallel plates given by (6.164a) can be used [6.21]. The wave field of the top plate subject to the external force F_0 and the bridge force F_{b1} , as well as that of supporting bottom plate subject to the additional bridge force F_{b2} can be written as

$$\begin{aligned} v_1(r) &= F_0 G_{11}(r | r_0) - F_{b1} G_{11}(r | r_b) + F_{b2} G_{21}(r | r_b) \\ v_2(r) &= F_0 G_{12}(r | r_0) - F_{b1} G_{12}(r | r_b) + F_{b2} G_{22}(r | r_b) \end{aligned} \quad (6.167)$$

The Green's functions G are those of the parallel plates obtained from (6.164a) for a unit force at a distance $|r - r_0|$ or $|r - r_b|$ respectively. The first index thereby, refers to the plate being excited whereas the second to the response plate. Hence, G_{11} and G_{12} are identical to (6.164a) with $F_0 = 1$ and r replaced by the respective distance. G_{22} and G_{21} result by interchanging the indices in (6.164a).

Since the plate velocity must equal the bridge velocity at the contact point, r can be set equal to r_b in (6.177) and the velocities $v_{b1} = v_1(r_b)$ and $v_{b2} = v_2(r_b)$ inserted in (6.166). The emerging set of equations yields the unknown forces F_{b1} and F_{b2} , by means of which all other quantities can be determined.

Of particular interest is the transmitted power due to the sound bridge

$$W_b = \frac{1}{2} \operatorname{Re} [F_{b2}^* v_{b2}]. \quad (6.168a)$$

If, for simplicity, a weak coupling is assumed for the elastic layer such that $G_{21} = G_{12} = 0$ and additionally

$$\begin{aligned} G_{11}(r_b | r_0) &= Y_1 \Pi(k_1 r_b), \\ G_{qq}(r_b | r_b) &= Y_q \quad ; \quad q = 1, 2, \end{aligned} \quad (6.168b)$$

where $Y_q = 1/(8\sqrt{B'_q m''_q})$ is the point mobility of the infinite plate and $\Pi(\cdot)$ the propagation function in Eq. (5.44a), substitution gives

$$W_b = F_0 Y_2 \frac{\left| \Pi(k_1 | r_b - r_0) \right|^2}{\left| (1 + Y_2 / Y_1) \cos k_b d + j(1/Y_1 Z_b + Z_b Y_2) \sin k_b d \right|^2}. \quad (6.169a)$$

This expression also allows for losses in the second bridge such that k_b and Z_b are complex. In the limiting case that $k_b d$ is small, (6.169a) reduces to

$$W_b = F_0^2 Y_2 \frac{\left| \Pi(k_1 | r_b - r_0) \right|^2}{\left(1 + Y_2 / Y_1 \right)^2 + (\omega / Y_1 s_b + \omega m_b Y_2)^2}. \quad (6.169b)$$

Equation (6.169b) reveals the possibilities to minimize the negative effect:

- a) The propagation function should be as small as possible. Upon considering material losses in the top plate, the propagation function can be approximated as

$$\left| \Pi(k_1 r_b) \right|^2 \approx \frac{2}{\Pi k_1 r_b} e^{-\eta_1 k_1 r_b / 2} \quad ; \quad k_1 r_b > 1, \quad (6.170a)$$

and becomes small for large distances between the external excitation and the sound bridge as well as for lossy materials [6.22].

- b) The bridge must be that elastic that [6.23]

$$\frac{\omega}{m_b} \gg Y_1 + Y_2, \quad (6.170b)$$

in other words, the mobility of the sound bridge, seen as a spring, must be larger than the sum of the plate mobilities.

- c) The bridge must be so heavy that

$$\omega m_b \gg \frac{1}{Y_1} + \frac{1}{Y_2}, \quad (6.170c)$$

or in other words, the mass impedance of the sound bridge should be bigger than the sum of the plate impedances. For thin plates, thus it can be beneficial to make the bridges as heavy as possible such that they act as blocking masses.

The observations listed above constitute additional examples of the validity of the fundamental rule: „A sound attenuating element must have acoustic properties (impedance or mobility), which differ as much as possible from those of the connected systems“. In this way the incident sound is terrified and turns rather round than dares to proceed into unknown territory.

This recipe is clear with respect to equal plates but for a combination of plates with widely differing mobilities it is not always possible to establish a solution that fully adheres to the rule.

6.9 Statistical Energy Analysis (SEA)

6.9.1 Analogies to Statistical Room Acoustics

In the statistical room acoustics, it is assumed that complicated wave fields, which are made up by many waves propagating here and there, can be well described by energy and power quantities. Prerequisites are that all directions of propagation are equally probable and all resonant modes are excited equally in a frequency average sense.

One application of statistical room acoustics, is the determination of power radiated by a source cf., Sect. 7.1. The expression

$$W = \frac{\overline{p^2} A}{\rho c^4} = \rho \overline{v^2} V \frac{13.8}{T} = m \overline{v^2} \omega \eta = E_{tot} \omega \eta \quad (6.171a)$$

underlies the measurement method [6.24]. $\overline{p^2}$ is the temporally and spatially averaged pressure squared and $\overline{v^2} = p^2 / (\rho c)^2$ the averaged velocity squared. A is the absorption area, determined by the room volume and the reverberation time. ρ is the medium density and c its speed of sound. E_{tot} is the total acoustic energy in the room, m the total mass and η the loss factor, related to the reverberation time as shown in Table 3.2. Essential for the problem treated in this section is that (6.171a) furnishes useful predictions for broad band sound, for room volumes $V > \lambda^3$ and for small losses such that the waves are multiply reflected before decaying. In the statistical room acoustic, moreover, is assumed that a sound source injects the

same power in every reverberation chamber as into an infinite space in frequency averaged sense. The power, thus, is independent of the room provided a minimum size is exceeded.

Upon transferring this to the structure-borne situation it is clear that the relation

$$W = mv^2 \omega \eta , \quad (6.171b)$$

also must be valid for structure-borne sound in an average sense since the medium is irrelevant for (6.171a). Applied for broad band, point excited structures, the power imparted is

$$W = \frac{1}{2} |F|^2 \operatorname{Re}[Y_\infty] = mv^2 \omega \eta . \quad (6.171c)$$

Herein, Y_∞ is the point mobility of the corresponding infinite structure cf., Sect. 5.7.3. Equation (6.171c) states that the transmitted power, on average in the stationary state, is independent of type of structure as well as its size and shape, again provided a minimum size is exceeded. For the power transmission, therefore, infinite systems can be used.

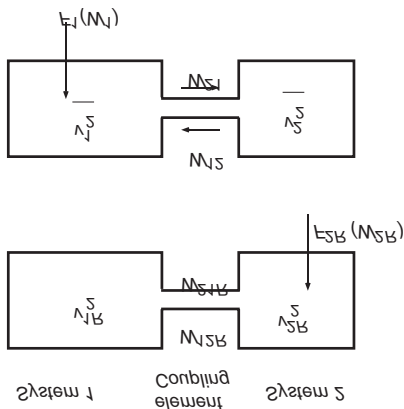


Fig. 6.37. Reciprocity analysis of coupled multi-modal systems with small losses

Considering next, the two coupled systems in the upper part of Fig. 6.37, for which the following power balance can be raised

$$\text{System1: } W_1 + W_{12} = W_{d1} + W_{21} \Leftrightarrow \frac{1}{2} |F_1|^2 \operatorname{Re}[Y_1] + W_{12} = m_1 \omega \eta_1 \overline{v_1^2} + W_{21}, \quad (6.172a)$$

$$\text{System2: } W_{21} = W_{2d} + W_{12} \Leftrightarrow W_{21} = m_2 \omega \eta_2 \overline{v_2^2} + W_{12},$$

since it is irrelevant in (6.171b) if the power is injected from an external source or from an adjacent system. In the expression, W_{12} and W_{21} are the power transmitted from system 2 to 1 and from 1 to 2 respectively. The order of indices is associated with the matrix notation. W_{d1} and W_{d2} are the dissipated powers in the two systems due to the loss factors η_1 and η_2 respectively. By adding the two expressions one obtains as expected $W_1 = W_{1d} + W_{2d}$.

For linearly behaving systems, the power transmitted is proportional to the energy and thence to the average velocity squared of the sending structure i.e.,

$$W_{21} = c_{21} \overline{v_1^2} \quad , \quad W_{12} = c_{12} \overline{v_2^2} . \quad (6.172b)$$

This means that (6.172a) yields

$$\frac{\overline{v_2^2}}{(|F_1|^2 / 2)} = \frac{c_{21} \operatorname{Re}[Y_1]}{m_1 \omega m_2 \omega \eta_1 \eta_2 + c_{21} m_2 \omega \eta_2 + c_{12} m_1 \omega \eta_1} . \quad (6.172c)$$

From a hypothetical experiment in which the second system is excited by means of a point force, as illustrated in the lower part of Fig. 6.37, the corresponding analysis gives

$$\frac{\overline{v_{1R}^2}}{(|F_{2R}|^2 / 2)} = \frac{c_{12} \operatorname{Re}[Y_2]}{m_1 \omega m_2 \omega \eta_1 \eta_2 + c_{21} m_2 \omega \eta_2 + c_{12} m_1 \omega \eta_1} . \quad (6.172d)$$

In view of the reciprocity principle, an interchange of excitation and response positions must deliver the same ratio of velocity to force. Since this must be true for every arbitrary position pair, it is accordingly also true for the mean value. Hence, the expressions (6.172c) and (6.172d) can be equated and the important reciprocity relation follows

$$c_{12} \operatorname{Re}[Y_2] = c_{21} \operatorname{Re}[Y_1] \Leftrightarrow \frac{c_{12}}{c_{21}} = \frac{\Delta N_1}{m_1} \frac{m_2}{\Delta N_2} . \quad (6.172e)$$

In the second part of this expression, Eq. (5.123) is employed, in which ΔN_1 and ΔN_2 are the number of modes in a specific frequency band. By considering the net power transmission

$$\begin{aligned} \overline{W_{21}} &= W_{21} - W_{12} = c_{21} \overline{|v_1|^2} / 2 - c_{12} \overline{|v_2|^2} / 2 \\ &= c_{21} \frac{\Delta N_1}{m_1} \left(\frac{m_1 \overline{|v_1|^2} / 2}{\Delta N_1} - \frac{m_2 \overline{|v_2|^2} / 2}{\Delta N_2} \right), \end{aligned} \quad (6.172f)$$

and introducing the energies contained in the two systems

$$E_1 = m_1 \overline{|v_1|^2} / 2, \quad E_2 = m_2 \overline{|v_2|^2} / 2, \quad (6.172g)$$

it follows that

$$\overline{W_{21}} = c_{12} \frac{\Delta N_1}{m_1} \left(\frac{E_1}{\Delta N_1} - \frac{E_2}{\Delta N_2} \right). \quad (6.172h)$$

This means that the net power transmitted is proportional to the difference in modal energies under the statistical prerequisites.

The ratio of squared velocities of the two systems when system 1 is directly excited, can be obtained from a substitution of (6.172f) in the second equation in (6.172a),

$$\frac{\overline{|v_2|^2}}{\overline{|v_1|^2}} = \frac{\Delta N_2 m_1}{\Delta N_1 m_2} \frac{1}{1 + m_2 \omega \eta_2 / c_{12}}, \quad (6.172i)$$

or

$$\frac{\overline{|v_2|^2} \operatorname{Re}[Y_1]}{\overline{|v_1|^2} \operatorname{Re}[Y_2]} = \frac{1}{1 + m_2 \omega \eta_2 / c_{12}} \frac{1}{1 + W_{d2} / W_{12}}.$$

Two limiting cases of Eq. (6.172i) are of particular interest.

- For the case where system 2 is lightly damped such that $W_{d2} < W_{12}$ i.e., when the dissipated power in system 2 is smaller than that transmitted back to system 1, the two systems are strongly coupled and

$$\frac{\overline{|v_2|^2}}{\overline{|v_1|^2}} \approx \frac{\operatorname{Re}[Y_2]}{\operatorname{Re}[Y_1]} \approx \frac{\Delta N_2 m_1}{\Delta N_1 m_2}. \quad (6.173a)$$

For strong coupling, accordingly, the velocity ratio depends only on the real parts of the mobilities and the energy becomes more or less uniformly distributed over the resonant modes irrespective of whether they are primarily associated with system 1 or 2. Owing to the fact that strong coupling often prevails in structure-borne sound, (6.173a) usually furnishes useful results in a rather simple way or, at least, an upper limit for $\overline{|v_2|^2}$.

- For the case that system 2 is highly damped and $W_{d2} > W_{12}$, on the other hand, the approximation

$$\frac{\left|v_2\right|^2}{\left|v_1\right|^2} \frac{\operatorname{Re}[Y_1]}{\operatorname{Re}[Y_2]} \frac{W_{12}}{W_{d2}} = \frac{\operatorname{Re}[Y_2]}{\operatorname{Re}[Y_1]} \frac{c_{12}}{m_2 \omega \eta_2} = \frac{c_{21}}{m_2 \omega \eta_2} \quad (6.173b)$$

applies. This means that the characteristics of the coupling control the velocity ratio. With the coupling factor c_{21} expressed in terms of the transmission efficiency, Eq. (6.173b) also can be considered as a guide for measurements of the transmission efficiency.

The considerations underlying Eqs. (6.172) and (6.173), moreover, can be extended to many coupled systems. If, for example, n systems are coupled, the power balance for each system can be written as

$$\begin{aligned} W_\mu + \sum_{\substack{v=1 \\ v \neq \mu}}^n W_{\mu v} &= W_{d\mu} + \sum_{\substack{v=1 \\ v \neq \mu}}^n W_{v\mu} ; \mu \in [1, n] \\ \Leftrightarrow \\ W_\mu + \sum_{\substack{v=1 \\ v \neq \mu}}^n c_{\mu v} \overline{|v_v|^2} &= m_\mu \omega \eta_\mu \overline{|v_\mu|^2} + \sum_{\substack{v=1 \\ v \neq \mu}}^n c_{v\mu} \overline{|v_\mu|^2} \end{aligned} \quad (6.174)$$

The case $\mu = v$ is excluded in the summations. Again, the reciprocity relation $c_{\mu v} \operatorname{Re}[Y_v] = c_{v\mu} \operatorname{Re}[Y_\mu]$ applies provided a „statistical state“ prevails. (6.174) establishes a set of linear equations. With the different coupling factors $c_{\mu v}$ as well as the power injections known, the energy flow and the velocity distribution can be computed for complicated, built-up systems.

The set of equations, however, can be used also for the inverse problem whereby the subsystems are successively excited one by one and the resulting velocity distributions are registered. In this way also, a possibly rather large set of equations is established, which can be solved for the unknown coupling factors. Commonly, the precision in solving such inverse problems is poor and any result should, therefore, be accompanied by the associated condition numbers to obtain an impression of the reliability of the results [6.25].

6.9.2 Energy Flow between Linearly Coupled Oscillators

In Sect. 5.7.3 was shown that averaging over several modes (oscillators) in a structure yields identical results as the energy relations, which are valid for diffuse „statistical“ vibration fields. Equations (5.121) to (5.124) demonstrate that under certain conditions, the modal energy on average is additive. The question is justified whether insight into the transmission process also can be gained from the opposite case of deterministic vibration fields.

In this pursuit, two oscillators will be considered and the energy distribution investigated when they are coupled. In this way, also the range of validity for the statistical approach is sought [6.26].

At first, the damped 2DoF-system in Fig. 6.38 is studied. The coupling is realized by means of a spring of stiffness s_{12} . From the free body diagrams or Lagrange's equations, supplementary accounting for the dampers, one obtains

$$\begin{aligned} m_1 \ddot{\xi}_1 + r_1 \dot{\xi}_1 + (s_1 + s_{12}) \xi_1 - s_{12} \xi_2 &= F_1, \\ m_2 \ddot{\xi}_2 + r_2 \dot{\xi}_2 + (s_2 + s_{12}) \xi_2 - s_{12} \xi_1 &= F_2. \end{aligned} \quad (6.175a)$$

With the usual assumption of harmonic oscillations, the velocity phasors become

$$\begin{aligned} v_1 &= \frac{-j\omega}{m_1 m_2 \text{Det}} \left[m_2 (\omega^2 - 2j\omega\delta_2 - \omega_2^2) F_1 + s_{12} F_2 \right], \\ v_2 &= \frac{-j\omega}{m_1 m_2 \text{Det}} \left[s_{12} F_1 + m_1 (\omega^2 - 2j\omega\delta_1 - \omega_1^2) F_2 \right], \end{aligned} \quad (6.175b)$$

where

$$\begin{aligned} \text{Det} &= \omega^4 - 2j\omega^3 (\delta_1 + \delta_2) - \omega^2 (\omega_1^2 + \omega_2^2 + 4\delta_1\delta_2) \\ &\quad + 2j\omega (\delta_1\omega_2^2 + \delta_2\omega_1^2) + \omega_1^2\omega_2^2 - s_{12}/(m_1 m_2) \end{aligned}$$

and $\omega_1 = \sqrt{(s_1 + s_{12})/m_1}$, $\omega_2 = \sqrt{(s_2 + s_{12})/m_2}$, $\delta_1 = r_1/(2m_1)$, $\delta_2 = r_2/(2m_2)$ are the eigen-frequencies and damping ratios of the two oscillators respectively when the other oscillator is blocked.

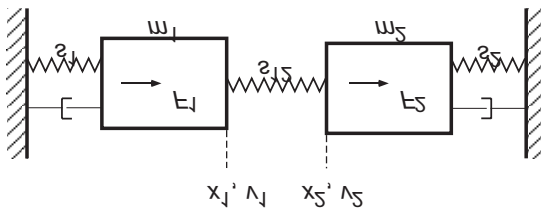


Fig. 6.38. Coupled oscillators

Of primary interest is the net energy flow $\overline{W_{12}}$ between the oscillators where the over bar denotes that the difference between the forwards and backwards transmitted power is understood. This quantity is given by

$$\begin{aligned}\overline{W_{12}} &= \frac{1}{2} \operatorname{Re} \left[F_{12} v_2^* \right] = \frac{1}{2} \operatorname{Re} \left[-s_{12} \frac{v_1 - v_2}{j\omega} v_2^* \right] \\ &= \frac{1}{2} \operatorname{Re} \left[\frac{-s_{12}}{j\omega} v_1 v_2^* \right] - \frac{1}{2} \operatorname{Re} \left[\frac{-s_{12}}{j\omega} |v_2|^2 \right] = \frac{1}{2} \operatorname{Re} \left[\frac{-s_{12}}{j\omega} v_1 v_2^* \right].\end{aligned}\quad (6.175c)$$

Herein, it is assumed that the stiffness s_{12} is purely real such that no dissipation takes place in the coupling element. Upon inserting (6.175b) in (6.175c) it is found that

$$\overline{W_{12}} = \frac{\omega^2 s_{12}^2}{m_1^2 m_2^2 |\operatorname{Det}|^2} \left[m_2 \delta_2 |F_1|^2 - m_1 \delta_1 |F_2|^2 \right] + \operatorname{Re} \left[A F_1^* F_2 + B F_1 F_2^* \right], \quad (6.175d)$$

where A and B are factors depending on ω , δ etc.

Based on the assumption that the forces F_1 and F_2 are independent of each other, the mixed products $F_1^* F_2$ and $F_1 F_2^*$ vanish on average. Additionally, it is assumed that the forces are broad band in nature, having flat spectra in the range comprising the two eigen-frequencies and decaying outside. By averaging (6.175d) over frequency, the net transmitted power in a band $\Delta\omega$ can be obtained. The integral involved is in the form

$$\begin{aligned}& \int_{-\infty}^{\infty} \frac{b_0 \omega^6 + b_1 \omega^4 + b_2 \omega^2 + b_3}{|a_0 \omega^4 + j a_1 \omega^3 + a_2 \omega^2 + j a_3 \omega + a_4|^2} d\omega \\ &= \pi j \frac{b_0 (-a_1 a_4 + a_2 a_3) + a_0 (a_1 b_2 - a_3 b_1) + a_0 b_3 (a_0 a_3 - a_1 a_2) / a_4}{a_0 (a_0 a_3^2 + a_1^2 a_4 - a_1 a_2 a_3)},\end{aligned}\quad (6.175e)$$

where the limits of integration have been extended to infinity for simplicity since it does not affect the result for the force spectra assumed. When the frequency band $\Delta\omega$ extends at least one octave beyond the resonances, the net averaged energy flow becomes

$$\overline{W_{12}} = \frac{\pi}{2\Delta\omega} \left[\frac{G_{F_1 F_1}}{m_1 \delta_1} - \frac{G_{F_2 F_2}}{m_2 \delta_2} \right] \frac{(\delta_1 + \delta_2) s_{12}^2}{m_1 m_2 Q}, \quad (6.176a)$$

where

$$Q = (\omega_1^2 - \omega_2^2)^2 + 4(\delta_1 + \delta_2)(\delta_1 \omega_2^2 + \delta_2 \omega_1^2) + 2(\delta_1 + \delta_2) \frac{s_{12}}{m_1 m_2},$$

and $G_{F_1 F_1}$ and $G_{F_2 F_2}$ are the average auto spectral density functions for the forces.

As the next step, the average energies are determined for the two oscillators

$$\overline{E_1} = \frac{1}{2} m_1 \overline{|v_1|^2} \quad , \quad \overline{E_2} = \frac{1}{2} m_2 \overline{|v_2|^2} . \quad (6.176b)$$

Upon substituting (6.175b) into (6.176b) and averaging in accordance with (6.175e), the difference in average energies is obtained as

$$\overline{E_1} - \overline{E_2} = \frac{\pi}{2\Delta\omega} \left[\frac{G_{F_1 F_1}}{m_1 \delta_1} - \frac{G_{F_2 F_2}}{m_2 \delta_2} \right] \frac{(\omega_1^2 - \omega_2^2)^2 / 2 + (\delta_1 + \delta_2)(\delta_1 \omega_2^2 + \delta_2 \omega_1^2)}{Q} .$$

This means that (6.176a) also can be written in the form

$$\overline{W_{12}} = \beta (\overline{E_1} - \overline{E_2}) = -\overline{W_{21}} . \quad (6.176c)$$

Herein, the proportionality constant amounts to

$$\beta = \frac{2}{m_1 m_2} \frac{(\delta_1 + \delta_2) s_{12}^2}{(\omega_1^2 - \omega_2^2)^2 + 4(\delta_1 + \delta_2)(\delta_1 \omega_2^2 + \delta_2 \omega_1^2)} . \quad (6.176d)$$

The analysis in Eqs. (6.176) shows that the power transmission between two coupled oscillators on average is proportional to the difference in average energies. This general finding is valid also for couplings realized by other additional linear elements. Thus, also a gyroscopic element, for example, could have been included. Such a coupling would have led to the additional term $B_{\zeta_2}^{\zeta_2}$ in the first equation in (6.175a) and $-B_{\zeta_1}^{\zeta_1}$ in the second. Even if the algebra would have grown, the proportionality in (6.176c) remains.

As is seen from a comparison of (6.176c) and (6.172h), the former constitute a special case of the latter, since there is only one mode per oscillator and hence, $\Delta N_1 = \Delta N_2 = 1$.

A comparison of β and $c_{21} \Delta N_1 / m_1$ shows that c_{21} will be a complicated function in the general case. Importantly, it is not only a function of the coupling element itself but depends also on the damping and on the separation of the eigen-frequencies. It is of interest, therefore, to seek manageable ways to assess the coupling factors and the conditions that have to be fulfilled. This issue is the most difficult one in statistical energy analysis.

6.9.3 Estimation of Coupling Loss Factors

In this chapter, almost exclusively infinitely extended structures are considered in the analysis of transmission of structure-borne sound power in built-up systems. It is thus suitable to investigate the relation between the coupling factors $c_{\mu\nu}$ and the transmission efficiencies τ , developed in pre-

vious sections. This problem formulation is also motivated by the fact that (6.172b) under statistical conditions tacitly requires a power transmission, which is independent of type of coupled systems. Accordingly, infinite continua are applicable, provided the material properties and cross-sectional dimensions are those of the finite systems.

In this context it is appropriate to change from coupling factors $c_{\mu\nu}$ to coupling loss factors $\eta_{\mu\nu}$, more commonly used in the literature. Since the energy flow from one system to another can be interpreted as a loss of energy for the emitting system, the coupling loss factor is defined in a similar way as the loss factor cf., Eq. (4.22),

$$\eta_{\mu\nu} = \frac{W_{\mu\nu}}{\omega E_v} = \frac{c_{\mu\nu} \overline{|v_v|^2} / 2}{\omega m_v \overline{|v_v|^2} / 2} = \frac{c_{\mu\nu}}{\omega m_v}. \quad (6.177a)$$

In turn, this means that the reciprocity relation in (6.172e) modifies into

$$\eta_{v\mu} \Delta N_\mu = \eta_{\mu v} \Delta N_v. \quad (6.177b)$$

6.9.3.1 One-Dimensional Configurations

Having treated the energy flow between two coupled oscillators in the previous section, the coupling will be addressed between the simplest case of continuous systems, in principle, possessing an infinite number of resonances. This kind of coupling exists for rods, beams and fluid-filled pipes or ducts at low frequencies. For the rigorous description of forces and velocities, the four-pole expressions in Eq. (4.41) apply. If the configuration in Fig. 6.39 is used as an example, the transmission of longitudinal waves across a blocking mass m can be obtained from the relations

$$\begin{aligned} F_1(l_1) &= F_0 c_1 - j Z v_0 s_1 \quad , \quad F_2(0) = F_1(l_1) - j \omega m v_1(l_1), \\ v_1(l_1) &= -j F_0 s_1 / Z_1 + v_0 c_1 \quad , \quad v_2(0) = v_1(l_1), \\ F_2(l_2) &= F_2(0) c_2 - j Z_2 v_2(0) s_2 \quad , \quad F_2(l_2) / v_2(l_2) = Z_T, \\ v_2(l_2) &= -j F_2(0) s_2 / Z_2 + j v_2(0) c_2. \end{aligned} \quad (6.178)$$

In the above relations $c_1 = \cos k_1 l_1$, $c_2 = \cos k_2 l_2$, $s_1 = \sin k_1 l_1$, $s_2 = \sin k_2 l_2$, $Z_1 = \rho_1 c_1 S_1$, $Z_2 = \rho_2 c_2 S_2$ and Z_T is a complex termination impedance. For the rods, S_1 and S_2 are the cross-sectional areas respectively. The wavenumbers k_1 and k_2 are taken to be complex to account for some material dissipation.

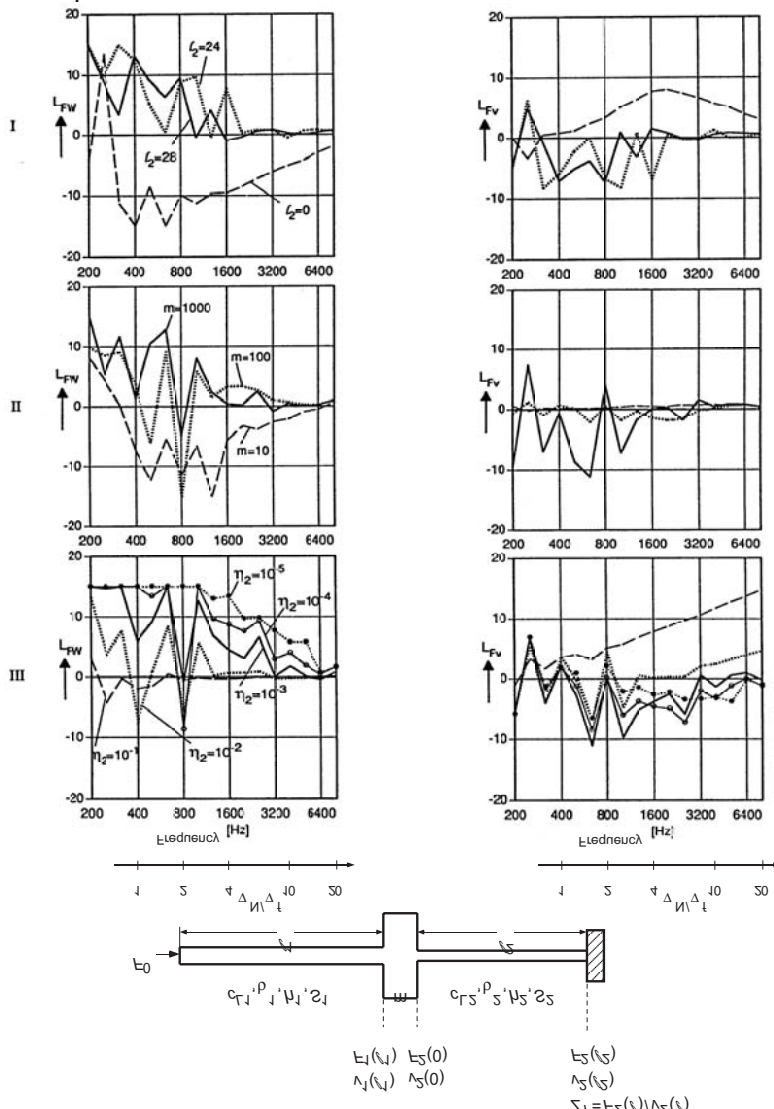


Fig. 6.39. Deviations of (6.172f) from (6.179e). For all cases $\rho_1 = \rho_2 = 8000 \text{ kg/m}^3$, $c_1 = c_2 = 5000 \text{ m/s}$, $S_1 = S_2 = 0.01 \text{ m}^2$, $l_1 = 20 \text{ m}$ and $Z_T = 0$, Diagram I: $\eta_1 = 0.003$, $m = 500 \text{ kg}$, $\eta_2 = 0.003$, Diagram II: $\eta_1 = 0.003$, $l_2 = 26 \text{ m}$, $\eta_2 = 0.003$, Diagram III: $\eta_1 = 0.001$, $l_2 = 26 \text{ m}$, $m = 500 \text{ kg}$

From the set of equations in (6.178), v_1 , v_2 and $F_2(0)$ can readily be solved for as functions of the external force F_0 . Thence, the spatially and frequency band averaged velocities squared as well as the net transmitted power to subsystem 2 can be developed i.e.,

$$\left(\frac{\overline{|v_1|^2}}{\overline{|v_2|^2}} \right)_{sim}, \quad \left(\overline{W_{12}} \right)_{sim} = \frac{1}{2} \operatorname{Re} [F_2(0)v_2^*(0)]. \quad (6.179a)$$

Upon combining the relation between the coupling loss factor and the coupling factor in (6.177) and the expression for the net energy flow between two subsystem in (6.172h), the numerically simulated coupling loss factor can be obtained as

$$\eta_{21_{sim}} = \frac{c_{21_{sim}}}{\omega m_1} \frac{2\overline{W_{21_{sim}}}/(\omega m_1)}{\overline{|v_1|^2} - \overline{|v_2|^2} \left[m_2 \Delta N_1 / (m_1 \Delta N_2) \right]}. \quad (6.179b)$$

The simulated results, based on a rigorous formulation, can be compared with those obtained employing the statistical formulation in Sect. 6.9.1, once the coupling factor is expressed in terms of the transmission efficiency $\tau_{\mu\nu}$, determined for the corresponding infinite structures. In this case, the special form of the definition of τ for one-dimensional systems is used

$$\tau_{\mu\nu} = \frac{W_{trans}}{W_{inc}} = \frac{W_{\mu\nu}}{W_{v+}} = \frac{W_{\mu\nu}}{\rho_v c_{gv} S_v |v_{v+}|^2}.$$

W_{trans} and $W_{\mu\nu}$ denote the transmitted power, and W_{inc} and W_{v+} the incident power, which can be expressed in terms of the density, the cross-sectional area, the group speed and the velocity amplitude squared of the incident wave. Since the velocity amplitude is composed of both the velocity of the incident wave and that of the reflected,

$$|v_{v+}|^2 = \frac{\overline{|v_v|^2}}{2 - \tau_{\mu\nu}}, \quad (6.179c)$$

from an energy conservation point of view cf., Sect. 6.1.1. From (6.179b), (6.179c) and a comparison with the definition in (6.172b), it is found that

$$c_{\mu\nu_{stat}} = \frac{W_{\mu\nu}}{\overline{|v_v|^2}} = \frac{\rho_v S_v c_{gv} \tau_{\mu\nu}}{2 - \tau_{\mu\nu}}, \quad (6.179d)$$

and

$$\eta_{\mu\nu_{stat}} = \frac{\rho_v S_v c_{gv}}{\rho_v S_v l_v \omega} \frac{\tau_{\mu\nu}}{2 - \tau_{\mu\nu}} = \frac{c_{gv}}{\omega l_v} \frac{\tau_{\mu\nu}}{2 - \tau_{\mu\nu}} \approx \tau_{\mu\nu} \frac{c_{gv}}{2\omega l_v}. \quad (6.179e)$$

The index ‘stat’ denotes that it is a result of statistical considerations. By employing the reciprocity relation in (6.177b) it can be demonstrated that $\tau_{\mu\nu} = \tau_{\nu\mu}$ since $\Delta N_v = \Delta \omega l_v (\pi c_{gv})$. This, previously frequently used equality is generally only valid in one-dimensional cases.

In the left part of Fig. 6.39 are shown the deviations of statistical estimates of the coupling loss factor from those of the numerical simulations

$$L_{DW} = 10 \log(\eta_{21stat} / \eta_{21sim}). \quad (6.180a)$$

The right-hand part of Fig. 6.39 similarly, present the deviations in velocity ratios

$$L_{Dv} = 10 \log \left(\frac{\overline{|v_1|^2}}{\overline{|v_2|^2}} \right)_{stat} - 10 \log \left(\frac{\overline{|v_1|^2}}{\overline{|v_2|^2}} \right)_{sim}. \quad (6.180b)$$

The statistical estimate is calculated from (6.172f) using c_{21stat} in (6.179d). In both sets of diagrams, averages over third octave bands are taken. In parallel with frequency as abscissa is displayed also the number of resonant modes per band for the receiving rod. For the example shown, $Z_T = 0$ is assumed, corresponding to a free end. Other, complex termination impedances as well as numerous other densities, wave speeds and cross-sectional areas, however, were included in the investigation.

For most of the cases investigated, the major portion, of which are not presented here, the statistical and simulated results agree within a few dB, provided that more than three resonant modes were encompassed in the frequency band. As is clearly highlighted in Fig. 6.39, however, there exist also exceptions, which can be explained by:

- When both subsystems are of equal dimensions and have the same boundary conditions, the eigen-frequencies are the same, give some small frequency shifts due to the coupling. Since the directly excited system acts like a filter for that indirectly excited, the excitation of the latter will be rather tonal than broad band. As can be expected, the transmission is stronger in such a case i.e., $\eta_{21sim} > \eta_{21stat}$ and $|v_2|_{sim}^2 > |v_2|_{stat}^2$. When so many modes are present in a band that the average modal distance is smaller than four times the their half-power bandwidth, the deviation becomes tolerable also for equal subsystems. In spite of this, SEA should not be employed for identical subsystems [6.27]. Usually, a variation in dimensions of 20% suffices, sometimes less, to separate the eigen-frequencies enough.

- When the coupling is very strong i.e., the coupling loss factor η_{12} is larger than about three times the loss factor η_2 , the coupling loss factor based on the statistical formulation is too high cf., the curves for $\eta_2 = 10^{-5}, 10^{-4}$ in Fig. 6.39. The velocity ratios, on the other hand, are approximately correct since the energy will be uniformly distributed among the modes, irrespective of the transmission. This result illustrates that for strong coupling where the net energy transport practically vanishes according to (6.172i), even an incorrect coupling factor c_{21} renders a correct velocity ratio. It should be noted that the loss factor η_2 encompasses the material dissipation and energy lost to the environment, exterior to the system but not that to the other subsystem.
- When the losses are very high, typically $\eta_2 k_2 l_2 > 2$, the system is practically no longer resonant since the amplitude of a wave has diminished more than 5 dB during a return trip and hence will not produce a resonance amplification. As a consequence, the spatially averaged velocity ratio will no longer be correctly described by the statistical approach. This case is represented by the curve $\eta_2 = 0.1$ in the right-hand part of Fig. 6.39. It is interesting to note that the coupling loss factor is well described by the statistical formulation although there is only one mode per frequency band cf., the left-hand part of Fig. 6.39. This can be referred to the coupling loss factor being principally independent of the averaged velocity and thence of the dissipation.
- For the sake of completeness, it must be pointed out that the SEA approach can be problematic when the excitation is not point-like but distributed as, for example, airborne sound excitation, which concentrates the power injected in a narrow wavenumber range.

6.9.3.2 Multi-Dimensional Configurations

Also for multi-dimensional configurations, a statistically based relation can be established between the coupling loss factor and the transmission efficiency of the corresponding infinite system. In analogy with (6.179c), the starting point is the definition of the transmission efficiency, averaged over all angles of incidence

$$\langle \tau_{\mu\nu} \rangle = \frac{\langle W_{\mu\nu} \rangle}{\langle W_{v+} \rangle}. \quad (6.181)$$

Upon combining (6.172b) and (6.177a),

$$\eta_{\mu\nu} = \frac{\langle \tau_{\mu\nu} \rangle \langle W_{v+} \rangle}{\omega m_v |v_v^2|},$$

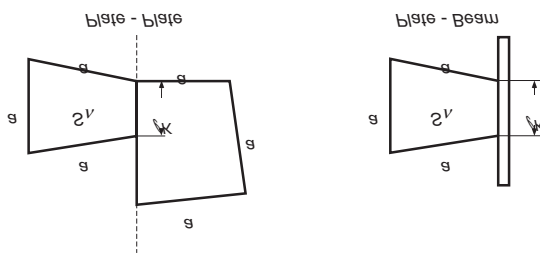
which leads to

$$\eta_{\mu\nu} = \langle \tau_{\mu\nu} \rangle \frac{c_{gv}}{\omega} \frac{l_c}{\pi S_v} \quad (6.182a)$$

in the two-dimensional case and

$$\eta_{\mu\nu} = \langle \tau_{\mu\nu} \rangle \frac{c_{gv}}{\omega} \frac{S_c}{4V_v} \quad (6.182b)$$

in the three-dimensional. Herein, c_{gv} , S_v and V_v are the group speed, the total area and the total volume of the sending subsystem respectively. l_c and S_c are the coupling length or area of the interface, as illustrated in Fig. 6.40. The factors $l_c/(\pi S_v)$ and $S_c/(4V_v)$ constitute the mean free path, which amounted to $2l_v$ in the one-dimensional case. The mean free path is the distance a wave propagates between two successive reflections at the coupling interface.



Two-dimensional source surfaces

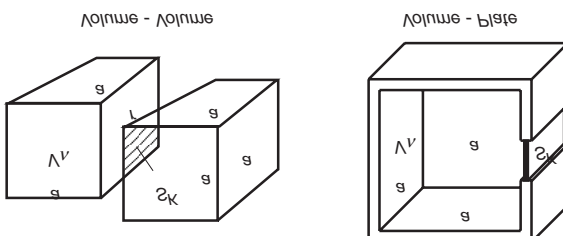


Fig. 6.40. Geometries for transformation of average transmission efficiency into coupling loss factor

Equations (6.182a) and (6.182b) realize a possibility to estimate the coupling loss factor when the transmission efficiency is known for the corresponding infinite system. In Fig. 6.40 this means that the boundaries denoted ‘a’ are made non-reflective whereas those denoted ‘r’ remain coupled as in the actual finite system.

With respect to validity and accuracy of (6.182), the considerations of the one-dimensional case hold cf., the end of Sect. 6.9.3.1. For multi-dimensional configurations, however, an interchange of indices in the average transmission efficiency is not possible since taking the average generally means that $\langle \tau_{\mu\nu} \rangle \neq \langle \tau_{\nu\mu} \rangle$. This does not represent a deficit of the reciprocity principle. Rather, the interchange of excitation and response positions can be used to show that $\langle \tau_{\mu\nu} \rangle \neq \langle \tau_{\nu\mu} \rangle$ follows from a correct application of the reciprocity principle. A simple example of this is the coupling of a room (index 1) to a duct (index 2). For such a system, the usual statistical formulation yields the relation between the average transmission efficiencies

$$\langle \tau_{21} \rangle = 8\pi \langle \tau_{12} \rangle / (k_1^2 S_2),$$

when the pressure resulting from a small volume velocity source is determined and the reciprocity principle applied. This means that the average transmission efficiency for the appropriate transmission direction always must be substituted in (6.182). Merely in the, regarding an SEA approach unfortunate, case of equal material properties and dimensions for the two subsystems, the average transmission efficiencies coincide in the two directions.

6.9.4 Application

Equations (6.172f) or (6.174) are the most important for the application of SEA. Accordingly, the quantities that have to be known are:

- The masses m_v of the subsystems,
- the loss factors η_v ,
- the number of modes ΔN_v in each frequency band and
- the coupling factors or coupling loss factors $\eta_{\mu\nu}$.

The determination of the masses and loss factors is usually not too cumbersome. The number of modes ΔN_v can be taken from Table 4.2 for many systems. An experimental assessment of ΔN_v from frequency response functions can be problematic since the identification of all the resonances often becomes difficult, particularly at high frequencies. The estimation of $c_{\mu\nu}$ or $\eta_{\mu\nu}$ was discussed in the previous section.

The SEA expressions become particularly simple when the dissipated power for a subsystem v is smaller than that re-transmitted to an adjacent subsystem i.e., $W_{dv} < W_{\mu v}$ or $\eta_v < \eta_{\mu v}$. This case is commonly termed strong coupling. In accordance with (6.172f), the velocity ratio is approximated by

$$\frac{\overline{|v_v|^2}}{\overline{|v_\mu|^2}} \approx \frac{\Delta N_v m_\mu}{\Delta N_\mu m_v}. \quad (6.183)$$

When it is clear that $\eta_v < \eta_{\mu v}$ or an upper limit for the velocity ratio is sought, meaningful predictions can be obtained without knowledge of the coupling quantities. Thereby, the mean square velocity of the indirectly excited subsystem, certainly, can be larger than that of the directly excited. Figure 6.41 shows two examples of the application of Eq. (6.183).

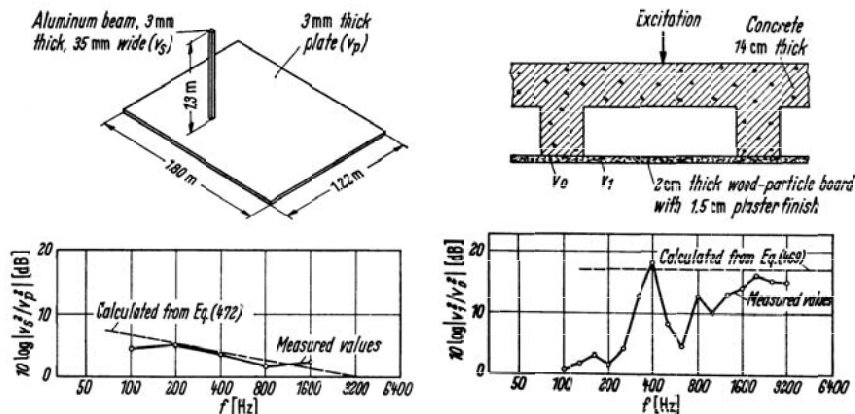


Fig. 6.41. Mean square velocity ratios for a rod-plate configuration and a lined waffle ceiling

For coupling between two structure-borne sound carrying subsystems or coupling between structure-borne and water-borne sound, the coupling loss factors are often rather large such that (6.183) is well suited for initial estimations. For coupling between structure-borne and airborne sound, however, the same expression mostly renders overestimates.

As an example of weak coupling, is considered the sound transmission from a fluid-filled volume V_F to a plane plate of area S_p . For the fluid, the density and speed of sound are ρ_F and c_F respectively. The density, thickness and bending wavenumber for the plate are ρ_p , h_p and k_p . It is assumed that only one side of the plate is in contact with the fluid. Otherwise the

area would have to be set to $2S_p$. In principle, the problem is solved when the radiation efficiency, defined in (7.9a), is known for the plate. With that known, the transmitted power can be written

$$W_{\mu\nu} = W_{Fp} = \rho_F c_F S_p \overline{|v_p|^2} \sigma. \quad (6.184a)$$

It follows that the coupling loss factor is

$$\eta_{\mu\nu} = \eta_{Fp} = \frac{W_{Fp}}{m_p \omega \overline{|v_p|^2}} = \frac{\rho_F c_F S_p \sigma}{m_p \omega}. \quad (6.184b)$$

If the mean square velocity is sought, resulting from a mean square pressure $\overline{|p_F|^2}$, again, Eq. (6.172i) can be used yielding

$$\begin{aligned} \frac{\overline{|v_p|^2}}{\overline{|v_F|^2}} &= \frac{\overline{|v_p|^2} (\rho_F c_F)^2}{\overline{|p_F|^2}} = \frac{\Delta N_p m_F}{\Delta N_F m_p} \frac{1}{1 + \eta_p / \eta_{Fp}} \\ &\approx \frac{\Delta N_p m_F}{\Delta N_F m_p} \frac{\eta_{Fp}}{\eta_p} \end{aligned} \quad (6.184c)$$

Here, the assumption is made that $\eta_p > \eta_{Fp}$, which normally is the case in conjunction with airborne sound problems. By introducing (6.184b), one finally obtains

$$\frac{\overline{|v_p|^2}}{\overline{|p_F|^2}} = \frac{\pi}{2} \left(\frac{1}{\omega \rho_p h_p} \right)^2 \left(\frac{f_c}{f} \right) \frac{\sigma}{\eta_p} \quad (6.184d)$$

This expression will be encountered also in the analysis of sound transmission loss in Sect. 7.9.

In particular, (6.184d) has proven applicable when $\sigma \approx 1$ i.e., when the frequency range of interest lies above the critical frequency f_c of Eq. (7.53). For small, weakly damped plate fields, (6.184d) gives satisfactory results also below the critical frequency, provided there are sufficient resonant modes. Problems can arise for big plates below the critical frequency since the excitation by fluid-borne sound does not result in an equipartition of energy among the resonant modes, thus violating the prerequisites for a statistical energy analysis. SEA can furnish highly erroneous results when applied to sound transmission loss problems for frequencies below the

critical frequency and the radiated sound at the other side is calculated using $\overline{|v_p|^2}$ in (6.184d). In that case, the non-resonant transmission due to forced vibrations is fully omitted, which is governed by the so called mass law in (7.81b).

References

- [6.1] Mugiono, 1955. Messungen der Reflexion von Biegewellen an Querschnittssprüngen auf Stäben. *Acustica*, 5, p. 182
- [6.2] Gösele K., 1965. Über Prüfstände zur Messung der Luftschalldämmung von Wänden und Decken. *Acustica*, 15, p. 317
- [6.3] Kurtze G., Tamm K. and Vogel S., 1955. Modellversuche zur Biegewellendämmung an Ecken. *Acustica*, 5, p. 223
- [6.4] Munjal M.L., 1987. Acoustics of ducts and mufflers. John Wiley & Sons, New York NY
- [6.5] Meyer E., 1956. Messungen zur Körperschallübertragung an Hand von Modellen. *Acustica*, 6, p. 51
- [6.6] Exner M-L. and Böhme W., 1953. Messung der Körperschalldämmung bei Biegewellen. *Acustica*, 3, p. 105
- [6.7] Cremer L., 1951. Propagation of structure-borne sound. Department of Scientific and Industrial Research report No.1, Series B. London
- [6.8] Müller H.L., 1957. Biegewellendämmung an symmetrischen und exzentrischen Sperrmassen. *Acustica*, 11, p. 342
- [6.9] Boerger G. and Cremer L., 1962. Ein mechanischer Kettenleiter für Verzögerungszwecke. Proc. 4th International Congress on Acoustics, Copenhagen, Paper N15
- [6.10] Cremer L. and Leilich H.O., 1953. Zur Theorie der Biegekettenleiter. Archiv der elektrischen Übertragung, 7, p. 261
- [6.11] Courant R. and Hilbert D., 1953. Methods of Mathematical Physics, Vol. I, Ch. IV. John Wiley & Sons, New York NY
- [6.12] Sommerfeld A., 1954. Mechanik der deformierbaren Medien, §12. Akademische Verlagsbuchhandlung, Leipzig
- [6.13] Kosten C.W., 1960. The mean free path in room acoustics. *Acustica*, 10, p. 245
- [6.14] Cremer L., 1952. Theorie des Klopfschalles bei Decken mit schwimmendem Estrich. *Acustica*, 2, p. 167
- [6.15] Gösele K., 1949. Zur Messmethodik der Trittschalldämmung. Gesundheitsingenieur, 70, p. 66
- [6.16] Gösele K., 1956. Trittschall – Entstehung und Dämmung. *Acustica*, 6, p. 67
- [6.17] Cremer L. and Heckl M., 1959. Ergänzungen zur Theorie des schwimmenden Estrichs. *Acustica*, 9, p. 200

- [6.18] Möser M., 1983. Eine Theorie zur Schalldämmung unter Berücksichtigung der Randeinspannungen. Fortschritte VDI, Reihe 4, 62
- [6.19] Meyer E., 1937. Versuche über Körperschallleitung (Schallbrücken). Akustische Zeitschrift, 2, p. 72
- [6.20] Gösele K., 1960. Über Schallbrücken bei schwimmenden Estrichen. Schalltechnik, 20, Heft 39/40, p. 5
- [6.21] Cremer L., 1954. Berechnung der Wirkung von Schallbrücken. Acustica, 4, p. 273
- [6.22] Cremer L., 1963. Akustische Versuche zu schwimmend verlegten Asphaltestrichen. Bitumen, Heft 5, p. 93
- [6.23] Heckl M., 1955. Experimentelle Untersuchungen an schwimmenden Estrichen mit Schallbrücken. Acustica, 5, p. 112
- [6.24] Cremer L. and Hubert M., 1982. Vorlesungen über Technische Akustik, 3. Auflage, §3.2. Springer Verlag, Berlin
- [6.25] Lewit M., 1995. Inverse Messung von Kräften und Leistungen in gekoppelten schwingenden Strukturen. Fortschritt-Berichte VDI, Reihe 11, 215
- [6.26] Lyon R.H. and deJong R.D., 1995. Statistical Energy Analysis (2nd ed.). Butterworth-Heinemann, Boston MA
- [6.27] Heckl M. and Seifert K., 1958. Untersuchungen über den Einfluss der Eigenresonanzen der Messräume auf die Ergebnisse von Schalldämmmessungen. Acustica, 8, p. 212

7 Sound Radiation from Structures

Any treatise of structure-borne sound would be incomplete without a thorough discussion of sound radiation. Generally, it is the audible impression that finally counts. In order to predict the sound radiation with some confidence, the vibration amplitude must be known as a function of frequency as well as its spatial distribution. For radiation into a relatively dense fluid, such as water, the fluid loading of the vibrating structure also often plays a significant role. Thus, a considerable amount of detail is required for the evaluation of the airborne sound resulting from structural vibration.

The present chapter begins with some general remarks. Then, the radiation process is discussed, first from elementary configurations, such as spherical sources and subsequently more complex structures such as finite plates. The main focus here is on the power radiated to light fluids where the fluid loading is of subordinate importance and can be neglected. The effects of fluid loading and the directivity of the radiated sound, however, are briefly discussed.

7.1 Measurement of Radiated Power

The sound power radiated from an object can be measured most simply by placing the object in a reverberant room of known volume V and with known reverberation time T . A room with a volume of slightly more than 50 m^3 suffices for most purposes. Only when the frequency range below 200 Hz is of concern, the room has to be bigger. In the latter case, also, the measurement object is often too big for a room of 50 m^3 . Preferably, the reverberation time should be about 2s and the walls non-parallel or the room equipped with several, distributed scatterers.

The radiated power W may be obtained from the spatially averaged mean-square sound pressure $|p|^2$ as

$$W = 13.8 \frac{V}{\rho c^2 T} \overline{|p|^2}, \quad (7.1)$$

where typically five to ten measurement positions are averaged. ρ and c are the density and wave speed of the medium. Associated with the power is the power level, defined as

$$L_W = 10 \log \frac{W}{W_{ref}} \text{ dB}, \quad (7.2)$$

with the reference $W_{ref} = 1 \text{ pW}$. Use of the power level is sometimes convenient in conjunction with the sound pressure level defined by

$$L_p = 10 \log \frac{\tilde{p}^2}{\tilde{p}_{ref}^2} \text{ dB}, \quad (7.3)$$

where the reference is standardized as $\tilde{p}_{ref} = 20 \mu\text{Pa}$ and the tilde denotes the rms-value.

The accuracy with which the sound power can be measured, employing the method described above, depends on the volume, shape and reverberation time of the reverberant room, the number of measurement positions and particularly on the character of the sound. For stationary, broadband noise, the third-octave or octave power can be determined within about $\pm 20\%$, corresponding to $\pm 1 \text{ dB}$. In situations with non-stationary or strong tonal contributions, for example, from rotating machinery, the error might be considerably larger.

A second possibility to measure the power radiated from an object consists of placing the object in free field conditions such as those of an anechoic chamber and measuring the sound pressure p_n at many points at a distance R . This distance must be significantly greater than the dimensions of the object. The radiated power is then obtained from

$$W = \frac{1}{2\rho c} \sum |p_n|^2 S_n, \quad (7.4)$$

where S_n is the surface element associated with the n th measurement point. The sum of all surface elements must equal that of a hemisphere or a sphere, depending on whether the object is located on a sound-reflective surface or not. In the special case that the measurement points are uniformly distributed over a hemispherical surface

$$W = \frac{\pi R^2}{\rho c} \frac{1}{N} \sum_{n=1}^N |p_n|^2 = \frac{\pi R^2}{\rho c} \overline{|p|^2} \quad (7.4a)$$

where $\overline{|p|^2}$ represents the average mean-square pressure.

It is evident that free field measurements are more tedious than those in a reverberation chamber, particularly if the radiation varies strongly in

various directions so that many points are required. Free field measurements moreover, might be influenced by weather and external noise.

If the directivity of the radiation is of interest, the measurements can be undertaken in free field conditions. Either a pivoted microphone is used or the measurement object is placed on a turn-table and the sound pressure is registered during rotation.

A third method exists which enables simultaneous directivity and power measurements. This is sometimes referred to as the intensity method and makes use of a probe incorporating two or more, equal microphones. In this way the velocity, proportional to the pressure gradient, can be approximated by a finite difference estimate. With three microphones, arranged in a Cartesian co-ordinate system, the intensity vector can be measured. The definition of the sound intensity vector in a shear stress-free medium is

$$\mathbf{J} = \overline{p\mathbf{v}}. \quad (7.5a)$$

From this definition, the power is obtained as

$$W = \oint_S \mathbf{J} d\mathbf{S} \approx \sum_n \mathbf{J}_n \Delta S_n \mathbf{e}_n, \quad (7.5b)$$

where \mathbf{e}_n is the normal unit vector of the surface element S_n . The intensity is most often measured normal to the surface element and accordingly the vector notation in (7.5b) can be omitted.

In principle, the intensity method can be employed also in the presence of adjacent noise sources and in arbitrary field conditions, such as in the nearfield. In this context, the ‘in principle’ is important since in presence of noise sources as in strong nearfields, the accuracy is markedly reduced [7.1, 7.2].

An often overlooked problem in conjunction with power measurements of parts of a source, is the influence of adjacent source parts. It is readily shown (e.g. [7.3]) that the power, measured on a surface enclosing the source part of interest, can vary almost arbitrarily. Whereas such a variation is easily found for a narrow frequency band, it is rather unlikely over broad range.

7.2 Definition and Measurement of Radiation Efficiency

In addition to the radiated power, also the relation between the structural vibrations and the power is usually of interest. In this pursuit, the radiation

efficiency σ is a useful but dangerous quantity in many cases. The definition reads [7.4]

$$\sigma = \frac{W}{\rho c S \overline{|v|^2} / 2}, \quad (7.6a)$$

where W is the power radiated from a structure with surface area S and vibrating with the spatially averaged, mean-square velocity $\overline{|v|^2}$.

For a rigid, vibrating surface, such as a piston, with dimensions much larger than the wavelength in the ambient fluid, the fluid cannot escape laterally, but its particle velocity must equal that of the surface, even outside its immediate vicinity. Since the radiation then occurs normal to the surface, the sound pressure produced in the fluid is given by

$$p = \rho c v. \quad (7.6b)$$

The radiated power thus becomes $W = S \rho c \overline{|v|^2} / 2$. This means that $\sigma = 1$ for large surfaces vibrating piston-like. Accordingly, the radiation efficiency reveals how much less and in exceptional cases how much more power an object radiates than a piston with the same area.

In Fig. 7.1 are shown some results of radiation efficiency measurements of plates in a baffle, of a free-standing steel duct excited by one or more shakers and of the blocks of some diesel engines. The engine data were obtained from the velocities measured at several points on resiliently mounted engines where the intake and exhaust were ducted to another room via isolated pipes to permit only radiation from the block [7.5].

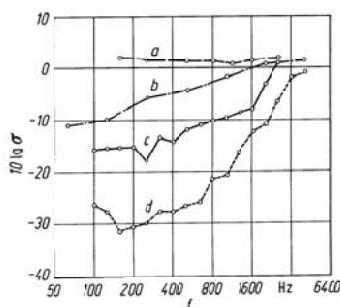


Fig. 7.1. Some experimental radiation efficiencies of (a) a 140mm concrete ceiling, (b) various diesel engine blocks, (c) 13mm plaster board on a lath grid and (d) a steel duct of 720mm diameter and 1.3mm wall thickness

The accuracy with which the radiation efficiency can be measured is 10% under most favourable conditions. It is limited primarily by how well the average mean square velocity can be determined. For lightly damped, homogeneous plates and the like, this measurement presents no particular problem but for inhomogeneous or highly damped structures difficulties arise. In the latter case, the velocity can vary considerably from point to point such that an average no longer is particularly meaningful. For point excited, highly damped structures, the velocity field can be so concentrated around the excitation point that an averaging is directly incorrect. Thus, radiation efficiency measurements should be measured only for relatively uniform velocity distributions.

The specification of a radiation efficiency gives the impression of a structural property. This is certainly not the case as is clearly demonstrated subsequently. The radiation efficiency can depend strongly on the boundary conditions, see Sect. 7.6.3.

7.3 Radiation Loss Factor

Besides the radiation efficiency, the radiation characteristics of structures can also be described by other quantities. One such alternative is realized by the ratio of radiated power into the ambient fluid W_{Rad} to that fed to the structure.

$$\zeta = \frac{W_{rad}}{W_s}. \quad (7.7)$$

Unfortunately, this, from a physics point of view, easily interpretable quantity is not easily measured. This is because the input power usually cannot be readily measured. Therefore, this ratio, which evidently cannot exceed unity, will be discussed only for point excitation.

Another quantity of interest is the radiation loss factor η_{rad} , which indicates to what extent the vibration of a structure are damped due to radiation to an ambient fluid. The radiation loss factor is defined as

$$\eta_{rad} = \frac{E_{rad}}{2\pi E_s}, \quad (7.8)$$

in complete analogy with the ordinary loss factor in (4.22) and where E_{rad} is the radiated energy within one period and E_s the reversible structural energy. By considering that E_{rad} equals the radiated power W_{rad} multiplied by the period $T = 1/f$, (7.8) can be rewritten as

$$\eta_{rad} = \frac{W_{rad}}{\omega E_S}. \quad (7.9)$$

For the structures of primary interest in this context namely beams, plates and shells, vibrating in flexure, $E_S = m''S|v|^2/2$. Combining this and (7.6a), a relation can be developed between the radiation loss factor and the radiation efficiency as

$$\eta_S = \frac{\rho c \sigma}{\omega m''}, \quad (7.10)$$

when a physically meaningful radiation efficiency can be determined. It should be noted that (7.10) pertains to single-sided radiation e.g., where there is air in front of the plate and vacuum behind it. For structures that are fully immersed in a fluid, Eq. (7.19) must be multiplied by 2 because the total radiating area is doubled.

The methods described in Chapter 4 are all suitable for the measurement of the radiation loss factor but the reverberation time technique has the advantage that there is no need to determine an average mean square velocity. This technique, moreover, also applies for irregular velocity fields, for example, due to inhomogeneities. An essential prerequisite for the reverberation time technique is that all other loss mechanisms are negligible. This is usually not the case with radiation into air. In contrast, the considerably larger wave impedance of water than of air leads to much higher radiation loss factors such that η_{rad} becomes measurably.

Two examples of the radiation loss factor are shown in Fig. 7.2. One refers to the hydro-acoustic radiation from a 10mm steel plate with web stiffeners. The second shows the radiation loss factor for a 4mm stiffened steel plate. As is seen, the losses due to radiation into water can be quite substantial, also for relatively thick plates.

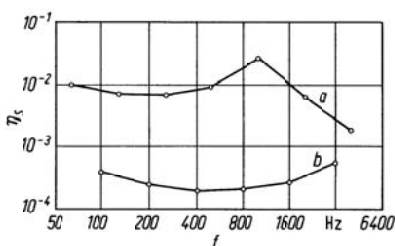


Fig. 7.2. Examples of measured radiation loss factors. (a) 10mm stiffened steel plate radiating to water and (b) 4mm stiffened steel plate radiating to air

By means of the radiation loss factor, the power ratio, (efficiency) defined in (7.7), can be determined. The total imparted structure-borne sound power obviously must equal the sum of radiated power W_{rad} and the power transformed into heat W_h . With a loss factor η_h representing that fraction of energy that is converted into heat, (5.124) gives

$$\zeta = \frac{W_{rad}}{W_{rad} + W_h} = \frac{1}{1 + \omega \eta_h E_S / W_{rad}} = \frac{1}{1 + \eta_h / \eta_{rad}} \quad (7.11)$$

The efficiency ζ , accordingly, is determined by the loss factor ratio. As expected, (7.11) tends to unity for very small inner losses $\eta_h \ll \eta_{rad}$. This means that all the power injected is radiated as fluid-borne sound. For air-borne sound, this condition never occurs but it is rather often encountered for radiation into water.

7.4 Elementary Radiators

7.4.1 Spherical Radiators

The simplest case of sound radiation is that of a sphere, which changes its volume with time in an unbounded, undisturbed, homogeneous fluid. Such a „breathing sphere“ or source of zero order is rarely encountered in practice but is of great theoretical importance. This is because complicated sound sources can often be considered as made up of a large number of spherical or hemispherical sources.

With the radial motion as function of time of a breathing sphere at a frequency ω given by $a + \text{Re}[\hat{\xi}_a e^{j\omega t}]$, the velocity of the spherical surface becomes

$$v_a(t) = \text{Re}\left[j\omega \hat{\xi}_a e^{j\omega t}\right] = \text{Re}\left[\hat{v}_a e^{j\omega t}\right]. \quad (7.12)$$

In the following the various symbols indicating phasors will be omitted. This velocity clearly must be identical to that of the ambient fluid at the interface $r = a$.



Fig. 7.3. Radiation from a spherical source

Mathematically, the problem consists of finding a solution to the wave equation

$$\nabla^2 p + k_0^2 p = 0, \quad (7.13)$$

subject to the boundary condition that the radial velocity of the fluid equals that at the surface of the sphere. In the above expression the viscosity of the fluid is neglected and $k_0 = \omega/c$ is the wavenumber. In spherical coordinates (r, ϑ, φ) the wave equation reads [7.6]

$$\begin{aligned} & \frac{1}{r^2} \frac{\partial}{\partial r} \left(r^2 \frac{\partial p}{\partial r} \right) + \frac{1}{r^2 \sin \vartheta} \frac{\partial}{\partial \vartheta} \left(\sin \vartheta \frac{\partial p}{\partial \vartheta} \right) \\ & + \frac{1}{r^2 \sin^2 \vartheta} \frac{\partial^2 p}{\partial \varphi^2} + k_0^2 p = 0. \end{aligned} \quad (7.13a)$$

The general relationship between pressure and velocity is obtained from the equation of conservation of momentum as

$$\mathbf{v} = -\frac{1}{j\omega\rho_0} \nabla p, \quad (7.14)$$

from which the radial component is given by

$$v_r = -\frac{1}{j\omega\rho_0} \frac{\partial p}{\partial r} \quad (7.14a)$$

For the present problem, radial symmetry exists such that the field quantities are independent of the angles ϑ and φ . Hence, the corresponding differentials in Eq. (7.13a) vanishes and one may assume a spatial pressure field in the form

$$p_r = \frac{C}{r} e^{-jk_0 r}. \quad (7.15)$$

This pressure field satisfies (7.13a) and represents an outwards propagating wave in the r -direction. The constant C is determined from the boundary condition at $r = a$. From (7.14a) the radial component of the velocity can be developed as

$$v_r = -\frac{C}{j\omega\rho_0} \left(-\frac{1}{r^2} - \frac{jk_0}{r} \right) e^{-jk_0 r}. \quad (7.16)$$

This means that

$$v_a = \frac{C(1+jk_0 a)}{j\omega\rho_0 a^2} e^{-jk_0 a} \Rightarrow C = \frac{j\omega\rho_0 a^2}{1+jk_0 a} v_a e^{jk_0 a}, \quad (7.17)$$

so that the velocity and pressure fields can be summarized as

$$\begin{aligned} v_r &= v_a \frac{a^2}{1+jk_0 a} \frac{1+jk_0 r}{r^2} e^{-jk_0(r-a)}, \\ p_r &= v_a \frac{j\omega\rho_0 a^2}{1+jk_0 a} \frac{e^{-jk_0(r-a)}}{r}. \end{aligned} \quad (7.18)$$

From these the radiated power can be found to be given by

$$W = \frac{1}{2} \operatorname{Re} \left[\int_S p_r v_r^* dS \right] = 2\pi a^2 |v_a|^2 \rho_0 c_0 \frac{(k_0 a)^2}{1+(k_0 a)^2}. \quad (7.19)$$

The integration involved is taken over a spherical surface at an arbitrary radius r and can simply be replaced by a multiplication by $4\pi r^2$ owing to symmetry.

The radiation efficiency for a breathing sphere can now be determined directly from (7.6) and (7.19) to be

$$\sigma = \frac{(k_0 a)^2}{1+(k_0 a)^2}. \quad (7.20)$$

Thus, the radiation efficiency of spherical radiators increases with the square of frequency for $k_a \ll 1$ i.e., for low frequencies and small radii. For high frequencies and large radiators, the radiation efficiency tends to unity.

The special case of very small spherical radiators, for which $k_a \ll 1$, is of particular importance with respect to the analysis that follows. For such

a radiator, which is called a „point radiator“ or monopole, one finds from Eq. (7.18) that

$$p = j\omega\rho_0 \frac{v_a 4\pi a^2}{4\pi r} e^{-jk_0 r} = j\omega\rho_0 q_0 \frac{e^{-jk_0 r}}{4\pi r}; k_0 a \ll 1. \quad (7.21)$$

Herein, q_0 represents the so-called volume velocity i.e., the product of velocity and surface area of the radiator. The introduction of this source strength has the advantage that the result can be applied to point radiators of arbitrary shape. With respect to the sound radiation, the shape of the small radiator is unimportant. Rather, it is the displaced volume that matters and hence q_0 . An influence of the shape is found only in the immediate vicinity of small radiators and thus, can be neglected.

7.4.2 Dipole Radiators and Radiation from Forces

Another very important elementary source is a fluctuating force directly applied to a homogeneous, infinite fluid. Such dipole sources are required for the general treatment of radiation, scattering and in flow acoustics.

The dipole radiator can be considered as a rigid sphere, oscillating forwards and backwards at a frequency ω as illustrated in Fig. 7.4. The position of the spherical surface or the radial velocity component are given by

$$a + \operatorname{Re} \left[\hat{\xi}_a \cos \vartheta e^{j\omega t} \right], \quad v_a(\vartheta) = \hat{v}_a \cos \vartheta. \quad (7.22a)$$

In these expressions appears only the angle ϑ , since the motion and the pressure are independent of the angle in the horizontal plane φ .

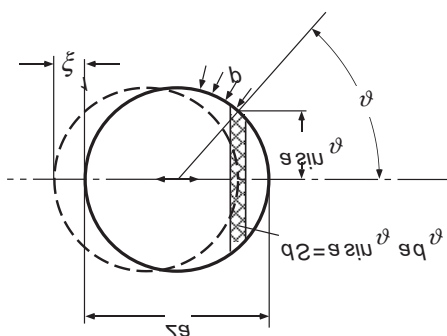


Fig. 7.4. Radiation from an oscillating, rigid sphere

The analysis is fully analogous to that in the preceding section. A valid solution to the wave equation in the absence of φ -dependence is

$$p(r, \vartheta) = C \left(\frac{1}{r^2} + \frac{j k_0}{r} \right) \cos \vartheta e^{-jkr}, \quad (7.22b)$$

as readily can be verified by substitution in (7.13a). By means of (7.14a), the radial component of the velocity can be determined and by choosing the constant C such that the velocity equals that of the source surface $v_a(\vartheta)$, the pressure and velocity fields are obtained as

$$\begin{aligned} p(r, \vartheta) &= C_a \left(\frac{1}{r^2} + \frac{j k_0}{r} \right) \cos \vartheta e^{-j k_0 (r-a)}, \\ v(r, \vartheta) &= \frac{C_a \cos \vartheta}{j \omega \rho_0} \left(\frac{2}{r^3} + \frac{2 j k_0}{r^2} - \frac{k_0^2}{r} \right) e^{-j k_0 (r-a)}, \end{aligned} \quad (7.22c)$$

where $C_a = j \omega \rho_0 \hat{v}_a a^3 / (2 + 2 j k_0 a - (k_0 a)^2)$. The resulting radiated power is given by

$$W = \frac{1}{2} \int_S \operatorname{Re} [p(r, \vartheta) v_r^*(r, \vartheta)] dS = \frac{\rho_0 c_0}{2} \frac{4 \pi a^2}{3} |\hat{v}_a|^2 \frac{(k_0 a)^4}{4 + (k_0 a)^4}, \quad (7.22d)$$

where the integration is made over the complete spherical surface. The surface element dS is detailed in Fig. 7.4.

In the derivation of (7.22c), the tangential velocity component is not considered. This means that the velocity of the fluid, in principle, could be different from that of the spherical surface. This contradicts the experience but has almost no influence on the sound radiation. The, in practice, observed equality of the tangential components (no slip condition) is related to the viscosity effects, which were omitted in the wave equation in (7.13). An inclusion of the viscosity effects, however, is hardly worthwhile since the viscous forces are localized to the very thin acoustic boundary layer (Stokes layer) [7.7] just outside the sphere. This boundary layer has the thickness

$$\delta = \sqrt{2 \nu / \omega} \quad (7.23)$$

cf., Eqs. (4.129). The kinematic viscosity ν is approx. $16 \cdot 10^{-6} \text{ m}^2/\text{s}$ for air and 10^{-6} for water, which means that δ in general is smaller than 0.1mm and hence unimportant for radiation problems.

In treating the monopole, the expressions for the pressure and velocity fields were furthered for the case of very small Helmholtz numbers $k_0 a \ll 1$. This was done by introducing the volume velocity such that arbi-

trarily shaped, small sources could be considered. A similar manipulation can be undertaken for dipoles when the force is considered, which is required for the excitation of the sphere. For this one may imagine an extremely lightweight small hollow sphere, which partitions the unbounded medium in interior and exterior parts. The hollow sphere must be significantly more lightweight than the fluid enclosed but still be non-deformable. For air, such a sphere is practically hard to conceive but for the markedly heavier water, such a device is realizable.

The hollow sphere is subject to an external force F_0 of frequency ω . To determine the motion of the oscillating sphere, it must be observed that the external force consists of two parts, the inertia force F_i of the enclosed fluid and the reaction force F_r from the exterior fluid i.e., the sound pressure on the spherical surface. The mass of the spherical shell is assumed negligible in this hypothetical experiment. Thus, equilibrium of forces gives

$$F_0 = F_i + F_r = m_i j\omega v_a + \int_S p(a, \vartheta) \cos \vartheta dS, \quad (7.24a)$$

where $m_i = \rho_0 4\pi a^3/3$ is the mass of the enclosed fluid and $j\omega v_a$ the acceleration. $p(a, \vartheta)$ is the sound pressure on the spherical surface, which exerts a force $p(a, \vartheta) \cos \vartheta dS$ on the surface element dS in the direction of motion. Upon substituting the pressure field in (7.22b) into (7.24a) it is found that

$$\begin{aligned} F_0 &= j\omega \rho_0 v_a \frac{4\pi a^3}{3} + \int \frac{j\omega \rho_0 v_a a^3}{2} \frac{1}{a^2} \cos^2 \vartheta 2\pi a^2 \sin \vartheta d\vartheta \\ &= j\omega v_a \left(\rho_0 \frac{4\pi a^3}{3} + \rho_0 \frac{2\pi a^3}{3} \right) = j\omega \rho_0 v_a 2\pi a^3, \end{aligned} \quad (7.24b)$$

for so small spheres that all terms involving $k_0 a$ in (7.22c) can be neglected. This means that (7.24b) is valid only for spheres of radius smaller than a sixth of the wavelength.

As is seen from (7.24b), the reaction force due to the sound pressure (the integral) appears as an additional mass. In this case with a spherical source, the hydro-dynamic mass or added mass is precisely half that of the enclosed fluid volume. For a small disc with thickness h and radius a , the added mass amounts to

$$m_a = \rho_0 \frac{8}{3} a^3 \left[1 - (4 - \pi) \frac{h}{8a} \right], \quad (7.24c)$$

which is slightly larger than that for a sphere when the disc thickness vanishes. From (7.24b) it follows that $j\omega \rho_0 v_a d^3 = F_0/2\pi$. By substituting this into (7.22c) and (7.22d), one obtains for small Helmholtz numbers

$$\begin{aligned} p(r, \vartheta) &= F_0 \cos \vartheta \left(\frac{1}{r} + jk_0 \right) \frac{e^{-jkr}}{4\pi r}, \\ v_r(r, \vartheta) &= F_0 \cos \vartheta \left(\frac{2}{r^2} + \frac{2jk_0}{r} - k_0^2 \right) \frac{e^{-jkr}}{4\pi r}, \\ W &= \frac{F_0^2}{2} \frac{\omega^2}{12\pi\rho_0 c_0^3}. \end{aligned} \quad (7.24d)$$

Thereby, relationships are established between a force acting on a very small area of the fluid and the resulting sound field.

7.4.3 Infinite Plates

Alike the point source, an infinitely extended plate, vibrating transversely represents an elementary case, which enables the analysis of radiation from more complicated systems by means of appropriate summations or integrations.

For a plate as sketched in Fig. 7.5, which has a velocity field given by

$$v(x) = v_0 e^{-jk_B x}, \quad (7.25a)$$

one may expect the sound pressure to be in the form

$$p(x, y) = p_0 e^{-jk_B x} e^{-jk_y y}. \quad (7.25b)$$

In the above expressions, k_B is the wavenumber of the flexural vibration and the wavelength is $\lambda_B = 2\pi/k_B$. The expression for the sound pressure must satisfy the wave equation in (7.13) and the normal component of the velocity, obtained from (7.14) with (7.25b) substituted must equal that of the plate surface. The first condition leads to

$$p_0 \left(-k_B^2 - k_y^2 \right) e^{-jk_B x} e^{-jk_y y} + p_0 k_0^2 e^{-jk_B x} e^{-jk_y y} = 0,$$

which is satisfied if

$$k_y^2 = k_0^2 - k_B^2, \quad (7.26a)$$

where, again, k_0 is the wavenumber of the fluid. The second condition yields

$$\left. \frac{-1}{j\omega\rho_0} \frac{\partial p}{\partial y} \right|_{y=0} = \frac{p_0 k_y}{\omega\rho_0} e^{-jk_B x} \Rightarrow p_0 = \frac{v_0 \rho_0 c_0 k_0}{k_y}. \quad (7.26b)$$

This means that the sound pressure in the positive half-space becomes

$$p(x, y) = \frac{v_0 \rho_0 c_0}{\sqrt{1 - k_B^2/k_0^2}} e^{-jk_B x} e^{-j\sqrt{k_0^2 - k_B^2} y}. \quad (7.26c)$$

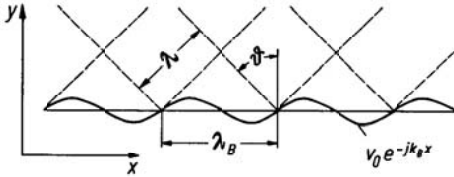


Fig. 7.5. Radiation from an infinite plate

Equation (7.26c) can be clarified physically by rewriting it in terms of the angle at which the sound is radiated. This angle must be such that the plate vibrations and the sound wave have the same x -dependence i.e., the trace of the acoustic wave along the plate must have the same wavelength as the plate wave. As is seen from Fig. 7.5, this equality occurs if $\lambda_0/\lambda_B = \sin \vartheta$, which is equivalent to $k_B/k_0 = \sin \vartheta$. Thus, Eq. (7.26c) can be rewritten as

$$p(x, y) = \frac{v_0 \rho_0 c_0}{\cos \vartheta} e^{-jk_B x} e^{-jk_0 y \cos \vartheta} ; \quad \lambda_B > \lambda. \quad (7.27a)$$

This expression only exists when the wavelength in the fluid is smaller than that of the plate. Otherwise, there exists no real angle at which the sound is radiated. Instead, a sound pressure is obtained which decreases exponentially with the distance from the plate and obeys

$$p(x, y) = \frac{jv_0 \rho_0 c_0}{\sqrt{(k_B/k_0)^2 - 1}} e^{-jk_B x} e^{-\sqrt{(k_B/k_0)^2 - 1} y} ; \quad \lambda_B < \lambda_0 \quad (7.27b)$$

in view of (7.26c). Accordingly, two fundamentally different regimes for the radiation from infinite plates must be distinguished. If the wavelength of the plate wave is larger than that in the fluid, then plane waves are radiated into the fluid at an angle determined by the ratio of the wavelengths. The sound pressure in the immediate vicinity of the plate is in phase with

the plate velocity. As may readily be determined, the radiation efficiency is given by

$$\sigma = \frac{1}{\cos \vartheta} = \frac{k_0}{\sqrt{k_0^2 - k_B^2}} \quad ; \quad k_B < k_0. \quad (7.28)$$

If, on the other hand, the wavelength in the plate is smaller than that in the fluid, a nearfield is formed. The larger the difference in wavelengths the faster is the decay with distance. In this regime, the plate velocity and the sound pressure are phase shifted 90° and hence no sound power is radiated. The radiation efficiency, therefore, is zero as shown in Fig. 7.6. The decay is rapid. For example, for $k_B = 0.7 \lambda_0$, the sound pressure at a distance of half a plate wavelength from the surface, the pressure is only 20% of its value at the surface, which corresponds to about 14 dB. Since the flexural wavelengths of practical interest are of the order of one meter or less, the nearfield can be neglected not only in conjunction with sound power but also with respect to the pressure.

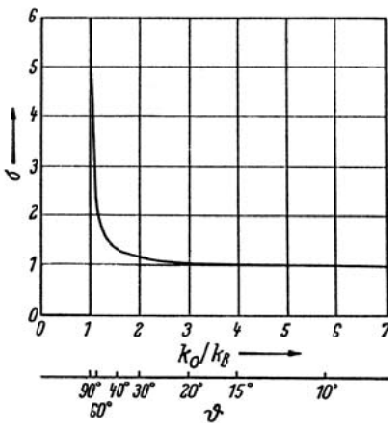


Fig. 7.6. Radiation efficiency for an infinite plate

As in the case of the oscillating sphere, is not considered the tangential motion, which differs at the plate and just outside. Again, only in a very thin boundary layer, the viscous effects, establishing tangential forces, can be observed cf., Eq. (7.23).

At the, up to now, excluded point where $k_B = k_0$ and where the structural and fluid wavelength are equal, the theory furnishes a radiation angle of

90° and an infinite sound pressure. In practice, the sound pressure remains finite, of course, both because structural areas are finite in practice and because the fluid loading of the structure is very high under this condition, making it impossible to generate the vibrations required [7.8]. The fact remains, however, that the radiation becomes strong. The effect is employed in many hydro-acoustic radiators. Such radiators, for which the desired velocity distribution of the radiating surface is obtained by appropriate transducer arrangements, radiate much sound power with high directivity nearly parallel to their surfaces.

Of interest is also the difference in air particle motion in the near- and far field. Whilst the air particles exhibit linear oscillations in the radiation direction for $\lambda_B > \lambda_0$, the x - and y -components of the velocity for $\lambda_B < \lambda_0$ are given by

$$\begin{aligned} v_x &= \frac{j k_B v_0}{\sqrt{k_B^2 - k_0^2}} e^{-j k_B x} e^{-\sqrt{k_B^2 - k_0^2} y}, \\ v_y &= v_0 e^{-j k_B x} e^{-\sqrt{k_B^2 - k_0^2} y}. \end{aligned} \quad (7.29a)$$

These components, accordingly, are phase shifted 90°. This means that the air particles generally undergo elliptic motions as depicted in Fig. 7.7. The elliptic orbits may be interpreted as the air particles escape compression. The compression necessary for generating a sound wave is thus avoided by moving laterally so that effectively all that remains is a back and forth sloshing of air from wave crest to trough; a hydro-dynamic short circuit.

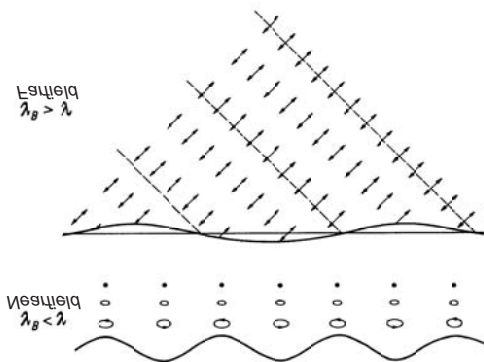


Fig. 7.7. Particle motions in far field and nearfield radiation

7.4.4 Cylindrical Radiators

To determine the radiation from vibrating pipes, tubes and ducts it is helpful to know the radiation properties of cylinders. Consider an infinitely long cylinder as an idealization of a vibrating pipe. The cylinder vibrates at a frequency ω , in-phase all along the whole length and the circumferential velocity distribution is

$$v(\varphi) = v_n \cos n\varphi, \quad (7.30)$$

as depicted left in Fig. 3.32. The task, again, is to find a function, which

- satisfies the wave equation in cylindrical co-ordinates i.e.,

$$\frac{1}{r} \frac{\partial}{\partial r} \left(r \frac{\partial p}{\partial r} \right) + \frac{1}{r^2} \frac{\partial^2 p}{\partial \varphi^2} + k_0^2 p = 0, \quad (7.31a)$$

- yields a dependence in the form

$$p \sim \frac{1}{\sqrt{r}} e^{-jk_0 r} ; \quad r \rightarrow \infty \quad (7.31b)$$

at large distances and hence describes outwards propagating cylindrical waves and

- satisfies the boundary condition

$$j\omega\rho_0 v(\varphi) = \left. \frac{\partial p}{\partial r} \right|_{r=a} \quad (7.31c)$$

at the surface of the radiator.

From the pertinent literature e.g., [7.6], the three requirements are fulfilled by

$$\begin{aligned} p(r, \varphi) &= -v_n \frac{j\rho_0 c_0}{H_n^{(2)\prime}(k_0 a)} \cos n\varphi H_n^{(2)}(k_0 r), \\ v(r, \varphi) &= -v_n \frac{\cos n\varphi}{H_n^{(2)\prime}(k_0 a)} H_n^{(2)\prime}(k_0 r). \end{aligned} \quad (7.31d)$$

Herein, $H_n^{(2)}(z)$ is the Hankel function of second kind and n th order and $H_n^{(2)\prime}(z)$ is the first derivative with respect to the argument. In very many applications, it is sufficient to work with the two limiting forms [7.9]

$$H_n^{(2)}(z) \approx \begin{cases} 1 - j \frac{2}{\pi} \ln\left(\frac{\gamma z}{2}\right) & ; \quad n = 0 \\ \left(\frac{z}{2}\right)^2 + j \frac{(n-1)!}{\pi} \left(\frac{2}{z}\right)^{2n} & ; \quad n \geq 1 \end{cases}; \quad k_0 r \ll n+1, \quad (7.31e)$$

and

$$H_n^{(2)}(z) \approx \sqrt{\frac{2}{\pi z}} e^{j\frac{\pi}{2}\binom{n+1}{2}} e^{-jz} \quad ; \quad k_0 r \gg n+1, \quad (7.31f)$$

where Euler's constant is $\gamma = 1.781\dots$

The radiated power can be determined, for example, from the sound pressure in the far field i.e., from Eq. (7.31d) using the asymptotic expression (7.31f)

$$W_{rad} = \frac{1}{2} \frac{1}{\rho_0 c_0} \int_0^{2\pi} |p(r, \varphi)|^2 r d\varphi = \frac{\rho_0 c_0 |v_n|^2}{\varepsilon_n |H_n^{(2)\prime}(k_0 a)|^2}, \quad (7.32a)$$

where

$$\varepsilon_n = \begin{cases} 1/2 & ; \quad n = 0 \\ 1 & ; \quad n \geq 1 \end{cases}.$$

Thus, the radiation efficiency, defined in (7.6a), becomes

$$\sigma_n = \frac{2}{\pi} \frac{\omega}{c_0} \frac{1}{|H_n^{(2)\prime}(k_0 a)|^2} \frac{1}{k_0^2 a}, \quad (7.32b)$$

for a cylindrical vibration with $2n$ nodes around the circumference.

A completely analogous analysis can be made for the case that the vibrations exhibit a periodicity with a wavelength λ_z also in the axial direction cf., the left part of Fig. 3.32. In such a case, the cylinder vibrations are given by

$$v(\varphi, z) = v_n \cos n\varphi e^{-jk_z z}. \quad (7.33a)$$

The associated radiation efficiency is given by (7.32b) when the wavenumber k_0 is replaced by the radial wavenumber component

$$k_r = \sqrt{k_0^2 - k_z^2}. \quad (7.33b)$$

When $k_z > k_0$, k_r becomes imaginary and the radiation efficiency, of course, vanishes; $\sigma_n = 0$.

In Fig. 7.8 are shown the radiation efficiencies as function of Helmholtz number for the nine first vibration modes of an infinite cylinder. From this graph and further studies of the governing equations, the following remarks can be made:

- When the axial component of the structural wavelength is smaller than the fluid wavelength i.e., $\lambda_z < \lambda_0$ the radiation efficiency vanishes; $\sigma = 0$. As for the plate, there occurs a hydro-dynamic short circuit cf., Figs. 7.6 and 7.7.
- When $\lambda_0 < 2\pi a/n$ and $\lambda_0 < \lambda_z$ or equivalently $k_r a > n$ i.e., the axial wavelength λ_z and also the circumferential wavelength $2\pi a/n$ are longer than that of the fluid, a comparatively strong radiation occurs with $\sigma = 1$. The maximum is reached at $k_r a \approx n$ and amounts to $\sigma_{\max} = \sqrt{n}$.
- When $k_r a < n$ or $\lambda_0 > 2\pi a/n$ but $\lambda_0 < \lambda_z$ so that the circumferential wavelength is smaller than that of the fluid, there is a hydro-dynamic short circuit in the circumferential direction, which, however, will not be complete due to the cylinder geometry. Hence, a small radiation efficiency is found for this range, which can be approximated by

$$\sigma_n \approx \begin{cases} \frac{\pi}{2} k_r a & ; \quad n=0, k_r a < 0.5 \\ \frac{\omega}{c_0 k_r} \frac{4\pi}{(n!)^2} \left(\frac{k_r a}{2}\right)^{2n+1} & ; \quad n \geq 1, k_r a < n/2 \end{cases} \quad (7.33c)$$

The larger the order n , the smaller is the radiation efficiency at small Helmholtz numbers.

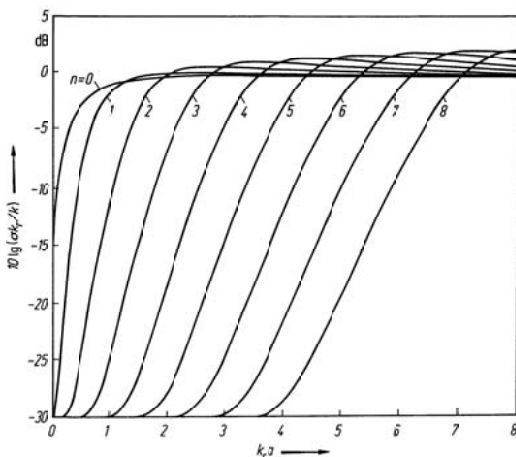


Fig. 7.8. Radiation efficiency for a cylindrical radiator for some different orders

Figure 7.9 visualizes the sound field in the vicinity of a cylindrical radiator. The expressions (7.30) to (7.33), which are valid for $2n$ nodes circumferentially and an axial wavenumber k_z , can be extended to accommodate arbitrary velocity distributions at the cylinder surface since the spatial functions $\cos n\varphi$ and $e^{-jk_z z}$ describe both the surface velocity and the sound pressure at an arbitrary receiver position. This means that the radiated modal power can be superimposed. If, therefore, the velocity field of the cylindrical surface is in the form

$$v(\varphi, z) = \sum_{n,m} [v_{cn}(k_{zm}) \cos n\varphi + v_{sn}(k_{zm}) \sin n\varphi] e^{-jk_{zm}z}, \quad (7.34a)$$

the radiated power becomes

$$W_{rad} = \frac{\rho_0 c_0}{2} S \sum_{n,m} [|v_{cn}(k_{zm})|^2 + |v_{sn}(k_{zm})|^2] \sigma(k_{zm}). \quad (7.34b)$$

In the latter expression, S means the (very large) cylinder surface.

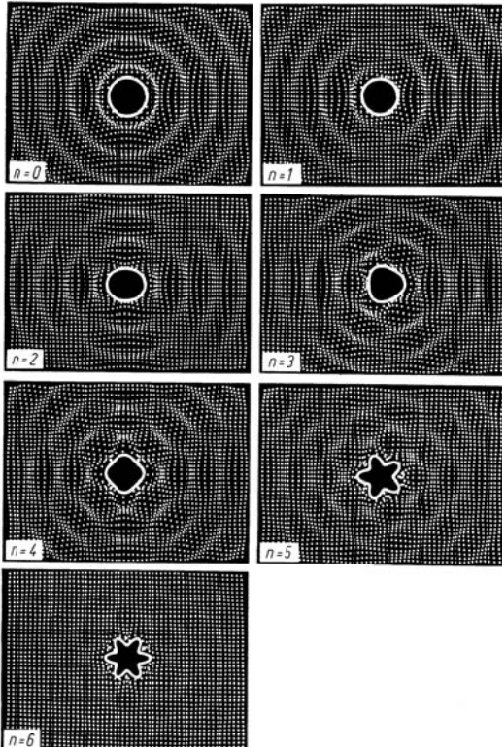


Fig. 7.9. Sound field in the vicinity of a cylindrical radiator at $ka = 4$, for some different orders $n = 0, 1, \dots, 6$. For $n = 6$ exists only a nearfield

It should be pointed out that the assessment of the modal amplitudes v_{cn} and v_{sn} , for example obtained from a modal analysis, must be very accurate, particularly for small n . This is so since with respect to the radiation, a strongly excited mode of large order n but low radiation efficiency can be fully shadowed by a low order mode that has a radiation efficiency close to unity.

7.4.5 Impulsive Sources

All previous analyses have addressed harmonic processes at a frequency ω . By employing Fourier transformations, the results and techniques can be applied also for arbitrary time histories as was shown in Sects. 5.4.5 and 5.8.1.

If, for example, a volume velocity has the time history $q_0(t)$, the pertinent spectrum as well as its inverse transform can be written as

$$q_0(\omega) = \int_{-\infty}^{+\infty} q_0(t) e^{-j\omega t} dt , \quad q_0(t) = \frac{1}{2\pi} \int_{-\infty}^{+\infty} q_0(\omega) e^{j\omega t} d\omega . \quad (7.35a)$$

For a compact source of typical dimension a , for which $k_0 a \ll 1$ in the range of interest, the radiated sound is given by (7.21) i.e.,

$$p(\omega) = \frac{\rho_0}{4\pi r} j\omega q_0(\omega) e^{-jk_0 r} . \quad (7.35b)$$

To perform the inverse transform, it must be observed that by differentiating (7.35a) with respect to time, the expression

$$\frac{dq_0(t)}{dt} = \frac{1}{2\pi} \int_{-\infty}^{+\infty} j\omega q_0(\omega) e^{j\omega t} d\omega$$

results. This means that the time history of the pressure at some distance r from the source is obtained as

$$\begin{aligned} p(r, t) &= \frac{1}{2\pi} \int_{-\infty}^{+\infty} p(\omega) e^{j\omega t} d\omega = \frac{\rho_0}{4\pi r} \frac{1}{2\pi} \int_{-\infty}^{+\infty} j\omega q_0(\omega) e^{j\omega(t-r/c_0)} d\omega \\ &= \frac{\rho_0}{4\pi r} \frac{dq_0(t-r/c_0)}{dt}, \end{aligned} \quad (7.35c)$$

where the substitution $\omega t - k_0 r = \omega(t - r/c_0)$ is made.

Fully analogously, (7.24c) yields the radiated pressure spectrum from a small force source as

$$p(r, \vartheta, \omega) = F_0(\omega) \frac{\cos \vartheta}{4\pi r} \left(\frac{1}{r} + \frac{j\omega}{c} \right) e^{-jk_0 r}. \quad (7.36a)$$

From an inverse transform is obtained

$$p(r, \vartheta, t) = \frac{\cos \vartheta}{4\pi r} \left[\frac{1}{r} F_0(t - r/c_0) + \frac{1}{c_0} \frac{d}{dt} F_0(t - r/c_0) \right], \quad (7.36b)$$

since a multiplication by $j\omega$ corresponds to a differentiation with respect to time. Upon integrating (7.35c) and (7.36b) over a large spherical surface, enclosing the sources, the powers radiated are given by

$$\begin{aligned} W_q &= \frac{1}{4\pi} \frac{\rho_0}{c_0} \overline{\left[\frac{dq_0(t)}{dt} \right]^2}, \\ W_F &= \frac{1}{12\pi} \frac{1}{\rho_0 c_0^3} \overline{\left[\frac{dF_0(t)}{dt} \right]^2}, \end{aligned} \quad (7.37)$$

for a compact volume velocity and force source respectively. These expression clearly highlights the very important noise control principle, which states that it is the temporal derivatives of the source strengths (q_0 , F_0) that govern the sound generation and not the actual amplitude of volume velocity or the force. Hence, it is the suddenness of the change in volume velocity or force that is important. In design, therefore, the endeavour should be to avoid or prolong every change in volume velocity or force e.g., by introducing resilient layers such that the few milliseconds are gained, which are necessary to ameliorate the most annoying high frequency components.

An important generating mechanism for impulsive sound is the so-called acceleration noise. It is the noise generated when a body suddenly is accelerated or decelerated without being deformed. As an example of such a source, a ball can be considered, which is decelerated from a velocity U to standstill in the short time period Δt . The associated time history and spectral expression can be found in Fig. 5.22. The force F_s must merely be replaced by the initial velocity U_0 .

By inserting the expression for the velocity spectrum in (7.22), the far field sound pressure spectrum is obtained as

$$p(r, \vartheta, \omega) = -\rho_0 c_0 \frac{a}{r} |v_a| \frac{(k_0 a)^2}{2 + 2jk_0 a - (k_0 a)^2} \cos \vartheta e^{-jk_0(r-a)} \quad (7.38a)$$

where

$$|v_a| = \frac{U_0}{\omega} \left| \frac{\sin(\omega \Delta t / 2)}{\omega \Delta t / 2} \right|.$$

In this context far field means that $1/r^2 \ll k_0/r$. As power is of little meaning for a single pulse, the sound energy will be determined for the deceleration. This is similar to the determination of the vibration energy due to an impact in Eq. (5.124). The only modification required is to replace the force by a surface integral of the pressure. Thus, the deceleration sound energy is obtained as

$$\begin{aligned} E_{Acc} &= \iint p(r, \vartheta, t) v(r, \vartheta, t) dt dS \\ &= \frac{1}{2\pi} \iint |p(r, \vartheta, \omega)|^2 \frac{1}{\rho_0 c_0} d\omega dS. \end{aligned} \quad (7.38b)$$

With (7.38a) introduced, the integration over the surface elements $dS = 2 \pi r \sin \vartheta r d\vartheta$ gives the energy density spectrum as

$$dE_{Acc} = \frac{\pi}{3} \rho_0 a^3 U_0^2 \frac{4 \sin^2(\omega \Delta t / 2)}{\pi} \frac{(\omega a/c_0)^2}{4 + (\omega a/c_0)^2} \frac{a}{c_0} d\omega. \quad (7.38c)$$

Herein is taken into account the fact that positive and negative frequencies render equal contributions to the spectrum and hence, $d\omega$ in (7.38c) only refers to positive frequencies. When the deceleration time Δt is so short that $c_0 \Delta t < 2a$ i.e., the sound propagation is smaller than the ball diameter, the methods of residues can be employed for the frequency integration. The poles, located at $\omega a/c_0 = 1 \pm j$, yield

$$E_{Acc} = \frac{\pi}{3} \rho_0 a^3 U_0^2 = \frac{1}{2} \rho_0 \frac{2\pi a^3}{3} U_0^2 = \frac{1}{2} m_a U_0^2. \quad (7.38d)$$

The mass m_a is the added mass defined in (7.24b).

The surprisingly simple result means that the radiated energy for a very short acceleration equals the kinetic energy of the added mass [7.10]. For known added masses, (7.38d) applies for non-spherical bodies. For example, the added mass for a thin disc is approximately given by (7.24c).

Upon substituting the data for a forge hammer into (7.38d) i.e., $V \approx 2 \cdot 10^{-2} \text{ m}^3$, $\rho_0 \approx 1.2 \text{ kg/m}^3$, $m_a \approx 0.024 \text{ kg}$ and $U_0 = 14 \text{ m/s}$, the acceleration noise energy amounts to $E_{Acc} \approx 2.4 \text{ Ws}$ per impact. For a rate of two impacts per second, this corresponds to an average power level of 127 dB. Although that is substantially less than the power radiated from the impact excited forge hammer casing, it is not that limited as intuitively could be expected. Relatively high acceleration noise is delivered also by slamming

doors. Again, it can be expected to be far below the noise radiated from the vibrating door blade and frame.

For not so short decelerations or accelerations, (7.38d) is invalid. Instead (7.38b) and (7.38c) yield curves that are exemplified in Fig. 7.10.

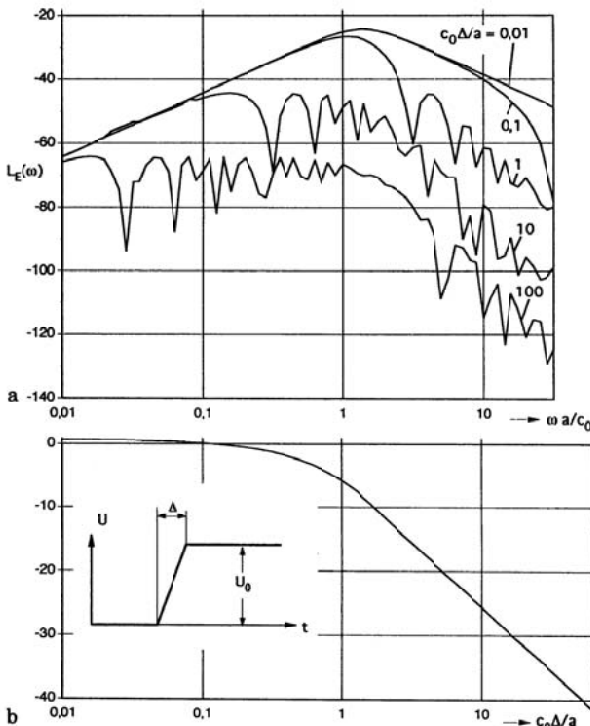


Fig. 7.10. Acceleration noise from a ball of radius a and acceleration time Δt . (a) Energy density spectrum $10 \log[(dE_{Acc}/d\omega)(c_0/aE_{max})]$ and (b) total energy $10 \log(E_{Acc}/E_{max})$, where $E_{max} = \pi\rho_0 a^3 U_0^2 / 3$

7.5 Plane, Baffled Radiators

Whilst the solution of the radiation problem can be rather complicated for an arbitrarily shaped structure, a solution on closed form is relatively simply found for the plane radiator in a rigid baffle. A prerequisite is that the radiator is located in a large baffle so that the velocity field is known over

an infinite plane. For the radiator, the velocity is $v = v(x, z)$ whereas it is zero elsewhere. This makes it possible to apply

- either the summation of many small volume velocity sources or
- to express the velocity distribution over the whole plane as a sum of plane waves.

Since both idealizations are treated already in Sects. 7.4.1 and 7.4.3, the results can be used as building blocks, which are summed or integrated to establish the complete solution.

7.5.1 The Plane Radiator as a Sum of Point Sources

Consider initially a small point source in a large baffle. It is readily confirmed that such a point source corresponds to a monopole owing to the symmetry and its pure radial motion. The only consideration is that the source in the baffle only offers half the volume velocity of the free source although the pressure at the baffle remains the same.

In accordance with (7.21), the pressure at a distance r from the source is given by

$$p = j\omega\rho_0 q_0 \frac{e^{-jk_0 r}}{2\pi r}. \quad (7.39a)$$

Again, it is irrelevant if the point source is semi-spherical or has any other shape. Important is the volume velocity $q_0 = v_0 \cdot S$. For a set of point sources such as in loudspeaker arrays and in sonar's, the contributions from each source are simply summed to establish the net pressure. With the notation of Fig. 7.11, the pressure can be written as

$$p = \frac{j\omega\rho_0}{2\pi} \left[\frac{q_1}{r_1} e^{-jk_0 r_1} + \frac{q_2}{r_2} e^{-jk_0 r_2} + \dots \right] = \frac{j\omega\rho_0}{2\pi} \sum \frac{q_n}{r_n} e^{-jk_0 r_n}. \quad (7.39b)$$

The step to a continuous velocity field is very small. Every surface element dS having the velocity $v(S)$ can be seen as a point source with the volume velocity $dq(S) = v(s)dS$. With the summation over source contributions replaced by an integration over the area, the pressure resulting from the complete radiator is given by

$$p = \frac{j\omega\rho_0}{2\pi} \int \frac{v(s)}{r} e^{-jk_0 r} dS. \quad (7.40)$$

This expression dates back to Lord Rayleigh [7.11].

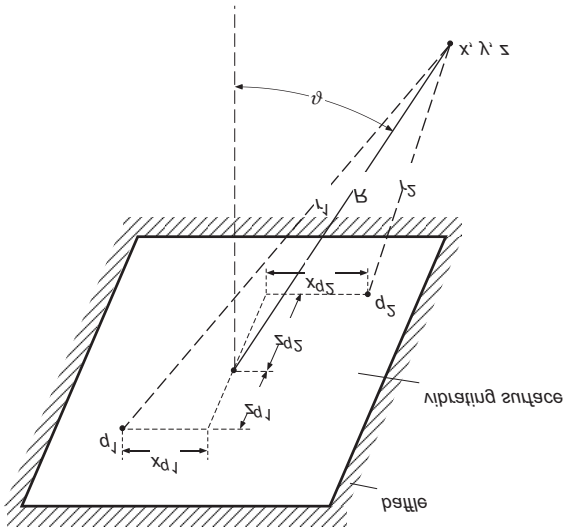


Fig. 7.11. Summation of point sources

If the directivity in the far field is sought, it is suitable to locate the origin for the spherical co-ordinate in (7.40) somewhere at the centre of the radiator such that the receiver point has the co-ordinates

$$x = R \sin \theta \sin \varphi , \quad y = R \cos \theta , \quad z = R \sin \theta \cos \varphi , \quad (7.41a)$$

as shown in Fig. 7.11. Here, θ is the angle between the y -axis and the vector to the receiver point whereas φ is the angle in the plane $y = 0$. For an arbitrary source point x_q, z_q , the distance to the receiver point becomes

$$\begin{aligned} r &= \left[(x - x_q)^2 + y^2 + (z - z_q)^2 \right]^{1/2} \\ &= R \left[1 - 2 \frac{x_q}{R} \sin \theta \sin \varphi - 2 \frac{z_q}{R} \sin \theta \cos \varphi + \frac{x_q^2 + z_q^2}{R^2} \right]^{1/2} \\ &\approx R - x_q \sin \theta \sin \varphi - z_q \sin \theta \cos \varphi + (x_q^2 + z_q^2)/2R. \end{aligned} \quad (7.41b)$$

For the approximation is used the binomial formula $(1 - 2\varepsilon)^{1/2} \approx 1 - \varepsilon$ when $\varepsilon \ll 1$, which is valid for x_q and z_q much less than R . With (7.41b) inserted into (7.40) and R assumed large, one obtains

$$p(R, \theta, \varphi) = \frac{j\omega\rho_0}{2\pi R} e^{-jk_0 R} \int v(x_q, z_q) e^{jk \sin \theta (x_q \sin \varphi - z_q \cos \varphi)} E_R dx_q dz_q , \quad (7.41c)$$

where $E_R = e^{-jk_0(x_q^2 + z_q^2)/2R} \approx 1$. This establishes a relatively manageable expression for the directivity of the radiated sound. The far field approximation developed is applicable if

$$\frac{k_0}{2R}(x_q^2 + z_q^2) = \frac{x_q^2 + z_q^2}{R\lambda_0} \pi \ll 1 \quad (7.41d)$$

in all of the integration range. The latter expression can be rewritten in the form $R > ND_q\pi$, where D_q is the maximum extension of the source and $N = D_q/\lambda_0$ is the number of wavelengths that equals the maximum extension. For sources, which are several wavelengths big, the distance R to the far field with respect to the directivity can become large.

Accordingly, it should be observed that the concept of far field has two meanings. The first is the acoustic far field meaning outside the hydrodynamic field and the second is the geometric far field referring to the region in which (7.41d) is satisfied.

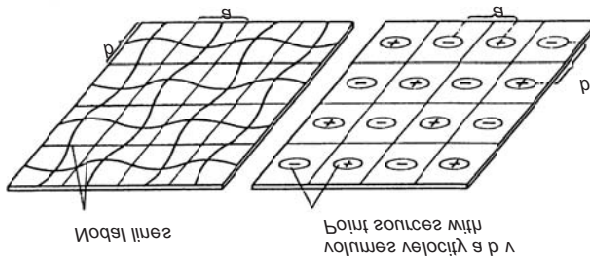


Fig. 7.12. Substitution of a modal vibration field by a periodic arrangement of point sources operating in anti-phase

Some findings from the application of (7.39) and (7.41c) with $E_R = 1$ are:

- a) For arrays of anti-phased point sources, which can be considered as approximations for modal velocity fields as illustrated in Fig. 7.12, the summation leads to

$$p(x, y, z) = \frac{j\omega\rho_0}{2\pi R} q_0 e^{-jk_0 R} \sum_{n=0}^{n_1-1} \left[e^{jk_0 ax/R} e^{j\pi} \right]^n \sum_{v=0}^{v_1-1} \left[e^{jk_0 bz/R} e^{j\pi} \right]^v, \quad (7.42a)$$

$$|p(x, y, z)| = \frac{\omega\rho_0}{2\pi R} q_0 \left| \frac{\sin n_1 \alpha}{\sin \alpha} \right| \left| \frac{\sin v_1 \beta}{\sin \beta} \right|,$$

where $2\alpha = \pi + k_0ax/R$, $2\beta = \pi + k_0bz/R$. The second form is obtained by summing the geometric series in the first. R is the distance between the point source $n = v = 0$ and the receiver point in the far field. For closely spaced point sources such that $k_0a \ll 1$ and $k_0b \ll 1$, the sines in the denominators tend to unity since $x < R$ and $z < R$. The remaining expression shows that such an array furnishes the sound pressure

$$|p(x, y, z)| = \frac{\omega\rho_0q_0}{2\pi R} |\sin n_1\alpha||\sin v_1\beta| \leq \frac{\omega\rho_0q_0}{2\pi R}, \quad (7.42b)$$

which is generally lower than that of a single point source due to the hydrodynamic short circuit. If, on the other hand, the separation of neighbouring point sources is larger than half a wavelength, the pressure contributions sum up to possibly substantial amplitudes. The maximum occurs when $k_0ax/R = \pi$, $k_0bz/R = \pi$ and amounts to

$$|p|_{\max} = \frac{\omega\rho_0q_0}{2\pi R} n_1 v_1, \quad (7.42c)$$

which corresponds to the sum of all point sources operating in phase. The associated radiation angle is simply found in that all incident wave contributions exhibit phase differences of 360° and interfere constructively. Some examples of computed directivities are shown in Fig. 7.13.

- b) For a rectangular piston with sides a and b and the velocity given by $v(x, z) = v_0$, the integral in (7.41c) yields the far field pressure

$$|p(R, \theta, \varphi)| = \frac{\omega\rho_0v_0}{2\pi R} \left| \frac{\sin(A/2)}{A/2} \right| \left| \frac{\sin(B/2)}{B/2} \right|, \quad (7.42d)$$

where $A = k_0a \sin \theta \sin \varphi$ and $B = k_0b \sin \theta \cos \varphi$. The radiation essentially occurs in the direction of the normal. The larger k_0a and k_0b , the more pronounced is the centre lobe. If, at all, side lobes appear, their zeroes are located at $A/2 = \pi, 2\pi, \dots$ and $B/2 = \pi, 2\pi, \dots$. To suppress the side lobes, the velocity must decay towards the edges.

- c) For a circular membrane of radius a , a rotationally symmetric velocity distribution can be expressed as a sum of functions in the form

$$v(r_M) = v_0 J_0(k_M r_M). \quad (7.42e)$$

Thereby, v_0 is the amplitude at the centre, $J_0(\dots)$ the zero order Bessel function, r_M the distance from the centre to a surface element and $k_M = 2\pi/\lambda_M$ is the membrane wavenumber, which is dependent on

the membrane properties and the type of excitation. λ_M is the associated wavelength. By introducing (7.42e) in (7.41c), the surface element is suitable chosen as $dx_q dz_q = 2\pi r_M dr_M$. Similarly can be employed $x_q \sin \varphi + z_q \cos \varphi = r_M$ since it is sufficient to consider a single direction in view of the rotational symmetry. With these substitutions, the integral in (7.41) gives

$$p(R, \vartheta) = \frac{j\omega\rho_0 a}{R} v_0 e^{-jk_0 R} \frac{k_M J_0(\gamma_0) J_1(\gamma_M) - k_0 \sin \vartheta J_0(\gamma_M) J_1(\gamma_0)}{k_M^2 - (k_0 \sin \vartheta)^2}, \quad (7.42f)$$

in which $\gamma_0 = k_0 a \sin \vartheta$ and $\gamma_M = k_M a$. To illustrate this result, Fig. 7.14 shows the directivity of four cases. Owing to symmetry, only half diagrams are presented.

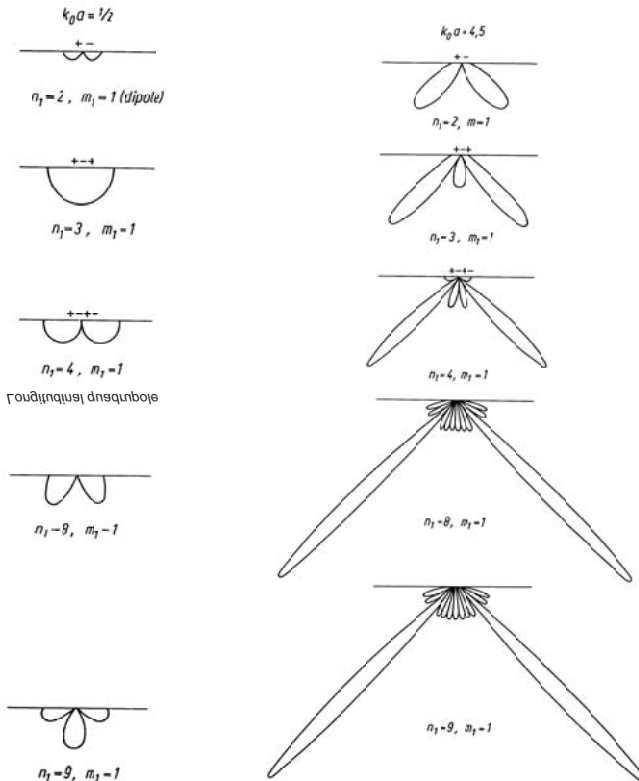


Fig. 7.13. Directivity of linear arrays of point sources

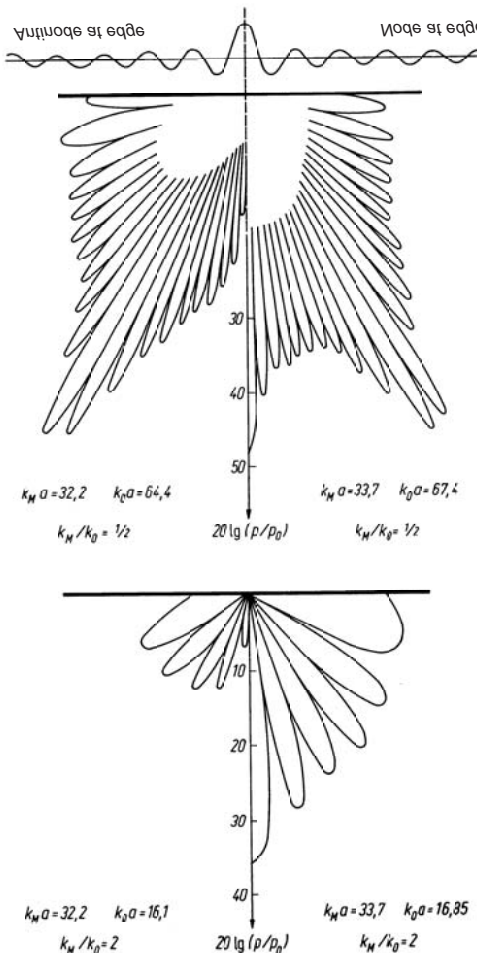


Fig. 7.14. Directivity of radiation from a circular membrane with the velocity distribution of (7.42e)

As can be seen, the radiation is comparatively high and directed for $k_M/k_0 = \gamma_0/\gamma_M < 1$. This is in agreement with the findings for infinite plates and planar arrays of sources when the fluid wavelength is shorter than that of the structure. The direction of the main radiation is close to that for which the denominator in (7.42f) vanishes i.e., $\sin \vartheta \approx k_M/k_0$. Also of interest is that the radiated sound pressure is relatively independent of whether there is a node or an anti-node at the periphery for $k_M/k_0 < 1$. The difference is seen essentially in the directivity where adjacent maxima are

slightly shifted whilst overall, the radiation patterns in the upper part of Fig. 7.14 are similar.

In contrast, the two patterns shown in the lower part of Fig. 7.14 pertain to cases where $k_M/k_0 = \lambda_0/\lambda_M = 2$ such that the fluid wavelength is larger than that of the membrane. It is seen that the two curves differ by some 15 dB at the centre although the membrane velocities are the same for the inner regions and only deviate at the peripheries cf., the uppermost part of the figure. The effect of the different boundary conditions for $k_M > k_0$ can also be determined from (7.42f) if $(k \sin \theta)^2$ is neglected and either is set $J_0(k_M a) = 0$ (node at the boundary) or $J_1(k_M a) = 0$ (anti-node at the boundary).

The observations discussed above are in agreement with those made for arrays of sources. Even for the present continuous velocity distributions, there occurs the hydro-dynamic short circuit effect, which leads to compensation of the fluid motions at the interior of the membrane such that only the radiation from the boundary remains. As is also indicated by the membrane result, the boundary radiation depends strongly on the details of the vibration at the periphery. Accordingly, one may affect the radiation significantly by rather small changes in the velocity distribution for $k_M/k_0 > 1$ but not for $k_M/k_0 < 1$.

7.5.2 Plane Radiators as Sum of Plane Waves

The plane radiator was already treated in Sect. 7.4.3 when vibrating in the form of a plane wave. The pertinent expressions in (7.25a) to (7.26d) can easily be extended to the two-dimensional case.

- a) Velocity distribution of the radiator:

$$v_B(x, z) = \hat{v}(k_x, k_z) e^{-jk_x x} e^{-jk_z z}. \quad (7.43a)$$

- b) Sound pressure from the boundary conditions:

$$p_B(x, y, z) = \frac{\rho_0 c_0 k_0 \hat{v}(k_x, k_z)}{\sqrt{k_0^2 - k_x^2 - k_z^2}} e^{-jk_x x} e^{-jk_z z} e^{-j\sqrt{k_0^2 - k_x^2 - k_z^2} y}; y > 0. \quad (7.43b)$$

- c) Particle velocity in the y -direction:

$$v_{yB} = \hat{v}(k_x, k_z) e^{-jk_x x} e^{-jk_z z} e^{-j\sqrt{k_0^2 - k_x^2 - k_z^2} y}. \quad (7.43c)$$

In order to establish a description of the radiation from a plane radiator with an arbitrary velocity field $v(x, z)$, Eqs. (7.43), again, are considered building blocks, from which the total solution can be constructed. The pro-

cedure is identical to that employed in Sect. 5.4. The velocity field of the radiator is described by the Fourier integral

$$v_B(x, z) = \frac{1}{4\pi^2} \int_{-\infty}^{\infty} \hat{v}(k_x, k_z) e^{-jk_x x} e^{-jk_z z} dk_x dk_z, \quad (7.44a)$$

which is applicable for all physically realizable distributions. The wavenumber spectrum $\hat{v}(k_x, k_z)$ is obtained from a transformation of the stationary velocity distribution

$$\hat{v}(k_x, k_z) = \int_{-\infty}^{\infty} v_B(x, z) e^{-jk_x x} e^{-jk_z z} dx dz. \quad (7.44b)$$

The integration is extended to infinity but since $v_s = 0$ outside the radiator surface, it suffices to encompass the radiator surface.

As (7.43b) is valid for every wavenumber pair k_x, k_z and the superposition principle applies, the sound pressure is obtained as the integral

$$p(x, y, z) = \frac{\rho_0 c_0 k_0}{4\pi^2} \int_{-\infty}^{\infty} \frac{\hat{v}(k_x, k_z)}{\sqrt{k_0^2 - k_x^2 - k_z^2}} e^{-jk_x x} e^{-jk_z z} e^{-j\sqrt{k_0^2 - k_x^2 - k_z^2}} dk_x dk_z. \quad (7.44c)$$

This expression can be used to determine the radiation from arbitrary plane radiators in a rigid baffle. It thus realizes an alternative to Eqs. (7.40) or (7.41c). The identity of the expressions can be proven with some mathematical exercise. In this context, however, it is sufficient to demonstrate that they establish the same intensity pattern in the far field. To do this, the power transmitted through a surface at $y = y_p$ is calculated as

$$\begin{aligned} W &= \frac{1}{2} \operatorname{Re} \left[\int_{-\infty}^{\infty} p(x, y_p, z) v_x^*(x, y_p, z) dx dz \right] \\ &= \frac{\rho_0 c_0 k_0}{32\pi^4} \operatorname{Re} \left[\left(\int \frac{\hat{v}(k_x, k_z) E}{\sqrt{k_0^2 - k_x^2 - k_z^2}} dk_x dk_z \right) \left(\int \hat{v}^*(k_x, k_z) E^* dk_x dk_z \right) \right] dx dz. \end{aligned} \quad (7.45a)$$

Herein, E is an abbreviation for the exponential functions in (7.44c). All integrals extend from $-\infty$ to $+\infty$. As shown in Sect. 5.5.1.2, the integral product reduces to a single double integral

$$\begin{aligned} W &= \frac{\rho_0 c_0 k_0}{8\pi^2} \operatorname{Re} \left[\int_{-\infty}^{\infty} \frac{\hat{v}(k_x, k_z) \hat{v}^*(k_x, k_z)}{\sqrt{k_0^2 - k_x^2 - k_z^2}} dk_x dk_z \right] \\ &= \frac{\rho_0 c_0 k_0}{8\pi^2} \int_{-k_c}^{k_c} \frac{|\hat{v}(k_x, k_z)|^2}{\sqrt{k_0^2 - k_x^2 - k_z^2}} dk_x dk_z. \end{aligned} \quad (7.45b)$$

The integral limits are given by the condition $k_c^2 = k_x^2 + k_z^2 = k_0^2$ since only in that range is the radical real valued. By means of the substitutions $k_x = k_0 \sin \vartheta \cos \varphi$ and $k_z = k_0 \sin \vartheta \cos \varphi$, the integrand is simplified through

$$\frac{dk_x dk_z}{\sqrt{k_0^2 - k_x^2 - k_z^2}} = \frac{k_0^2 \sin \vartheta \cos \vartheta d\vartheta d\varphi}{k_0 \cos \vartheta} = k_0 \sin \vartheta d\vartheta d\varphi.$$

This means that the radiated power is obtained as

$$W = \frac{\rho_0 c_0 k_0^2}{8\pi^2} \int_0^{\pi/2} \int_0^{2\pi} |\hat{v}(k_0 \sin \vartheta \sin \varphi, k_0 \sin \vartheta \cos \varphi)|^2 \sin \vartheta d\vartheta d\varphi. \quad (7.45c)$$

The radiated power in (7.45c) can now be compared with that transmitted to the far field given by (7.41c). After changing to polar co-ordinates, the far field expression reads

$$\begin{aligned} W_p &= \frac{1}{2\rho_0 c_0} \int_0^{\pi/2} \int_0^{2\pi} |p(R, \vartheta, \varphi)|^2 R^2 \sin \vartheta d\vartheta d\varphi \\ &= \frac{\omega^2 \rho_0}{8\pi^2 c_0} \int_0^{\pi/2} \int_0^{2\pi} |v_I(\vartheta, \varphi)|^2 \sin \vartheta d\vartheta d\varphi. \end{aligned} \quad (7.45d)$$

In these expressions, the factor E_R is set equal to unity such that

$$v_I(\vartheta, \varphi) = \int v(x_q, z_q) e^{jk_0 \sin \vartheta \sin \varphi x_q} e^{jk_0 \sin \vartheta \cos \varphi z_q} dx_q dz_q. \quad (7.45e)$$

By comparing (7.45e) with (7.44b), it is clear that v_I is precisely the transformed radiator velocity for $k_x = k_0 \sin \vartheta \sin \varphi$ and $k_z = k_0 \sin \vartheta \cos \varphi$. Hence, it is proven that (7.45c) is identical with (7.45d). Since this identity not only refers to the integral but is also valid for every ϑ and φ , the very important result is established that the wavenumber spectrum of the radiator velocity is directly proportional to the directivity. This means that with the wavenumber spectrum of the radiator velocity according to (7.44b), the directivity of the radiated sound is determined. Even the complete wavenumber spectrum is not required but only the portion in which $k_x^2 + k_z^2 < k_0^2$ yielding radiation to the far field. From the fact that the wavenumber spectrum and the directivity are closely related, some additional conclusions can be drawn.

- To realize a radiator with a prescribed directivity, a wavenumber spectrum for the radiator velocity must be formed that is prescribed in the range $k_x^2 + k_z^2 < k_0^2$ but can be arbitrary in the range of larger wavenumbers. The velocity distribution associated with the prescribed directivity can be achieved in many ways. In principle, it is possible to realize a very sharp lobe with, for example, a radiator

that is very small in comparison with the wavelength of the medium. The efficiency of such a radiator, however, is rather small. Also, the radiator generates an extremely strong nearfield, which, in case of some small inhomogeneity, totally alters the directivity. The design of radiators with prescribed directivity and low energy consumption is treated in [7.12].

- Conversely to the above conclusion, it follows that the velocity distribution of a radiator cannot be fully reconstructed from measurements in the far field. This is so since an arbitrary nearfield can be superimposed on the measured long waves in the far field.
- By applying Parseval's theorem

$$\frac{1}{4\pi^2} \overline{|v|^2} S = \frac{1}{4\pi^2} \int_S |v(x, z)|^2 dx dz = \int_{-\infty}^{\infty} |\hat{v}(k_x, k_z)|^2 dk_x dk_z,$$

the radiation efficiency, defined in (7.6a), can be written as

$$\sigma = \frac{\int_{-k_c}^{k_c} |\hat{v}(k_x, k_z)|^2 \frac{k_0}{\sqrt{k_0^2 - k_x^2 - k_z^2}} dk_x dk_z}{\int_{-\infty}^{\infty} |\hat{v}(x, z)|^2 dk_x dk_z}. \quad (7.45f)$$

The numerator is integrated over the range $-k_0 = -|k_c| \leq \sqrt{k_x^2 + k_z^2} \leq |k_c| = k_0$. The imaginary part of the radiation impedance corresponding to the apparent mass can be assessed from a similar expression where the numerator is integrated over $|k_c| \leq \sqrt{k_x^2 + k_z^2} \leq \infty$.

- In the direction perpendicular to the radiator surface, the sound pressure is given by the mean square velocity of the radiator.
- For small sources, compared with the wavelength, the exponential functions in (7.44b) can be expanded such that

$$\begin{aligned} \hat{v}(k_x, k_z) &= \int v_s(x, z) dx dz - jk_x D_x - jk_z D_z \\ &\quad - \frac{k_x^2}{2} D_{xx} - k_x k_z D_{xz} - \frac{k_z^2}{2} D_{zz} \end{aligned} \quad (7.45g)$$

where $D_x = \int x v_s(x, z) dx dz$, $D_{xx} = \int x^2 v_s(x, z) dx dz$ etc. corresponds to the dipole and quadrupole moments for the radiator.

- When $v_s(x, z)$ is composed of standing waves, then $\hat{v}(k_x, k_z)$ is a symmetric function in k_x and k_z . Accordingly, also the directivity is symmetric. To obtain a non-symmetric directivity, $v_s(x_q, z_q)$ must contain a portion of propagating waves.

7.6 Radiation from Bending Waves

The radiation from baffled plates can be calculated from (7.40), (7.41c), (7.44c) or (7.45b, d) for all possible cases provided the vibration field is known. The justification of a separate section on bending waves lies in the importance of bending wave radiation for noise control and in its interesting features.

7.6.1 Semi-infinite plate

In many cases, the vibration of a (one-dimensional) plate can be described as a sum of forwards and backwards propagating and evanescent waves. Consider at first, a semi-infinite plate as depicted in Fig. 7.15, where the physics is most easily presented. For all values of z , the velocity is given by

$$v_s = \begin{cases} A[e^{-jk_B x} + re^{jk_B x} + r_j e^{k_B x}] & ; \quad x \leq 0 \\ 0 & ; \quad x \geq 0 \end{cases}, \quad (7.46a)$$

in accordance with Sect. 6.1.2. A is the wave amplitude, k_B is the bending wavenumber, r and r_j are the reflection coefficients of the reflected propagating and evanescent waves respectively.

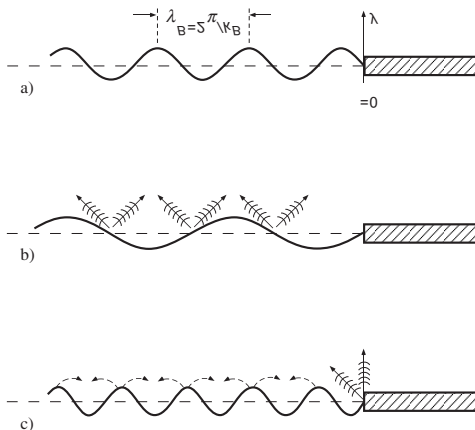


Fig. 7.15. Bending wave radiation from a semi-infinite plate. (a) vibration field, (b) radiation from long and (c) short bending waves

Upon inserting (7.46a) in (7.44b), the wavenumber spectrum is obtained as

$$\hat{v}(k_x) = A \left[\frac{j}{k_B + k_x} - j \frac{r}{k_B - k_x} + \frac{r_j}{k_B - jk_x} \right]. \quad (7.46b)$$

With the wavenumber spectrum substituted in (7.45b), the radiated power becomes

$$W' = \frac{\rho_0 c_0 k_0}{4\pi} |A|^2 \int_{-k_0}^{k_0} \frac{T^2 dk_x}{\sqrt{k_0^2 - k_x^2}}, \quad (7.46c)$$

where

$$T = \left| \frac{k_B^2 (j - jr + r_j) - k_B k_x (j - 1 + r + jr) + k_x^2 (-1 - r - r_j)}{(k_B^2 - k_x^2)(k_B - jk_x)} \right|.$$

Owing to the fact that here a one-dimensional transform is considered, the denominator in (7.46c) is altered to 4π . Accordingly, W' is the radiated power per unit width.

The integral is critically dependent on whether the poles at $k_x = \pm k_B$ are located inside or outside the integration range. For long wavelengths, for which $k_B < 0.9 k_0$, the integral is practically solely determined by the behaviour of the integrand around $k_x = \pm k_0$. A calculation would furnish an infinite power, however, since the radiating surface is assumed semi-infinite but the radiation efficiency can be meaningfully determined by means of (7.45f). Thereby, the radical $\sqrt{k_0^2 - k_x^2}$ is approximated by $\sqrt{k_0^2 - k_B^2}$ and brought outside the integral such that the limits can be extended to infinite. This leads to

$$\sigma = \frac{k_0}{\sqrt{k_0^2 - k_B^2}} \quad ; \quad k_B < 0.9k_0 \quad (7.46d)$$

For short wavelengths, where $k_B > k_0$, (7.46c) contains no poles and the integral yields a finite result also for infinite surfaces. A few examples, computed by means of (7.46c), are presented in Fig. 7.16, for which the following remarks can be made:

- Below the critical frequency, the radiation depends strongly on the boundary condition at $x = 0$.
- When the factor to k_B^2 can be made to vanish through suitable choices of r and r_j , the radiation is of dipole type, or, when also the factor to $k_B k_x$ is made to vanish, quadrupole type (curves 2 and 4).

- For a vanishing velocity at $x = 0$, $v_s(0) = 0$, a dipole type of nearfield radiation can be established through a suitable choice of the reflection coefficient r_j (curve 5). This leads to less radiation than that for a simply supported or clamped boundary.
- Since by otherwise unaltered conditions, a change of the nearfield i.e., a change of r_j , affects the radiated power, it can be concluded that the origin of the radiation lies close to the discontinuity. This is also confirmed by intensity measurements.
- The fact that the sound radiation can be reduced by the reflected propagating and evanescent waves for frequencies below the critical frequency, demonstrates the possibility to (actively) reduce the radiation by means of forces and moments applied at the boundaries.
- The sound radiation mechanism for the semi-infinite plate below the critical frequency can be interpreted as a non-radiating plate field due to the hydro-dynamic short circuit but a radiating edge since the short circuit there is incomplete. The strength of the edge radiation depends on the „completeness“ of the short circuit and thus on the details of the boundary conditions.

	r	r_j	v_s	End condition
1	-1	0	0	simply supported
2	1	0	$\neq 0$	guided
3	$-j$	$-1+j$	0	clamped
4	$-j$	$1-j$	$\neq 0$	free
5	j	$-1-j$	0	—

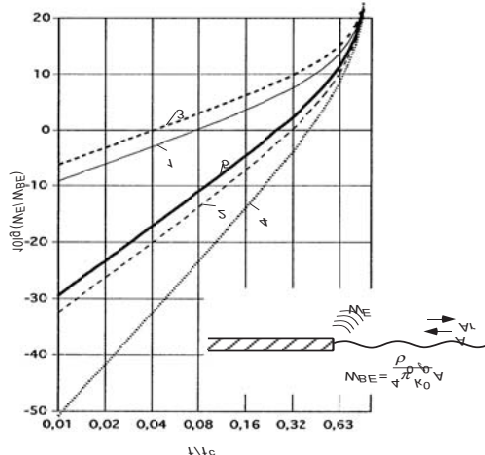


Fig. 7.16. Influence of the boundary conditions on the radiation from flexural waves below the critical frequency

7.6.2 The Critical Frequency

As was found for the infinite plate, the previous section demonstrated that the strength of the radiation from a plate substantially depends on how large the wavelength of the radiator is compared with that of the ambient fluid. For large radiator wavelengths, $k_B < k_0$, the radiation is strong whereas short wavelengths $k_B > k_0$ lead to weak radiation.

The critical frequency, defined through equality of the wavelengths or wavespeeds involved, thus, is highly important for the radiation from bending waves. Since the bending wavelength of a plate is given by

$$\lambda_B = 2\pi\sqrt[4]{B'/\omega^2 m''},$$

the critical frequency is obtained from $k_B = k_0$ or $\lambda_B = \lambda_0 = c_0/f_c$ i.e.,

$$f_c = \frac{c_0^2}{2\pi} \sqrt{\frac{m''}{B'}}. \quad (7.47a)$$

If, instead of the ratio m''/B' , the longitudinal wave speed for the material c_L and the plate thickness h are introduced, the expression for the critical frequency can be rewritten as

$$f_c = \frac{c_0^2}{1.8c_L h}. \quad (7.47b)$$

A simple method for measuring the critical frequency consists of assessing the ratio of mass to bending stiffness from a statical experiment. The centre displacement ξ of a simply supported beam of length l , due to its mass per unit length m' , is $\xi = 5 m'l^4 g / 384B$ where g is the gravitational acceleration. This means that the critical frequency can be estimated from

$$f_c = \frac{c_0^2}{2\pi l^2} \sqrt{\frac{384\xi}{5g}}. \quad (7.47c)$$

The static displacement of a one metre long, horizontally supported beam must amount to 10 mm for the critical frequency to be about 5000 Hz. Although such high critical frequencies often are hard to achieve in practice, due to strength of materials aspects, it is good noise control practice to design for an as high critical frequency as possible. In particular this applies for linings and enclosures etc. where statical considerations are of subordinate importance. A critical frequency of 3 kHz or more is thereby fully possible.

The critical frequencies by radiation to air are shown for some plate materials in Fig. 7.17. For radiation to water, the critical frequencies are approximately 20 times higher. A more exact calculation in the case with radiation into water cannot be made with (7.47c) since, in particular for

diation into water cannot be made with (7.47c) since, in particular for thin plates, the fluid loading shifts the critical frequency yet higher. The fluid loading acts as a frequency dependent mass layer and the critical frequency is mostly so high that the ordinary bending theory is invalid. Hence, the wavenumber must be determined by means of (3.196a).



Fig. 7.17. Critical frequencies for radiation into air

Besides the homogeneous plates treated here, also flexurally vibrating, multi-layered plates and anisotropic plates are encountered in practice. For multi-layered plates, such as sandwich plates, the critical frequency can be determined by means of (7.47a) but not by means of (7.47b, c). It must be noted, however, that the bending stiffness varies with frequency cf., (4.90). Naturally, the wavenumbers calculated from the more involved dispersion equation e.g., (4.106) and (4.116), can be equated to the fluid wavenumber to obtain the critical frequency. For a correctly designed multi-layered plate, the critical frequency is at least twice that of the statically corresponding homogeneous plate. Such plates not only radiate less but present also a relatively good sound transmission loss, as will be seen in Sect. 7.8.2, since a plate also is less excited by airborne sound when the radiation is small. Correctly designed multi-layered plates, therefore, are suitable as walls and liners where a low sound transmission is sought. Excep-

tions are, for instance, the sandwich configurations commonly used in aircrafts with their relatively stiff core.

For orthogonally corrugated plates, the critical frequency can be calculated from (7.47a) provided that the distance between the corrugations are smaller than the flexural wavelength at that frequency. Moreover, the bending stiffnesses in all directions must be approximately equal. Since the ratio of mass to bending stiffness of a plate can be altered by means of recesses e.g., milled slits or by attaching masses, the critical frequency can be shifted to high frequencies. Such measures, therefore, serve to control the sound radiation from and increase the sound transmission loss of linings and enclosures.

The situation is slightly more involved for plates that are corrugated only in one direction. As was shown in Sect. 3.7.4.3 on orthotropic plates, the bending wavenumber and hence the wavelength varies with the direction of propagation. In the stiff direction, the wavelength is obtained as

$$\lambda_{Bx} = 2\pi \sqrt[4]{B'_x / m''} / \sqrt{\omega}.$$

The associated critical frequency lies at

$$f_{cx} = \frac{c_0^2}{2\pi} \sqrt{\frac{m''}{B'_x}}. \quad (7.47d)$$

With B'_x representing the maximum stiffness, f_{cx} constitutes the lower limit and the critical frequencies are higher for waves in other directions.

In the orthogonal direction i.e., across the corrugation, the critical frequency is given by

$$f_{cz} = \frac{c_0^2}{2\pi} \sqrt{\frac{m''}{B'_z}}. \quad (7.47e)$$

Above this frequency the bending wavelength in any direction are longer than that of the ambient fluid. Accordingly, the radiation from the corrugated plate becomes that of a homogeneous above its critical frequency.

The complicated radiation characteristics between the two frequencies f_{cx} and f_{cz} will not be discussed in detail but it is sufficient to point out that the radiation is already above f_{cx} almost as strong as beyond f_{cz} . Thus, plates corrugated in one direction are not particularly suitable as sound reducing walls. It follows from this discussion, moreover, that recesses or attached masses are beneficial only when made in two orthogonal directions. With slits, for example, in one direction only, the static properties of the plate deteriorate whereas the sound transmission is hardly affected.

7.6.3 Modal Radiation

With the normal component of the radiator velocity expressed as a sum of eigen-functions or modes cf., Sect. 5.7.1,

$$v(x, z) = \sum v_n \varphi_n(x, z), \quad (7.48)$$

the radiation from the individual modes can be determined from (7.40) or (7.44c). The total sound pressure is obtained after summation. The total radiated power, in general, cannot be obtained from a summation of the modal contributions since the superposition principle does not apply for the power.

There are, however, several examples where no error is introduced by adding the individual modal contributions. To clarify this, a plate is considered of infinite extent in the z -direction but simply supported at $x = 0$ and $x = l_x$. The vibration is composed of two modes of complex amplitudes \underline{v}_1 and \underline{v}_2 . Hence, the vibration field is described by

$$\underline{v}(x) = \begin{cases} \frac{\underline{v}_1 \sin \frac{n_1 \pi x}{l_x} + \underline{v}_2 \sin \frac{n_2 \pi x}{l_x}}{l_x} & ; \quad 0 \leq x \leq l_x \\ 0 & ; \quad -\infty < x < 0, \quad l_x < x < \infty \end{cases}. \quad (7.49a)$$

Upon forming the wavenumber spectrum according to (7.44b) and developing the power radiated per unit width in analogy with (7.46c), one finds that

$$W' = \frac{\rho_0 c_0}{4\pi} \int_{-k_0}^{k_0} \frac{k_0}{\sqrt{k_0^2 - k_x^2}} |\underline{v}_1 A_1 E_1 + \underline{v}_2 A_2 E_2|^2 dk_x, \quad (7.49b)$$

where $A_\nu = 2 j n_\nu \pi l_x \sin[(k_x l_x - n_\nu \pi)/2]/(k_x^2 l_x^2 - n_\nu^2 \pi^2)$ and $E_\nu = e^{-j(k_x l_x - n_\nu \pi)/2}$ for $\nu \in [1, 2]$. This can be developed into

$$\begin{aligned} W' = & \frac{\rho_0 c_0}{4\pi} |\underline{v}_1|^2 \int_{-k_0}^{k_0} \frac{k_0 |A_1|^2}{\sqrt{k_0^2 - k_x^2}} dk_x + \frac{\rho_0 c_0}{4\pi} |\underline{v}_2|^2 \int_{-k_0}^{k_0} \frac{k_0 |A_2|^2}{\sqrt{k_0^2 - k_x^2}} dk_x \\ & + \frac{\rho_0 c_0}{2\pi} |\underline{v}_1 \underline{v}_2| \cos \left(\varphi_1 - \varphi_2 + \frac{n_1 - n_2}{2} \pi \right) \int_{-k_0}^{k_0} \frac{k_0 |A_1 A_2|^2}{\sqrt{k_0^2 - k_x^2}} dk_x, \end{aligned} \quad (7.49c)$$

which can be abbreviated

$$W' = W'_1 + W'_2 + W'_{12}. \quad (7.49d)$$

In this expression, W'_1 and W'_2 are the radiated powers from the individual modes. W'_{12} is a modal interaction term. Its magnitude and sign vary with the phase shift between the modes.

The principal behaviour of $|A_\nu|^2$ is plotted in Fig. 7.18. Essentially, these are functions in the form $(\sin x)/x$ with maxima at $k_x l_x = \pm n_\nu \pi$ and of period π/l_x . From the behaviour of $|A_\nu|^2$, the following remarks can be made for the modally radiated power.

- a) When $k_0 l_x \ll n_\nu \pi$ i.e., the distance between successive nodes of the plate vibration is smaller than the fluid wavelength, the integration range does not encompass the maxima of $|A_\nu|^2$ cf., range α in Fig. 7.18. Thus, little radiation occurs and the radiation efficiency is low, as shown in the diagrams a) and b) in Fig. 7.19.
- b) When $k_0 l_x \gg n_\nu \pi$ i.e., the nodal separation is large compared with the fluid wavelength, the integration extends over a large range, within which $|A_\nu|^2$ exhibits its maxima cf., range β in Fig. 7.18. Approximately, the power is given by

$$W'_\nu \approx \frac{\rho_0 c_0 l_x}{4} \sum |v_\nu|^2 ; \quad \sigma_\nu \approx 1. \quad (7.50a)$$

- γ) When $k_0 l_x \approx n_\nu \pi$, the integration becomes more intricate. Useful approximations are

$$W'_\nu \approx \frac{\rho_0 c_0 l_x}{6} \sqrt{\frac{k_0 l_x}{\pi}} |v_\nu|^2 ; \quad \sigma \approx \frac{2}{3} \sqrt{\frac{k_0 l_x}{\pi}} = \frac{2}{3} \sqrt{n_\nu}. \quad (7.50b)$$

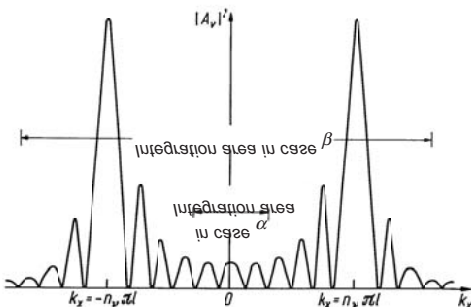


Fig. 7.18. Principal behaviour of $|A_\nu|^2$

The development of approximations for the interaction term is difficult since the integrand contains two sinusoids with differing arguments. Therefore, are included in Fig. 7.19 some examples of the influence of this term. Thereby, the net radiated power W' is compared with the sum of

powers of the two modes $W'_1 + W'_2$. For the examples in Fig. 7.19, the amplitudes of the two modes are taken to be equal. Diagram c) in Fig. 7.19 illustrates the influence of the phase shift between the modes and diagram d) the reduction in radiation when the two modes have opposite phases. The critical frequencies are given by $k_0 l_x = n\pi$.

Perhaps the most interesting observations from Fig. 7.19 is the possibility to reduce the radiation due to mode n below its critical frequency by exciting another mode $n+2, n+4$ etc.. By means of some suitable artificial excitation, other modes, in principle, can be brought to lower the radiation although the average mean square velocity will increase. By excitation of several modes, it can be expected the radiation can be further suppressed than that demonstrated in diagram d).

Above the critical frequency, it is questionable if „anti-modes“ will offer some radiation reduction.

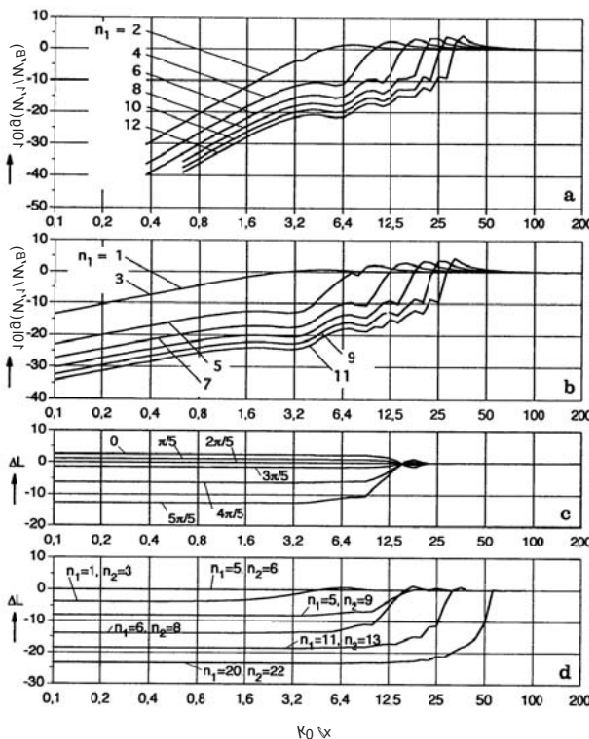


Fig. 7.19. Radiation from a plate with the vibration given by (7.49a). a) and b) radiation from a single mode, $W'_B = \rho_0 c_0 l |v_v|^2 / 4$. c) Influence of the phase of a second mode of equal amplitude as the reference mode, $n_1 = 5$ and $n_2 = 7$. d) Radiation reduction due to a second mode in anti-phase, $\Delta L = 10 \log [W' / (W'_1 + W'_2)]$.

7.6.4 Radiation from Externally Excited Bending Waves

7.6.4.1 Basic Equations

The previously considered cases show that the radiation from bending waves depends on the boundary conditions and on the details of the vibration field, in particular below the critical frequency. It is thus necessary to know the vibration field precisely to calculate the sound radiation. Due to the difficulties in establishing such precise knowledge, the question can be posed if the radiation can be directly developed from the usually much simpler excitation field without an explicit calculation of the velocity field [7.13].

This kind of analysis is particularly simple for infinite plates. Hence, this case will be considered initially whereby also the fluid reaction will be taken into account.

In Sects. 5.4.1 and 5.4.2 the wave mobilities of plate-like structures were detailed. For the infinite homogeneous plate, Eq. (5.49b) yields

$$\hat{v}(k_x, k_z) = \frac{j\omega}{B} \frac{\hat{p}(k_x, k_z)}{(k_x^2 + k_z^2) - k_B^4} = \hat{p}(k_x, k_z) Y_\sim. \quad (7.51)$$

The wavenumber spectrum of the exerted pressure can be determined from (5.55a). This pressure comprise the external excitation p_e and the pressure reaction p_f from the ambient fluid. Equation (5.55a), therefore, can be written in the form

$$\begin{aligned} \hat{p}(k_x, k_z) &= \int p_e(x, z) e^{jk_x x} e^{jk_z z} dx dz \\ &\quad - \int p_f(x, z) e^{jk_x x} e^{jk_z z} dx dz \\ &= \hat{p}_e(k_x, k_z) - \hat{p}_f(k_x, k_z). \end{aligned} \quad (7.52)$$

The wavenumber spectrum \hat{p}_f need not be calculated here since it was determined in (7.52). With $y = 0$ in Eq. (7.44c), the fluid reaction on one side of the plate is obtained. The magnitude of the spectrum is revealed by the integrand in (7.44c). Another possibility is to take $p(x, 0, z) = p_f(x, z)$ in (7.52) and use the orthogonality of the exponential functions. Either way, the result becomes

$$\hat{p}_f(k_x, k_z) = \frac{\rho_0 c_0 k_0}{\sqrt{k_0^2 - k_x^2 - k_z^2}} \hat{v}(k_x, k_z) = Z_{rad} \hat{v}(k_x, k_z). \quad (7.53)$$

Equation (7.44c) yields the radiation from a single-sided, fluid loaded plate where the fluid properties are ρ_0 and c_0 . For a double-sided fluid loading, the radiation impedance in (7.53) is replaced by $Z_{rad1} + Z_{rad2}$ i.e., the sum of

the fluid impedances on the two sides of the plate. In this analysis, single-sided radiation and fluid loading is assumed.

Upon combining (7.51), (7.52) and (7.53), the wavenumber spectrum of the plate velocity is found to be given by

$$\hat{v}(k_x, k_z) = Y_{\sim} \hat{p}_e(k_x, k_z) / (1 + Y_{\sim} Z_{rad}). \quad (7.54)$$

By substitution in (7.44c), (7.45b) and (7.45d), one obtains for the sound pressure, the radiated power and the far field directivity respectively

$$p(x, y, z) = \frac{1}{4\pi} \int_{-\infty}^{\infty} Z_{rad} \frac{\hat{p}_e(k_x, k_z) Y_{\sim}}{(1 + Y_{\sim} Z_{rad})} e^{-jk_x x} e^{jk_z z} e^{-j\sqrt{k_0^2 - k_x^2 - k_z^2} y} dk_x dk_z, \quad (7.55a)$$

$$W = \frac{1}{8\pi^2} \int \text{Re}[Z_{rad}] \left| \frac{\hat{p}_e(k_x, k_z) Y_{\sim}}{1 + Y_{\sim} Z_{rad}} \right|^2 dk_x dk_z, \quad (7.55b)$$

$$|p(R, \vartheta, \varphi)|^2 \approx \frac{\omega^2 \rho_0^2}{4\pi^2 R^2} \left| \frac{\hat{p}_e(k_0 \sin \vartheta \sin \varphi, k_0 \sin \vartheta \cos \varphi) Y_{\sim}(\vartheta, \varphi)}{1 + Y_{\sim}(\vartheta, \varphi) Z_{rad}(\vartheta, \varphi)} \right|^2. \quad (7.55c)$$

In the expressions for the directivity, the arguments of the wave mobility and impedance are translated as $k_x = k_0 \sin \vartheta \sin \varphi$ and $k_z = k_0 \sin \vartheta \cos \varphi$. The three expressions are remarkably simple in that they establish direct relations between the excitation and the radiated sound without recourse to the radiator velocity. It can be noted, moreover, that insight can be gained into the directivity directly from the wavenumber of the excitation, filtered by the wavenumber characteristics of the plate and the fluid, without some integration but taking the fluid loading into account.

Equations (7.55) are written such that they can be applied also for orthotropic plates, prestressed plates, plates on a Winkler bed and the elastic semi-infinite continuum. The corresponding wave mobilities are given in Sect. 5.4.2 and in Eqs. (3.148d) and (4.109).

7.6.4.2 Examples

The sound radiation from an infinite plate, subject to a point force F_0 at $x = z = 0$ constitute an important and simple example. From (5.56b), the excitation wavenumber spectrum is

$$\hat{p}_e(k_x, k_z) = F_0. \quad (7.56a)$$

The power radiated to one side is obtained from (5.50a), (7.53) and (7.55b), using the substitutions $k_x = k_r \sin \psi$, $k_z = k_r \cos \psi$ and $dk_x dk_z = k_r dk_r d\psi$,

$$W = \frac{|F_0|^2 \rho_0 c_0 k_0}{4\pi} \int_0^{k_0} \frac{k_r dk_r}{\sqrt{k_0^2 - k_r^2} \left[\omega^2 m''^2 \left(1 - k_r^4/k_B^4\right)^2 + \rho_0^2 c_0^2 k_0^2 / (k_0^2 - k_r^2) \right]}. \quad (7.56b)$$

Herein, the integration over the angle ψ undertaken simply leads to 2π .

For the frequency range below the critical frequency, $k_B^2 \gg k_0^2$ and the ratio k_r^4/k_B^4 can be neglected. With such an approximation

$$W = \frac{|F_0|^2 \rho_0 c_0 k_0^2}{4\pi \omega^2 m''^2} \left(1 - \frac{\rho_0 c_0}{\omega m''} \arctan \frac{\omega m''}{\rho_0 c_0} \right); \quad f \ll f_c. \quad (7.56c)$$

In a case with a light fluid such as air, normally $\omega m'' \gg \rho_0 c_0$. This means that for negligible fluid loading, a point excited, infinite plate emits the power

$$W = \frac{\rho_0}{4\pi m''^2 c_0} |F_0|^2. \quad (7.57a)$$

By considering the factor in front of the force as the real part of the system mobility in view of Eq. (5.23), the real part for the system constituted by plate and fluid half-space, is found frequency independent. The radiation, moreover, is omni-directional, as can be seen from (7.55c). The efficiency of such a radiator, however, is rather small. It follows from (7.7), (5.85a) and Table 5.1 that it amounts to

$$\zeta = \frac{2W}{|F_0|^2 \operatorname{Re}[Y]} = \frac{2\rho_0 c_0}{\pi^2 m'' f_c}. \quad (7.57b)$$

Instead of relating the radiated power to the force but to the resulting velocity v_0 at the excitation point, one finds for vanishing fluid loading that

$$W = \frac{16\rho_0 c_0 k_0^2}{\pi k_B^4} |v_0|^2 = \frac{4}{\pi^3} \rho_0 c_0 |v_0|^2 \lambda_c^2, \quad (7.57c)$$

where $\lambda_c = c_0/f_c$ is the wavelength at the critical frequency.

In the radiation expression (7.56c), the most important quantity for the velocity field over the major part of the plate, namely the flexural wavelength is not involved. From this observations and other from additional analyses, it can be deduced that the hydro-dynamic short circuit prevents radiation from the major part of the plate. Only the incomplete short-circuiting remains in the vicinity of the excitation point, which supplies the radiated power.

To associate the sound radiation from point excited large plates below the critical frequency with the nearfield would not reveal the physics completely. It can be shown that also for point-excited membranes where no

exponentially decaying nearfield arise, radiation only occurs from a small area around the excitation point for short wavelengths.

It is interesting to compare the power in (7.57c) with that from a point source in a baffle, given by (7.19) for $k_0 a \ll 1$. Such a comparison shows that the incomplete hydro-dynamic short circuit at the excitation point supplies the same amount of radiated power as that of a point source with the volume velocity $q_0 = 8 v_0/k_B^2$. Since $k_B = 2\pi/\lambda_B$, this corresponds to a piston with velocity v_0 and radius $\lambda_B \sqrt{2/\pi^3}$ i.e., approximately a radius of $\lambda_B/4$.

This surprisingly simple result can be used to assess the radiation in cases where the excitation is no longer point-like but distributed over a small area with a characteristic dimension (radius) a . It can be expected that the radiation resembles that of a piston with radius $a + \lambda_B/4$, for which the power amounts to

$$W \approx \frac{\rho_0 c_0}{4} k_0^2 \pi |v_0|^2 \left(a + \frac{\lambda_B}{4} \right)^4. \quad (7.57d)$$

From (7.56c) also, a simple expression can be derived for heavy fluid loading such as a thin plate floated on a water surface. With the truncated expansion $\arctan x \approx x - x^3/3$ substituted, the radiated power becomes

$$W \approx \frac{|F_0|^2}{12\pi} \frac{\omega^2}{\rho_0 c_0^3}. \quad (7.58a)$$

In this expression, appears neither the bending wavelength nor the plate mass. Furthermore, except for a factor of two, it is identical to (7.24d), describing the radiated power from a force (dipole) acting directly on the fluid. If the value for double-sided fluid loading would have been substituted in (7.56c) instead of $\rho_0 c_0 / \omega m''$, valid for single-sided fluid loading, the missing factor of two would have been recovered. Accordingly, the two expressions are equal under equal conditions. The fact that point excited plates radiates as dipoles for heavy fluid loading below the critical frequency can be seen also from (7.55c). With the approximation $Z_{\perp}(\vartheta, \phi) \ll Z_{rad}(\vartheta, \phi)$, valid under such circumstances, it follows that

$$|p(R, \vartheta, \phi)|^2 \approx |F_0|^2 \frac{k_0^2}{4\pi^2 R^2} \cos^2 \vartheta. \quad (7.58b)$$

In a similar way as for a point force, the sound radiation from the excitation region of a line force can be developed. For such an excitation, the power per unit length can be found to be given by

$$W' = \frac{|F'_0|^2 \rho_0 c_0 k_0}{4 \left[(\omega^2 m''^2 + \rho_0^2 c_0^2) + \rho_0 c_0 \sqrt{\omega^2 m''^2 + \rho_0^2 c_0^2} \right]} ; \quad f \ll f_c. \quad (7.59)$$

Here, F'_0 is the force per unit length. Also in this case, the radiation is of omni-directional, monopole type for vanishing fluid loading but of dipole type for heavy fluid loading.

As a second case, the radiation due to a moment excitation will be analysed. For a plate subject to $F_0/2$ at $(x, z) = (-a, 0)$ and $-F_0/2$ at $(x, z) = (a, 0)$, the excitation wavenumber spectrum becomes $\hat{p}_e(k_x, k_z) = jF_0 \sin(k_x a)$. Substituted in (7.55b), the power radiated is obtained as

$$W = \frac{|F'_0|^2 \rho_0 c_0 k_0^4 a^2}{16\pi 4\omega^2 m''^2} \left[2(1+\varepsilon^2) \left(1 - \varepsilon \arctan \frac{1}{\varepsilon} \right) - \frac{2}{3} \right], \quad (7.60a)$$

where the abbreviation $\varepsilon = \rho_0 c_0 / \omega m''$ is introduced. The approximations for small ($\varepsilon \rightarrow 0$) and large ($\varepsilon \rightarrow \infty$) fluid loading are given by

$$W \approx \begin{cases} \frac{|F'_0|^2 \rho_0}{4\pi m''^2 c_0} \frac{(k_0 a)^2}{3} & ; \quad \varepsilon \rightarrow 0 \\ \frac{|F'_0|^2 \omega^2}{12\pi \rho_0 c_0^3} \frac{(k_0 a)^2}{3} & ; \quad \varepsilon \rightarrow \infty \end{cases}, \quad (7.60b)$$

respectively, when arctan is expanded to fifth order. The analysis of the directivity shows that the radiation is of dipole type for light fluid loading but corresponds to that of a longitudinal quadrupole for heavy.

Owing to the many interesting phenomena, the radiation below the critical frequency has been treated relatively comprehensive. In comparison, radiation above the critical frequency is more straightforward and can be described as follows. For $f > f_c$, $k_B < k_0$ in view of (7.47a). Thence, the locus for $(k_x^2 + k_z^2) = k_B^2$ is inside the range of integration of (7.55). At $(k_x^2 + k_z^2) = k_B^2$, the wave mobility of the plate tends to infinite as this is the condition for free waves irrespective of structure. When the locus of infinite wave mobility or conversely, vanishing wave impedance, is within the range of integration and the radiation impedance is not extremely large, the integral is determined by this maximum of the integrand. It follows that the radiation principally occurs in the direction given by

$$k_B^2 = k_x^2 + k_z^2 = k_0^2 \sin^2 \vartheta (\sin^2 \varphi + \cos^2 \varphi) = k_0^2 \sin^2 \vartheta. \quad (7.61)$$

A calculation of the power radiated by means of (7.55b) is not necessary since the undamped infinite plate intuitively radiates all the transmitted, structure-borne power.

To establish the, for many applications, important radiation loss factor for flexural waves in plates, Y_{\sim} and Z_{rad} are introduced explicitly in (7.54). By means of (7.51) and (7.53) one obtains

$$\frac{\hat{p}(k_x, k_z)}{\hat{v}(k_x, k_z)} = j\omega m'' \left[1 - \frac{(k_x^2 + k_z^2)^2}{k_B^4} - j \frac{\rho_0}{m''} \frac{1}{\sqrt{k_0^2 - k_x^2 - k_z^2}} \right]. \quad (7.62a)$$

From a comparison of this expression with the wave impedance of a plate in absence of fluid loading but in presence of a fictitious loss factor η_{rad} i.e.,

$$\frac{\hat{p}(k_x, k_z)}{\hat{v}(k_x, k_z)} = j\omega m'' \left[1 - \frac{(k_x^2 + k_z^2)^2}{k_B^4} (1 + j\eta_{rad}) \right], \quad (7.62b)$$

it is seen that by equating the imaginary parts of the two brackets, the radiation loss factor is given by

$$\eta_{rad} = \frac{\rho_0}{m''} \frac{k_B^4}{(k_x^2 + k_z^2)^2} \frac{1}{\sqrt{k_0^2 - k_x^2 - k_z^2}} \approx \frac{\rho_0}{m''} \frac{1}{\sqrt{k_0^2 - k_B^2}} \quad ; \quad f > f_c \quad (7.62c)$$

in the range where $(k_x^2 + k_z^2) = k_B^2$ governs the radiation. For light fluids such as air, (7.62c) mostly renders small values. This means that the decay of the bending waves almost exclusively is controlled by the geometrical attenuation, $|v(r)|^2 \sim 1/r$, for frequencies above the critical frequency. Correspondingly, the surface contribution to the radiation is large and the directivity is concentrated to the angle $\theta = \arcsin(k_B/k_0)$. In contrast, (7.62c) yields rather large values for heavy fluid loading such that the bending waves decay exponentially with distance from the excitation. In this case, the directivity is not pronounced. It should be emphasized that for heavy fluids such as water, the critical frequency is high, implying that the ordinary bending theory might not be valid.

7.6.5 Comparison with Experiments

In Fig. 7.20 are shown examples of measurements of radiation from three different wall designs. At the top of the figure is a diagram presenting the radiation efficiency of unity of a brick wall with the critical frequency at the low end of the range considered. The diagram in the middle displays

the logarithm of the radiation efficiency of a point excited, lightly damped plate. For such a system accordingly, the edge radiation is dominant. The bottom example refers to a thin plate on a wooden frame. In this measurement, every plate field subdivided was excited by means of a shaker such that, in principle, the result is the sum of the contributions from five partial plate fields.

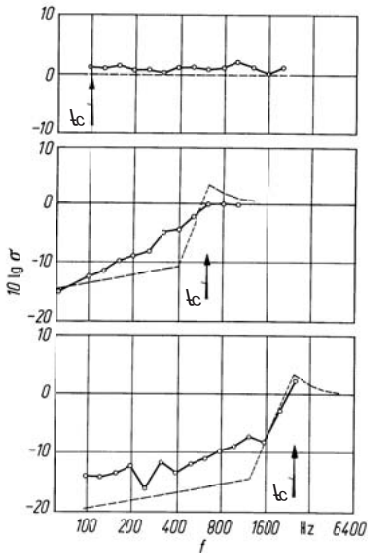


Fig. 7.20. Radiation efficiency for point force excited, weakly damped plates. Dashed curves denote predictions according to Eq. (7.63). 240mm brick wall of 12 m^2 area (top), 70mm lightweight concrete of 4 m^2 area (centre) and 13mm gypsum board wall on frames of 0.8 m^2 area (bottom)

For comparison are included in Fig. 7.20 the predictions using the radiation efficiencies in (7.50) at and above the critical frequency. A prediction below the critical frequency is markedly more difficult. As shown in Sects. 7.6.1 and 7.6.3, the boundary conditions or the form, amplitude and phase of the each excited mode must be known. This information can only be obtained with great effort and are not available under normal circumstances where the mean square velocity is determined. This means that more or less appropriate assumptions must be made. In the present case, a rather lengthy analysis [7.14] is used, which is based on the following presumptions:

- For point excitation, only those modes contribute to the radiation having eigen-frequencies within the range of excitation.
- The amplitudes of the resonant modes are equal on average and their phases are randomly distributed.
- The radiating plate is situated in a rigid baffle and simply supported along the edges.

The following approximations emerge from the analysis:

$$\sigma \approx \begin{cases} \frac{\lambda_c^2}{S} \left(2g_1 + \frac{U}{\lambda_c} g_2 \right) & ; \quad f < f_c \\ \sqrt{l/\lambda_c} + \sqrt{b/\lambda_c} & ; \quad f \approx f_c \\ \text{Min} \left[1/\sqrt{1-f_c/f}, \sqrt{\lambda/\lambda_c} + \sqrt{b/\lambda_c} \right] & ; \quad f > f_c \end{cases} . \quad (7.63)$$

l and b are the length and width of the radiating surface respectively. $S = l \cdot b$ and $U = 2(l+b)$ are the area and perimeter. The two functions g_1 and g_2 are defined by

$$g_1 = \begin{cases} \frac{4}{\pi^4} (1-2\alpha^2) \frac{1}{\alpha \sqrt{1-\alpha^2}} & ; \quad f < f_c/2 \\ 0 & ; \quad f_c/2 < f < f_c \end{cases},$$

$$g_2 = \frac{1}{4\pi^4} \frac{(1-\alpha^2) \ln[(1+\alpha)/(1-\alpha)] + 2\alpha}{(1-\alpha^2)^{3/2}},$$

where $\alpha = \sqrt{f/f_c}$. The aforementioned estimates are valid for radiators of dimensions larger than a quarter wavelength of the fluid wave.

As is seen from Fig. 7.20, the estimations are satisfactory in the range $f > f_c$ and acceptable for $f < f_c$, bearing in mind the many assumptions. Nonetheless, it should be pointed out that the radiation efficiency is a hazardous quantity in the latter range. Its definition and the commonly used measurement method convey an impression of a quantity only dependent on frequency, radiator dimensions and material properties. This is, however, not the case. Also the boundary conditions and the energy partition amongst the modes and thence the type of excitation play important roles, as has been discussed. The differences resulting can be substantial. As an example, point force excited thin plates usually exhibit radiation efficiencies ranging from 10^{-3} to 10^{-2} below the critical frequency whilst this quantity is approximately unity for the same plates when exposed to airborne

sound excitation over a large part of the surfaces. A phase constant line excitation leads to efficiencies somewhere between those values.

The previously discussed theoretical and experimental results yield the practical conclusion that to minimize the radiation, not only should the material be chosen such that the critical frequency becomes as high as possible but also folds and stiffeners should be avoided. Such discontinuities enlarge the effective perimeter and thus enhance the radiation. In particular, these issues are of importance with respect to the stiffened hulls in aircraft and ship building [7.4].

A measurement result is exemplified in Fig. 7.21 of the radiation from the excitation area at a large plate. The example refers to a gypsum board of 10mm thickness, which is unstiffened over an area of 5.1 m^2 and which is driven by a shaker with third-octave band noise. The resulting velocity field decays with increasing distance from the point of excitation such that a representation by means of the mean square velocity would have limited meaning as would a radiation efficiency from (7.6a). In the diagram, the abscissa is the band centre frequency and the ordinate is 10 times the logarithm of the ratio $W/(\rho_0 c_0 \lambda_c^2 |v_0|^2/2)$, where v_0 is the velocity at the excitation point. As can be seen, the measured and calculated results from (7.57c) are close for frequencies below critical frequency.

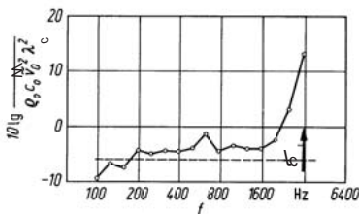


Fig. 7.21. Bending wave radiation from a point force excited 10mm gypsum board wall of $1.7 \cdot 3 \text{ m}^2$ area. Dashed curve denotes prediction according to (7.57c)

In this context it is interesting to analyse the effect of additional damping on the radiation. For frequencies above the critical, the question is easily answered since the radiation efficiency is independent of the loss factor. Thus, the reduction in radiation is proportional to that of the mean square velocity and the power radiated diminishes in general as $1/\eta$. In the vicinity of the critical frequency, the same is true, in principle, although it should be observed that an added damping layer leads to elevated bending stiffness such that the critical frequency is lowered. In practice, however,

the frequency shifts seldom exceeds 10 %. Below the critical frequency, the situation is somewhat more complicated because the total radiation is composed of contributions from the bending wave field and the edge radiation. By adding these two parts as given by (7.57a) and (7.6a) respectively, one obtains

$$W = \frac{\rho_0 c_0 k_0^2}{2\pi\omega^2 m''^2} |F|^2 / 2 + \rho_0 c_0 S \sigma |v_0|^2 / 2. \quad (7.64a)$$

With the relationship between the exciting point force and the averaged mean square pressure according to (5.118a), the expression for the radiated power can be rewritten as

$$W = \frac{\rho_0 c_0 k_0^2}{2\pi\omega^2 m''^2} \frac{|F|^2}{2} \left(1 + \frac{\pi}{4} \frac{f_c}{f} \frac{\sigma}{\eta} \right). \quad (7.64b)$$

Since only the second term depends on the loss factor, it is realized that a damping treatment is meaningful only when $f_c \sigma/(f\eta) > 1$. For a quadratic plate of dimensions 10 times the bending wavelength, an increase of the loss factor above $3 \cdot 10^{-2}$ will be wasted with respect to radiation.

For built-in plates i.e., plates with energy loss at the boundaries, the loss factors usually reach 10^{-2} . In practice, therefore, the experience is that although a damping treatment reduces the mean square velocity, the radiation remains unaffected. From such measurement results commonly, the conclusion is drawn that damping enhances radiation. As seen from (7.64b), this conclusion is incorrect. Rather, damping is, at most, inconsequential for radiation below the critical frequency and prescribed force excitation.

7.6.6 Additional Remarks on Structure-Borne Sound Radiation

7.6.6.1 Cylindrical Radiators with Prescribed Excitation

For the analysis of the relation between the radiation from infinitely extended cylindrical structures and an exciting force, the same procedure can be employed as for the plate in Sect. 7.6.4.1. With the wave impedance for the cylinder, introduced in Sect. 3.8.3.4, the radial component of the shell velocity, due to an excitation with a wave with $2n$ nodes in the circumferential direction and a wavenumber k_z in axial direction, can be written in the form

$$\hat{v}_n(k_z) = \hat{p}_n(k_z) / Z_{-n}. \quad (7.65a)$$

Here, $Z_{\sim n}$ is the wave impedance given by Eqs. (3.208) or (3.209) and $\hat{p}_n(k_z)$ the pressure amplitude. The latter is made up by the external excitation $\hat{p}_e(k_z)$ and the pressure reactions $\hat{p}_{ni}(k_z)$ and $\hat{p}_{no}(k_z)$ at the inner and outer cylinder surfaces respectively. By expressing the pressure reactions in terms of the shell velocity and the associated radiation impedances, the total pressure field becomes

$$\hat{p}_n(k_z) = \hat{p}_e(k_z) - \hat{v}_n(k_z)(Z_{n,rad,i} + Z_{n,rad,o}). \quad (7.65b)$$

For an unbounded fluid outside the cylinder, the radiation impedances are given by

$$\begin{aligned} Z_{n,rad,o} &= \frac{\hat{p}_{no}(k_z)}{\hat{v}_n(k_z)} = -\frac{-j\omega\rho_0 a}{(k_r a)} \frac{H_n^{(2)}(k_r a)}{H_n^{(2)\prime}(k_r a)}, \\ Z_{n,rad,i} &= \frac{\hat{p}_{ni}(k_z)}{\hat{v}_n(k_z)} = -\frac{-j\omega\rho_0 a}{(k_r a)} \frac{J_n(k_r a)}{J'_n(k_r a)}. \end{aligned} \quad (7.65c)$$

The outer radiation impedance follows from (7.31d) whereby the radial wavenumber k_r is defined by (7.33b). The inner radiation impedance is developed from an inner sound pressure field assumed in the form of Bessel functions $\hat{p}_n(r) = \hat{p}_n J_n(k_r r)$ and proceeding as in Sect. 7.4.4.

From (7.65), the wavenumber spectrum of the cylinder velocity can be determined as a function of the external excitation. The radiated power to the external fluid is obtained with the aid of Eqs. (7.32) and (7.33), in analogy with (7.55), as

$$W = \frac{\rho_0 c_0}{4\pi^2 a} \sum_{n=0}^{\infty} \mathcal{E}_n \int_{-k_0}^{k_0} \left| \frac{\hat{p}_{ne}(k_z)}{Z_{\sim tot}} \right|^2 \sigma_n(k_z) dk_z. \quad (7.65d)$$

Herein,

$$\begin{aligned} Z_{\sim tot} &= Z_{\sim n} + Z_{n,rad,i} + Z_{n,rad,o}, \\ \hat{p}_{ne}(k_z) &= \int_0^{2\pi} \int_{-\infty}^{\infty} p_e(\varphi, z) \cos n\varphi e^{jk_z z} ad\varphi dz, \end{aligned} \quad (7.65e)$$

and σ_n is the radiation efficiency according to (7.32b) whereby k_0 is replaced by k_r . $p_e(\varphi, z)$ is the spatial distribution of the external excitation.

The far field directivity for the individual modes is given by

$$|p_n(R, \vartheta, \varphi)| \approx \frac{\rho_0 c_0 \mathcal{E}_n}{2\pi^2 a R} \left| \frac{\cos \varphi}{H_n^{(2)\prime}(k_0 a \sin \vartheta)} \right| \left| \frac{\hat{p}_{ne}(k_0 \cos \vartheta)}{Z_{\sim tot}} \right|. \quad (7.65f)$$

The distance R is measured from the „centre“ of the excited area to the observation point. ϑ is the angle between the normal to the cylinder axis and the vector \mathbf{R} . Accordingly, a transformation is undertaken from cylindrical to spherical co-ordinates.

It should be observed that a direct relationship is again established between the wavenumber spectrum of the excitation and the directivity. This expression becomes particularly simple for point excitation since then $\hat{p}_{ne}(k_z) = F_0$.

7.6.6.2 Stiffened Plates

The expressions derived in Sect. 7.6.4.1 concern plane, infinite homogeneous plates. With some effort these can be elaborated to account for single stiffeners or other kinds of discontinuities through substitution of equivalent forces and moments. Thereby, the plate with discontinuities is brought into the form of a plate with several „external“ forces and moments. Fig. 7.22 illustrates the procedure cf., Fig. 6.23.

The steps of the analysis are:

- In the modelling, all stiffeners, boundaries etc. are initially removed so that an infinitely, homogeneous plate is established.
- The homogeneous infinite plate is considered excited by the truly external excitation p_e and the equivalent forces and moments F_n, F_R, M_n, M_R etc., resulting from the removed obstructions. In the latter group, there are point forces and moments for which the point of application is known whereas amplitudes and phases are not. For line-like forces and moments an approximation in form of a discretization can be used to avoid integral equations. As a rule of thumb, the line reaction is replaced by equivalent, discrete forces or moments, separated by less than a sixth of the governing wavelength or a tenth, when a high accuracy is desired.
- The wavenumber spectrum of the external excitation is determined. By adding the wavenumber spectra of the equivalent forces and moments is obtained in a one-dimensional example

$$\hat{p}_{tot}(k_x) = \hat{p}_e(k_x) + (F_1 + jk_x M_1)e^{jk_x x_1} + (F_2 + jk_x M_2)e^{jk_x x_2} + \dots, \quad (7.66a)$$

which readily can be extended to two dimensions.

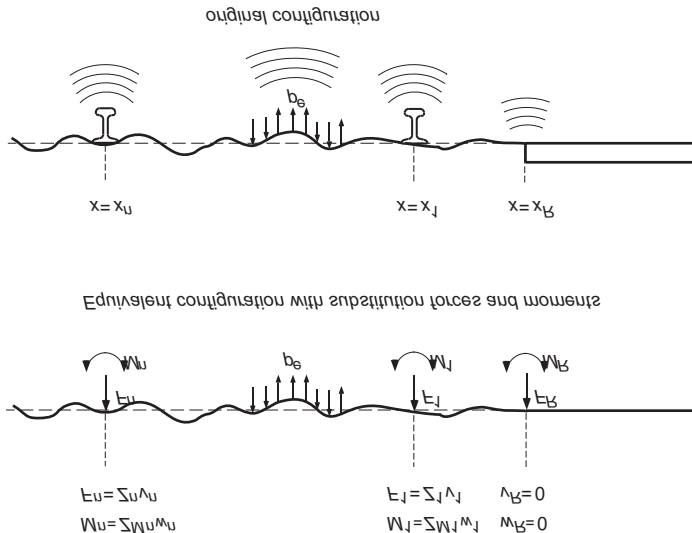


Fig. 7.22. Substitution of stiffeners and boundaries by equivalent forces and moments

As in (7.54), the wavenumber spectrum of the plate velocity is

$$\check{v}(k_x) = \frac{\check{p}_{tot}(k_x)}{Z_{\sim} + Z_{rad}}, \quad (7.66b)$$

from which the vibration field is obtained as

$$v(x) = \frac{1}{2\pi} \left[\int \frac{\check{p}_e(k_x)}{Z_{\sim} + Z_{rad}} e^{jk_x x} dk_x + \int \frac{F_1 e^{jk_x(x_1-x)}}{Z_{\sim} + Z_{rad}} dk_x + j \int \frac{M_1 k_x e^{jk_x(x_1-x)}}{Z_{\sim} + Z_{rad}} dk_x + \int \frac{F_2 e^{jk_x(x_2-x)}}{Z_{\sim} + Z_{rad}} dk_x + \dots \right]. \quad (7.66c)$$

From (7.66c) the plate moments and shear forces are developed according to (3.184c) and (3.184e). By sequentially substituting x_1, \dots, x_n and x_R for x in the equations for moments and shear forces, a set of linear expression is established, which can be related to the conditions at the discontinuities e.g., the mobilities of the stiffeners. In this way, a system of linear equations is developed with as many equations as there are unknown forces F_q and moments M_q cf., end of Sect. 6.5.3. The possibly large set of equations is solved for the unknown equivalent forces and moments. Thence, Eqs. (7.66a, b) do not contain any unknown and the wavenumber spectra can be calculated and employed in (7.55).

The procedure outlined presents a few numerical difficulties. All integrals extend from $-\infty$ to ∞ , which means that some consideration must be paid their truncation. Z_+ , moreover, is function with a narrow maximum such that its discretization must be made very fine, particularly for low damping. As for similar analyses, it is suitable to substitute the angle for the wavenumber such that the singularity of Z_{rad} can be avoided. Finally, it should be pointed out that especially for line-like obstructions and boundary conditions, the set of equations to solve can become very large due to the discretized relations.

The procedure can be employed also for cylinders with discontinuities whereby the expressions discussed in Sect. 7.6.6.1 apply.

For plates or cylinders partitioned by the discontinuities into more or less independently vibrating sections, the comprehensive procedure described above is unnecessary. When the vibrations of the sections are known, these can be treated approximately as small plane baffled radiators and the radiated powers summed.

7.6.6.3 Radiation from Arbitrary Shaped Structures with Prescribed Vibrations

The complete solution of the radiation problem from arbitrarily shaped structures is only available by means of integral equations. Therefore, approximations usually are required. In this context their basic principles will be discussed. Figure 7.23 outlines the problem. The radiation is sought from a structure with an arbitrary equilibrium form and a prescribed surface velocity v_n in the normal direction. The tangential component, again, is left without consideration since the fluid viscosity is neglected.

For the commonly called „Rayleigh-method“ [7.15], illustrated in Fig. 7.23b, the vibrating surface is subdivided into small surface elements ΔS , realising the volume velocity

$$q_n = v_n \Delta S. \quad (7.67a)$$

The vibrating structure, then, is thought removed from the fluid and the sound radiation is calculated for the small volume velocity sources. These sources are assumed to behave as monopoles such that they do not act as scattering objects, influencing the radiation of each other. It is thus possible to write the pressure as

$$p(x, y, z) = \sum_{n=1}^N \frac{j\omega\rho_0 v_n}{4\pi r_n} e^{-jk_0 r_n} \Delta S, \quad (7.67b)$$

in analogy with (7.39b), where r_n is the distance from the n th monopole to the receiver position. In this expression no consideration is taken of the

fact that the structure itself constitute a scatterer for the radiated sound. Were the velocity field such, for instance, that only $q_1 \neq 0$ but all other sources would have vanishing volume velocity, the directivity certainly would be incorrect. This is most easily realized from the unconsidered shadowing effect of the structure at its rear side. Hence, the Rayleigh-method is unsuitable for directivity analysis. In contrast, the method readily yields useful estimates of the power radiated, provided the structure is „curved“. A flat structure, such as a finite plate, enables adjacent sources in the approximation to compensate each other, which would be prevented in reality by the structure.

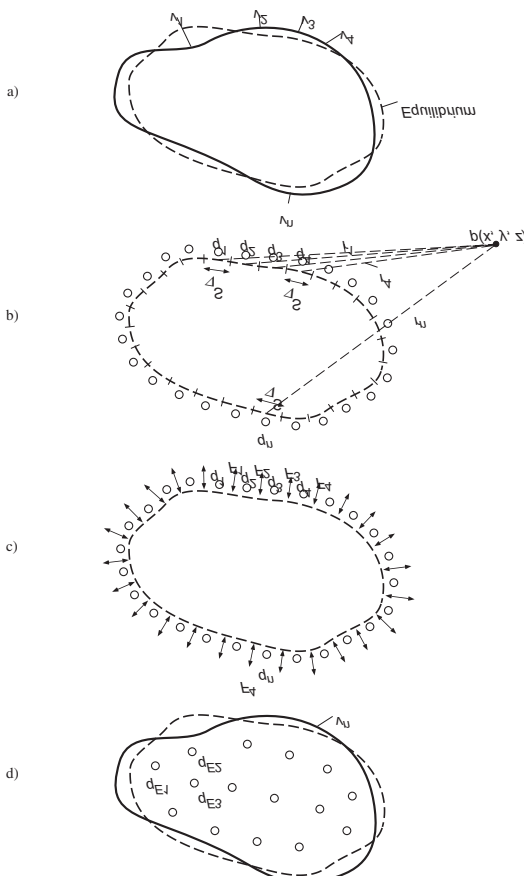


Fig. 7.23. Illustration of methods for estimation of radiation from arbitrary shaped structures with normal velocity component v_n . a) original situation, b) „Rayleigh-method“, c) boundary element method and d) multi-pole method

For the application of the Rayleigh-method as well as for the other methods discussed subsequently, it is necessary to keep the distance between the sources sufficiently small. As a rule of thumb, the dimensions of ΔS should be smaller than a third of the distance between regions vibrating out-of-phase. In addition, the dimensions should be smaller than a sixth of the fluid wavelength. It is appropriate, moreover, to modify the denominator for large structures. This means that the mirror source effect is taken into account simply by replacing the 4 by a 2, as in Eq. (7.39b).

The fact that the vibrating structure not only radiates sound but also acts as a scatterer can be considered by distributing dipole sources F_n at the surface, in addition to the monopoles q_n , see Fig. 7.23c. The strength of the dipoles is given by

$$F_n = p_n \cdot \Delta S \quad (7.68a)$$

where p_n is the spatial average of the sound pressure at the elemental surface ΔS . Also with this modelling the structure is absent from the fluid. This means that an unbounded homogeneous fluid is assumed, which encompasses a control surface coincident with the structural contour. Over the control surface, numerous monopoles and dipoles are distributed, having finite volume velocities q_n and exerting finite forces F_n respectively and being small enough not to cause any scattering themselves. According to (7.21) and (7.24d) the resulting pressure for the radiator configuration depicted in Fig. 7.23c becomes

$$p(x, y, z) = \sum_{n=1}^N \frac{j\omega\rho_0}{4\pi r_n} v_n \Delta S e^{-jk_0 r_n} + \sum_{n=1}^N \frac{\cos \vartheta}{4\pi r_n} \left(\frac{1}{r_n} + jk_0 \right) p_n \Delta S e^{jk_0 r_n} \quad (7.68b)$$

Herein, ϑ is the angle between source and receiver positions.

In the limiting case of infinitesimally small surface elements, Eq. (7.68b) turns into the Kirchhoff-Helmholtz integral equation, which establishes a complete description of the sound field in the presence of prescribed boundary conditions. The expression thus, is the discrete form of the rigorous solution of the radiation problem. Equation (7.68b) involves the complication that the pressure p_n is not known a priori. In a slightly modified form, however, the equation can be applied also for the centre points of the surface elements. Thereby, a set of N linear equations between the N unknown pressures is obtained. Due to coincidence of source and receiver positions i.e., $r_n \approx 0$ and the singularity of the coefficient matrix at certain frequencies, the solution is not straightforward. By means of the procedure developed for the boundary element method, BEM, the complications can be circumvented and a solution established. The numerical effort certainly can be large, particularly when a large frequency

range should be covered but with commercially available computer programmes, the method is frequently employed [7.16 – 7.18].

In Fig. 7.23d yet another approximation is illustrated. This, not yet commercially available, procedure [7.19 – 7.22] again, employs one or more elementary sources such as monopoles, dipoles, quadrupoles etc.. The elementary sources are substituted for the real radiating structure. Their amplitudes and phases are adjusted such that the resulting sound field outside the radiator contour becomes equivalent to that of radiator. Two schemes exist for the adjustment, which both lead to a set of linear equations to be solved by means of linear algebraic techniques. One advantage of this procedure with multi-pole sources is that when the equation of motion is known for the radiator, the radiation can be determined directly from the exciting forces or moments.

7.7 Fluid-Borne Sound Excitation of Structures

It can appear somewhat misplaced to analyse excitation of structures by sound waves in a chapter on sound radiation. In view of the reciprocity principle, however, this is not so strange. As is discussed in the Sect. 6.9, there is a close relationship between radiation and fluid excitation.

7.7.1 Transmission Loss of Single Leaf Wall

Consider a very large, flat plate on which there impinges a plane sound wave at an angle ϑ as depicted in Fig. 7.24. The incident wave is partly reflected by, partly transmitted through the plate such that the pressure field and the y -component of the velocity can be expressed as

$$p(x, y) = \begin{cases} (p_i e^{-jk_0 y \cos \vartheta} + p_r e^{jk_0 y \cos \vartheta}) e^{-jk_0 x \sin \vartheta} & ; \quad y < 0 \\ p_z e^{-jk_0 y \cos \vartheta} e^{-jk_0 x \sin \vartheta} & ; \quad y > 0 \end{cases},$$

$$v_y(x, y) = \begin{cases} \frac{\cos \vartheta}{\rho_0 c_0} (p_i e^{-jk_0 y \cos \vartheta} - p_r e^{jk_0 y \cos \vartheta}) e^{-jk_0 x \sin \vartheta} & ; \quad y < 0 \\ \frac{\cos \vartheta}{\rho_0 c_0} p_t e^{-jk_0 y \cos \vartheta} e^{-jk_0 x \sin \vartheta} & ; \quad y > 0 \end{cases}. \quad (7.69)$$

The relation between v_y and p is derived from conservation of momentum cf. (7.26b).

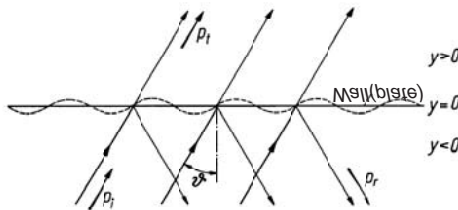


Fig. 7.24. Excitation of a plate by plane sound waves

If the fluids differ on the two sides of the plate, the expression remains almost the same, only the different characteristic impedances and angles of incidence and transmission must be taken into account. The angles are obtained from Snell's law of refraction.

The exciting pressure is made up of the incident, reflected and transmitted waves such that

$$p(x, 0) = (p_i + p_r - p_t) e^{-jk_0 x \sin \theta}. \quad (7.70)$$

Since the pressure distribution is in the form of a plane wave, the wave impedances or mobilities given in Sects. 5.4.1 and 5.4.2 for several cases can be directly employed to get the velocity as

$$v_p(x) = (p_i + p_r - p_t) Y_{\sim} (k_0 \sin \theta) e^{-jk_0 x \sin \theta}. \quad (7.71)$$

Herein, Y_{\sim} is the wave mobility of the plate at $k_x = k_0 \sin \theta$ because the excitation occurs at this wavenumber component over the whole domain. The wavenumber component in the z -direction can be set equal to zero since the presently treated problems do not involve any direction dependence in the plane of the plate. For orthotropic plates on the other hand, such a procedure is obviously not admissible.

By using the additional boundary condition that the normal components of the velocities on the two sides of the wall must equal that of the wall, one obtains at $y = 0$

$$\frac{\cos \theta}{\rho_0 c_0} (p_i - p_r) = (p_i + p_r - p_t) Y_{\sim}, \quad \frac{\cos \theta}{\rho_0 c_0} p_t = (p_i + p_r - p_t) Y_{\sim}, \quad (7.72)$$

This means that the plate velocity and the transmitted sound pressure can be expressed as

$$\nu_p = \frac{2p_i Y_{\sim}}{1 + 2\rho_0 c_0 / (Y_{\sim} \cos \vartheta)} , \quad \frac{p_t}{p_i} = \frac{Y_{\sim}}{Y_{\sim} + \frac{\cos \vartheta}{2\rho_0 c_0}} . \quad (7.73)$$

From the latter of these expressions, the transmission efficiency can be determined i.e. the ratio of transmitted to incident power.

$$\tau = \frac{W_t}{W_i} = \left| \frac{p_t}{p_i} \right|^2 = \left| \frac{2\rho_0 c_0 Y_{\sim}}{2\rho_0 c_0 Y_{\sim} + \cos \vartheta} \right|^2 \quad (7.74)$$

In turn, the transmission loss R in dB is readily obtained from the transmission efficiency as $R = 10 \log (1/\tau)$.

As is seen, the fundamental quantity is the wave mobility in all the relations. Of particular importance is the question whether the wave mobility tends to infinity or not in the frequency and angular ranges considered. Each such singularity of the mobility implies that total transmission occurs i.e., $\tau = 1$.

Equations (7.73) and (7.74) are valid for infinitely extended structures with known wave impedances or wave mobilities. Accordingly, plates with finite shear stiffness (5.50c), orthotropic plates (5.50b) and prestressed plates or membranes (5.50e) are also included. Also parallel plates with an interlayer acting in shear (4.109) or with an elastic interlayer without lateral coupling (Y_{-2} in (6.163a)) can be treated by the aforementioned expressions. In the following, the analysis is confined to thin plates, however, for which the wave mobility at an exciting wavenumber $k_x = k_0 \sin \vartheta$ is given by

$$Y_{\sim} = 1 / \left[j\omega m'' \left(1 - (k_0 \sin \vartheta / k_B)^4 \right) \right] . \quad (7.75a)$$

In the range $k_0 \ll k_B$, well below the critical frequency, the second term in the parenthesis can be neglected. The resulting transmission loss is the so called mass law for airborne sound transmission,

$$R = 10 \log \left(1 + \frac{\omega^2 m''^2 \cos^2 \vartheta}{4\rho_0^2 c_0^2} \right) ; \quad f \ll f_c \quad (7.75b)$$

The sound transmission loss of plates below the critical frequency, thus, is the higher the higher the mass reactance compared with the radiation resistance. It is also seen that the transmission loss vanishes for grazing incidence ($\vartheta = 90^\circ$). Fortunately, grazing incidence does not play a substantial role in conjunction with finite walls. This means that for uniformly distributed angles of incidence, the squared cosine term in (7.75b) can be ap-

proximated by a half, $\cos^2 \vartheta \approx 1/2$. In Fig. 7.25, the transmission losses calculated with this approximation are shown together with measurement results for a plate of 16 kg/m^2 . As is seen, the predictions satisfactory illustrate what can be achieved in practice provided the critical frequency is not exceeded. In general, the mass controlled transmission loss does not furnish more than 45 dB. Exceptions are only realized by very heavy and flexible materials such as lead, rubber and the like.

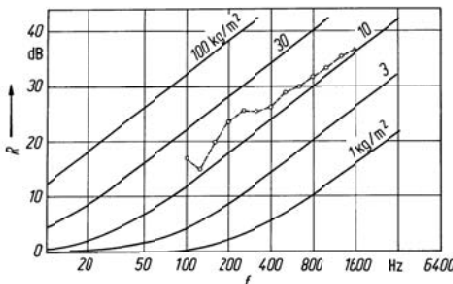


Fig. 7.25. Sound transmission loss below the critical frequency calculated for an angle of incidence of 60° . Dashed curve represents measured results for a plate of 16 kg/m^2

For frequencies above the critical frequency, Eq. (7.75a) shows that there is always an angle $\vartheta = \arcsin(k_B/k_0)$, for which Y_- tends to infinity and the plate offers no resistance to the sound, which thus is totally transmitted. This effect occurs when the free bending wavelength equals the trace wavelength $\lambda_0/\sin \vartheta$ of the incident sound. Accordingly, the effect is termed trace wave matching [7.23]. As a consequence, the very important equality of the directions of maximum excitation and radiation follows cf., Sect. 7.4.3.

Since the angle at which trace wave matching occurs also can be written as

$$\vartheta = \arcsin\left(\sqrt{\frac{f_c}{f}}\right) \quad (7.75c)$$

for homogeneous plates, an increase in frequency causes the trace matching angle to approach that of normal incidence. For angles smaller than the critical angle given by (7.75c), the wave mobility is mass controlled whereas the approximation

$$Y_{\sim} \approx \frac{j\omega}{B'k_0^4 \sin^4 \vartheta} = \frac{jc_0^4}{\omega^3 B' \sin^4 \vartheta}$$

applies for larger angles. This means that beyond the critical angle, the wave mobility is controlled by an angle dependent stiffness and is inversely proportional to the cube of the frequency.

For sound that impinges uniformly from all directions, the transmission loss and the plate velocity primarily depend on the conditions in the vicinity of the critical angle. The corresponding analysis, which is meaningful only if damping is taken into account, will be considered in Sect. 7.8.4 by means of an entirely different approach.

7.7.2 Double Walls with Sound Bridges

Besides the previously discussed single-leaf walls, also double walls are of great practical importance. In the ideal case with two infinite parallel plates separated at some distance without introducing connecting sound bridges, the transmission efficiency is obtained by inserting $Y_{\sim 2}$ from (6.163a) in (7.74). Upon limiting the analysis to the range below the critical frequency, the approximation leading to Eq. (7.75b) can be employed and one obtains

$$R_{ideal} = 10 \log \left[1 + \frac{\omega^2 m_l'' \cos^2 \vartheta}{4 \rho_0^2 c_0^2} \left(1 - \frac{\omega^2}{\omega_1^2 - \omega_2^2} \right)^2 \right]. \quad (7.76a)$$

The frequencies ω_1 and ω_2 are given by (6.162b).

Of yet greater practical importance is the stiff wall with a thin, flexible lining plate as depicted in Fig. 7.26. The critical frequency of the stiff wall is assumed to lie below the frequency range of interest so that its radiation efficiency can be taken to be unity irrespective of whether the plate is mechanically excited or excited by fluid-borne sound. Let R_1 denote the transmission loss of the stiff wall, given by the ratio of incident power W_i to that transmitted W_{t1} in Eq. (7.74). Because $\sigma = 1$, the transmitted power can be written in terms of the wall velocity v_1 and area S as

$$R_1 = 10 \log \frac{W_i}{W_{t1}} = 10 \log \frac{W_i}{\rho_0 c_0 S |v_1|^2 / 2}. \quad (7.76b)$$

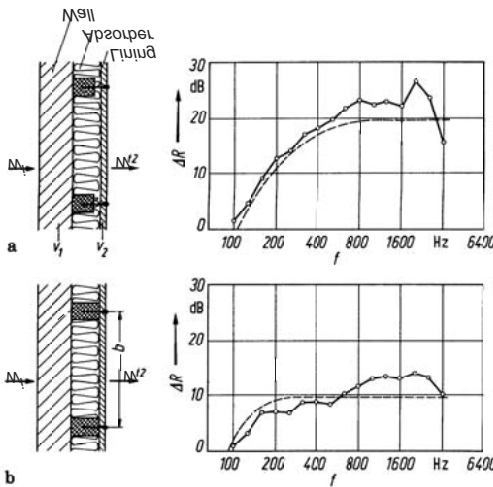


Fig. 7.26. Improvement of sound transmission loss resulting from a flexible lining of 10mm gypsum board. a) point connections calculated according to Eq. (7.76e) and b) line connections calculated according to Eq. (7.76f)

If it is assumed now that the transmission from the stiff to the flexible plate occurs only via point-like sound bridges and the latter plate is so large and so heavily damped that the bending nearfield radiation dominates, the power radiated from the lining can be expressed as

$$W_{t2} = \frac{8}{\pi^3} \rho_0 c_0 n \lambda_c^2 |v_2|^2 / 2, \quad (7.76c)$$

in view of Eq. (7.57c). In this expression v_2 is the velocity at the bridge location, n is the number of bridges and λ_c is the wavelength at the critical frequency of the flexible lining.

By means of (7.76c), the transmission loss of the complete wall system can be obtained as

$$\begin{aligned} R &= 10 \log \frac{W_i}{W_{t2}} = \left[10 \log \frac{W_i}{W_{t1}} + 10 \log \frac{W_{t1}}{W_{t2}} \right] \\ &= R_1 + 10 \log \frac{|v_1|^2 S \pi^3}{8 |v_2|^2 n \lambda_c^2}. \end{aligned} \quad (7.76d)$$

The second term in this expression obviously represents the improvement resulting from the lining. The improvement is seen to be bigger the softer

the bridges i.e., the bigger the ratio $|v_1|^2/|v_2|^2$. Also, fewer sound bridges and as high as possible a critical frequency of the lining enhances the improvement.

At low frequencies, however, sound transmission via the enclosed air or mineral wool in the cavity becomes significant. This additional transmission is of an entirely different character, corresponding to plane waves, which leads to an apparent increase of the transmission loss approximately obeying $40 \log(f/f_2)$. f_2 is the resonance frequency of the lining mass supported by the enclosed fluid or layer. The net result is that the improvement of the transmission is given by

$$\Delta R = \text{Min} \left\{ 40 \log(f/f_2) , 10 \log \left[|v_1|^2 S \pi^3 / \left(8 |v_2|^2 n \lambda_c^2 \right) \right] \right\}. \quad (7.76e)$$

This is exemplified in the upper part of Fig. 7.26.

A completely analogous analysis can be made for flexible linings that are connected to the primary wall along lines. For such a case the bending wave nearfield radiation follows from (7.59) for $\omega m'' \gg \rho_0 c_0$ and the beam impedance from (5.21) and is given by

$$W_{t2} = \frac{2}{\pi} \rho_0 c_0 n l_b \lambda_c \frac{|v_2|^2}{2}.$$

Again, $|v_2|^2$ is the velocity at the line contact, n the number of line contacts and l_b the length of each bridge. The improvement is thus found to be given by

$$\Delta R = \text{Min} \left\{ 40 \log(f/f_2) , 10 \log \frac{\pi |v_1|^2 S}{2 |v_2|^2 n l_b \lambda_c} \right\}. \quad (7.76f)$$

The lower part in Fig. 7.26 shows an example of the transmission loss improvement for rigidly connected line bridges. The improvement in this case is constant at high frequencies but less than that obtained for point bridges. The improvement that can be achieved by means of reasonably flexible linings, attached via rigid line bridges is of the order 5 to 10 dB. It is less for stiff linings and for materials with low losses, even a reduced transmission loss may arise. Such an example was discussed in conjunction with strongly coupled subsystems as illustrated in Fig. 6.41. Further examples occur only too often in practice where stiff panels are attached at many locations by means of mortar, plaster grouting etc. cf., Sect. 7.9.3.

7.8 Relation between Radiation and Response

7.8.1 Reciprocity

In the course of the earlier discussion of plate responses, it was pointed out that in the analysis of the transmitted structure-borne sound power there arise expressions that are very nearly the same as those encountered in analysing the radiated power. Furthermore, in the previous section it was found that the direction of maximum radiation coincides with that of maximum excitation. These similarities are not coincidental. Rather, they are manifestations of the reciprocity principle, which is commonly encountered in physics and which also has been applied several times in previous chapters.

For acoustics, this principle may be stated as follows: If a force F_1 , acting at point P_1 , produces a velocity v_{12} at point P_2 , then the same force ($F_2 = F_1$) acting at point P_2 will produce the velocity $v_{21} = v_{12}$ at point P_1 . Thus, the ratio of observed velocity to the force extended remains the same if the excitation and response positions are interchanged, provided also the directions of force and velocity are interchanged.

Since rather far-reaching conclusions will be drawn from the reciprocity principle in the following, some additional remarks are appropriate at this point. The theoretical basis for the reciprocity principle was provided by Lord Rayleigh [7.24] who demonstrated that the principle holds for all systems which have a finite number of degrees of freedom and for which the energy can be described in a symmetric quadratic form. More recent studies [7.25] of coupled continuous systems with infinite numbers of degrees of freedom have led to principally the same results. The studies have shown that the reciprocity principle applies whenever the governing differential equation is symmetric in the spatial variables. Since the differential equations, of linear acoustics processes always are symmetric, provided no flow is present, the reciprocity principle is valid. There are indeed non-symmetric differential equations in the literature, for example, the equation of motion for cylindrical shells and the wave equation for porous materials. In those cases, however, always approximations are introduced where the asymmetry is due to omissions of small quantities. The reciprocity principle, thus, can be applied for all usual acoustic problems.

Use of the principle in practice occasionally lead to difficulties, which invariably can be ascribed to some violation of the prerequisites. In air-borne sound measurements, for example, interchanging the source and receiver positions is only admissible when the source and receiver transducers have the same directivity. To avoid confusion, only the simple

formulation of the principle given above will be used. Also the loading by the transducers can perturb the reciprocity.

It should be pointed out that the reciprocity principle can be extended to encompass also several sources and receivers. This leads to Heaviside's law of mutual energies cf., Fig. 2.11. For several measurement problems the law is very useful.

7.8.2 Response and Radiation in a Reverberant Room

A general relation between response and radiation can be obtained from a series of hypothetical experiments. Let the structure of interest, such as a curved plate, be mounted in a reverberant fluid-filled room. The structure is excited by a point force F in the hypothetical experiment A as illustrated in Fig. 7.27. On the plate a certain velocity field will result, which, in turn, will lead to sound radiation. As long as the system is linear, the sound power radiated into the reverberant room is proportional to the mean square of the velocity and thus, proportional to the mean square of the exciting force,

$$W = \alpha |F|^2 / 2 \quad (7.77a)$$

where α is a parameter that characterize the radiation.

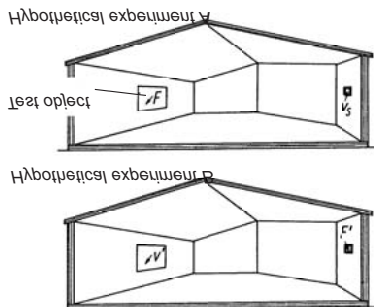


Fig. 7.27. Hypothetical experiments for deriving Eq. (7.78)

According to Eq. (7.1), there results the mean square pressure in the room

$$\frac{|p|^2}{2} = \frac{\rho_0 c_0^2 T}{13.8V} W, \quad (7.77b)$$

when the power W is supplied. The room has a volume V and a reverberation time T . Due to reflections, the mean square pressure at the walls is twice that given by (7.77b), provided the walls are heavy enough. If a moveable disc of mass m and area S is set into one wall, the mean square pressure $|p|^2$ will act on the disc, again, provided it is heavy enough. If the dimensions of the disc are significantly smaller than the fluid wavelength at all frequencies of interest, an assumption that can be made in a hypothetical experiment but is not easily realized in practice, the disc can be considered as a mass subject to a force $S|p|$. The disc velocity squared therefore, is given by

$$|v_s|^2 = \frac{2S^2 |p|^2}{\omega^2 m^2}. \quad (7.77c)$$

By combining Eqs. (7.77a) to (7.77c), one obtains the ratio

$$\frac{|v_s|^2}{|F'|^2} = \alpha \frac{\rho_0 c_0^2 T S^2}{6.9 V \omega^2 m^2}. \quad (7.77d)$$

In the inverse hypothetical experiment, denoted B in Fig. 7.27, the moveable disc is excited by the point force F' resulting in the disc velocity

$$|v_s|^2 = |F'|^2 / (\omega m)^2. \quad (7.77e)$$

The square of the resulting acoustic strength or volume velocity then becomes $|q|^2 = S^2 |v_s|^2$. Since the dimensions of the source are small compared with the fluid wavelength, the radiated power is given by Eq. (7.19) with $k_0 a \ll 1$. The power radiated from the small disc thus, is given by

$$W' = \frac{\rho_0 c_0}{2\pi} k_0^2 S^2 |v_s|^2 / 2. \quad (7.77f)$$

This power leads to a mean square sound pressure

$$\frac{|p'|^2}{2} = \frac{\rho_0 c_0^2 T}{13.8V} W', \quad (7.77g)$$

which, in turn, excites the initially discussed structure. In view of linearity, the structural response is proportional to the excitation such that by introducing a parameter β to characterize the excitation, the velocity can be written as

$$|v'|^2 = \beta |p'| \quad (7.77h)$$

By combining now (7.77e) to (7.77h), it follows that

$$\frac{|v'|^2}{|F'|^2} = \frac{\beta}{2\pi} \frac{\rho_0^2 c_0^3 T k_0^2 S^2}{13.8 V \omega^2 m^2}. \quad (7.77i)$$

Because the two hypothetical experiments involve point forces and the excitation and response positions are interchanged, the reciprocity can be applied. Thus, by equating (7.77d) and (7.77i) it is found that

$$\frac{\alpha}{\beta} = \frac{k_0^2 \rho_0 c_0}{4\pi}. \quad (7.78)$$

This equation states that the velocity of a structure that is excited by a randomly distributed sound field can be directly determined from the acoustic power radiated by the same structure when it is subject to a point force excitation. In other words, the response of a structure may be determined from its radiation and vice versa, provided a point force is employed and the incident sound field is random i.e., all directions of incidence are equally probable.

Before applying (7.78), it must be emphasized that α and β in general are location dependent. For a beam stiffened plate, for example, the quantity α , associated with the power radiated, is substantially different for an excitation point on a stiffener or between the stiffeners. Analogously, β , which is related to the airborne excitation highly differs if the response is registered at a stiffener or between them. For inhomogeneous structures care must be taken that the quantities α and β are measured at the same point. The situation is somewhat simpler for homogeneous structures because the power radiated due to a point force excitation is relatively independent of the excitation position in a frequency average sense, except for the areas close to the boundaries.

The fact that Eq. (7.78) applies for every point on the walls of a reverberant room may also be used to find the „least sensitive“ positions to point force excitation. One merely needs to excite the room acoustically and map the walls with an accelerometer with respect to the smallest response and thus the least excitation. In view of (7.78), α and hence also the power radiated due to a point force will also be smallest. A point located in this way would thus be an appropriate installation point for structure-borne sound generating equipment. The procedure, of course, is particularly useful in cases where the walls are inhomogeneous such as in ships and aircrafts.

7.8.3 Directivity by Excitation and Radiation

For the application of the reciprocity principle on excitation and radiation problems, the reverberant room involved in the hypothetical experiments in the previous section is not essential. Also the hypothetical experiment outlined in Fig. 7.28 can be used. A structure is considered in an unbounded fluid. In part A of the hypothetical experiment, the structure is excited at a position by a point force F_A . In the far field, the sound pressure, which is proportional to the force, diminishes with distance R such that it can be written as

$$|p_A|^2 = \gamma |F_A|^2 / R^2. \quad (7.79a)$$

Herein, γ is a proportionality constant, which depends on the material properties and the dimensions of the structure, the properties of the ambient fluid and the angle θ to the receiver position. The velocity resulting in the direction of a line between the excitation and response position is given by

$$v_A = p_A / (\rho_0 c_0). \quad (7.79b)$$

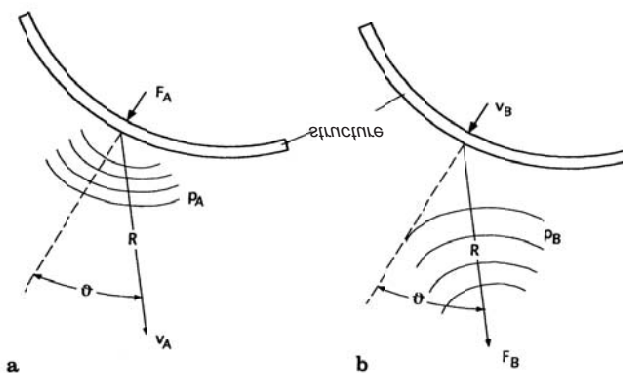


Fig. 7.28. Hypothetical experiments for deriving Eq. (7.80a)

In the second part B of the hypothetical experiment, a force F_B is exerted directly on the fluid giving the far field pressure at the distance R

$$|p_B|^2 = \frac{|F_B|^2 k_0^2}{16\pi^2 R^2}, \quad (7.79c)$$

according to (7.24b). p_B is the pressure of the wave, incident on the structure which establishes the excitation. For linear systems and processes, of course, the resulting structural velocity is proportional to the pressure of the incident wave, such that

$$|v_B|^2 = \varepsilon |p_B|^2. \quad (7.79d)$$

In this proportionality, ε is a quantity, which generally depends on receiver position, the properties of the structure and fluid as well as on the angle ϑ . By combining Eqs. (7.79) and applying reciprocity i.e., $v_A/F_A = v_B/F_B$, it is found that

$$\frac{\gamma}{\varepsilon} = \frac{\rho_0^2 c_0^2 k_0^2}{16\pi^2}. \quad (7.80a)$$

As is seen, the sound radiated to the far field from a point force excitation, represented by γ , is intimately linked to the sensitivity of the structure to acoustic plane wave excitation. By using (7.79d) for an infinitely extended structure with the wave impedance Z_\sim and an angle of incidence ϑ , it follows from (7.73) that

$$\varepsilon = \frac{|v_p|^2}{|p_i|^2} = \frac{4}{|Z_\sim + 2\rho_0 c_0 / \cos \vartheta|^2}. \quad (7.80b)$$

With this substituted into (7.80a), a relation between a point force and the far field pressure is obtained, which readily can be shown to be identical to (7.55c). As an alternative, Eq. (7.56c) could have been obtained also from an integration of (7.73) over all angles of incidence ϑ , provided $Z_\sim = j\omega m$ and $\rho_0 c_0$ instead of $2\rho_0 c_0$ were substituted since fluid is only present on one side of the plate in (7.56c).

7.8.4 Sound Transmission above the Critical Frequency

Sound transmission through walls involves essentially two phenomena, excitation of the wall by incident sound and radiation from the resulting wall vibrations. Thus, Eq. (7.78) also applies in this context since the „excitation“ is characterized by the quantity β . By considering that the average mean square pressure $|p|^2$ in a reverberant room leads to an incident power on an area S of $W_i = |p|^2 S / (8\rho_0 c_0)$ whereas the wall vibrating with the average mean square velocity $|v|^2$ results in the radiated power at the other side $W_t = |v|^2 \rho_0 c_0 S \sigma / 2$. The transmission efficiency, thus, can be expressed as

$$\tau = \frac{W_t}{W_i} = \frac{4|v|^2 \rho_0^2 c_0^2 \sigma}{|p|^2} = 4\rho_0^2 c_0^2 \sigma \beta. \quad (7.81a)$$

Generally, σ is the most uncertain parameter because the radiation efficiency depends strongly on the type of excitation. Therefore, the expression above pertaining to point excitation cannot be applied à priori. Only in one frequency range, the radiation is the same irrespective of excitation and approximately equal to unity, namely that above the critical frequency. This means that with Eq. (7.78), the transmission efficiency becomes

$$\tau = 4\rho_0^2 c_0^2 \beta = 16\pi\rho_0 c_0 \alpha / k_0^2 \quad ; \quad f > f_c. \quad (7.81b)$$

The transmission efficiency of a homogeneous wall thus, can be directly determined from its radiation when subject to a point excitation. According to Eq. (5.115a), however, the average plate velocity resulting from a point force excitation is given by

$$|v|^2 = \frac{|F|^2 k_B^2}{8\omega^2 m'^2 \eta S},$$

where η is the loss factor. This means that the power radiated above the critical frequency becomes

$$W = \alpha |F|^2 / 2 = \rho_0 c_0 S |v|^2 / 2 = \frac{\rho_0 c_0 k_B^2}{8\omega^2 m'^2 \eta} \frac{|F|^2}{2}, \quad (7.81c)$$

since $\sigma = 1$. By substituting the value of α obtained from the above expression into (7.81b), one obtains the transmission efficiency

$$\tau = \frac{2\pi(\rho_0 c_0)^2 k_B^2}{(\omega m')^2 \eta k_0^2} \quad ; \quad f > f_c, \quad (7.82a)$$

which is identical to the result derived by Cremer [7.22] by means of an entirely different approach. If the loss factor is expressed in terms of the corresponding structural reverberation time T_S , see Table 4.2, the transmission loss is obtained as

$$R = 20 \log \frac{\omega m'}{2\rho c} - 10 \log f_c T_S + 1.5 \quad ; \quad f > f_c. \quad (7.82b)$$

The transmission loss calculated on the basis of this expression is compared with experimental data in Fig. 7.29 [7.26]. Such an experiment normally involves generation of a sound pressure p_S in a reverberant „send-ing“ room by one or more loudspeakers, measurements of the sound

pressure in 5 to 10 different points as well as measurements of the sound pressure p_R and reverberation time in the „receiving“ room in a number of points. The sending room pressure constitutes a measure of the power incident on the wall whereas that of the receiving room and its reverberation time represent the power transmitted and absorbed respectively. With the volume of the receiving room V and the area of the wall S known, the transmission loss can be calculated from the experimental data by means of Eq. (7.1) as

$$R = 10 \log \frac{|p_s|^2 S}{4|p_R|^2} \frac{c_0 T}{13.8V}. \quad (7.83a)$$

The requirements on size and shape of the rooms used for transmission loss measurements are the same as those for sound power measurements cf., [7.27].

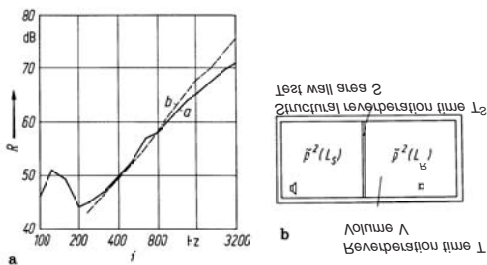


Fig. 7.29. Transmission loss of a 220mm thick brick wall ($m'' = 450 \text{ kg/m}^2$, $f_c = 170 \text{ Hz}$). a) Measured results and b) calculated results according to (7.82b) taking into account the reverberation times T_s of the mounted wall

With respect to practice, it should be noted that also above the critical frequency the attenuation increases with increasing wall mass. Besides this, the attenuation also is affected significantly by the location of the critical frequency as well as the losses. Since the losses not only depends on the material of the wall but also on the boundary conditions, the attenuation provided above the critical frequency can be predicted only with limited reliability. For the same reasons, transmission loss measured on differently mounted but otherwise identical walls can differ up to 6 dB [7.28].

Frequently, the one-dimensional version of (7.82a) is used for comparisons with measurements results. This version is obtained with the same

procedure by applying a line excitation and Eq. (7.78) in a somewhat modified form. The result is

$$\tau_E = \frac{2(\rho_0 c_0)^2}{(\omega m'')^2 \eta} \sqrt{\frac{f_c}{f}}. \quad (7.83b)$$

As is evident, the difference is small between (7.82a) and (7.83b) for commonly encountered walls. Surprisingly, (7.83b) often is in better agreement with measured results. This, however, does not rule out the possibility that (7.83b) compensates the error often introduced by assuming a frequency independent loss factor.

Regarding the location of the critical frequency, it follows from (7.82a) that it should be as far below the frequency range of interest as possible to achieve the highest possible transmission loss. When, therefore, it is practically difficult to realize a critical frequency which is above the frequency range of interest i.e. when the mass controlled attenuation is not available, then the wall must be designed so stiff that the critical frequency becomes as low as possible, below the lower frequency limit. The loss factor, moreover, should be sought as large as possible. Fully unsatisfactory is a critical frequency that falls in the frequency range of interest. In such a case the radiation is not only a maximum but also the excitation is a maximum as a consequence of reciprocity. The transmission loss hence is reduced by two effects simultaneously. In the building acoustic context where the frequency range is standardized to 100-3200 Hz, homogeneous partitioning walls of thicknesses between 2 and 10 cm should be avoided since the corresponding critical frequencies falls between 150-1500 Hz for commonly used materials. Accordingly, to achieve the transmission loss required only those possibilities remains with relatively thick, homogeneous partitions or inhomogeneous wall with special measures taken to elevate the critical frequency or double walls.

In practice there is often a conflict between the heavy, flexible plates required for the airborne sound insulation and the lightweight, stiff plates desirable from a static strength perspective. Hence, the question is justified if there exists such a parameter set, which leads to smaller transmission efficiencies in (7.82a) than those given by the mass law. Since the mass law is contained in (7.82a) one would be inclined to believe that it is achievable as long as $(2\eta f/\pi f_c)$ could be made larger than unity. Unfortunately, this appears not to be possible in practice. The reasons are:

- If f_c is set very low, very stiff partitions must be used. At the same time, the loss factor must be of the order 0.1 or larger. There are no known materials which have both these properties.

- A few octaves above the critical frequency the ordinary bending theory becomes invalid. The wave impedance or mobility must hence be determined using thick plate theories leading to an expression similar to (5.50c) introduced in (7.74). The corresponding analysis [7.29] shows that the transmission efficiency becomes somewhat higher than that predicted by (7.82a), which makes it difficult to overbid the mass law.
- Another alternative would be to apply a substantial prestress and thence the wave impedance or mobility according to Eq. (5.50e). Thereby, the critical frequency theoretically can be shifted markedly. From calculations it is seen, however, that the critical frequency can be shifted only weakly when the prestress is kept within a realistic range from a material strength point of view. Equally unsuccessful is the attempt with a negative prestress i.e. precompression of the material to increase the critical frequency. The buckling load for the partitioning element is reached before a noticeable effect is achieved on the transmission loss.

7.8.5 Transmission Loss in the Vicinity of the Critical Frequency

When frequencies in the vicinity of or below the critical frequency are of interest, the application of the reciprocity principle to obtain the transmission loss is problematic. It follows from (7.63b) and (7.78), however, that the plate velocity is given by

$$\frac{|v_p|^2}{|p|^2} = \beta = \frac{2}{(\omega m'')^2} \left(1 + \frac{\pi}{4} \frac{f_c}{h} \frac{\sigma}{\eta} \right), \quad (7.84a)$$

but this does not automatically lead to a formula for the transmission efficiency. The reason is that different vibration patterns and thence different radiation efficiencies are associated with the two terms in the parenthesis. The first term represents the so called forced vibrations having wavelengths equal to the trace wavelengths of the incident waves $\gamma_0/\sin \theta$. The second term, in contrast, is linked to the free bending waves. For the forced vibrations, the radiation efficiency $\sigma_E \geq 1$ whilst for the free $\sigma_F < 1$ below the critical frequency. Modifying (7.84a) with the radiation efficiencies σ_E and σ_F and substituting into (7.81a) leads to the transmission efficiency

$$\tau = \frac{8(\rho_0 c_0)^2}{(\omega m'')^2} \left(\sigma_E + \frac{\pi f_c \sigma \sigma_F}{4f\eta} \right) \quad (7.84b)$$

For $\sigma = \sigma_F = 1$ and $f_c/\eta f \gg 1$, this expression turns into (7.82a), as expected.

With $\sigma_E \approx 1$ and $\sigma = \sigma_F$ approximated by means of (7.63), a formula is obtained with which the transmission efficiency can be estimated. The estimates are uncertain, however, in those ranges where the approximated radiation efficiency is uncertain. With the properties of commonly encountered walls inserted in (7.84b) and (7.63) it is found that:

- Far below the critical frequency, the term involving $\sigma \sigma_F$ can be neglected such that the mass law is recovered, particularly if the wall possesses some losses.
- Close to the critical frequency, the transmission efficiency is a maximum (a trough in the transmission loss), which is associated with $\sigma = \sigma_F$ exceeding unity. This maximum is the more pronounced the larger the wall dimensions, measured in the wavelength at the critical frequency, as is seen from (7.73).

7.9 Application of Statistical Energy Analysis

A part of the analysis in the previous section could also have been undertaken with the aid of SEA. In Sect. 6.9, a general relation was derived between coupling quantities for the energy transport in opposite directions using the reciprocity principle cf., Eqs. (6.172e) and (6.177b). The SEA formulae, however, are confined to systems where the average mean square velocities are determined by the amplitudes of the resonant modes [7.30, 7.31]. For SEA, accordingly, only the free vibrations are considered but not the forced. This is in contrast to Eqs. (7.78) and (7.80c) where both free and forced waves are encompassed. Therefore, the application of SEA in this section on airborne sound transmission problems is confined to the frequency range above the critical frequency where the free waves predominate.

7.9.1 Flanking Transmission

In built-up structures, such as vehicles and buildings, airborne sound is transmitted not only through the direct partitioning area but also via flanking side walls, floors and ceiling cf., Fig. 7.30. These flanking paths are

usually as important as the direct for homogeneous partitions. Even more important is the flanking path when the primary partitioning structure is a high quality double wall whereas the sidewalls and ceilings consist of homogeneous plates. It is then to anticipate that the flanking transmission dominates.

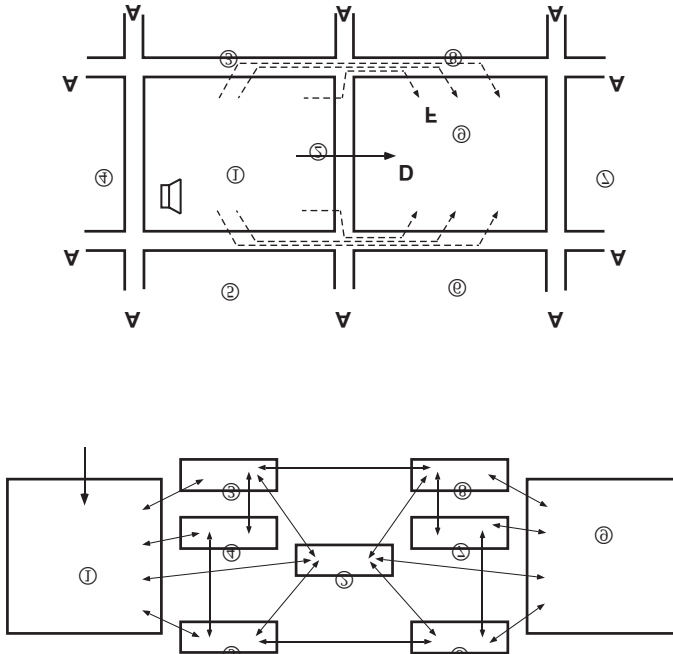


Fig. 7.30. Flanking transmission. a) wall configuration (2) – (8) and cavities (1), (9) and b) SEA modelling

To calculate the transmission via the different flanking paths, SEA is highly suitable for frequencies above the critical frequency. Since built-up structures such as ships and buildings consist of several cavities, walls, floors and ceilings, the set of equations for an SEA modelling of the complete system usually becomes very big. It is common, therefore, to consider only a section, such as depicted in Fig. 7.30. From Eq. (6.174) with $c_{\mu\nu} = m_\nu \omega \eta_{\mu\nu}$ according to (6.177a), one obtains

$$\omega \Delta \omega \begin{bmatrix} C_{11} & C_{12} & C_{13} & C_{14} & C_{15} & 0 & 0 & 0 & 0 \\ C_{21} & C_{22} & C_{23} & 0 & C_{25} & C_{26} & 0 & C_{28} & C_{29} \\ C_{31} & C_{32} & C_{33} & C_{34} & 0 & 0 & 0 & C_{38} & 0 \\ C_{41} & 0 & C_{43} & C_{44} & C_{45} & 0 & 0 & 0 & 0 \\ C_{51} & C_{52} & 0 & C_{54} & C_{55} & C_{56} & 0 & 0 & 0 \\ 0 & 0 & 0 & 0 & 0 & C_{66} & C_{67} & 0 & C_{69} \\ 0 & 0 & 0 & 0 & 0 & C_{76} & C_{77} & C_{78} & C_{79} \\ 0 & 0 & C_{83} & 0 & 0 & 0 & C_{87} & C_{88} & C_{89} \\ 0 & 0 & 0 & 0 & 0 & C_{96} & C_{97} & C_{98} & C_{99} \end{bmatrix} \begin{bmatrix} E_1^m \\ E_2^m \\ E_3^m \\ E_4^m \\ E_5^m \\ E_6^m \\ E_7^m \\ E_8^m \\ E_9^m \end{bmatrix} = \begin{bmatrix} W_1 \\ 0 \\ 0 \\ 0 \\ 0 \\ 0 \\ 0 \\ 0 \\ 0 \end{bmatrix} \quad (7.85)$$

where $C_{pp} = n_1 \left(\eta_{11} + \sum_{q=2}^5 \eta_{q1} \right)$ is the loss due to conversion into heat and the losses due to transmission into adjacent coupled subsystems, $C_{qp} = -n_q \eta_{qp}$ represents the transmission from adjacent, coupled subsystems p to a subsystem q and $E_q^m = m_q |v_q|^2 / (2n_q \Delta \omega)$ is the average modal energy of subsystem q . η_{qp} denotes the coupling loss factors, which can be calculated from the transmission efficiencies by means of Eq. (6.172a) when no more detailed information is available. For the configuration described by (7.85) is assumed that the airborne sound radiation only results in negligible damping for walls and floors.

If all elements are assumed to be equal, (7.85) can be solved analytically. In such a situation it is found that:

- The power transmitted to wall 2, from a reverberant field with the mean square pressure $|p_1|^2$, is

$$W_{21} = \frac{\pi}{2} S_2 \frac{f_{c2}}{f} \frac{\overline{|p_1|^2}}{\omega \rho_2 h_2} \quad (7.86a)$$

- Corresponding expressions can be found for walls 3 and 5 and when all walls are alike, their mean square velocity ratios are given by

$$\overline{|v_2|^2} \approx \overline{|v_3|^2} \approx \overline{|v_5|^2}, \quad \overline{|v_6|^2} \approx \overline{|v_8|^2} \approx \overline{|v_2|^2} / 4 \quad (7.86b)$$

- The mean square velocity of the partitioning wall becomes

$$\frac{\overline{|v_2|^2}}{|p_1|^2} = \frac{\pi}{2} \left(\frac{1}{\omega \rho_2 h_2} \right)^2 \frac{f_{c2}}{f} \frac{1}{\eta_2} \quad (7.86c)$$

This means that each flanking surface radiates a factor of 4 less power to the receiving room than the partitioning wall in the present case. Since the total flanking wall area is substantially bigger than that of the partitioning wall, one may use as a rule of thumb that the two power contributions are roughly the same provided that the walls are identical.

For non-identical building elements, (7.85) is suitably solved numerically. The resulting data agree with those from measurements in a frequency averaged sense [7.32].

7.9.2 Double Walls

Upon applying the power balance relations in (6.174) on the double wall system depicted in Fig. 7.31, where no sound bridges and no flanking paths are present, the two equations

$$\begin{aligned} m_2 \overline{|v_2|^2} \omega (\eta_{22} + \eta_{32}) - m_3 \overline{|v_3|^2} \omega \eta_{23} &= W_{21}, \\ m_3 \overline{|v_3|^2} \omega (\eta_{33} + \eta_{23}) - m_2 \overline{|v_2|^2} \omega \eta_{32} &= 0 \end{aligned} \quad (7.88)$$

result. As in conjunction with (7.85), the radiation losses are neglected. An elimination of v_2 gives

$$m_3 \overline{|v_3|^2} \omega (\eta_{22}\eta_{33} + \eta_{22}\eta_{23} + \eta_3\eta_{32}) = W_{21}\eta_{32}. \quad (7.89a)$$

η_{22} and η_{33} represent the inner losses and the structure-borne sound transmission to adjacent structures not included in the system analysed. η_{23} and η_{32} are the coupling loss factors. For the continued analysis it is appropriate introduce the transmission efficiencies τ_2 and τ_3 defined by (7.74). These transmission efficiencies refer to those of single leaf walls and from (7.82a) one obtains

$$\tau_q = \frac{4\rho_1^2 c_1^2 \pi f_{cq}}{\omega^2 m_q''^2 2\eta_q f} \quad ; \quad q = 2, 3. \quad (7.89b)$$

Herein, m_q'' is the mass per unit area such that $m_q = Sm_q''$. The power transmission W_{21} is already given by (7.86a). Together with (7.89b) it can be rewritten in the form

$$W_{21} = \tau_2 \frac{m_2'' S_2 \omega \eta_2}{4\rho_0^2 c_0^2} \overline{|p_1|^2}. \quad (7.89c)$$

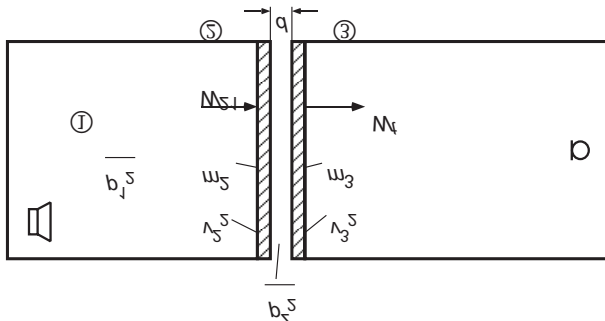


Fig. 7.31. Schematic double wall. 1) sending room and 2), 3) parts of the double wall

To assess η_{32} , the power W_{32} transmitted from wall 2 to 3 is estimated using (7.86a). Thereby, it must be observed that the mean square pressure $\overline{|p_z|^2}$ at a wall is twice that in (7.86a) representing the mean square pressure averaged over the whole sending room. In analogy with (7.89c) this power transmission can be written as

$$W_{32} = m''_2 S_2 \omega \eta_{32} \overline{|v_2|^2} = \tau_3 \frac{m''_3 S_3 \omega \eta_3}{4\rho_0^2 c_0^2} \frac{\overline{|p_z|^2}}{2}. \quad (7.89d)$$

Upon inserting (7.89c) and (7.89d) in (7.89a), it is found after some manipulations that

$$\frac{\overline{|p_1|^2}}{\overline{|v_3|^2}} = \frac{4\rho_0^2 c_0^2}{\tau_2 \tau_3} = \frac{4\rho_0^2 c_0^2 2\overline{|v_2|^2}}{\overline{|p_z|^2}} \left(1 + \frac{\eta_{23}}{\eta_3} + \frac{\eta_{32}}{\eta_2} \right), \quad (7.89e)$$

and from the second relation in (7.88) that

$$\frac{\overline{|v_3|^2}}{\overline{|v_2|^2}} = \frac{\tau_3}{4\rho_0^2 c_0^2} = \frac{\overline{|p_z|^2}}{2\overline{|v_2|^2}} \frac{1}{1 + \eta_{23}/\eta_3}. \quad (7.89f)$$

In analogy with (7.81a), it follows from (7.89e) that the transmission efficiency of the double wall is given by

$$\tau_D = \frac{\tau_2 \tau_3}{8(\rho_0 c_0)^2} \frac{\overline{|P_z|^2}}{\overline{|v_2|^2}} \frac{1}{1 + \frac{\eta_{23}}{\eta_3} + \frac{\eta_{32}}{\eta_2}} \quad (7.89g)$$

With the aid of (7.89f), one may therefore also write

$$\tau_D = \tau_2 \frac{\overline{|v_3|^2}}{\overline{|v_2|^2}} \frac{1 + \eta_{23} / \eta_3}{1 + \eta_{23} / \eta_3 + \eta_{32} / \eta_2} \quad (7.89h)$$

For the further analysis, the frequency range is suitably divided into two regions by introducing a double wall resonance frequency f_D . Well below this frequency i.e., roughly $f < f_D / \sqrt{2}$, the two panels are strongly coupled such that they behave like a single leaf wall. In this range the transmission efficiency is best estimated by using Eq. (6.82a) where the compound mass per unit area is inserted as m'' . For η and f_c , the less favourable values of the thickest panels should be used.

Well above the frequency f_D , say $f > \sqrt{2}f_D$, only a weak coupling remains between the panels and hence the double wall character is manifested. At least in the context of airborne sound attenuation, one may presume in this range that the power transmitted from one panel to the other is substantially smaller than that dissipated in the panels. This means that $\eta_{32} \ll \eta_2$ and $\eta_{23} \ll \eta_3$ and hence the last fraction in (7.89g) can be omitted, leaving only the ratio $\overline{|P_z|^2} / \overline{|v_2|^2}$ to be determined.

By considering first a thin interlayer of a locally reacting elastic material or a thin layer of air, which at least partially is equipped with some absorbing material, a stiffness per unit area s'' can be assigned. For a layer thickness of d , the stiffness is given by

$$s'' = K / d, \quad (7.90a)$$

where the compressional modulus is $K = \rho_0 c_0^2$ for a thin air layer. As before, ρ_0 is the density but c_0 is the speed of sound for an isothermal rather than adiabatic compression, which means a 20% reduction compared with the normal sound speed. Equation (7.90a) is applicable as long as the interlayer can be considered thin compared with the interlayer wavelength, usually up to about a sixth of a wavelength.

Owing to the weak coupling assumed, $\overline{|v_3|^2} \ll \overline{|v_2|^2}$ and it is reasonable to consider the pressure p_z determined solely by the stiffness s'' and the displacement of wall 2. This means that

$$\overline{|P_z|^2} = \left(\frac{s''}{\omega} \right) \overline{|v_2|^2}. \quad (7.90b)$$

Accordingly, the transmission efficiency in the range above f_D becomes

$$\tau_D = \frac{\tau_2 \tau_3}{2} \left(\frac{s''}{2\rho_0 c_0 \omega} \right)^2 ; \quad f > \sqrt{2} f_D \quad (7.90c)$$

By introducing the stiffness for an air layer, the term within parenthesis is always larger than unity provided the condition for thin cavities, $d < c_0/\omega$, is satisfied. Apart from the factor of two in the denominator, (7.90c) is derived in [7.34] following a different approach, where also good agreement with measured data is demonstrated. This suggests that the present version, also, would compare favourably with measurement results.

Secondly, the interlayer, which most commonly consists of air, can be considered thick compared with the wavelength. In that situation, (7.90b) does not hold anymore since standing waves can form in the cavity. As a coarse approximation, the cavity can be considered as a reverberant space resulting in a power transmission of

$$W_z = \rho_0 c_0 S_z \overline{|v_2|^2} \quad (7.90d)$$

to the cavity above the critical frequency. The power transmitted yields a sound pressure

$$\overline{|p_z|^2} = (\rho_0 c_0)^2 \frac{c_0}{\omega d \eta_z} \overline{|v_2|^2} ; \quad d > c_0 / 2f \quad (7.90e)$$

in the cavity, where η_z is the associated loss factor. After substitution of (7.90e) into (7.89g), a double wall formula results, containing the rather problematic dissipation in the cavity.

Regarding the frequency f_D , hitherto used only as a conceptual divider between the two ranges, it can be approximately estimated from the double wall system seen as two masses connected via a spring such that

$$f_D \approx \frac{1}{2\pi} \sqrt{\frac{s''(m_2'' + m_3'')}{m_2'' m_3''}}.$$

7.9.3 Multi-Layered Walls with Several Rigid Connections

It is known that a wall consisting of multiple layers, which are rigidly connected as illustrated in Fig. 7.32, overall exhibits a higher transmission efficiency than an equally heavy, single leaf wall of the same material, particularly at high frequencies. A principal explanation to this phenomenon, which is particularly pronounced for weakly damped materials, can be ob-

tained from a statistical energy analysis. With the notations of Fig. 7.32, the energy flow equations read,

$$\begin{aligned} m_2 \overline{|v_2|^2} \omega (\eta_{22} + \eta_{32}) &= W_{21} + m_3 \overline{|v_3|^2} \omega \eta_{23}, \\ m_3 \overline{|v_3|^2} \omega (\eta_{33} + \eta_{23} + \eta_{43}) &= m_2 \overline{|v_2|^2} \omega \eta_{32} + m_4 \overline{|v_4|^2} \omega \eta_{34}, \\ m_4 \overline{|v_4|^2} \omega (\eta_{44} + \eta_{34} + \eta_{54}) &= m_3 \overline{|v_3|^2} \omega \eta_{43} + m_5 \overline{|v_5|^2} \omega \eta_{45}, \\ m_5 \overline{|v_5|^2} \omega (\eta_{55} + \eta_{45}) &= m_4 \overline{|v_4|^2} \omega \eta_{54}. \end{aligned} \quad (7.91a)$$

Hereby, it is assumed that the distance between the sound bridges are larger than at least half a flexural wavelength. Otherwise, the subsystems are not resonant, which is a prerequisite for SEA.

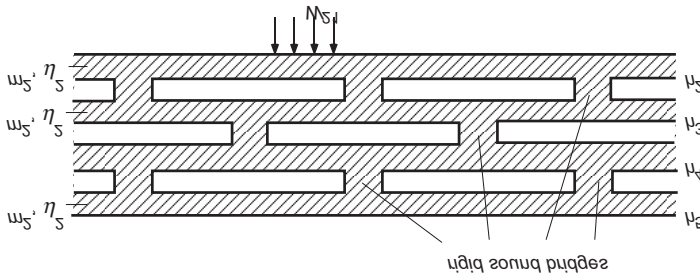


Fig. 7.32. Principal layout of a multi-layered wall with several sound bridges

In principle, the coupling loss factor for a rigid sound bridge should now be determined from the expressions in Sect. 6.8.2 and then substituted into (7.91a) to solve the set of linear equations. Since the principal behaviour is of primary interest, it is reasonable to assume that strong coupling in an SEA sense prevails, as is often the case in practice, such that the dissipative loss factors are smaller than the coupling loss factors. In accordance with Eq. (6.183), this means that the velocity ratios can be written as

$$\frac{\overline{|v_\nu|^2}}{\overline{|v_\mu|^2}} = \frac{\Delta N_\nu m_\mu}{\Delta N_\mu m_\nu}. \quad (7.91b)$$

By adding all equations in (7.91a), the terms involving coupling loss factors compensate each other. If, for simplicity, it is furthermore assumed that all layers are equal ($m_2 = m_3 = \dots$, $\eta_2 = \eta_3 = \dots$, $\Delta N_2 = \Delta N_3 = \dots$), the four-layer wall of Fig. 7.32 leads to

$$\Xi m_5 \overline{|v_5|^2} \omega \eta_5 = \frac{\pi}{2} S_2 \frac{f_{c2}}{f} \frac{\overline{|p_1|^2}}{\omega \rho_2 h_2}, \quad (7.91c)$$

where, again, Eq. (7.86a) is employed. Ξ is the number of layers, which in this case is 4. Following the usual procedure, the transmission efficiency of the multi-layered wall is obtained as

$$\tau_\Sigma = \frac{4\rho_0^2 c_0^2 \overline{|v_5|^2}}{\overline{|p_1|^2}} = \frac{4\rho_0^2 c_0^2}{\omega^2 \rho_2^2 h_2^2} \frac{\pi f_{c2}}{2\eta_2 f} \frac{1}{\Xi} = \frac{\tau_2}{\Xi}, \quad (7.91d)$$

provided all layers are the same. In the last form, τ_2 represents the transmission efficiency of the primary layer (indexed 2) in isolation.

Upon comparing transmission efficiency in (7.91d) with that of a single leaf wall of thickness Ξh_2 , it is seen that the former is Ξ^2 bigger than the theoretical transmission efficiency of the equally heavy single leaf wall. In this, account is taken of the fact that the larger thickness results in a bigger mass and thence a lower critical frequency ($f_{c2} \sim 1/h_2$), both of which leading to a reduced transmission efficiency.

This simple estimation clarifies why partitions involving several resonant subsystems, which are rigidly connected and encompassing large cavities, exhibit higher transmission than the corresponding single leaf wall. The increase in transmission is the more pronounced the smaller the material losses.

References

- [7.1] DIN 45635, Parts 1 and 2: Geräuschmessungen an Maschinen; Luftschall-emission. Rahmen – Messverfahren. Beuth Vertrieb, Berlin 1988
- [7.2] Fahy F.J., 1995. Sound intensity (2nd ed.). E & FN Spon, London
- [7.3] Crighton D.G., Dowling A.P., Ffowcs Williams J.E., Heckl M. and Lepping-ton F.G., 1992. Modern methods in analytical acoustics, § 9.3.3.3. Springer Verlag, London
- [7.4] Gösele K., 1953. Schallabstrahlung von Platten die zu Biegeschwingungen angeregt sind. Acustica, 3, p. 243
- [7.5] Hempel W. and Siedel T., 1970. Statistische Erhebung über Dieselmotorengeräusche. Motortechnische Zeitschrift, 31, p. 153
- [7.6] Morse P.M., 1948. Vibration and sound, Ch. VII. McGraw-Hill, New York NY
- [7.7] Lighthill J., 1978. Waves in Fluids, Ch. 27. Cambridge University Press, Cambridge
- [7.8] Kurtze G. and Bolt R.H., 1959. On the interaction between plate bending waves and their radiation load. Acustica, 9, p. 238

- [7.9] Abramowitz M. and Stegun I.A., 1972. Handbook of mathematical functions. Dover Publications, New York NY
- [7.10] Lighthill J., 1986. An informal introduction to theoretical fluid mechanics, §8.3. Clarendon Press, Oxford
- [7.11] Rayleigh J.W.S., 1945. The theory of sound, Vol. 2, §278. Dover Publications, New York NY
- [7.12] Möser M., 1988. Analyse und Synthese akustischer Spektren. Springer Verlag, Berlin
- [7.13] Heckl M., 1959. Schallabstrahlung von Platten bei punktförmiger Anregung. *Acustica*, 9, p. 371
- [7.14] Maidanik G., 1962. Response of ribbed panels to reverberant acoustic fields. *Journal of the Acoustical Society of America*, 34, p. 809
- [7.15] Klemenz M., v. Estorff O. and Heckl M., 1995. Schallabstrahlung eines Katalysators mit der BEM und dem „Rayleigh-Verfahren“. *Proc. DAGA*, Saarbrücken, vol. II, p. 683
- [7.16] Colton C. and Kress R., 1983. Integral equation methods in scattering theory. John Wiley & Sons, New York NY
- [7.17] Shenk H., 1968. Improved integral formulation for acoustic radiation problems. *Journal of the Acoustical Society of America*, 44, p. 41
- [7.18] Seybert A.F., Soenorko B., Rizzo F.J. and Shippy D.J., 1985. An advanced computational method for radiation and scattering of acoustic waves in three dimensions. *Journal of the Acoustical Society of America*, 77, p. 362
- [7.19] Cremer L., and Wang M., 1985. Die Synthese eines von einem beliebigen Körper in Luft erzeugten Feldes aus Kugelschallfeldern und deren Realisierung in Durchrechnung und Experiment. *Acustica*, 65, p. 53
- [7.20] Bobrovnikskii Y.I. and Tomilina T.M., 1990. Calculation of radiation from finite elastic bodies by the method of auxiliary sources. *Soviet Physics Acoustics*, 36, p. 334
- [7.21] Heckl M., 1989. Bemerkung zur Berechnung der Schallabstrahlung nach der Methode der Kugelfeldsynthese. *Acustica*, 68, p. 251
- [7.22] Ochmann M., 1990. Die Multipolstrahlersynthese – ein effektives Verfahren zur Berechnung der Schallabstrahlung von schwingenden Strukturen beliebiger Oberflächengestalt. *Acustica*, 72, p. 233
- [7.23] Cremer L., 1942. Theorie der Schalldämmung dünner Wände bei schrägem Schalleinfall. *Akustische Zeitschrift*, 7, p. 81
- [7.24] Heckl M., 1961. Untersuchungen über die Luftschalldämmung von Doppelwänden mit Schallbrücken. *Proc. 3rd International Congress on Acoustics*, Stuttgart, p. 1010
- [7.25] Rayleigh J.W.S., 1945. The theory of sound, Vol. 1, §104-110. Dover Publications, New York NY
- [7.26] Belousov Y.I. and Rimskii-Korsakov A.V., 1975. The reciprocity principle in acoustics and its application to the calculation of sound field of bodies. *Soviet Physics Acoustics*, 21, p. 103
- [7.27] Josse R. and Lamure L., 1964. Transmission du son par une paroi simple. *Acustica*, 14, p. 266

-
- [7.28] ISO/DIS 140-1: Akustik – Messung der Schalldämmung in Gebäuden und von Bauteilen. Beuth Vertrieb, Berlin 1990
 - [7.29] Gösele K., 1961. Luftschalldämmung. Proc. 3rd International Congress on Acoustics, Stuttgart, 1959, p. 989. Elsevier Publishing Company, Amsterdam
 - [7.30] Heckl M. and Donner U., 1985. Schalldämmung dicker Wände. Rundfunktechnische Mitteilungen, 29, p. 287
 - [7.31] Lyon R.H. and de Jong R.G., 1995. Theory and application of statistical energy analysis (2nd ed.). Butterworth-Heinemann, Boston MA
 - [7.32] Crocker M.J. and Price A.J., 1969. Sound transmission using statistical energy analysis. Journal of Sound and Vibration, 9, p. 469
 - [7.33] Wöhle W., 1984. Statistische Energieanalyse der Schalltransmission, §1.10. Taschenbuch Akustik (Fasold, Kraak, Schirmer eds.). VEB Verlag, Berlin
 - [7.34] Gösele K. and Schüle W., 1989. Schall Wärme Feuchte, 9. Auflage, § 4.2.3. Bauverlag, Wiesbaden
 - [7.35] Gösele K., 1980. Zur Berechnung der Luftschalldämmung von doppelschaligen Bauteilen (ohne Verbindung der Schalen) Acustica, 45, p. 218

8 Generation and Measurement of Structure-Borne Sound

8.1 Mechanical Measurement Methods

8.1.1 Registration of Motion

Most “structure-borne sound sensors” respond to kinematic variables such as displacement, velocity or acceleration. Dynamic quantities such as stresses are usually deduced from differences of the former. The reason for this is in part that the kinematic variables are normally simpler to register than tensor quantities like stresses and strains despite their directional dependencies. Moreover, usually only the exterior of some structure-borne sound field is accessible for measurements whereas the field is disturbed if the structure is penetrated to reach interior points.

The measurement technique that is simplest to visualize consists of direct observation of the excursion i.e., of the displacement of the test object relative some fixed body, supporting a scale, as sketched in Fig. 8.1. Because these excursions generally are very small, only some enlarged or amplified observation can be made. Such a direct observation therefore is limited largely to calibration instruments in the laboratory.

Optical amplification of excursions from an equilibrium position can be primitively obtained by means of a mirror deflecting a light beam. If one

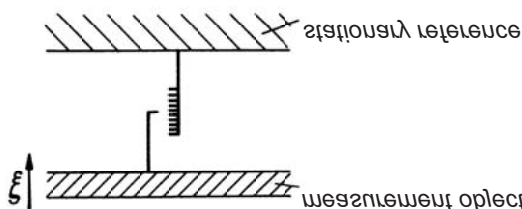


Fig. 8.1. Arrangement for direct observation of test object displacement

edge of a mirror of length l is displaced by an amount ξ , while the other edge pivots about a fix axis as depicted in Fig. 8.2, the mirror rotates an angle ξ/l . An impinging light beam accordingly is deflected twice that angle and a spot of the light, reflected at a screen at a distance L , is displaced by

$$\Delta = \xi (2L/l), \quad (8.1)$$

relative the equilibrium reflection point. Since an amplification of $2L/l = 500$ can be readily achieved, a test object displacement of 0.01mm not only can be measured but also the time history can be registered.

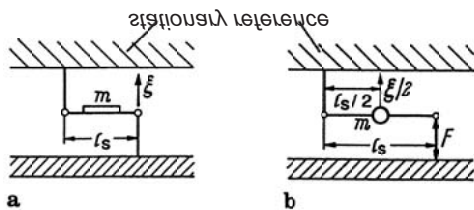


Fig. 8.2. Observation of displacement by means of a pivoted mirror. a) mirror attached to a lever and b) mass lever substitution

The rotating mirror sensor differs in one important aspect from the direct observation. Whereas a direct observation leads to no reaction force on the test object, the mirror inertia results in a force

$$F = -\frac{1}{l} \left(\frac{\omega^2 m}{2} \frac{l}{2} \right) \xi = -\frac{\omega^2 m}{4} \xi. \quad (8.2)$$

A similar relation applies to any instrument, with which a displacement is to be registered by means of a system of levers.

Because the reaction force produced by the sensor varies with frequency squared for a given displacement, such tilting mirrors and mechanical lever systems clearly are useful only for low frequencies. This limitation, also, becomes apparent if one notes that as for airborne sound, the square of the particle velocity but not the square of the displacement is proportional to the energy in the structure-borne sound context. Thus, for given energy, the displacement is inversely proportional to frequency. The dynamic variables force and strains associated with propagating waves, also, are proportional to the particle velocities and the products of forces and

portional to the particle velocities and the products of forces and velocities constitute the corresponding power quantities.

The most appropriate way to assess the reaction of a vibration sensor on a measurement object is to compare the mobility of the sensor \underline{Y}_a with that of the object \underline{Y} at the point of measurement. The latter mobility determines the velocity of the object induced by the force. This velocity alters the velocity of the unloaded object from the initial v_0 to

$$\underline{v} = \underline{v}_0 - \underline{Y} F = \underline{v}_0 - (\underline{Y}/\underline{Y}_a) \underline{v}. \quad (8.3)$$

The relative difference between the velocity sought v_0 and the actually measured velocity v , therefore, obeys

$$(\underline{v}_0 - \underline{v})/\underline{v} = \underline{Y}/\underline{Y}_a. \quad (8.3a)$$

For the previously described pivoted mirror, the sensor mobility is given by

$$\underline{Y}_a = 4/(j\omega m), \quad (8.4)$$

which thus is proportional to frequency. The factor $-j$ indicates that the velocity lags the force by a phase angle of $\pi/2$.

8.1.2 Comparison with Known Mobilities

If the sensing edge of the pivoted mirror of the previous section is kept in contact with the object only by gravity and the vibration of interest is in the vertical direction, the mirror cannot follow downward accelerations that exceed the acceleration of gravity. The force exerted by the object on the edge of the mirror cannot be negative,

$$F = m(g + \ddot{\xi}) > 0. \quad (8.5)$$

This ‘1g’ acceleration threshold is useful for absolute calibration of vibration sources such as shakers and vibration tables. Moreover, different thresholds can be achieved by using preloaded springs to force a known mass against the vibrating object as depicted in Fig. 8.3. Such a device also applies in the case of horizontal motion. In the vertical case, the force, which again cannot become negative, obeys

$$F = F_s + m(g + \ddot{\xi}) + s\xi > 0, \quad (8.6)$$

where s denotes the spring stiffness. By considering harmonic motion and introducing the natural frequency $\omega_0 = \sqrt{s/m}$, the displacement amplitude is found from Eq. (8.6) to be given by

$$\xi = \frac{F_s/m + g}{\omega^2 - \omega_0^2}. \quad (8.7)$$

A mass that is pressed by a prestressed spring against a measurement object, thus, can serve as an acceleration sensor only if the excitation frequency is substantially larger than the natural frequency of the mass-spring system. Accordingly, the mass cannot be too small and the spring cannot be too stiff. In spite of these limitations, early measurements were successfully carried out on membranes [8.1].

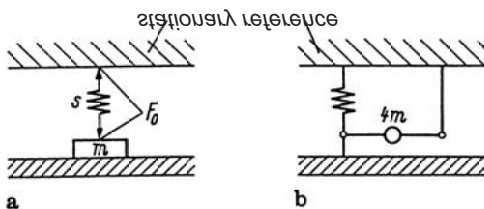


Fig. 8.3. Spring-loaded mass used as an acceleration threshold indicator. a) mechanical configuration and b) mechanical ‘circuit’ using a mass lever

At resonance i.e., when the excitation frequency coincides with the natural frequency of the sensor, the displacement amplitude tends to infinity. This condition, however, does not result in a particularly large reaction force on the measured object. Rather, the oppositely phased spring and inertia forces, making up the force F acting on the sensor

$$F = \left(j\omega m + \frac{s}{j\omega} \right) v, \quad (8.8)$$

cancel each other. This means that the sensor mobility tends to infinity at this frequency.

From Fig. 8.3, it would be tempting to term the mass and spring connected in series. Such a description must not be confused with a series connection in an electrical sense. Clearly, the same force as given by (8.8) also results when the mass and spring are attached side by side to the vibrating object. The lower and upper side of the mass in Fig. 1.4a, moreover, do not correspond to the “input” and “output” of an electrical two-pole. Rather, the force here is exerted at the same pole of the mass, with the opposite pole being the inertial reference for the acceleration.

The topology of the mechanical system can readily be translated to an electrical circuit when the mass is replaced by a mass lever [8.2] with a point mass at its midpoint, as depicted in Fig. 1.4b. From the considerations of the pivoted mirror, the point mass must be $4m$ to result in an inertia force of $j\omega m$. Accordingly, the “mechanical circuit” in Fig. 1.4b much better displays the physics of the mass and spring being connected in parallel. This is also in accordance with the electrical analogy where the branching forces correspond to the branching currents. The force “flow” in the mass lever, however, differs in one respect from the current in a branch of an electrical circuit. Although the force has the same magnitude before and after the mass, its algebraic sign is reversed. This effect is important if the other pivot rests on a mobile body instead of being fixed in space such that the mass lever acts as a coupling element. The sign of the force may be reversed once more by replacing the single mass lever by two such levers, mechanically in series.

The fact that a mechanical series connection provides no information regarding the topology of the analogous electrical circuit is also illustrated by the observation that the mobility is fully altered when the configuration shown in Fig. 8.4a is considered instead of the previously discussed sensor design of Fig. 8.3a. Here, the spring is situated between the vibrating object and the mass. In this arrangement no branching force occurs but the force at the “input” flows unperturbed through the spring to the mass. In contrast, the displacement of the mass differs from the compression of the spring. This difference becomes very clear when the two “mechanical circuits” in Figs. 8.3b and 8.4b, employing mass levers, are compared.

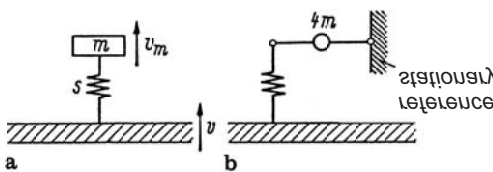


Fig. 8.4. Simple oscillator representing a sensor. a) mechanical system and b) mechanical circuit

By adding the two relations

$$\underline{v}_m = \underline{F}/(j\omega m) \quad , \quad \underline{v} - \underline{v}_m = j\omega \underline{F}/s \quad (8.9)$$

the mobility can be established of the sensor at the contact point with the object,

$$\underline{Y} = \left(\frac{j\omega}{s} + \frac{1}{j\omega m} \right), \quad (8.10)$$

which vanishes at the mass-spring resonance. The velocity of the mass, on the other hand, tends to infinity for a given velocity of the object, as seen from the relation

$$\underline{v}_m = \frac{\underline{v}}{1 - (\omega/\omega_0)^2}, \quad (8.11)$$

also obtained from (8.9). This result indicates that small motions, invisible to the naked eye, in principle, can be enlarged by resonant systems and not only by microscopes and optical levers.

8.1.3 Mechanical Transducers as Damped Mass-Spring Systems

The mechanical systems considered in the previous section must be augmented by the inevitable dissipation to realistically represent transducers for structure-borne sound. As discussed in Chapter 4, many different types of dissipation exist but only the most simple, namely the viscous element, will be considered in this context, realizing a force proportional to the velocity

$$F_r = -rv. \quad (8.12)$$

Herein, r is the viscous damping coefficient, which depends on the shape of the moving body and the ambient fluid. As introduced in Fig. 8.5, the viscous element is represented by a symbol that should associate to a piston in a cylinder, a “dash-pot”. Again, the viscous element acts physically in parallel with the mass, as is evident from the mechanical circuit in Fig. 8.5b.

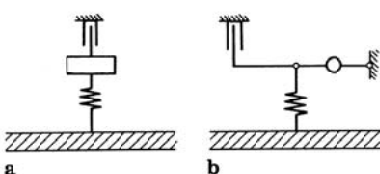


Fig. 8.5. Simple oscillator with linear frictional resistance. a) mechanical system and b) mechanical circuit

The input mobility of the sensor can be found to be given by

$$\underline{Y} = \frac{1 - (\omega/\omega_0)^2 + j\omega r/s}{j\omega m + r}, \quad (8.13)$$

which does not vanish at resonance. Instead, it takes on the real value

$$\underline{Y}_0 = \frac{r}{sm} \quad (8.14)$$

at the resonance for small enough damping coefficients, satisfying the inequality $r \ll \omega_0 m$. The mobility, therefore, is the larger the smaller the mass and spring stiffness and the larger the damping coefficient.

The transmissibility $\underline{v}_m / \underline{v}$ can be derived as

$$\frac{\underline{v}_m}{\underline{v}} = \frac{1}{1 - (\omega/\omega_0)^2 + \frac{j\omega r}{s}}, \quad (8.15a)$$

which has the magnitude squared

$$\left| \frac{\underline{v}_m}{\underline{v}} \right|^2 = \frac{sm}{r^2} \quad (8.15b)$$

at resonance. In principle, it thus appears possible to observe the displacement ξ_m , corresponding to v_m , from which the displacement of the test object ξ can be determined. This measurement method is not practical, however, not only because the dissipation usually is due to mechanisms other than pure viscous damping and is difficult to assess but foremost because the resonance peak is very narrow.

In order to describe the resonance peak in more general form, Eq. (8.15a) can be rewritten in terms of the decay constant, characterizing the decay of free oscillations

$$\xi = \hat{\xi} e^{-\delta t} \cos(\omega t + \phi_{\xi}) = \operatorname{Re} \left[\hat{\xi} e^{-(\delta + j\omega)t} \right] \quad (8.16)$$

of the system depicted in Fig. 8.5 with the oscillating object held fix. By introducing (8.16) in the equation of motion

$$m\ddot{\xi} + r\dot{\xi} + s\xi = 0, \quad (8.17)$$

one finds that the decay constant is related to the damping coefficient as

$$\delta = \frac{r}{2m} \quad (8.18a)$$

and that the eigen-frequency reduces to

$$\omega = \sqrt{\omega_0^2 - \delta^2} \quad (8.18b)$$

The transmissibility, which can be rewritten as

$$\frac{v_m}{v} = \frac{1}{1 - (\omega/\omega_0)^2 + j\omega \frac{2\delta}{\omega_0}}, \quad (8.19)$$

is shown in Fig. 8.6 for a damping ratio of $r/r_c = \delta/\omega_0 = 0.1$ where $r_c = 2\sqrt{sm}$ is the critical damping. The graph does not exhibit a pole but a pronounced peak at the damped eigen-frequency. By differentiating the square of the denominator magnitude with respect to ω^2 , the peak frequency can be found to obey

$$\omega = \sqrt{\omega_0^2 - 2\delta^2} \approx \omega_0(1 - \delta^2/\omega_0^2). \quad (8.20)$$

For small enough damping ratios, the difference between the undamped and the damped eigen-frequency can be neglected such that $\omega \approx \omega_0$ and the magnitude follows

$$v_{m,\max} \approx \frac{\omega_0}{2\delta} v \quad (8.21)$$

in the vicinity of the peak.

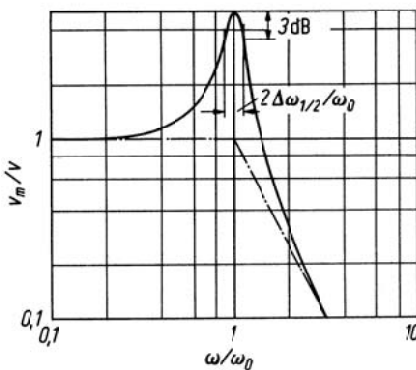


Fig. 8.6. Motion transmissibility of the simple oscillator in Fig. 8.5

With the frequency deviation $\Delta\omega = \omega - \omega_0$ introduced and neglecting terms of the order $(\Delta\omega)^2$, the ratio of oscillator velocity to maximum velocity

$$\frac{v_m}{v_{m,\max}} = \frac{1}{1 + j\Delta\omega/\delta} \quad (8.22a)$$

is obtained. Such a relation between a field variable and its maximum resonance value as function of the frequency deviation can be viewed as a definition of the “resonance function”. This function not only describes the parabolic region in the vicinity of the peak

$$\left| \frac{v_m}{v_{m,\max}} \right| \approx 1 - \frac{1}{2} \left(\frac{\Delta\omega}{\delta} \right)^2, \quad (8.22b)$$

but is valid also below the inflection points for small enough δ . The function thus describes the “bell-shaped” amplitude curve versus frequency deviation, which is common for all resonance phenomena. On a logarithmic scale, the inflection points occur where the magnitude squared and thus the power is half of the peak value. The corresponding frequency deviation is found from Eq. (8.22) to be

$$\Delta\omega_{1/2} = \delta. \quad (8.23a)$$

Twice this deviation can be considered a reasonable measure of the width of the resonance peak and is termed the half-value or half-power bandwidth. This bandwidth is usually given in Hz such that

$$2\Delta f_{1/2} = \delta/\pi \quad (8.23b)$$

Measured from the amplitude, the bandwidth is obtained at $1/\sqrt{2}$ of the maximum amplitude.

In order to obtain large peak velocities, small damping coefficients, decay constants or damping ratios are required. The small damping means, however, that the half-value bandwidth is limited. The associated strong variation with frequency of the response of lightly damped systems near their resonances makes them unsuitable as structure-borne sound sensors.

On the other hand, lightly damped mechanical systems are well suited for use as frequency indicators. In this respect, mechanical systems are usually better than electrical because their damping can be made much smaller.

8.1.4 Interaction of Transducer and Measurement Object

Any measurement implies that the object or its behaviour is affected, albeit ever so little. Since this general law naturally applies also for structure-borne sound measurements and the effect is not always evident, the issue will be analysed in this section through some examples.

The first situation considered is outlined in Fig. 8.7. It involves an oscillator attached to a vibrating object with a prescribed velocity \underline{v} . The oscillator mass m_M is connected to the object via springs of total stiffness s_M . On top of the oscillator, a transducer of mass m is attached via some spring-like fixture of stiffness s .

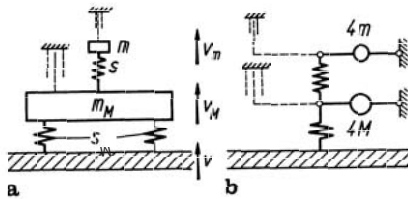


Fig. 8.7. Simple transducer model on top of a simple oscillator. a) mechanical configuration and b) mechanical circuit

For pure harmonic processes of frequency ω , the spring forces are given by

$$F_{s_M} = \frac{s_M}{j\omega} (\underline{v} - \underline{v}_M), \quad F_s = \frac{s}{j\omega} (\underline{v}_M - \underline{v}_m), \quad (8.24)$$

for the lower and upper masses respectively. The inertia forces of the masses are obtained from the accelerations $j\omega\underline{v}_M$ and $j\omega\underline{v}_m$ respectively as $F_M = j\omega m_M \underline{v}_M$ and $F_m = j\omega m_m \underline{v}_m$. The force balances require

$$\underline{F}_M = \underline{F}_{s_M} - \underline{F}_s \Rightarrow \frac{s_M}{j\omega} (\underline{v} - \underline{v}_M) - \frac{s}{j\omega} (\underline{v}_M - \underline{v}_m) = j\omega m_M \underline{v}_M \quad (8.25a)$$

and

$$\underline{F}_m = \underline{F}_s \Rightarrow \frac{s}{j\omega} (\underline{v}_M - \underline{v}_m) = j\omega m_m \underline{v}_m. \quad (8.25b)$$

This yields the coupled system of equations

$$\begin{aligned} (-\omega^2 m_M + s_M + s) \underline{v}_M - s \underline{v}_m &= s_M \underline{v}, \\ -s \underline{v}_M + (-\omega^2 m + s) \underline{v}_m &= 0, \end{aligned} \quad (8.26)$$

from which the transmissibilities

$$\frac{\underline{v}_M}{\underline{v}} = \frac{1 - (\omega/\omega_0)^2}{\left(1 + \frac{s}{s_M} - \frac{\omega^2}{\omega_M^2}\right)\left(1 - \frac{\omega^2}{\omega_m^2}\right) - \frac{s}{s_M}}, \quad (8.27a)$$

and

$$\frac{\underline{v}_m}{\underline{v}} = \frac{1}{\left(1 + \frac{s}{s_M} - \frac{\omega^2}{\omega_M^2}\right)\left(1 - \frac{\omega^2}{\omega_m^2}\right) - \frac{s}{s_M}} \quad (8.27b)$$

are obtained. Herein, $\omega_m = \sqrt{s/m}$ and $\omega_M = \sqrt{s_M/m_M}$ are the eigenfrequencies of the separated mass-spring systems.

Equation (8.27a) shows that the presence of the small mass m considerably affects the motion of the oscillator mass m_M at certain frequencies:

- At the zeroes of the denominator i.e., for frequencies above ω_m and below ω_M respectively provided $\omega_m < \omega_M$, resonances appear

$$\omega_{I,II}^2 = \frac{1}{2} \left[\omega_m^2 + \omega_M^2 + \frac{s}{m_M} \pm \sqrt{\left(\omega_m^2 + \omega_M^2 + \frac{s}{m_M}\right)^2 - 4\omega_m^2\omega_M^2} \right], \quad (8.28)$$

which would not occur in the absence of the transducer mass m .

- At the frequency $\omega = \omega_m$, the mass m_M is completely stopped i.e., an antiresonance occurs and $\underline{v}_M = 0$. In the special case of $s_M/m_M = s/m$ such that $\omega_M = \omega_m$, the biggest alteration is introduced, namely a transition from an infinitely large to a vanishingly small velocity since the resonance frequency ω_M , would equal ω_m in the absence of the transducer mass m .

Although the effects mentioned above still occur when dissipation is taken into account, they are not so pronounced. The corresponding analysis for the system sketched in Fig. 8.7 with the dashpot included, fixed to some inertial frame, simply means that the viscous forces are added on the right-hand side of Eqs. (8.25). Such a modelling to some extent, would represent the friction associated with the motion of the masses in the ambient medium. In a case where the dissipation is associated essentially with material losses in the springs, the dashpots must be re-arranged parallel to

the former. This would mean that $s/j\omega$ in Eq. (8.25) would be replaced by $r + s/j\omega$ and $s_M/j\omega$ by $r_M + s_M/j\omega$.

Figure 8.8 shows the transmissibility v_M/v as function of frequency, with and without the transducer. In the example is assumed equal eigenfrequencies for the two cascaded oscillators i.e., $s_M/m_M = s/m$ and $r_M/m_M = r/m$. The small mass and the damping ratio, moreover, are set to be $m = m_M/10$ and $\delta/\omega_0 = r/2$ $sm = 0.1$. Strong interaction is clearly seen in the vicinity of the resonance whereas the effect is negligible elsewhere for small ratios m/m_M .

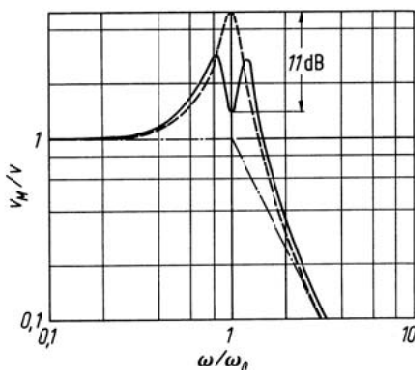


Fig. 8.8. Motion transmissibility of the simple oscillator. (—) with and (---) without a tuned transducer

All the drawbacks associated with resonance phenomena of a tuned transducer could be ameliorated by making the damping ratio so large that no or only little resonant amplification would arise. Such a damping is difficult to achieve, however, for the relatively large masses of structure-borne sound transducers. In practice, therefore, tuned transducers are only designed with their resonances either well above or well below the frequency range of interest.

The mechanical system depicted in Fig. 8.7 not only is of great significance for structure-borne sound measurement techniques. It is also a model for the so-called dynamic absorber i.e., small mass-spring systems, which are mounted on resonantly vibrating structures, in this case a large mass. As is observed, the resonance amplitude can be reduced substantially already with a relatively small dynamic absorber.

As a second example, Fig. 8.9 presents an idealization of a useful structure-borne sound exciter. It consists of a small coil mass m_1 , which is connected to the test object by means of a stiff spring s_1 , for example, representing some adhesive. The coil, moreover, is connected via some soft spring s_2 to centre the magnet mass m_2 , which, in turn, resiliently rests on the test object on soft springs s_0 .

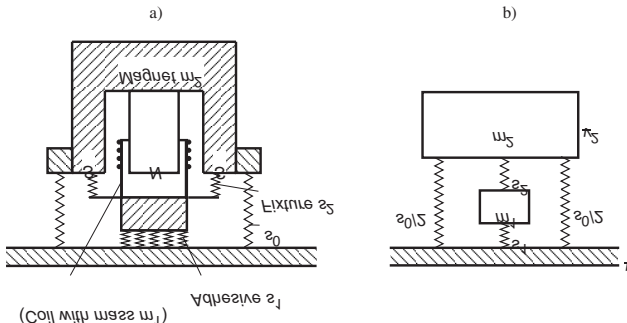


Fig. 8.9. Mechanical configuration of an electro-dynamic exciter. a) principal construction and b) model

Upon temporarily disregarding the electro-dynamic interaction, the system of equations corresponding to (8.26) is obtained from the force balances

$$\begin{aligned} s_0(\underline{v} - \underline{v}_2) + s_2(\underline{v}_1 - \underline{v}_2) &= -\omega^2 m_2 \underline{v}_2, \\ s_1(\underline{v} - \underline{v}_1) + s_2(\underline{v}_1 - \underline{v}_2) &= -\omega^2 m_1 \underline{v}_1. \end{aligned} \quad (8.29)$$

Solving for \underline{v}_1 and \underline{v}_2 brings no difficulties and after some manipulation one finds, for example, the relative difference between the test object velocity and that of the coil as

$$\frac{\underline{v} - \underline{v}_1}{\underline{v}} = \frac{v^2(v^2\mu - \mu - \sigma_2)}{v^4\mu - v^2(\mu + \sigma_1 + \sigma_2) + \sigma_1 + \sigma_2 - \sigma_2^2}. \quad (8.29a)$$

In this expression are used the abbreviations

$$\mu = \frac{m_1}{m_2}, \quad \sigma_1 = \frac{s_1}{s_0 + s_2}, \quad \sigma_2 = \frac{s_2}{s_0 + s_2}, \quad v^2 = \frac{\omega^2}{\omega_2^2} = \frac{\omega^2 m_2}{s_0 + s_2}.$$

From an interaction point of view, the mobility of the exciter, as seen from the test object, is more interesting. This is obtained as

$$\underline{Y}_{exc} = \frac{\underline{v}}{\underline{F}} = \frac{\underline{v}}{\underline{F}_0 + \underline{F}_1}, \quad (8.30)$$

where \underline{F} means the total force exerted, composed of the two spring forces $\underline{F}_0 = s_0 (\underline{v} - \underline{v}_2)/j\omega$ and $\underline{F}_1 = s_1 (\underline{v} - \underline{v}_1)/j\omega$. By carrying out the simple but tedious algebra, it is found that

$$\underline{Y}_{exc}\omega m_2 = j \frac{\nu^4 \mu - \nu^2 (\mu + \sigma_1 + \sigma_2) + \sigma_1 + \sigma_2 - \sigma_2^2}{\nu^2 \mu (1 + \sigma_1 - \sigma_2) - (1 + \mu)(\sigma_1 + \sigma_2 - \sigma_2^2)}, \quad (8.30a)$$

where the same abbreviations are used as in Eq. (8.29a).

The magnitude of the exciter mobility, normalized with respect to the mass mobility of the backing magnet, is plotted in Fig. 8.10 for a specific design. For the computations, some small amount of damping is included, which limits the resonance and antiresonances. As expected, the mobility equals the mass mobility of the magnet at low frequencies ($\nu < 1$). In an intermediate range, the exciter mobility essentially is that of the light-weight coil mass but increases rapidly at frequencies there above. The latter range, however, is of little interest from a transducer point of view since the coil is dynamically decoupled and therefore has a significantly smaller amplitude than the test object.

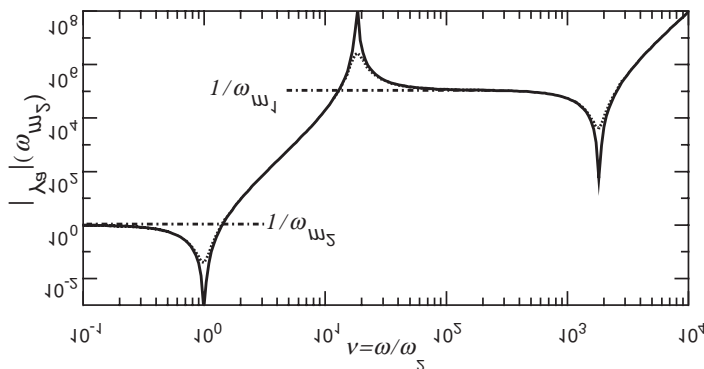


Fig. 8.10. Normalized input mobility of the structure-borne sound exciter in Fig. 8.9. Calculated from Eq. (8.30a) with $\mu = 0.003$, $\sigma_1 = 10000$, $\sigma_2 = 0.95$. (-----) loss factor $\eta = 0.01$, (· · ·) loss factor $\eta = 0.1$, (- - -) mass mobility of m_1 and $0 m_2$

The idealized design is outlined in Fig. 8.11 of another transducer of great practical value. It concerns the mechanical configuration of piezoelectric transducers where the piezo-electric material constitutes the spring

s. Since the electrical charge is proportional to the acting force $F_1 = s(\underline{v} - \underline{v}_2)/j\omega$, the velocities must be known of the seismic mass m_2 and of the house m_1 .

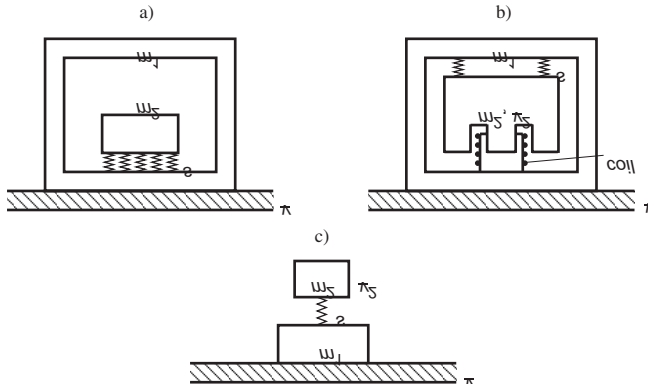


Fig. 8.11. Encapsulated structure-borne sound transducers with “seismic” masses m_2 . a) piezoelectric transducer, b) geophone and c) model

For the so-called geophone in Fig. 8.11b, m_2 represents the mass of a magnet with a coil fitted in the air gap. The coil is rigidly connected with the house whereas the magnet is suspended in the soft springs of stiffness s . With the voltage proportional to the velocity difference $\underline{v} - \underline{v}_2$, the latter must be determined.

The starting point for the continued analysis, again, is a force balance, which reads

$$s(\underline{v} - \underline{v}_2)/j\omega = j\omega m_2 \underline{v}_2 .$$

From this, both the velocity ratio $\underline{v}_2/\underline{v}$ and the velocity difference in the magnetic field can readily be developed,

$$(\underline{v} - \underline{v}_2) = \underline{v} \frac{1}{1 - (\omega_2/\omega)^2} . \quad (8.31a)$$

For the piezo-electric spring, similarly, the acting force is

$$\underline{F}_1 = j\omega m_2 \underline{v} \frac{1}{1 - (\omega/\omega_2)^2} , \quad (8.31b)$$

where, in both the above expressions, $\omega_2^2 = s/m_2$.

As can be seen, the velocity difference registered by the magnetic transducer approximates well the velocity of the test object for $\omega \gg \omega_2$. Accordingly, the geophone is tuned as low frequent as possible to obtain a voltage proportional to the velocity. This means that the spring s is made very soft and the mass m_2 as big as is admissible in view of its mobility.

Contrary, the force \underline{F}_1 proves proportional to the acceleration $j\omega\underline{v}$ of the test object in the range $\omega \ll \omega_2$ and a high frequency tuning is pursued for the piezo-electric transducer.

Finally also, the input mobility of the transducer design is of importance. It is composed of the mass mobility of the house and the reaction from the seismic mass such that

$$\underline{Y}_{transd} = \frac{\underline{v}}{\underline{F}} = \frac{1}{j\omega m_1 + \frac{1}{j\omega m_2} + \frac{j\omega}{s}} = \frac{1}{j\omega m_1 + \frac{j\omega m_2}{1 - (\omega/\omega_2)^2}}. \quad (8.32)$$

The last part of (8.32) shows that the mobility vanishes for $\omega^2 = s/m_2$, i.e., the transducer exhibits an antiresonance whereas it tends to infinity and a mass-spring-mass resonance occurs at

$$\omega_{12}^2 = s \left(\frac{1}{m_1} + \frac{1}{m_2} \right).$$

By means of the input mobility of a transducer, its interaction with the test object can be treated in a general way. To see this is considered the situation outlined in Fig. 8.12, where the undisturbed test object exhibits the velocity \underline{v}_0 and mobility \underline{Y}_0 at the measurement position. Due to the loading from the transducer, the test object's velocity changes from \underline{v}_0 to \underline{v}_m since the transducer reacts with the force $\underline{F} = \underline{v}_m / \underline{Y}_{transd}$. This means that

$$\underline{v}_m = \underline{v}_0 - \underline{F} \underline{Y}_0 = \underline{v}_0 - \frac{\underline{Y}_0}{\underline{Y}_{transd}} \underline{v}_m \Leftrightarrow \underline{v}_m = \underline{v}_0 \frac{1}{1 + \underline{Y}_0 / \underline{Y}_{transd}}. \quad (8.33)$$

As is observed, an as unperturbed measurement as possible is obtained for $|\underline{Y}_{transd}| \gg |\underline{Y}_0|$. Structure-borne measurement devices, therefore, should be as small and light-weight as possible or as weakly coupled dynamically to the test object as possible. Also, internal transducer resonances should be avoided since they may lead to low mobilities at certain frequencies, which can be difficult to predict. The inevitable interaction mainly leads to a reduction of the vibration velocity. For $|\underline{Y}_{transd}| \approx |\underline{Y}_0|$, however, also an increase is possible since the two mobilities can have opposite signs.

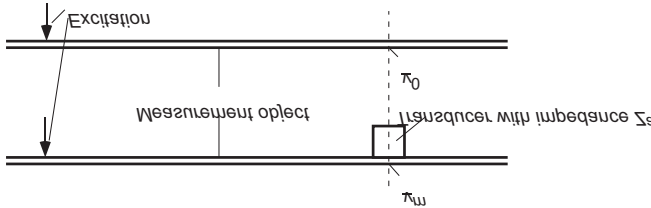


Fig. 8.12. Influence of the transducer mobility on the motion of a measurement object. Only one component of motion is considered

It should be noted that the quantities in Eq. (8.33) usually are complex, which means that the interaction also yields some phase distortion. When such phase errors must be kept small, for instance in conjunction with intensity measurements, the requirements on the condition $|Y_{transd}| \gg |Y_0|$ becomes much more rigorous than for ordinary magnitude or amplitude based measurements.

8.1.5 Immobile Reference and Rigid Termination

For the structure-borne sound transducers illustrated in Figs. 8.1 and 8.2 as well as for numerous other optical and electrical sensors, an “immobile” reference is required. Naturally, this is an ideal condition, which is hardly realizable for frequencies above some hundred Hz since immobile means an absolute motion less than 10^{-6}m or even 10^{-10}m .

A similar, principally unsolvable, problem is the “rigid termination”, which is desirable for some structure-borne sound measurement techniques, for example, in conjunction with stiffness measurements. Also in this case an ideal condition is sought that becomes the more insuperable the higher the frequency.

A way out of this dilemma is offered by transducers built according to the mass-spring-mass design cf., Sect. 4.4.1.2 or employing a seismic mass as a reference, as in Fig. 8.11. The basic idea is to replace the unfeasible immobile reference with an element for which the motion can be predicted precisely and thence can be used as the reference. Obviously, not only seismic masses are suitable for this purpose but also any configuration with a known mobility for the component of motion considered.

8.2 Controllable Sensors

For all types of measurements, particularly of oscillatory quantities, it is usually useful to convert any non-electrical quantity to an electrical current or a voltage change. This is so since use can then be made of the entire signal conditioning and processing capabilities provided by modern electronics. For example, the signals can be amplified, filtered, recorded and displayed in many ways and, above all, fed to computers for post-processing and, eventually, the manipulated signals can react on the test object.

Structure-borne sound transducers that convert mechanical quantities to proportional electrical ones may be divided into two groups. For the first, under consideration in this section, the motion of some mechanical element acts on an electrical or optical source without any reaction, except for such small effects as the radiation pressure or the local rise in temperature. The transduction phenomena on which such sensors are based, thus, cannot be used for the conversion of electrical or optical signals to mechanical. Accordingly, they are unsuitable for the generation of structure-borne sound.

In contrast, the phenomena underlying the second group of sensors, the so-called electro-mechanical transducers, are reciprocal and, hence, can be used both as sensors and excitors, disregarding the phase. As an inevitable consequence, this group always is accompanied by some reaction from the electrical side onto the mechanical.

8.2.1 Electrical Sensors

Sensors that control electrical circuits without producing a mechanical reaction act on the electrical circuits by virtue of a relative displacement $\Delta\xi$, which, in principle, is frequency independent even down to the static state.

The most commonly employed principles involve a change in one of the basic electrical two-poles, a resistor, an inductance or a capacitance.

A carbon microphone such as those previously used in telephones, is an example of a sensor that depends on a change in electrical resistance. The displacement of a membrane compresses the carbon aggregates against a rigid housing and this compression increases the aggregate contact area, which thus reduces the resistance. With a few volts from a battery across the aggregate, the $\Delta\xi$ quantities may be converted to directly measurable current changes Δi . Although the sensitivity is so high that no additional amplifier is required, it is rather unstable and generates so much self-noise that it is not useful for structure-borne sound measurements. On the other

hand, sheets of pressure-moulded carbon or graphite are occasionally used for this purpose. Because such sheets are relatively stiff, they are suitable for high frequency tuned acceleration sensors or load transmitting force transducers if their modulus of elasticity is known.

Such a transducer configuration used as a force gauge suffers from the fundamental disadvantage that the electrical resistance

$$R = \rho_{el} \frac{l}{S}, \quad (8.34a)$$

where ρ_{el} denotes the resistivity, and the reciprocal of the stiffness i.e., the compliance

$$\frac{1}{s} = \frac{l}{ES}, \quad (8.34b)$$

depend on the length l and cross-sectional area S in the same way. For force measurements, however, the compliance usually should be small and the resistance large. It is therefore advantageous to separate the resistance element from that determining the extension. Thereby, the resistance element can be made of a thin wire with a large effective length in the direction of the extension, obtained by folding the wire as a serpentine. This design is employed in the modern strain gauge, a typical example of which is shown in Fig. 8.13. For the nine back-and-forth folds shown in the figure, the effective length to be used in (8.34a) is $l = 19l_1$. The lengths l or l_1 appear only, however, in the absolute length changes but not in the strain

$$\frac{\Delta\xi}{l_1} = \frac{\Delta l}{l} = \varepsilon. \quad (8.34c)$$

The sensitivity of a strain gauge, defined as the relative change in resistance per unit change of strain, is made up of three contributions, as can be found from Eq. (8.34a)

$$k = \frac{1}{R} \frac{dR}{d\varepsilon} = \frac{1}{l} \frac{\partial l}{\partial \varepsilon} - \frac{1}{S} \frac{\partial S}{\partial \varepsilon} + \frac{1}{\rho_{el}} \frac{\partial \rho_{el}}{\partial \varepsilon}. \quad (8.35a)$$

The first term is equal to unity, as follows from the definition of strain. The cross-sectional contraction accounted for by the second term, amounts to 2μ . This means that the sensitivity reduces to

$$k = 1 + 2\mu + \frac{1}{\rho_{el}} \frac{\partial \rho_{el}}{\partial \varepsilon}, \quad (8.35b)$$

giving typical sensitivities between 1.6 and 5.

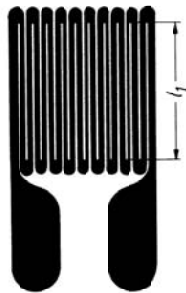


Fig. 8.13. Typical resistance strain gauge

The primary use of strain gauges is the direct sensing of strains of test objects and not in special force transducers. The additional force required to induce a strain in such a gauge itself is generally negligible. Similarly, only for measurements on very thin plates in bending, the slightly elevated location of the gauge from the plate surface of primary interest may require some consideration.

It is common practice to use a strain gauge as one branch of a balanced Wheatstone resistance bridge as depicted in Fig. 8.14 and to find the strain by measuring the bridge current. By appropriate use of several strain gauges in different branches of the Wheatstone bridge, also, various types of deformation can be separated. For example, strain gauges I and II that are glued to the top and bottom of a bar or plate, as shown in Fig. 8.14b, yield the extensional strain if they are connected in branches A and D of the bridge in Fig. 8.14a but indicate the bending strain if they are connected in neighbouring branches such as A and B.

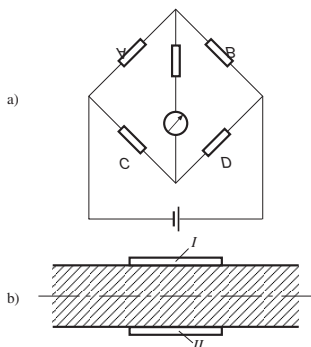


Fig. 8.14. Two resistance strain gauges a) in a bridge circuit and b) attached to a plate

The sensitivity is substantially increased by use semi-conductors. This is on behalf of larger temperature sensitivity than for resistors or common resistance strain gauges.

Sensors making use of inductance changes involve somewhat heavier elements, even if they consist of only two coils that move relative to each other. By using ferrous elements, greater inductance changes, of course, can be obtained but then also the non-linearities and losses resulting from the associated hysteresis phenomena.

Test objects of iron or steel may serve as mobile armatures, the motion of which change the resistance of a magnetic circuit as further discussed in Sect. 8.3.4.

A more reliable and easily implemented system makes use of a rod that is pressed lightly against the test object by a soft pre-compressed spring. Only the end of the rod need be magnetic. When the test object is at rest, this magnetic end should be approximately equally entered in the two coils that constitute the two neighbouring branches of an inductance bridge cf., Fig. 8.15. If the rod is displaced by an amount ξ that is not too large, the inductance of one branch is increased whereas the other is decreased and the current in the bridge is proportional to the displacement ξ or to the practically equally large differential displacement ξ_Δ for a sensor with a low natural frequency.

Since the reactance changes are observed, an alternating voltage must be supplied to the bridge. The frequency of this voltage is called the “carrier

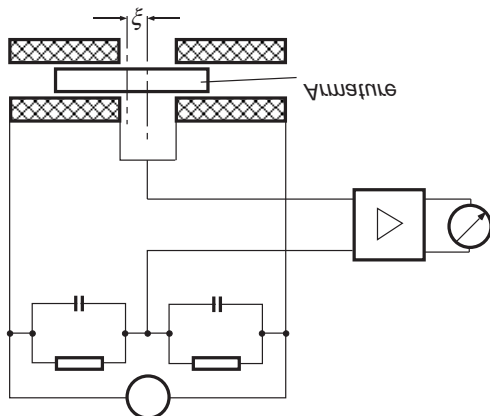


Fig. 8.15. Configuration and circuit of a variable inductance sensor

frequency". The displacement ξ thus is observed in terms of a change in the amplitude of an alternating current at the carrier frequency.

This carrier frequency approach has such great advantages that it is also used for resistance strain gauges. By use of appropriate frequency band filters, the interference or noise at other frequencies can be largely eliminated. In this process, however, the three components making up the "modulated" carrier current must be taken into account, as is seen from the identity

$$(A + a \cos \omega t) \cos \Omega t = A \cos \Omega t + \frac{a}{2} (\cos(\Omega - \omega)t + \cos(\Omega + \omega)t). \quad (8.36)$$

This means that the filters must be chosen such that the entire band $(\Omega - \omega)/2\pi$ to $(\Omega + \omega)/2\pi$ is passed. The carrier frequency, also, always must be kept considerably above the highest frequency to be measured in order to minimize distortion. With a carrier frequency of 4000 Hz, for example, events of frequencies of up to 1000 Hz can be reproduced without distortion.

Instead of using a variable inductance as an element in a circuit, connected to a constant frequency alternating voltage source, the inductance can be used as part of an electric oscillator circuit, the natural frequency of which depends on the inductance L and the capacitance C as

$$\omega_0 = 1/\sqrt{LC}. \quad (8.37)$$

A feedback amplifier may be employed to keep the circuit oscillating at its natural frequency. Because of the non-linearities mentioned above, such arrangements are used less with variable inductances than with variable conductances, as illustrated in Fig. 8.16.

A variable capacitance sensor in its simplest form consists of two metal surfaces of area S , parallel to each other, one of which may be part of the test object or simply a glued-on foil. For small displacements ξ , the changes in the capacitance can be considered approximately linear such that one can write

$$C = C_{eq} \frac{d}{d - \xi} \approx C_{eq} \left(1 + \frac{\xi}{d} \right), \quad (8.38)$$

where C_{eq} represents the equilibrium value of the capacitance. Variations of ξ thus leads to alterations of the capacitance and thence a frequency modulation, which can be further processed by means of a signal analyser.

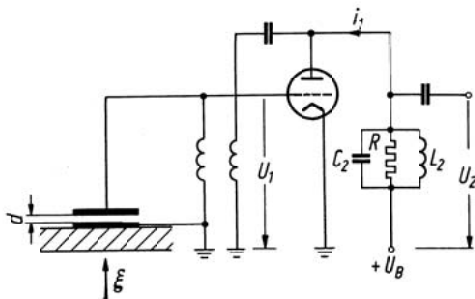


Fig. 8.16. Configuration and circuit of a variable capacitance sensor

This technique, which originally was developed for microphones, allows measurements of excursions as small as 10^{-8} m. The utility of the method, however, is restricted essentially to laboratory investigations, because the equilibrium separation d has a very important effect and must be accounted for by calculations or by electrical compensation. In addition, the capacitance of the sensor is usually so small that unavoidable capacity changes in cables can induce spurious modulations.

In fact, it is important to note that all the phenomena that can be harnessed for sensors, also, can contribute to extraneous signals. From this point of view, a carbon microphone is simply a random aggregate of knife switches.

8.2.2 Optical Sensors

In conjunction with the rather simplified arrangements in Figs. 8.1 and 8.2, it was pointed out that optical means allow measurements of vibration amplitudes using microscope, mirror or stroboscopic light. Also interferometric arrangements can be used, in particularly for calibration purposes. The reflected light beams from an immobile and a vibrating, reflecting surface, are brought to interference so that a fringe pattern results and the amplitude can be determined from the number of fringes and knowledge of the wavelength of the light.

With the laser and the fibre optics, a new avenue for measurements of structure-borne sound is opened. The so-called laser-doppler-vibrometer (LDV) establishes a robust equipment. It uses the fact that a moving reflector realizes a frequency shift due to the Doppler effect. With f_{light} being the frequency of the impinging light, f_{refl} that of the reflected light, v the vibra-

tion velocity of the reflector and c_{light} the phase velocity of the light, one may write

$$f_{refl} = f_{light} \left(1 \pm \frac{v}{c_{light}} \right). \quad (8.39)$$

Since v is of the order of 10^{-3} m/s or smaller and the phase velocity of the light is $3 \cdot 10^8$ m/s, the frequency deviation is extremely small. Modern opto-electronic devices, however, can discriminate such small differences and furnish an electrical signal, which similar to signals from electrodynamic transducers, can be amplified, filtered and stored [8.3].

Figure 8.17 shows the principal design of an LDV. The complete optics is enclosed in a manageable measurement head, which can be used as a non-contacting and interaction-free device in the vicinity of the vibrating object. It should be noted that, again, an immobile reference or a seismic mass is required since a velocity difference is registered between the measurement head and the test object.

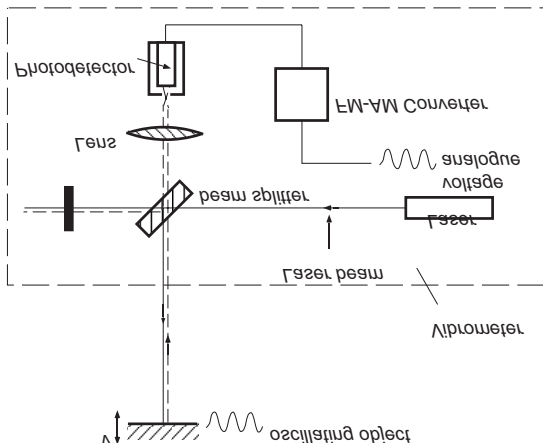


Fig. 8.17. Principle design of a laser-doppler-vibrometer

In Fig. 8.18, yet another principle is outlined for structure-borne sound measurements. In this case a vibrating surface deflects a narrow light beam and establishes a modulation of the light energy impinging on the second optical fibre.

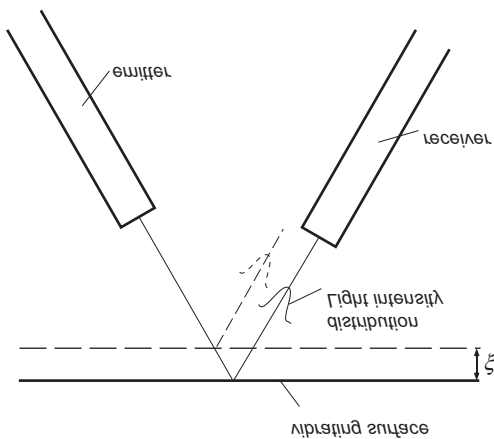


Fig. 8.18. Amplitude modulation of a narrow light beam from a reflecting vibrating surface

In conjunction with optical methods, also, the vibration holograms should be mentioned. Such holograms are either developed as time averaged or double-pulse holograms, which yields more or less easily interpretable pictures of the vibration field. Whereas all other measurement techniques furnish the vibration at a single measurement position, a vibration hologram 'in one go' offers the distribution of an area. Despite this obvious advantage, the snarl in post-processing the holograms has promoted the scanning technique, for instance, employing the laser-doppler-vibrometer, yielding a very good representation of the vibration process.

8.3 Excitation and Measurement of Structure-Borne Sound

For most measurements of structure-borne sound, reciprocal, electro-mechanical transducers are used in practice. They are based on the electrodynamic, piezo-electric, electro-static or magnetostrictive principles. Their performance is principally determined by the associated transducer constant. Important are additionally their inevitable inner mechanical and electrical impedances as well as the properties of connected elements [8.4-8.6].

8.3.1 Electro-Dynamic Transducers

The fundamental electro-technical principle, upon which, for example, the dynamo is based, states that a loss-free lead of length l_L , which moves with a velocity v_w , perpendicular to its length and to a magnetic field of strength B , establishes a transducer voltage

$$U_w = -Bl_L v_w . \quad (8.40a)$$

The velocity v_w is the velocity relative to the magnetic field cf., Fig. 8.19. The transducer constant Bl_L , in this case, has the units Vs/m = Ws/Am and a typical value is 10 Vs/m for structure-borne sound excitors and sensors. The sign is principally arbitrary but in this context it is chosen such that both the electric and the mechanical powers are positive when transmitted to the transducer.

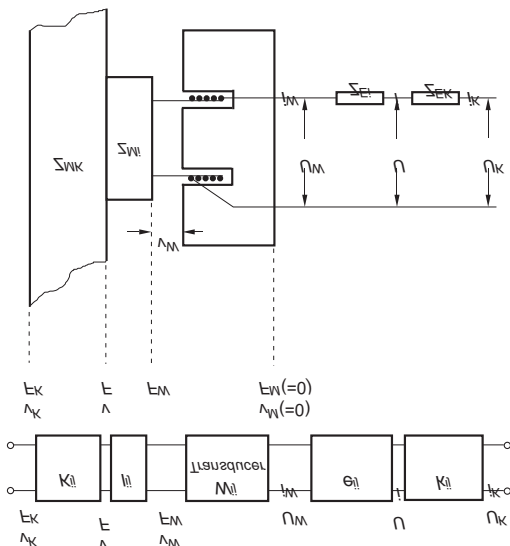


Fig. 8.19. Electrical and mechanical impedances for an electro dynamic transducer. a) Configuration outline and b) generalization as cascaded four-poles

Another fundamental electro-technical principle, underlying, for instance, the electro-motor, states that a current i_w that is passed through a lead of length l_L at rest, perpendicular to magnetic field of strength B , induces a transducer force

$$F_w = Bl_L i_w, \quad (8.40b)$$

acting perpendicular to B and i_w .

In phasor notation, Eqs. (8.40) can be rewritten in matrix form as the four-pole equations

$$\begin{Bmatrix} F_w \\ v_w \end{Bmatrix} = \begin{bmatrix} Bl_L & 0 \\ 0 & -1/Bl_L \end{bmatrix} \begin{Bmatrix} i_w \\ U_w \end{Bmatrix}. \quad (8.40c)$$

By means of this expression, however, the physical transducer is not described adequately since the loss-free and the motion-less lead clearly is an idealization. The description thus must be augmented by the effects of the mechanical and electrical impedances of the transducer.

For the electrical part, the situation is relatively simple because the transducer is connected in series to the inner electrical impedance consisting of a self-inductance L_i and a resistance R_i such that $Z_{Ei} = j\omega L_i + R_i$. According to Fig. 8.19 the relation

$$\begin{Bmatrix} i_w \\ U_w \end{Bmatrix} = \begin{bmatrix} 1 & 0 \\ -Z_{Ei} & 1 \end{bmatrix} \begin{Bmatrix} i \\ U \end{Bmatrix} \quad (8.41a)$$

exists between the transducer quantities i_w and U_w and the physically measurable voltage and current. This relation states that the current through the coil remains unaltered whereas the transducer voltage differs from the measurable by the voltage drop over the inner impedance. Usually, there is externally yet another impedance to consider, for example, that of the measurement equipment connected. Aligned with the arrangements outlined in Fig. 8.19 this means that

$$\begin{Bmatrix} i \\ U \end{Bmatrix} = \begin{bmatrix} 1 & 0 \\ -Z_{EK} & 1 \end{bmatrix} \begin{Bmatrix} i_K \\ U_K \end{Bmatrix}. \quad (8.41b)$$

For the mechanical part, the influence of the inner impedance is somewhat more involved. Therefore, the simple case of a rigidly fixed magnet ($v_M = 0$) is considered first and subsequently the more general case.

8.3.1.1 Impedances and Transfer Functions for Immobile Magnets

By excitation of light-weight structures, it is possible to presume that the magnet in Fig. 8.19 is so heavy or fixed to a rigid body such that the magnet velocity v_w equals zero. This is particularly true for loudspeakers, which are nothing but structure-borne sound excitors driving a light membrane and the fluid in front.

With the assumption that the different elements are rigidly connected i.e., the coil and membrane of impedance Z_{Mi} are connected to the measurement object of impedance Z_{MK} , the arrangement in Fig. 8.19 leads to

$$\underline{F}_K - \underline{F} = \underline{Z}_{MK} \underline{v}_K, \quad \underline{F} - \underline{F}_w = \underline{Z}_{Mi} \underline{v}_w, \quad \underline{v} = \underline{v}_K = \underline{v}_w. \quad (8.41c)$$

This can also be rewritten in matrix form as

$$\begin{Bmatrix} \underline{F}_K \\ \underline{v}_K \end{Bmatrix} = \begin{bmatrix} 1 & \underline{Z}_{MK} \\ 0 & 1 \end{bmatrix} \begin{Bmatrix} \underline{F} \\ \underline{v} \end{Bmatrix}, \quad \begin{Bmatrix} \underline{F} \\ \underline{v} \end{Bmatrix} = \begin{bmatrix} 1 & \underline{Z}_{Mi} \\ 0 & 1 \end{bmatrix} \begin{Bmatrix} \underline{F}_w \\ \underline{v}_w \end{Bmatrix}. \quad (8.41d)$$

Herein, Z_{Mi} is an inherent part of the transducers. It is given by the mass of the coil and membrane m_i and the lossy stiffness of the suspension s_i ,

$$Z_{Mi} = j\omega m_i + s_i / j\omega. \quad (8.41e)$$

Upon combining Eqs. (8.41a), (8.41b) and (8.41d), one obtains

$$\begin{Bmatrix} \underline{F}_K \\ \underline{v}_K \end{Bmatrix} = \frac{1}{Bl_L} \begin{bmatrix} [(Bl_L)^2 + Z_{MS} Z_{ES}] & -Z_{MS} \\ Z_{ES} & -1 \end{bmatrix} \begin{Bmatrix} \underline{i}_K \\ \underline{U}_K \end{Bmatrix}, \quad (8.41f)$$

where $Z_{MS} = Z_{Mi} + Z_{MK}$ and $Z_{ES} = Z_{Ei} + Z_{EK}$ are the sums of the inner and external mechanical and electrical impedances respectively.

Since the expressions above are written in a form of linked four-poles, which can be combined by means of matrix multiplication, the formulae are readily generalizable to

$$\begin{aligned} \begin{Bmatrix} \underline{F}_K \\ \underline{v}_K \end{Bmatrix} &= \begin{bmatrix} K_{11} & K_{12} \\ K_{21} & K_{22} \end{bmatrix} \begin{Bmatrix} \underline{F} \\ \underline{v} \end{Bmatrix} = \begin{bmatrix} K_{11} & K_{12} \\ K_{21} & K_{22} \end{bmatrix} \begin{bmatrix} I_{11} & I_{12} \\ I_{21} & I_{22} \end{bmatrix} \begin{Bmatrix} \underline{F}_w \\ \underline{v}_w \end{Bmatrix} \\ &= \begin{bmatrix} K_{11} & K_{12} \\ K_{21} & K_{22} \end{bmatrix} \begin{bmatrix} I_{11} & I_{12} \\ I_{21} & I_{22} \end{bmatrix} \begin{bmatrix} W_{11} & W_{12} \\ W_{21} & W_{22} \end{bmatrix} \begin{bmatrix} \varepsilon_{11} & \varepsilon_{12} \\ \varepsilon_{21} & \varepsilon_{22} \end{bmatrix} \begin{bmatrix} \kappa_{11} & \kappa_{12} \\ \kappa_{21} & \kappa_{22} \end{bmatrix} \begin{Bmatrix} \underline{i}_K \\ \underline{U}_K \end{Bmatrix}. \end{aligned} \quad (8.42)$$

Thereby, the input quantities of one transducer element connect to those at the output of the adjacent one. This cascading may involve mass-spring elements, wave guides and electrical circuits.

From (8.41f) and (8.42), all the impedances and transfer functions of interest can be computed. For an immobile magnet of an electro-dynamic structure-borne sound transducer, operated short-circuited, the impedance, for example, is obtained as

$$\left. \frac{\underline{F}_K}{\underline{v}_K} \right|_{\underline{U}_K=0} = Z_{MS} + \frac{(Bl_L)^2}{Z_{ES}}. \quad (8.43a)$$

The mechanical impedance thus consists of a pure mechanical part $Z_{MS} = Z_{Mi} + Z_{MK}$ and the electrical reaction, the latter of which becomes the

more pronounced, the bigger the transducer constant Bl_L and the smaller the electrical load Z_{ES} . For a typical constant of $Bl_L = 10 \text{ Vs/m}$ and short circuited operation such that $Z_{ES} \approx Z_{Ei} = 1\Omega$ due to an inner coil resistance, the electrical part of the measured total mechanical impedance would amount to 10 Ns/m . As a comparison, a 16 g mass at 100 Hz also presents an impedance of about 10 Ns/m . One may thus conclude that the electrical reaction predominantly is of significance for light-weight structures and low frequencies. It is possible, however, that the impedance at a resonance becomes that small for big and weakly damped structures that the electric part appears as a noticeable additional damping.

For the electrical impedance of a structure-borne sound exciter with no external forces acting i.e., $\underline{F}_K = 0$, the relation in (8.41f) yields

$$\left. \frac{\underline{i}_K}{\underline{U}_K} \right|_{\underline{F}_K=0} = \frac{Z_{MS}}{(Bl_L)^2 + Z_{MS}Z_{ES}}. \quad (8.43b)$$

This expression is composed of one pure electrical part and a mechanical reaction. Hence, it is, in principle, possible to infer the mechanical impedance from the voltage and current.

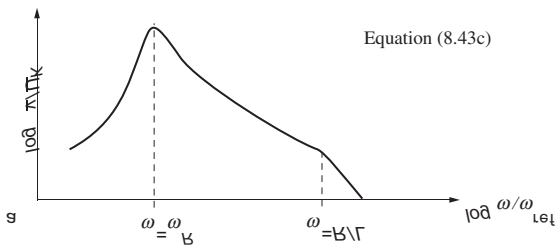
The transfer function during operation is also found from (8.41f), again, with no external forces present,

$$\left. \frac{\underline{v}_K}{\underline{U}_K} \right|_{\underline{F}_K=0} = \frac{-Bl_L}{(Bl_L)^2 + Z_{MS}Z_{ES}}. \quad (8.43c)$$

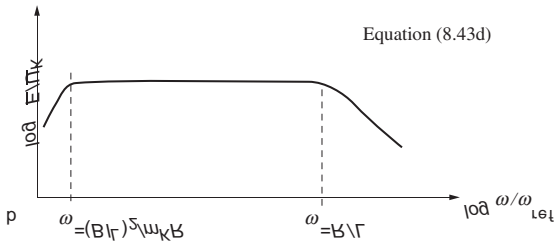
Furthermore, it follows from (8.41c) that $\underline{F} = -Z_{MK} \underline{v}_K$ and by substitution in (8.43c), the force exerted by the moving coil on a structure with the impedance Z_{MK} is found to be given by

$$\left. \frac{\underline{F}}{\underline{U}_K} \right|_{\underline{F}_K=0} = \frac{Bl_L Z_{MK}}{(Bl_L)^2 + Z_{MS}Z_{ES}}. \quad (8.43d)$$

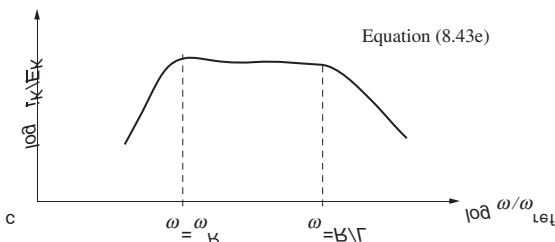
For loudspeakers and exciters, acting on very light-weight structures i.e., $Z_{MS} \approx Z_{Mi}$, the resulting velocity is of primary interest. It is given by (8.43c). With a softly suspended moving coil of impedance $Z_{MS} = j\omega m (1 - \omega_R^2/\omega^2)$, a frequency characteristic is obtained as outlined in Fig. 8.20, assuming an electric impedance as given by (8.43b). In the graphs, ω_R is the resonance frequency of the mass-spring system made up by the moving coil and the stiffness of the suspension.



Equation (8.43c)



Equation (8.43d)



Equation (8.43e)

Fig. 8.20. Transfer function of electro-dynamic transducers. a) Exciter ($F_K = 0$) with negligible mechanical load, b) exciter ($F_K = 0$) with high mechanical load and c) sensor ($U_K = 0$) with negligible mechanical load. For high mechanical load, the transfer function is uniform cf., Eq. (8.43f)

For structure-borne sound exciters acting on heavy structures, $Z_{MK} = j\omega m_K \gg Z_{Mi}$ and with $Z_{ES} = R + j\omega L$, Eq. (8.43d) renders the middle graph in Fig. 8.20.

Operated as a sensor, the describing transfer function can also be developed from (8.41f). In this situation, however, $U_K = 0$ and

$$\left. \frac{i_K}{F_K} \right|_{U_K=0} = \frac{Bl_L}{(Bl_L)^2 + Z_{MS}Z_{ES}}. \quad (8.43e)$$

With the exception of the sign, the right-hand side is identical to that of (8.43c) owing to reciprocity. The design criteria, however, lead to different

transition frequencies. Whereas comparatively large masses can be tolerated for excitors such that ω_R , where $Z_{MK} \rightarrow 0$, can be tuned to low frequencies, this is not possible for sensors designed to be very light-weight. In the latter case, the resonance frequency is placed at the centre of the frequency range of interest and the mechanical and electrical damping is made that high that the frequency characteristics in the bottom graph in Fig. 8.20 result. The most important example is the condenser microphone where the exciting force is given by the pressure. Such microphones can be made extremely small owing to the limited load Z_{MS} from the ambient air.

For structure-borne sound sensors, aimed at measuring the velocity of heavy structures, (8.41f) gives

$$\left. \frac{i_K}{v_K} \right|_{U_K=0} = \frac{Bl_L}{Z_{ES}} , \quad \left. \frac{U}{v_K} \right|_{U_K=0} = \frac{Bl_L Z_{EK}}{Z_{ES}}. \quad (8.43f)$$

Up to the decay above $\omega = R/L$, a uniform signature can be established.

8.3.1.2 Energy Balance

In this section it is demonstrated that the equality of the transducer constants in (8.40a) and (8.40b) is a consequence of energy conservation. In this pursuit, quite generally one may write

$$F_w = \alpha i_w, \quad U_w = \beta v_w. \quad (8.44a)$$

In combination with (8.41a) and (8.41c), the physically measurable quantities are obtained as

$$\begin{aligned} F &= F_w + Z_{Mi} v = \alpha i + Z_{Mi} v, \\ U &= U_w - Z_{Ei} i = \beta v - Z_{Ei} i. \end{aligned} \quad (8.44b)$$

The mechanical power transmitted is obtained as

$$W_M = \frac{1}{2} \operatorname{Re} [F v^*] = \frac{1}{2} \operatorname{Re} [\alpha i v^* + Z_{Mi} |v|^2], \quad (8.44c)$$

and, similarly, the electrical power is

$$W_E = \frac{1}{2} \operatorname{Re} [U i^*] = \frac{1}{2} \operatorname{Re} [\beta^* i v^* + Z_{Ei} |i|^2]. \quad (8.44d)$$

In these expressions, $\operatorname{Re}[Z_{Mi}]|v|^2/2$ and $\operatorname{Re}[-Z_{Ei}]|i|^2/2$ are the dissipated powers by inner mechanical and electrical impedances. The two remaining terms must sum up to zero given the sign convention since ideal transducers neither produce nor dissipate power. Accordingly, one obtains

$$0 = \frac{1}{2} \operatorname{Re} [\alpha i \underline{v}^*] + \frac{1}{2} \operatorname{Re} [\beta^* i \underline{v}^*], \\ -\alpha = \beta^*, \quad (8.44e)$$

respectively. If therefore, $\alpha = Bl_L$ it follows that $\beta = -Bl_L$ in accordance with (8.40a).

8.3.1.3 Impedances and Transfer Functions for Mobile Magnets

Upon trying to excite a concrete plate or a heavy machine at low frequencies by means of a handheld, several kg heavy exciter, it is realized that the assumptions made in the previous section of $v_M = 0$ or equivalently $v_w = v$ cf., Fig. 8.18, do not reflect reality. It is obvious that the important effect in exciting low mobility structures at low frequencies, must be taken into account. Whilst all other elements of the transducer remain, only new coefficients I_{ij} in the chain of matrices need be established, linking F_w , v_w and F, v .

For this purpose, Fig. 8.21 presents the essential parts of the transducer together with the forces and velocities. Additionally is introduced a common spring of stiffness s , representing the moving coil suspension s_1 and that suspending the magnet s_2 . This means that

$$\underline{F} - \underline{F}_w = Z_{M1} \underline{v} + \frac{s}{j\omega} (\underline{v} - \underline{v}_M), \\ \underline{F}_w - \underline{F}_M = Z_{MM} \underline{v}_M - \frac{s}{j\omega} (\underline{v} - \underline{v}_M), \\ \underline{v}_w = \underline{v} - \underline{v}_M. \quad (8.45)$$

Herein, \underline{F}_w again is the transducer force and \underline{v}_w the velocity difference between that of the moving coil and the magnet. Z_{MM} is the impedance of the magnet. In the following it is assumed that $F_M = 0$, which does not imply any restrictions since if the magnet is supported by another structure merely the value of Z_{MM} must be raised and additional resonances considered.

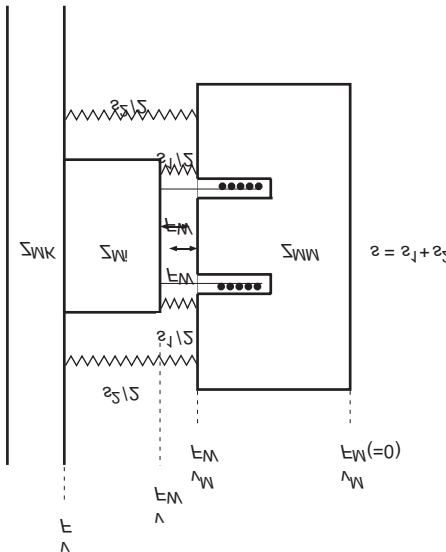


Fig. 8.21. Velocities and forces associated with an electro-dynamic transducer with a mobile magnet

By eliminating v_M in (8.45) and rewriting the equations such that F and v only appears on the left-hand side and F_w and v_w on the right, the desirable four-pole is established,

$$\begin{Bmatrix} \underline{F} \\ \underline{v} \end{Bmatrix} = \begin{bmatrix} \frac{Z_{Mi} + Z_{MM}}{Z_{MM}} & \frac{s}{j\omega} \frac{Z_{Mi} + Z_{MM}}{Z_{MM}} + Z_{Mi} \\ \frac{1}{Z_{MM}} & 1 + \frac{s}{j\omega Z_{MM}} \end{bmatrix} \begin{Bmatrix} \underline{F}_w \\ \underline{v}_w \end{Bmatrix}. \quad (8.45a)$$

This expression must be substituted in the chain of matrices (8.42) for I_{ij} . The multiplication by the other already known matrices principally yields

$$\begin{Bmatrix} \underline{F}_K \\ \underline{v}_K \end{Bmatrix} = \begin{bmatrix} A_{11} & A_{12} \\ A_{21} & A_{22} \end{bmatrix} \begin{Bmatrix} \underline{i}_K \\ \underline{U}_K \end{Bmatrix}. \quad (8.45b)$$

Of the rather lengthy expressions for the elements A_{ij} , only

$$A_{11} = \frac{1}{Bl_L} \left[(Bl_L)^2 \frac{Z_{MS} + Z_{MM}}{Z_{MM}} + Z_{ES}Z_{MS} \left(1 + \frac{s}{j\omega} \frac{Z_{MS} + Z_{MM}}{Z_{MS}Z_{MM}} \right) \right]$$

and

$$A_{21} = \frac{Z_{ES}}{Bl_L} \left(1 + \frac{s}{j\omega} \frac{1}{Z_{MM}} \right) + \frac{Bl_L}{Z_{MM}}$$

are required for the transfer function. As before, $Z_{MS} = Z_{Mi} + Z_{MK}$ and $Z_{ES} = Z_{Ei} + Z_{EK}$ with the notation given in Fig. 8.19. Upon assuming that Z_{MS} and Z_{MM} can be approximated as mass impedances, one obtains

$$A_{11} = \frac{1}{Bl_L} \left[(Bl_L)^2 \frac{m_{MS} + m_{MM}}{m_{MM}} + Z_{ES} j\omega m_{MS} \left(1 - \frac{\omega_{MS}^2}{\omega^2} \right) \right]. \quad (8.45c)$$

The resonance frequency ω_{MS} is that of the mass-spring-mass system constituted by the mass m_{MS} of the structure and the moving coil, the stiffness s of the spring and the mass m_{MM} of the magnet.

The transfer functions when the transducer is operated as exciter, follow from (8.45b) as

$$\begin{aligned} \left. \frac{\underline{v}_K}{\underline{U}_K} \right|_{\underline{F}_K=0} &= \frac{-A_{12}A_{21}}{A_{11}} + A_{22} = \frac{A_{11}A_{22} - A_{12}A_{21}}{A_{11}} = -\frac{1}{A_{11}}, \\ \left. \frac{\underline{F}}{\underline{U}_K} \right|_{\underline{F}_K=0} &= \frac{Z_{MK}}{A_{11}} \end{aligned}, \quad (8.45e)$$

and operated as sensor

$$\begin{aligned} \left. \frac{\underline{i}_K}{\underline{F}_K} \right|_{\underline{U}_K=0} &= \frac{1}{A_{11}} \\ \left. \frac{\underline{i}_K}{\underline{v}_K} \right|_{\underline{U}_K=0} &= \frac{1}{A_{21}}, \quad \left. \frac{\underline{U}}{\underline{v}_K} \right|_{\underline{U}_K=0} = \frac{Z_{EK}}{A_{21}}. \end{aligned} \quad (8.45f)$$

In the first of these expressions, use is made of the fact that the determinant of the transducer matrix in (8.40c) equals -1 . The other matrices in (8.42) have all unity determinants. This means that the determinant of the chain of matrices becomes

$$A_{11}A_{22} - A_{12}A_{21} = (+1) \cdot (+1) \cdot (-1) \cdot (+1) \cdot (+1) = -1.$$

From the transfer functions in (8.45e,f), the following conclusions can be drawn:

- When the spring is very stiff, ω_{MS} falls relatively high. In the range $\omega < \omega_{MS}$ almost nothing moves and almost no force is exerted on the test object.

- When ω_{MS} is tuned sufficiently low in frequency, which is the usual design, the transfer functions turns into the corresponding expressions in (8.43d) to (8.43f) for $Z_{MM} > Z_{MS}$.
- For structure-borne sound excitors, the motion of the magnet leads to an elevation of the lower frequency limit at $|Z_{MS}| = (Bl_L)^2 / |Z_{ES}|$ in Fig. 8.20b by a factor of $|1 + Z_{MS} / Z_{MM}|$. This means that the force diminishes towards low frequencies, which is due to the counter voltage increase induced by the magnet motion. Differently described, the effective electrical resistance increases with the enlarged motion of the magnet through the reaction in (8.43a). In the upper range, the transducer has the frequency characteristics depicted in the figure.

For structure-borne sound sensors according to Fig. 8.11b, the same applies as for excitors. By means of soft springs is pursued, a mass-spring-mass resonance as low as possible. A resonance frequency of 5 Hz or below is fully realistic.

From the expressions and the associated discussion it follows that electro-dynamic transducers should be designed with an as large transducer constant and an as low mass-spring-mass resonance as possible. These guide lines become slightly contradictory in practice. A low mass-spring-mass resonance requires a very soft spring and a large Bl_L product requires a very narrow air gap in the magnet, which can be achieved only by means of a stiff coil suspension in order to prevent the coil from touching the magnet. This problem is usually solved through a multi-stage suspension, which is soft in the direction of motion but avoids sidewise and rocking motion of the moving coil.

For modern electro-dynamic excitors, one may typically assume a maximum long-term force of 5 to 10 N per kg exciter mass. A larger force could be achieved, in principle, through a higher current but this would result in too high a heat release without external cooling.

In many applications it is interesting to know the relation between the transducer force F_w and magnet velocity v_M . It is presumed thereby that the transducer is operated as a sensor such that Eqs. (8.45) takes the form

$$\begin{aligned} Z_{MK} \underline{v} - F_w &= Z_{Mi} \underline{v} + \frac{s}{j\omega} (\underline{v} - \underline{v}_M) \\ F_w - 0 &= Z_{MM} \underline{v}_M - \frac{s}{j\omega} (\underline{v} - \underline{v}_M). \end{aligned} \tag{8.46}$$

By eliminating \underline{v} , the relation is obtained

$$\underline{v}_M = \underline{F}_w \frac{Z_{MS}}{Z_{MS}Z_{MM} + \frac{s}{j\omega}(Z_{MS} + Z_{MM})} = \frac{\underline{F}_w}{Z_{MM}} \frac{1}{1 + \frac{s}{j\omega} \frac{Z_{MS} + Z_{MM}}{Z_{MS}Z_{MM}}}. \quad (8.46a)$$

The second denominator can also be brought in the form $1 - \omega_{MS}^2/\omega^2$. Equation (8.46a) thus states that above the mass-spring-mass resonance, the transducer force \underline{F}_w can simply be determined from the easily measured magnet velocity, multiplied by Z_{MM} cf., Sect. 4.2.

In the present analysis is left aside the mechanical reaction onto the test object by the transducer. This problem was considered in Sect. 8.2.4, particularly in Eq. (8.33). Merely the remark should be made that the transducer impedance required in this context can be obtained from the chain of matrices as $Z_{acc} = \underline{F}/\underline{v}$, which consists of one mechanical and one electrical part as exemplified in Eq. (8.43a). As in many other situations, the analysis demonstrates that splitting a complicated problem in “independent parts”, as here in mechanical and electrical parts, certainly conforms to human perception and often performs successfully. At the end of the day, however, the “parts” are coupled and the behaviour and performance always must be assessed for the integrated system.

8.3.2 Piezo-Electric Transducers

Thanks to their manageability, almost exclusively piezo-electric sensors are used for structure-borne sound measurements. The designs of the most important types are outlined in Fig. 8.22. One is here concerned with a transducer responding to acceleration, which up to its resonance frequency has an almost flat response and can be manufactured robust and very small, down to a tenth of a gram. As rough guides can be used a sensitivity of 100 to 1000 m_{acc} [Vs²/m] and a resonance frequency of $100/m_{acc}$ to $600/m_{acc}$ [Hz] where m_{acc} is the total mass of the transducer.

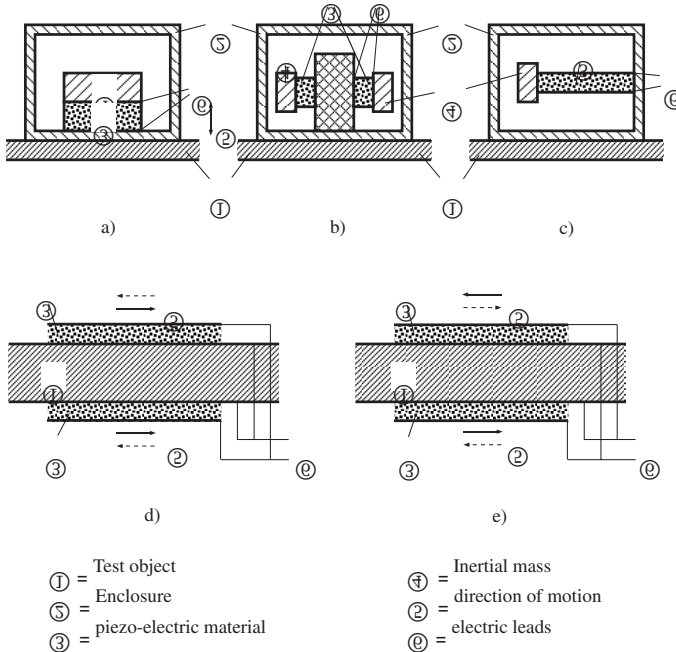


Fig. 8.22. Examples of piezo-electric transducers. a) compressional, b) shear and c) flexural design, d) longitudinal and e) flexural PVDF transducers

The piezo-electric transducer is suitable as exciter only when small displacements but large forces are required. Hence, the transducer must face large impedances on both sides and large voltages must be employed.

More recently, thin piezo-film (PVDF) has become commercially available, which can be glued to the test object and used both as sensor and exciter. As illustrated in Fig. 8.22, longitudinal and flexural waves can be excited with a good bonding. The advantage is that no large masses or stiff suspensions are required as support for the exciter [8.7]. Such piezo-film is manufactured in different thicknesses and thereby, almost non-loading transducers can be achieved. The reproducibility, however, can still be significantly improved.

To understand the piezo-electric effect, one can imagine different positive and negative ions, which are displaced in the material such that a net charge is realized as sketched in Fig. 8.23. In an undeformed state, the ions are in electrical equilibrium so that no charge appears at the externally attached electrodes. This equilibrium is disturbed if the lattice is compressed or stretched corresponding to compressive or tensile strains as in Fig.

8.23b and c respectively. Electric charges then collect at the electrodes, without the requirement of an external source of charges. Due to the Poisson contraction, also a displacement η along the crystal (y direction), perpendicular to the crystal axis (x direction) can produce such a change in charge. One may therefore assume [8.8] that

$$\underline{Q}_w = -K_{xx}\xi, \quad Q_w = -K_{xy}\eta, \quad (8.47)$$

where Q_w is the transducer charge established. ξ and η are the compression and cross-sectional contraction respectively with the associated transducer constants K_{xx} and K_{xy} , dependent on the material, patch size, patch form and alignment with the crystal axis.

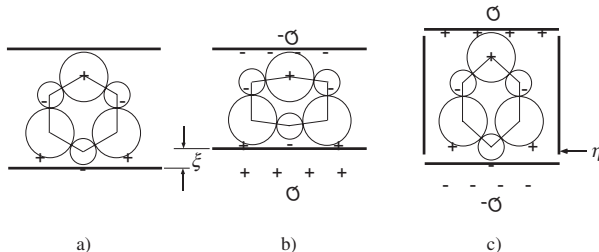


Fig. 8.23. Behaviour of piezo-electric materials [8.4]. a) undeformed state, b) deformation in the direction of (axial) and c) perpendicular to the current (lateral)

In the following only one direction of motion will be considered and therefore a single transducer constant K is sufficient. For the analysis must be considered, moreover, that the temporal change in charge is proportional to the current $i = dQ/dt$ and the temporal change in displacement is proportional to the velocity $v = d\xi/dt$. Upon introducing the phasor notation, the first fundamental relation

$$\underline{i}_w = -K\underline{v}_w \quad (8.47a)$$

is obtained for piezo-electric transducers. The reciprocal piezo-electric effect implies that an applied voltage gives rise to a proportional expansion of the material, leading to a mechanical transducer force

$$\underline{F}_w = K\underline{U}_w. \quad (8.47b)$$

The fact that the same constant K appears in both (8.47a) and (8.47b) is again a consequence of energy conservation. The proof proceeds exactly as for electro-dynamic transducers in (8.44c) to (8.44e).

By combining the last two equations, the four-pole description is obtained as

$$\begin{Bmatrix} \underline{F}_w \\ \underline{v}_w \end{Bmatrix} = \begin{bmatrix} 0 & K \\ -1/K & 0 \end{bmatrix} \begin{Bmatrix} \underline{i}_w \\ \underline{U}_w \end{Bmatrix} \quad (8.48)$$

Since the velocity is proportional to current and force to voltage for piezoelectric transducers whereas the situation is the opposite for electrodynamic ones, the distinction is made between N -transducers in the former case and M -transducers in the latter.

Another difference between the two types of transducers is the role of the inner impedance. In Fig. 8.19, this impedance is in series with the transducer, rendering an inevitable voltage drop. For the piezo-electric transducers, in contrast, the capacitance of the transducer is parallel to the current source i_w and, thus, yields a drop in current. Therefore, the transducer circuit is that shown in Fig. 8.24. The associated electrical relations can be compiled as

$$\begin{Bmatrix} \underline{i}_w \\ \underline{U}_w \end{Bmatrix} = \begin{bmatrix} 1 & -1/Z_{Ei} \\ 0 & 1 \end{bmatrix} \begin{Bmatrix} \underline{i} \\ \underline{U} \end{Bmatrix}. \quad (8.49)$$

Herein, Z_{Ei} essentially represents the relatively large impedance of the capacitance realized by the transducer

$$Z_{Ei} = 1/j\omega C. \quad (8.49a)$$

Thereby, the matrices in the four-pole chain in Fig. 8.24 are known since the mechanical and electrical loads, again can be taken from (8.41d) and (8.43a) and (8.41b) respectively. By carrying out the matrix multiplication, the mechanical part is found to be described by

$$\begin{Bmatrix} \underline{F}_K \\ \underline{v}_K \end{Bmatrix} = \begin{bmatrix} \frac{Z_{MS} + Z_{MM}}{Z_{MM}} & \frac{s}{j\omega} \frac{Z_{MS} + Z_{MM}}{Z_{MM}} + Z_{MS} \\ 1/Z_{MM} & 1 + \frac{s}{j\omega Z_{MM}} \end{bmatrix} \begin{Bmatrix} \underline{F}_w \\ \underline{v}_w \end{Bmatrix}, \quad (8.49b)$$

and the electrical part by

$$\begin{Bmatrix} \underline{F}_w \\ \underline{v}_w \end{Bmatrix} = \begin{bmatrix} -KZ_{EK} & K \\ -\frac{1}{K} \left(1 + \frac{Z_{EK}}{Z_{Ei}} \right) & \frac{1}{KZ_{Ei}} \end{bmatrix} \begin{Bmatrix} \underline{i}_K \\ \underline{U}_K \end{Bmatrix}. \quad (8.49c)$$

In the mechanical part, $Z_{MS} = Z_{Mi} + Z_{MK}$ is the sum of the mechanical sensor impedance, essentially given by the mass of the housing, and the im-

pedance of the test object. In contrast to the electro-dynamic transducer, Z_{MM} here represents the impedance of the seismic mass.

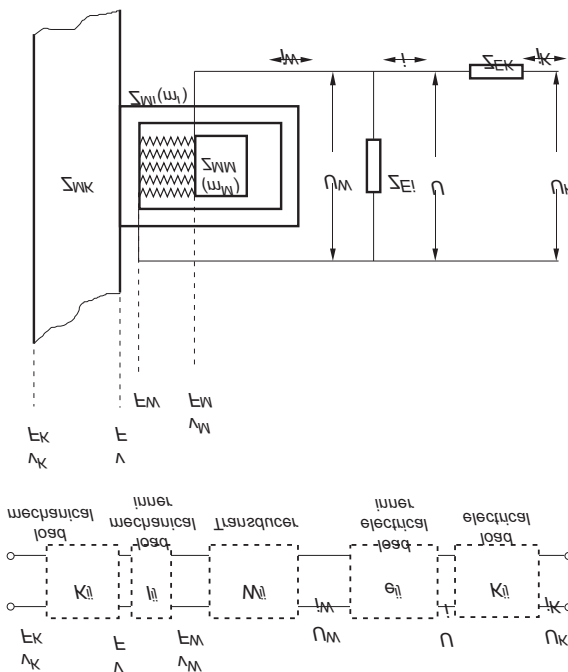


Fig. 8.24. Electrical and mechanical impedances for a piezo-electric transducer. a) Configuration outline and b) generalization as cascaded four-poles

Upon comparing Figs. 8.19 and 8.24, the following correspondences can be made, cf., Sect. 8.3.6.1:

Electro-dynamic transducer	Piezo-electric transducer
Voltage source	Current source
Series connected inner impedance	Parallel connected inner impedance
Magnet impedance Z_{MM}	Seismic mass impedance Z_{MM}
$Z_{MM} \approx j\omega m_{MM}$	
Soft suspension s	Stiff piezo crystal s
Moving coil impedance Z_{Mi}	Transducer housing impedance Z_{Mi}
$Z_{Mi} \approx j\omega m_{Mi}$	

$$Z_{MM} \approx j\omega m_{MM} \quad (8.49d)$$

$$\begin{aligned} &\text{Soft suspension } s \\ &\text{Moving coil impedance } Z_{Mi} \end{aligned} \quad \begin{aligned} &\text{Stiff piezo crystal } s \\ &\text{Transducer housing impedance } Z_{Mi} \end{aligned}$$

$$Z_{Mi} \approx j\omega m_{Mi} \quad (8.49e)$$

A multiplication of (8.49b) and (8.49c) yields the complete matrix, again, in the form of (8.45b). Also in this case, the individual determinants equal ± 1 . In analogy with (8.45f), the sensor sensitivity is obtained as

$$\frac{\underline{U}}{\underline{v}_K} \Big|_{\underline{U}_K=0} = \frac{Z_{EK}}{A_{21}} = \frac{-K}{\left(\frac{1}{Z_{EK}} + \frac{1}{Z_{Ei}} \right) \left(1 + \frac{s}{j\omega Z_{MM}} \right) + \frac{K^2}{Z_{MM}}}. \quad (8.50a)$$

For the subsequent discussion it is suitable to let $Z_{MM} = j\omega m_{MM}$, $Z_{Ei} = 1/j\omega C$, $Z_{EK} = R$, which correspond to the usual experience with piezo-electric transducers and to convert from velocity to acceleration. Accordingly, (8.50a) becomes

$$\frac{\underline{U}}{\underline{a}_K} \Big|_{\underline{U}_K=0} = \frac{m_{MM} K}{sC} \frac{-1}{\left(1 + \frac{1}{j\omega CR} \right) \left(1 - \frac{\omega^2 m_{MM}}{s} \right) + \frac{K^2}{sC}}. \quad (8.50b)$$

The second term in the denominator is very small and plays only a role at the resonance frequency $\omega^2 = s/m_{MM}$. In Fig. 8.25a are shown the frequency characteristics of Eq. (8.50b). Since R can be made extremely high with modern charge amplifiers and also the ratio s/m will be high for small accelerometers, the frequency response is essentially constant in a wide frequency range.

Piezo-electric materials are also frequently employed for measurements of dynamic forces. A design of the transducer is shown schematically in Fig. 8.26. The transfer function can be developed from (8.49a) and (8.49b) to be given by

$$\frac{\underline{U}}{\underline{F}_K} \Big|_{\underline{U}_K=0} = \frac{-1}{K} \frac{1}{\frac{Z_{MM} + Z_{MS}}{Z_{MM}} + \frac{1}{K^2} \left(\frac{1}{Z_{EK}} + \frac{1}{Z_{Ei}} \right) \left(Z_{MS} + \frac{s}{j\omega} \frac{Z_{MM} + Z_{MS}}{Z_{MM}} \right)} \approx \frac{-1}{K}. \quad (8.50c)$$

The rather simple approximation in the last part of (8.50c) is admissible for the following conditions:

- For force transducers, one is concerned with making the mechanical element between the force to be registered and the piezo-electric element as small but stiff as possible. Therefore, $Z_{MS} = Z_{MK} + Z_{Mi} \ll Z_{MM}$, where Z_{MM} is the impedance of the excited structure.
- The transducer constant K as well as the electrical impedances Z_{Ei} and Z_{EK} are numerically very large.

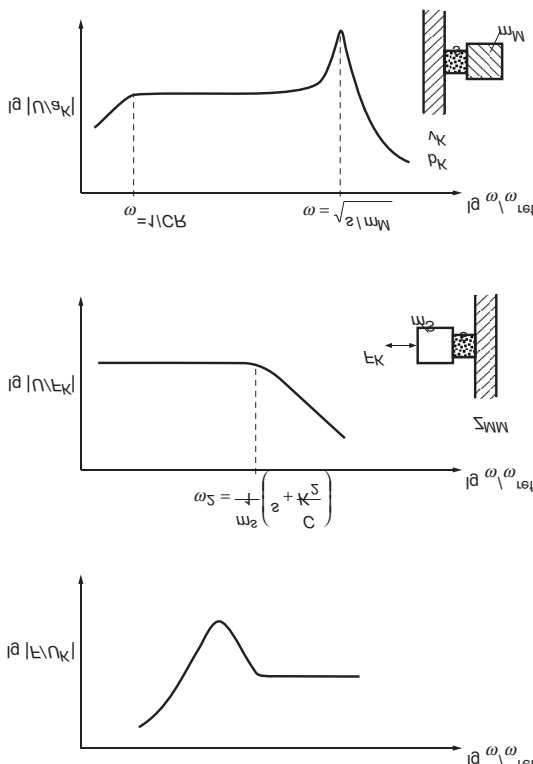


Fig. 8.25. Frequency response of piezo-electric transducers. a) accelerometer as in Fig. 8.23, b) force transducer as in Fig. 8.26 and c) piezo-electric exciter

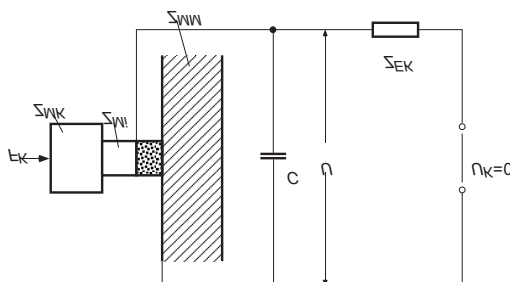


Fig. 8.26. Principle design of piezo-electric force transducer

As pointed out, the piezo-electric materials can also be used for structure-borne sound exciters. In such a case the transfer function is determined from (8.49b) and (8.49c) as

$$\left. \frac{F}{U_K} \right|_{F_K=0} = \frac{Z_{MK}}{Z_{MS}} \frac{-K}{\left(1 + \frac{Z_{EK}}{Z_{Ei}}\right) \left(1 + \frac{s}{j\omega Z_T}\right) + \frac{K^2 Z_{EK}}{Z_T}}, \quad (8.50d)$$

where $Z_T = (Z_{MK} + Z_{Mi} + Z_{MM})/Z_{MM}$ ($Z_{Mi} + Z_{MK} \approx Z_{MK}$) and $Z_{MS} = Z_{Mi} + Z_{MK} \approx Z_{MK}$. By substitution of typical data, one can readily convince oneself that piezo-electric excitors do not offer large forces at low frequencies cf., Fig. 8.25c. For frequencies above the mass-spring-mass resonance, where the piezo-electric material acts as a spring, Eq. (8.50d) reduces to $-K$ in a wide frequency range.

The choice of suitable piezo-electric materials as well as electrical and mechanical impedances is a crucial aspect of the transducer design. Additionally, a series of other considerations must be made. In this context should be mentioned, the sensitivity to disturbing electrical and magnetic fields, temperature stability (pyro-electric effects), minimal deformation of the transducer housing etc. as well as directional sensitivity.

8.3.3 Electro-Static Transducers

Electrostatic or dielectric transducers most often consist of two plate-like electrodes across which a dc-voltage is supplied. One of the electrodes is very thin and is fixed (glued) to the test object. In accordance with applications in practice, only the situation with an immobile backing electrode as depicted in Fig. 8.27 will be considered. A situation with a mobile backing electrode can be treated as in Sect. 8.3.1.3.

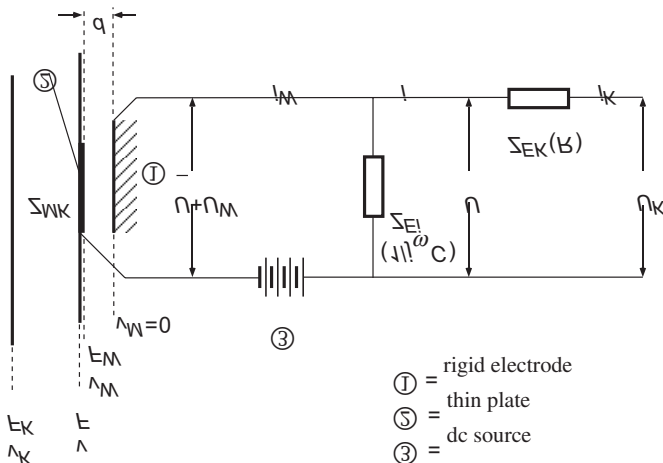


Fig. 8.27. Principle configuration of an electro-static transducer

The condenser microphone for airborne sound is also an electrostatic transducer. It consists of a thin, firmly prestressed membrane constituting one of the electrodes and the rigid housing forming the other. The membrane is forced to vibrations by incident sound whereby its amplitude is converted to an electrical signal by the transducer [8.9].

The electro-mechanical relation underlying this transducer is Coulomb's law of electro-static attraction. Applied on two plates at a distance d with the equilibrium capacitance \bar{C} , the attraction force is given by

$$F = \frac{QU}{2d} = \frac{\bar{C}\bar{U}^2}{2d} = \frac{\bar{C}}{2d}(\bar{U} + \tilde{U})^2 \approx \frac{\bar{C}}{2d}\bar{U}^2 + \frac{\bar{C}}{d}\bar{U}\tilde{U}. \quad (8.51a)$$

Herein, Q is the charge of the condenser, \bar{U} the dc voltage supplied and \tilde{U} the ac voltage.

In the acoustics context, the approximation in (8.51a) corresponding to a linearization is legitimate since the dc voltage supplied usually is of the order of 100 V or more whilst the induced ac voltage is less than a hundredth thereof. The linearization is also valid for the so-called electret transducers, often employed in microphones, for which no external dc voltage is supplied but the transducer material furnishes an internal polarization voltage.

For the exciter problem, only the alternating voltage is of interest and in phasor notation, the transducer force can be written as

$$\underline{F}_w = \frac{\bar{C}\bar{U}}{d}\underline{U}_w. \quad (8.51b)$$

This force is exerted on the test object for a constant capacitance \bar{C} . In the opposite situation with the transducer as sensor, where the membrane is brought to vibrate with the velocity \underline{v}_w , the transducer current amounts to

$$\underline{i}_w = -\frac{\bar{C}\bar{U}}{d}\underline{v}_w. \quad (8.51c)$$

In this development, again, the equality of magnitudes of transducer constants, proven in (8.44a) to (8.44e), is used. In the four-pole representation, the equation for ideal electro-static transducers reads

$$\begin{Bmatrix} \underline{F}_w \\ \underline{v}_w \end{Bmatrix} = \begin{bmatrix} 0 & \bar{C}\bar{U}/d \\ -d/\bar{C}\bar{U} & 0 \end{bmatrix} \begin{Bmatrix} \underline{i}_w \\ \underline{U}_w \end{Bmatrix}. \quad (8.51d)$$

Disregarding the symbols, (8.51d) is identical to the representation for piezo-electric transducers. The close relationship between the two types of transducers is also valid for the influence of the inner electrical impedance.

Also for electro-static transducers, one part of the resulting current passes the inner impedance Z_{Ei} connected in parallel as shown in Fig. 8.27. The inner impedance is essentially capacitive such that Eqs. (8.49) and (8.49d) can be adopted directly.

Regarding the inner mechanical impedance there is a small difference, however. In contrast to electro-dynamic and piezo-electric transducers, a polarization voltage is supplied resulting in an attraction force according to (8.51a). During operation, this force varies, a fact that also can be expressed in terms of an additional, electrically induced stiffness

$$\begin{aligned} s_E &= \frac{dF}{d\xi} = \frac{1}{2d} \frac{d\cancel{Q}U}{d\xi} = \frac{\overline{Q}}{2d} \frac{dU}{d\xi} + \frac{\overline{U}}{2d} \frac{d\cancel{Q}}{d\xi} = \frac{\overline{Q}}{2d} \frac{d}{CU} \frac{dF}{d\xi} + \frac{\overline{U}^2}{2d} \frac{dC}{d\xi} \\ &= \frac{1}{2} \frac{dF}{d\xi} + \frac{\overline{U}^2 \overline{C}}{2d} \frac{d(1-\xi/d)}{d\xi} = \frac{1}{2} \frac{dF}{d\xi} - \frac{\overline{U}^2 \overline{C}}{2d^2} \Leftrightarrow s_E = -\frac{\overline{U}^2 \overline{C}}{d^2} = -\left(\frac{\overline{U}\overline{C}}{d}\right)^2 \frac{1}{\overline{C}} \end{aligned} \quad (8.51e)$$

as developed from (8.51a). Herein, ξ is the change in electrode distance and the variable capacitance is approximated by

$$C = \frac{\overline{C}}{1+\xi/d} \approx \overline{C}(1-\xi/d). \quad (8.51f)$$

As can be expected, s_E is negative since compression implies an enlarged attraction, in contrast to an ordinary mechanical spring. Accordingly, the additional mechanical impedance, resulting in this way, becomes

$$Z_{ME} = \frac{s_E}{j\omega} = -\frac{1}{j\omega \overline{C}} \left(\frac{\overline{U}\overline{C}}{d} \right)^2. \quad (8.51g)$$

In this expression, the transducer constant squared appears. This is typical for the mechanical effect of an electrical element as observed in (8.43a).

For the remaining analysis, all the relations, previously derived for the piezo-electric transducers, can be adopted. Only the inner mechanical impedance must be replaced by

$$Z'_{Mi} = Z_{Mi} - \frac{1}{j\omega \overline{C}} \left(\frac{\overline{U}\overline{C}}{d} \right)^2. \quad (8.51h)$$

In this way, the chain of matrices becomes

$$\begin{aligned} \begin{Bmatrix} F \\ v \end{Bmatrix} &= \begin{bmatrix} 1 & Z'_{Mi} \\ 0 & 1 \end{bmatrix} \begin{bmatrix} 0 & \alpha \\ -1/\alpha & 0 \end{bmatrix} \begin{bmatrix} 1 & -1/Z_{Ei} \\ 0 & 1 \end{bmatrix} \begin{Bmatrix} i \\ U \end{Bmatrix} \\ &= \begin{bmatrix} Z'_{Mi}/\alpha & \alpha + Z'_{Mi}/\alpha Z_{Ei} \\ -1/\alpha & 1/\alpha Z_{Ei} \end{bmatrix} \begin{Bmatrix} i \\ U \end{Bmatrix}, \end{aligned} \quad (8.52a)$$

in case of an immobile backing electrode. With $Z_{MM} \rightarrow \infty$, the transfer function of the transducer operated as a sensor is obtained by means of (8.50a) as

$$\left. \frac{\underline{U}}{\underline{v}_K} \right|_{\underline{U}_K=0} = \frac{\overline{C} \overline{U} Z_{Ei}}{d(1 + Z_{Ei}/Z_{EK})} \rightarrow \frac{-\overline{U}}{j\omega d(1 + 1/j\omega \overline{C} R)}. \quad (8.52b)$$

In this development are used the impedances $Z_{Ei} = 1/j\omega \overline{C}$ and $Z_{EK} = R$, in accordance with applications in practice. Upon multiplying both sides by $j\omega$, the left-hand side becomes the ratio of voltage to displacement $\xi = v_K/j\omega$. This means that for high impedance signal analysis equipment such that $\omega > 1/RC$, the electro-static transducer constitutes a displacement sensor.

The transducer relations derived in these sections can also be established by means of Hamilton's principle, once again proving its generality. The procedure will be exemplified in this section of electro-static transducers whereby are required the energy of a charged condenser

$$E_C = \frac{1}{2} \frac{\underline{Q}^2}{C}, \quad (8.53a)$$

and that of an inductance

$$E_L = \frac{1}{2} L i^2 = \frac{1}{2} L \dot{Q}^2, \quad (8.53b)$$

both of which can be obtained from textbooks.

For the model sketched in Fig. 8.28, where the displacement ξ_K is assumed prescribed, the kinetic energies to be considered are $m_K \dot{\xi}^2/2$ and $L \dot{Q}^2/2$ whilst the potential energies read $s_\xi \xi^2/2$, $s_K (\xi - \xi_K)^2/2$ and $(\overline{Q} + \tilde{Q})^2/2(\overline{C} + \tilde{C})$. This means that the Hamiltonian becomes

$$\frac{1}{2} \left[m_K \dot{\xi}^2 + L \dot{Q}^2 - s_\xi \xi^2 - s_K (\xi - \xi_K)^2 - \frac{(\overline{Q} + \tilde{Q})^2}{\overline{C}} (1 - \xi/d) \right], \quad (8.53c)$$

where both the charge and the capacitance are split in dc and ac components and the vanishing time derivative of \tilde{Q} is omitted. In the last term, moreover, the displacement dependent ac component of the capacitance is approximated according to (8.51d).

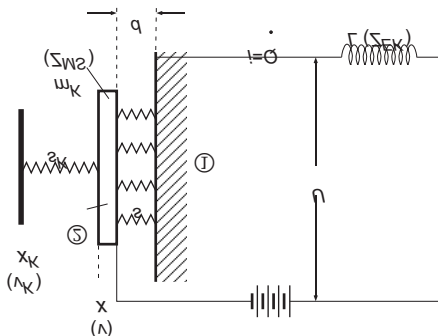


Fig. 8.28. Model of electro-static transducer showing the notation used in Eqs. (8.51) to (8.54). The backing electrode (1) and the mass (2) form a capacitor

Upon carrying out the variation with respect to the unknown coordinates ξ and \tilde{Q} , one obtains

$$\begin{aligned} m_K \ddot{\xi} + s_K (\xi - \xi_K) - \frac{(\bar{Q} + \tilde{Q})^2}{2\bar{C}d} &= 0, \\ L \ddot{\tilde{Q}} + \frac{1}{C} (\bar{Q} + \tilde{Q})(1 - \xi/d) &= 0. \end{aligned} \quad (8.54a)$$

The subsequent manipulations are:

- Omission of terms of second order e.g., $\xi \dot{\tilde{Q}}$.
- Change to velocity $v = \dot{\xi}$ and current $i = \dot{\tilde{Q}}$ implying that all dc components vanish.
- Introduction of phasor notation i.e., $\ddot{\xi} = j\omega \underline{v}$, $\ddot{\tilde{Q}} = j\omega \underline{i}$.
- Substitution of the inductive impedance $j\omega L$ by Z_{EK} and the mass and spring impedance by Z_{Mi} such that, simultaneously, the result becomes more general and losses can be taken into account.

The outcome of these operations is

$$\begin{aligned} Z_{Mi} \underline{v} + \frac{s_K}{j\omega} \underline{v} - \beta \underline{i} &= \frac{s_K}{j\omega} \underline{v}_K, \\ \beta \underline{v} - \left(Z_{EK} + \frac{1}{j\omega C} \right) \underline{i} &= 0, \end{aligned} \quad (8.54b)$$

where the abbreviation $\beta = \bar{Q}/j\omega d\bar{C} = \bar{U}/j\omega d$ has been introduced. Clearly the first expression has the dimension of force whereas the second that of voltage. Therefore, this set of equations can be compared with that in (8.52a). By observing that the force and the voltage are $F = s_K(v_K - v)/j\omega$ and $\underline{U} = Z_{EK} \underline{i}$ respectively, Eq. (8.54b) can be rewritten as

$$\begin{aligned}\underline{F} &= Z_{Mi} \underline{v} - \beta \underline{i}, \\ \underline{U} &= \beta \underline{v} + i/j\omega \bar{C}.\end{aligned}\quad (8.54c)$$

It is somewhat laborious to bring (8.54c) in the form of (8.52a) since the difference between Z_{Mi} and Z'_{Mi} need be considered. If, in spite of that, the algebra is undertaken, it is found that both methods yield the same result with the exception of the sign of the current i , associated with the sign convention.

A comparison of the two procedures shows that the one based on Hamilton's principle is the least transparent and that, in the present formulation, the electrical and mechanical losses can be taken into account only afterwards. On the other hand, however, it has the advantage of starting from very fundamental relations as well as automatically accounting for the equality in transducer constants, the influence of the inner impedances and the significance of the additional, electrically induced stiffness.

8.3.4 Electro-Magnetic Transducers

For electro-magnetic transducers, the ferromagnetic armature is located in a magnetic field with a large flux as depicted in Fig. 8.29. The force acting between the magnet and the armature, is proportional to the flux squared,

$$F \propto \Phi^2 \propto (\bar{\Phi} + \tilde{\Phi})^2. \quad (8.55a)$$

To establish a linear relationship between the electrical and mechanical variables, again, a large dc component Φ is required. It can be achieved by means of a permanent magnet or a coil supplied with a direct current. Superimposed on the direct component is an alternating. Operated as an exciter, the latter is the alternating current through the coil and as a sensor, it is ultimately the perturbations of the reluctance due to the changes in the distance d , which give rise to an alternating flux $\tilde{\Phi}$. Because the transducer is reversible, the ideal transducer relations are given by

$$\begin{Bmatrix} \underline{F}_w \\ \underline{v}_w \end{Bmatrix} = \begin{bmatrix} \gamma & 0 \\ 0 & -1/\gamma \end{bmatrix} \begin{Bmatrix} \underline{i}_w \\ \underline{U}_w \end{Bmatrix}, \quad (8.55b)$$

where γ is the transducer constant, dependent on the distance d , the strength of the magnetic field and the geometry.

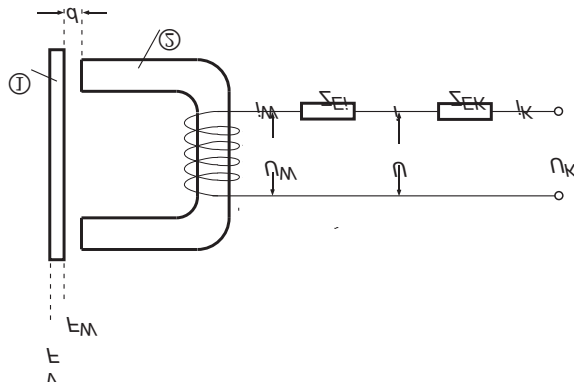


Fig. 8.29. Principle configuration of an electro-magnetic transducer. Ferromagnetic armature (1) and permanent magnet (2)

A comparison with Eq. (8.40c) shows that save the numerical values, the transducer relations equal those of ideal electro-dynamic transducers. Also the role of the inner electrical impedance is the same since it results in a voltage drop. In both cases, the inner impedance consists of an inductance L_i and a resistance. Regarding the inner mechanical impedance, there is a small difference. Similar to the electro-static transducer, there is an attraction force which depends on the distance between the magnet and the armature and thus on their relative motion. As before, this leads to a negative stiffness cf., (8.51e). This means that Eq. (8.42d), again, can be adopted albeit with Z_{Mi} replaced by

$$Z'_{Mi} = Z_{Mi} - \frac{s_E}{j\omega} = Z_{Mi} - \frac{\gamma^2}{j\omega L_i}. \quad (8.55c)$$

As seen, the pivotal quantity with respect to the reaction of an electrical element on the mechanical impedance is, as always, the square of the transducer constant.

By multiplying the matrices (8.41d), (8.55b) and (8.41a), the relation for the physical electromagnetic transducer with an immobile magnet is obtained as

$$\begin{Bmatrix} F \\ v \end{Bmatrix} = \begin{bmatrix} (\gamma^2 + Z'_{Mi} Z_{Ei})/\gamma & -Z'_{Mi}/\gamma \\ Z_{Ei}/\gamma & -1/\gamma \end{bmatrix} \begin{Bmatrix} i \\ U \end{Bmatrix}. \quad (8.55d)$$

From this relation, all the quantities of interest can be developed. If the motion of the magnet must be taken into account, the procedure demonstrated in Sect. 8.3.1.2 applies.

Electro-magnetic as electro-static transducers essentially are employed in the laboratory. Their advantage is that they are only weakly coupled to the test object and realize hardly any loading, also allowing for investigations of very light-weight systems.

8.3.5 Magnetostrictive Transducers

A magnetostrictive transducer most often consists of a rod of magnetostrictive material inserted in a coil as illustrated in Fig. 8.30. The primary magnetostrictive materials are nickel, some ferrites and, more recently, special alloys termed “giant magnetostrictive alloys” [8.10].

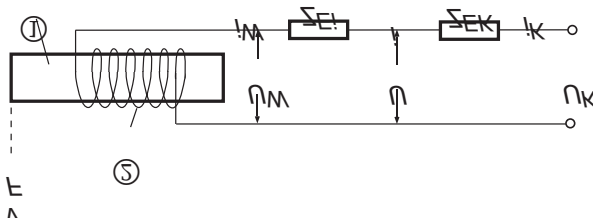


Fig. 8.30. Principle configuration of a magnetostrictive transducer. Magnetostrictive rod (1) and coil (2)

By passing a current i through the coil, the magnetic forces in the magnetostrictive material either shorten or lengthen the rod and constraining the rod at its ends results in a relatively large force. As stated previously, the force is proportional to the square of the magnetic flux. To achieve an alternating force, proportional to some supplied alternating current, a dc component is again required, such that the total and the transducer forces can be written as

$$F \propto \Phi^2 = \frac{1}{2} \gamma_s i^2 = \frac{1}{2} \gamma_s (\bar{i} + \tilde{i})^2 \approx \frac{1}{2} \gamma_s \bar{i}^2 + \gamma_s \bar{i} \tilde{i}, \quad (8.56a)$$

$$F_w = \gamma_s \bar{i} \dot{i}_w.$$

Since the transducer is reciprocal for $\bar{i} \gg \tilde{i}$, an alternating voltage arises when the magnetostrictive transducer is compressed with the velocity v_w , which is given by

$$U_w = -\gamma_s \bar{i} v_w. \quad (8.56b)$$

With the exception of the altered symbols, these relations are the same as those for the electro-magnetic transducers. Moreover, since the effects of inner electrical and mechanical impedances are the same, the formulae of the previous section can be directly adopted.

Magnetostrictive transducers essentially are used in underwater acoustics. The attainable displacement amplitudes are very small. For nickel, the maximum relative elongation is of the order of 10^{-6} and for the giant magnetostrictive alloys 10^{-4} to 10^{-3} .

Despite the very simple design, the magnetostrictive transducers are only employed for special structure-borne sound problems [8.11]. Typically, there is a use when large force and small displacements are required such as at high frequencies. A disadvantage is the direct current required which is accompanied by resistive losses.

8.3.6 Elaboration on Reciprocal Transducers

8.3.6.1 M- and N-Transducers

By summarizing the transducer expressions for immobile magnets and backing electrodes respectively, those dependent on magnetic fields in (8.41f) and (8.55c) are described by

$$\begin{aligned} \left\{ \frac{F}{v} \right\} &= \frac{1}{Bl_L} \begin{bmatrix} (Bl_L)^2 + Z_{Mi}Z_{Ei} & -Z_{Mi} \\ Z_{Ei} & -1 \end{bmatrix} \left\{ \frac{i}{U} \right\}, \\ \left\{ \frac{F}{v} \right\} &= \frac{1}{\gamma} \begin{bmatrix} \gamma^2 + Z'_{Mi}Z_{Ei} & -Z'_{Mi} \\ Z_{Ei} & -1 \end{bmatrix} \left\{ \frac{i}{U} \right\}, \end{aligned} \quad (8.57a)$$

for the electro-dynamic and electro-magnetic as well as magnetostrictive transducers respectively. When all displacements are blocked, the force is proportional to the alternating current for this class of transducers.

For the transducers dependent on electro-static forces, (8.48), (8.49), (8.41a) and (8.52a) apply. One finds

$$\begin{aligned} \left\{ \frac{F}{v} \right\} &= \frac{1}{K} \begin{bmatrix} -Z_{Mi} & K^2 + Z_{Mi}/Z_{Ei} \\ -1 & 1/Z_{Ei} \end{bmatrix} \left\{ \frac{i}{U} \right\}, \\ \left\{ \frac{F}{v} \right\} &= \frac{1}{\alpha} \begin{bmatrix} Z'_{Mi} & \alpha^2 + Z_{Mi}/Z_{Ei} \\ -1 & 1/Z_{Ei} \end{bmatrix} \left\{ \frac{i}{U} \right\}, \end{aligned} \quad (8.57b)$$

for the piezo-electric and electro-static transducers. For this class of transducers, the forces are proportional to the alternating voltage as the displacements vanish.

Two of the relations in (8.57a) and (8.57b) still contains the flaw that the electrically induced, negative stiffness must be considered in the inner mechanical impedance Z'_{Mi} . By substituting (8.51f) and (8.55c) in (8.57b) and (8.57a) respectively, the electro-static description becomes

$$\left\{ \begin{array}{c} F \\ v \end{array} \right\} = \frac{1}{\alpha Z_{Ei}} \begin{bmatrix} (\alpha Z_{Ei})^2 + Z_{Mi} Z_{Ei} & Z_{Mi} \\ -Z_{Mi} & 1 \end{bmatrix} \left\{ \begin{array}{c} i \\ U \end{array} \right\}. \quad (8.57c)$$

Upon letting $Bl_L \rightarrow \alpha Z_{Ei}$, (8.57c) but the sign becomes identical to the formula for the electro-dynamic transducer. The electro-static and electro-dynamic transducers are categorized as M -transducers (equivalent voltage source). The description in (8.57c), moreover, would have been established directly from Eq. (8.54c), developed from Hamilton's principle.

In a similar way, one obtains

$$\left\{ \begin{array}{c} F \\ v \end{array} \right\} = \frac{1}{\gamma} \begin{bmatrix} Z_{Mi} & \gamma^2 + Z_{Mi}/Z_{Ei} \\ 1 & -1/Z_{Ei} \end{bmatrix} \left\{ \begin{array}{c} i \\ U \end{array} \right\}, \quad (8.57d)$$

for the electro-magnetic and magnetostrictive transducers from (8.57a) with (8.55c). Aside for the sign, this is also valid for the piezo-electric transducer. The latter electromagnetic and the magnetostrictive transducers are categorized as N -transducers (equivalent current source). Ultimately, however, the categorization is of a formal nature.

8.3.6.2 Reciprocity Calibration

The reciprocity of reciprocal transducers can be used also to calibrate electro-mechanical transducers without absolute measurements of dynamic quantities. The procedure is illustrated in two steps in Fig. 8.31 [8.12].

In the first step, a mass is given a velocity v_1 by means of an auxiliary exciter. Instead of a mass, any other mechanical structure can be used provided its impedance is well defined. The voltage proportional to the velocity is measured at the transducer W to be calibrated and the reciprocal transducer R ,

$$U_{W1} = \alpha_W v_1, \quad U_{R1} = \alpha_R v_1. \quad (8.58a)$$

For the second step, the auxiliary exciter is turned off and the mass driven by the reciprocal transducer. The force F_2 and velocity v_2 resulting for a current i_{R2} are related by

$$|v_2| = |F_2/Z| = |\alpha_R i_{R2}/Z|, \quad (8.58b)$$

where Z is the known impedance. In this relation is used that the reciprocity principle or the law of mutual energies are valid such that

$$\left| \frac{\underline{U}_{R1}}{v_1} \right| = \left| \frac{\underline{F}_2}{\underline{i}_{R2}} \right|, \quad \underline{U}_{R1} \underline{i}_{R2} = \underline{F}_2 v_1, \quad (8.58c)$$

respectively. Since the transducer to be calibrated should be linear, the voltage offered is

$$\underline{U}_{w2} = \alpha_w v_2. \quad (8.58d)$$

By substitution of (8.58a) and (8.58b), v_2 , α_R and v_1 can be eliminated and

$$|\alpha_w|^2 = \left| \frac{\underline{U}_{w1} \underline{U}_{w2}}{\underline{U}_{R1} \underline{i}_{R2}} Z \right|. \quad (8.58e)$$

Thus, the determination of the calibration factor α_w sought is transferred to measurements of electrical voltages and currents besides the knowledge of a well-defined impedance.

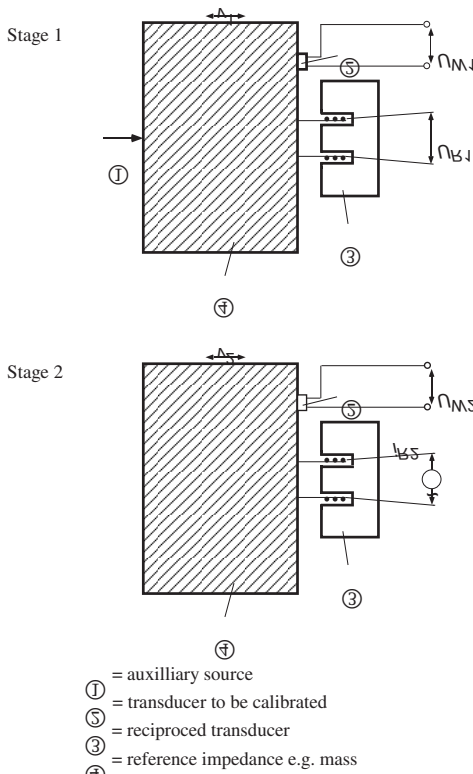


Fig. 8.31. Measurement of combined quantities associated with bending motion

Precise measurements of currents and voltages are usually straightforward as long as the reciprocal transducer is sufficiently strong to achieve a measurable signal over the entire range of interest. A well-defined impedance can be more cumbersome, however, since also for compact masses, the suspension may lead to deviations from the basic $Z = j\omega m$. Additionally, it must be taken into account that for small masses, all connected electrical equipment can noticeable affect the impedance.

8.4 Combined Quantities

With the transducers hitherto described, the displacement, velocity, acceleration or strain can be measured directly. In addition to these primary measurement quantities, more and more often some further are required, which can be derived from the former. For bending motion, for example, the first and second derivatives, corresponding to the cross-sectional rotation and the curvature respectively can be of interest. Those derived quantities can be obtained from finite differences formed from the signals from two or three identical or carefully calibrated transducers, as illustrated in Fig. 8.32. In this it is important that the distance Δx , on the one hand, does not become too small but, on the other, not too big. In the former situation, signals are subtracted of almost the same magnitude with enhanced errors as a risk whereas, in the latter, the finite difference will not be a satisfactory approximation of the corresponding differential. A reasonable compromise is to set Δx somewhere between a twentieth and a tenth of the wavelength.

Without strain gauges, strain can be measured also by using two adjacent sensors and approximating the spatial derivative in e.g., (3.1) by a finite difference.

A substantial problem for the structure-borne sound measurement technique as a whole is the fact that with the exception of optical methods in transparent structures, there are no means to undertake measurements in the interior of a structure without causing serious disturbances of the vibration field. Accordingly, one is forced to extract the interior motion from the results of measurements on the surfaces. As long as the structure is thin i.e., its thickness typically less than a sixth of the governing wavelength, such an extraction is principally possible. In that case, it can be assumed that all quantities are linearly related. Nonetheless, such measurements can prove rather laborious when different wave types must be distinguished. In Fig. 8.33 is exemplified the extraction of displacement, rotation, strain and cross-sectional contraction from measurements of eight displacement

quantities on two sides of a thin structure. Fortunately, such extensive and error prone measurements are only necessary on rare occasions since frequently, the most dominant component of motion can be identified and a proper transducer configuration devised.

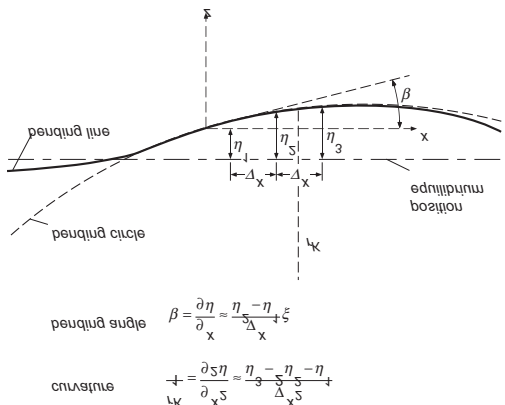


Fig. 8.32. Estimation of different components of motion from surface measurements

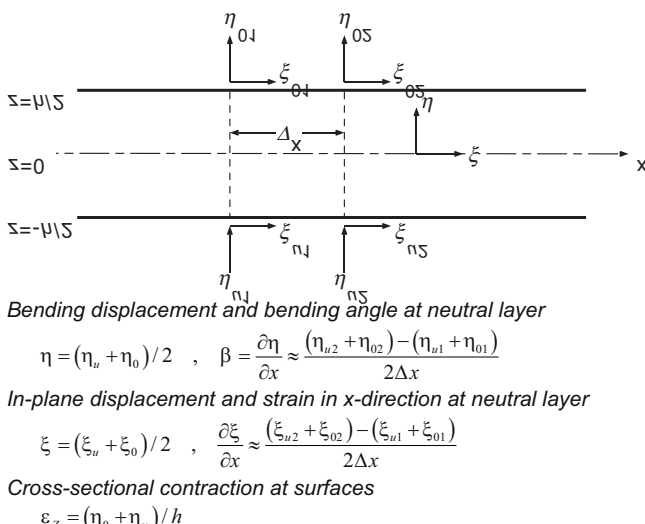


Fig. 8.33. Determination of various motion components from measurements on the surfaces of a plate or shell structure

In conjunction with measurements of structure-borne sound intensity, registration of stress and velocity is required as indicated by the expression in Sect. 3.9. Again, the velocity registration is comparatively straightforward, at least as far as the necessary quantities representing the interior motion can be deduced from measurements at the surfaces. In contrast, the determination of stresses is more intricate from two aspects [3.27,3.28]:

- The stress-strain relations comprise several strain components cf., (3.119) and (3.162a), such that a set of finite differences would have to be formed. Due to the complicated and error prone finite difference operators, simple states of deformation are assumed, for which simple stress-strain relations are available, (3.2), (3.42), (3.54), (3.73) and (3.223f).
- The stresses can be calculated from the strains only when some properties such as Young's modulus or shear modulus are known for the material at the measurement position. This means that certain knowledge must be present in advance.

At present, measurement of structure-borne sound intensity in slender rods and beams as well as in thin plates and shells is practicable in the laboratory. The employment of the technique in everyday practice will probably take a while although the insight gain from knowledge of the intensities and power transmissions would be of great help in many practical applications.

References

- [8.1] Bragg W., 1929. An instrument for measuring small amplitudes of vibrations. *Journal of Scientific Instruments*, 6, p. 196
- [8.2] Cremer L. and Klotter K., 1959. Neuer Blick auf die elektrisch-mechanischen Analogien. *Ingenieur-Archiv*, 28, p. 27
- [8.3] Halliwell N.A., 1979. Laser-doppler measurement of vibrating surfaces: A portable instrument. *Journal of Sound and Vibration*, 62, p. 312
- [8.4] Neubert H., 1975. Instrument transducers: An introduction to their performance and design. Clarendon Press, Oxford
- [8.5] Lenk A., 1977. Elektromechanische Systeme, Band 1,2. VEB Verlag, Berlin
- [8.6] Harris C.M. and Crede C.E., 1976. Shock and vibration handbook, Ch. 13-22. McGraw-Hill
- [8.7] Crawley E.F. and de Luis J., 1987. Use of piezoelectric actuators as elements of intelligent structures. *AIAA Journal*, 25, p. 1373
- [8.8] Hertz H., 1884. Die Principien der Mechanik in neuem Zusammenhang dargestellt. Drei Arbeiten von Heinrich Hertz mit einem Vorwort von H.von Helmholtz. Akademische Verlagsanstalt, Leipzig

- [8.9] Meyer E. and Guicking D., 1974. Schwingungslehre Ch. 3. Vieweg, Braunschweig
- [8.10] Savage H.T., Abbundi R., Clark A.E. and McMasters O.D., 1979. Permeability, magnetomechanical coupling and magnetostriction in grain-oriented rare earth-iron alloys. Journal of Applied Physics, 50, B3, p. 1674
- [8.11] Petersson B.A.T., 1987. On the use of giant magnetostrictive devices for moment excitation. Journal of Sound and Vibration, 116, p. 191
- [8.12] Beranek L.L., 1954. Acoustics, part XXIX. McGraw-Hill, New York NY

List of Symbols and Notation

A	Amplitude, absorption area [m^2]
B	Bending stiffness of beam [Nm^2], strength of magnetic field [Vs/m]
B'	Bending stiffness of plate [Nm],
C	Capacitance [F], specific heat [$\text{J}/(\text{kg}\cdot\text{K})$], rotational stiffness
D	Modulus of elasticity (longitudinal stiffness) [N/m^2]
D'	Real part of complex longitudinal stiffness \bar{D}
D''	Imaginary part of complex longitudinal stiffness \bar{D}
E	Young's modulus [N/m^2], energy [J]
$E(\dots)$	Abbreviation for exponential function
E_x, E_z	Young's modulus in x - and z -directions
E_{kin}	Kinetic energy
E_{pot}	Potential energy
F	Force [N]
F_0	Exciting point force
$F_{x, y, z}$	Force components in x -, y - and z -directions
F_W	Transducer force
F'	Force per unit length
G	Shear modulus [N/m^2]
H	Hamiltonian
$H_n^{(2)}(\dots)$	Hankel function of second kind and order n
I	Second area moment [m^4], impulse [Ns]
I'	$\hbar^2/12$
J	Intensity [W/m^2]
$J_{x, y, z}$	Intensity components in x -, y - and z -directions
$J_n(\dots)$	Bessel function of order n
K	Piezoelectric transducer constant, compressional modulus [N/m^2], shear stiffness
L	Level [dB], inductance [H]
L_p	Sound pressure level
L_W	Sound power level
M	Moment [Nm]

N	Integer number, number of modes
Q	Electrical charge [C], complex power [W]
Q_x, Q_z	Cross-sectional force components
R	Electrical resistance [Ω], transmission loss, radius, distance
S	Area [m^2]
T	Period, reverberation time [s], torsional stiffness [Nm^2], tensional force
U	Voltage [V], flow velocity, speed [m/s]
U_W	Transducer voltage
V	Reactive power [W]
W	Active power [W], work [J]
W_{diss}	Dissipated power
W'	Power per unit length [W/m]
Y	Mobility
Y_\sim	Wave mobility
Z	Impedance
Z_\sim	Wave impedance
Z_E	Electrical impedance [Ω]
a	Radius of cylinder or sphere [m], acceleration [m/s^2]
a_{11}, a_{12}, \dots	Auxiliary quantities
b	Width [m], half-power bandwidth
c	Wave and phase speed [m/s]
c_0	Wave speed in ambient fluid
c_B	Bending wave speed
c_g	Group speed
c_L	Longitudinal wave speed (3D)
c_{LI}	Longitudinal wave speed (2D)
c_{LII}	Longitudinal wave speed (1D)
c_R	Rayleigh wave speed
c_T	Transversal or shear wave speed
$c_{\mu\nu}$	Coupling factor
d	Thickness [m]
e	Base of natural logarithm, energy density [J/m^3]
f	Frequency [Hz]
f_n	n-th resonance frequency
f_c	Critical frequency, coincidence frequency
g	Gravitational acceleration, shear parameter, propagation constant
h	Plate thickness [m]

i	Electrical current [A]
i_W	Transducer current
j	Imaginary unit
k	Integer number, wavenumber [1/m]
k'	Real part of complex wavenumber \underline{k}
k''	Imaginary part of complex wavenumber \underline{k}
$k_{x,y,z}$	Wavenumber components in x -, y - and z -directions
k_0	Wavenumber in ambient fluid
k_B	Bending wavenumber
k_L	Longitudinal wavenumber
k_r	Wavenumber in radial direction
k_R	Rayleigh wavenumber
k_T	Shear wavenumber
$\mathbf{i}, \mathbf{j}, \mathbf{k}$	Unit vectors in x -, y - and z -directions
l	Length [m]
l_m	Mean free path [m]
m	Mass [kg]
m'	Mass per unit length [kg/m]
m''	Mass per unit area [kg/m ²]
n	Refraction index, integer number
p	Pressure, force per unit area, sound pressure [N/m ²]
q	Volume velocity [m ³ /s]
r	Frictional resistance [Ns/m], radius [m], reflection factor
r_{LL}, r_{LT}, r_{TT}	Reflection factors for longitudinal and transversal waves
r_0, r_l	Reflection factors at the ends of a rod
r_j	Reflection factor for evanescent wave
s	Stiffness [N/m], arc length [m]
s''	Stiffness per unit area [N/m ³]
\mathbf{s}	Displacement vector
t	Time [s], transmission coefficient
t_j	Near-field transmission coefficient
u	General field variable
v	Particle velocity [m/s]
$v_{x,y,z}$	Particle velocity components
v_w	Transducer velocity
w	Rotational or angular particle velocity [1/s]
∇^2	Laplace operator
Δ	Difference, time step, thickness ratio

ΔN	Number of modes in a frequency band
Θ	Mass moment of inertia [kgm^2]
Θ'	Mass moment of inertia per unit length [kgm]
Λ	Logarithmic decrement, norm of eigenfunction [kg], thermal conductivity [$\text{W}/(\text{m}\cdot\text{K})$]
$\Pi(\dots)$	Propagation function
Φ	Scalar potential, magnetic flux [Vs]
Ψ	Vector potential
α	Eigen-value, transducer constant, absorption factor, radiation parameter, auxiliary quantity
β	Cross-sectional rotation, excitation parameter, auxiliary quantity
γ	Shear angle, phase shift, transducer constant, Green's function
δ	Variation, decay constant, dilatation, acoustic boundary layer thickness
$\delta(\dots)$	Dirac's delta function
ε	Strain, auxiliary quantity
$\varepsilon_{x, y, z}$	Strain in x -, y - and z -directions
ζ	Displacement in z -direction [m], radiation fraction
η	Displacement in y -direction, lossfactor
$\eta_{\mu\nu}$	Coupling lossfactor
ϑ	Angle of incidence, auxiliary quantity
κ	Auxiliary quantity
λ	Wavelength [m]
λ_B	Bending wavelength
λ_L	Longitudinal wavelength
λ_c	Wavelength at the critical frequency
λ_v	Lagrange's multiplier
μ	Poisson's ratio, auxiliary quantity
ν	Kinematic viscosity [m^2/s], non-dimensional frequency, integer number, auxiliary quantity
ξ	Displacement in x -direction
ρ	Density [kg/m^3], reflection efficiency
ρ_0	Density of ambient fluid
$\rho_{LL}, \rho_{LT}, \rho_{TT}$	Reflection efficiencies for longitudinal and transversal waves

σ	Normal stress [N/m^2], relaxation time, thickness ratio
$\sigma_{x, y, z}$	Stress components in x -, y - and z -directions
τ	Shear stress [N/m^2], radiation efficiency, transmission efficiency
$\tau_{xy}, \tau_{yz}, \tau_{zx}$	Shear stress components
φ	Phase angle
$\varphi(\dots)$	Eigen-function
ϕ	Phase angle
χ	Angle of rotation
ψ	Angle, auxiliary quantity
ω	Angular frequency
$\underline{\omega}_n$	Resonance frequency
\underline{x}	Averaged quantity
x	Complex quantity
\hat{x}	Peak value, Fourier transformed variable
\dot{x}, \ddot{x}	First and second time derivative
$ x' , x'' $	First and second spatial derivative
$ x $	Absolute value
x^*	Complex conjugated quantity
$\text{Re}[\dots]$	Real part
$\text{Im}[\dots]$	Imaginary part
x, y, z	Cartesian co-ordinates
r, φ, z	Cylindrical co-ordinates
R, ϑ, φ	Spherical co-ordinates

Index

- absorption coefficient 243
- acceleration noise 470
- accelerometer 238
- acoustic boundary layer 459
- acoustic far field 475
- active part of the power 327
- added system 221
- adiabatic 192
- after-effect functions 150
- airborne sound radiation 450
- analogy force - current 540
- angle of incidence 85
- angular velocity 49, 51
- anti-node 478
- antiresonance 178, 551
- apparent mass 482
- arbitrarily shaped structures 505
- attached layers 197
- attenuation 149
- attenuation constant 378
- attenuation region 379
- audible frequency range 1
- average absorption efficiency 403
- average modal energy 527
- average transmission efficiency 403, 412
- bandwidth 172, 217, 544
- beam excited normally by an impacting mass 249
- beams
 - vibrations 60
- bending moment 53
- bending stiffness 51
 - measurement 188
 - measurement of 184
- bending wave equation 54
- bending waves 49
 - effect of discontinuities 345
 - effect of interlayers 359
 - effect of masses 369
 - equation for beams 54
 - equation for plates 115
- Bessel function 289
- blocking masses 368
- body or bulk waves 93
- Boltzmann model 153
- boundary element method 507
- boundary layer noise 323
- branching junctions 354
- breathing mode 135
- bulk modulus of air 422
- capacitance sensor 557
- carbon microphone 553
- carrier frequency approach 557
- carrier wave 56
- centre lobe 476
- characteristic equation 5, 113, 137
- characteristic frequencies 65
- characteristic impedance 31, 237, 244
- characteristic impedance bending wave 346
- characteristic mobility 237
- coincidence 420, 485
- coincidence excitation 325
- complex conjugate 21
- complex exponential 5
- complex modulus 153
- complex modulus of elasticity 153
- complex nearfields 157
- complex power 327
- complex propagation speed 156

- complex wavenumber 156
compression modulus 422
condenser microphone 579
constant force source 330
constant velocity source 329
constrained layer 204
constrained layer configurations 201
contact stiffness 266
contact time 308
conversion 400
corners 348
corrected bending wave 121
corrected flexural wave 126
Coulomb friction 231
coupled oscillators 435
coupled plates 422
coupling
 of bending waves 424
 of flexural and longitudinal waves 373
coupling loss factors 438, 527
critical angle 90
critical frequency 486
cross-contractional modulus 118
cross-mobility 273
cross-sectional contraction 52
cross-sectional contractions 34
cross-sectional discontinuities 343
curvature 51
cut-on frequencies for propagating modes 269
cylindrical radiator 468
cylindrical shells 126
- damped beams 161
 bending waves 169
 quasi-longitudinal waves 162
 torsional waves 162
damping 149
 by resonant systems 217
 complex parameters 153
 data 191
 dry friction 231
 effect on vibration sensor 543,
 547
 energy variations 158
 measurements 173
 measurements beam 172
 measures 161
 mechanisms 192
 of attached layers 197
 of building materials 195
 of flexural waves 198
 of granular materials 224
 of interfaces 226
 of longitudinal waves 198
 of metals 191
 of plastics 193
 phase angle 175
 ratio 6, 543
 viscous 5, 150
 with spacer 200
damping due to relative motion
 normal 226
damping for built-up systems 225
damping layer 197
damping layers 208
damping material 197
damping mechanisms 193
damping quantities 161
dash-pot 541
decay time 186
decrement
 logarithmic 161, 179
degenerate 297
degenerate modes 297
dielectric transducer 578
dilatation 77
dilatational waves 80
dipole 482, 495
dipole sources 458
dipole type 496
Dirac's delta function 250, 280
directivity 475, 481, 493
 axially symmetric membrane 478
directivity of the radiation 451
discontinuity 345
dislocation processes 192
dispersion 55
 for waves on shells 134
 for waves on strips 140

- dispersion diagram 102, 105, 109,
135
dispersion equation 104
displacement vector 77
dissipation 149
divergence 77
divergence-free 79
Donell-Mushtari equation 132
double wall 512, 528
double wall resonance frequency
530
double-plate structures 422
doubly curved shells 140
driving-point impedance 162
dry friction 231
dry joints 232
dynamic absorber 547
- eccentric blocking mass 373
edge radiation 498
effect of damping 500
eigen-frequencies 20, 65, 290
eigen-function expansion theorem
293
eigen-functions 137, 139, 291, 294
eigen-values 5
eigen-vectors 20
eight-pole description 386
eight-pole equations 171
elastic half-space 93
elastic interlayers 359
elastic layer 360
elastic semi-infinite continuum 493
electrical circuit 540
electrical sensors for vibrations
capacitative type 558
inductance type 556
strain gauge 554
electro dynamic transducer 561
electro-dynamic exciter 570
electro-dynamic transducer 570
electro-magnetic transducer 583
electro-mechanical analogy 540
electro-mechanical circuit 540
electro-mechanical transducer 553,
560
- electro-mechanical transfer function
563
electro-static transducer 578
energy
in beams with attached springs
and waves 221
in plates with attached layers
197, 201
energy conservation 365, 369
energy density 29, 31
in bending waves 59
energy distribution 59
in bending waves 59
energy distributions
in longitudinal waves 32
equation of motion 4
orthotropic plates 117
thin plates 109
three-layer system 214
two-layer beam 211
equipartition 446
equivalent absorption length 404
error function 250
Euler's constant 466
exciting impulse 307
extensional strain 27
extensions 75
- far field 475
fillers 194
finite difference 589
finite element method 13
flanking paths 525
flanking transmission 525
flexural stiffness 51
measurement 185, 187
flexural waves 49
floating floor 422
flow resistance 423
fluid half-space the wave impedance
259
fluid loaded plate 492
fluid loading 464
fluid reaction 492
foot-fall noise 309
force - current analogy 540

- force gauge 554
 force transducer 238
 forced vibrations 524
 four-pole 168
 four-pole equations 168
 four-pole matrix 562
 four-pole representation 363, 384
 free bending waves 524
 free field 450
 free plate waves 101
 free surface 84
 free vibrations
 bending 67
 longitudinal 63
 free waves 260
 frequency modulation 557
 frequency response function 6
 frequency response of piezo-electric
 transducer 577
 friction dry 230
- gas pumping 226
 Gaussian error integral 250
 generation 2
 geometric far field 475
 geometric non-linearities 15
 geophone 550
 glass-transition temperature 194
 grazing incidence 403
 Green's function 311
 Green's function for thin plate 276
 group speed 57, 60
 gyroscopic element 437
- half-power bandwidth 161, 544
 half-value bandwidth 166, 172, 181,
 544
 Hamilton's principle 22, 120, 130,
 209, 392
 Hankel function 252, 465
 heat conduction phenomena 192
 high-polymer materials 193
 Hooke's law 28
 hydro-acoustic radiators 464
 hydro-dynamic mass 460
- hydro-dynamic short circuit 415,
 464, 467, 494
- ideal boundary conditions 68
 ideal reflection 62
 imaginary part of moment mobility
 275
 immobile reference 552
 impact duration or contact time 308
 impact excitation 306
 impedance 236
 driving point 236
 half space 265
 head 238, 239
 mass 163
 matrix 273
 measurement 238
 radiation 492
 simply supported rectangular
 plate 303
 spring 164
 transducer 545
 tube 243
- impedance formulae 286
 impulse of impacting mass 250, 307
 impulse response 311
 impulsive sound 470
 index of refraction 88
 inductance bridge 556
 inductive sensors 556
 infinitely long beam 273
 input mobility of an infinitely long
 rod 244
 input point mobilities of beams in
 flexure 245
 input point mobility of force excited
 plate 255
 input point mobility of semi-infinite
 beams 247
 intensity 29
 intensity method 451
 intensity structure-borne 140
 intensity vector 141
 interlayers 359
 inverse problem 434
 irrotational 79

- isothermal case 192
- Kelvin-Voigt model 150
- kinematic viscosity 226
- kinetic 10
- kinetic energy 10, 28
- Kirchhoff's bending theory 123
- Kirchhoff-Helmholtz integral equation 507
- Lagrange's equations 10
- Lagrange's multiplier 392, 397
- Laplace operator 78
- laser-doppler-vibrometer 558
- law of refraction 88
- level
- power 450
 - sound pressure 450
- limiting angle 91
- limiting angle for total reflection 91, 407, 412, 415
- loading transducer 551
- local elasticity 266, 306
- logarithmic decrement 161, 179
- longitudinal periodic system 376
- longitudinal vibrations 61
- longitudinal wave 27
- effect of elastic interlayers 360
 - effects of blocking masses 368, 373
 - effects of discontinuities 342
 - in beams and plates 36
 - in periodic structures 380
- loss factor 153, 160
- beams with attachments 221
 - definition 153
 - measurements 173
 - metals 191
 - plastics 195
 - plates with attached layers 197
 - relations to other damping measures 161
- loss factor and modulus of elasticity
- for high polymers 195
- loudspeaker, electro-dynamic 564
- low-pass filter for longitudinal and torsional waves 379
- L-waves 84
- magnetostrictive transducer 585
- mass controlled 8
- mass impact
- bending waves 249
 - input power 309
 - quasi-longitudinal waves 244
- mass law 510
- mass moment of inertia 46
- masses 368
- material properties 192
- Maxwell model 152
- mean free path 405
- measurement of complex modulus 175
- measurement of frequency response functions 177
- measurements on beams 183
- mechanical circuit diagram 238
- mechanical circuits 540
- damped mass 541
 - spring-loaded mass 539
 - spring-supported mass 541
 - two-mass system 545
- mechanical impedance 236
- mechanical mobility 236
- mechanical properties of metals 191
- membrane equation of shell 132
- metals
- damping mechanisms 192
 - mechanical properties 191
- method of residues 262
- Mindlin plate theory 263
- mobilities 7, 390
- formulae 286
 - matrix 273
 - measurements 239
 - of a tube 270
 - of half-space 265
- modal
- analysis 20
 - density 302
 - energies 433

- lattice 304
- power 468
- modal interaction term 489
- mode shapes 291
- modes 20
- modified shear stiffness 126
- modulus of elasticity 36
 - measurement 173
- moment
 - excitation 273
 - mobilities 272, 273, 274
- monopole 458
- M*-transducer 587
- multi-layered wall 533
- multiple-degree-of-freedom 20
- multi-pole sources 508
- mutual energies 19
- natural frequencies 65, 290
- natural vibrations 63
- Navier-Stoke's equations 226
- near fields 69
- node 478
- non-contacting device 559
- non-linearity 16
- norm 293
- N*-transducer 587
- number of modes and modal densities 302
- oblique incidence
 - airborne sound 508
 - flexural plate waves 402
 - on free surface 85
- orthogonality 291, 365, 369, 492
- orthogonality relation 280
- orthotropic plates 117, 266, 282, 488, 493, 510
- parametric excitation 322
- Parseval's theorem 482
- particular solution 5
- pass- and stop bands 383, 387
- period 32
- periodic bending wave-guide 385
- periodic longitudinal wave-guide
 - 381
- periodic structures 376
- phase
 - angle 6
 - constant 378
 - jump 70
 - speed of bending waves 55
- phasor notation 17, 64
- piezo-electric
 - effect 572
 - sensors 571
 - transducers 549, 572, 575
- piezo-film 572
- piston 452
- plane radiator 473
- plasticizers 195
- plastics
 - damping mechanisms 193
 - glass transition 194
 - temperature frequency equivalence 194
- plate 38
- plate strip 267
- plates
 - attached layers 197
 - bending stiffness 107, 115, 199, 206, 208
 - bending waves 113, 121
 - corrugated 119
 - design for high damping 200
 - flexural waves 114, 121
 - Green's function 276, 313
 - loss factor 198, 199, 202, 203, 206
 - moment mobility 274
 - multi-layer 208
 - orthotropic 117, 257
 - point mobility 255
 - power consideration 277
 - radiation from
 - finite plates 473, 499
 - infinite plates 461
 - response to
 - airborne sound 508

- response to distributed excitation 277, 283
response to point excitation 255
simple layer 197
spacer 200
thick 258
waves free 101
plates on a Winkler bed 493
playback of the surface roughness 319
point excited infinite beam 390
point excited thick plate 263
point impedance 236
point mobility 236, 263
Point mobility of a homogeneous plate 251
point mobility of a plate 267
point mobility of a plate strip 268
point source 457
Poisson's ratio 34
porosity 422
potential and kinetic energy 59
potential energies 10
potential energy 10, 29
power 451
airborne sound 449
balance 431
bending waves 49, 58
flow 50
level 450
quasi-longitudinal waves 37, 38
transmitted 248, 273
transmitted to infinitely extended structures 277
transmitted to plate-like structures 282
pressure level 450
prestressed plates 493
prestressed plates or membranes 510
propagation 2
constant 378
function 253
pure longitudinal waves 33, 36
pure transverse waves 41
quadrupole 496
quadrupole moments 482
quasi-longitudinal wave propagation 38
quasi-longitudinal waves 35, 162
 plates 38
 rods 37, 162
radian frequency 32
radiated power 449
radiation 2
 array of sources 473
 baffled plates 483
 cylindrical structures 501
 dipole 458
 efficiency 452, 466, 482
 cylinders 466
 finite plates 498
 point excited plates 499
 finite plates 473
 flexural nearfields 500
 impedance 492, 502
 infinite plates 461
 loading 494
 loss factor 453, 497
 measurements 452
 modes 489
 radius of gyration 142
 Rayleigh quotient 24
 Rayleigh wave 98
 Rayleigh wave at the surface of an elastic half-space 260
 Rayleigh wave speed 98
 Rayleigh-method 505
 reactive part of the complex power 327
 receiver 2
 reciprocity 587
 reciprocity principle 18, 334, 336, 515
 reciprocity relation 438
 reduction with distance 189
 reflection
 coefficient 343, 346
 efficiency 90, 91, 344

- factor 88, 92
reflection and transmission efficiencies 353
reflections and transmissions factors 351
refraction 407
refraction index 88
relaxation function 150
relaxation process 192
relaxation time 151, 192
resilient transmission elements 332
resonance frequency 181, 290
resonance function 544
resonant vibrations 161
 beams 161
 damping measurement 181
resonantly or resistively controlled 8
reverberant room 449
reverberation time 186, 404
reversible mechanical energy 160
rigid termination 552
ring frequency 134, 138
ring resonances 270
rolling noise 319
rotating mirror sensor 537
rotational
 inertia 46
 operator 77
 stiffness 364
rotations 76
rubber 195

sandwich plates 487
 damping 206
scatterer 507
scattering 406
second moment of area 52
secular solution 323
seismic mass 552
seismic waves 33
semi-conductors 556
semi-infinite beam 246
semi-infinite continuum 259
sensor
 acceleration 550
capacitative 557
displacement 554
force 554
inductive 556
strain 554
velocity 558
shear 75
 angle 39
 force 53
 modulus 40
 parameter 203
 stiffness 364
 strain 40
shell 126
 equation 133
 radiation 465
 wave speed 133
side lobes 476
Snell's law 88, 407
Sommerfeld radiation condition 251
sound bridges 427, 513
sound power level 450
sound pressure 450
sound pressure level 450
sound transmission 520
source 2
source of zero order 455
source volumes 286
source-free 80
source-free field 81
spacer 200
spatial average of the square of the velocity 298
spatial decay 187
spatial period 32
spatially periodic masses 376
specific heat 192
spherical radiator 455
spherical sound source 455
spring impedance 164
spring stiffness 10
squeeze film damping 226
St. Venant's principle 408
statistical energy analysis 430
steady-state response 6
stick and slip 231

- stick-slip motion 319
stiffness
 bending 51
 longitudinal 36
 shear 43
 torsional 45
stiffness controlled 8
Stokes layer 459
strain
 extensional 27
 gauge 554
 history 150
stress
 normal 28
 radial 128
 shear 45
stress-strain relation
 damping measurement 174
 elastic 150
 viscoelastic 159
strip 267
strong coupling 433, 445
structure-borne sound
 definition 1
 sensors 536
 transducer 560
structure-borne sound exciter 548
sudden release 317
sudden release of potential energy 317
surface wave 93
systems attached 217
- tensile stress 28
tensor formalism 81
thermal conductivity 192
thick plate 258
thin plate 274
three-layer systems 213
Timoshenko-Mindlin correction 123
torsional
 angle 44
 moment 46
 pendulum 179
 stiffness 45, 180
- stiffnesses of rectangles 47
wave impedance 419
waves 44, 47, 162
total attenuation 365
total reflection 368
total transmission 365, 368
trace speed 86
trace velocity 101, 406
trace wave matching 511
trace wavelength 85
transducer
 acceleration 550
 constant 561, 573, 580, 583
 crystal 573
 electro-dynamic 561
 electro-magnetic 583
 electrostatic 578
 force 577
 inductive 556
 magnetostrictive 585
 matrix 562
 piezoelectric 571
 strain 554
 structure-borne sound 561
 velocity 558
transfer function 177
transfer function of electro-dynamic transducer 565
transfer impedance 335
transfer mobilities 336
transition region 193, 195
transmissibility 542
transmission 2
transmission coefficient 347
transmission efficiency 343, 347, 351, 361, 368, 410, 510, 521, 524
 average 403
 bending waves 347
 blocking masses 368, 373
 corners 351, 353
 elastic interlayers 361
 longitudinal waves 343
 multi-layered wall 533
 plates 510
 stiffeners 410
transmission elements 326, 334

- transmission loss 344, 366
 transmission region 378
 transmitted power 255
 transverse motion
 quasi-longitudinal waves 34
 transverse waves 40
 transverse velocity 49
 transverse waves 40, 41
 trapped modes 366, 370
 tube 126, 145, 270, 465
 tuned damping resonators 217
 T-wave 86
 two-layer system 209
- vector potential 82
 velocity of the free source 329
 velocity sensor 558
 vibration
 holograms 560
 isolators 332
 vibration decay technique 180
 vibration exciter
 electro-dynamic 570
 electro-magnetic 583
 magnetostrictive 585
 piezoelectric 577
 viscoelastic 197
 viscosity 459
 viscous
 boundary layer 227
 damping 5
 damping coefficient 541
 film 230
 fluid 260
 friction force 150
 medium 226
 volume velocity 458
- wave conversion 86, 90, 349, 413
 wave equation
 beams with locally acting
 attachments 218
 general three-dimensional 78
 shell 131
- wave field 80
 wave impedance 136, 213, 237,
 256, 258
 wave impedance for a prestressed
 plate on a Winkler bed 259
 wave impedance of the thin plate
 257
 wave mobility 237, 256, 259
 orthotropic plate 257
 thin plate 257
 wave speed
 bending 55
 longitudinal 30
 quasi-longitudinal 37
 torsional 48
 transverse 40
 wave trace matching 319
 wave train closure principle 66
 wavelength 32
 bending waves 56
 wavenumber 31
 bending waves 55
 complex 156
 longitudinal 31
 spectrum 283
 waves
 bending 49
 body 93
 longitudinal 27
 Rayleigh 98
 surface 93, 96
 torsional 44
 transverse 39
 wave-train closure principle 65, 163
 weak coupling 445
 Wheatstone bridge 555
 Winkler bed 119
- Young's modulus 52
 complex 153
 measurement 174
- Zener model 152